Retarded sorption in wood : experimental study, analyses and modeling

Håkansson, Håkan

1998

Lund University • Sweden
Lund Institute of Technology
Department of Building Science
Report TABK--98/1012

RETARDED SORPTION IN WOOD

Experimental study, analyses and modelling

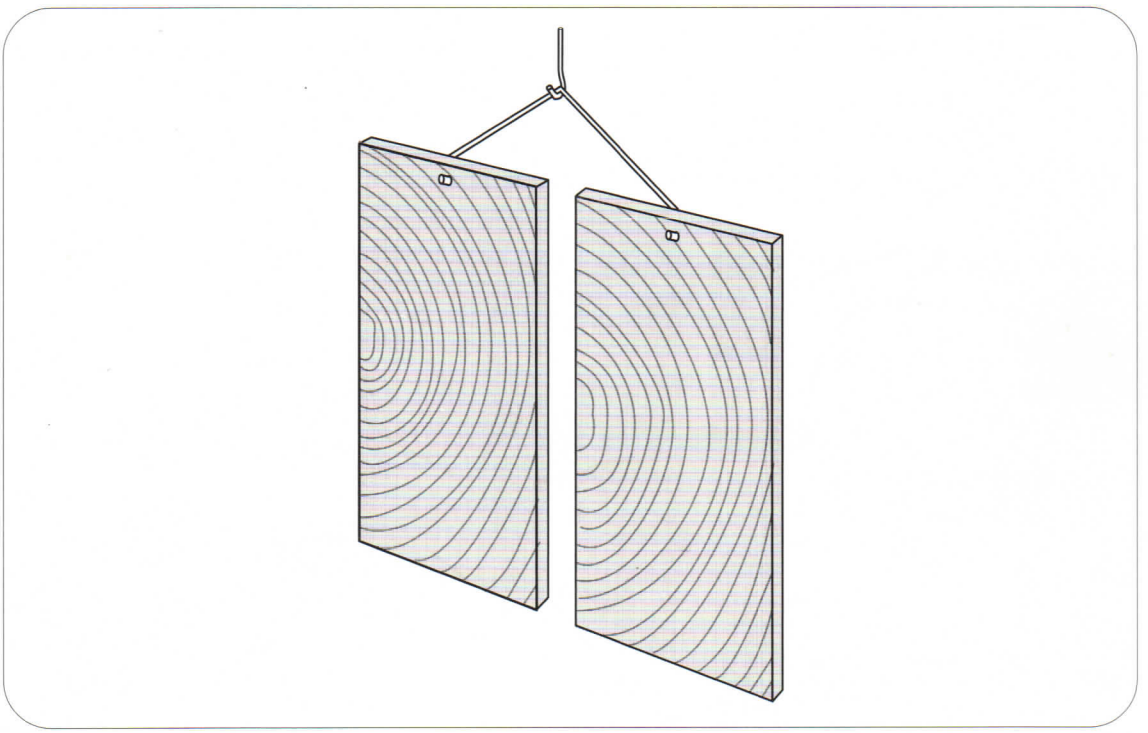

Håkan Håkansson

Building Science

Lund University

Lund University, with eight faculties and a number of research centres and specialized institutes, is the largest establishment for research and higher education in Scandinavia. The main part of the University is situated in the small city of Lund which has about 97 600 inhabitants. A number of departments for research and education are, however, located in Malmö. Lund University was founded in 1666 and has today a total staff of 5 850 employees and 38 200 students attending 50 degree programmes and 850 subject courses offered by 170 departments.

Department of Building Science

The Department of Building Science is part of the School of Architecture within the Faculty of Technology. The Department has two professorial chairs, Building Science and Building Services. Research at the Department is concentrated on energy management, climatic control and moisture problems. The main areas of research are:

- design and preformance of new low-energy buildings
- energy conservation in existing buildings
- utilization of solar heat
- climatic control
- climatic control in foreign climates
- moisture research

RETARDED SORPTION IN WOOD

Experimental study, analyses and modelling

Håkan Håkansson

This report relates to Research grant No 930272-7 from the Swedish Council for Building Research to the Department of Building Science, Lund University, Lund Institute of Technology, Lund, Sweden.

Keywords

moisture, wood, measurements, retarded sorption, non-Fickian, anomalous sorption, history-dependent sorption, latent heat effect, swelling-shrinkage, non-linear model, transient

Printed by KFS AB, Lund 1998

Report TABK- -98/1012
Retarded Sorption in Wood. Experimental study, analyses and modelling.

Lund University, Lund Institute of Technology,
Department of Building Science, Lund, Sweden.

ISSN 1103-4467
ISRN LUTADL/TABK- -1012- -SE

Lund University,
Department of Building Science
P.O. Box 118
SE-221 00 LUND
Sweden

Telephone: + 46 46 222 73 45
Telefax: + 46 46 222 47 19
E-mail: bkl@bkl.lth.se
Homepage: http://www.bkl.lth.se

Abstract

Models of moisture flow processes in wood are normally based on a Fickian approach. In many instances, there are considerable discrepancies between modelling and experimental results. It is shown in this thesis that a major cause for these discrepancies is a so-called retarded sorption which is not accounted for in conventional theories.

This retarded sorption occurs in the wood cell wall. A special experimental set-up to isolate and measure this process has been developed. Extensive series of sorption response measurements with different sequences of relative humidities have been performed on very thin, well exposed wood samples. The results show that the sorption often has an intricate dependence on moisture history. Two small steps may not give the same sorption as the corresponding single larger step. The process is not linear. The part of the sorption that is retarded is especially large at high relative humidities. The retarded sorption increases with decreasing temperature. In special cases, retarded sorption for single cell walls with a time scale of more than a month has been observed.

Different models to reproduce the measured results have been tested. It is shown that models with one added internal node are not sufficient. A few internal nodes are needed. The conductances between the nodes must be decreasing inwards. Non-linear conductances, where the conductance increases with the difference in moisture state between the nodes, are required to reproduce the result for more irregular sequences of relative humidity. The best agreement was obtained with a non-linear model with five internal nodes, where the innermost node accounted for hysteresis.

Tangential and radial swelling (and shrinkage) was measured in parallel for two series. The ratio between radial and tangential swelling was quite constant throughout the whole series with their many and varied changes of relative humidity. The variation in time of tangential swelling and moisture content followed each other quite well along lines with a constant slope, in particular for cyclic steps. A somewhat higher slope was obtained in all cases where the sorption contained a larger retarded part.

Contents

Acknowledgements

This work was initiated by my supervisor professor Johan Claesson. We have been in close contact resulting in many fruitful discussions during the whole period of this work. The basic type of measurements that were performed and the structure of the models are based on his ideas. The introduction of Section 1.1 follows closely a presentation by him where this work was a part, Claesson (1997). The mathematical model in Chapter 3 is originally due to him. I am deeply indebted for his patient efforts to help me structure my work.

I wish to thank Tech. Dr. Lars Wadsö for introducing me to the field of wood research and also for many suggestions regarding the experiments.

The members of the Moisture Research Group have provided a good base for my work by giving suggestions and ideas. I also wish to thank my colleagues at the Department of Building Science for their support.

The research was funded by the Swedish Council for Building Research. The support is gratefully acknowledged.

Lund, April 1998

Håkan Håkansson

1 Introduction

Wood is an excellent building material. In comparison with other building materials, it has good strength and stiffness relative to its weight. Wood has good thermal insulation properties in comparison with its load bearing capacity. Wood is easy to cut, tool and join together. The fact that wood has different properties in different directions can be exploited for more optimal designs. It is possible to produce wood in a cost-effective, environmentally friendly way. The tactile quality of wood makes it popular for furniture and interior design. It is perceived as a soft and inviting material for facades. There certainly is a potential for a widespread use of this versatile material. At the same time, the limits of function for wood has to be established, in order to avoid that unsuitable use will bring it into disrepute.

However attractive, the hygroscopic properties of wood have constantly to be addressed, so that moisture-related problems can be avoided. It is an important task to deepen and enlarge the knowledge of moisture behaviour in wood.

The interest of modelling of moisture processes in wood has increased during the last decade due to various problems related to moisture in wood. A few examples of such problems are rot and mould growth in painted exterior wood panels, dimensional changes with changing moisture content, and cracks caused by initial drying.

The possibilities of using advanced computer models have increased considerably due to the rapidly increasing computer capabilities. However it is still a main challenge is to establish proper, experimentally verified models, and in particular to determine the data needed in the models.

Many authors report discrepancies between measured and modelled moisture processes in wood. It is claimed in this thesis that the main reason for these discrepancies is that the sorption in the wood cell wall is not modelled in a correct way. The conventional use of the sorption isotherm implies that the moisture uptake is virtually instantaneous in small parts of the cell wall. But a closer analysis of experiments shows that the sorption process is much more complicated in many cases. It depends on the moisture history and, in a non-linear way, on the size of the change of relative humidity.

This sorption in the cell wall with its complicated behaviour and varying time scales will be referred to as *retarded sorption.*

A large part of the work in this thesis has been devoted to experimental studies of this retarded sorption under various conditions. The experiments are described and analysed in Part I. The second part reports the result from sequences of measurements. In the third part tentative models for the retarded sorption are described.

The swelling and shrinkage in the tangential and radial directions were measured on twin samples in the climate chamber. Accurate comparisons are hence possible.

An effect, peculiar for wood, is the substantially increased creep that is obtained when wood is subjected to load combined with humidity variations. This phenomenon is often referred to as the mechano-sorptive effect. A proper description of the temporal variations of the moisture content including the retarded sorption should have an important bearing on the mechano-sorptive effect. The mechano-sorptive effect is not dealt with in this thesis except when touched upon in connection with swelling and shrinkage.

1.1 Moisture flow in wood. Cell wall sorption

The modelling of moisture flow in wood involves particular problems. This will be discussed, and examples of results from this work will be presented.

1.1.1 Failure of Fickian models

Conventional models for isothermal moisture flow processes in wood are based on Fick's equation for the moisture flow g [kg/(m^2·s)], a sorption isotherm for the moisture content by volume $w(\varphi)$ [kg/m^3] and the mass conservation equation. In the one-dimensional case, using water vapour content v [kg_{water}/m^3] as independent variable, we have:

$$g = -D_v(\varphi)\cdot\frac{\partial v}{\partial x} \qquad w = w(\varphi) \qquad \frac{\partial w}{\partial t} = \frac{\partial}{\partial x}\left(D_v(\varphi)\cdot\frac{\partial v}{\partial x}\right) \qquad (1.1)$$

The water vapour content is $v = \varphi \cdot v_{sat}$ where φ is the relative humidity and v_{sat} is the water vapour content in saturated air. For wood the moisture content u [kg_{water}/kg_{wood}] usually is used. The moisture content is related to the dry mass of wood $w = \rho \cdot u$.

The equilibrium moisture content $u(\varphi)$ is measured for different relative humidities φ. The moisture flow coefficient $D_v(\varphi)$ which depends strongly on the relative humidity for high humidities, may be measured with the Cup-method. A steady-state flow is established over a slab of the material and the water flow is measured by weighing. Another common method to determine $D_v(\varphi)$ is to weigh continuously the moisture uptake after a step change of φ. This sorption method is discussed in great detail in Wadsö (1993). The problem is that the two methods often give quite different results, in particular for relative humidities above 70%. This type of discrepancies is reported in Nilsson (1990). A clear example of the discrepancy is shown in Figure 1.1, which is taken from Wadsö (1993). The full curves 1-4 show measured moisture uptake in samples of pine sapwood after a change of the relative humidity from 75% to 84%.The flow direction and the thickness of the samples are given in the table. The time to absorb half of the equilibrium moisture content is around 100 hours although the samples are quite thin. The corresponding dashed curves give the result of a calculation according to Eq. (1.1). The moisture flow coefficient has been measured with the Cup method for duplicate samples of pine sapwood. The time to half-absorption lies between 2 and 15 hours. There is a large discrepancy. There is something *fundamentally wrong* in our models.

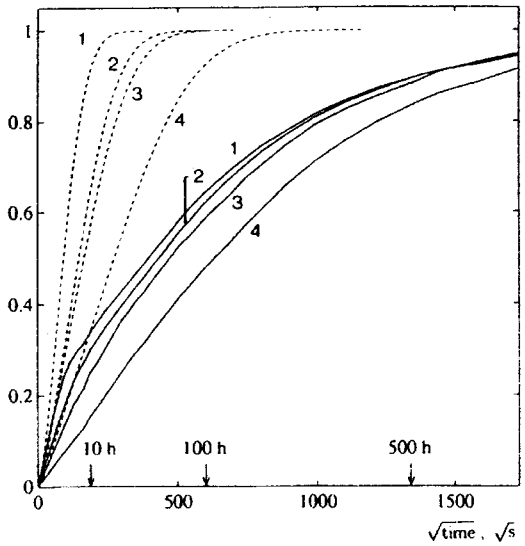

sample number	flow direction	half thickness mm
1	longitudinal	6,7
2	longitudinal	11,4
3	tangential	4,8
4	tangential	8,1

Figure 1.1 Relative moisture uptake in a sample of pine after a change of relative humidity from 75% to 84%. The dashed lines are the result from calculations. From Wadsö (1993).

1.1.2 Possible explanations of the discrepancies

The measurements cited above are carefully performed so the discrepancies are certainly not due to measuring errors.

The moisture changes are much slower than those predicted by Cup measurements A possible explanation is that there is a *surface resistance* over the wood surface. The conventional resistance from humid air to the outer wood surface, which is quite well known, is not sufficient. In order to fit the sorption measurements, one has to assume a much higher moisture flow resistance. The wood surface must in some way or another bloc the moisture transfer. A problem is that the discrepancies increase with increased relative humidity.

The curves 1, 2 (longitudinal flow) and 3 (tangential flow, thin sample) in Figure 1.1 lie quite close to each other after 10 hours and onwards. Suppose that a surface resistance is the major cause for the slow uptake of moisture. Sample 2 is twice as thick as 1 and 3. Then the relative uptake (per unit volume) would be only half of that of the other two. Curve 2 should lie much lower than the other two, if a surface resistance is dominating the uptake. This *proves* that a surface resistance cannot explain the long time-scales. The lag of curve 4 (tangential flow, thicker sample) is of the same size in measurements and calculations. The lag is due to the slower moisture migration in tangential direction.

We are forced to consider the single cell or wood fibre in order to find an explanation of the slow uptake. The moisture uptake in single cell walls was studied by Christensen in the Fifties. She in some cases used extremely thin slices of wood. Pure water vapour was used in order to reduce as much as possible any outside resistance between air and sample. She measured very clearly these long time-scales, Christensen (1965). The curves were similar to those in Figure 1.1 .

1.1.3 Retarded cell wall sorption

Thus, it is an experimental fact that there exists a *retarded cell wall sorption* with a wide range of time-scales of days and even much longer, in particular at higher relative humidities. This is a third elementary process that has to be measured and accounted for in the models. The *three elementary processes*, which are to be used in the models and must be measured, are:

- sorption isotherm $u(\varphi)$
- moisture flow coefficient $D_v(\varphi)$
- model for the retarded cell wall sorption

In Eq. (1.1), it is the left hand term $\partial w/\partial t$ that must be modified. The change of moisture content in the cell wall depends on the actual value of φ but also on the previous history, i.e. on $\varphi(t')$, $t' \leq t$. The problem is to find a description that reproduces experimental values with sufficient accuracy. The problem of transient cell wall sorption is touched upon in some references from Christensen (1965) and onwards, but a standard reference for models of moisture flow in wood like Siau (1984) does not mention these problems.

1.1.4 Measurements of retarded cell wall sorption

In order to study the transient cell wall sorption a precision climate chamber is used, Figure 1.2. The relative humidity $\varphi(t) = RH(t)$ is carefully controlled. The weight $u(t)$ of the sample is measured continuously. The tangential and radial free strain due to changes in moisture state, ε_t and ε_r , are measured on separate twin samples.

We want to reduce the moisture flow resistance from air to sample and through the sample as much as possible in order to obtain the transient cell wall sorption only. There is a strong air circulation in the chamber in order to reduce the air-to-sample resistance to a minimum. The samples of pine are very thin (1.7 mm), and they are cut perpendicular to the fibres. The moisture transport occurs in the fast fibre direction. The relative humidity is changed in steps. The response $u(t)$ of moisture content [kg_{water}/kg_{wood}] is measured continuously. The time-scale for the chamber to establish a new constant relative humidity after a step-change with these samples is below a few hours. Extensive sequences of measurements was performed. Figure 1.5 shows one of the six sequences. A survey of the measurements is given in Chapter 5. The first measurements, which involved sequences during almost a year, are shown in detail in Section 6.1 .

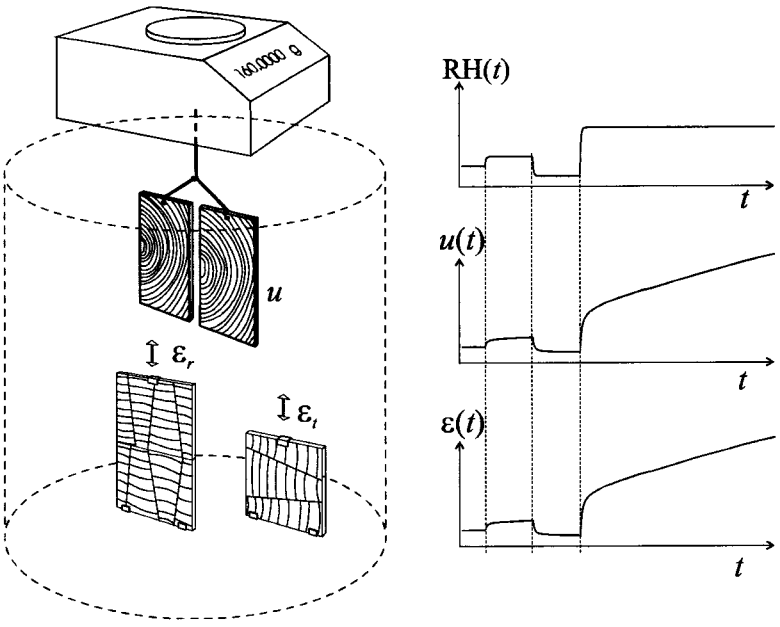

Figure 1.2 Measurements of retarded sorption and swelling.

1.1.5 Modelling of retarded cell wall sorption

In order to simulate these various moisture processes including the transient moisture uptake in the cell walls, different models with increasing complexity have been tested. Let us first consider an ordinary Fickian model. In the numerical solution we divide the porous material in nodes or cells. Each node has a moisture capacity. The moisture flow is determined by the moisture conductances between the nodes. We get a moisture flow network with capacities that are coupled to neighbouring nodes and boundary nodes by conductances. The top left picture in Figure 1.3 illustrates this Fickian moisture flow network in the one-dimensional case with four nodes inside the material.

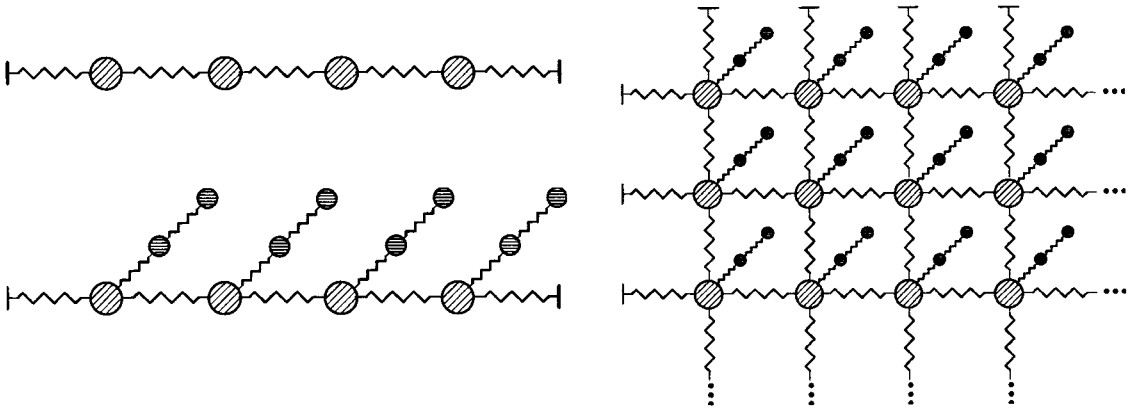

Figure 1.3 Left: Fickian moisture flow network and a corresponding network with two internal nodes to account for cell wall sorption. Right: The corresponding network in two dimensions.

The retarded, transient sorption in the cell wall will, tentatively, be modelled by "internal" nodes. The case with a single internal node has been studied by for example Cunningham (1995). It will be shown that this is not sufficient in many cases. We have to use two or more inner nodes. The simplest possibility is to couple the internal nodes in series. We have for each Fickian node an outer node and a line of inner nodes. Figure 1.3, bottom left, shows the modification of the top left Fickian network in the case with two internal nodes. The corresponding network in two dimensions is shown to the right. Internal nodes coupled to different neighbouring external nodes may exchange moisture directly. This would require further moisture conductances. The complexity of the model would increase drastically. This additional complication has not been studied here.

In a Fickian model, it would be sufficient to use a single node for our very thin samples. The wood sample is in our measurements represented by a single outer node coupled to the boundary via an outer conductance to the humid air in the precision chamber. See Figure 1.4, left. A few tested networks with capacities and conductances are shown in Figure 1.4 . Both linear and non-linear conductances have been used for the internal nodes or levels in the cell wall. The outermost conductance connected to the ambient climate chamber is the same for all models. This conductance accounts for the surface resistance and (to some extent) the Fickian diffusion within the thin sample. Several models have been tested and measured sequences have been compared to simulated ones. This is described in Chapter 11. Three of the models are presented in this introduction, simulating one of the measured sequences (at 5°C).

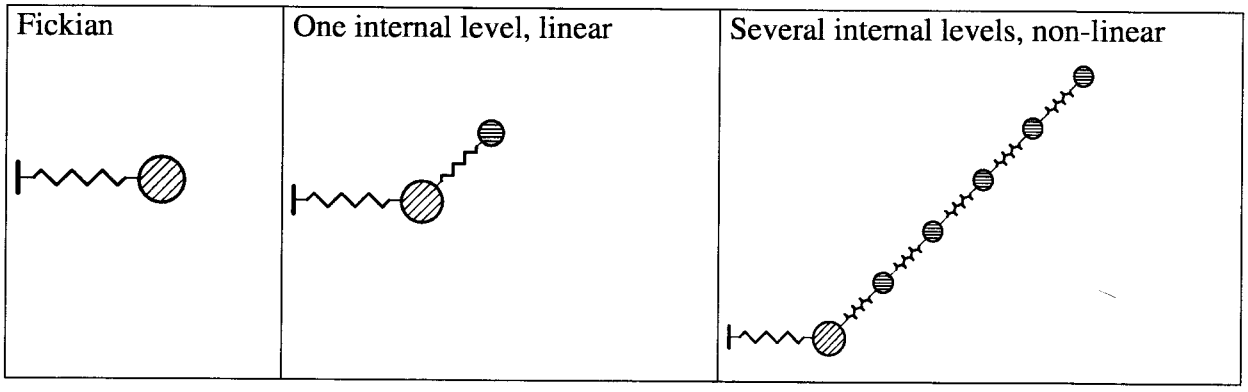

Figure 1.4 Networks with capacities and conductances for a few tested models. Very thin sample.

First a *traditional Fickian model* is tested. The network is shown in Figure 1.4, top left. The result is shown in Figure 1.5, where the result of the simulations is compared to the measured values. The simulated sorption reaches equilibrium very fast, whereas there is a drift in all measured sorption curves, especially at high RH. For cyclic steps the measured sorption amplitude is much smaller than the result from the Fickian model. The Fickian model is generally poor in reproducing the measured values.

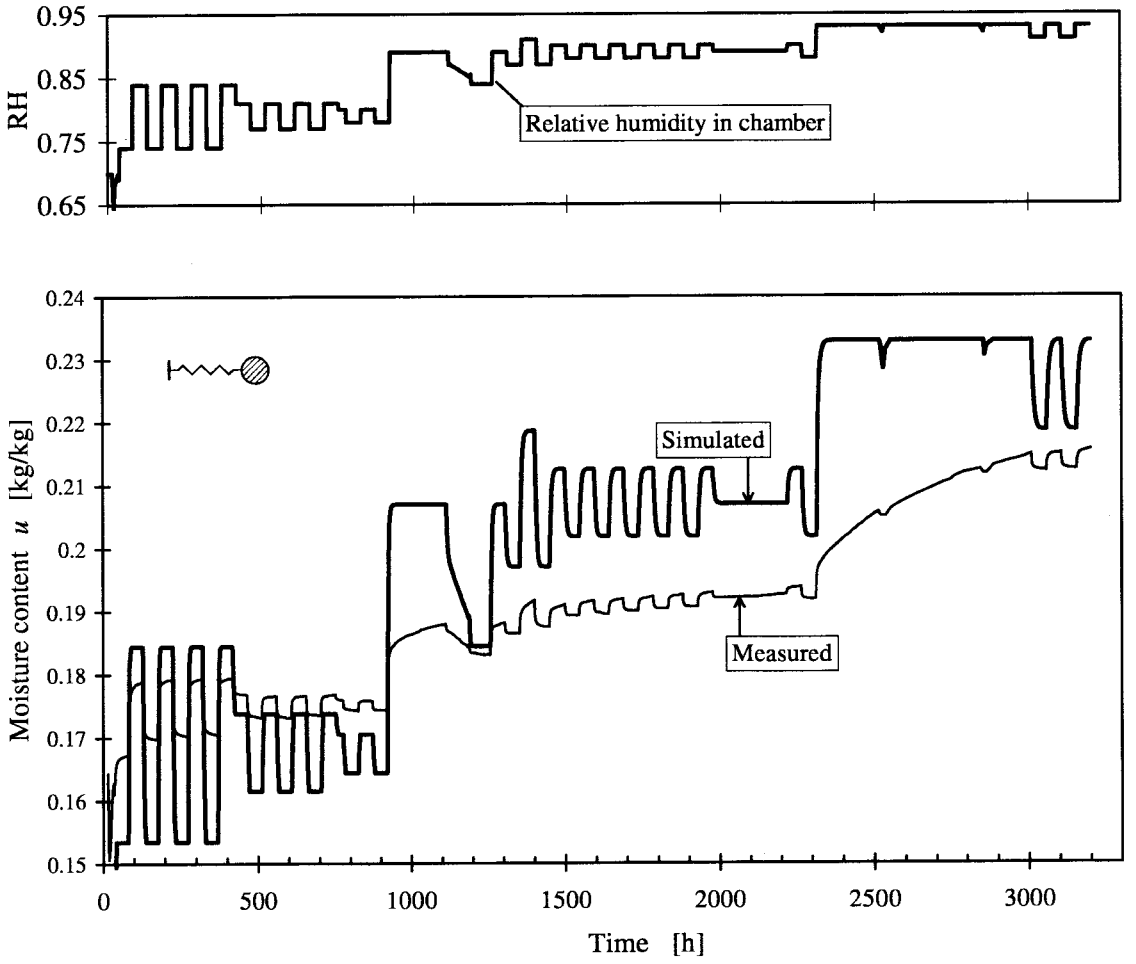

Figure 1.5 Simulation compared to measurements. Fickian model.

The first step for describing the retarded sorption is to add *one internal level* connected with a moisture conductance. The network is shown in Figure 1.4, centre. Comparison between simulated and measured sorption can be made in Figure 1.6. The measured response contains a wide range of time-scales, but this model basically produces responses from the internal level with only one time-scale

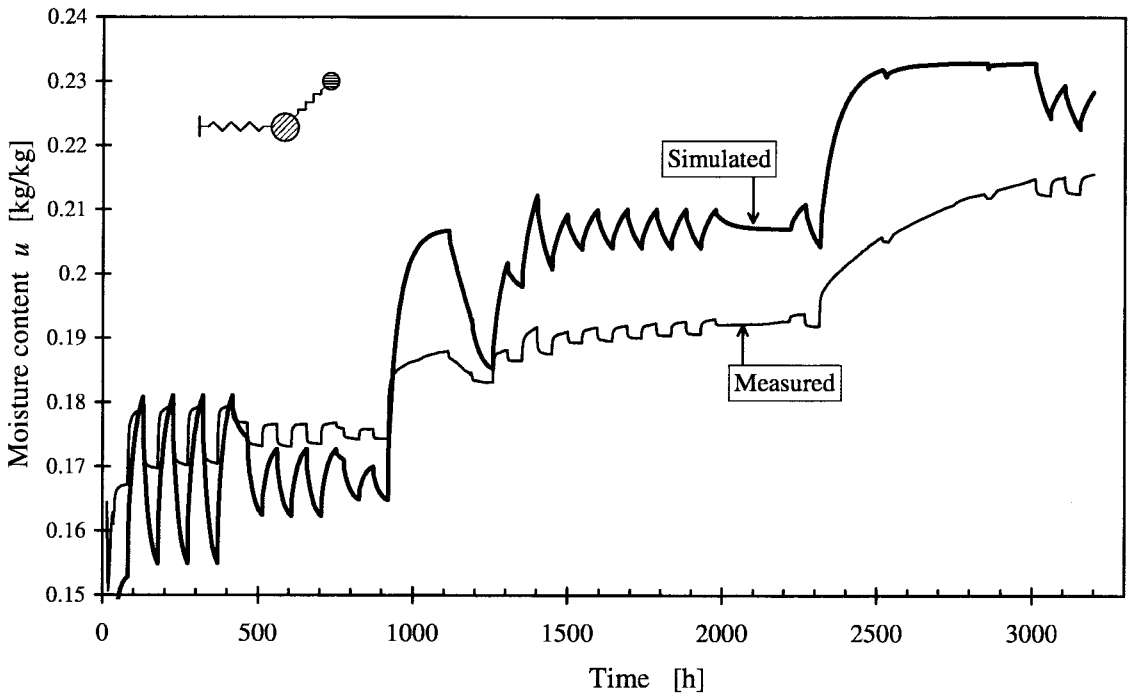

Figure 1.6 *Simulation compared to measurements. Model with one internal level, linear conductance.*

A further step is to use *non-linear conductances* in the model and combine it with *several internal levels*. An example is shown in Figure 1.4, right. The result from this simulation reproduces quite well the responses both for the long and short time-scales and with different combinations of steps. This is shown in Figure 1.7.

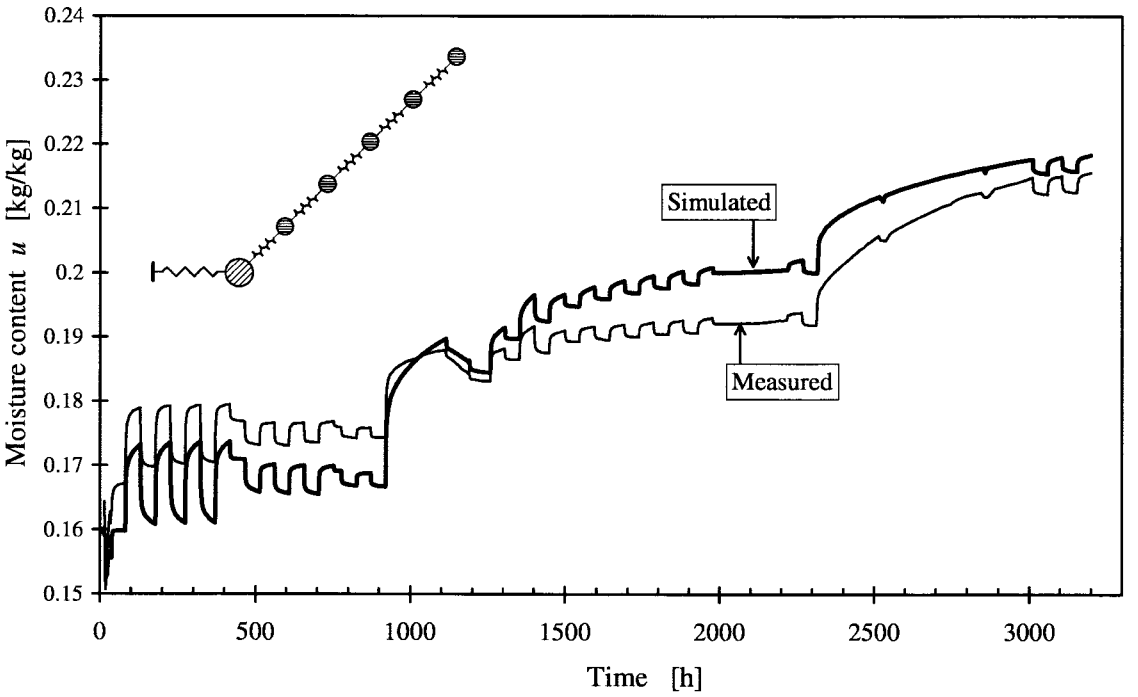

Figure 1.7 *Simulation compared to measurements. Model with five internal levels, non-linear conductances.*

These few examples and the results to come lead to the following *conclusions*. To model the sorption in wood in detail, also the transient sorption in the cell walls has to be considered. In order to investigate this process, particularly designed experiments are needed.

The measured step-responses exhibit a complex behaviour. Responses have non-linear properties. There is an intricate dependence on the moisture history. The most readily available moisture capacity has a different (smaller) variation versus RH than the capacity for the remaining time-dependent sorption.

Models of different complexity to simulate these processes have been tested. It is only the models where the time-dependent sorption in the cell wall is modelled with non-linear conductances combined with several internal levels that have been able to reasonably well reproduce all situations in the tested sequences.

1.1.6 Radial and tangential swelling and shrinkage

Swelling (and shrinkage) in the tangential and radial directions is measured at the same time as the sorption on samples of the same thickness. This enables close comparison. The swelling in the two directions perpendicular to the fibre direction was proportional to one another with the same time-pattern. The swelling and sorption responses were also similar, but there was a certain difference. An example is seen in Figure 1.8 (from a sequence different from the one previously shown).

Subtle differences of proportionality and time-lag can be seen more easily in Figure 1.9 which shows the relation between u and ε_t . In the diagram consecutive points are connected by a thin trajectory. The first step to a previously not attained moisture level has a higher slope. This is a situation where the measurements have proved to give a large portion of retarded sorption and thus a pronounced non-Fickian behaviour. The tangential swelling is somewhat lagging behind the sorption for this initial step in the diagram.

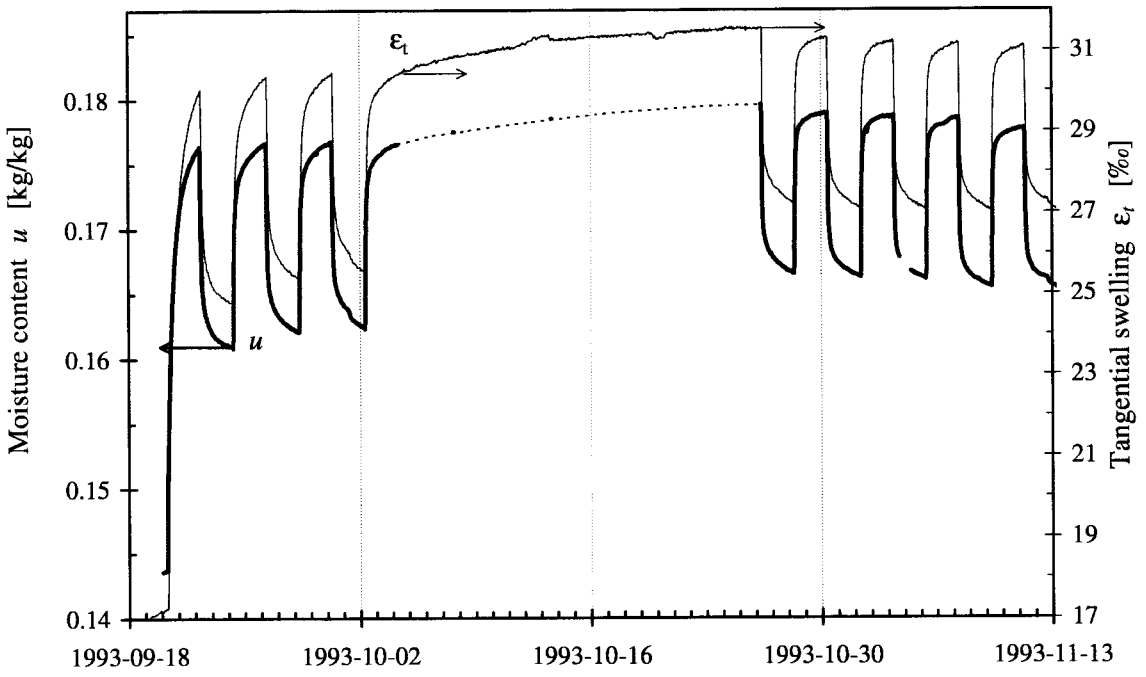

Figure 1.8 Example of sorption and tangential swelling during a cyclic sequence.

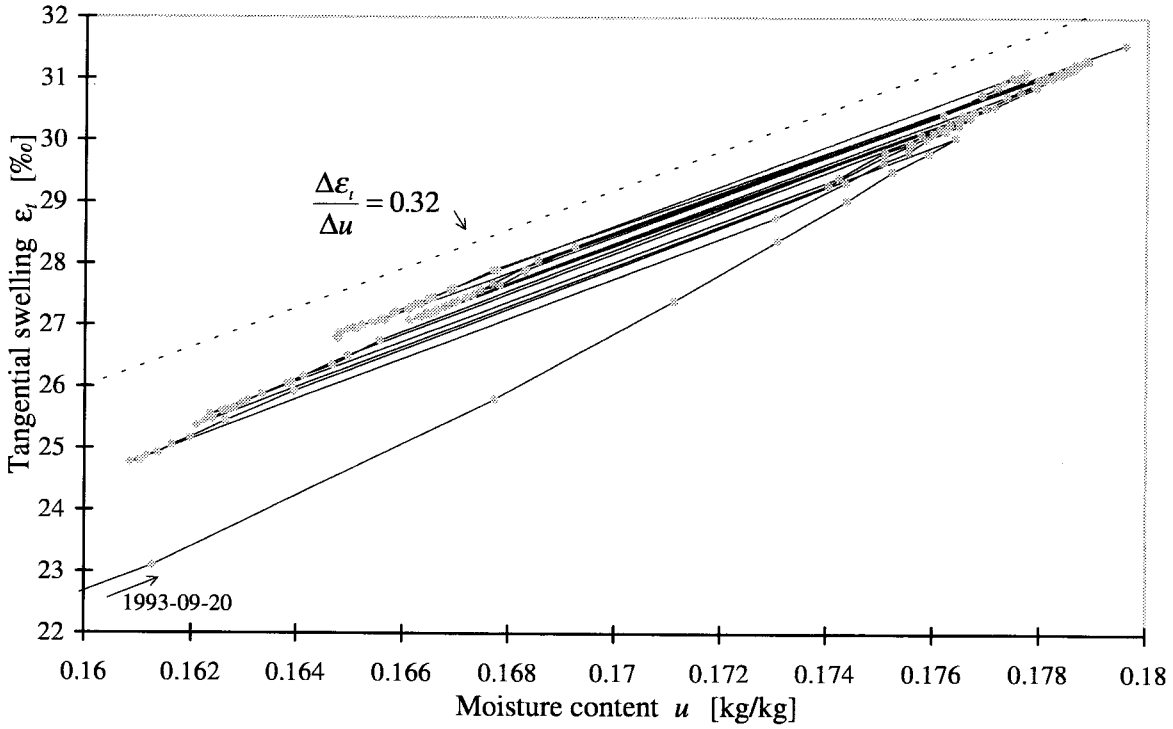

Figure 1.9 Relation between u and ε_t for the sequence of Figure 1.8.

1.2 Progress reports and presentations

The work of this thesis has been going on during some years. Four reports for a Licentiate thesis was presented during 1994-95:

Håkansson H. 1994
Experimentella studier av transient sorption i cellväggen i trä. (Experimental studies of transient sorption in the cell wall of wood). (Report TABK--94/3021). Lund Institute of Technology, Dept. of Building Science.

Håkansson H. 1995
Experimentella studier av transient sorption i cellväggen i trä. Del II —Fortsatta mätningar. (Experimental studies of transient sorption in the cell wall of wood. Part II —Continued measurements). Report TABK--95/3030, Lund Institute of Technology, Dept. of Building Science.

Håkansson H. 1995
A non-linear model for time-dependent moisture sorption in wood. Report TABK--95/3031, Lund Institute of Technology, Dept. of Building Science.

Håkansson H. 1995
Time-dependent moisture sorption in wood. Report TABK--95/1005, Lund Institute of Technology, Dept. of Building Science.

For this thesis, the material in the first two reports in Swedish on measurements have been rewritten and supplemented rather thoroughly. The third report concerning modelling is essentially unaltered and presented as Part III of this thesis. The fourth report is an overview of the work at the present time intended primarily for the Licentiate dissertation.

The progress of the work has been presented at the following conferences:

Claesson J. Håkansson H. 1993
Modelling of Moisture Flow in Wood. Fundamental Experiments and Analyses. *Proc. of the 3rd symposium, Building Pysics in the Nordic Countries,* Thermal Insulation Laboratory, Technical University of Denmark.

Håkansson H. 1994
Time-dependent sorption and swelling in wood. *Proc. from Nordic Workshop, Moisture in Building materials and Constructions,* Norges byggforskningsinstitutt, Universitetet i Trondheim.

Håkansson H. 1995
Measurements of time-dependent sorption in wood. *Proc. from W40 Symposium on Moisture problems in Building Walls*, Porto, Portugal.

Håkansson H. 1995
Time-dependent sorption in wood. *Proc. from a Nordic Conference, Wood – Paint – Moisture,* University of Luleå, Skellefteå Campus, Sweden.

Claesson J. Håkansson H. 1996
Modelling, measurements and analyses of transient sorption and moisture flow in wood. *Proc. of the 4th symposium, Building Pysics in the Nordic Countries,* VTT Building Technology, Espoo, Finland.

Claesson J. Håkansson H. Arfvidsson J. 1996
Modelling of moisture flow in coated wood – recent results. *Proc. from a Nordic Conference, Wood – Paint – Moisture*, Swedish Institute for Wood Technology Research, Stockholm.

Claesson J. 1997
Mathematical modelling of moisture transport. *Proc. from COST Action E8, Mechanical performance of Wood and Wood products, Theme: Wood – water relations.* Dept. of Structural Engineering and Materials. Technical University of Denmark.
(Only a part of this conference paper deals with retarded sorption and the work of this thesis).

1.3 Literature survey

This literature survey concentrates on anomalous sorption in wood and movements (swelling /shrinkage) related to this sorption. For general discussions on wood structure, moisture transport and sorption see Siau (1984) and Skaar (1988).

Fick originally investigated a stationary case of diffusion and found a proportionality between flow and gradient. A conventional model for the transient case, where also the capacity is involved, is sometimes referred to as Fick's second law. These laws have been extensively used for moisture transport in wood and other materials.

Over the years a number of researchers have reported on anomalous (non-Fickian, time-dependent, two-stage, retarded) sorption in wood, e. g. Christensen (1960), Comstock (1963), Prichananda (1966), McNamara et al. (1971), Rogers (1965), Park (1968), Kelly and Hart (1970), Wadsö (1993) and Wadsö (1994).

The first and also most important work on non-Fickian behaviour in wood was made by *Christensen* and co-workers. They subjected thin samples to rapid steps in water vapour pressure in absence of air. In a pure water vapour environment the diffusion resistance basically is eliminated and the response times will become very short if non-Fickian effects are not present. The sample thickness is usually very thin in the experiments. In all Christensen's studies however, large non-Fickian effects are seen. The only exception is when the sorption starts

from a dry sample. The steps are generally absorption steps in the works of Christensen and the most common evaluation point is the half-time, $t_{0.5}$.

Christensen found that the non-Fickian effects were nullified when starting from a dry sample. The consistency of this, from an example taken from Christensen (1959), is further verified by calculations made in Section 4.5.1.

In Christensen (1959) different degrees of *delignification and processing* was investigated with respect of the anomalous effects. The largest delayed sorption was obtained for untreated wood followed by delignified wood. Further smaller effects were found for pulp made from the same wood. In Christensen (1965) tests were run on regenerated cellulose of different thicknesses . Non-Fickian effects were found at least to some degree on all wood and wood derivatives.

In the present thesis, only the retarded sorption of one species of softwood, Scots pine, is investigated. In Christensen and Kelsey (1959) non-Fickian effects were found on another softwood, Klinki pine. Similar effects were found for hardwoods: Eucalyptus, Christensen (1960), Balsa and Satin box, Christensen (1965). In Wadsö (1993), non-Fickian effects were found with little variation for the two softwoods and four hardwoods that were investigated.

The *step size* has a very strong influence on the retarded sorption. In Christensen (1959), (1960), (1965) and (1967) a special evaluation is used that illustrates and quantifies the influence from the step size in a distinct way. The used time parameter is $t_{0.5}$, the time when half the sorption has taken place. The inverse of the half-time, $1/t_{0.5}$, proves for many cases to be closely proportional to the logarithm of the quotient of the two relative humidities for the step, $\ln(\varphi_1/\varphi_2)$. This means that if the response process is simplified to be governed by a single conductance, it is proportional to $\ln(\varphi_1/\varphi_2) = \ln(\varphi_1) - \ln(\varphi_2)$. This means that the conductance is proportional to the step size (for small steps where $\ln(\varphi_1/\varphi_2) \sim (\varphi_1 - \varphi_2)$). The moisture flow is with this assumption proportional to the square of the difference in humidity. The measurements of Christensen are discussed more in detail in Section 4.5.

A drastic, related example of the influence from a special step was found by Christensen and Hergt (1969). Samples were kept at the same humidity for a long time. They were then dried also for a long time, but some of the moisture was still retained. If liquid water was added to the samples, it was possible to dry them completely in a comparatively short time.

In Toratti and Svensson (1998), also Svensson (1997), wood is subjected to compression and tension cycles perpendicular to grain combined with moisture cycles. It is observed that a single large step in relative humidity results in larger free shrinkage than corresponding smaller steps. Thus the step size influences *mechano-sorptive effects*.

In some instances a *fraction of the sorption* after a step has a markedly *faster response* than the remaining more retarded sorption, especially at high levels of relative humidity. An example is response curve 1 in Figure 1.1. The time axis is represented by the square root of time in the diagram. The ideal (Fickian) step response for a semi-infinite body becomes a straight line in such a diagram. The way in which the time scale is expressed influences of course a visual evaluation. In Christensen, the response curves are usually given for the square root of time. It is hard to physically motivate this representation since the diffusion process over the thickness of the sample is practically eliminated in the pure water vapour environment. The samples are also very thin. In many response curves at high RH a distinct knick-point is apparent in some of the curves when only a fraction of the sorption has taken place. In Section 9.1 in this thesis a method for thin samples is devised and tested to evaluate the fraction of the sorption associated with a moisture capacity that is readily accessible.

The term *moisture history* can have several meanings. It may refer to any time-variable set of moisture distributions. Here, we are interested in the previous moisture at any considered

point in the wood. In Christensen and Hergt (1969) a special form of moisture history is demonstrated. The samples were initially dry. The samples were then subjected to an intermediate step to 0.52 RH. Different samples were exposed to the intermediate humidity for a wide range of time periods, however all did come to apparent equilibrium. After that the samples were subjected to another step (smaller, from 0.52 to 0.69 RH), and the sorption responses were registered. The equilibrium levels were consistently higher for *shorter* exposure to the intermediate level (at 0.52 RH). The half-time $t_{0.5}$ for the following step was distinctly longer for those samples that were exposed to the intermediate step for longer time. In fact there was a nearly linear relationship between the logarithm of the exposure time and the logarithm of the half-time. This is shown in Figure 1.10, the upper line. This is an example of memory in the material that is not reflected in instantaneously measurable properties, since the moisture content was the same for the different samples at the intermediate point. Also a larger second step from 0.52 to 0.80 in relative humidity was tested for some samples. A similar linear relationship between the two logarithms was obtained. However, the influence on the half-times was not so large as seen in Figure 1.10, the lower line.

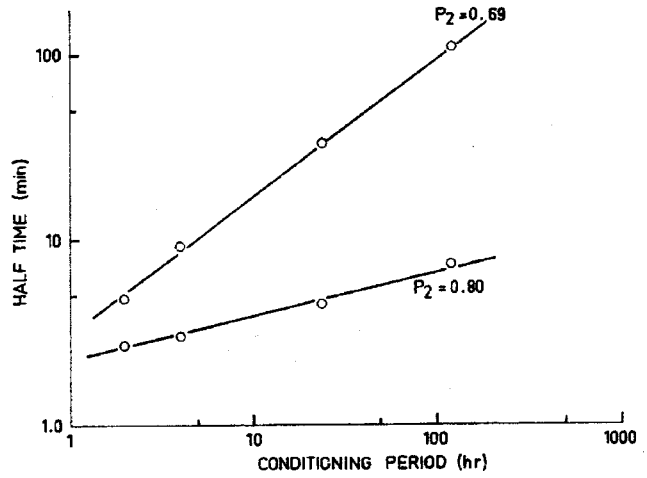

Figure 1.10 Dependence of sorption half time at relative humidity p_2 on conditioning period at relative humidity p_1 = 0.53. From Christensen and Hergt.

In Christensen (1965) the influence from *cell wall thickness* on absorption speed was investigated. A species with thin cell walls (Balsa, 1 μm) and a species with thick cell walls (Satin box, 4 μm) were selected. A relatively small step at high RH gives a very slow absorption but nevertheless practically identical for the two different cell wall thicknesses. If the retarded sorption is thought to be confined to separate regions, they are much smaller than the cell wall thicknesses. The regions are with this way of reasoning surrounded by a pore system that is comparatively more penetrable.

A similar discussion is pursued in Bazant (1985). First Bazant puts the attention on similarities between the behaviour of stressed wood and cement-based concrete and presents some similarities. A broad range of pore sizes including subcapillary pores of molecular dimensions, *gel-type pores*, and strongly hydrophilic pore walls. Bazant makes a reasoning about the the orders of magnitude between the coarser pore system and the gel-type pores. Assuming viscous flow with a conductivity proportional to the cube of the pore width, he concludes that the water enters the finest pores equally from all directions. The flow in coarse pores, driven by a gradient in water vapour pressure, is called macrodiffusion. The macroscopic transport of water tends to pass through the passages of least resistance. The transport from

the coarse pore system to the gel-type sorption sites is accordingly called microsorption. The driving force for this water migration is thought to be differences in chemical potential.

The focal point of the paper of Bazant is a discussion in what way the structure of wood accelerates the creep caused by moisture. Early experiment with a steady-state diffusion on a stressed specimen of wood did not seem to accelerate creep and such an influence was ruled out. Bazant points out that the width of the gel-type pores is only a few molecules and that the water is able to interact with the adjacent walls and take part in transmitting of loads. Bazant assumes *flat pores* in this reasoning.

Much of the stiffness and strength of wood is provided by the microfibrils situated in the S_2 layer in the cell wall. They also have a limited longitudinal swelling and contribute to the fact that the longitudinal swelling of for instance pine is only about one fourteenth of the tangential swelling. The average angle between the microfibrils and the longitudinal axis of the wood has a profound influence on the distribution of the swelling between different directions. A typical value for pine is a microfibrillar angle of 10° to 20°. In Meylan (1972) the longitudinal swelling of radiata pine for a wide range of *microfibrillar angles* is investigated. Meylan also measured the swelling in the radial and tangential directions and found proportionality with the moisture content. Based on the measurements, he could not draw conclusions whether hysteresis occurred or not.

In Persson (1997), variation of properties of wood is investigated, both the distribution over the tree trunk to a individual growth ring. Both mechanical and moisture (swelling /shrinkage) properties are investigated. Models are presented that account for the mechanical properties of the components in wood. This is also done in Petersson, Dahlblom, Ormarsson and Persson (1997).

A remarkable transient temporary effect of the *longitudinal swelling* is demonstrated in Hunt (1989). Thin samples of 0.5 mm thickness of Scots pine were subjected to steps in RH under zero load while the axial swelling and the absorption were registered. For steps at high RH there is a large 'overshoot' of the axial swelling seen in Figure 1.11(b). In Figure 1.11(a) the axial swelling is shown versus moisture uptake. A proportionality between axial swelling and moisture uptake would have produced a straight line. Instead the moisture uptake is lagging behind. In Figure 1.9 it is shown that there is a rather close proportionality between tangential swelling and sorption for the measurements in this thesis.

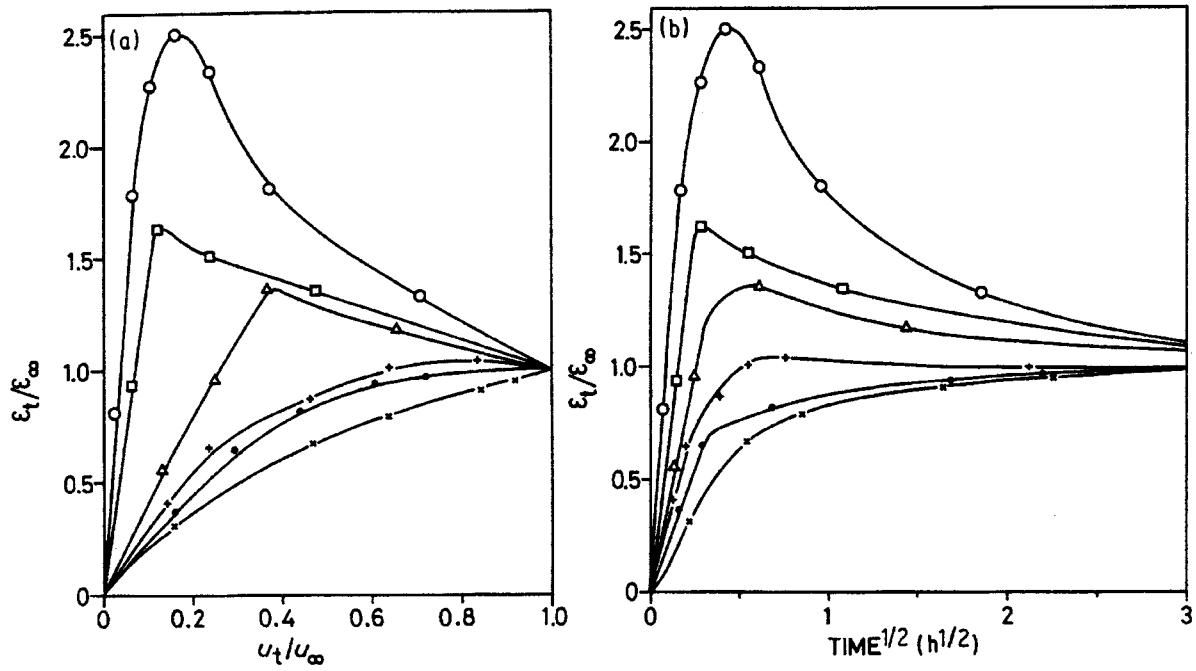

*Figure 1.11 Step increase in air humidity under zero load; relative humidity (×) 32 to 42%, (•) 42 to 51%, (+) 51 to 62%, (Δ) 62 to 70%, (1) 70 to 77.5% and (°) 77.5 to 90%. (**a**) Fraction of equilibrium axial strain increase $\varepsilon_t/\varepsilon_\infty$ plotted against fraction of equilibrium moisture increase u_t/u_∞ . (**b**) Fraction of equilibrium axial strain increase $\varepsilon_t/\varepsilon_\infty$ plotted against the square root of time. From Hunt (1989).*

The hysteresis of the moisture content is rather large for wood when subjected to large scans in absorption-desorption. The longitudinal moisture-related strain however, does not follow the moisture content in this respect, but it has rather the same value for the same RH, independent of absorption or desorption. This is measured by Hunt (1990) in Figure 1.12. It is also illustrated in the figure that the longitudinal swelling strain is larger at low RH.

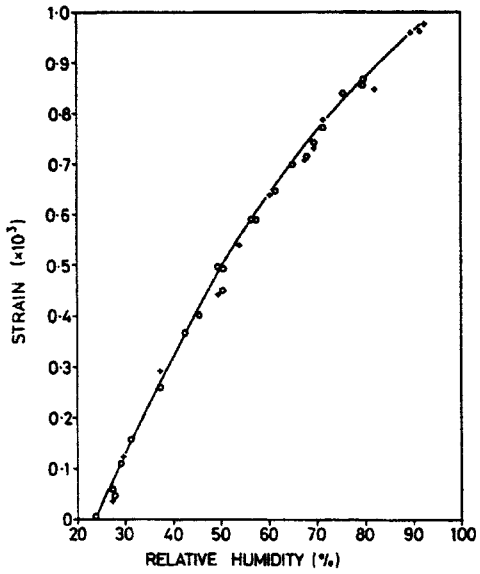

Figure 1.12 Zero-load axial equilibrium dimensional changes plotted against relative humidity. (+) absorption, (°) desorption. From Hunt (1990).

In Hunt (1989) two classical theories of stress and sorption are combined. The first is Barkas' (1949) thermodynamically based theory that states that a tensile stress applied to wood will cause an increase in the moisture equilibrium content and a compression stress the reverse. The second is the lenticular trellis theory of Boyd (1982) in which the structure of wood is simplified into a lentil shape with a stiff envelope surrounding a hygroscopic interior.

A retarded sorption may be interpreted as caused by an increased *surface resistance*. It has been thought that non-Fickian or retarded response sorption curves could be corrected by the introduction of a large surface moisture transfer coefficient. This is based on the work by Choong and Skaar (1969), who fitted an empirical relationship for diffusion coefficient and surface resistance to Fick's second law. It was meant to be applied on drying of wood. The equation is based on the time $t_{0.5}$ when half the sorption has taken place after a step change.

Although there certainly is a surface resistance, it cannot account for the observed, large deviation from Fick's law. An example of this is Avramidis and Siau (1987) who obtained diffusion coefficients and surface emission factors from measured sorption responses where sample thickness, temperature and moisture level were varied. The result gives a wide range of surface emission factors for the same drying situation. For instance, the factor increases threefold at a relative humidity of 30% compared to 90% (at high temperature). The diffusivities have an equally large variation with thickness (5mm and 20 mm, at 30°C and 90% relative humidity). Moreover, the individual coefficients are widely scattered. It is hard to find any consistent features for the coefficients derived in this way. However, the coefficients are obtained solely by the $t_{0.5}$ point in time and some of the response curves actually show a "two-stage non-Fickian situation", Avramidis and Siau (1987).

In the present thesis, not only consecutive absorption steps and consecutive desorption steps are measured, but also cyclic steps. Substantially less moisture capacity is found to be active than determined by the slope of a mean moisture equilibrium curve. In Time (1998) it is emphasised that including hysteresis in the moisture equilibrium curve for a transient moisture transport calculation gives a better result. The less steep slope of the intermediate curves between absorption and desorption of the moisture equilibrium curve gives the desired reduction in moisture capacity.

Part I Experimental set-up and introductory modelling

2 The experiment

2.1 Method

In order to isolate the retarded sorption, especially designed measurements were made. The samples were thin and cut perpendicular to the grain, so that the moisture transport took place in the fast longitudinal direction. The air was agitated around the samples to reduce surface resistance. The samples were undisturbed by being continuously suspended from balances in precision moisture chambers. An outline of the arrangement is shown in Figure 2.1. Well defined steps in relative humidity (RH) were made. The samples were weighed by high precision balances (of the analysis type with 0.1 mg as the last digit).

The measurements were made at 20°C and 5°C temperature. This made it possible to study the temperature influence on the retarded sorption.

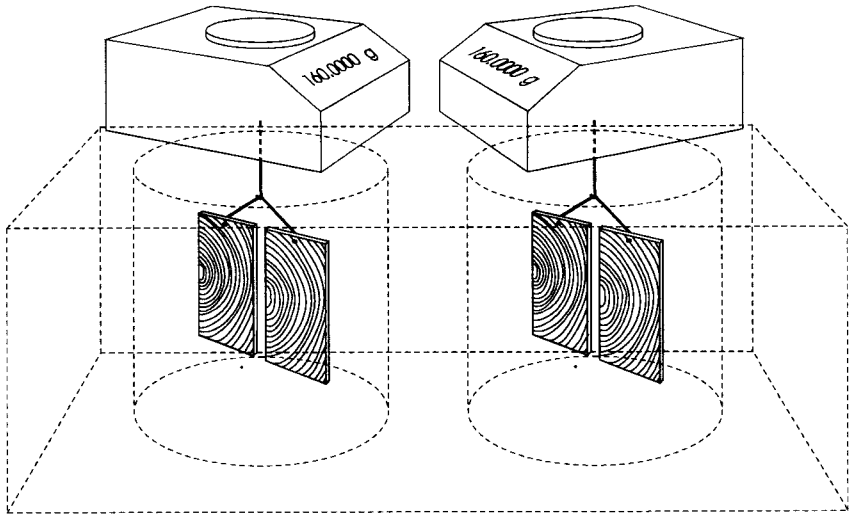

Figure 2.1 Arrangement for weighing of samples in precision moisture chambers.

2.2 Wood material

The wood used is pine (*Pinus sylvestris*) from southern Sweden which was felled around 1990. Transient sorption studies on this wood were published by Wadsö (1994). Villadsen et al. (1993) have also conducted steady-state cup measurements on the same material (cf. Wadsö 1994b). The sections used for the samples consisted of 90% to 95% sapwood. The dry density was determined for an adjacent larger sample. This value, 530 kg/m^3, is used in the following only to calculate relative volumetric swelling. The sorption is given in moisture content in this report, where the dry density is not involved.

2.3 Samples

The samples designated Sample 1 and Sample 2 were composed of several sheets of 3 mm thickness mounted in parallel as Figure 2.2 shows. These samples were used during the first series of measurements.

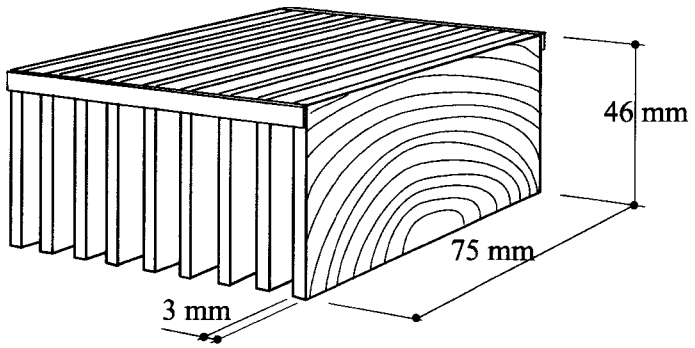

Figure 2.2 Array of wood for Sample 1 and Sample 2

The other series of measurements (second to sixth) have been carried out on thinner samples, designated Sample 3 and Sample 4. The sample arrangement with two sheets of 1.7 mm thickness is shown in Figure 2.3. As seen in the figure the surfaces are freely exposed to the circulating air.

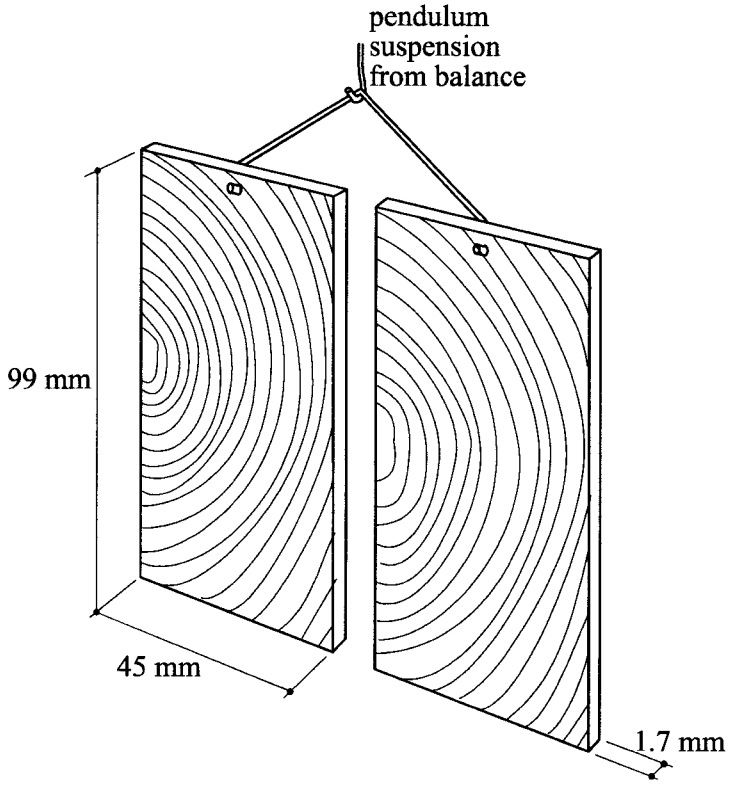

Figure 2.3 Array of wood for Sample 3 and Sample 4

The results from the sorption tests in this report are shown in the diagrams as variation of moisture content $u(t)$ with time. Let $m_w(t)$ be the measured weight of the wet sample at any time t, and let m denote the weight of the dry sample. Then we have for the moisture content $u(t)$ (water content /dry mass [kg/kg]):

$$u(t) = \frac{m_w(t) - m}{m} \qquad [\mathrm{kg_{water}}/\mathrm{kg_{wood}}]$$

The dry weight m was determined in the following way. After the tests the samples were dried by being surrounded by a drying agent of the molecular-sieves type in a closed container at 60°C for 10 days. The high temperature accelerates the drying process several times compared to room temperature. At the same time it is low enough to avoid resin flow and to restrict the emission of volatile compounds. A drying process exhibits retarded properties. The final part of the drying takes very long time to accomplish compared with what could be expected from the first fast phase. This is illustrated by the measurements themselves, which have shown retarded effects at room temperature, also at low relative humidities. This was the background for the used thorough drying procedure for the thin samples.

A specific problem when weighing dried thin samples with high precision in ambient air is the fast absorption during the inevitable handling time. The error was minimized by doing the drying procedure in two steps. First, the drying was done with unwrapped, freely exposed samples. In a second drying, the samples were wrapped with aluminium foil, leaving an opening that was easy to seal rapidly. This second drying lasted for an extra day. Most of the small amounts of water unintentionally absorbed during the wrapping handling time could escape through this opening during the second drying.

The measurements have been reported in previous reports in Swedish, Håkansson (1994a) and (1995a). The final measurements of the dry weights were not available at that time. Therefore assumed dry weights were used. Those differ about one percent or less from the new ones. This explains the small differences in u between the previous reports and this one.

2.4 Measurements of swelling

Measurements of swelling (and shrinkage) was conducted on twin samples simultaneously with sorption on Sample 3 in the same chamber. In the following, the word swelling is used to include shrinkage also. This common chamber makes accurate comparison between sorption and swelling possible since the samples are subjected to the same climate, including deviations from the intended RH-level. It is also important that the same sequence of RH-steps are used for comparison as the retarded sorption proves to be dependent on the moisture history.

The swelling was measured in tangential and radial directions on two separate samples. They were made from adjacent wood to the sorption samples, and they had the same thickness (1.7 mm). The samples were divided by radial cuts, made perpendicular to the annual rings, and then glued together to straighten out the annual rings as Figure 2.4 shows. The glue lines were kept thin and attention was paid to avoid excessive glue. Polyurethane adhesive was used, the type curing by the ambient moisture. Three metal plates were also glued on to serve as fastening points.

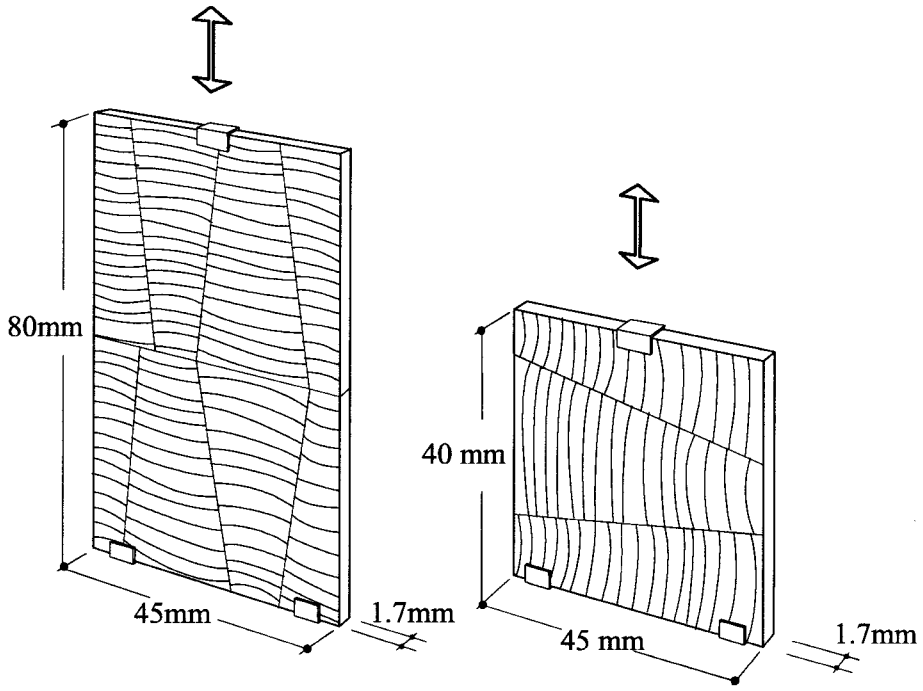

Figure 2.4 Samples for measuring radial, (left) and tangential swelling, (right)

The device for measuring swelling is shown schematically in Figure 2.5. The two points on the lower base were fixed to the frame by four thin metal rods, allowing free movements also perpendicular to the measured vertical direction.

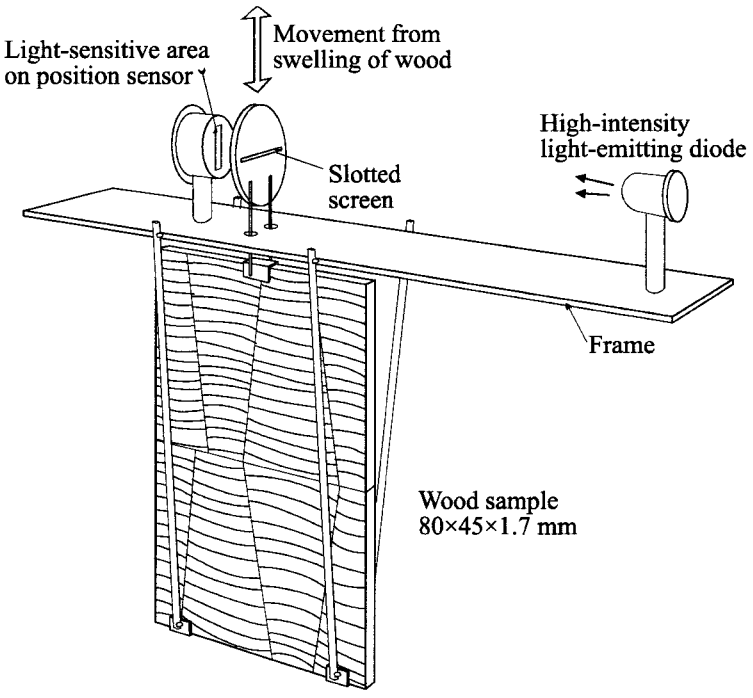

Figure 2.5 Device for measuring swelling using an optical position sensor

The vertical movement was prevented from lateral deviation by being guided by thin horizontal wires arranged in a cross. This is not shown in the figure. This allowed for reasonable guidance and still maintaining the device friction free.

The upper moving point on the sample was connected to a screen with a horizontal slot. This slot altered the position of a beam of light falling on an optical position sensor. The screen was made from copper foil with a dark, matt surface facing the sensor. The width of the slot was approximately 0.1 mm.

The components in the device was soldered together to be easy adjustable, and still provide rigid connections.

The position sensor was a Hamamatsu S 3979. The light-sensitive surface has an area of 1×3 mm and consists of a photo-diode with common cathode and two separate anodes. In the data-sheet for the sensor x is the distance from the centre of the sensitive area to the centre of the spot of incident light. The distance x as a function of the two currents through the anodes is given by the expression:

$$x = \frac{L}{2} \cdot \frac{I_1 - I_2}{I_1 + I_2}$$

x	distance between light-spot and centre of sensor
L	the length of the sensitive area (3 mm for S 3979)
I_1, I_2	the currents through the two anodes

The error of position based on the equation above is given in the data sheet as typically ±15 µm and ±60 µm as a maximum. The error of position is given with the nominal value of the length L in the expression. Judging from the good linearity for the sensor according to the examples in the data sheet, a better accuracy can be achieved if a calibration is made in two points as it is done here. The examples in the data sheet show smooth curves. The relative error can then be assumed to be small even for minor intervals. As the currents are small in the used application, the output signal is noisy. This was counteracted by recording the mean value in a one minute interval.

Since the sensor is measuring the centre of gravity of the spot of incident light, it is important to have a distinct spot, well within the boundaries of the length of the sensitive area. The slotted screen was therefore adjusted close to the sensor, but with a clearance to avoid friction.

2.5 Precision moisture chambers

Two precision moisture chambers were used. They had a cylindrical shape with 0.295 m in diameter and 0.32 m height, giving 22 l of volume each. The chambers were submerged in a large common constant-temperature bath. Access to the chambers were by top-mounted lids. The principle of the apparatus is shown in Figure 2.6.

The precision moisture chambers were of the two-pressure principle. In such an apparatus, saturated air at a total absolute pressure of p_1 is allowed to expand to a pressure of p_2 . The relative humidity in the expanded air is given by the relation p_2/p_1 (constant temperatures are implied). This is valid for perfect gases, but the deviation for water/air is only 0.1% at 65% RH and it decreases at higher RH-levels. In the study, no correction was applied.

In a two-pressure apparatus, the saturation of the air to a well defined temperature is achieved by letting saturated air at an elevated temperature pass a condenser. With sufficient surface area in the condenser, an equilibrium with the desired temperature is attained and the

saturation is still maintained. The produced condensed water must be allowed to be separated from the air stream to be drained off.

After passage through the valve reducing the pressure from p_1 to p_2 , the air is unintentionally cooled by the adiabatic expansion and has again to be brought to the desired temperature by an additional heat exchanger.

The apparatus was originally constructed in the 1970's and a version is described by Ahlgren (1972). A two-pressure apparatus described by Amdur & White (1965) has to some extent served as a model for the design.

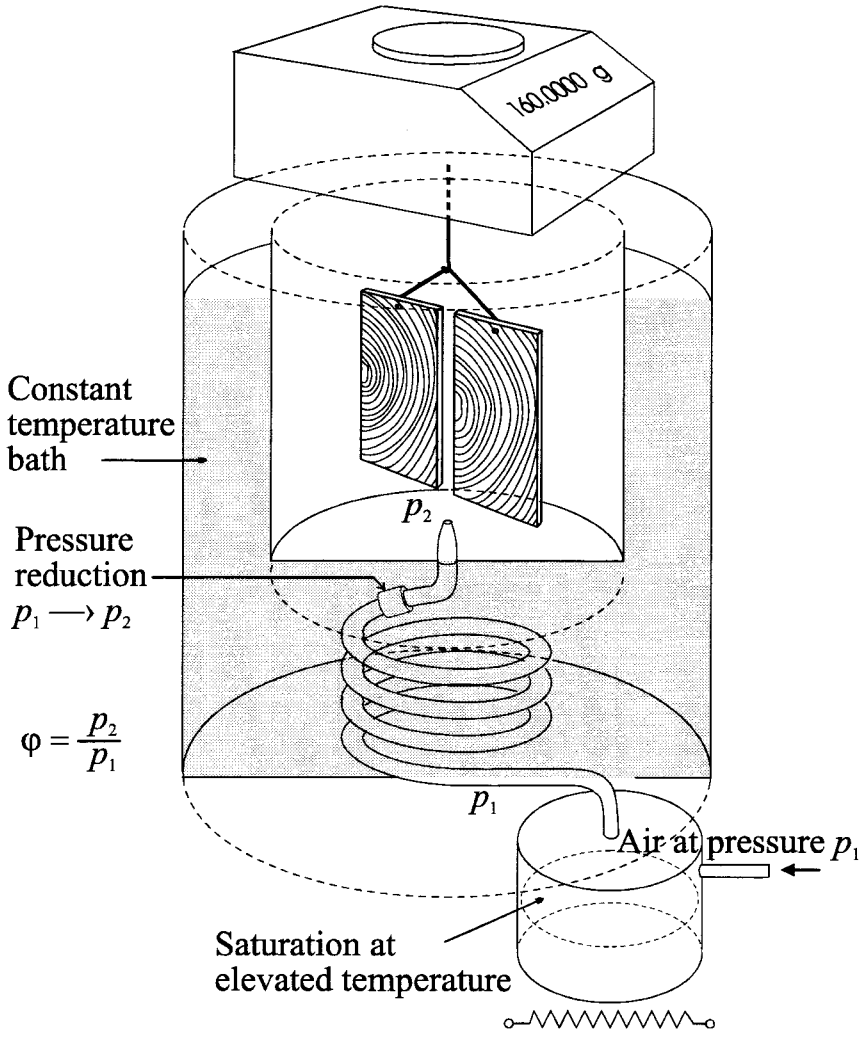

Figure 2.6 Precision moisture chamber. Outline of the basic components in the two-pressure apparatus.

In the used apparatus the condensers and the additional heat exchangers were composed of copper tubes coiled around the chambers. The close thermal contact between sample and surfaces defining the saturation pressure provided by the constant temperature bath, ensured that only minor errors were caused by temperature differences. The top lid was well insulated to minimize influence from the surroundings.

Air has to be allowed to escape, corresponding to the entered volume into the chambers. Sufficiently wide exit openings for the air stream in the top lid made the pressure difference negligible. At the same time they were narrow and long enough to ensure that external air did not enter the chambers. In one of these openings the suspension for the sample under the balance was placed. The suspension consisted of a thin wire to minimize influence from the air stream. The small air stream passing the opening was diverted to avoid turbulence around the sensitive parts of the balance.

The low pressure difference over the lid meant that the pressure p_2 was the atmospheric pressure. The pressure p_1 was actively controlled according to barometric changes. This was achieved by pressure transducers controlling a servo motor adjusting a pressure regulator valve connected to the compressed air supply. The two chambers were controlled independently. A common pressure transducer measured the barometric pressure. However the first series of measurements were made with mechanical pressure regulators only, without the aid of active control. The pressures were manually monitored on mercury or water column pressure gauges.

When the expanded air entered the chamber, it passed a nozzle and a jet was produced that was directed towards the sample. This provided a good mixing within the chamber and reduction of surface resistance at the sample with minimal temperature disturbances. If an alternative with a fan had been used, a substantial heat source would have been introduced and a risk of changing the RH. This possibility of producing agitation without a fan is an advantage with the two-pressure principle. In order to avoid disturbances during weighing, the jet was diverted at these times and diffused through a perforated plate by a screen attached to a solenoid.

The rate of air flow was determined by the setting of the expansion valve and the pressure over the valve, $p_1 - p_2$. This pressure difference varied over a wide range for the used RH-values. The apparatus was not equipped with air flow meters, but a reasonably constant flow was kept by an indirect method. The vertical jet blowing on the sample and its suspension created an uplift that could be seen on the balance (0.1 g was used). The air flow was determined when the measurements were finished by a volumetric method normally used for calibrating tracer gas. The flow was captured in a bag for a certain period of time and the volume measured by a piston.

2.6 Weighing

The samples were weighed continuously suspended from balances. See Figure 2.6. The pendulum suspension was made from a 0.2 mm in diameter resistance wire that was made straight by being heated electrically and stretched. It was possible to dislocate the suspension from a hook on the balance to facilitate zeroing of the drift of the balance without disturbing the sample.

The balances were of the analytical type Mettler AK160, with 160 g range and 0.0001 g resolution. An estimate of the maximal drift during a period of a month was 0.0030 g . This corresponds to a moisture content of 0.04% [kg_{water} / kg_{wood}] for the smaller samples used.

A malfunction in the control circuitry occurred for one balance (sample 3, the second series). The symptom was an unexpected diurnal variation. It was therefore discovered and the fault is not thought to have been going on for a long time. The balances were with regular intervals controlled by placing a calibrated weight on the weighing pan and a check was done for the correct increment on the scale.

The weight result was logged once every hour. A separate clock has controlled the deflection of the air stream for a couple of minutes around the logging time.

3 Analysis of the response for a small body

In order to distinguish properly the non-Fickian part of the dynamic response, an estimate of the theoretical Fickian behaviour for the experiment is needed. An understanding of the rate with which the step-change inside the sample is taking place for a theoretical Fickian process is the base for evaluating the non-Fickian, retarded sorption. For this objective and these measurements, some reasonable simplifications are made, discussed in this chapter. This is also done in Section 9.1, where also numerical examples are presented.

The air flow rate to the chamber that is given the desired step change was limited with the used apparatus. One disadvantage was that this resulted in a less steep step of relative humidity in the air of the chamber. However, this effect is completely analogue with an added surface resistance and when the flow of the supply air is known, thus well defined. This calculation is showed in Section 3.1.1 below. The less steep step in the ambient air is further dampened out inside the sample by diffusion. How this is treated for the analysis of these measurements is mentioned in Section 3.1.2.

A way to estimate the influence from latent heat is suggested in Section 3.2. This influence is not considered in Håkansson (1995b).

The mass of water vapour per unit volume, v [kg/m^3], in humid air is in SI-standard to be called humidity by volume. It is called water vapour content in this thesis.

Notations:

Latin letters

A	surface area of sample (area of both sides)	[m^2]
c	heat capacity of the wood	[J/(kg ·K)]
c_{pa}	heat capacity of the air	[J/(kg ·K)]
D_v	vapour transport coefficient	[m^2/s]
G	moisture uptake rate of the sample	[kg$_{water}$ / s]
h_e	latent heat of evaporation	[J/kg]
L	halv thickness of the sample	[m]
L_{eq}	average diffusion length in sample	[m]
m	dry mass of sample	[kg]
T	temperature in sample	[K]
T_{ch}	ambient chamber temperature	[K]
u	average moisture content in sample	[kg$_{water}$ / kg$_{wood}$]
$\dot{V}_{air}$	air flow rate	[m^3/s]
V_{ch}	volume of chamber	[m^3]
v	average water vapour content for air phases inside the sample	[kg/m^3]
v_{sat}	water vapour content in saturated air	[kg/m^3]
v_{inlet}	water vapour content in in-flowing air	[kg/m^3]
v_{ch}	water vapour content in mixed air in chamber	[kg/m^3]
v_{surf}	water vapour content on surface of sample	[kg/m^3]

Greek letters

α_c	convective heat transfer coefficient	[W/(m^2 ·K)]
α_r	radiative heat transfer coefficient	[W/(m^2 ·K)]
α_{tot}	total heat transfer coefficient $\alpha_{tot} = \alpha_c + \alpha_r$	[W/(m^2 ·K)]
β	air-to-surface moisture transfer coefficient	[m/s]
β_{vtot}	total moisture transfer coefficient	[m/s]
$\rho_a \cdot c_{pa}$	volumetric heat capacity of the air	[J/(m^3 ·K)]

3.1 Isothermal case

In the isothermal analysis, we assume that the sample temperature is equal to the chamber air temperature: $T = T_{ch}$.

3.1.1 Moisture flow resistance over boundary layer

The variables concerning the chamber and boundary layer are shown in Figure 3.1.

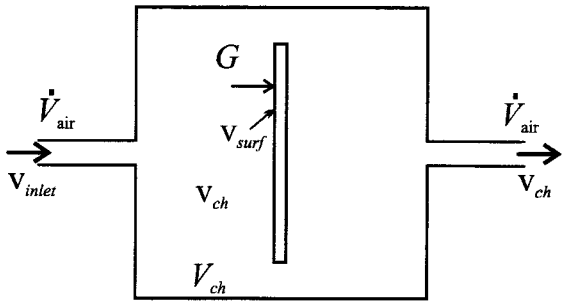

Figure 3.1 Variables for moisture exchange into sample in chamber

The moisture balance for the air in the chamber is:

$$(v_{inlet} - v_{ch}) \cdot \dot{V}_{air} = G \qquad (3.1)$$

For simplicity the moisture capacity of the air is neglected, being only a small fraction of the moisture capacity of the sample. A numerical example of this is given in Section 4.1.5 in Håkansson (1995b).

We can now calculate the moisture balance of the surface. Let β [m/s] denote the air-to-surface moisture transfer coefficient, and A [m^2] the total exposed area of the sample (both sides). The balance of the surface becomes:

$$(v_{ch} - v_{surf}) \cdot \beta \cdot A = G \qquad (3.2)$$

These two equations may be written:

$$v_{inlet} - v_{ch} = G \cdot \frac{1}{\dot{V}_{air}} \qquad (3.3)$$

$$v_{ch} - v_{surf} = G \cdot \frac{1}{\beta \cdot A} \qquad (3.4)$$

Addition of the two equations gives:

$$v_{inlet} - v_{surf} = G \cdot \left(\frac{1}{\dot{V}_{air}} + \frac{1}{\beta \cdot A}\right)$$

3.1.2 Moisture resistance associated with sample thickness

The effect of the moisture transport within the thin sample is here dealt with in the following way. Let $2 \cdot L$ be the thickness of the sample, Figure 3.2. Let L_{eq} denote an estimated average length for the diffusion within the sample. This length must be a fraction of L: $0 < L_{eq} < L$. The sorption experiments were executed with steps and the analysis is based on this. Let furthermore D_v denote the vapour transport coefficient in wood for the direction in question (longitudinal) and v the average water vapour content in the sample. See Figure 3.2. The index v indicates that the moisture flow is obtained from a difference in water vapour content v.

Then we have:

$$D_v \cdot \frac{v_{surf} - v}{L_{eq}} \cdot A = G \qquad \text{or,}$$

$$v_{surf} - v = G \cdot \frac{L_{eq}}{A \cdot D_v} \tag{3.5}$$

The length of L_{eq} is shown in Figure 3.2. We will choose the fraction, L_{eq} /L to 0.8 below: $L_{eq} = 0.8 \cdot L$.

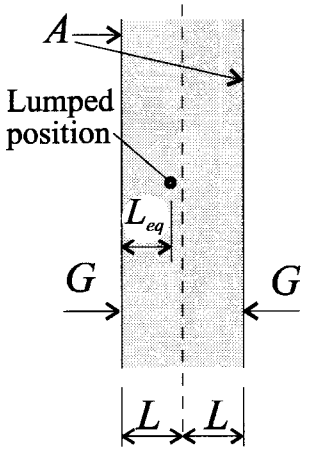

Figure 3.2 Estimated average diffusion length into the sample

We can now combine the equations for the complete moisture flow. To the previous moisture resistances representing the dampening effect of the limited flow of supply air, Equation 3.3, and the surface-to-air resistance, Equation 3.4, the last approximate resistance in the material can be added, Equation 3.5.

$$v_{inlet} - v = G \cdot \left(\frac{1}{V_{air}} + \frac{1}{A \cdot \beta} + \frac{L_{eq}}{A \cdot D_v}\right) \tag{3.6}$$

This may be written in the following way:

$$G = A \cdot \beta_{vtot} \cdot (v_{inlet} - v) \tag{3.7}$$

Here we have introduced a total moisture transfer coefficient, β_{vtot}:

$$\frac{1}{\beta_{vtot}} = \frac{A}{\dot{V}_{air}} + \frac{1}{\beta} + \frac{L_{eq}}{D_v} \qquad \beta_{vtot} = \frac{1}{\frac{A}{\dot{V}_{air}} + \frac{1}{\beta} + \frac{L_{eq}}{D_v}} \tag{3.8}$$

The above equation may be written in the following way:

$$\frac{1}{\beta_{vtot}} = \frac{A}{\dot{V}_{air}} + \frac{1}{\beta} + \frac{L_{eq}}{L} \cdot \frac{L}{D_v}$$

The factor L_{eq}/L must lie between 0 and 1. It may be close to zero during a first rapid period. But the value of L_{eq} does not matter much if the moisture resistance L/D_v of half the sample is small compared to the outer resistance. The internal flow in the sample is of secondary importance when the following criterion is fulfilled:

$$\frac{A}{\dot{V}_{air}} + \frac{1}{\beta} > \frac{L}{D_v}$$

From a reference case in Section 4.2.3 the corresponding terms are: 270 + 100 > 212. At the late part of the step-response ("late regime") the shape of the distribution of moisture gradient is more established and the transfer can with good accuracy be described by a constant moisture resistance and a lumped moisture capacity. For a not too precise calculation, it is reasonable to assume a constant resistance after roughly half of the sorption has taken place. This assumption holds even for thick samples, also when the surface resistance not is dominating.

3.1.3 Equation and time constant for isothermal moisture uptake $u(t)$

The moisture uptake G results in a change of moisture content u of the sample:

$$G = m \cdot \frac{du}{dt} \tag{3.9}$$

Combining Eq. (3.7) and (3.9), we have:

$$v_{inlet} - v = \frac{m}{A \cdot \beta_{vtot}} \cdot \frac{du}{dt} \tag{3.10}$$

The average moisture content is related to the average humidity by volume v of the sample by the sorption isotherm:

$$u = u(\varphi) \qquad \varphi = \frac{v}{v_{sat}} \tag{3.11}$$

Here, $v_{sat} = v_{sat}(T)$ is the saturation water vapour content at the concerned temperature.
It is shown in Figure 4.1. Here we use the chamber temperature. The complication with different chamber and sample temperatures is discussed in Section 3.2. We insert Eq. (3.11) in (3.10) and multiply the equation by $du/d\varphi$. Then we have:

$$v_{sat} \cdot \frac{du}{d\varphi} \cdot (\varphi_{inlet} - \varphi) = \frac{du}{d\varphi} \cdot \frac{m}{A \cdot \beta_{vtot}} \cdot \frac{du}{dt} \tag{3.12}$$

We use a linear approximation of the sorption isotherm. See Figure 3.4. Then we have:

$$u_{inlet} - u = \frac{du}{d\varphi} \cdot (\varphi_{inlet} - \varphi)$$

Here, u_{inlet} is the moisture content of the sample for the inlet relative humidity: $u_{inlet} = u(\varphi_{inlet})$. Inserting this in (3.12) gives the following equation for $u(t)$:

$$u_{inlet} - u(t) = t_1 \cdot \frac{du}{dt} \qquad (3.13)$$

Here we have got a time constant t_1 for the response of the sample moisture uptake:

$$t_1 = \frac{m}{\beta_{vtot} \cdot A \cdot v_{sat}} \cdot \frac{du}{d\varphi}$$

The moisture transfer coefficient β_{vtot} is given by Eq. 3.8. The time constant t_1 is then:

$$t_1 = \left(\frac{A}{\dot{V}_{air}} + \frac{1}{\beta} + \frac{L_{eq}}{D_v} \right) \cdot \frac{m}{A \cdot v_{sat}} \cdot \frac{du}{d\varphi} \qquad (3.14)$$

The solution for a constant u_{inlet} and a given $u(0)$ at $t = 0$ is readily obtained from 3.13:

$$u(t) = u(0) + (u_{inlet} - u(0)) \cdot (1 - e^{-t/t_1}) \qquad (3.15)$$

or in dimensionless form:

$$u'(t) = \frac{u(t) - u(0)}{u_{inlet} - u(0)} = 1 - e^{-t/t_1}$$

The dimensionless moisture content $u'(t)$ starts at zero and increases exponentially to +1 with a time constant t_1. This solution is shown in Figure 3.3.

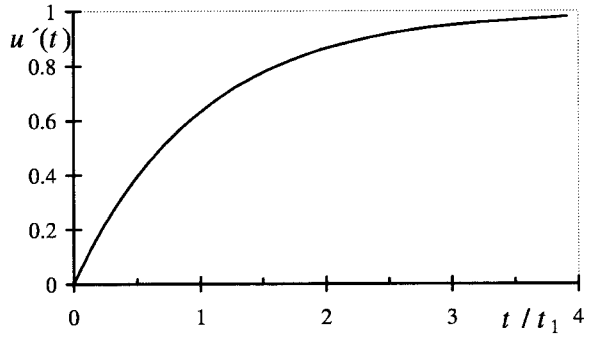

Figure 3.3 Step response in dimensionless form

Half of the change from $u(0)$ to u_{inlet} occurs at $u' = 0.5$:

$u' = 0.5 = 1 - e^{-t/t_1}$ or $t / t_1 = \ln(2) = 0.69$.

The half-time $t_{0.5}$ corresponding to $u' = 0.5$ is then:

$$t_{0.5} = t_1 \cdot \ln(2) = 0.69 \cdot t_1. \qquad (3.16)$$

A numerical example is shown in Section 4.2.3 with data in (4.6) for a typical case from the measurements. The sample thickness is $2 \cdot L$ = 1.7 mm. The step is from 70% to 85% relative humidity and the temperature is 20°C. The resulting time-constant t_1 is 1.41 [h] for this

case. The contribution to the time-constant from the effect of the restricted air flow is rather big.

3.2 Effect of latent heat on response time

The temperature T in the sample will vary in time if the latent heat of evaporation is accounted for. We will in this section consider this effect. The heat capacity of the sample is still neglected. This effect will be considered in the next section.

The other assumptions from the previous section are retained. The transport in the sample is modelled by a lumped moisture capacity and an average diffusion length. The influence from the moisture capacity of the air in the chamber is ignored.

3.2.1 Different sample and chamber temperatures

The three equations for moisture balance with humidity by volume as the driving force are still valid for different sample and chamber temperatures. Equations (3.3), (3.4) and (3.5) are:

$$v_{inlet} - v_{ch} = \frac{1}{\dot{V}_{air}} \cdot G$$

$$v_{ch} - v_{surf} = \frac{1}{\beta} \cdot \frac{G}{A}$$

$$v_{surf} - v = \frac{L_{eq}}{D_v} \cdot \frac{G}{A}$$

The sum of these equations gives:

$$v_{inlet} - v = \left(\frac{A}{\dot{V}_{air}} + \frac{1}{\beta} + \frac{L_{eq}}{D_v} \right) \cdot \frac{G}{A} \qquad (3.17)$$

or as in the preceding section, Eq. 3.7, with β_{vtot} defined by (3.8):

$$G = A \cdot \beta_{vtot} \cdot (v_{inlet} - v)$$

The moisture uptake increases the moisture content:

$$G = m \cdot \frac{du}{dt} \qquad (3.18)$$

We have:

$$v_{inlet} - v = \frac{m}{A \cdot \beta_{vtot}} \cdot \frac{du}{dt}$$

The water vapour content is given by the product of relative humidity and saturation vapour content. The temperature dependence of the saturation moisture content is illustrated in Figure 4.1. We have, using the temperatures T_{ch} and T:

$$v_{inlet} = \varphi_{inlet} \cdot v_{sat}(T_{ch}) \qquad v = \varphi \cdot v_{sat}(T) \qquad (3.19)$$

From equations (3.17 – 3.19) we get:

$$\varphi_{inlet} \cdot \mathrm{v}_{sat}(T_{ch}) - \varphi \cdot \mathrm{v}_{sat}(T) = \frac{m}{A \cdot \beta_{vtot}} \cdot \frac{\mathrm{d}u}{\mathrm{d}t} \qquad (3.20)$$

From the sorption isotherm we have that the relative humidity is a function of the moisture content u. We use a linear relation between u and φ locally in the considered RH-region. See Figure 3.4.

$$u = u_{inlet} + \frac{\mathrm{d}u}{\mathrm{d}\varphi} \cdot (\varphi - \varphi_{inlet})$$

or

$$\frac{\mathrm{d}u}{\mathrm{d}\varphi} \cdot \varphi = u - u_{inlet} + \frac{\mathrm{d}u}{\mathrm{d}\varphi} \cdot \varphi_{inlet} \qquad (3.21)$$

Here $\frac{\mathrm{d}u}{\mathrm{d}\varphi}$ is the slope of the equilibrium sorption curve for the inlet value.

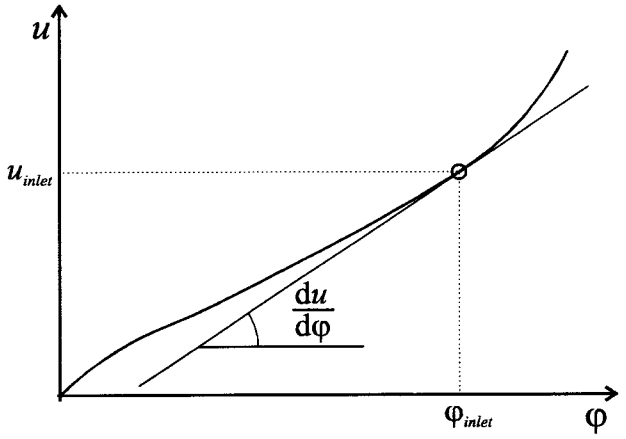

Figure 3.4 Linearization of the sorption isotherm

We multiply (3.20) by $\frac{\mathrm{d}u}{\mathrm{d}\varphi}$ and divide it by $\mathrm{v}_{sat}(T_{ch})$. Then we get, inserting Eq. (3.21), the following equation for $u(t)$:

$$\frac{\mathrm{d}u}{\mathrm{d}\varphi} \cdot \varphi_{inlet} - \left(u - u_{inlet} + \frac{\mathrm{d}u}{\mathrm{d}\varphi} \cdot \varphi_{inlet} \right) \cdot \frac{\mathrm{v}_{sat}(T)}{\mathrm{v}_{sat}(T_{ch})} = t_1 \cdot \frac{\mathrm{d}u}{\mathrm{d}t} \qquad (3.22)$$

Here, t_1 again is a time constant, Eq. (3.14):

$$t_1 = \left(\frac{A}{\dot{V}_{air}} + \frac{1}{\beta} + \frac{L_{eq}}{D_v} \right) \cdot \frac{m}{A \cdot \mathrm{v}_{sat}(T_{ch})} \cdot \frac{\mathrm{d}u}{\mathrm{d}\varphi} \qquad (3.23)$$

Equation (3.22) is our basic equation for the response $u(t)$ when φ_{inlet} is changed in time. In the case $T = T_{ch}$, the last factor before the equality sign in (3.22) is +1, and we regain the isothermal equation (3.13). Now, we need to relate the temperature T to $u(t)$.

3.2.2 Equation for the temperature $T(t)$

The temperature factor $\mathrm{v}_{sat}(T)/\mathrm{v}_{sat}(T_{ch})$ in (3.22) is obtained in the following way. The phase change of the moisture flow G from vapour to liquid results in a heat production on the sur-

face determined by the latent heat of evaporation h_e [J/kg$_{water}$]. We neglect the heat capacity of the sample. The heat of condensation balances the convective heat flow from the sample:

$$G \cdot h_e = A \cdot \alpha_c \cdot (T - T_{ch}) \qquad [\,W\,] \qquad (3.24)$$

Here, α_c is the convective heat transfer coefficient.

We now have two transfer coefficients α_c and β. Lewis' relation, which relates β to α_c , Eq. (3.60), may often be used with good accuracy.

The temperature difference due to moisture flow is obtained from Eqs. (3.24) and (3.18):

$$T - T_{ch} = \frac{h_e}{\alpha_c} \cdot \frac{G}{A} = \frac{h_e}{\alpha_c} \cdot \frac{m}{A} \cdot \frac{du}{dt} \qquad (3.25)$$

The function $v_{sat}(T)$ is locally linearized:

$$v_{sat}(T) = v_{sat}(T_{ch}) + \frac{dv_{sat}}{dT} \cdot (T - T_{ch}) \qquad (3.26)$$

Combining these two equations, the temperature factor in (3.22) may be written:

$$\frac{v_{sat}(T)}{v_{sat}(T_{ch})} = 1 + \gamma_1 \cdot \frac{du}{dt} \qquad (3.27)$$

Here, the constant γ_1 is given by:

$$\gamma_1 = \frac{1}{v_{sat}(T_{ch})} \cdot \frac{dv_{sat}}{dT} \cdot \frac{h_e}{\alpha_{tot}} \cdot \frac{m}{A} \quad [\text{s, kg}_{wood}/\text{kg}_{water}] \qquad (3.28)$$

The factor containing the derivative of $v_{sat}(T)$ divided by $v_{sat}(T)$ is plotted in Figure 4.2.

Radiation is neglected in the above formulas. If a parallel heat exchange by radiation also is taken into account with a radiative heat transfer coefficient, α_r , the balance (3.24) becomes:

$$G \cdot h_e = A \cdot (\alpha_c + \alpha_r) \cdot (T - T_{ch}) \qquad (3.29)$$

If also the radiative heat transfer coefficient is taken into account, we have to add α_r to α_c . Eq. (3.25) becomes:

$$T - T_{ch} = \frac{h_e}{\alpha_c + \alpha_r} \cdot \frac{G}{A} = \frac{h_e}{\alpha_c + \alpha_r} \cdot \frac{m}{A} \cdot \frac{du}{dt}$$

The constant γ_1 , Eq. (3.28), becomes:

$$\gamma_1 = \frac{1}{v_{sat}(T_{ch})} \cdot \frac{dv_{sat}}{dT} \cdot \frac{h_e}{\alpha_c + \alpha_r} \cdot \frac{m}{A} \quad [\text{s, kg}_{wood}/\text{kg}_{water}]$$

In all formulas to follow we will use α_{tot} to account for the total heat transfer $Q(t)$ [W] due to convection and radiation:

$$\alpha_{tot} = \alpha_c + \alpha_r \qquad (3.30)$$

The heat flow $Q(t)$ [W] to the sample is given by:

$$Q = A \cdot \alpha_{tot} \cdot (T_{ch} - T) \qquad (3.31)$$

3.2.3 Equation for moisture content $u\,(t)$

The final equation for $u(t)$ is now from Eq. (3.22) and (3.27).

$$\frac{du}{d\varphi}\cdot\varphi_{inlet}-\left(u(t)-u_{inlet}+\frac{du}{d\varphi}\cdot\varphi_{inlet}\right)\cdot\left(1+\gamma_1\cdot\frac{du}{dt}\right)=t_1\cdot\frac{du}{dt} \qquad (3.32)$$

or

$$u_{inlet}-u(t)=\frac{du}{dt}\cdot\left[t_1+\gamma_1\cdot\left(u(t)-u_{inlet}+\frac{du}{d\varphi}\cdot\varphi_{inlet}\right)\right] \qquad (3.33)$$

This is our general equation for $u(t)$. The initial value $u(0)$ is given. The inlet relative humidity is a given function of time.

3.2.4 Solution for a constant step

We consider a constant φ_{inlet} for $t > 0$, and a given initial value $u = u(0)$ at $t = 0$.

We have to integrate Eq. (3.33)for constant φ_{inlet} (and constant u_{inlet}). The solution is obtained by direct integration if we consider t as a function of u. We have:

$$\frac{dt}{du}=\frac{t_1+\gamma_1\left(u(t)-u_{inlet}+\frac{du}{d\varphi}\cdot\varphi_{inlet}\right)}{u_{inlet}-u(t)}=-\gamma_1+\frac{t_1+\gamma_1\cdot\frac{du}{d\varphi}\cdot\varphi_{inlet}}{u_{inlet}-u(t)} \qquad (3.34)$$

Integration from $u(0)$ to $u(t)$ gives:

$$t=-\gamma_1\cdot(u(t)-u(0))-\left(t_1+\gamma_1\cdot\frac{du}{d\varphi}\cdot\varphi_{inlet}\right)\cdot\ln\left(\frac{u_{inlet}-u(t)}{u_{inlet}-u(0)}\right) \qquad (3.35)$$

We introduce the dimensionless moisture content $u'(t)$:

$$u'(t)=\frac{u(t)-u(0)}{u_{inlet}-u(0)} \qquad (3.36)$$

The above equation is then:

$$t=-\gamma_1\cdot(u_{inlet}-u(0))\cdot u'-\left(t_1+\gamma_1\cdot\frac{du}{d\varphi}\cdot\varphi_{inlet}\right)\cdot\ln(1-u') \qquad (3.37)$$

The equation may be written:

$$t=-t_\gamma\cdot u'-(t_1+t_2)\cdot\ln(1-u') \qquad (3.38)$$

Here, two new time constants t_2 and t_γ are introduced:

$$t_2=\gamma_1\cdot\frac{du}{d\varphi}\cdot\varphi_{inlet}\,, \qquad (3.39)$$

$$t_\gamma=\gamma_1\cdot(u_{inlet}-u(0)) \qquad (3.40)$$

Dividing (3.38) by t_1+t_2, we get the following final dimensionless equation:

$$t' = \frac{t}{t_1 + t_2} = -\gamma \cdot u' - \ln(1 - u') \tag{3.41}$$

This dimensionless equation between $t' = t/(t_1 + t_2)$ and u' involves a single parameter γ:

$$\gamma = \frac{t_\gamma}{t_1 + t_2} \tag{3.42}$$

Division by γ_1 in Eq. (3.39) and (3.40) gives:

$$\gamma = \frac{u_{inlet} - u(0)}{\frac{t_1}{\gamma_1} + \frac{du}{d\varphi} \cdot \varphi_{inlet}} \tag{3.43}$$

Here, we have from Eq. (3.23) and (3.28):

$$\frac{t_1}{\gamma_1} = \frac{du}{d\varphi} \cdot \left(\frac{A}{\dot{V}_{air}} + \frac{1}{\beta} + \frac{L_{eq}}{D_v} \right) \cdot \frac{\alpha_{tot}}{\frac{dv_{sat}}{dT} \cdot h_e} \tag{3.44}$$

The value $u(0)$ may be the equilibrium value for a previous $\varphi = \varphi^-_{inlet}$ for t < 0. Then we have, using (3.40), (3.43) and (3.44):

$$u(0) = u(\varphi^-_{inlet})$$

$$u_{inlet} - u(0) = u(\varphi_{inlet}) - u(\varphi^-_{inlet}) = \frac{du}{d\varphi} \cdot (\varphi_{inlet} - \varphi^-_{inlet})$$

$$t_\gamma = \gamma_1 \cdot \frac{du}{d\varphi} \cdot (\varphi_{inlet} - \varphi^-_{inlet})$$

$$\gamma = \frac{\varphi_{inlet} - \varphi^-_{inlet}}{t_1 / (\gamma_1 \cdot \frac{du}{d\varphi}) + \varphi_{inlet}}$$

$$\gamma = \frac{\varphi_{inlet} - \varphi^-_{inlet}}{\left(\frac{A}{\dot{V}_{air}} + \frac{1}{\beta} + \frac{L_{eq}}{D_v} \right) \cdot \frac{\alpha_{tot}}{h_e \cdot \frac{dv_{sat}}{dT}} + \varphi_{inlet}}$$

The heat of evaporation is neglected by putting $h_e = 0$ or $\gamma = 0$. For $\gamma = 0$, we have the pure exponential response, Figure 3.3.

$$t' = -\ln(1 - u') \qquad e^{-t'} = 1 - u'$$

or:

$$u' = 1 - e^{-t'}$$

The basic equation (3.41) is illustrated in Figure 3.5. The dotted lines show $t' = \gamma \cdot u'$ for a few different γ. The difference between the curve $-\ln(1-u')$ and curve $\gamma \cdot u'$ gives t' as a function of u'.

The relation (3.41) with u' as a function of t' is shown in Figure 3.6 for different γ.

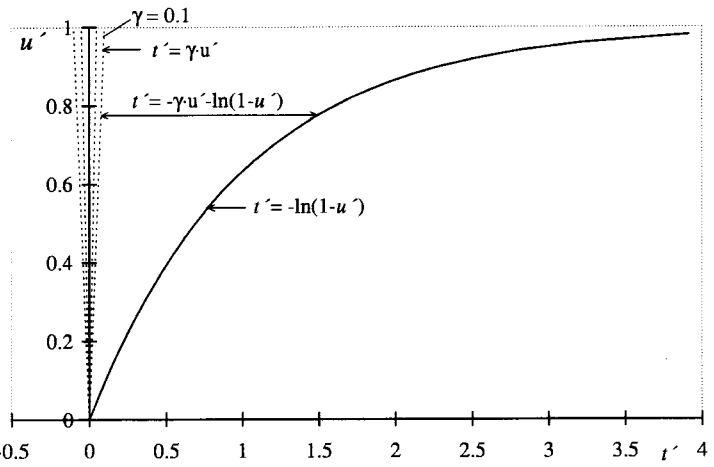

Figure 3.5 Illustration of Eq. (3.41).

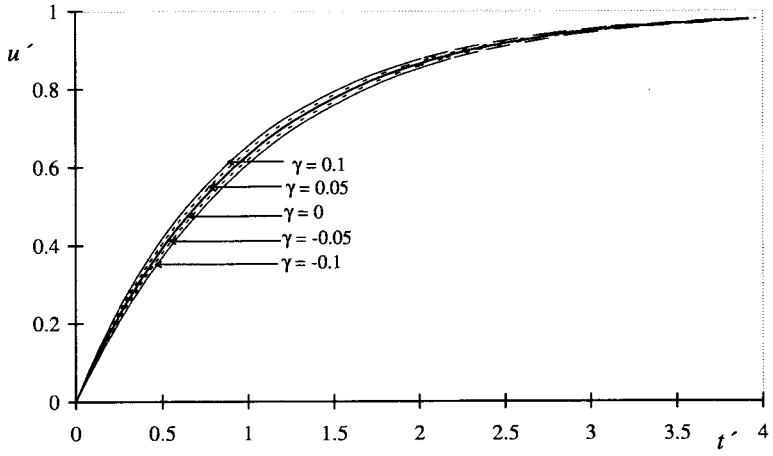

Figure 3.6 The relation (3.41) between u' and t' for different γ.

A good measure of the response time, is
the time $t_{0.5}$ for which u' equals 0.5. Equation (3.38) gives:

$$t_{0.5} = t_\gamma \cdot 0.5 - (t_1 + t_2) \cdot \ln(1 - \tfrac{1}{2})$$

or

$$t_{0.5} = \ln(2) \cdot (t_1 + t_2) - 0.5 \cdot t_\gamma = 0.69 \cdot (t_1 + t_2) - 0.5 \cdot t_\gamma$$

3.2.5 Equation for the sample temperature T

We consider the case of constant chamber temperature T_{ch}. The sample temperature, $T = T(t)$, will vary in time. We have from Eq. (3.25), (3.36) and (3.41) :

$$T(t) - T_{ch} = \frac{h_e \cdot m}{\alpha_{tot} \cdot A} \cdot \frac{du}{dt} = \frac{h_e \cdot m}{\alpha_{tot} \cdot A} \cdot \frac{u_{inlet} - u(0)}{t_1 + t_2} \cdot \frac{du'}{dt'} \qquad (3.45)$$

For $t = 0$ we have:

$$T(0)-T_{ch}=\frac{h_e\cdot m}{\alpha_{tot}\cdot A}\cdot\frac{u_{inlet}-u(0)}{t_1+t_2}\cdot\frac{\mathrm{d}u'}{\mathrm{d}t'}(0)$$

The derivative $\frac{\mathrm{d}t'}{\mathrm{d}u'}$ is, Eq. (3.41) :

$$\frac{\mathrm{d}t'}{\mathrm{d}u'}=-\gamma+\frac{1}{1-u'}\qquad\frac{\mathrm{d}u'}{\mathrm{d}t'}=\frac{1-u'}{1-\gamma+\gamma\cdot u'}\tag{3.46}$$

From this we have:

$$T(t)=T_{ch}+(T(0)-T_{ch})\cdot\frac{(1-u')\cdot(1-\gamma)}{1-\gamma+\gamma\cdot u'}$$

or

$$T(t)=T_{ch}+(T(0)-T_{ch})\cdot\frac{(1-u')}{1+\frac{\gamma}{1-\gamma}\cdot u'}\tag{3.47}$$

Here, the factor $T(0)$ - T_{ch} is the temperature difference at $t = 0$:

$$T(0)-T_{ch}=\frac{h_e\cdot m}{\alpha_{tot}\cdot A}\cdot\frac{u_{inlet}-u(0)}{t_1+t_2}\cdot\frac{1}{1-\gamma}\tag{3.48}$$

or, inserting Eq. (3.42):

$$T(0)-T_{ch}=\frac{h_e\cdot m}{\alpha_{tot}\cdot A}\cdot\frac{u_{inlet}-u(0)}{t_1+t_2-t_\gamma}\tag{3.49}$$

Equation (3.47) involves the factor $\gamma/(1-\gamma)$, which may be written, Eq. (3.42):

$$\frac{\gamma}{1-\gamma}=\frac{t_\gamma}{t_1+t_2-t_\gamma}$$

A dimensionless excess sample temperature is introduced:

$$T'=\frac{T(t)-T_{ch}}{T(0)-T_{ch}}=\frac{1-u'}{1+\frac{\gamma}{1-\gamma}\cdot u'}\tag{3.50}$$

This function is shown in Figure 3.7 for different γ.

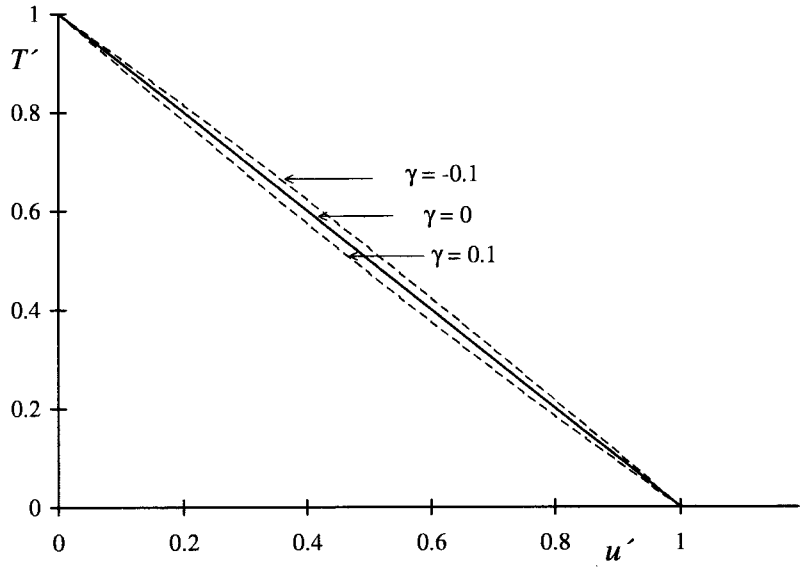

Figure 3.7 The dimensionless excess sample temperature, (3.50).

The above equation gives T' as a function of u'. In order to obtain the time dependence, we have to combine Figure 3.7 and Figure 3.6 as it is done in Figure 3.8. An example of connected values t', u' and T' for $\gamma = 0.1$ is shown by the dotted lines.

3.2.6 Summary

Let us summarize the obtained result. The dimensionless equation between u' and t' is, (3.41):

$$t' = \frac{t}{t_1 + t_2} = -\gamma \cdot u' - \ln(1 - u')$$

Here, u' is the dimensionless moisture content.

$$u' = \frac{u(t) - u(0)}{u_{inlet} - u(0)}$$

Here, $u_{inlet} = u(\varphi_{inlet})$, is the equilibrium moisture content for $\varphi = \varphi_{inlet}$. The time t_1 is the time-constant for an isothermal step response, (3.23):

$$t_1 = \left(\frac{A}{\dot{V}_{air}} + \frac{1}{\beta} + \frac{L_{eq}}{D_v} \right) \cdot \frac{m}{A \cdot v_{sat}(T_{ch})} \cdot \frac{du}{d\varphi} \quad [s]$$

The dimensionless variable γ involves two new time-constants, (3.42):

$$\gamma = \frac{t_\gamma}{t_1 + t_2}$$

The additional time constants t_2 and t_γ for the non-isothermal case are, (3.39) and (3.40):

$$t_2 = \gamma_1 \cdot \frac{du}{d\varphi} \cdot \varphi_{inlet} \quad [s]$$

$$t_\gamma = \gamma_1 \cdot (u_{inlet} - u(0)) \quad [s]$$

The constant γ_1 involves the effects of latent heat, (3.28):

$$\gamma_1 = \frac{1}{v_{sat}(T_{ch})} \cdot \frac{dv_{sat}}{dT} \cdot \frac{h_e}{\alpha_{tot}} \cdot \frac{m}{A} \quad [s, kg_{wood}/kg_{water}]$$

A linear relation between u and φ is used:.

$$u(\varphi) = u_{inlet} + \frac{du}{d\varphi} \cdot (\varphi - \varphi_{inlet})$$

The temperature development in the sample, $T = T(t)$, is, (3.47):

$$T(t) = T_{ch} + (T(0) - T_{ch}) \cdot \frac{1-u'}{1+\frac{\gamma}{1-\gamma} \cdot u'} \quad [°C]$$

The temperature difference at $t' = 0$, is, (3.49):

$$T(0) - T_{ch} = \frac{h_e \cdot m}{\alpha_{tot} \cdot A} \cdot \frac{u_{inlet} - u(0)}{t_1 + t_2 - t_\gamma} \quad [°C]$$

The dimensionless excess sample temperature T' is:

$$T' = \frac{T(t) - T_{ch}}{T(0) - T_{ch}} = \frac{1-u'}{1+\frac{\gamma}{1-\gamma} \cdot u'}$$

The above relations between u', T' and t' are shown in Figure 3.8 for different γ.

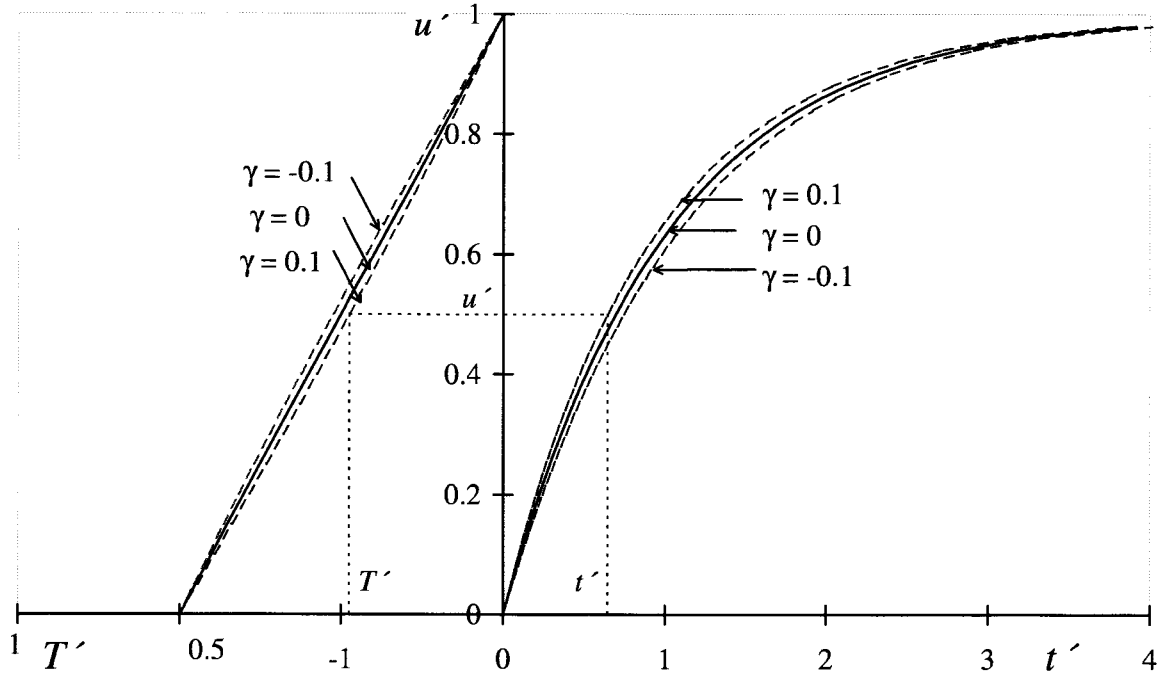

Figure 3.8 The relations between T', u' and t' for different γ.

3.3 General equations for moisture and temperature

In the above section we neglected the heat capacity of the sample. A linear approximation for the sorption isotherm $u(\varphi)$ was used. We also used a linear approximation in temperature for the saturation water vapour content $v_{sat}(T)$. We will here consider a more general case with-

out these restrictions. We still consider a "small" sample, which is described by a single (average) moisture content $u(t)$ and a single (average) temperature $T(t)$. The solution of the equations will be obtained numerically using the mathematical package Mathcad.

The moisture flow $G(t)$ is given by (3.7):

$$G = A \cdot \beta_{vtot} \cdot (\mathrm{v}_{inlet} - \mathrm{v})$$

The heat flow $Q(t)$ [W] is given by (3.31):

$$Q = A \cdot \alpha_{tot} \cdot (T_{ch} - T)$$

The mass and heat balance equations are:

$$m \cdot \frac{\mathrm{d}u}{\mathrm{d}t} = G \tag{3.51}$$

$$m \cdot c \cdot \frac{\mathrm{d}T}{\mathrm{d}t} = Q + h_e \cdot G \tag{3.52}$$

Here, c [J/(kg,K)] is the heat capacity of the sample, and h_e the latent heat of evaporation.

We now have two coupled differential equations for $u(t)$ and $T(t)$:

$$\frac{\mathrm{d}u}{\mathrm{d}t} = \frac{A \cdot \beta_{vtot}}{m} \cdot (\mathrm{v}_{inlet} - \mathrm{v})$$

$$\frac{\mathrm{d}T}{\mathrm{d}t} = \frac{A \cdot \alpha_{tot}}{m \cdot c} \cdot (T_{ch} - T) + \frac{A \cdot \beta_{vtot} \cdot h_e}{m \cdot c} \cdot (\mathrm{v}_{inlet} - \mathrm{v})$$

The water vapour concentration v is related to the relative humidity, Eq. (3.11):

$$\varphi = \frac{\mathrm{v}}{\mathrm{v}_{sat}(T)}$$

For the sorption isotherm $u = u(\varphi)$, we may use the inverse $\varphi = \varphi(u)$. From this we get v as a function of u and T:

$$\mathrm{v}(u,T) = \varphi(u) \cdot \mathrm{v}_{sat}(T) \tag{3.53}$$

We also have:

$$\mathrm{v}_{inlet} = \varphi_{inlet} \cdot \mathrm{v}_{sat}(T_{ch}) \tag{3.54}$$

The equation system involving only u and T is now:

$$\frac{\mathrm{d}u}{\mathrm{d}t} = -\frac{A \cdot \beta_{vtot}}{m} \cdot (\mathrm{v}(u,T) - \mathrm{v}_{\mathrm{inlet}}) \tag{3.55a}$$

$$\frac{\mathrm{d}T}{\mathrm{d}t} = -\frac{A \cdot \alpha_{tot}}{m \cdot c} \cdot (T - T_{ch}) - \frac{A \cdot \beta_{vtot} \cdot h_e}{m \cdot c} \cdot (\mathrm{v}(u,T) - \mathrm{v}_{inlet}) \tag{3.55b}$$

The initial values of moisture content, $u(0)$, and temperature, $T(0)$, must be prescribed. The function $\mathrm{v}(u,T)$ is given by (3.53), and v_{inlet} by (3.54).

This equation system for $u(t)$ and $T(t)$ will be solved using the Mathcad program for computer solution of mathematical problems. A number of results will be given in Chapter 4. A complete solution in Mathcad for a particular case is given in Appendix A.

3.4 Basic response time constants

The above equations, (3.55a) and (3.55b), for $u(t)$ and $T(t)$ involve two basic time constants for the moisture and thermal response to a change of the outside humidity φ_{inlet} and/or temperature T_{ch}. In order to obtain formulas for these time constants, we have to linearize the equation system.

The water vapour content $v = v(u,T)$ is linearized:

$$v(u,T) = v(u_{inlet},T_{ch}) + \frac{\partial v}{\partial u}\cdot(u-u_{inlet}) + \frac{\partial v}{\partial T}\cdot(T-T_{ch})$$

Here, the derivatives of $v(u,T)$, Eq. (3.53), are taken at the point of linearization:

$$\frac{\partial v}{\partial u} = \frac{d\varphi}{du}(u_{inlet})\cdot v_{sat}(T_{ch}) = \frac{v_{sat}(T_{ch})}{\frac{du}{d\varphi}}$$

$$\frac{\partial v}{\partial T} = \varphi(u_{inlet})\cdot\frac{dv_{sat}}{dT}(T_{ch}) = \varphi_{inlet}\cdot\frac{dv_{sat}}{dT}(T_{ch})$$

Insertion of the linearized approximation of $v(u,T) - v_{inlet}$ in the equations (3.55) gives:

$$\frac{du}{dt} = -\frac{A\cdot\beta_{vtot}}{m}\cdot\frac{v_{sat}(T_{ch})}{\frac{du}{d\varphi}}\cdot(u-u_{inlet}) - \frac{A\cdot\beta_{vtot}}{m}\cdot\varphi_{inlet}\cdot\frac{dv_{sat}}{dT}\cdot(T-T_{ch}) \qquad (3.56a)$$

$$\frac{dT}{dt} = -\frac{A\cdot\alpha_{tot}}{m\cdot c}\cdot(T-T_{ch}) - \frac{h_e}{c}\cdot\left(\frac{A\cdot\beta_{vtot}}{m}\cdot\frac{v_{sat}(T_{ch})}{\frac{du}{d\varphi}}\cdot(u-u_{inlet}) + \frac{A\cdot\beta_{vtot}}{m}\cdot\varphi_{inlet}\cdot\frac{dv_{sat}}{dT}\cdot(T-T_{ch})\right) \qquad (3.56b)$$

The factor before $u - u_{inlet}$ in (3.56a) is $1/t_1$, Eq. (3.14):

$$t_1 = \frac{m}{A\cdot\beta_{vtot}\cdot v_{sat}(T_{ch})}\cdot\frac{du}{d\varphi}(\varphi_{inlet})$$

The factor before $T - T_{ch}$ in the first term of the equation for $T(t)$ gives the time constant t_3 for a pure thermal response:

$$t_3 = \frac{m\cdot c}{A\cdot\alpha_{tot}} \qquad (3.57)$$

The factor before $T - T_{ch}$ in the equation for $u(t)$ may be written in the following way:

$$\frac{A\cdot\beta_{vtot}}{m}\cdot\varphi_{inlet}\cdot\frac{dv_{sat}}{dT} = \frac{1}{t_1}\cdot\varphi_{inlet}\cdot\frac{du}{d\varphi}\cdot\frac{\frac{dv_{sat}}{dT}}{v_{sat}(T_{ch})} =$$

$$= \frac{1}{t_1}\cdot\frac{c}{h_e}\cdot\frac{1}{t_3}\cdot\varphi_{inlet}\cdot\frac{du}{d\varphi}\cdot\frac{h_e}{c}\cdot\frac{m\cdot c}{A\cdot\alpha_{tot}}\cdot\frac{\frac{dv_{sat}}{dT}}{v_{sat}(T_{ch})} =$$

$$= \frac{c}{h_e}\cdot\frac{1}{t_1\cdot t_3}\cdot\varphi_{inlet}\cdot\frac{du}{d\varphi}\cdot\gamma_1 = \frac{c}{h_e}\cdot\frac{t_2}{t_1\cdot t_3}$$

Here, γ_1, is given by (3.28) and t_2 by (3.39).

The two linearized equations (3.56a) and (3.56b) are now:

$$\frac{du}{dt} = -\frac{1}{t_1}\cdot(u - u_{inlet}) - \frac{c}{h_e}\cdot\frac{t_2}{t_1 \cdot t_3}\cdot(T - T_{ch}) \qquad (3.58a)$$

$$\frac{dT}{dt} = -\left(\frac{1}{t_3} + \frac{t_2}{t_1 \cdot t_3}\right)\cdot(T - T_{ch}) - \frac{h_e}{c}\cdot\frac{1}{t_1}\cdot(u - u_{inlet}) \qquad (3.58b)$$

The equations involve the factor c/h_e and the three times t_1, t_2 and t_3. The solution for any initial values $u(0)$ and $T(0)$ is well known. See for example Claesson and Hagentoft (1994). We will not give the solution in detail here. Our main interest is the time constants of the response to a change of φ_{inlet} (and/or T_{ch}). The solution consists of two exponentials $\exp(-\lambda_+ \cdot t)$ and $\exp(-\lambda_- \cdot t)$. The exponents involve the two eigenvalues of equation system (3.58). These are the solution of the determinant:

$$\begin{vmatrix} \lambda - \frac{1}{t_1} & -\frac{c}{h_e}\cdot\frac{t_2}{t_1 \cdot t_3} \\ -\frac{h_e}{c}\cdot\frac{1}{t_1} & \lambda - \frac{1}{t_3} - \frac{t_2}{t_1 \cdot t_3} \end{vmatrix} = 0$$

or

$$\left(\lambda - \frac{1}{t_1}\right)\cdot\left(\lambda - \frac{1}{t_3} - \frac{t_2}{t_1 \cdot t_3}\right) - \frac{h_e}{c}\cdot\frac{1}{t_1}\cdot\frac{c}{h_e}\cdot\frac{t_2}{t_1 \cdot t_3} = 0$$

$$\lambda^2 - \lambda\cdot\left(\frac{1}{t_1} + \frac{1}{t_3} + \frac{t_2}{t_1 \cdot t_3}\right) + \frac{1}{t_1 \cdot t_3} = 0$$

We multiply this equation by the factor $\frac{t_1 \cdot t_3}{\lambda^2}$:

$$t_1 \cdot t_3 - \frac{1}{\lambda}\cdot(t_1 + t_2 + t_3) + \frac{1}{\lambda^2} = 0$$

The solutions for $\frac{1}{\lambda}$ are:

$$\frac{1}{\lambda} = \frac{t_1 + t_2 + t_3}{2} \pm \sqrt{\left(\frac{t_1 + t_2 + t_3}{2}\right)^2 - t_1 \cdot t_3}$$

We have obtained the two time constants of the exponentials:

$$t_+ = \frac{1}{\lambda_+} = \tfrac{1}{2}\cdot\left(t_1 + t_2 + t_3 + \sqrt{(t_1 + t_2 + t_3)^2 - 4 \cdot t_1 \cdot t_3}\right) \qquad (3.59a)$$

$$t_- = \frac{1}{\lambda_-} = \tfrac{1}{2}\cdot\left(t_1 + t_2 + t_3 - \sqrt{(t_1 + t_2 + t_3)^2 - 4 \cdot t_1 \cdot t_3}\right) \qquad (3.59b)$$

The solutions for $u(t) - u_{inlet}$ and $T(t) - T_{ch}$ are linear combinations of the two exponentials:

$$e^{-t/t_+} \qquad e^{-t/t_-}.$$

The coefficients are determined from the initial conditions.

The larger time constant t_+ determines the exponential approach towards $u = u_{inlet}$ and $T = T_{ch}$. It is our *basic response time*:

$$t_+ = \frac{1}{\lambda_+} = \tfrac{1}{2}\cdot\left(t_1 + t_2 + t_3 + \sqrt{(t_1 + t_2 + t_3)^2 - 4\cdot t_1 \cdot t_3}\right)$$

Let us summarize the results. We have three time parameters:

$$t_1 = \frac{m}{A\cdot \beta_{vtot}\cdot \mathrm{v}_{sat}(T_{ch})}\cdot\frac{\mathrm{d}u}{\mathrm{d}\varphi}(\varphi_{inlet})$$

$$t_2 = \frac{\mathrm{d}u}{\mathrm{d}\varphi}(\varphi_{inlet})\cdot\varphi_{inlet}\cdot\frac{m\cdot h_e}{A\cdot\alpha_{tot}}\cdot\frac{\frac{\mathrm{dv}_{sat}}{\mathrm{d}T}(T_{ch})}{\mathrm{v}_{sat}(T_{ch})}$$

$$t_3 = \frac{m\cdot c}{A\cdot\alpha_{tot}}$$

These times are combined in (3.59) to give the smaller time constant t_- and the larger, basic response time t_+.

3.5 Heat and moisture transfer coefficients

A crucial part of the above theory for the moisture and temperature response of the thin samples of the type used in the experiments is the transfer coefficients α_{tot} and β for heat and moisture. We will here discuss them in some detail.

3.5.1 Lewis' relation

Lewis' relation, Eckert and Drake (1959), relates the surface moisture coefficient β to the convective heat transfer coefficient α_c :

$$\beta = \frac{\alpha_c}{\rho_a\cdot c_{pa}} \quad [\mathrm{m/s}] \qquad (3.60)$$

The relation is based on an analogy between heat and water vapour diffusion in flowing gas at a solid boundary.

The following value for the volumetric heat capacity of the air will be used:

$\rho_a \cdot c_{pa} = 1200$ [J/(m^3, K)]

3.5.2 Heat transfer coefficients

The heat transfer consists of a part due to radiation, α_r , and a part due to convective heat transfer, α_r . The total heat transfer coefficient α_{tot} is the sum of these two. See Eq. (3.30).

Radiative heat transfer coefficient α_r

For the samples placed in a single flat layer, the heat transfer coefficient from radiation, α_r , is calculated with a view factor F = 1, since every part of the sample is openly exposed to a

hemisphere of chamber wall. For a view factor of 1, an approximate expression for the coefficient for a moderate temperature difference is:

$$\alpha_r = 4 \cdot \varepsilon \cdot \sigma \cdot \left(T + 273\right)^3 \quad [\text{ W/(m}^2\cdot\ ^\circ\text{C) }] \qquad (3.61)$$

Here, the Stefan–Boltzmann constant is $\sigma = 5.67 \cdot 10^{-8}$ [W/(m^2·K^4)]. The combined emissivity ε is with the emissivities ε_1 and ε_2 of the surfaces of the sample and the chamber:

$$\frac{1}{\varepsilon} = \frac{1}{\varepsilon_1} + \frac{1}{\varepsilon_2} - 1 \qquad (3.62)$$

The emissivity for wood is around 0.9, and the same value was chosen for the walls of the chamber. This gives with (3.62) a combined emissivity of 0.82.

Convective heat transfer coefficient α_c

For the convective heat transfer coefficient, α_c , a rough estimate based on an assumed speed in the surrounding air is made. The air blows parallel to the sample.

The Colburn analogy between wall friction and heat transfer, given in Bejan (1993), is:

$$\text{Nu}_y = 0.0296 \cdot \text{Re}_y^{4/5} \cdot \text{Pr}^{1/3}$$

Nu_y	the local Nusselt number,	$\text{Nu}_y = \dfrac{\alpha_c \cdot y}{\lambda}$
λ	heat transfer coefficient [W/(m·K)],	$\lambda = 0.025$ for air at 20°C
y	distance from the edge to the local point in question [m]	
Pr	Prandtl number for the gas,	Pr = 0.72 for air (at 0–30°C)
Re_y	the local Reinolds number,	$\text{Re}_y = \dfrac{u_\infty \cdot y}{\nu}$
u_∞	the speed of the surrounding air [m/s]	
ν	kinematic viscosity [m^2/s]	

The air speed is assumed to be 1.5 m/s. A point on the middle of the sample, 0.05 m from the edge, is investigated.

$$\text{Re}_y = \frac{1.5 \cdot 0.05}{15 \cdot 10^{-6}} = 5000 \qquad \text{Nu}_y = 0.0296 \cdot 5000^{4/5} \cdot 0.72^{1/3} = 24$$

$$\alpha_c = \frac{24 \cdot 0.025}{0.05} = 12 \quad [\text{W/(m}^2\cdot\text{K)}]$$

Here, $\nu = 15 \cdot 10^{-6}$ m^2/s is the kinematic viscosity for air at 20°C. This reference value for α_c is varied in Sections 4.3.6 and 4.4.3.

3.5.3 Heat transfer coefficient in a pure water vapour environment

In Section 0 examples from the experiments of Christensen in pure water vapour are evaluated. The heat transfer coefficient is required in the calculations. Only natural convection is assumed to take place. (It should be noted that there is no diffusion of water vapour here. This means that Lewis' law is not applicable).

The following notations are used in this section:

g	gravitational acceleration [m/s^2]
β_{ex}	coefficient of volumetric thermal expansion [K^{-1}]
T_{surf} -T_{ch} = ΔT	temperature difference between sample and chamber [K]
L_y	height of the vertical surface [m]
ρ	density [kg/m^3]
ρ_{sat}	density of saturated water vapour [kg/m^3]
c_p	heat capacity for the gas [J/(kg·K)]
μ	dynamic viscosity [kg/(s·m)]
ν	kinematic viscosity [m^2/s] $\nu = \frac{\mu}{\rho}$
α_c	convective heat transfer coefficient [W/(m^2, K)]
Pr	Prandtl number for the gas, $\mathrm{Pr} = \frac{\nu \cdot \rho \cdot c_{pa}}{\lambda} = \frac{\mu \cdot c_{pa}}{\lambda}$

The convective heat transfer coefficient, α_c , is calculated with help of the Nusselt number. The average Nusselt number for a "wall" of height L is defined as:

$$\overline{\mathrm{Nu}}_L = \frac{\alpha_c \cdot L_y}{\lambda} \qquad \alpha_c = \frac{\overline{\mathrm{Nu}}_L \cdot \lambda}{L_y} \ [\mathrm{W/(m^2, K)}] \qquad (3.63)$$

A representative sample size is 10×10×1 mm for many experiments made by Christensen and coauthors. The Grashof number gives a relation between buoyancy forces from natural convection versus viscous forces. The Grashof number, Gr_L , related to the total height of the sample is, Bejan (1993):

$$\mathrm{Gr}_L = \frac{g \cdot \beta_{ex} \cdot (T_{surf} - T_{ch}) \cdot L_y^3}{\nu^2} \qquad (3.64)$$

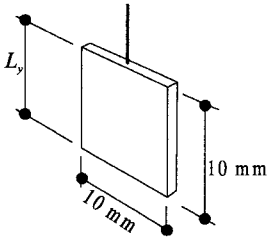

For water vapour at the actual pressures far away from the pressure at the critical point, the dynamic viscosity is highly independent of the pressure. The value of the dynamic viscosity for water vapour, μ, is shown in Table 3.1 and Figure 3.9. On the other hand the kinematic viscosity, defined as $\nu = \mu/\rho$, is inversely proportional to the density and thus inversely proportional to the pressure (if the gas acts as a perfect gas). This is illustrated in Figure 3.9 for $\varphi = 1$ and $\varphi = 0.5$.

$$\varphi = \frac{\nu}{\nu_{sat}} = \frac{\rho}{\rho_{sat}} \qquad \nu(T) \cong \frac{\mu(T)}{\rho_{sat}(T) \cdot \varphi} \qquad \nu(\varphi) \cong \frac{\nu(\varphi = 1)}{\varphi}$$

The conductivity, λ, is highly constant with pressure for pressures in the actual range. This means that the values in can be used for all φ. This also applies for the Prandtl number for the gas also shown in Table 3.1.

Table 3.1 Density, dynamic viscosity, thermal conductivity and Prandtl number for saturated water vapour at different temperatures

T [°C]	ρ_{sat} [kg/m^3]	μ [kg/(m·s)]	λ [W/(m·K)]	Pr
0	$4847 \cdot 10^{-6}$	$884 \cdot 10^{-8}$	0.0167	0.9816
10	$9396 \cdot 10^{-6}$	$917 \cdot 10^{-8}$	0.0174	0.9812
20	$1729 \cdot 10^{-5}$	$952 \cdot 10^{-8}$	0.0181	0.9805
30	$3037 \cdot 10^{-5}$	$986 \cdot 10^{-8}$	0.0190	0.9730
40	$5116 \cdot 10^{-5}$	$1018 \cdot 10^{-8}$	0.0197	0.9741
50	$8302 \cdot 10^{-5}$	$1051 \cdot 10^{-8}$	0.0204	0.9784
60	$1302 \cdot 10^{-4}$	$1088 \cdot 10^{-8}$	0.0212	0.9833
70	$1982 \cdot 10^{-4}$	$1128 \cdot 10^{-8}$	0.0222	0.9837

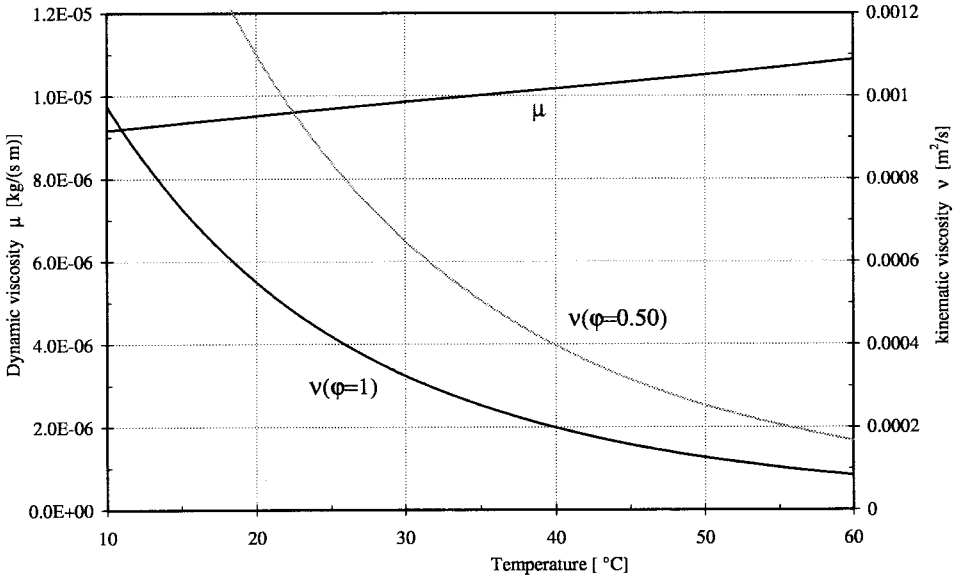

Figure 3.9 Viscosity of water vapour as a function of RH and temperature

A empirical correlation to calculate the Nusselt number for an isothermal vertical surface is shown in Figure 3.10, Pitts and Sissom (1977). The lower range in the diagram is applicable for the conditions here where conduction is dominating. A rough estimate of pure conduction in stagnant gas with the sample size and a chamber diameter of 0.1 m gives a corresponding value of ln(Nu) = 0.1 . This figure is used as an extrapolation of the diagram for low values.

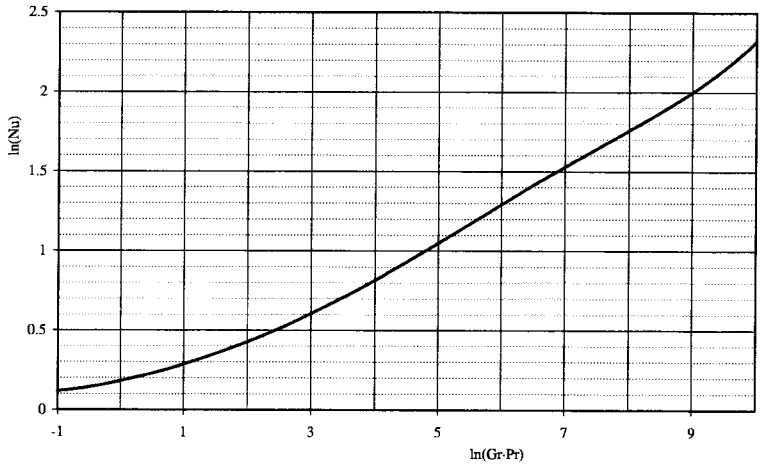

Figure 3.10 Correlation between Gr·Pr *and* Nu *numbers for heated vertical plates*

The product of Gr·Pr is used in Figure 3.10. It can be expressed as:

$$\mathrm{Gr}\cdot\mathrm{Pr}=\frac{g\cdot\beta_{ex}\cdot\Delta T\cdot L_y^3}{\nu^2}\cdot\frac{\nu\cdot\rho\cdot c_p}{\lambda}=\frac{g\cdot\beta_{ex}\cdot\Delta T\cdot L_y^3\cdot\rho^2\cdot c_p}{\lambda\cdot\mu}$$

Exchanging ρ with $\rho_{sat}\cdot\varphi$ and grouping the temperature depending variables we get:

$$\mathrm{Gr}\cdot\mathrm{Pr}=g\cdot L_y^3\cdot\frac{\beta_{ex}\cdot\rho_{sat}^2\cdot c_p}{\lambda\cdot\mu}(T)\cdot\varphi^2\cdot\Delta T$$

At 20°C the product of Gr·Pr is:

$$\mathrm{Gr}\cdot\mathrm{Pr}=9.81\cdot 0.01^3\cdot\frac{0.0173^2\cdot 1866}{(20+273)\cdot 0.0181\cdot 952\cdot 10^{-8}}\cdot\varphi^2\cdot\Delta T=0.108\cdot\varphi^2\cdot\Delta T$$

At 60°C the product of Gr·Pr is:

$$\mathrm{Gr}\cdot\mathrm{Pr}=9.81\cdot 0.01^3\cdot\frac{0.1302^2\cdot 1916}{(60+273)\cdot 0.0212\cdot 1088\cdot 10^{-8}}\cdot\varphi^2\cdot\Delta T=4.15\cdot\varphi^2\cdot\Delta T$$

The Prandtl number is very close to 1 as seen in Table 3.1. The convective heat transfer coefficients are calculated from Equation. (3.63) for a few values in below.

Table 3.2 Convective heat transfer coefficients for different temperature differences, RH-levels and temperature levels for the examples

	$T = 20°C$			$T = 60°C$		
RH	$\Delta T = 0.1°C$	$\Delta T = 1°C$	$\Delta T = 10°C$	$\Delta T = 0.1°C$	$\Delta T = 1°C$	$\Delta T = 10°C$
$\varphi = 0.2$	2.04	2.04	2.04	2.39	2.50	2.64
$\varphi = 0.5$	2.04	2.04	2.06	2.39	2.52	3.49
$\varphi = 0.8$	2.04	2.04	2.09	2.42	2.79	4.18

As seen in the table, α_c is close to constant with temperature difference. It is only at high temperature combined with a large temperature difference that there is a significant influence.

4 Numerical studies of step responses

We will in this chapter apply the theory developed in Chapter 3 for the thin samples used in the experiments reported in this thesis.

4.1 Saturation water vapour content

The formulas of the preceding chapter involve the saturation water vapour content, $v_{sat}(T)$, and its derivative. These functions are shown in Figure 4.1. The strong temperature dependence of the saturation vapour content is illustrated in the diagram. The ratio used in for example in Equation 3.28 between the temperature derivative of the saturation water vapour content and the function itself, is plotted in Figure 4.2. Its variation with temperature is small.

The expression to be used for the saturation water vapour content is given by (4.1). The principle for the expression is taken from The Institute of Measurement and Control (1996) adopted from vapour pressure to vapour content to values from Grigull (1979). The fitted range is $0 < T < 80°C$.

$$v_{sat} = \exp\left[\frac{a_1}{T+273.15} + a_2 + a_3 \cdot (T+273.15) + a_4 \cdot (T+273.15)^2 + a_5 \cdot \ln(T+273.15)\right]$$

where: $a_1 = -6050$ $a_2 = 14.835$ $a_3 = -0.0268$ $a_4 = 0.0000172$ $a_5 = 1.43$ (4.1)

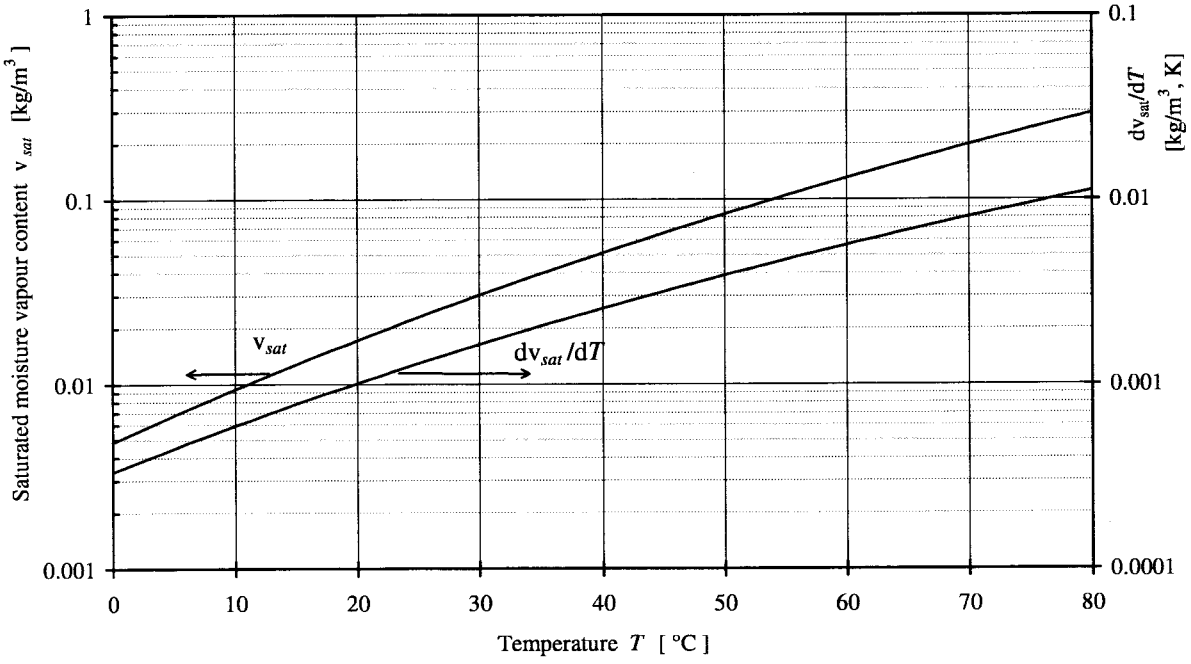

Figure 4.1 Saturation moisture content v_{sat} and its temperature derivative dv_{sat}/dT as a function of temperature.

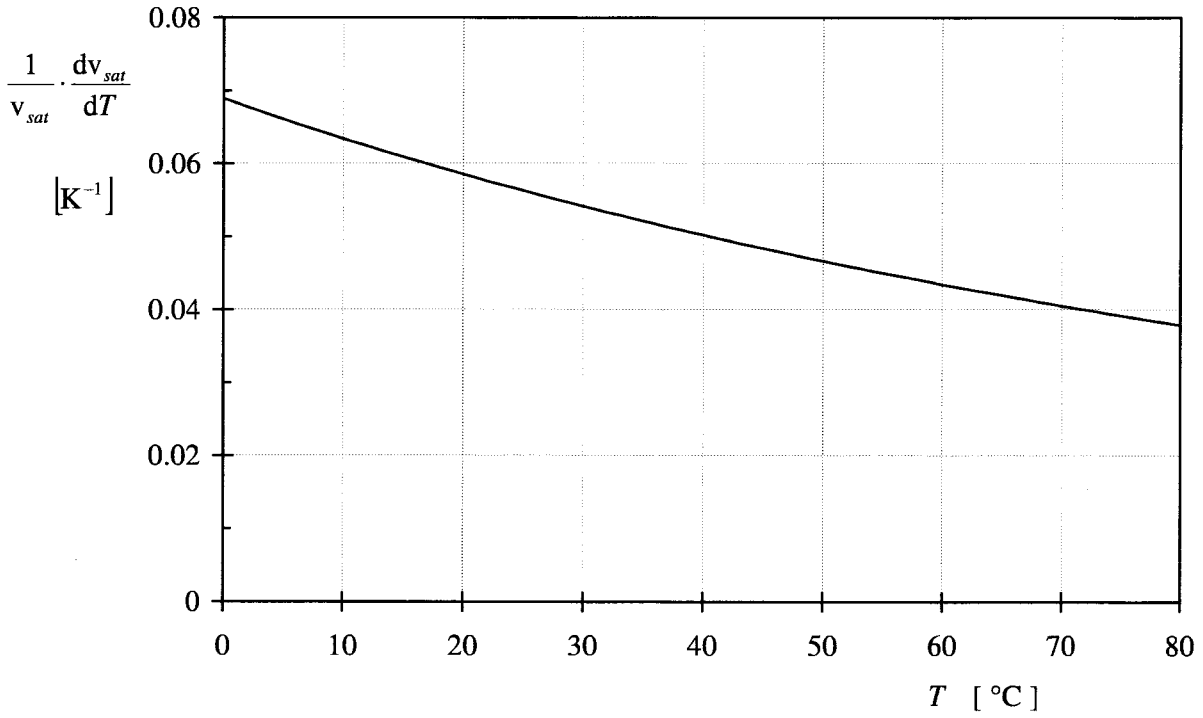

Figure 4.2 *Ratio between the temperature derivative* dv_{sat}/dT *and the saturation moisture content* v_{sat} *as a function of temperature.*

4.2 Reference case

The calculations in this chapter will concern a reference case and variations of some parameters of this case.

4.2.1 Sorption isotherm

It is very convenient to have a formula for the sorption isotherm that is easy to work with. The following simple expression has an overall shape with a rather good agreement for wood in general:

$$u(\varphi) = \frac{A - \ln[-\ln(\varphi)]}{B} \qquad 0.08 \le \varphi \le 0.98$$

The φ-interval is however limited since the function is not finite at both extremes of the interval. If additional constants C and D are added the algorithm can be made finite.

$$u(\varphi) = \frac{A - \ln[-\ln(C \cdot \varphi + D)]}{B} \qquad 0 \le \varphi \le 1 \qquad (4.2a)$$

The constant D is chosen so that $u(0) = 0$. Furthermore C is chosen so that $u(1) = u_{max}$. We thus have three variables A, B and u_{max} for the sorption formula. The constants D and C become:

$$D = e^{-e^{A}} \qquad C = e^{-e^{A - B \cdot u_{max}}} - e^{-e^{A}} \qquad (4.2b)$$

We will also need the inverse of the sorption isotherm: $\varphi = \varphi(u)$. We have from (4.2a):

$$\varphi(u) = \frac{1}{C} \cdot \{\exp[-\exp(A - B \cdot u)] - D\} \qquad 0 \le u \le u_{max} \qquad (4.2c)$$

The derivative of the sorption isotherm and its inverse are readily obtained from(4.2a) and (4.2c). We get:

$$\frac{du}{d\varphi} = \frac{C}{B} \cdot \frac{1}{-\ln(C \cdot \varphi + D)} \cdot \frac{1}{C \cdot \varphi + D} \qquad 0 \le \varphi \le 1 \qquad (4.2d)$$

$$\frac{d\varphi}{du} = \frac{B}{C} \cdot \exp[A - B \cdot u - \exp(A - B \cdot u)] \qquad 0 \le u \le u_{max} \qquad (4.2e)$$

The following values will be used at 20°C for Scots pine (*Pinus sylvestris*):

$A = 1.5 \qquad B = 19.2 \qquad u_{max} = 0.5 \qquad (4.2f)$

The values for C and D become:

$D = 0.01131 \qquad C = 0.98838$

It is somewhat difficult to obtain good sorption data from literature (they seem to vary more between specimens of researchers than between specimens of wood). Fitting has been made to absorption data from Ahlgren (1972) given in Kielsgaard-Hansen (1986). The moisture content values are somewhat high compared to data by others. Kielsgaard-Hansen presents two series of measurements. The one with smaller values was used to obtain the above values. The fitted value of u_{max} became high. It was reduced to conform with other data.

The sorption isotherm depends somewhat on the temperature also: $u = u(\varphi,T)$. The temperature dependency of the sorption isotherm is not too well established. The temperature dependence is obtained by fitting in the following way:

$$A = 1.7 - 0.01 \cdot T$$

$$B = 19.1 + 0.00025 \cdot T^2$$

$$u_{max} = 0.52 - 0.001 \cdot T \qquad (4.2g)$$

Here, T is given in °C. The temperature dependence is not obtained by fitting of specific data for Scots pine only, but also on properties for wood in general described in the literature. The above fitting is therefore somewhat uncertain. The temperature dependency for u_{max} , which is mostly influencing the relative humidity range close to 100%, was selected to be – 0.1% per °C. This is based on the temperature dependency for the fibre saturation point which is considered to have this value generally for wood, Nilsson (1988). By adding a linear term to the constant A , the desired effect of having a rather uniform du/dT distribution over a wide range of the centre φ -interval is achieved. Due to the special properties of the algorithm, to maintain this desired effect over a wide range of temperature levels, a non-linear term have to be added to the constant B. The uniform du/dT distribution is based on data from Stamm (1964). Both Stamm (1964) and Krischer (1963) show a slight increase in the du/dT values for a range around $\varphi = 0.8$ for high temperatures. The same tendency is seen in data from Kelsey (1957) discussed in Wadsö (1997). This effect could be achieved by increasing the non-linear term in constant B but it is not done here. A moderate temperature dependence is used in the analyses in this chapter.

The sorption isotherm $u(\varphi,T)$ (4.2a, b, f and g) for Scots pine is shown in Figure 4.3.

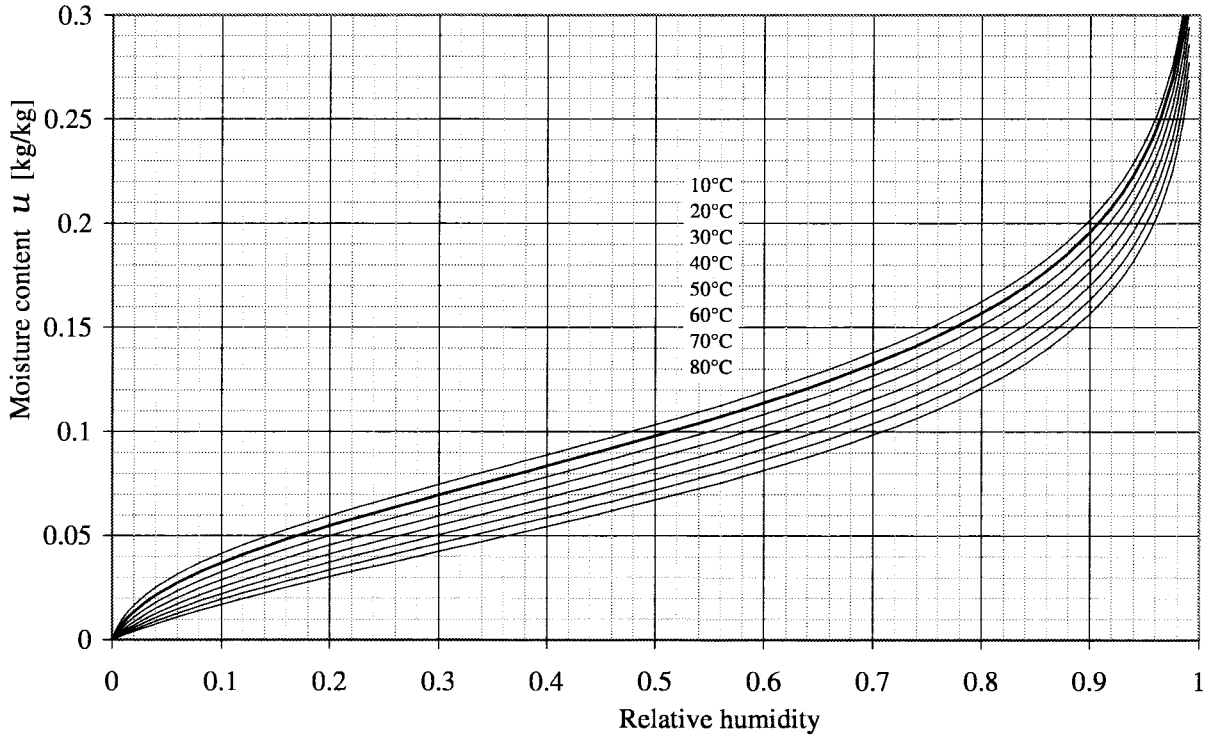

Figure 4.3 Sorption isotherm (4.2) for Scots pine

The sorption isotherm , fitted for Scots pine at 20°C, is rather similar for other species such as Norwegian spruce, Sifka spruce and Klinki pine. The temperature dependence in the expression is taken from several kinds of wood. The group of sorption curves for the whole temperature range are therefore not so related to Scots pine specifically, but more to wood in general.

4.2.2 Latent heat of evaporation and heat of sorption

The latent heat of evaporation, h_e , has a slight dependence with temperature. A linear expression for this dependence is given in (4.3), taken from Nevander and Elmarsson (1996). The expression yields $h_e = 2.45 \cdot 10^6$ [J/kg$_{water}$] for 20°C and $h_e = 2.49 \cdot 10^6$ [J/kg$_{water}$] for 5°C.

$$h_e(T) = 2.5 \cdot 10^6 \cdot (1 - 0.001 \cdot T) \quad \text{[J/kg}_{water}\text{]} \qquad (4.3)$$

The latent heat of sorption is the difference in enthalpy between vapour and free liquid water. The enthalpy at the free, liquid state is zero by definition. There is also a difference in enthalpy between the free and the sorbed state. In Figure 4.4 the heat of sorption, designated h_{sorp} , is shown as a function of the moisture content for wood. The arrow in the figure shows the differential heat of sorption produced by absorption at a constant level of humidity (an infinitesimal amount of water sorbed to the material). In the calculations, an average over the step interval in moisture content is used. No temperature dependence for the heat of sorption is included. The total heat of sorption becomes:

$$h_{e,tot} = h_e(T) + h_{sorp}(u) \qquad (4.4)$$

The heat of sorption in Figure 4.4 is taken from a diagram in Wadsö (1997) (from Skaar 1988). A fitting with a simple expression, (4.5), was done.

$$h_{sorp}(u) = 1.15 \cdot 10^6 \cdot \exp\left(-\frac{u}{0.07}\right) \qquad (4.5)$$

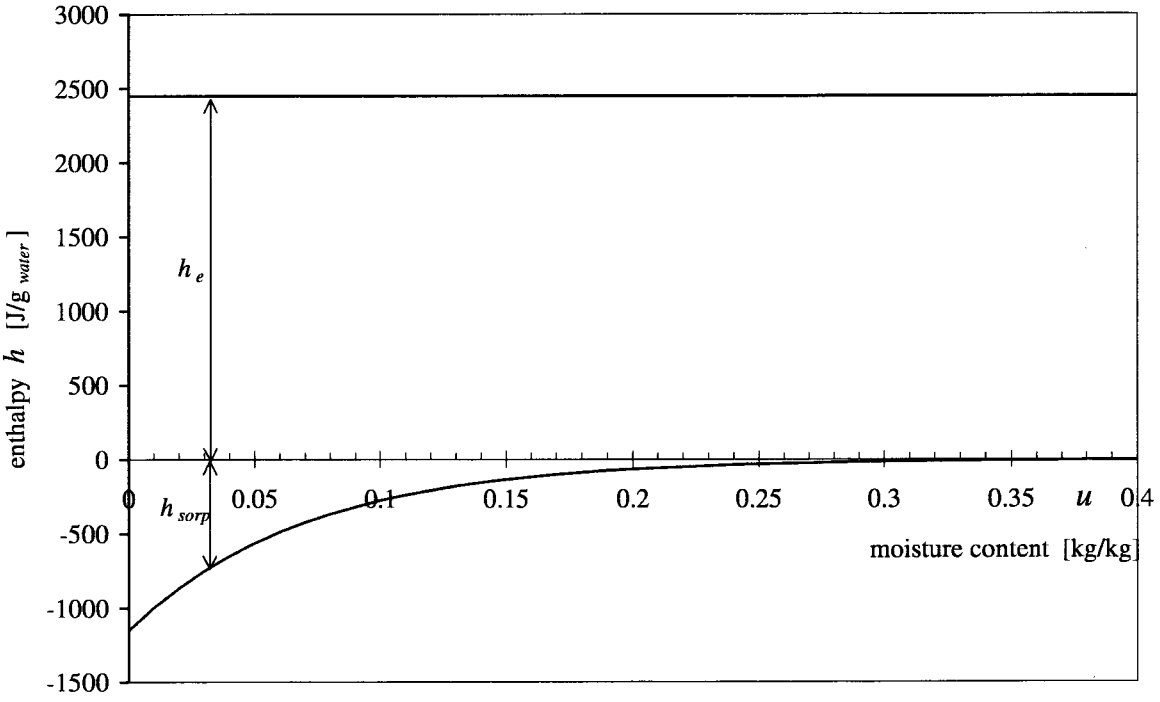

Figure 4.4 Latent heat of evaporation, h_e (at 20°C), and heat of sorption, $h_{sorp}(u)$, as a function of moisture content for wood. (J per gram of water).

4.2.3 Data for reference case

As a first numerical example we consider the following case which is quite typical for the experiments. The temperature is 20°C. The initial relative humidity in the sample is 75%, and the inlet air relative humidity is 85%. The sample is subjected to a step from 75% to 85%. The dry weight of the sample is m = 0.0077 [kg] and the total area of the sample is A = 0.0178 [m^2]. The sample thickness, $2 \cdot L$, is 1.7 mm. The average diffusion length, L_{eq} , is chosen to $L_{eq} = 0.8 \cdot L = 0.68 \cdot 10^{-3}$ [m] . See Figure 3.2. The air exchange into the chamber is $\dot{V}_{air} = 0.066 \cdot 10^{-3}$ [m^3/s]. Longitudinal transport coefficient is $D_v = 4 \cdot 10^{-6}$ [m^2/s] according to Villadsen et al (1993). The radiative heat transfer coefficient is with a emissivity of 0.9 on the sample and the chamber wall, Eqs. (3.61) and (3.62), α_r = 4 [W/(m^2,K)]. An estimate for the convective coefficient is α_c = 12 [W/(m^2,K)] according to Section 3.5.2. The latent heat of evaporation is $h_e = 2.45 \cdot 10^6$ [J/kg] and the heat of sorption is estimated to $h_{sorp} = 0.10 \cdot 10^6$ [J/kg] according to Section 4.2.2 (for u = 0.17). The heat capacity for dry wood is estimated to 1300 [J/(kg_{wood}, K)]. To this capacity the added mass of water is contributing with 4180 [J/(kg_{water}, K)]. At this moisture level the combined heat capacity becomes 2000 [J/(kg_{water}, K)].

We have the following primary input data:

$\varphi_{inlet} = 0.85$ $\varphi(0) = 0.75$ $T_{ch} = 20°C$

$T(0) = 20°C$ $m = 0.0077$ kg $A = 0.0178$ m^2

$L_{eq} = 0.68 \cdot 10\text{-}3$ m $\dot{V}_{air} = 0.066 \cdot 10\text{-}3$ m3/s $D_v = 4 \cdot 10\text{-}6$ m/s

$\alpha_r = 4$ W/(m2,K) $\alpha_c = 12$ W/(m2,K)

$h_e = 2.55 \cdot 10^6$ J/kg $c = 2000$ J/(kg,K) 4.6a)

The total heat transfer coefficient becomes, (3.30):

$\alpha_{tot} = 16$ [W/(m^2, K)]

We use Lewis' law, (3.60), to get the surface moisture transfer coefficient:

$$\beta = \frac{12}{1200} = 0.01 \text{ [m/s]}$$

The total moisture transfer coefficient β_{vtot} becomes, (3.8):

$$\frac{1}{\beta_{vtot}} = \frac{0.0178}{0.066 \cdot 10^{-3}} + \frac{1}{0.01} + \frac{0.68 \cdot 10^{-3}}{4 \cdot 10^{-6}} \qquad \beta_{vtot} = 0.001853 \text{ [m/s]}$$

The saturation moisture content at 20°C and its temperature derivative can be obtained from Figure 4.1, $v_{sat} = 17.29 \cdot 10^{-3}$ [kg/m^3] and $dv_{sat}/dT = 1.012 \cdot 10^{-3}$ [kg/(m^3,K)]. The moisture capacity for the wood at $\varphi_{inlet} = 0.85$ is $du/d\varphi = 0.3759$ [kg_{water}/kg_{wood}].

We have the following auxiliary data for the reference case:

$\alpha_{tot} = 16$ [W/(m^2, K)] $\beta_{vtot} = 0.001853$ [m/s]

$v_{sat}(20) = 17.29 \cdot 10^{-3}$ kg/m^3 $\frac{dv_{sat}}{dT}(20) = 1.012 \cdot 10^{-3}$ kg/m^3,K $\frac{du}{d\varphi}(0.85) = 0.3759$ kg/kg

$u(0) = 0.1436$ kg/kg $u_{inlet} = 0.1733$ kg/kg (4.6b)

4.2.4 Comparison of the different solutions for the reference case

In the preceding chapter, we have presented three solutions involving different assumptions. It is of interest to compare these.

In Section 3.1, the temperature changes were neglected. By assumption the sample temperature was equal to the chamber temperature: $T = T_{ch}$. The time constant t_1 , (3.14), becomes:

$$t_1 = \left(\frac{0.0178}{0.066 \cdot 10^{-3}} + \frac{1}{0.01} + \frac{0.68 \cdot 10^{-3}}{4 \cdot 10^{-6}} \right) \cdot \frac{0.0077 \cdot 0.3759}{0.0178 \cdot 17.29 \cdot 10^{-3}}$$

$$t_1 = (270 + 100 + 170) \cdot 9.405 = 5077 \text{ [s]} \quad t_1 = 1.41 \text{ [h]}$$

The solution $u(t)$ is given by the simple exponential expression (3.15). Figure 4.5 shows $u(t)$ for the reference case.

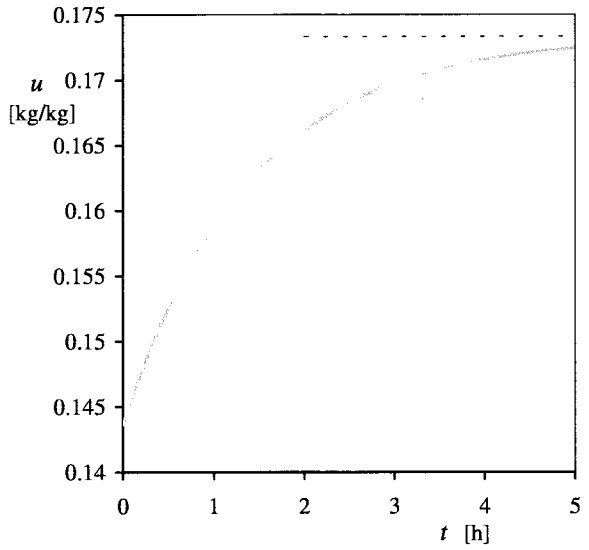

Figure 4.5 The moisture content u(t) for the reference case using the first, isothermal solution from Section 3.1.

In Section 3.2, the effect of latent heat was considered, but the heat capacity of the sample was neglected. The constant γ_1 concerning the latent heat and the total heat transfer, Eq. (3.28), is:

$$\gamma_1 = \frac{1.012 \cdot 10^{-3}}{17.29 \cdot 10^{-3}} \cdot \frac{2.55 \cdot 10^{6}}{16} \cdot \frac{0.0077}{0.0178} = 4032 \quad [\mathrm{s, kg_{wood}/kg_{water}}]$$

The time constant t_2, (3.39), is:

$$t_2 = \gamma_1 \cdot \frac{\mathrm{d}u}{\mathrm{d}\varphi} \cdot \varphi_{inlet} = 4032 \cdot 0.3759 \cdot 0.85 = 1288 \ [\mathrm{s}] \quad t_2 = 0.36 \ [\mathrm{h}]$$

The time constant t_γ, which depends on the step size, Eq. (3.40), becomes:

$$t_\gamma = 4032 \cdot (0.1733 - 0.1436) = 120 \ [\mathrm{s}] \quad t_\gamma = 0.03 \ [\mathrm{h}]$$

The dimensionless parameter γ from Eq. (3.42), involving t_γ, t_1 and t_2, is:

$$\gamma = \frac{120}{5077 + 1288} = 0.0188$$

The excess temperature at $t = 0$ is, Eq. (3.49):

$$T(0) - T_{ch} = \frac{2.55 \cdot 10^{6} \cdot 0.0077}{16 \cdot 0.0178} \cdot \frac{0.1733 - 0.1436}{5077 + 1288 - 120} = 0.327 \ [\mathrm{K}]$$

The solution $u(t)$ is given by (3.38). It is shown in Figure 4.6, left. The shaded line shows the solution of Figure 4.5 from Section 3.1. The essential difference of the two curves is that the time constant in the exponential is changed from $t_1 = 1.41$ h to $t_1 + t_2 = 1.41 + 0.36$ h. The correction due to the small γ-value of 0.0188 is secondary. The right hand figure shows the temperature as a function of time, Eq. (3.47).

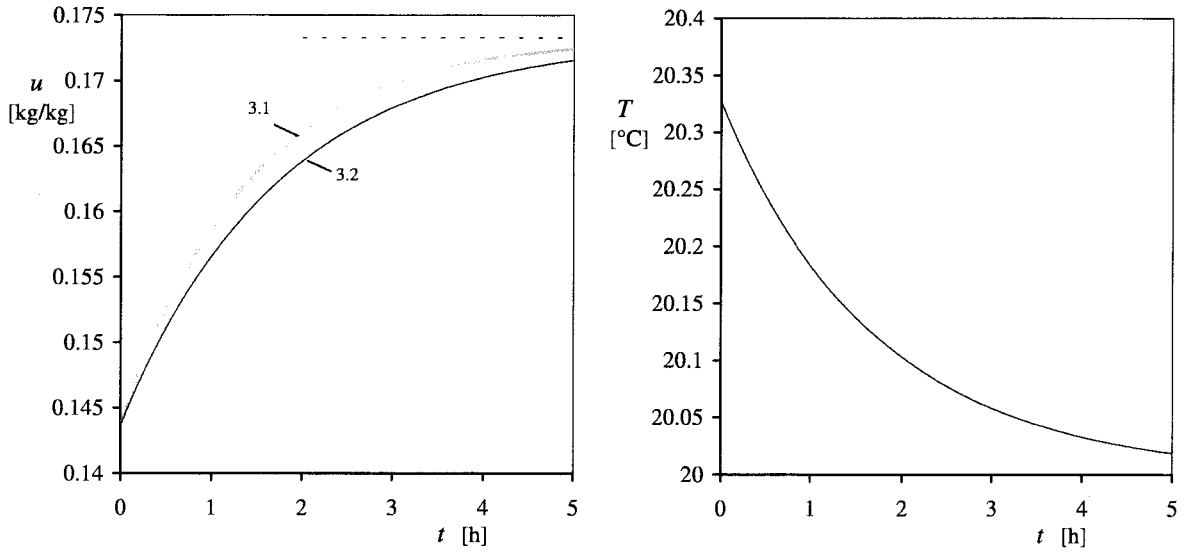

Figure 4.6 *The moisture content, u(t) (left figure) and the temperature T(t) (right figure) for the reference case using the second solution from Section 3.2. The shaded line shows the solution from Figure 4.5.*

The general solution for a small sample was given in Section 3.3. The two coupled, nonlinear equations for $u(t)$ and $T(t)$ are given by (3.55a) and (3.55b). The equations have been solved using the mathematical package Mathcad. A numerical routine based on the Runge-Kutta method is used. The complete work sheet for the general solution is given in Appendix A. A few comments are added in order to explain the different steps in the solution. The Mathcad solution is shown in Figure 4.7

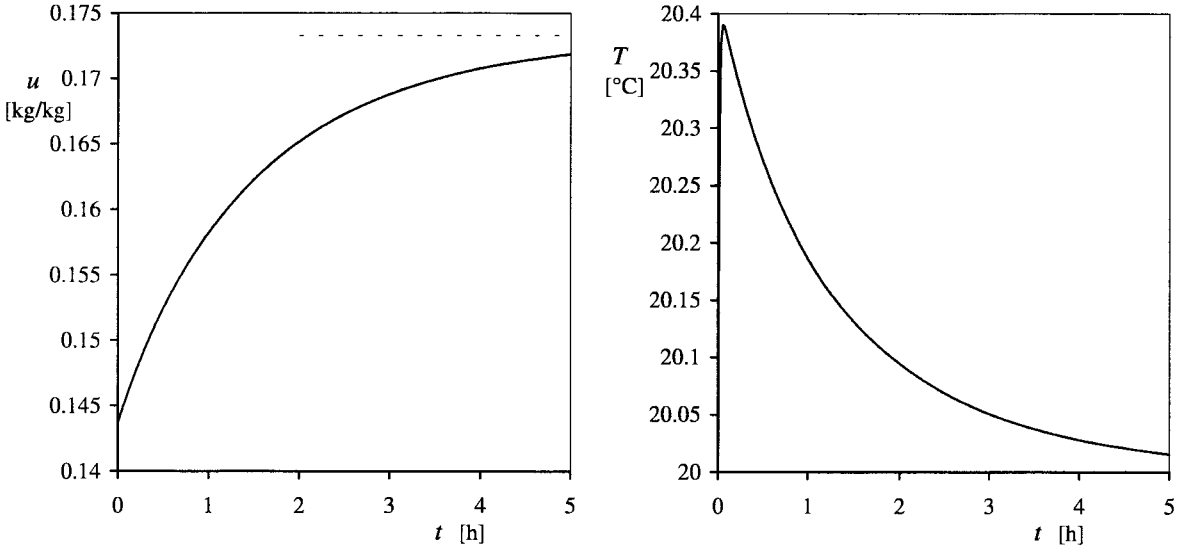

Figure 4.7 *The moisture content u(t) (left figure) and the temperature T(t) (right figure) for the reference case using the third, general solution from Section 3.3.*

The thermal response involves a much shorter time constant. Figure 4.8 shows this initial period with its rapid temperature change to a maximum and a following, slow thermal decline. The maximum temperature $T = 20.390$ occurs at $t = 200$ sec.

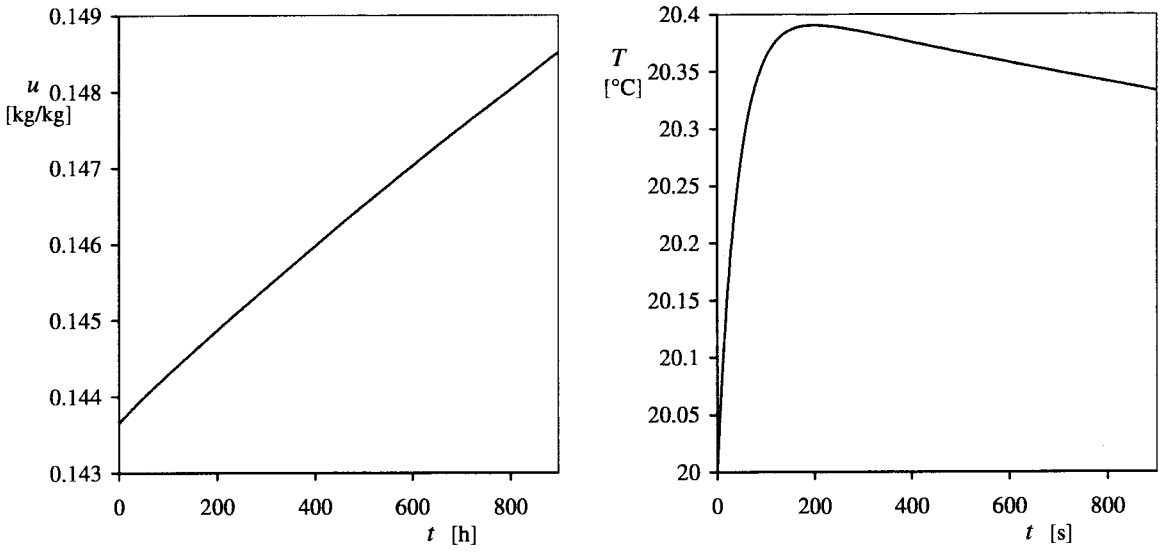

Figure 4.8 The moisture content u(t) (left figure) and the temperature T(t) (right figure) for the solution from Figure 4.7 for the initial period.

The three solutions of Figure 4.5 to Figure 4.8 are shown for comparison in Figure 4.9.

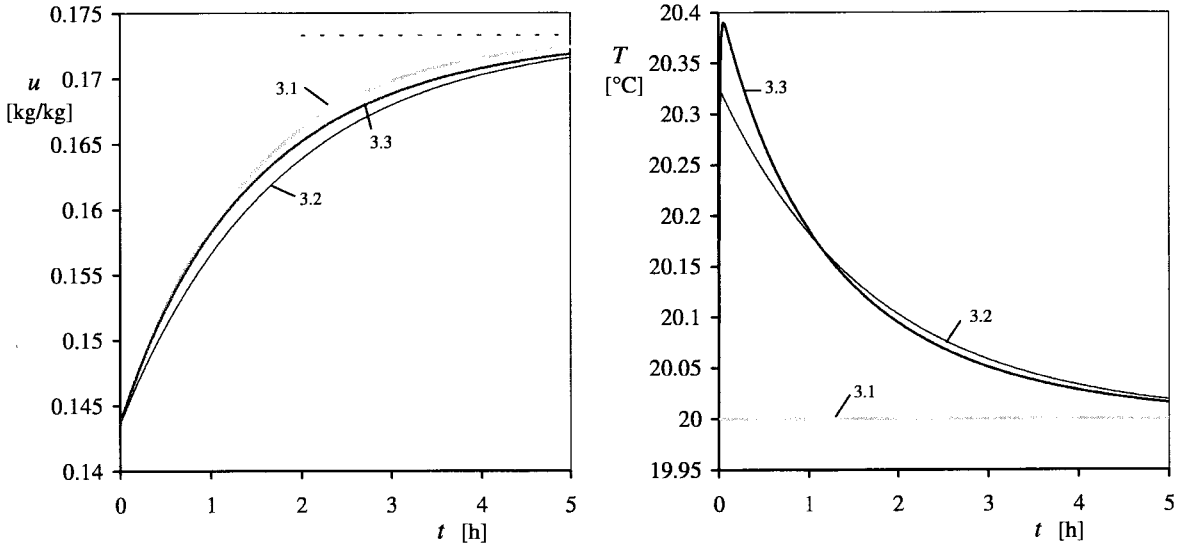

Figure 4.9 The moisture content u(t) (left figure) and the temperature T(t) (right figure) for the three solutions of Sections 3.1 – 3.3.

The nonlinear equations were linearized in Section 3.4. We obtained a time constant t_3 for a pure thermal response, and two basic time constants t_+ and t_-. The value of t_3 is for the reference case, Eq. (3.57):

$$t_3 = \frac{0.0077 \cdot 2000}{0.0178 \cdot 16} = 54 \text{ [s]} \quad t_3 = 0.015 \text{ [h]}$$

The three time constants t_1 , t_2 and t_3 are combined to give the two time constants for the solution. The time constant t_+ from Eq. (3.59a) is the basic response time:

$$t_+ = \tfrac{1}{2}\cdot\left(5077+1288+54+\sqrt{(5077+1288+54)^2-4\cdot 5077\cdot 54}\right) = 6377 \text{ [s]} \quad t_+ = 1.77 \text{ [h]}$$

Time constant t_- from Eq. (3.59b) is short and basically only influencing the initial phase:

$$t_- = \tfrac{1}{2}\cdot\left(5077+1288+54-\sqrt{(5077+1288+54)^2-4\cdot 5077\cdot 54}\right) = 43 \text{ [s]}$$

The linear equations may be solved analytically. For simplicity, we have used the mathcad solution linearized in v(u, T) as is shown in Section 3.4. In Figure 4.10 the linearized and exact solutions for $u(t)$ and $T(t)$ are shown. The linearized solution is shown as thin lines. The full lines show the general solution from Section 3.3. We see that the solutions at first are somewhat different, but later they follow each other quite well. There is a certain difference for the temperature during the first period with rapidly changing temperature. This is shown in Figure 4.11, left. These initial differences are due to different conditions for the two solutions. The solution from Section 3.4 uses a linearization for the moisture capacity and the saturation vapour content in the equilibrium point. The general model on the other hand uses the exact moisture capacity and the saturation vapour content at the present moisture content and temperature. These differences are largest at the start of the step.

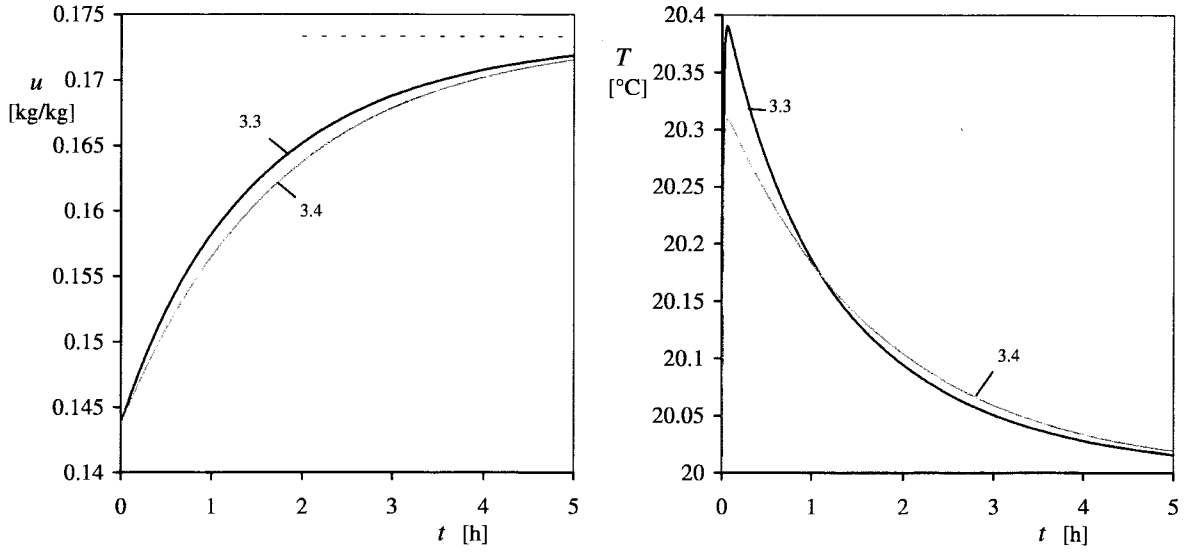

Figure 4.10 The moisture content u(t) (left figure) and the temperature T(t) (right figure) for the linearized solution from Section 3.4. The full lines are the general solution from Section 3.3.

The driving force behind the moisture transport is differences in moisture vapour content. To illustrate how the vapour content evolves during the initial phase with rapidly changing temperature, a diagram with v(t) is plotted. See Figure 4.11, right. At the starting point of the step the two curves of moisture vapour content differ since curve 3.4 is derived from a linearisation at φ_{inlet} and curve 3.3 uses the correct vapour content. The two response curves converge at equilibrium.

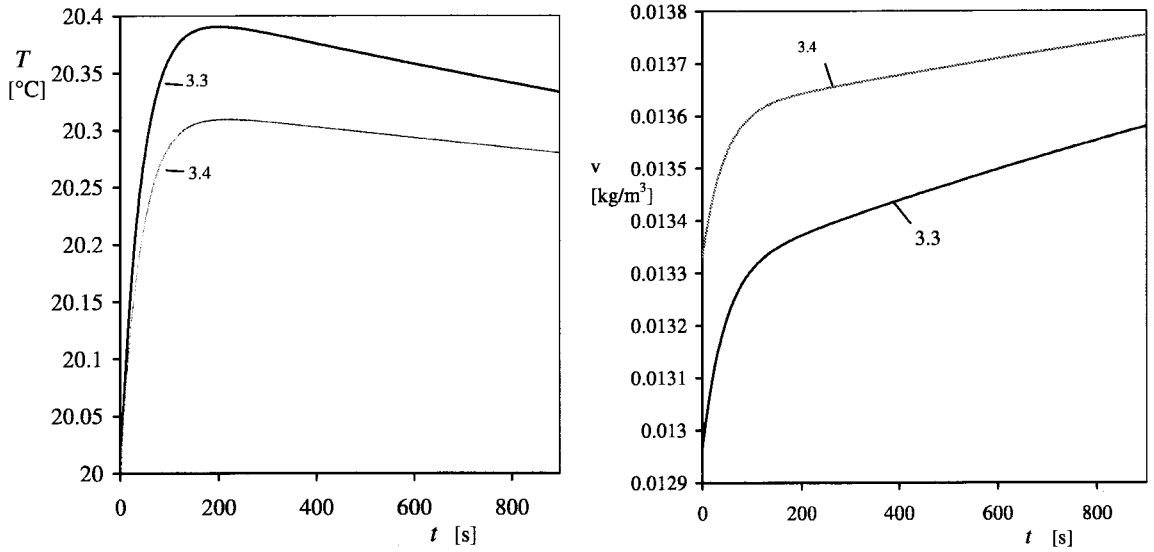

Figure 4.11 The temperature T(t) for the initial period in Figure 4.10, (left figure). The development of the water vapour content, v(t), for the initial period is shown in the right hand figure.

4.3 Changes of key parameters for the reference case

4.3.1 Temperature altered to 5°C

The experiments have been carried out, besides at 20°C as in the reference case, at 5°C. It is of interest to consider the reference case with the temperature altered to 5°C. The primary data of reference case (4.6a) are valid except for:

$T_{ch} = 5°C$ $T(0) = 5°C$

The auxiliary data, (4.6b), have the following changes:

$v_{sat}(5) = 6.80 \cdot 10^{-3}$ kg/m^3 $\frac{dv_{sat}}{dT}(5) = 4.49 \cdot 10^{-4}$ kg/m^3,K $h_e = 2.49 \cdot 10^6$ J/kg

$\frac{du}{d\varphi}(0.85) = 0.378$ kg/kg $u(0) = 0.1519$ kg/kg $u_{inlet} = 0.1817$ kg/kg

The time constant t_1, (3.14), becomes:

$$t_1 = \left(\frac{0.0178}{0.066 \cdot 10^{-3}} + \frac{1}{0.01} + \frac{0.68 \cdot 10^{-3}}{4 \cdot 10^{-6}} \right) \cdot \frac{0.0077 \cdot 0.378}{0.0178 \cdot 6.8 \cdot 10^{-3}}$$

$t_1 = (270 + 100 + 170) \cdot 24.1 = 12990$ [s] $t_1 = 3.61$ [h]

The constant γ_1 is changed somewhat , Eq. (3.28):

$$\gamma_1 = \frac{4.49 \cdot 10^{-4}}{6.8 \cdot 10^{-3}} \cdot \frac{2.57 \cdot 10^{6}}{16} \cdot \frac{0.0077}{0.0178} = 4599 \quad [\mathrm{s, kg_{wood}/kg_{water}}]$$

The time constant t_2 , (3.39), is:

$$t_2 = \gamma_1 \cdot \frac{du}{d\varphi} \cdot \varphi_{inlet} = 4599 \cdot 0.378 \cdot 0.85 = 1478 \ [\mathrm{s}] \quad t_2 = 0.41 \ [\mathrm{h}]$$

The difference in the moisture content in the equation for time constant t_γ is changed slightly because of the minor temperature dependence of the slope of the sorption isotherm. Eq. (3.40) gives:

$t_\gamma = 4599 \cdot (0.1817 - 0.1519) = 137$ [s] $t_\gamma = 0.04$ [h]

In Table 4.1 the constants for 5°C are shown together with the previous ones for the reference case.

Table 4.1 Time constants for the lower temperature at 5°C and for the reference case (4.6) at 20°C.

	lower temp.	ref. case
	T_{ch} = 5°C	T_{ch} = 20°C
t_1 [s]	12990	5077
t_2 [s]	1478	1288
γ	0.0095	0.0188
t_γ [s]	137	120
t_+ [s]	14470	6377
t_- [s]	49	43
$T(0) - T_{ch}$ [°C]	0.145	0.327

We see that significant changes take place for t_1 , γ and $T(0) - T_{ch}$ whereas t_2 and t_γ are changed insignificantly. The saturation water vapour content, v_{sat} , is a factor of the denominator in Eq. (3.23) for t_1 . This explains the change of t_1 . The expressions for $T(0) - T_{ch}$ and γ, (3.49) and (3.42), have the time constant t_1 in the denominator, which explains the change.

The time constants t_2 and t_γ are changed insignificantly with temperature. They both contain γ_1 as a factor, (3.39) and (3.40). The expression for γ_1 , (3.28), contains a factor $(dv_{sat}/dT)/v_{sat}$ shown in Figure 4.2. Its variation with temperature is small.

The solutions $u(t)$ and $T(t)$ were calculated in the previous section for the reference case (at 20°C). Corresponding results for the reference case at 5°C are shown in Figure 4.12 and Figure 4.13.

Figure 4.12 shows the second solution given by (3.38). The shaded, upper line shows the isothermal solution from Section 3.1. The corresponding Figure 4.6 at 20°C has a substantially faster development. The excess temperature is also substantially lower at 5°C, since it is driven by the moisture flow. This is seen in Eq. (3.49) of the excess temperature where the step in the moisture content is in the numerator and the time constants are in the denominator.

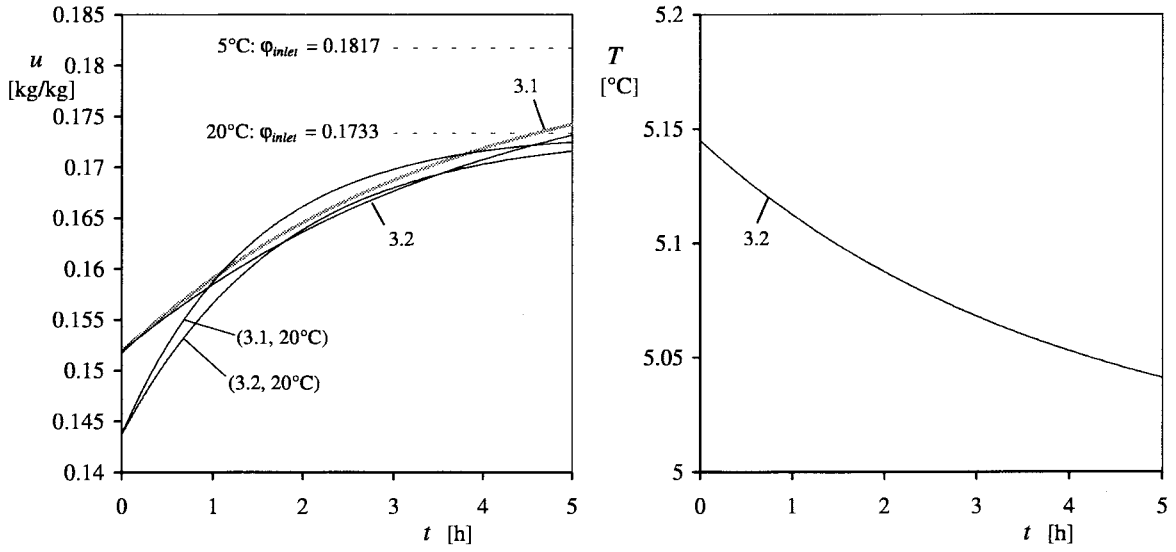

Figure 4.12 The moisture content, u(t) (left figure) and the temperature T(t) (right figure) for the reference case altered to 5°C, using the second solution from Section 3.2. The shaded line is the first, isothermal solution from Section 3.1. The corresponding lines at 20° C from Figure 4.6 are thin.

The step response basically takes place with an exponential decline with a time constant of $t_1 + t_2$, and with the time constant of t_1 for a response where the latent heat is ignored. This means that the relative importance from the latent heat is less at lower temperature where t_1 is relatively larger.

The three solutions from Sections 3.1, 3.2 and 3.3 are shown in Figure 4.13. The corresponding curves for the reference case at 20°C are given in Figure 4.9.

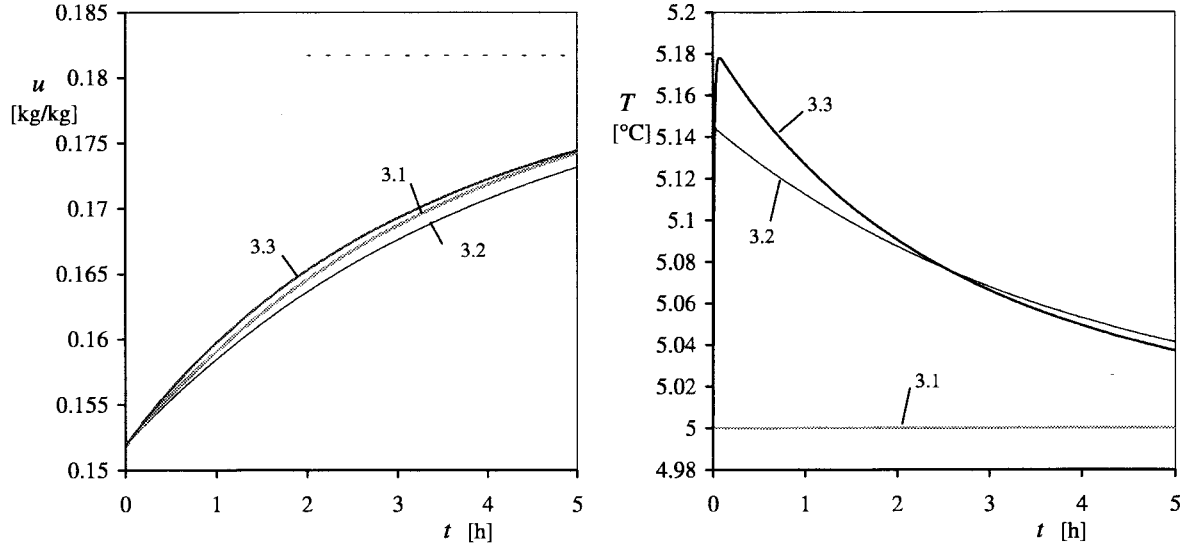

Figure 4.13 The moisture content u(t) (left) and the temperature T(t) (right) for the three solutions of Sections 3.1 – 3.3.

The influence from the temperature is illustrated further in the parameter study in Section 4.4.1 for a wider interval of temperature.

4.3.2 Smaller step in relative humidity

Instead of the step from $\varphi(0) = 0.75$ to $\varphi_{inlet} = 0.85$ in the reference case, a smaller step from $\varphi(0) = 0.83$ to $\varphi_{inlet} = 0.85$ is calculated.

In the analytical solution, time constants t_1 and t_2 are not changing with the step change since they depend on $du/d\varphi$, v_{sat} and φ_{inlet}, which remain the same. The primary and auxiliary data only have the following changes:

$\varphi(0) = 0.83$ $u(0) = 0.1662$ kg/kg

Time constant t_γ is proportional to the step size, Eq. (3.40):

$$t_\gamma = \gamma_1 \cdot (u_{inlet} - u(0)) = 4032 \cdot (0.1733 - 0.1662) = 29 \text{ [s]}$$

The constant γ_1 is not changing with the step size, Eq. (3.28).

Table 4.2 *Time constants for a step response for a small step from $\varphi(0) = 0.83$ to $\varphi_{inlet} = 0.85$ in reference case (4.6), 20°C.*

	small step	ref. case
	83% -> 85%	75% -> 85%
t_1 [s]	5077	5077
t_2 [s]	1288	1288
γ_1	4034	4599
γ	0.0045	0.0188
t_γ [s]	29	120
t_+ [s]	6377	6377
t_- [s]	43	43
$T(0) - T_{ch}$ [°C]	0.077	0.327

In Figure 4.14 the linearized solution from Section 3.4 is compared with the general solution from Section 3.3. For this small step, the two solutions of $u(t)$ are virtually identical. There is a very small difference for the temperature around the temperature peak.

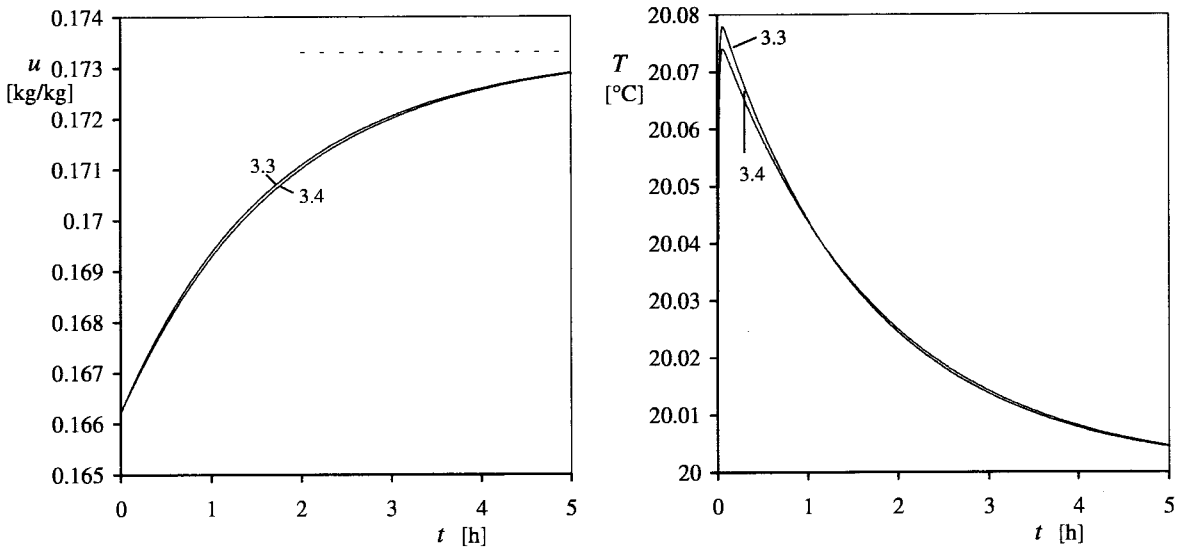

Figure 4.14 The moisture content u(t) (left figure) and the temperature T(t) (right figure) for the linearized solution from Section 3.4. The upper lines are the general solution from Section 3.3 (virtually the same). Small step size.

4.3.3 Step at higher relative humidity

Instead of the step from $\varphi(0) = 0.75$ to $\varphi_{inlet} = 0.85$ in the reference case, a step at higher relative humidity but with the same magnitude, (in RH), is tested. The step is from $\varphi(0) = 0.85$ to $\varphi_{inlet} = 0.95$. The heat of sorption is changed insignificantly at this high moisture level. The primary data of reference case (4.6) are valid except for:

$\varphi_{inlet} = 0.95$ $\varphi(0) = 0.85$

The auxillary data have the following changes:

$$\frac{du}{d\varphi}(0.95) = 1.062 \text{ kg/kg} \qquad u(0) = 0.1733 \text{ kg/kg} \quad u_{inlet} = 0.2331 \text{ kg/kg}$$

The moisture capacity, $du/d\varphi$, is substantially larger at 95% . The expressions for both t_1 and t_2 contains the moisture capacity as a factor.

$$t_\gamma = \gamma_1 \cdot (u_{inlet} - u(0)) = 3578\ (0.2331 - 0.1733) = 214 \text{ [s]}$$

Table 4.3 Time constants for a step response at higher humidity from $\varphi(0) = 0.85$ to $\varphi_{inlet} = 0.95$ in reference case (4.6), 20°C.

	high RH-level	ref. case
	85% -> 95%	75% -> 85%
t_1 [s]	14350	5077
t_2 [s]	3980	1288
γ_1 [s·kg/kg]	3944	4599
γ	0.0129	0.0188
t_γ [s]	236	120
t_+ [s]	18340	6377
t_- [s]	43	43
$T(0) - T_{ch}$ [°C]	0.223	0.327

In Figure 4.15 the differences between the responses at higher relative humidity compared to the reference case are shown. We see that initially there is the same sorption rate resulting in the same excess temperature. Later the responses are slower due to the higher moisture capacity at the higher humidity level.

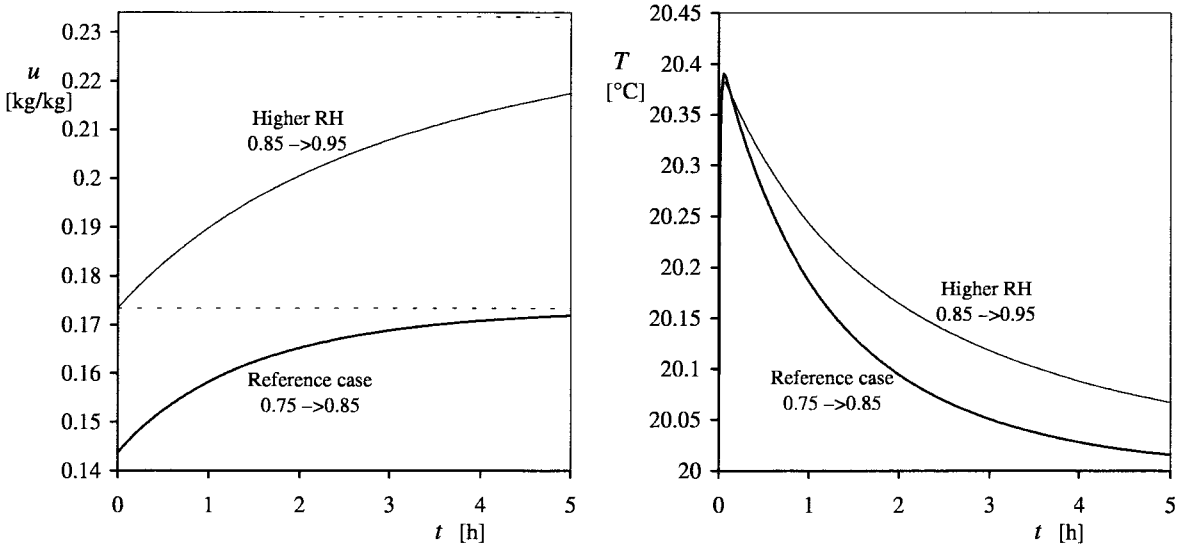

Figure 4.15 The moisture content u(t) (left figure) and the temperature T(t) (right figure) at higher relative humidity using the general solution from Section 3.3. The reference case is included for comparison.

The influence of relative humidity is illustrated further in Section 4.4.2, where the relative humidity is varied in a wider range. Also an investigation of a combination of the levels of relative humidity and temperature is shown.

4.3.4 Variations of the resistance of diffusion

The uncertainties of the moisture resistance due to internal diffusion are represented by the equivalent length for the diffusion L_{eq} in the sample, Figure 3.2. In the example in this section

the resistance of diffusion is halved and doubled compared to the reference case to investigate the influence. To test the influence from the chosen fraction $L_{eq}/L = 0.8$, the fraction is given its largest possible value, 1.0 , in one case. A case with zero diffusion resistance in the material is also included. The time constants are shown in Table 4.4 below.

Table 4.4 Time constants for different moisture diffusion values in reference case (4.6).

	zero resistance	low resistance	reference case	$L_{eq} = 1 \cdot L$	high resistance
L_{eq}/D_v	0	85	170	212.5	340
t_1 [s]	3478	4278	5077	5477	6676
t_2 [s]	1288	1288	1288	1288	1288
γ	0.0251	0.0215	0.0188	0.0177	0.0150
t_γ [s]	120	120	120	120	120
t_+ [s]	4781	5579	6377	6776	7974
t_- [s]	39	44	43	44	45
$T(0)$-T_{ch} [°C]	0.439	0.375	0.327	0.307	0.260

The contribution from the resistance of diffusion, L_{eq}/D_v , to the total moisture resistance, $1/\beta_{vtot}$, in Eq. (3.8) is less than half for the reference case. The variation of the internal diffusion does not have a large influence in the examples. We have the important conclusion that the response time scales are not influenced significantly by this somewhat uncertain factor.

4.3.5 Supply air flow

The flow rate of air into the chamber is limited. This makes the step in the air inside the chamber less steep. To test the influence, the air flow is doubled and halved. The obtained time constants are shown in Table 4.5. A case where the step in the chamber is thought to take place instantaneously is also included.

Table 4.5 Time constants for different amounts of supply air in reference case (4.6).

	instant. step	high air flow	ref. case	low air flow
$\dot{V}_{air}$ [m^3/s]	∞	$0.132 \cdot 10^{-3}$	$0.066 \cdot 10^{-3}$	$0.033 \cdot 10^{-3}$
t_1 [s]	2540	3809	5077	7614
t_2 [s]	1288	1288	1288	1288
γ	0.0312	0.0235	0.0188	0.0134
t_γ [s]	120	120	120	120
t_+ [s]	3847	5111	6377	8911
t_- [s]	36	40	43	46
$T(0) - T_{ch}$ [°C]	0.551	0.410	0.327	0.233

The effect of the restricted air flow influences the moisture flow through a term in the total moisture resistance, $1/\beta_{vtot}$, in Eq. (3.8). It influences β_{vtot} in the same way as the diffusion resistance in the material. The contribution to the total moisture resistance in the reference

case is a little larger than that from the resistance from internal diffusion and hence a variation in supply airflow has a little more influence than a variation of the internal diffusion parameters.

The measurement of the supply air flow was rather accurate and the uncertainty of this term in Eq. (3.8) is relatively small.

4.3.6 Convective heat transfer coefficient

A change of the convective heat transfer coefficient α_c is more complicated than the effect from variations of the resistance of diffusion and the effect of variations in air supply, which both influence through the total moisture resistance, $1/\beta_{vtot}$. An increased heat transfer coefficient primarily decreases the thermal resistance and reduces the excess temperature and thus the effects from latent heat. The heat transfer is somewhat complicated by working in parallel with the radiative heat transfer. Besides the thermal effect, an increased convective heat transfer coefficient also has a direct influence on the moisture flow by reducing the surface moisture resistance and thereby reducing the total moisture resistance.

The time constant t_3 for the thermal response is inversely proportional with α_{tot} as seen in Eq. (3.57). The time constant is included in Table 4.6 to illustrate this.

Table 4.6 Time constants for different convective heat transfer coefficient in reference case (4.6).

	low convection	reference case	high convection
α_c	6	12	24
t_1 [s]	6018	5077	4607
t_2 [s]	2062	1288	736
γ	0.0237	0.0188	0.0128
t_γ [s]	191	120	68
t_3 [s]	87	54	31
t_+ [s]	8102	6377	5347
t_- [s]	64	43	27
$T(0) - T_{ch}$ [°C]	0.414	0.327	0.221

The influence from the surface transfer coefficient is illustrated further in Section 4.4.3, where the variations in intervals of transfer coefficient and temperature are extended.

4.3.7 Effect of heat of sorption

To illustrate the influence from the moisture dependence of the heat of sorption, Eq. (4.5) the variation for the interval in the reference case is investigated. The influence on the latent heat of evaporation from the small temperature change during the step is also tested.

The moisture content for the interval in the reference case, (4.6b), is between $u(0) = 0.1436$ and $u_{inlet} = 0.1733$ [kg/kg]. The differential heat of sorption from Section 4.2.2 is at those points $0.148 \cdot 10^6$ and $0.097 \cdot 10^6$ [J/kg], respectively. The temperature variation during the course of the step for the reference case is between 20°C and 20.38°C. The latent heat of evaporation is $2.450 \cdot 10^6$ and $2.449 \cdot 10^6$ [J/kg] for these two temperatures, Eq. (4.3). By adding the absolute values for the differences for the two variations, the upper limit for a possible

variation on the total heat of evaporation and sorption is obtained. The variation becomes 2.0%. This corresponds to a change of t_+ of only 4.2‰.

In the calculations in this chapter, an average heat of sorption for the interval in question and the latent heat of evaporation at the equilibrium temperature are used.

4.4 Parameter variations

Larger parameter variations of temperature, humidity level and convective heat transfer coefficient are made in this section, far beyond the conditions for the measurements. Only a small step is considered and the heat capacity of the sample is ignored. The comparisons in this section is focused on the primary time constants t_1 and t_2. The time constants t_1 and t_2 are not depending on the step size. The governing time constant becomes the sum of t_1 and t_2 under these conditions. Under isothermal conditions when the latent heat is ignored, the governing time constant becomes t_1 only.

In this section the radiative heat transfer is assumed to be zero, contrary to the previous calculations for the reference case. The reason for this is to demonstrate a more pure and large latent heat effect. The conditions without radiative transfer occur for instance inside a pile of wood during convective kiln drying. Samples 1 and 2 measured in the first series of measurement in Section 5.1 consists of several layers, as shown on the picture in Figure 2.2. The radiative transfer is limited for the centre parts in those samples.

The expressions for the time constants t_1 and t_2 are repeated in Eqs. (4.7) and (4.8) below for the discussions in this section:

$$t_1 = \left(\frac{A}{\dot{V}_{air}} + \frac{1}{\beta} + \frac{L_{eq}}{D_v} \right) \cdot \frac{m}{A \cdot v_{sat}(T_{ch})} \cdot \frac{du}{d\varphi} \quad [s] \qquad (4.7)$$

$$t_2 = \frac{1}{v_{sat}(T_{ch})} \cdot \frac{dv_{sat}}{dT} \cdot \frac{h_e}{\alpha_{tot}} \cdot \frac{m}{A} \cdot \frac{du}{d\varphi} \cdot \varphi_{inlet} \quad [s] \qquad (4.8)$$

4.4.1 Variation of the temperature

The conditions are basically assumed to be the same as in the reference case, (4.6). The radiative heat transfer is however set to zero. The expressions for the time constants are evaluated at the same moisture level, φ , as the equilibrium humidity in the reference case. $\varphi = \varphi_{inlet} = 0.85$. The temperature level T is the varied parameter.

$\alpha_r = 0$

$\varphi = \varphi_{inlet} = 0.85$

$T = T_{ch} = T(0)$ is varied

The values of the two time constants as a function of temperature level are shown in Figure 4.16. We see that the time constant t_1 decreases strongly with temperature. The second time constant t_2 is rather constant (it decreases slightly with T). These results are quite clear from the formulas (4.7) and (4.8) for t_1 and t_2 . The strong variation of v_{sat} with temperature affects t_1 . The factor in the formula for t_2 , dv_{sat}/dT divided by v_{sat} , varies only slightly with temperature. A graph of the variation with temperature for this factor is shown in Figure 4.2.

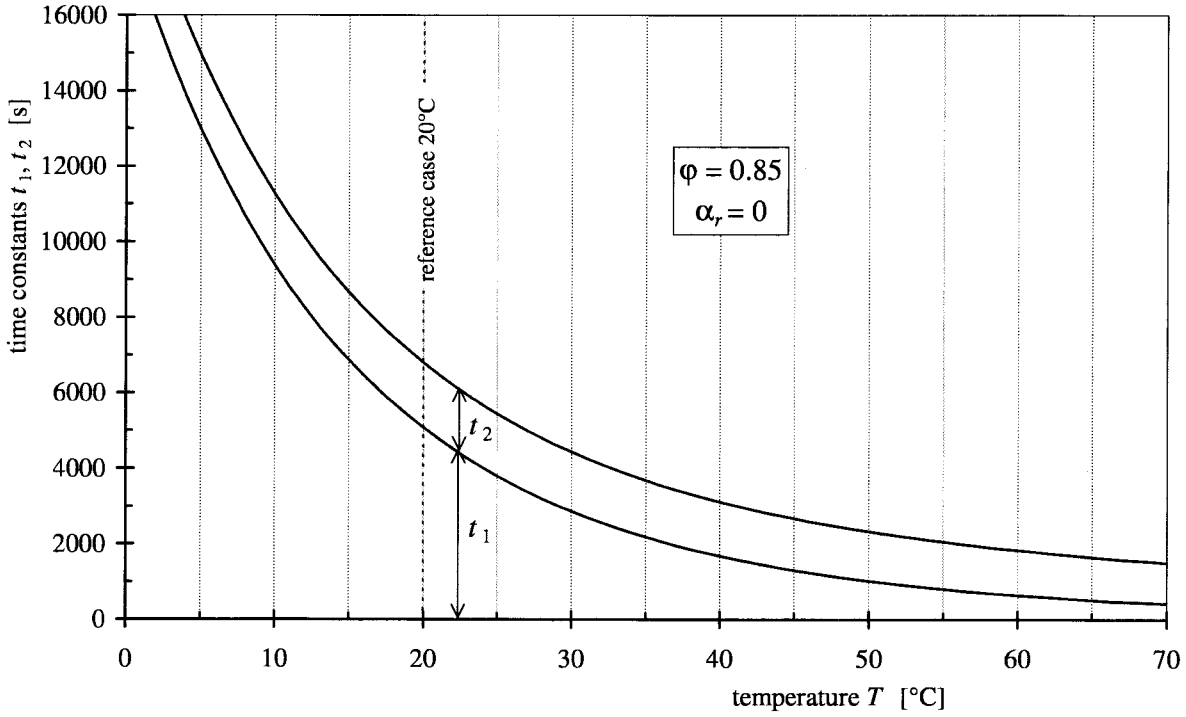

Figure 4.16 Time constants t_1 and t_2 as a function of temperature for the reference case (with the exception $\alpha_r = 0$).

4.4.2 Variation of the relative humidity

The conditions are basically the same as in the reference case, (4.6) with the exception that the radiative heat transfer is set to zero. The expressions for the time constants are evaluated at the same temperature level, $T = T_{ch} = T(0) = 20°C$, as in the reference case. The humidity level, $\varphi = \varphi_{inlet}$ is the varied parameter.

$\alpha_r = 0$

$\varphi = \varphi_{inlet}$ is varied

$T = T_{ch} = T(0) = 20°C$

The variation with relative humidity level for the two time constants is shown in Figure 4.17. The variation of t_1 is a direct reflection of the moisture capacity variation, $du/d\varphi$, in the equation for t_1 , (4.7). In the equation for t_2 , (4.8), φ is a factor. This explains the growing value of t_2 with relative humidity.

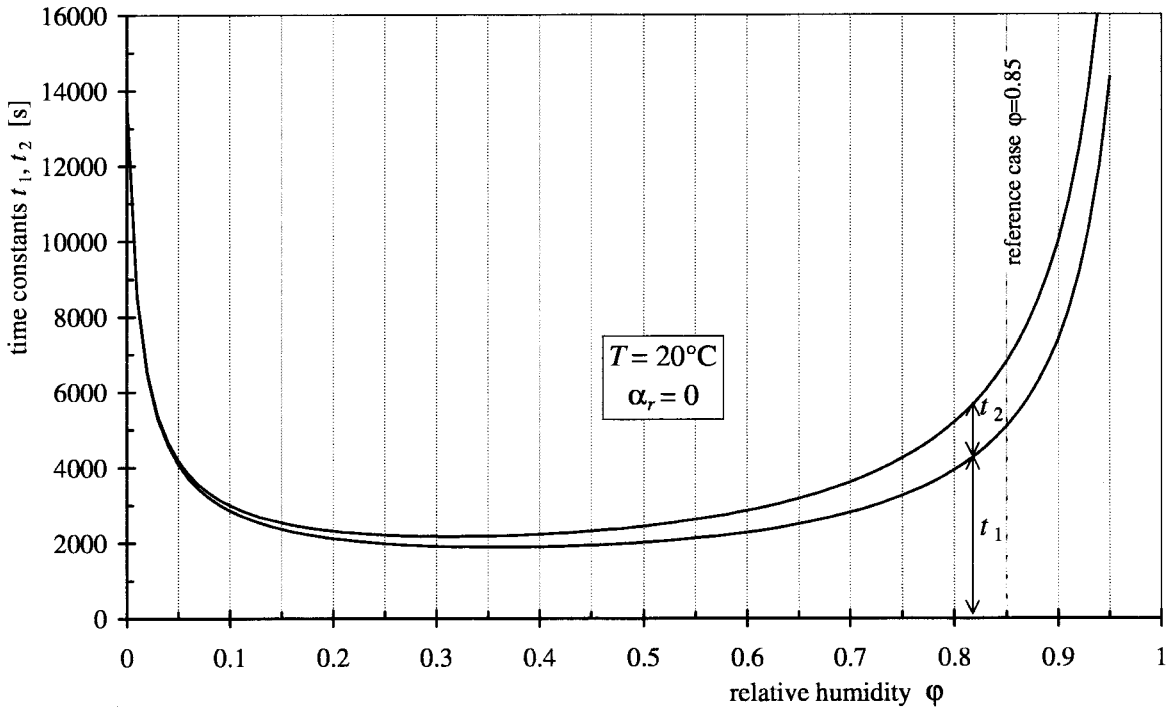

Figure 4.17 Time constants t_1 and t_2 as a function of the relative humidity level for the reference case (with the exception $\alpha_r = 0$).

To further illustrate the relative importance of including latent heat in calculations of a moisture change, the ratio between ($t_1 + t_2$) and t_1 is formed. This ratio is thus the relation of the response time scale where the latent heat is included compared to when it is ignored. The result is shown in Figure 4.18 for the combined variation of temperature and relative humidity levels.

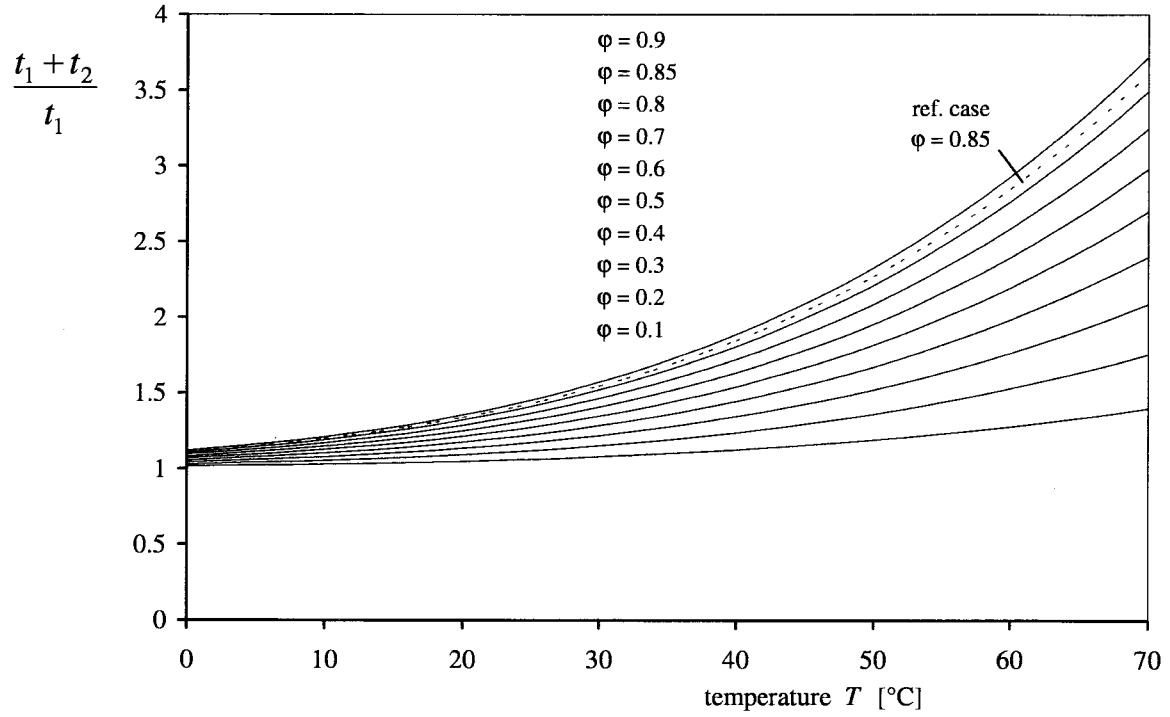

Figure 4.18 Ratio between the time constants when the influence from latent heat is included and when it is ignored, as a function of temperature and relative humidity level for the reference case (with the exception $\alpha_r = 0$).

We see that the importance of latent heat increases with temperature and relative humidity. At 20°C the factor varies between 1 and 1.39 for the whole humidity interval between 0 to 100%. The relation between surface moisture resistance and total moisture resistance is constant in the reference case. That relation is varied in the next section.

4.4.3 Variation of the heat transfer coefficient

The relation between the surface moisture transfer coefficient and the convective heat transfer coefficient is obtained by Lewis' law, (3.60), where $\rho_a \cdot c_{pa} = 1200$ is selected.

$$\beta \cdot \rho_a \cdot c_{pa} = \alpha_c \quad [\mathrm{W/(m^2, K)}]$$

The constant relation between β and α_c makes it possible to have both coefficients in the same diagram in Figure 4.19, where the upper x-axis has the surface moisture transfer coefficient and the lower the convective heat transfer coefficient. The diagram is only applicable for the reference case (4.6) with the exception for the change to $\alpha_r = 0$.

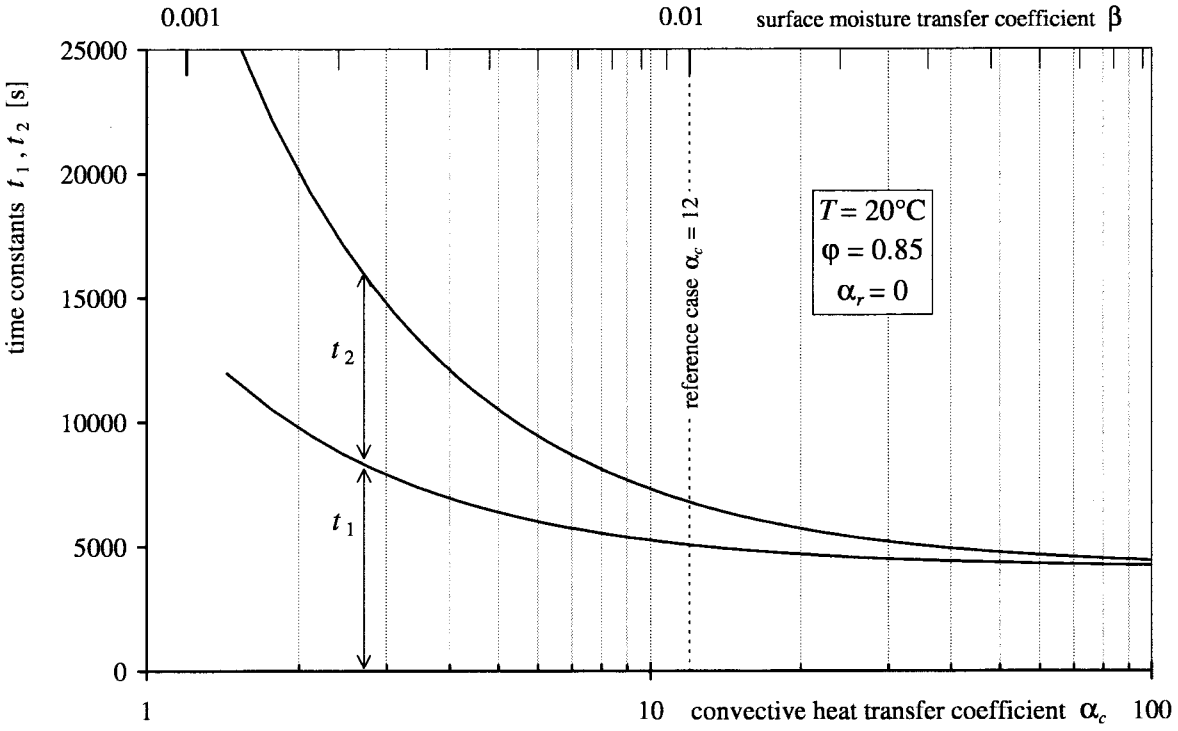

Figure 4.19 Time constants t_1 and t_2 as a function of humidity level and heat convective transfer coefficients for the reference case (with the exception $\alpha_r = 0$).

Let us now consider the effect of variation of α_c and temperature T not only for thin but also for thick wood samples. The total moisture resistance is $1/\beta_{vtot}$, Eq. (4.9).

$$\frac{1}{\beta_{vtot}} = \frac{A}{\dot{V}_{air}} + \frac{1}{\beta} + \frac{L_{eq}}{D_v} \qquad (4.9)$$

To obtain a more general picture of the influence from convection, a dimensionless convection related parameter ξ is created to be used in Figure 4.20. If the moisture resistance at the surface, $1/\beta$, is subtracted from the total moisture resistance, the remaining moisture resistance is $A/\dot{V}_{air} + L_{eq}/D_v$ [s/m]. The parameter ξ is the ratio between this moisture resistance and the surface moisture resistance, $1/\beta$:

$$\xi = \frac{1/\beta_{vtot} - 1/\beta}{1/\beta} = \frac{A/\dot{V}_{air} + L_{eq}/D_v}{1/\beta} \qquad (4.10a)$$

This fraction in moisture resistances can be expressed in α_c through Lewis' law:

$$\xi = \frac{\alpha_c}{1200} \cdot \left(\frac{A}{\dot{V}_{air}} + \frac{L_{eq}}{D_v} \right) \qquad (4.10b)$$

The dimensionless parameter ξ gets very small for the combination of small convection and thin wood, and very large for high agitation and thick wood. It could thus vary in a wide range under different conditions. The reference case with high convection and thin sample thickness has a intermediate value and the parameter becomes $\xi = 4.4$. In kiln drying with low convection combined with large wood thickness a similar intermediate value could be assumed to apply.

The ratio $(t_1 + t_2)/t_1$ as a function of T and ξ is shown in Figure 4.20. We see that the combination of high T and low ξ gives a high ratio.

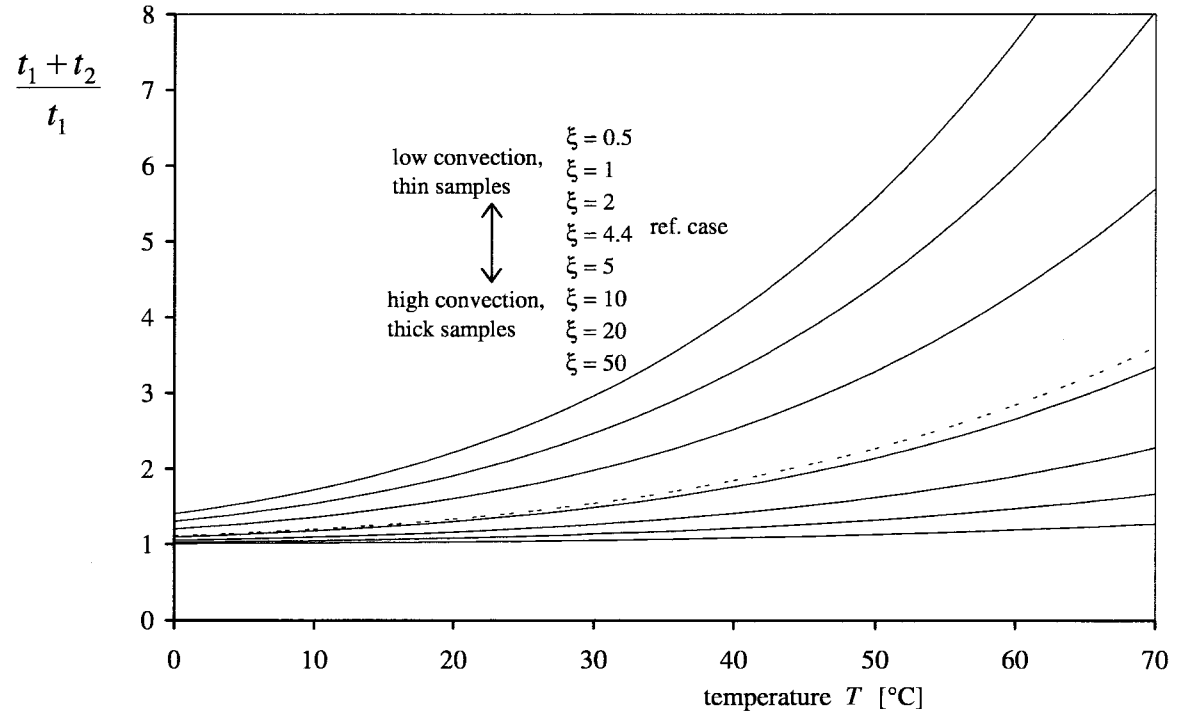

Figure 4.20 Ratio between the time constants when the influence from latent heat is included versus when it is ignored, as a function of temperature level and the convective parameter ξ from Eq. (4.10).

4.5 The experiments of Christensen in pure water vapour

The response times for a Fickian process vary strongly with the level of relative humidity due to the influence from the moisture capacity and the effect of latent heat. In this section, simulations with the complete set of equations from Section 3.3 are made for a selection of Christensen's measurements in pure water vapour. The objective is to be able to, with more certainty, identify responses that exhibit a non-Fickian behaviour.

4.5.1 Different step sizes starting from a dry sample

In the experiments in pure water vapour made by Christensen and co-authors, some of the time scales of the step responses are very short. In other instances, when non-Fickian effects are prominent, the time scales are remarkably extended. One occasion with short time-scales is when a step starts from a dry sample. The time-lag emanating from non-Fickian behaviour seems to be very small for this case. This is the reason why these tests are selected to be used for fitting for a rough moisture resistance. It is then examined in Section 4.5.2 how consistent this fitted moisture resistance is with another measurement in pure water vapour.

The development of the moisture uptake from steps starting with a dry sample with a wide range of step amplitudes is tabulated in Christensen (1959), expressed in fractions of moisture

change. The step responses are shown in diagrams in Figure 4.21 and Figure 4.22. The samples, made of klinki-pine, were cut in 1 mm thick slices in the grain direction. The temperature was 25°C in this experiment.

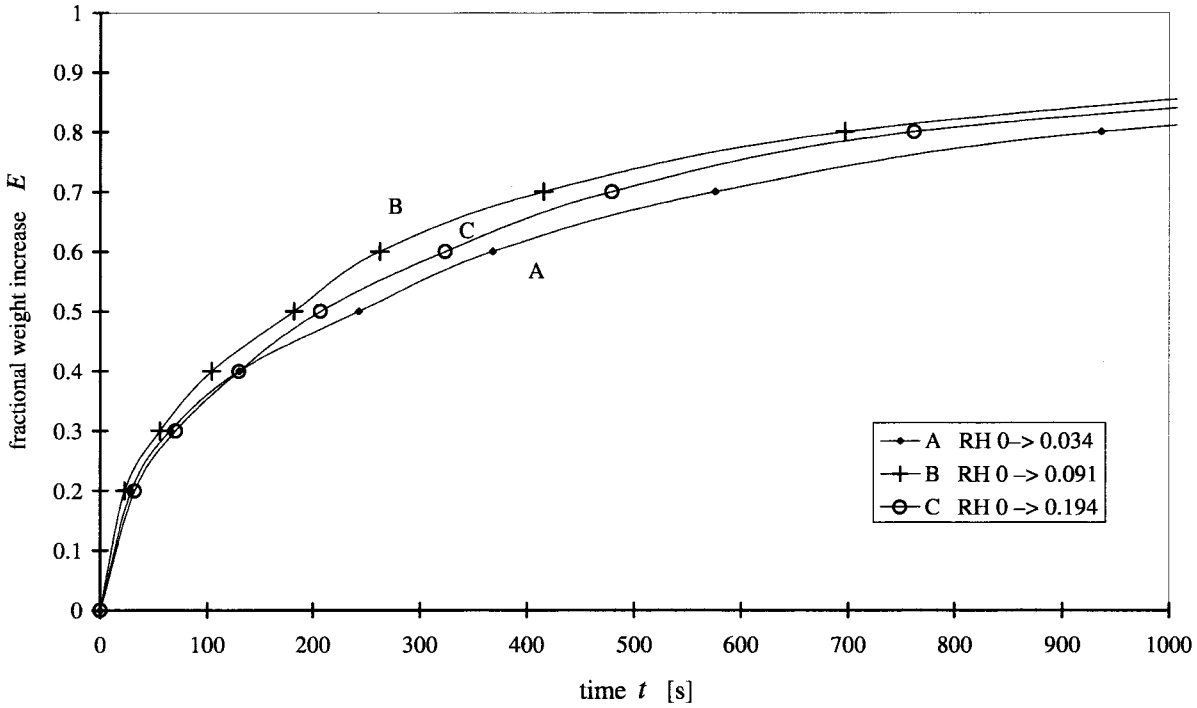

Figure 4.21 Step responses for 1 mm samples in pure water vapour, starting from a dry sample. From Christensen (1959). Steps A to C with increasing amplitudes.

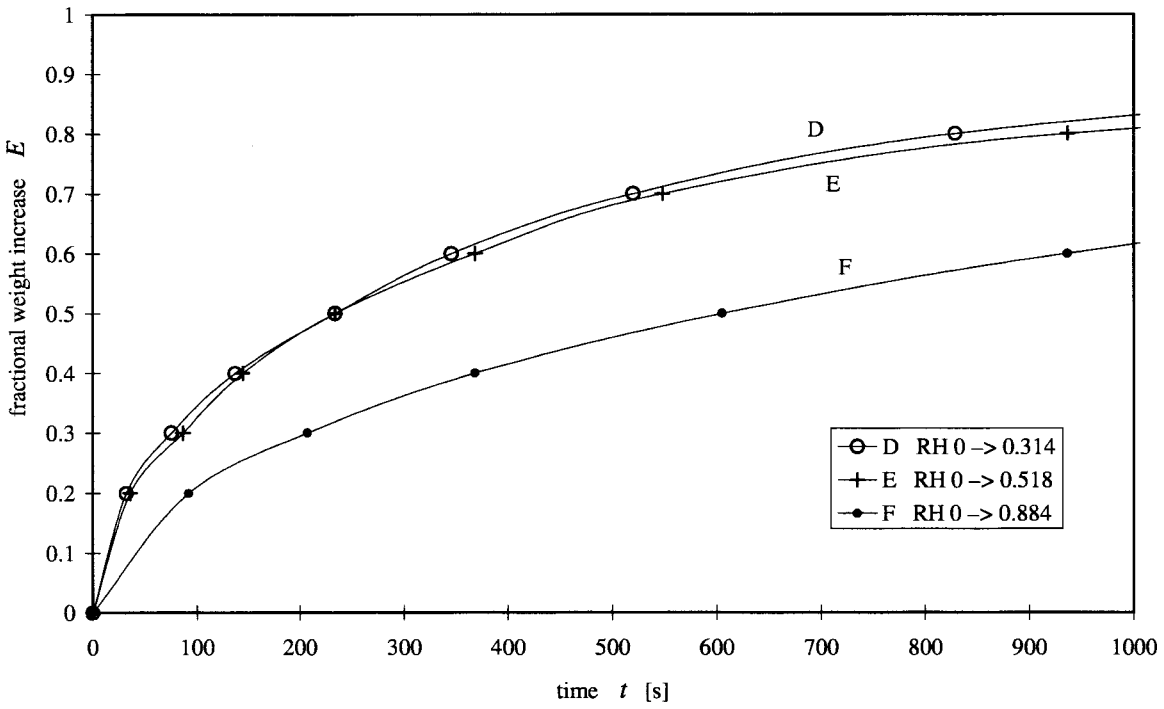

Figure 4.22 Step responses for 1 mm samples in pure water vapour, starting from a dry sample. From Christensen (1959). Steps D to F with increasing amplitudes.

A simulation for the six steps with the general solution from Section 3.3 is shown in Figure 4.23. The transfer coefficients β_{vtot} and α_{tot} are critical for the calculation results. The moisture transfer coefficient is particularly uncertain, since Lewis' law is not applicable in pure water vapour. This variable has therefore been varied. Two values of the total moisture conductance, $\beta_{vtot} = 0.01$ and $\beta_{vtot} = 0.006$ are used in the simulations. In Section 3.5.3 the value of the convective heat transfer coefficient α_c in pure water vapour is discussed in detail. The values of α_c are chosen according to the relations given there. In Table 3.2 some examples of α_c are shown. The used radiative heat transfer coefficient α_r is given by (3.61) (the used emissivity is $\varepsilon = 0.82$).

We see that there is a large discrepancy in the shape of the response curves for the first steps, A and B. For the last curves D, E and F however, there is a better agreement. One explanation could be that the resistance to diffusion is lower at low relative humidity, but that is contrary to common experience for wood. If the starting point is displaced, a better agreement is obtained but only for the first steps.

One thing that differs between the first steps and the later ones is that the amount of water engaged in the first steps is much less than in the later ones. An explanation for the very fast response for the first fraction of moisture uptake for the first step could be that the step producing part of the apparatus is not ideal. Instead one small amount of water could be readily available and the rest accessible with a moisture resistance. This moisture resistance is incorporated in the fitting with the one node simulation and gives a reasonable agreement in the last steps where the small amount of water that is readily available from the apparatus is not dominating.

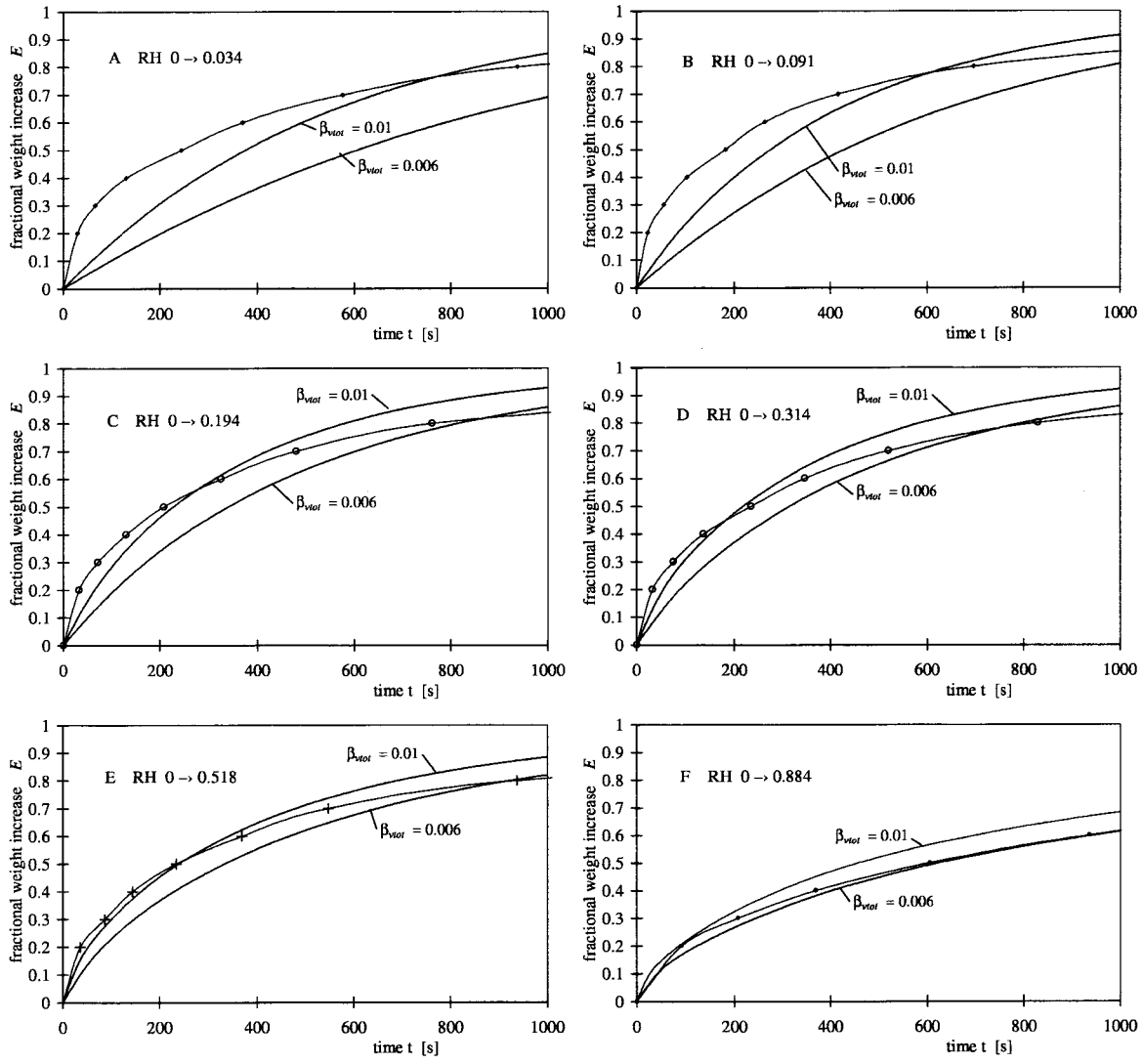

Figure 4.23 Simulated step responses for the cases A to F in Figure 4.21 and Figure 4.22.

4.5.2 Temperature rise from absorption step

In Christensen and Kelsey (1959) the temperature development at the surface of the sample is shown for a sequence of absorption steps. Klinki pine was used as in Section 4.5.1. The ambient temperature was 40°C in this test. The samples were cut parallel to the grain. The smaller of the total moisture conductances in Figure 4.23, β_{vtot} = 0.006 , is used for the simulations. The direction of transport is different from the cases in Section 4.5.1. In pure water vapour the moisture diffusion resistance could be thought to be eliminated, at least in the coarser pores. The anisotropy of the wood looses its meaning in a pure water vapour atmosphere (without trapped air). Instead the assumed moisture resistance is thought to emanate mainly from sources such as the sorption in the cell wall or in the apparatus itself. The direction of transport is then not a decisive factor.

The measured excess temperature is shown in Figure 4.24. Note that the scale of the axis is as a function of the square root of time. The temperature peak occurring at 0.12 [$h^{1/2}$] corresponds to 52 [s]. Figure 4.25 presents the corresponding temperatures calculated with the general model. The first curve has the best agreement. For the remaining curves, the similarities

are best in the initial period. For the rest of the response time a smaller excess temperature is measured. The difference increases for steps at high RH.

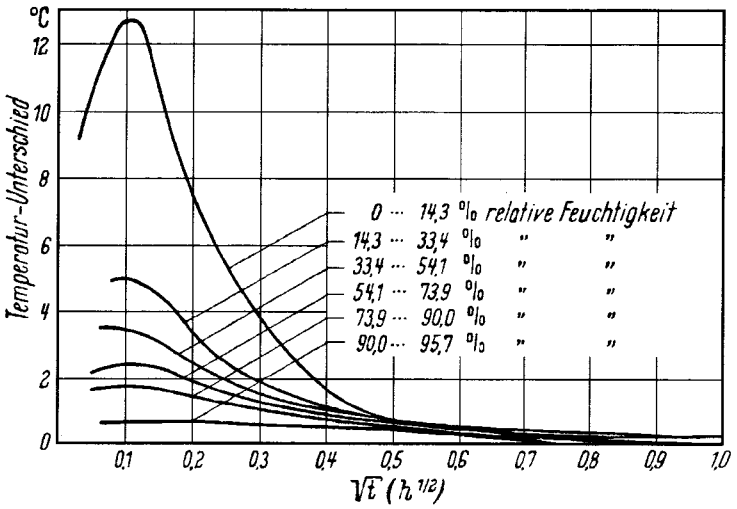

Figure 4.24 Measured excess temperature responses for 1 mm samples in pure water vapour, consecutive steps. From Christensen and Kelsey (1959). (Legends in German: relative Feuchtigkeit = RH, Temperatur-Unterschied = excess temperature.)

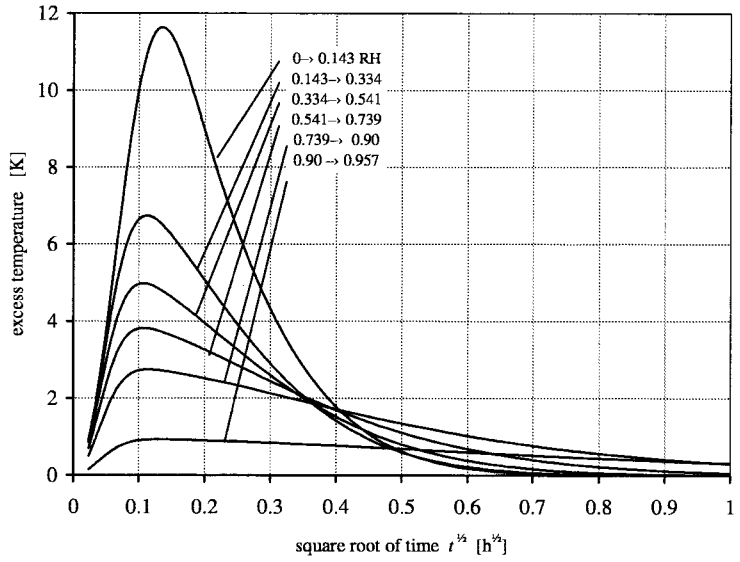

Figure 4.25 Simulated excess temperature responses for the step sequence in Figure 4.24. A total moisture transfer coefficient β_{vtot} = 0.006 is used.

In Christensen and Kelsey (1959) also the sorption responses are given for similar samples measured simultaneously with the samples for temperature. The diagram is shown in Figure 4.26.

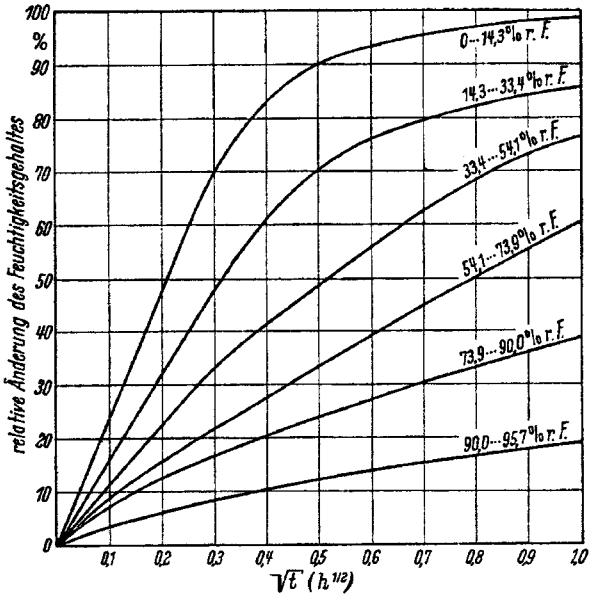

Figure 4.26 Measured sorption responses corresponding to the temperature responses in Figure 4.24. From Christensen and Kelsey (1959). (Legends in German: r. F. = RH, relative Änderung des Feuchtigkeitsgehaltes = fractional weight increase)

The simulated sorption curves are shown in Figure 4.27. We see that only the first curve, starting from 0% RH, has a reasonable agreement. The other curves have longer response times with increasing differences for each step.

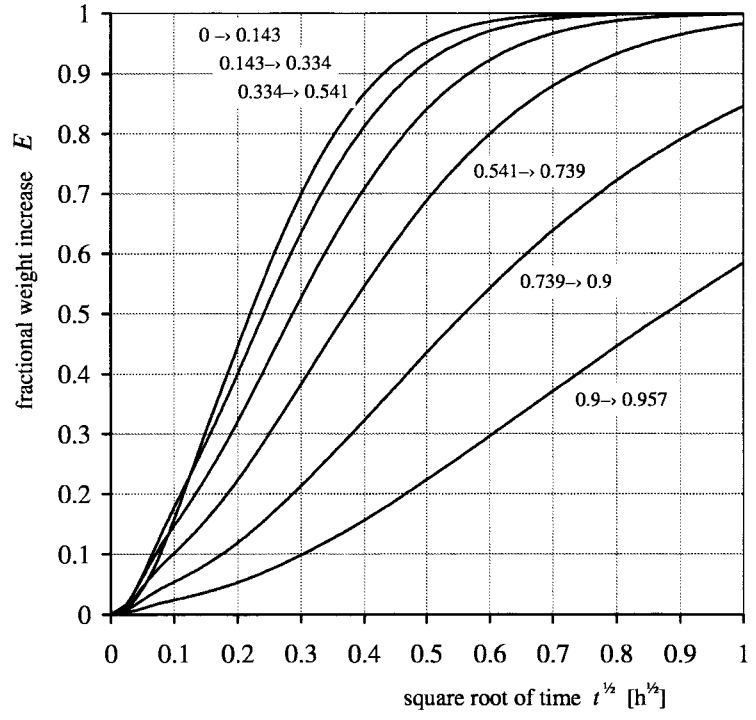

Figure 4.27 Simulated sorption responses for the step sequence in Figure 4.26. A total moisture transfer coefficient β_{vtot} = 0.006 is used.

To illustrate the influence from the latent heat on the time scales and also the influence on the shape of the response curves, a simulation is made where the latent heat is ignored (isothermal case). The curves where the latent heat is ignored are shown in Figure 4.28. We see that including the influence from the latent heat in the calculations is crucial for this case. This is explained by the fast response obtained in the pure water vapour environment and the ensuing higher relative importance from the latent heat. The latent heat is slowing down the response with increasing relative humidity as illustrated in for instance in Figure 4.18 and the time scales for the responses are increasing for each step at growing relative humidity in Figure 4.27. The time scales for the isothermal responses in Figure 4.28 are basically determined by the moisture capacity only and they are consequently shortest at mid range RH where the capacity is at its lowest.

Not only the time scale but also the shape of the response curve are different from the isothermal case. This is due to that a separate time scale for the heat response also is involved. This is also the case for the general solution for the reference case in humid air in Section 4.2.4 where the effect from the thermal response is barely noticeable and where the time constant for the thermal response is very much shorter than the moisture one.

Initially, before the excess temperature is established, the moisture uptake is the same in Figure 4.27 and in the isothermal case in Figure 4.28. Very soon the temperature rises as seen in Figure 4.25 and the responses slow down compared to the isothermal case.

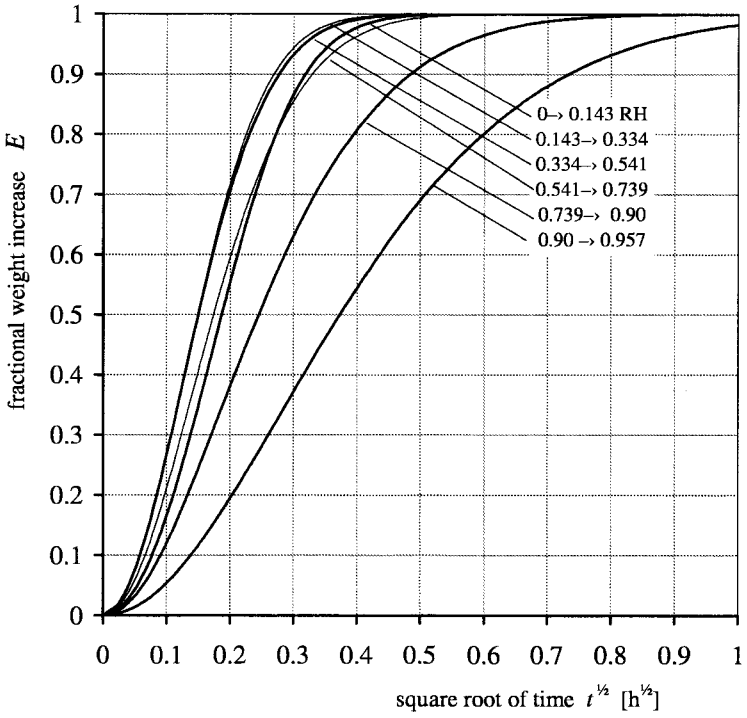

Figure 4.28 Sorption responses for the step sequence in Figure 4.27. The effects of latent heat are ignored in the simulation.

The response curves in Figure 4.28 have basically the shape of an exponential decline with the time scales depending on the moisture capacity of the present humidity interval of the step.

The time axis as a function of square root of time is somewhat deceptive for comparison at different points in time. To compare the three time scales of sorption between the measured

and simulated responses with and without latent heat, the time when half the sorption has occurred is transferred to Table 4.7.

Table 4.7 The time $t_{0.5}$ when half the sorption has taken place, (E = 0.5), in Figure 4.26 and Figure 4.27.

Step in φ	$t_{0.5}$ [h] measured	$t_{0.5}$ [h] simulated	$t_{0.5}$ [h] simulated, latent heat ignored
0 -> 0.143	0.042	0.048	0.035
0.143 -> 0.334	0.094	0.058	0.031
0.334 -> 0.541	0.28	0.083	0.022
0.541 -> 0.739	0.65	0.138	0.022
0.739 -> 0.900	~2	0.315	0.059
0.900 -> 0.957	~10	0.767	0.137

We see that the measured and simulated values of $t_{0.5}$ closely is the same for the first step but with ever larger differences for each following step. This can be compared to the reasonably good agreement for the simulations at high RH in Section 4.5.1.

The difference between the tests in the previous section and this one is the wide range of step sizes in Section 4.5.1 but also that the tests are starting from zero moisture content which seems to nullify the influence from retarded sorption. Smaller steps have normally larger portion of retarded sorption, but the measurements of steps starting from zero in Section 4.5.1 rather the opposite seems to be the case (maybe attributed to the measurement circumstances).

4.5.3 Conclusion for the simulations in pure water vapour

In pure water vapour the diffusion resistance is reduced to zero since no collisions take place with air molecules. In finer pores in a material however, the walls form a resistance when the pore size is in the same magnitude or smaller than the mean free path of the water molecules. Trapped air is also a possible hindrance. The vapour generating device is a potential source of resistance in the experiment as well.

Even if the transport resistance was reduced to zero, the slowing effect of latent heat still remains that is controlling the moisture transfer. In the example here in pure water vapour the influence from latent heat is very important.

For the steps starting from zero humidity, the effects of retarded sorption are hard to detect independently if the higher levels of RH are included in the interval or not. For smaller steps in the higher range of RH however, substantially longer time scales of sorption are measured than simulated.

5 Overview of the measurements

In this chapter, an overview of the measurements is given. The relative humidity, (RH), in the precision chamber was kept constant during a certain period, and then changed to a new value. The samples experience a sequence of step changes in relative humidities. The weight, and hence the moisture uptake, was measured continuously.

These measurements were organised in a number of series, usually starting and ending in a relatively dry state. Two samples in separate chambers were tested simultaneously. Samples of two different thickness was used. In the first series the thickness of the samples was 3 mm (Sample 1 and Sample 2). In the remaining second to sixth series, the thickness of the samples was 1.7 mm (Sample 3 and Sample 4). The wood was pine (*Pinus silvestris*).

5.1 The first series

The total time for the first series was 9 months. The sample thickness was 3 mm. The sequence of relative humidities is shown in Figure 5.1 for Sample 1 and in Figure 5.2 for Sample 2. The sequence of steps consists of continuous absorption steps from dry (~30% RH) to very moist (98% RH), followed by continuous desorption steps. In principle, the two sequences differ in the following way. There are essentially twice as many steps for Sample 1. Each (larger) step for Sample 2 corresponds to two steps for sample 1.

The temperature was constant and equal to 20°C during the whole measurement. All measurements of the first four series was at 20°C. The temperature in the last two series was mostly held constant at 5°C, but there were a few shifts between 20°C and 5°C.

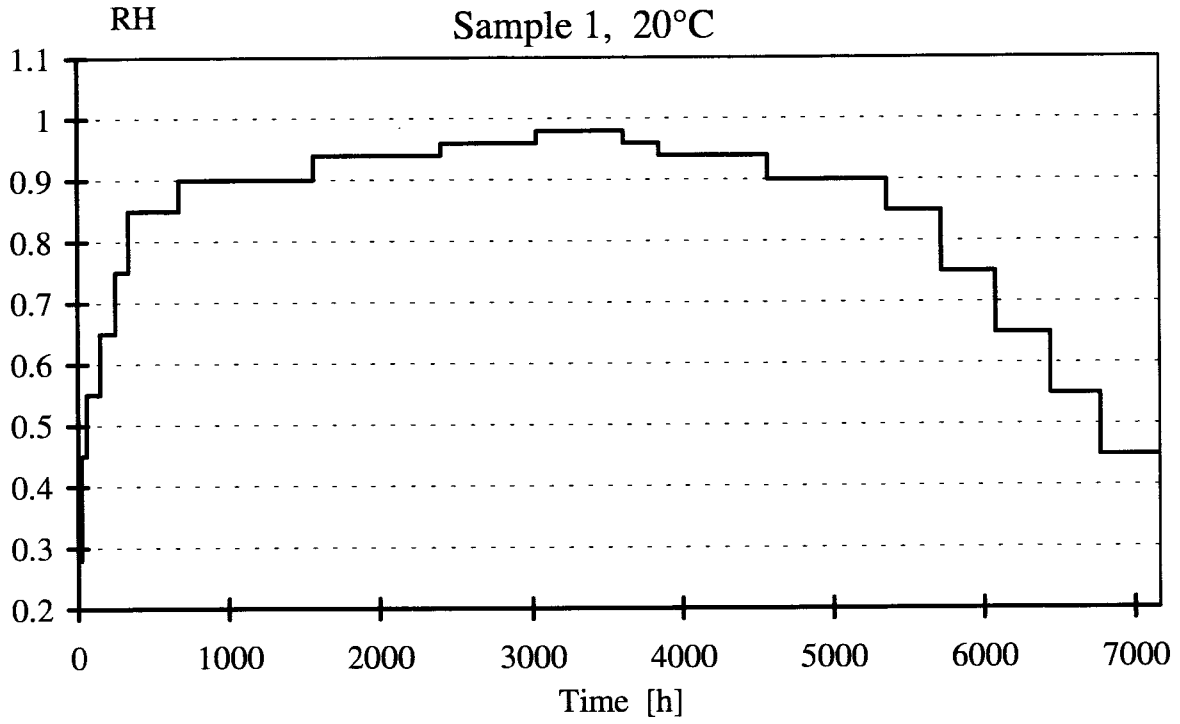

Figure 5.1 Relative humidities for the first series of measurements, Sample 1

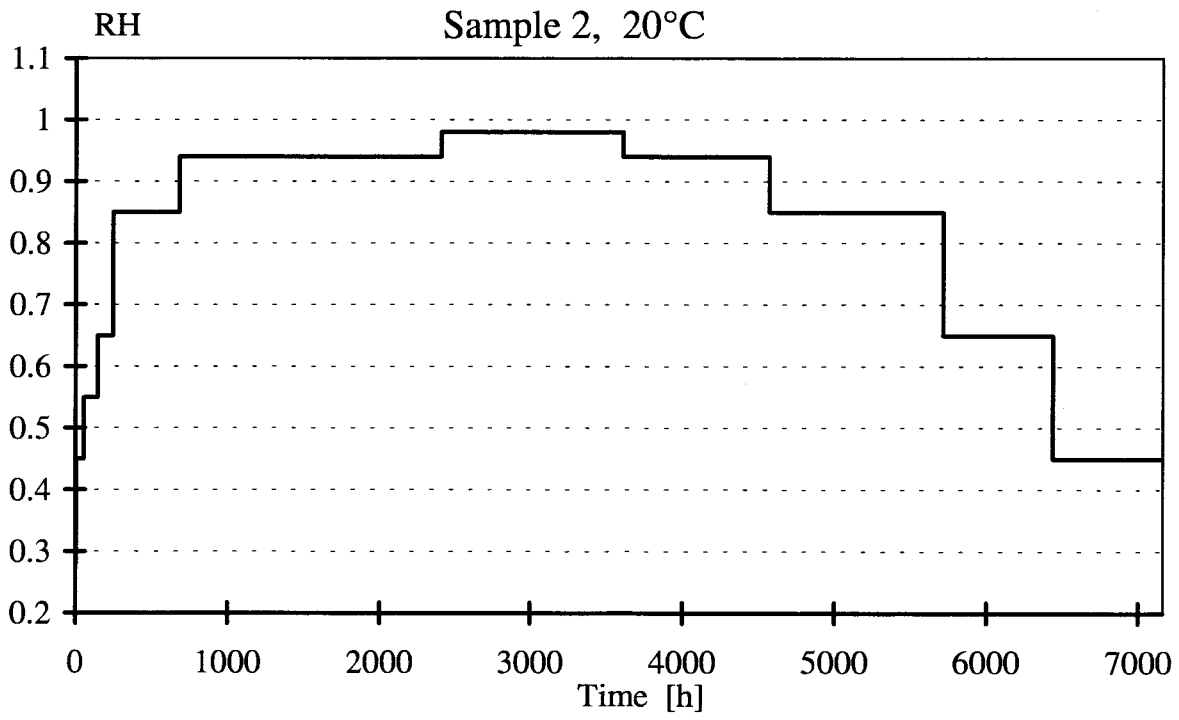

Figure 5.2 Relative humidities for the first series of measurements, Sample 2

5.2 The second series

In this series and the following ones, a thinner sample thickness of 1.7 mm was used. This facilitated the analyses of the first period after a step change. The quantity of wood was substantially less. This results in a faster step change in the air in the chamber, since the limited air supply is not affected so much by a large moisture capacity from the wood

The step sequence pattern from the first series is copied, but the total time is shortened to 2 months. The step pattern for Sample 3 in Figure 5.3 is similar to the previous steps in Figure 5.1, and the pattern for Sample 4 in Figure 5.4 is similar to the steps in Figure 5.2.

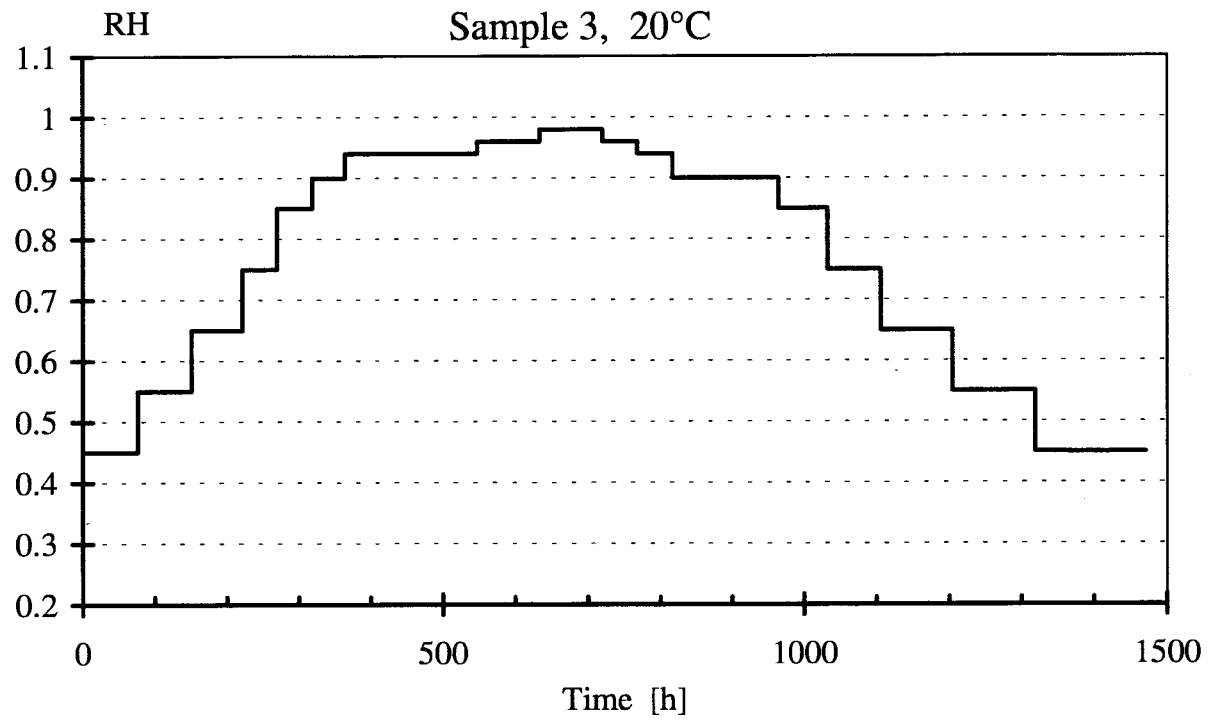

Figure 5.3 Relative humidities for the second series of measurements, Sample 3

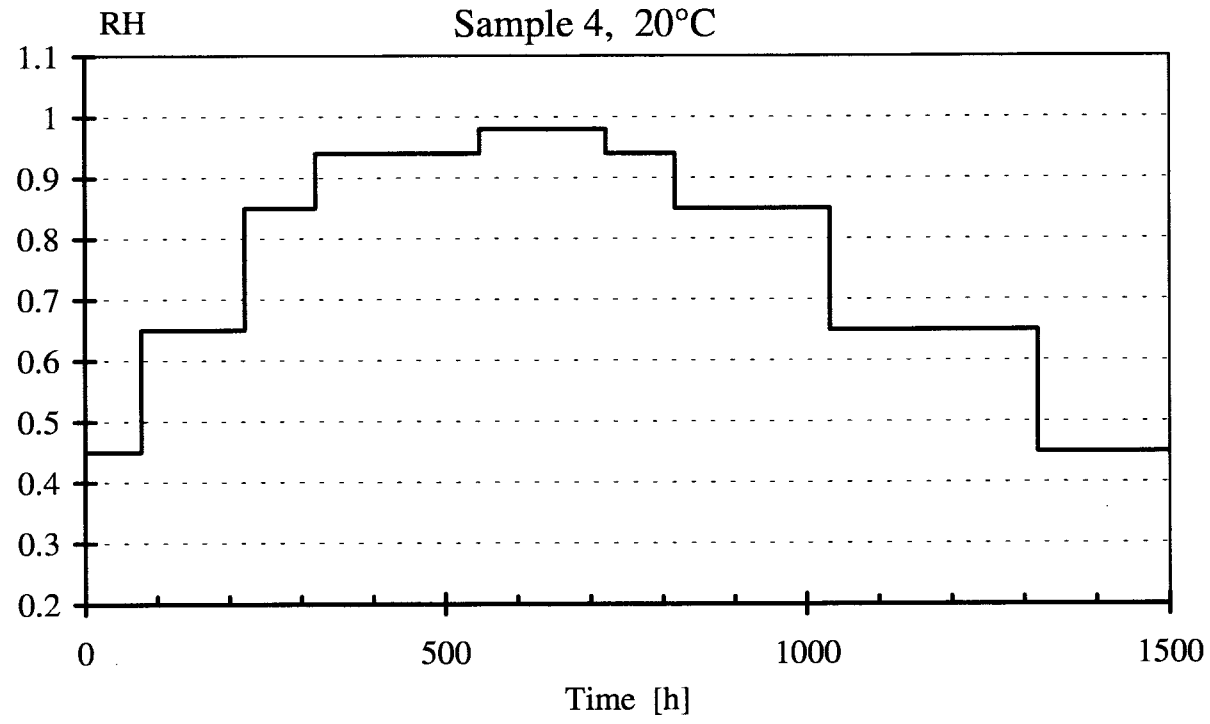

Figure 5.4 Relative humidities for the second series of measurements, Sample 4

5.3 The third series

The sequence of humidities for the third series of measurements for Sample 3 is shown in Figure 5.5. The step sequence for Sample 3 was divided further compared to Figure 5.3 in the previous series. Each step in Figure 5.3 is divided into two smaller steps in Figure 5.5. The time for each individual step was relatively short.

During the desorption step to 35% RH, substantial retarded sorption effects were found, unexpected at such a dry state. This interval was therefore prolonged to investigate this further. After the desorption and the long equilibrium time at 35% RH, the opportunity to add an absorption step without disturbing the sample was utilised.

The step sequence for Sample 4 shown in Figure 5.6 started with a step with very large amplitude to investigate the influence from the size of the step. The succeeding desorption steps were chosen to make up for such desorption intervals in the second series, where the measurement results were lost due to recording problems.

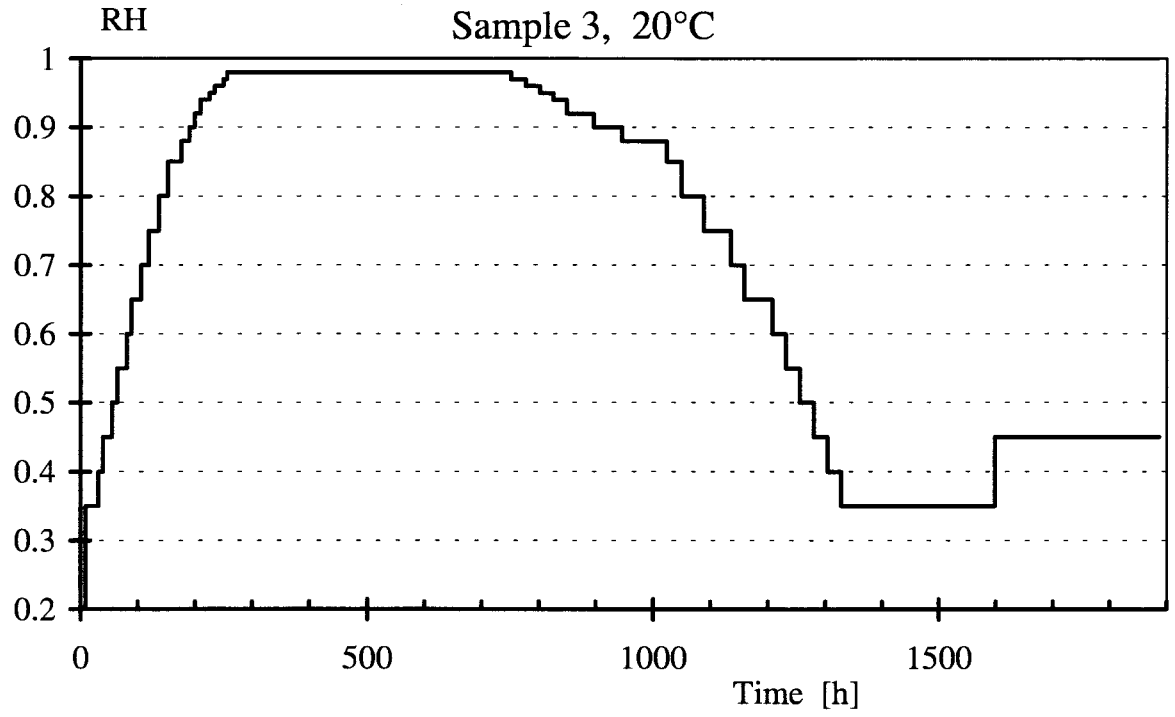

Figure 5.5 Relative humidities for the third series of measurements, Sample 3

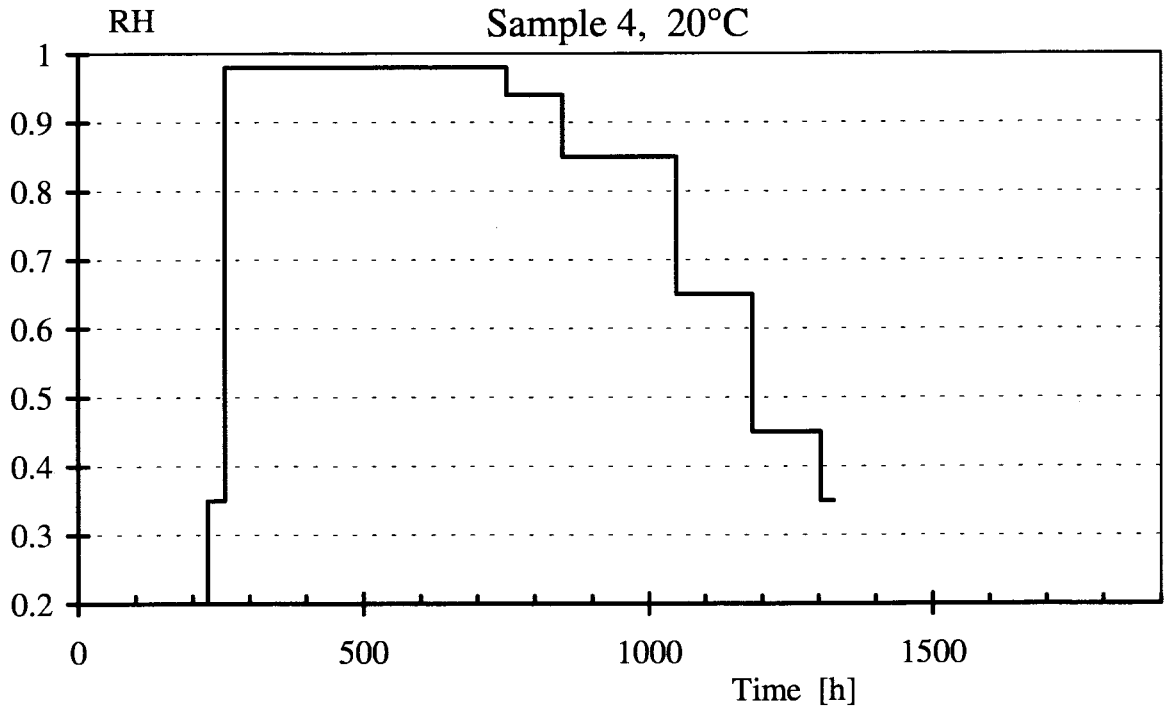

Figure 5.6 Relative humidities for the third series of measurements, Sample 4

5.4 The fourth series

In the fourth series, cyclic steps were introduced. The sequence of humidities for the fourth series of measurements is the same for Sample 3 and Sample 4. This is shown in Figure 5.7.

In this fourth series and the remaining fifth and sixth ones, the two samples have undergone (practically) the same step sequences, but in separately controlled chambers. This gives an added safety from errors, and it has in some instances been used to increase precision in the analyses by averaging the two results.

The first few cycles, at medium-range relative humidity, consisted of a daily step change. At higher RH the sorption is slower, and two days between step changes were chosen. The cycle time is 96 hours. This cycle time is used for the remaining sequences.

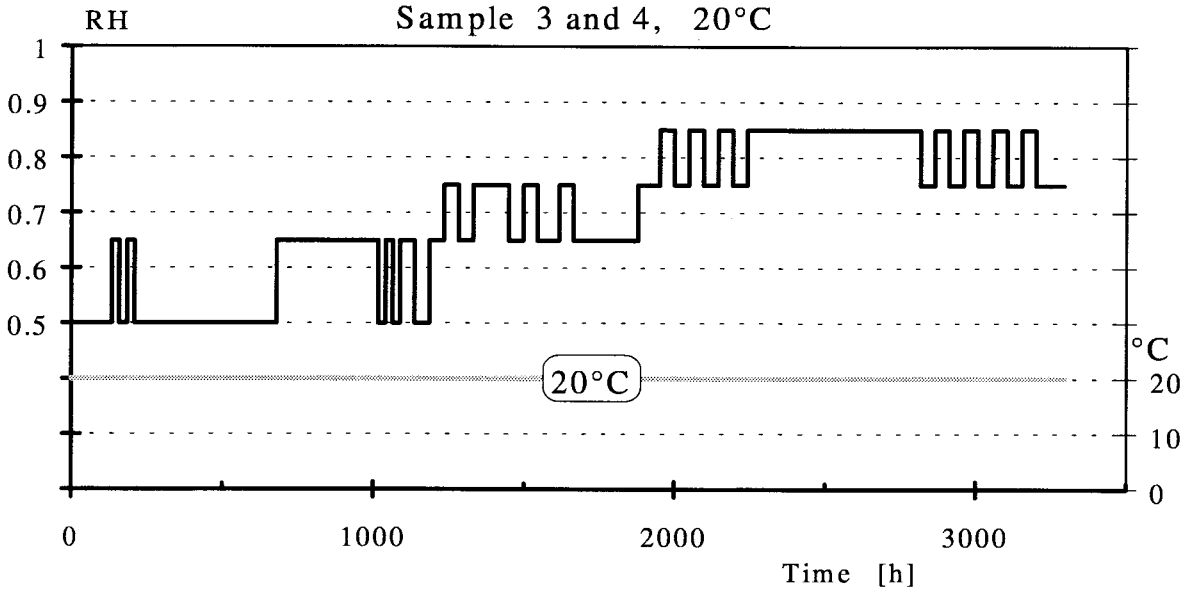

Figure 5.7 Relative humidities for the fourth series of measurements, Samples 3 and 4

5.5 The fifth series

All measurements in the preceding series were performed at 20°C. At lower temperature, larger effects from retarded sorption were expected. A lower temperature, 5°C, was therefore introduced in the fifth series. The sequence of humidities for the fifth series of measurements is shown in Figure 5.8. Cyclic steps were used, interspersed with larger single absorption steps, resulting in a high RH-level at the end of the series.

At the end, a temperature shift to 20°C was made and a few cyclic steps were repeated.

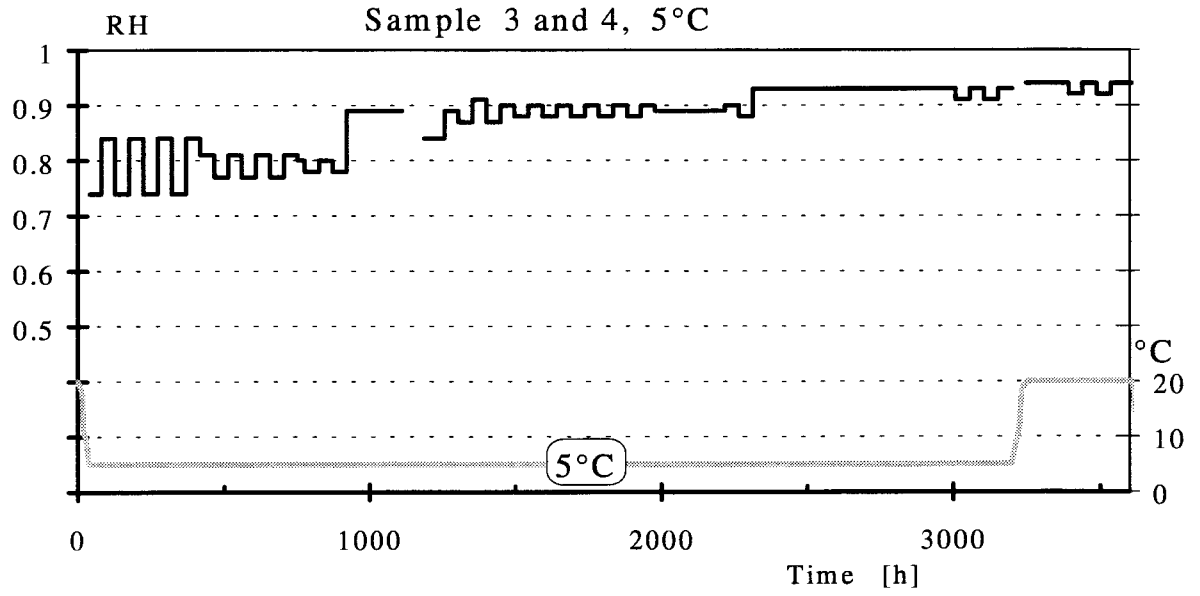

Figure 5.8 Relative humidities for the fifth series of measurements, Samples 3 and 4

5.6 The sixth series

The sequence of humidities and temperatures for the sixth series of measurements is shown in Figure 5.9. The temperature of 20°C at the end of the previous series (Figure 5.8) was shifted to 5°C at the starting point for this series. This was followed by a number of RH-cycles and a desorption step at 5°C. Next two temperature shifts between 5°C to 20°C and back were tested. During these shifts the relative humidity was kept constant at 85%. After the temperature shifts a number of RH-cycles, followed by some consecutive desorption steps, were performed at 5°C. At the end of the series, another temperature shift from 5°C to 20°C was made, but this time the RH-level during the change was adjusted in accordance to zero sorption in the samples. This gives an estimate of the temperature dependence for the equilibrium moisture sorption curve.

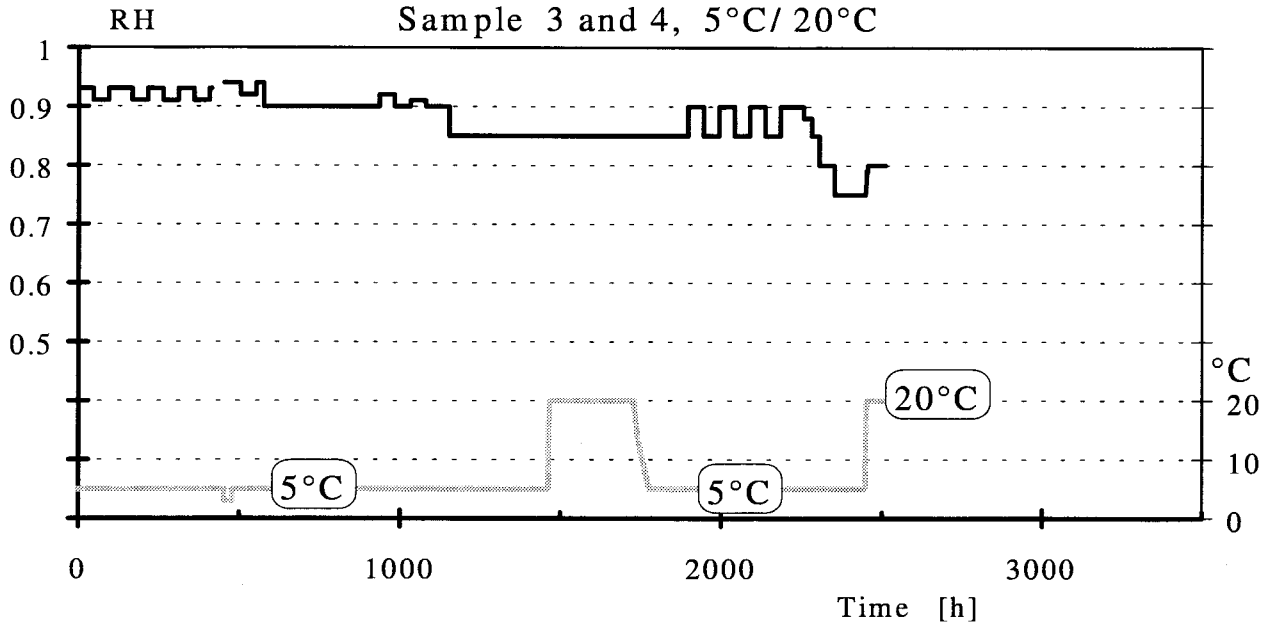

Figure 5.9 Relative humidities for the sixth series of measurements, Samples 3 and 4

6 Measured result

In this chapter the directly measured sorption for the different sequences is shown in diagrams as a function of continuous time. Using the dry weight of the samples, the weight results are converted to moisture content, u [kg_{water} / $kg_{dry\ wood}$], in the diagrams. The formula is given in Section 2.3. The sorption was recorded with one-hour interval. When dots are used on the sorption response curves, hourly values are shown. The first hours after a step change, the curves usually are steep. The individual dots representing hourly values are distinguishable in these parts. This facilitates evaluation and comparison between curves during the first hours after a step change.

During these long sequences of measurements, some failures occurred. These are reported, and curves from sequences, where a part of the measured values are missing, are still presented. The parts, where problems occurred, are indicated in the curves.

6.1 The first series

The first series of measurements was performed with Sample 1 and Sample 2. The sequences of relative humidity steps are shown in Figures 5.1 and 5.2. The wood samples are described in Section 2.3 and in Figure 2.2. The thickness of the samples was 3 mm. The temperature was 20°C.

The measurements started with the samples at room conditions with an estimated RH of around 28%. The first absorption steps to 65% RH in the sequence served as a test of the experiment procedure. Absorption was also established. These initial steps are shown separately in Section 6.1.1.

A survey of the result is shown in Figure 6.1 for sample 1 and in Figure 6.2 for sample 2. The initial steps are not included. The relative humidity during each step is shown by straight thin lines.

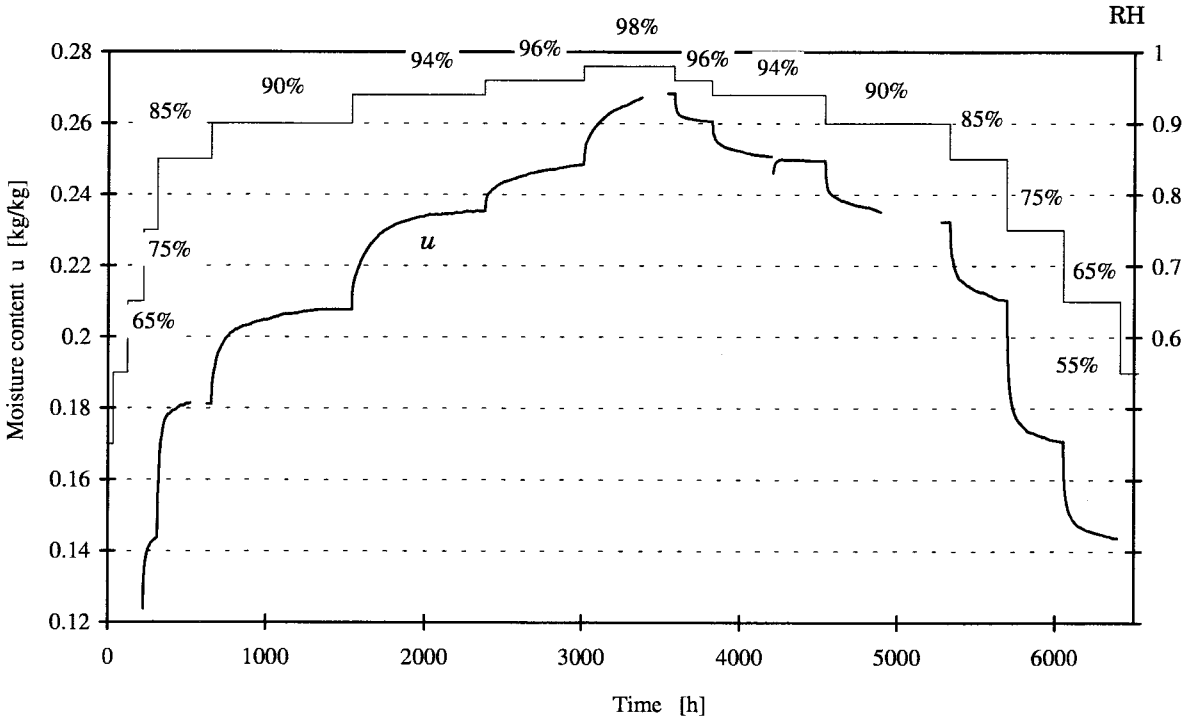

Figure 6.1 Survey of sorption response in the first series, Sample 1

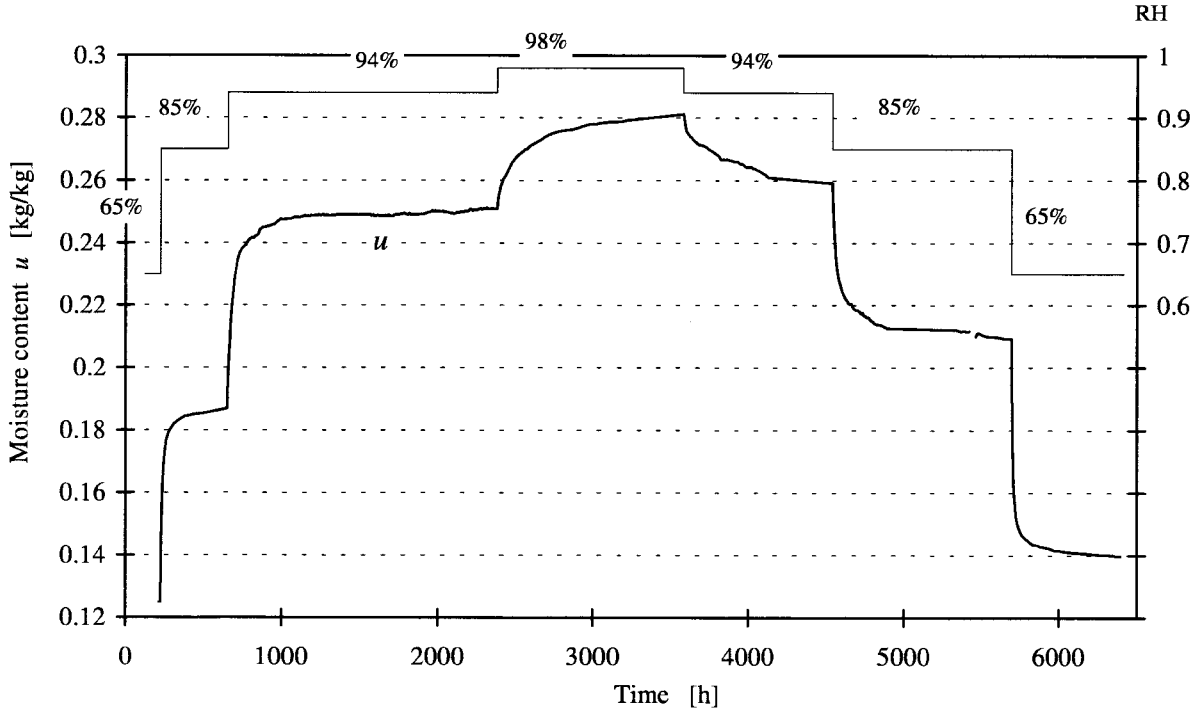

Figure 6.2 Survey of sorption response in the first series, Sample 2

6.1.1 Initial absorption steps

The samples were not dried totally prior to the tests in order to avoid drying damages of the structure of the wood. The measurements started with the samples at room conditions. The relative humidity was estimated to be around 28%. The first three absorption steps to 65% RH

in the sequence served as a test of the experimental procedure. Absorption was also established for the following steps.

During the 65% RH-step, the chamber was opened, the samples isolated and nozzles producing air agitation in the chambers were installed. The set-up is described in Section 2.5.

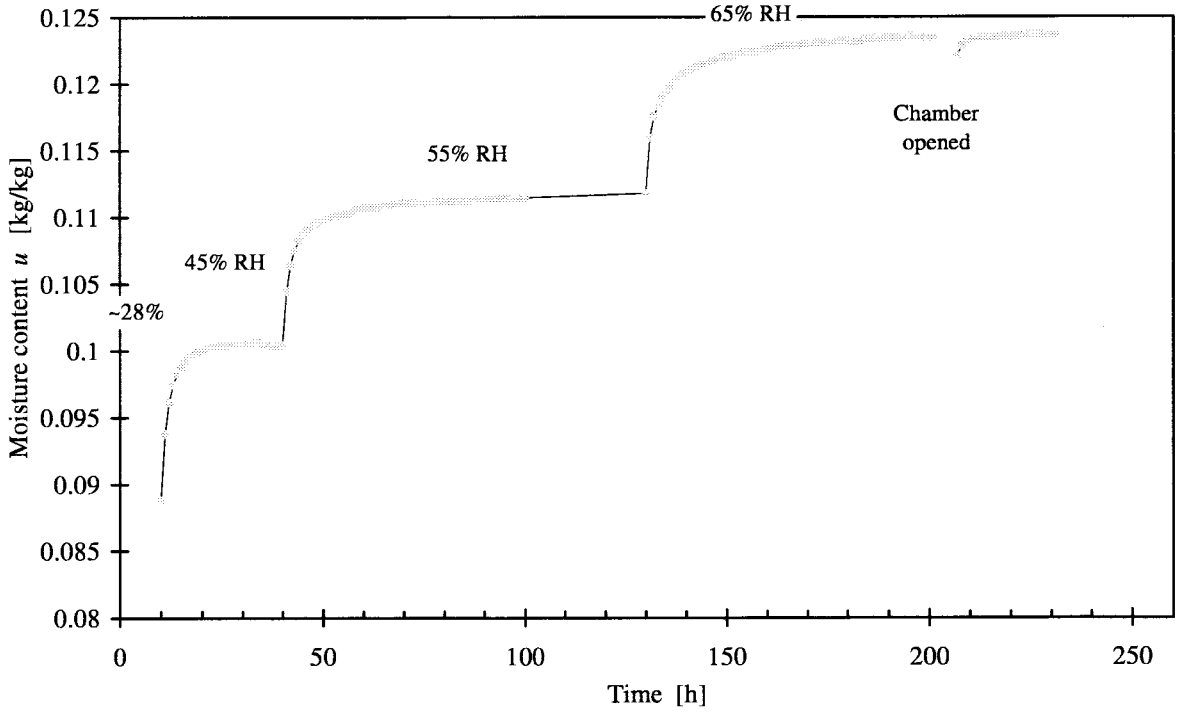

Figure 6.3 Initial steps. Sorption response, Sample 1, 28% –› 65% RH-interval.

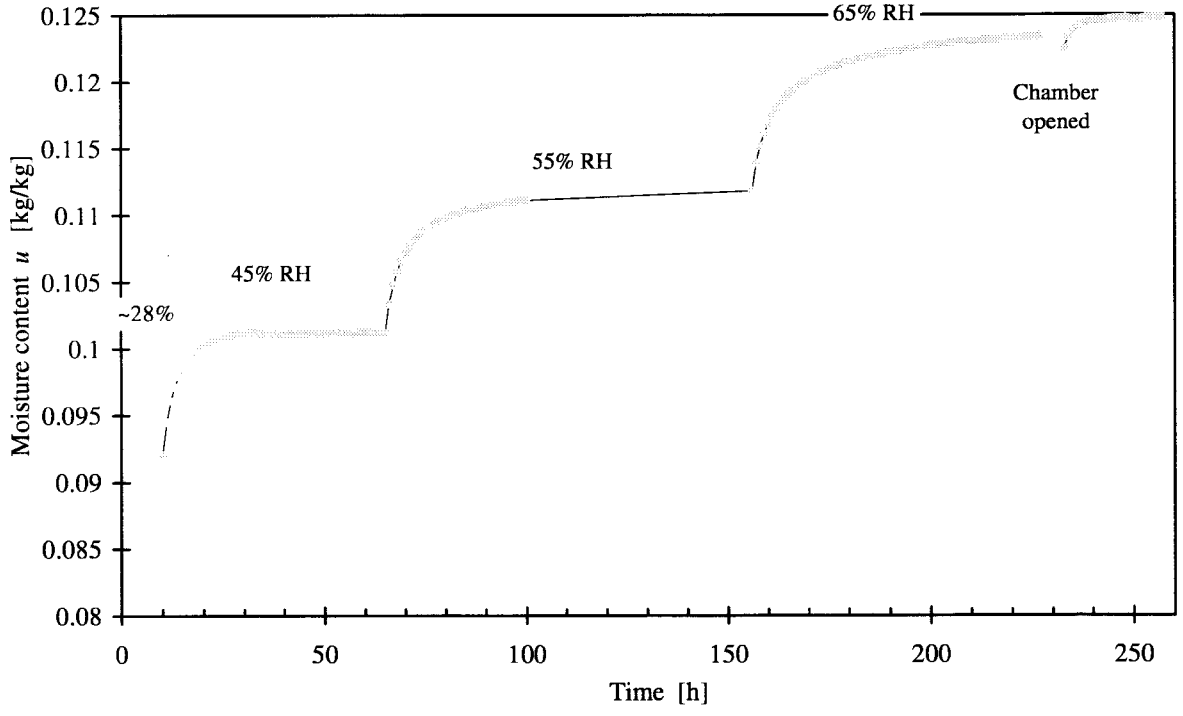

Figure 6.4 Initial steps. Sorption response, Sample 2, 28% –› 65% RH-interval.

6.1.2 Absorption steps

For the remainder of the first series, the measured sorption response is shown together for the two samples in Figure 6.5 to Figure 6.11. The measurements have taken place simultaneously in the same interval of relative humidity for the two samples. Sample 1 however, was undergoing two steps during the interval where Sample 2 only had one step. In order to make the whole curves stand out separated from one another in the diagrams, minor displacements on the time axis have been made.

The sorption responses for steps in the RH-interval from 65 to 85% are shown in Figure 6.5. The samples do not come to a distinct equilibrium. Instead a distinct retarded sorption is taking place, clearly visible for instance about 80 hours after a step. It was not possible at this stage to keep the RH-levels sufficiently constant to get a quality of measurement, allowing evaluation of the whole period.

In Figure 6.6 the absorption steps in the interval from 85% to 94% are shown. Also here several disturbances were encountered, e. g. slightly lost control of temperature in the surrounding bath. The undisturbed parts of the curves however, are possible to evaluate. The response curves show an increasing effect of retarded sorption compared with the previous curves at lower relative humidity.

In Figure 6.7 the final absorption steps in the interval from 94% to 98% are shown. The step size in relative humidity is only 2% for Sample 1. Here a division of moisture uptake in a first fast phase and a second retarded phase is especially distinguishable.

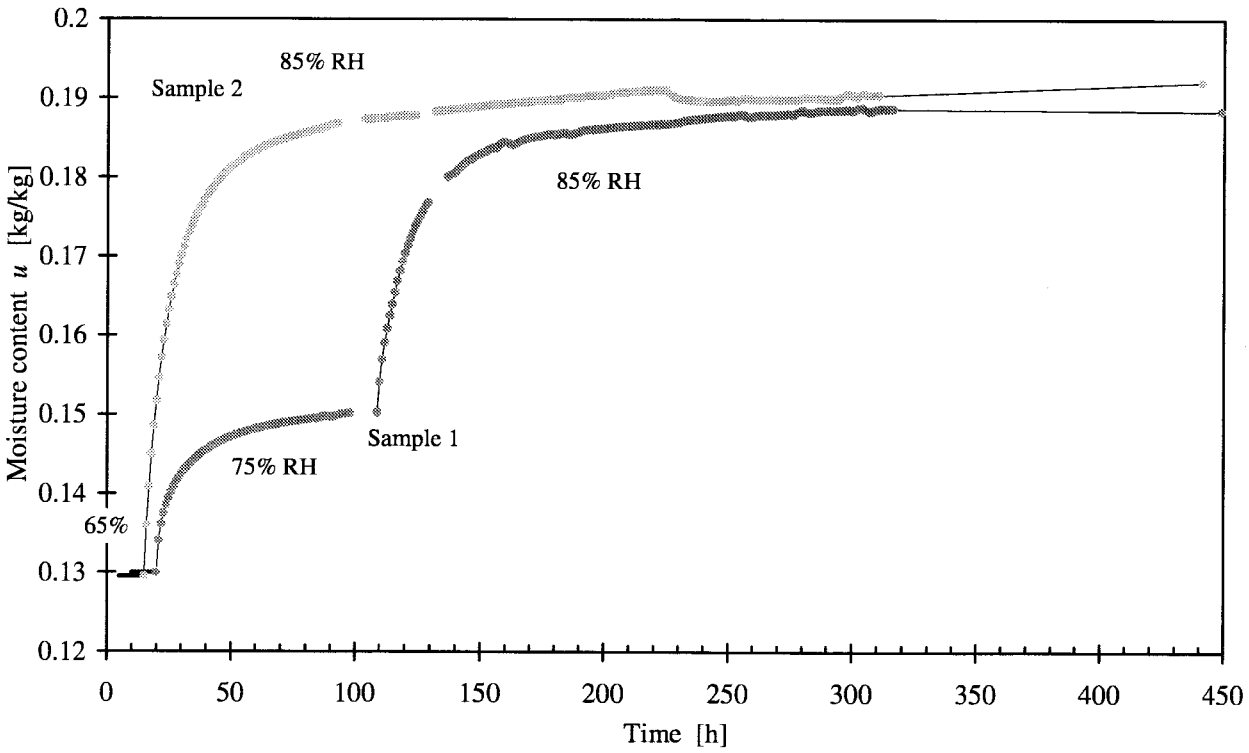

Figure 6.5 Sorption response, Sample 1 and Sample 2, 65% –› 85% RH-interval.

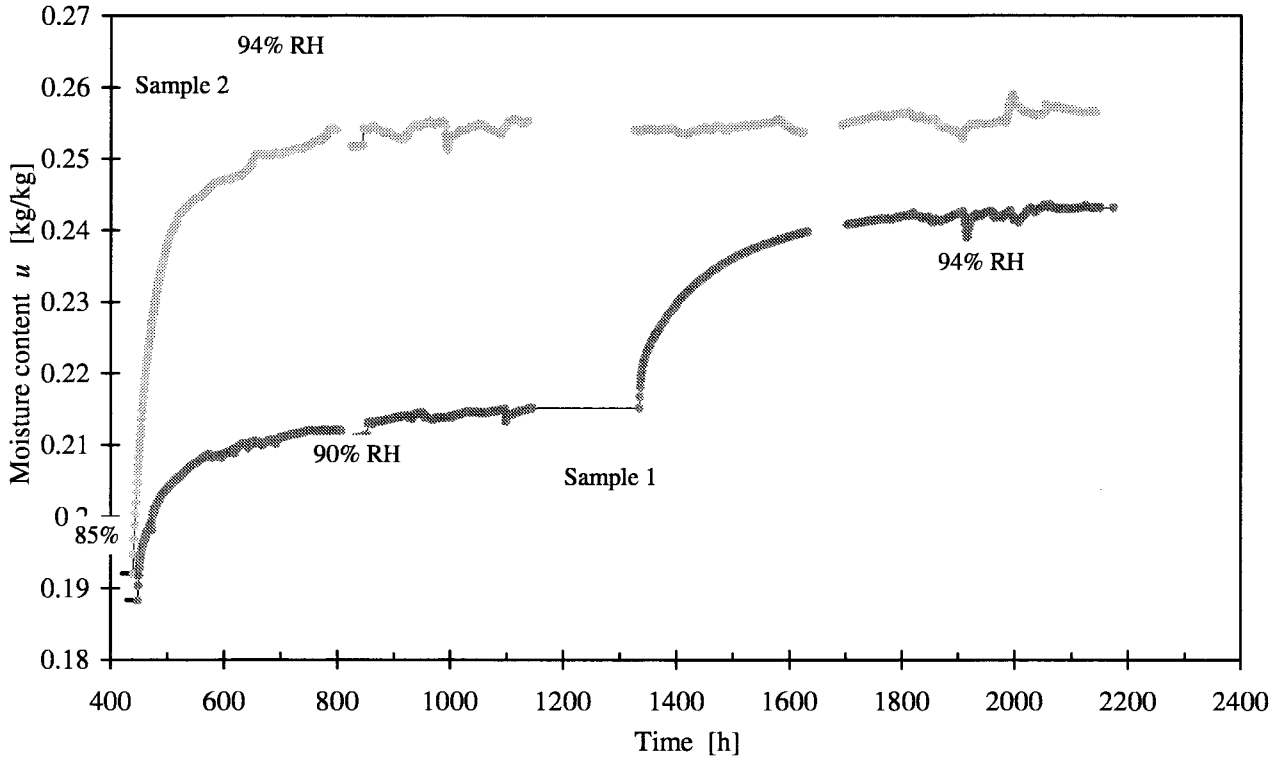

Figure 6.6 Sorption response, Sample 1 and Sample 2, 85% –› 94% RH-interval.

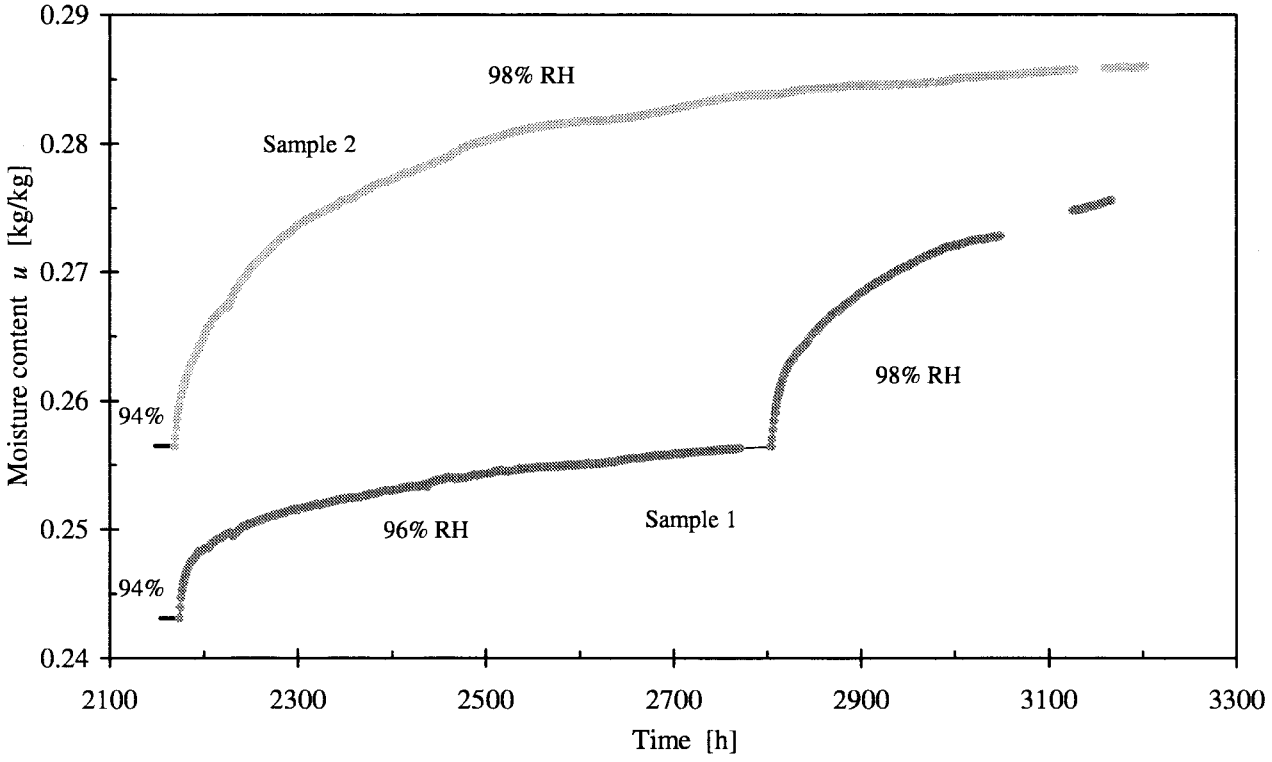

Figure 6.7 Sorption response, Sample 1 and Sample 2, 94% –› 98% RH-interval.

6.1.3 Desorption steps

The first desorption steps in the interval from 98% to 94% are shown in Figure 6.8. The chamber for Sample 2 unfortunately had a problem of leakage from the temperature bath. The deviation from an expected response curve is not so large, hence the effect from the deviation on the following desorption step is thought to be small. Sample 1 was taken out of the chamber and isolated for a short period. The short disturbance in the sorption seems to recover almost totally.

In Figure 6.9 the desorption steps in the interval from 94% to 85% are shown. Data was lost for a long period, fortunately the first responses after step changes were recorded.

Figure 6.10 shows the desorption responses in the interval from 85% to 65%. Several of the previous problems were sorted out and undisturbed measurements were obtained. The slope of the response curves when the first sorption after a step has taken place is rather similar for the two samples, though the step size is different. The amount of desorbed water differs between the two samples subjected to the same RH-interval. The two smaller steps of desorption for Sample 1 yields totally less change in moisture content than one larger step for Sample 2. When, as in this case, the two samples are subjected to the same overall interval change during the same period, the conditions are that Sample 1 is experiencing half of the time between step changes, compared to Sample 2.

In Figure 6.11 the final desorption steps in the interval from 65% to 45% are shown. Also in this curves the sorption responses after the initial sorption after a step has taken place is rather similar for larger and smaller RH-steps. It is noticeable that the retarded sorption is clear even at such dry conditions as 45% relative humidity. Influencing factors could be that the samples have been exposed for high relative humidities and for long periods.

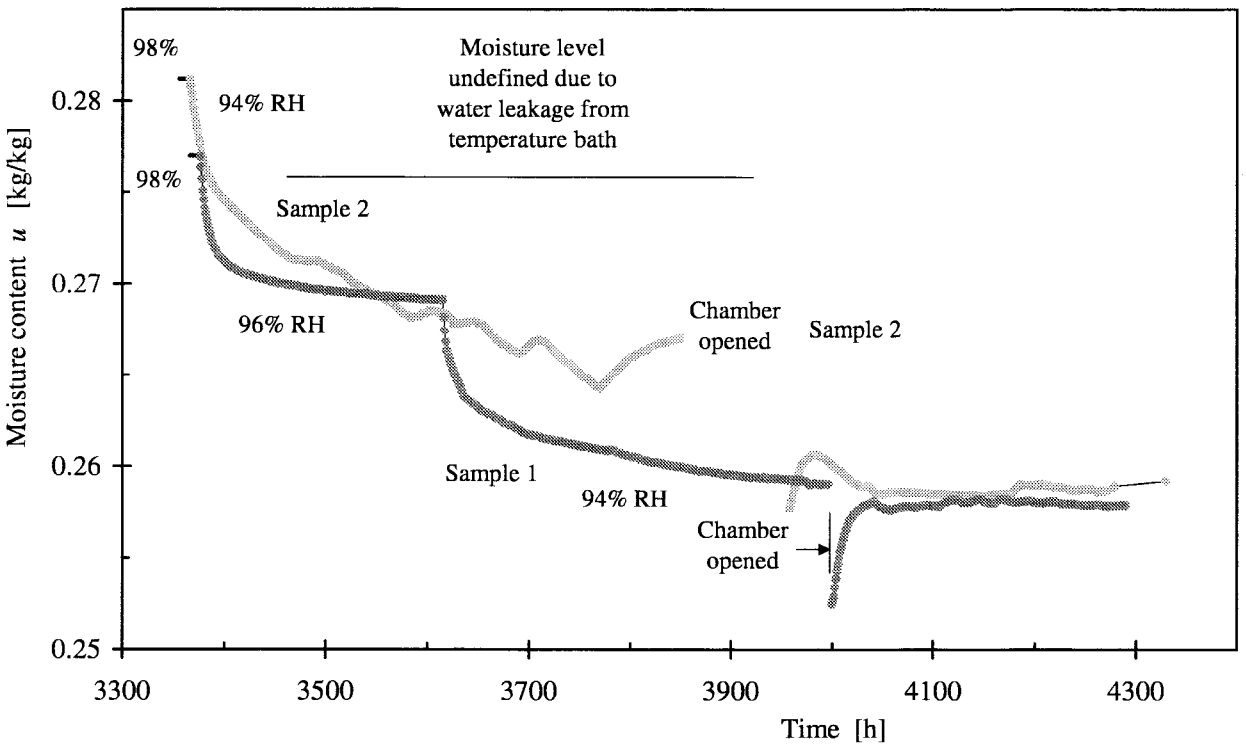

Figure 6.8 Sorption response, Sample 1 and Sample 2, 98% –› 94% RH-interval.

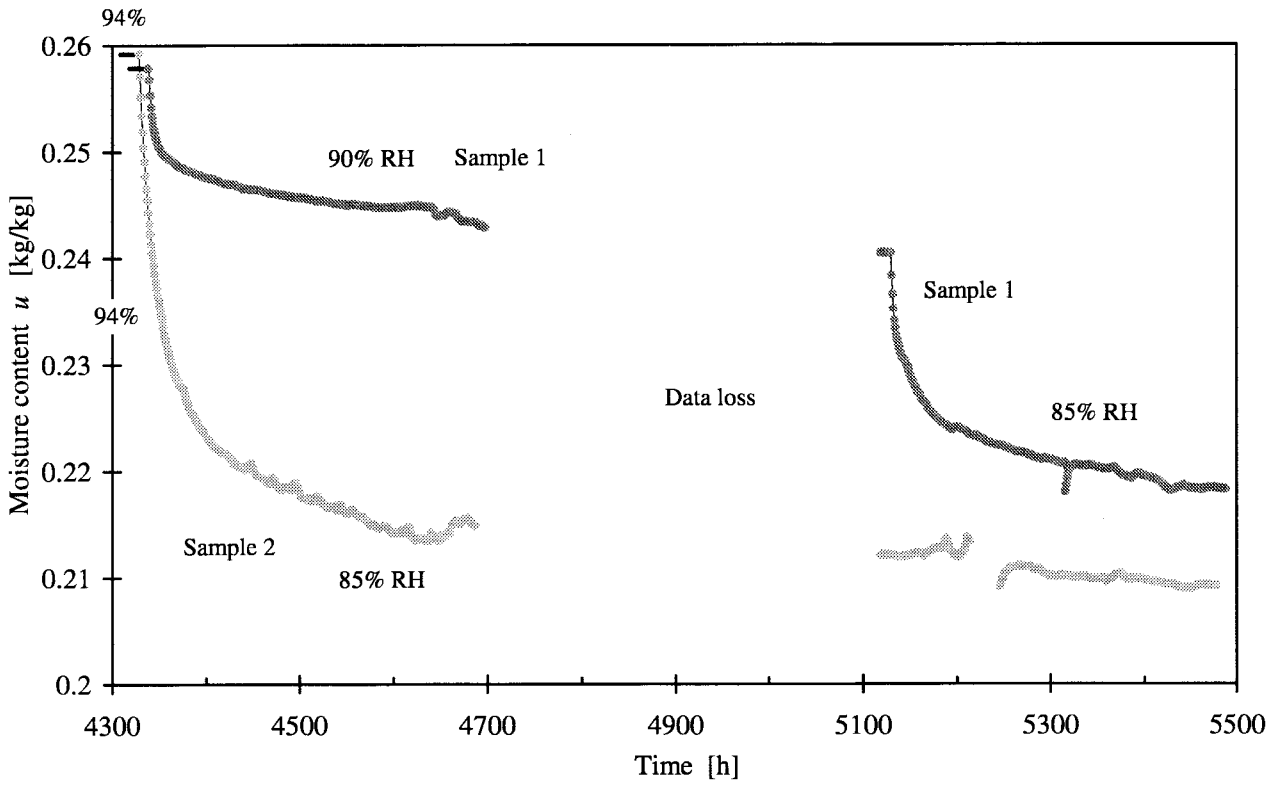

Figure 6.9 Sorption response, Sample 1 and Sample 2, 94% –› 85% RH-interval.

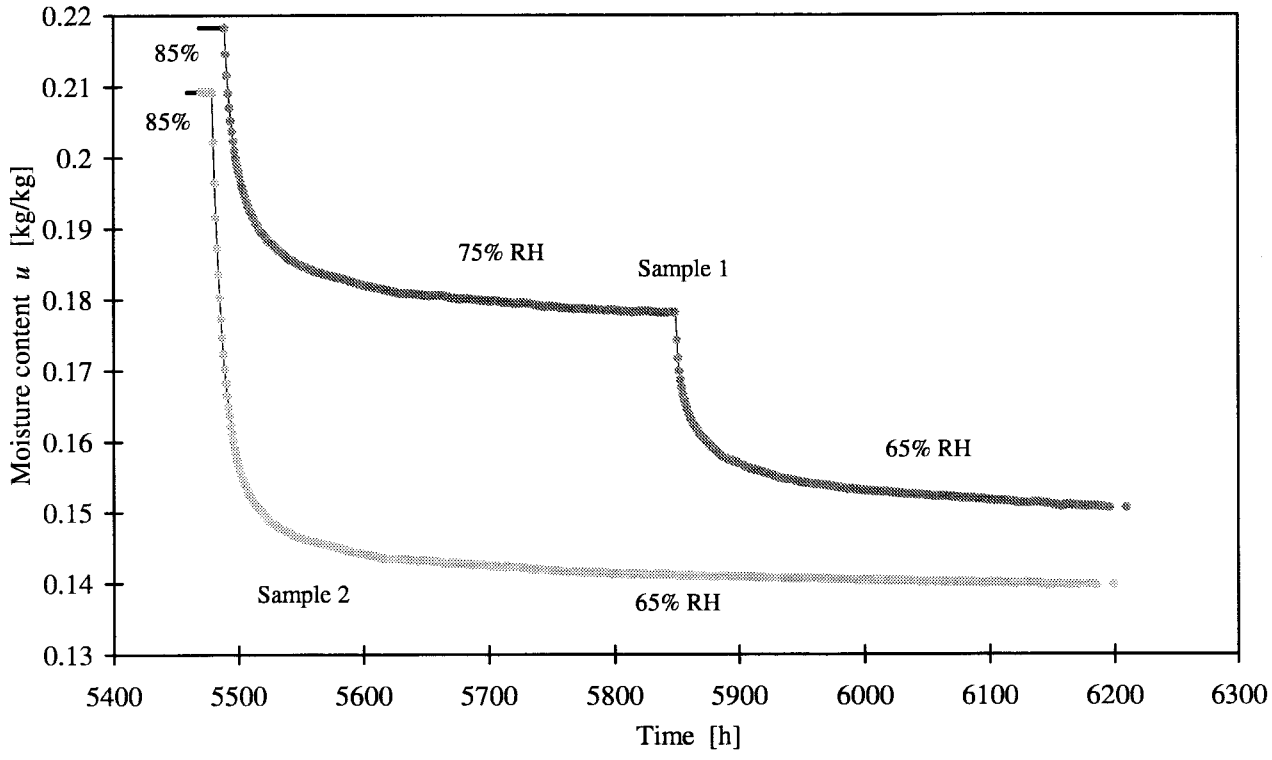

Figure 6.10 Sorption response, Sample 1 and Sample 2, 85% –› 65% RH-interval.

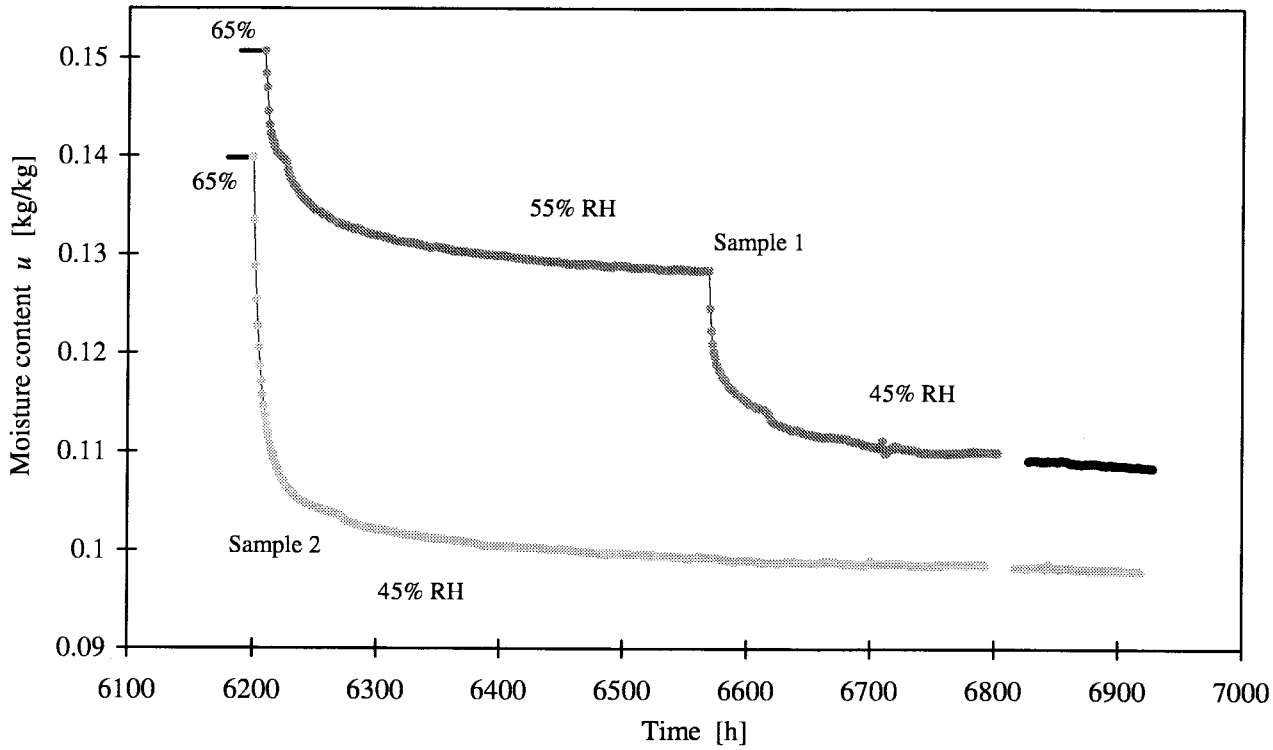

Figure 6.11 Sorption response, Sample 1 and Sample 2, 65% –› 45% RH-interval.

6.2 The second series

The first series of measurements was performed with samples of 3 mm thickness. In this series and the following ones, a thinner sample thickness of 1.7 mm was used. The wood samples are described in Section 2.3 and shown in Figure 2.3. The samples are designated Sample 3 and Sample 4, and they were used in the remainder of the measurements. The first series of measurements consisted of continuous absorption steps followed by desorption steps. The total period was 9 months. In this series the sequence pattern from the first series is repeated, but the total time is shortened to 2 months. The sequences of relative humidities are shown in Figure 6.3 and Figure 6.4. Surveys of the result are shown in Figure 6.12 and Figure 6.13 for the absorption steps and in Figure 6.17 and Figure 6.18 for the desorption steps. The relative humidities are shown over each curve segment. The dotted lines represent lost sorption data. The temperature was 20°C.

6.2.1 Absorption steps

The measured sorption responses with two steps for Sample 3, simultaneous with a single step for Sample 4, are shown together in the same diagram in the common RH-interval. The same kind of presentation was used in the first series.

A survey of the sorption responses for Sample 3 is shown in Figure 6.12 and for Sample 4 in Figure 6.13. At the end of the absorption sequence large parts of the measurement data were lost. The sorption is then hinted by dotted lines to show the duration of the RH-steps.

The first sorption responses for steps in the RH-interval from 45% to 65% are shown in Figure 6.14.

In Figure 6.15 the sorption responses for steps in the RH-interval from 65% to 85% are shown. The same sequence in the first series with thicker samples is shown in Figure 6.5. In both diagrams the dots represent hourly values, and a comparison is possible of the sorption speed the first period after a step change. This gives an idea of the thickness dependence of the swiftness of the step response. The time for half the sorption to take place takes roughly 8 hours for the thicker samples compared to 2 hours for the thinner, for the step from 65% to 85%.

Figure 6.16 shows the sorption responses in the interval from 85% to 94% RH. Corresponding curves for the first series with thicker samples are found in Figure 6.6. Unfortunately the quality of the measurements are not so good in this interval, with missing data and small jumps on the curves.

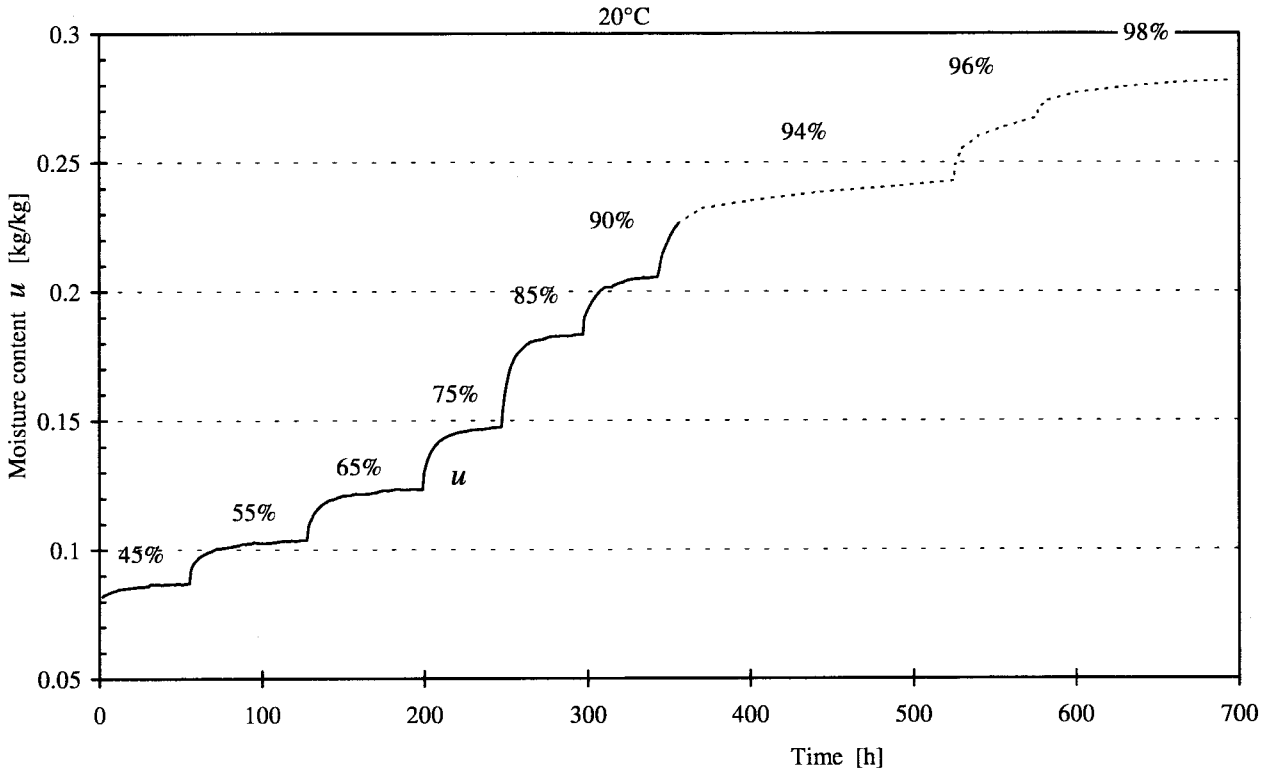

Figure 6.12 Survey of absorption response in the second series, Sample 3

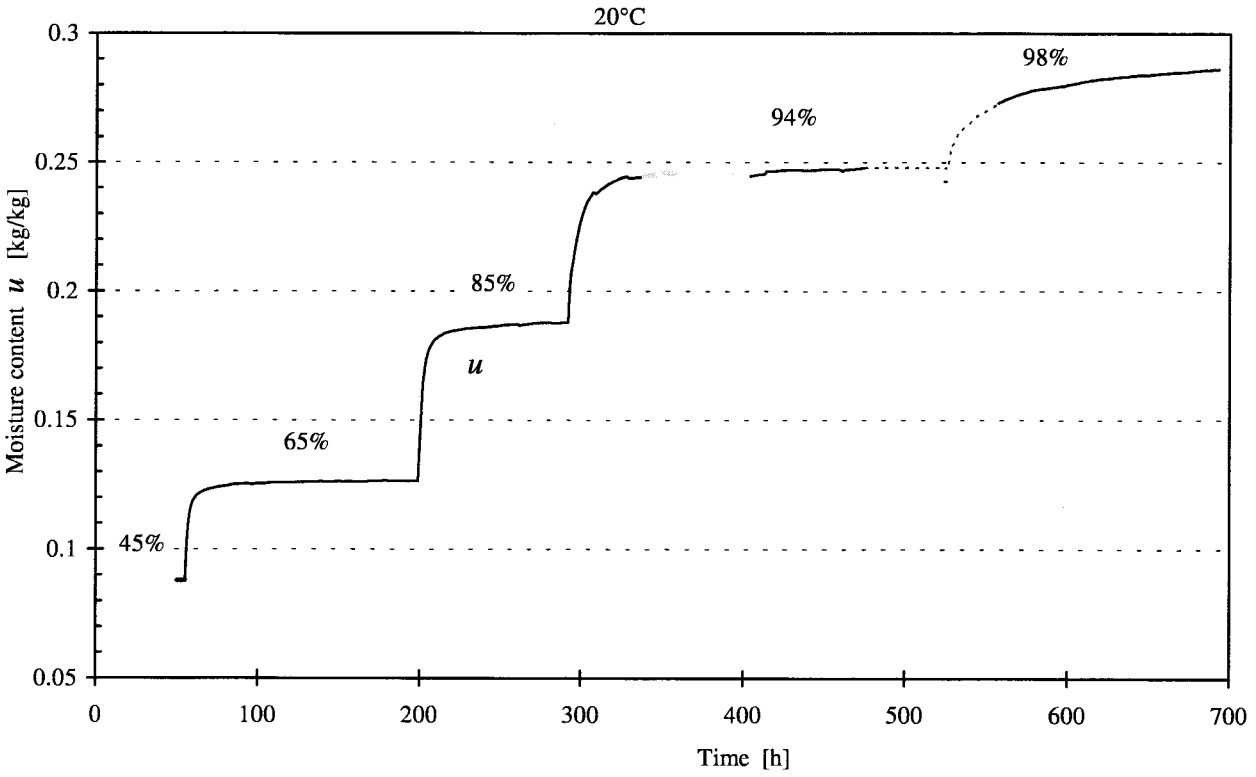

Figure 6.13 Survey of absorption response in the second series, Sample 4

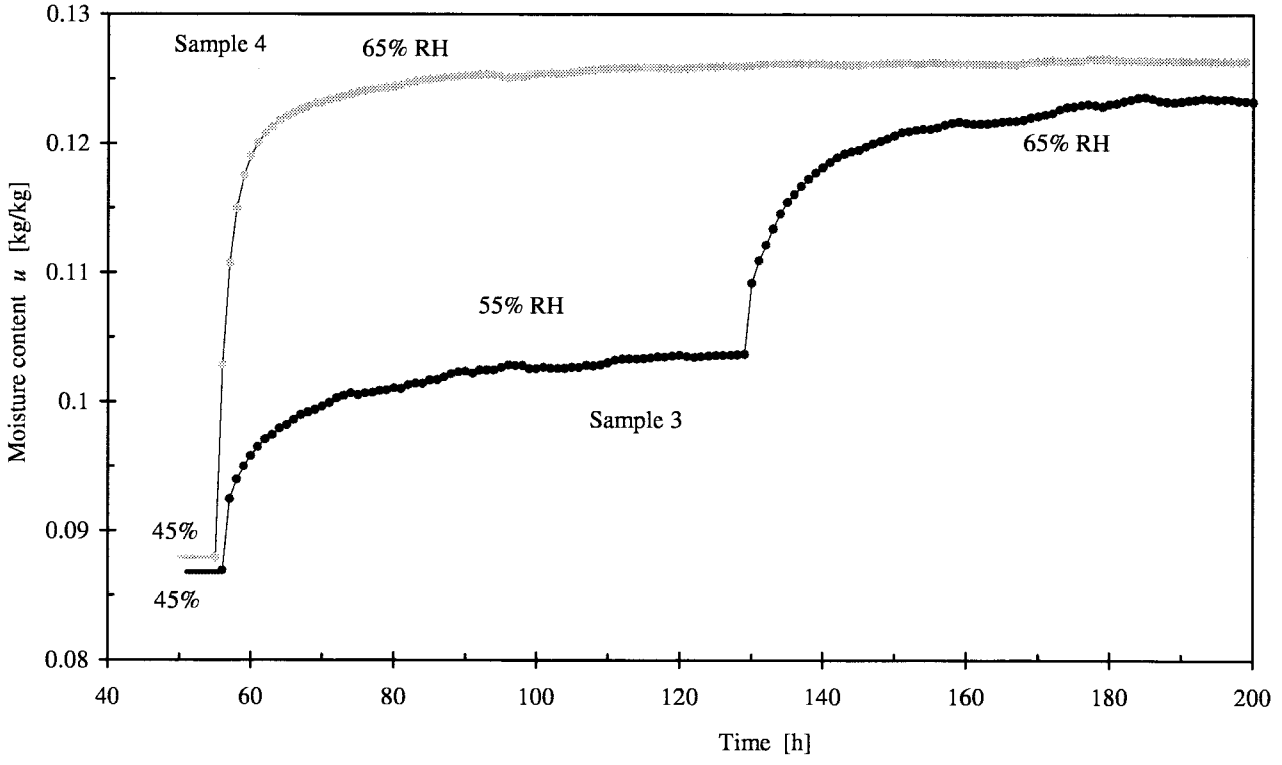

Figure 6.14 Sorption response, Sample 3 and Sample 4, 45% –› 65% RH-interval.

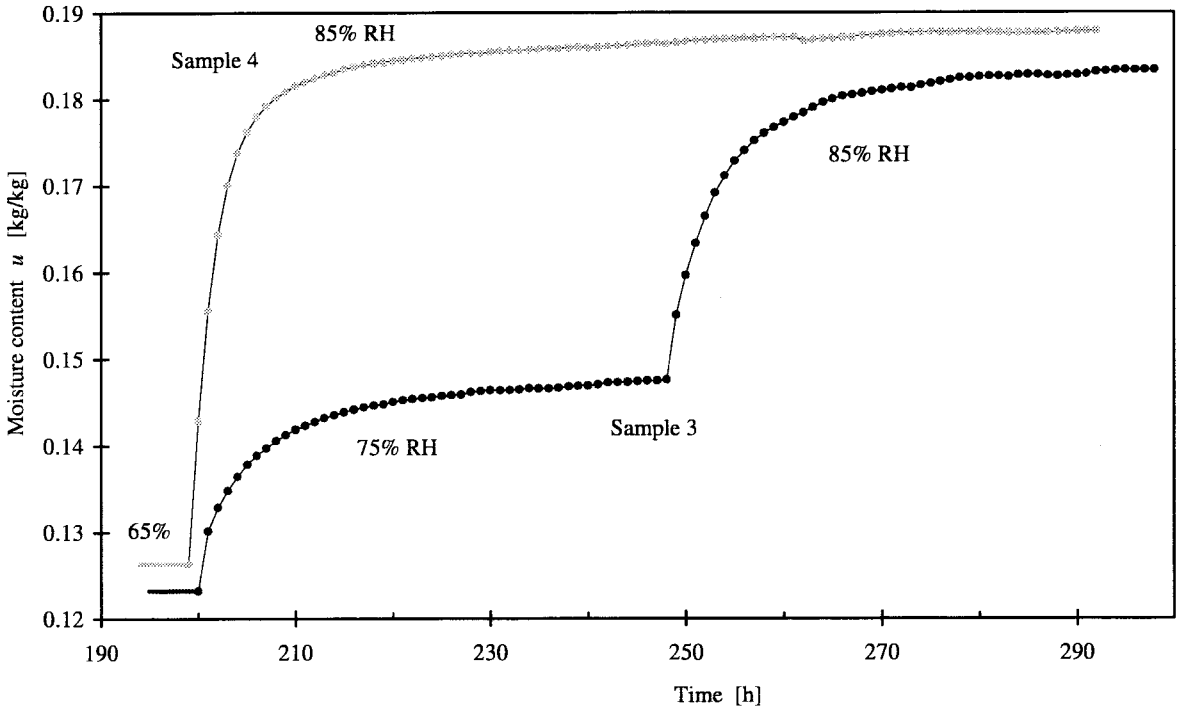

Figure 6.15 Sorption response, Sample 3 and Sample 4, 65% –› 85% RH-interval.

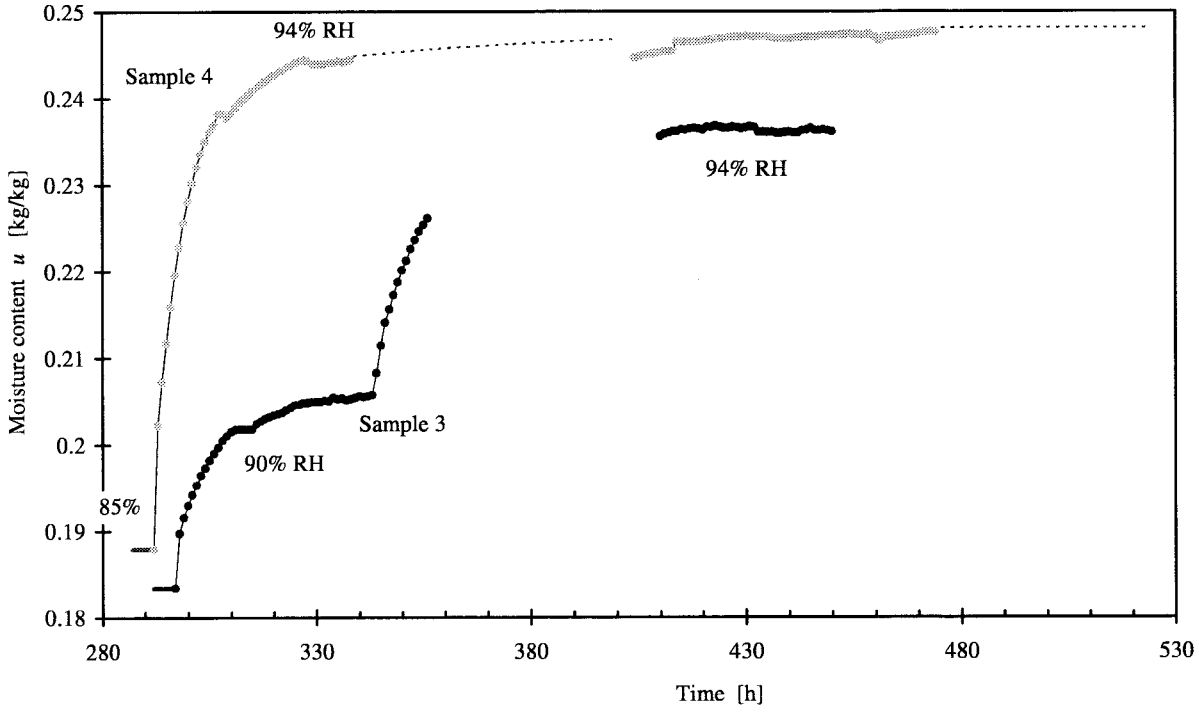

Figure 6.16 Sorption response, Sample 3 and Sample 4, 85% –› 94% RH-interval.

6.2.2 Desorption steps

A survey of the sorption responses for Sample 3 is shown in Figure 6.17 and for Sample 4 in Figure 6.18. For Sample 4 large parts of the measurement data were lost. Sorption response

when the data were lost is hinted by dotted lines to show the duration of the RH-steps. At one instance, Sample 4 had to be removed from the chamber and isolated. The event is noted in Figure 6.18. To maintain desorption for the following measurements, a few drops of water were added inside the container where the sample was isolated.

Only in the first desorption interval described in Figure 6.19, measurement data were obtained for both of the samples. In Figure 6.20 to Figure 6.22 only the sorption response for Sample 3 is available. In Figure 6.23 the sorption response for the last interval of Sample 4 is shown. The same interval for Sample 3 is shown in Figure 6.22. The step changes were not made simultaneously and because of this the measurements are shown separately.

An insidious fault occurred in the electronic balance weighing Sample 3. The optical system guiding the control had a flaw and the performance of the balance was slightly deteriorating. Fortunately it had a diurnal variation and was therefore eventually discovered, but not until the end of the series.

In Figure 6.19 the first desorption responses for steps in the RH-interval from 98% to 94% are shown. The same sequence in the first series with a thicker sample is shown in Figure 6.8.

Measurements in the RH-interval from 94% to 85% for Sample 3 are shown in Figure 6.20. Corresponding interval in the first series is shown in Figure 6.9. The sorption response in the RH-interval from 85% to 65% for Sample 3 is shown in Figure 6.21. Corresponding interval in the first series is shown in Figure 6.10. The last sorption response for Sample 3 in the RH-interval from 65% to 45% is shown in Figure 6.22. Corresponding interval in the first series is shown in Figure 6.11

In Figure 6.23 the desorption step for Sample 4 from 65 to 45% RH is shown. Sample 3 was subjected to the same interval in two steps, shown in Figure 6.22. Additional manually readings for an extended period at 45% RH are shown in the overview of the desorption response for Sample 4 in Figure 6.18.

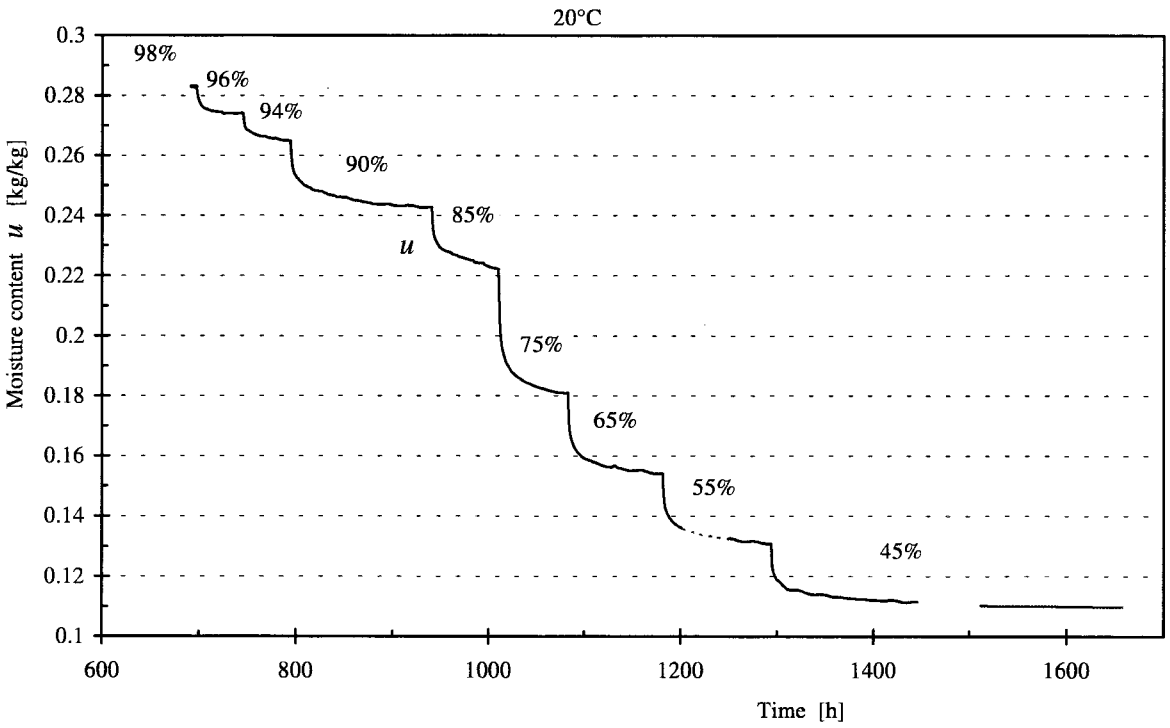

Figure 6.17 Survey of desorption response in the second series, Sample 3.

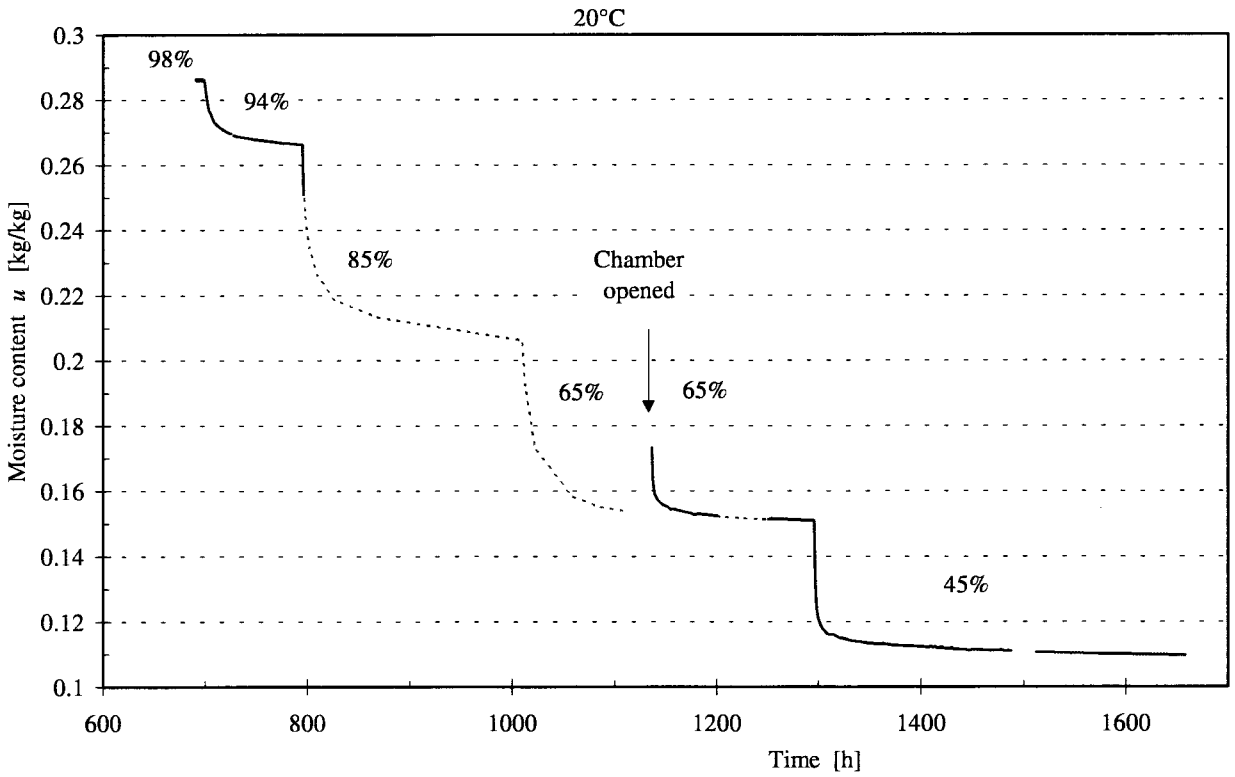

Figure 6.18 Survey of desorption response in the second series, Sample 4.

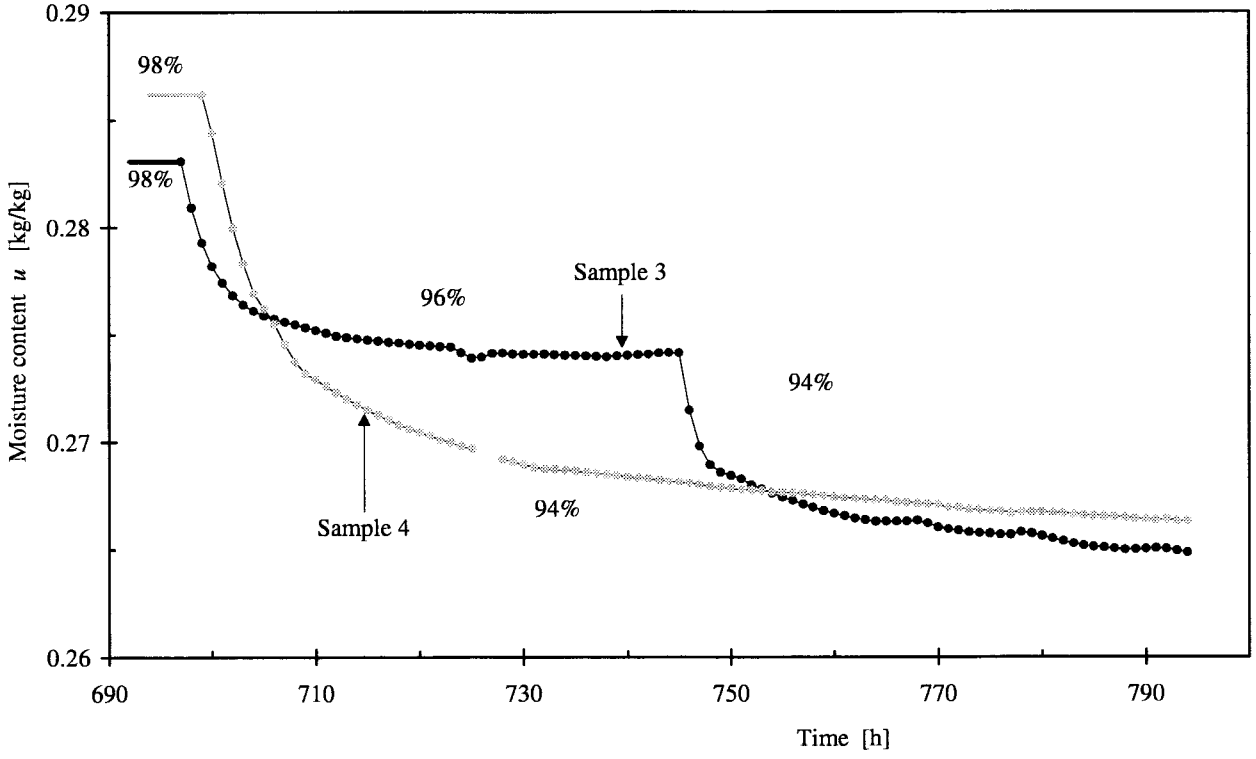

Figure 6.19 Sorption response, Sample 3 and Sample 4, 98% –› 94% RH-interval.

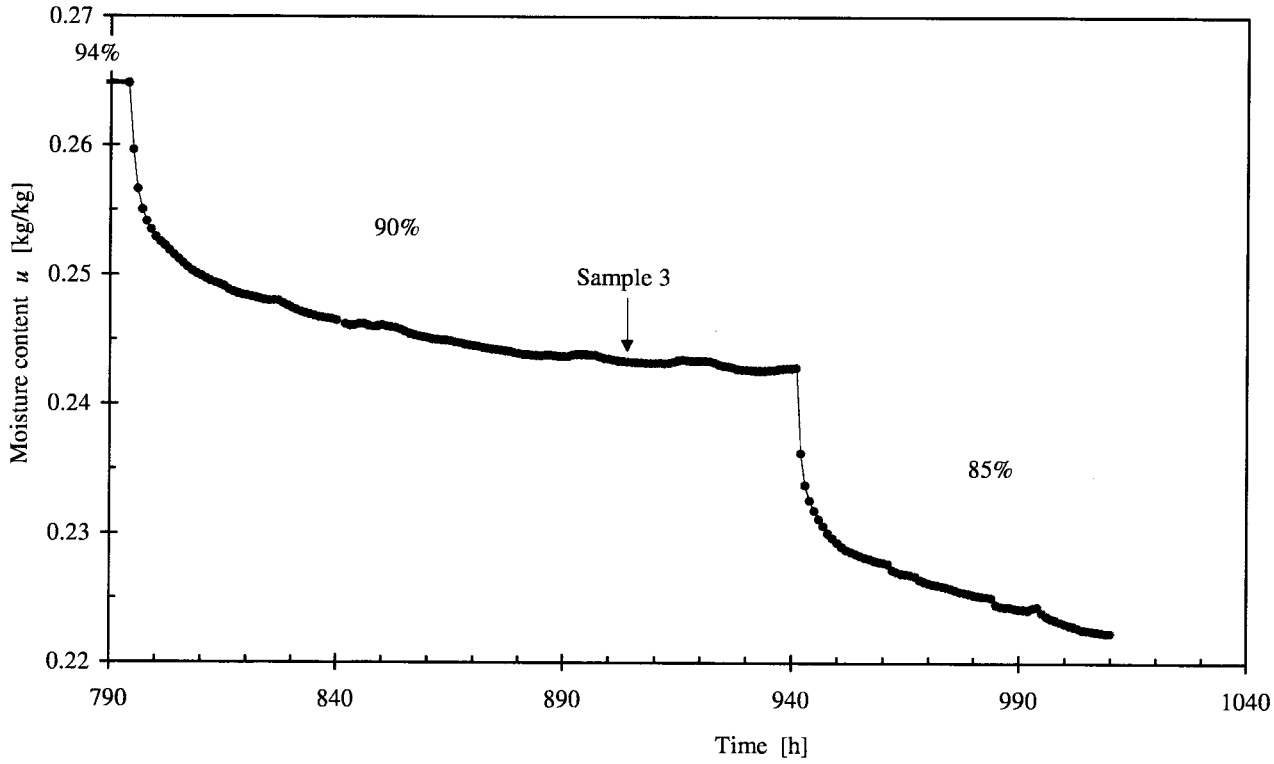

Figure 6.20 Sorption response, Sample 3, 94% –› 85% RH-interval.

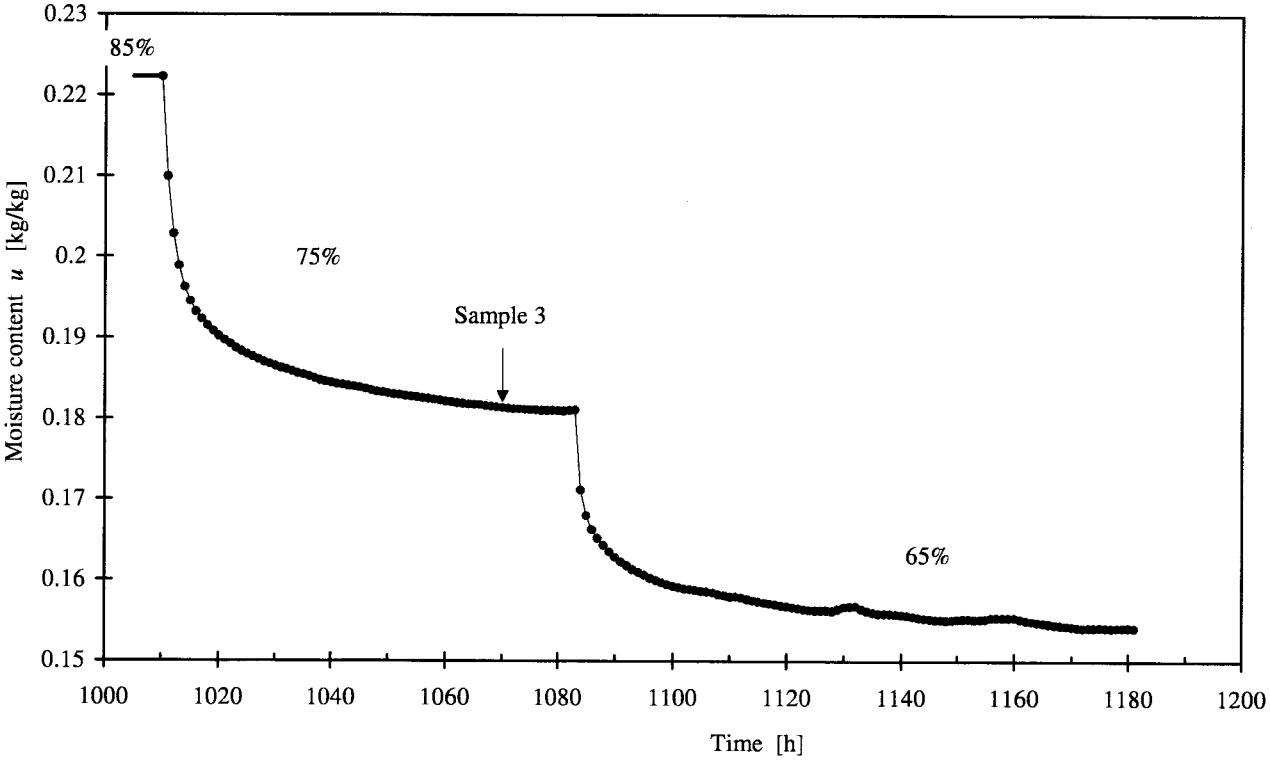

Figure 6.21 Sorption response, Sample 3, 85% –› 65% RH-interval.

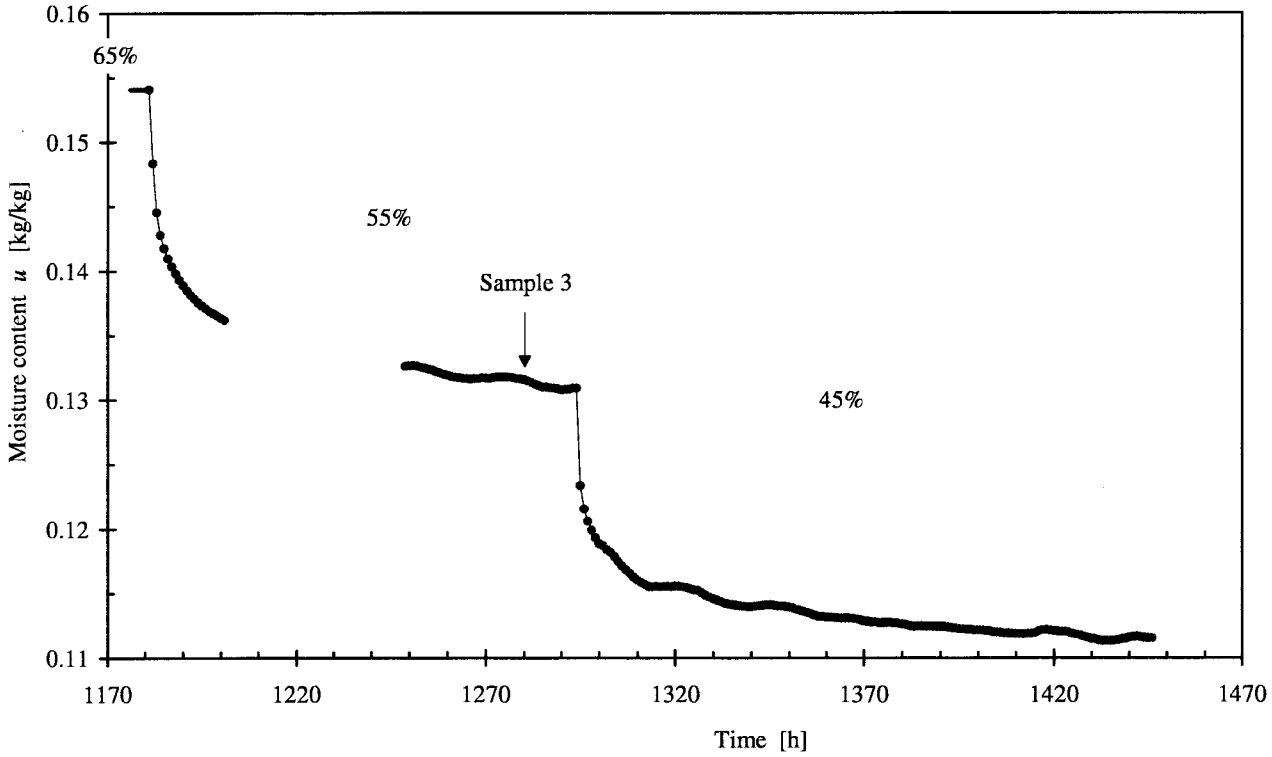

Figure 6.22 Sorption response, Sample 3, 65% –› 45% RH-interval.

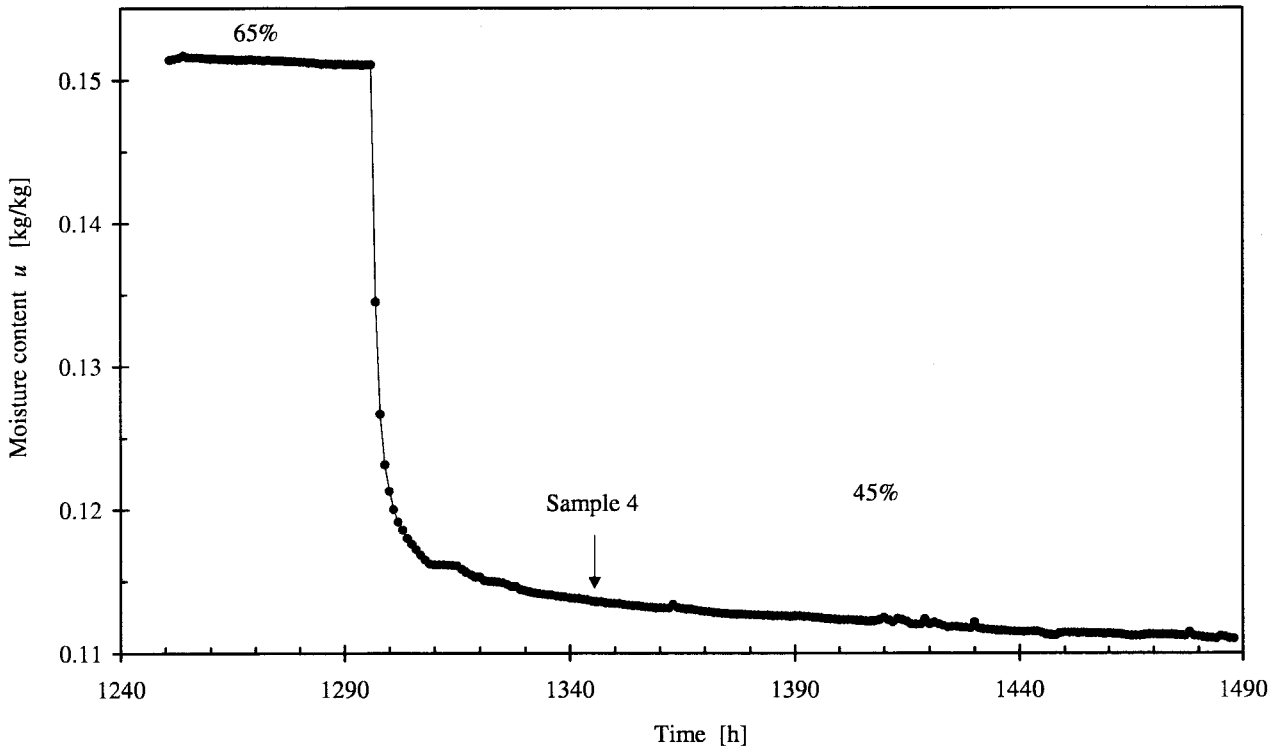

Figure 6.23 Sorption response, Sample 4, 65% –› 45% RH-interval.

6.3 The third series

The sequences of relative humidities are shown by Figure 5.5 (Sample 3) and Figure 5.6 (Sample 4). A survey of the absorption response for Sample 3 is shown in Figure 6.24, and the absorption response for Sample 4 is shown in Figure 6.28. Surveys of the desorption responses are shown in Figure 6.29 for Sample 3 and in Figure 6.30 for Sample 4.

For Sample 3, the absorption step sequence in Figure 6.24 and the desorption step sequence in Figure 6.29 was divided further compared to the steps in the previous series. Each step in Figure 6.12 and Figure 6.17 in the previous second series is divided into two smaller steps in Figure 6.24 and Figure 6.29. The time for each individual step was relatively short.

6.3.1 Absorption steps

In Figure 6.25 the sorption response for the first steps are shown. The wood does not come to an equilibrium at all between steps. This is specially the case in the responses for steps at high RH shown in Figure 6.26. Note that for step responses calculated by a traditional Fickian process, equilibrium is established after rather few hours for these tin samples.

Figure 6.27 shows the last absorption step. The 98% RH-level was kept for 500 hours. The origin for the tree disturbances, marked with vertical lines, are known .The reason is that the air jet was diffused more than the time around weighing by mistake. It resulted in a somewhat different temperature pattern in the chamber.

The intention was to subject Sample 4 to a single, very large step, from 35% to 98% RH. Unfortunately, the control of the mechanical pressure regulator was lost some time after the step and the deviation was not found and corrected until 64 hours after the step. The 98% RH-level was then kept for about 500 hours. The sorption response is shown in Figure 6.28.

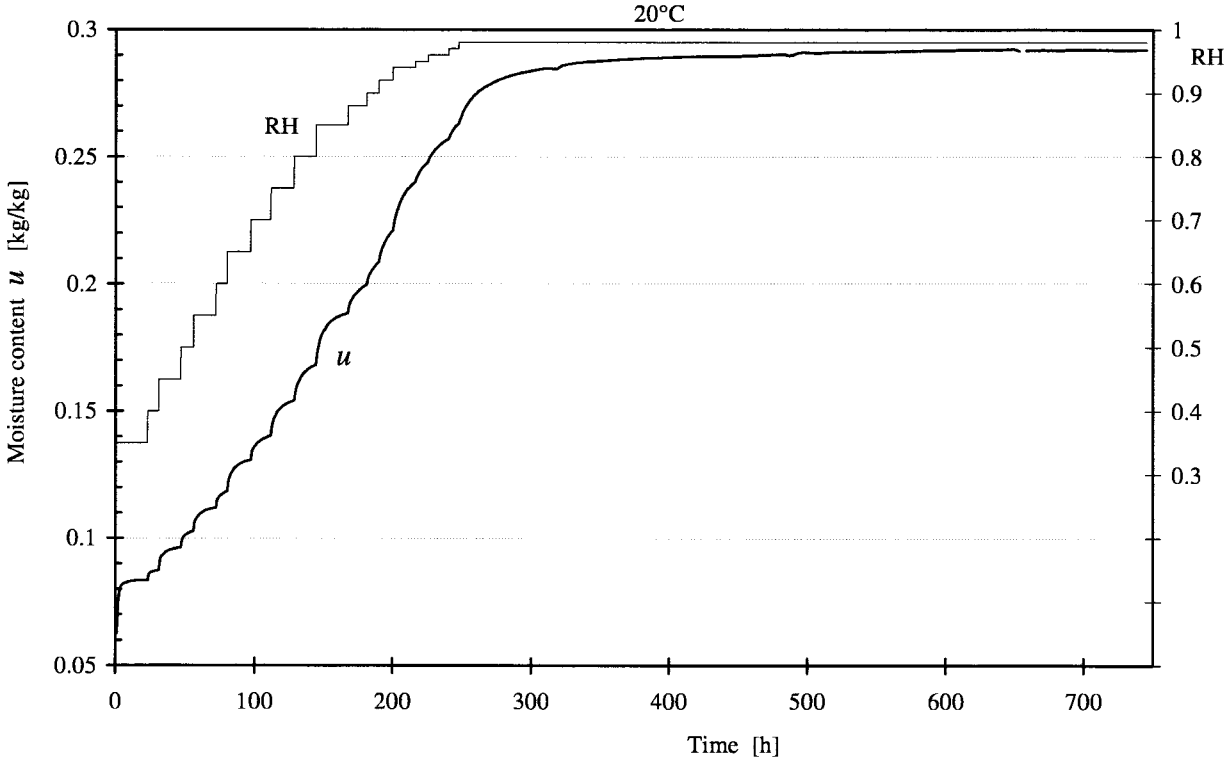

Figure 6.24 Survey of absorption response in the third series, Sample 3.

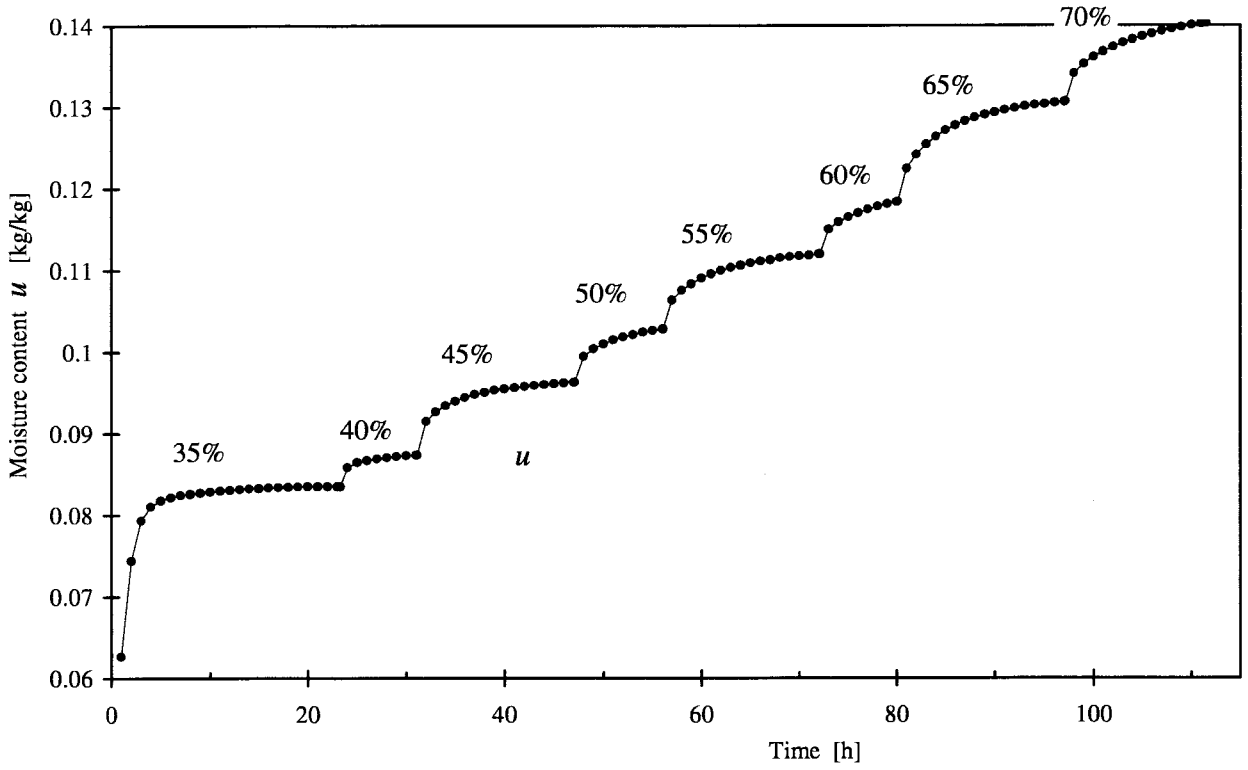

Figure 6.25 Sorption response, Sample 3, 35% –› 70% RH-interval.

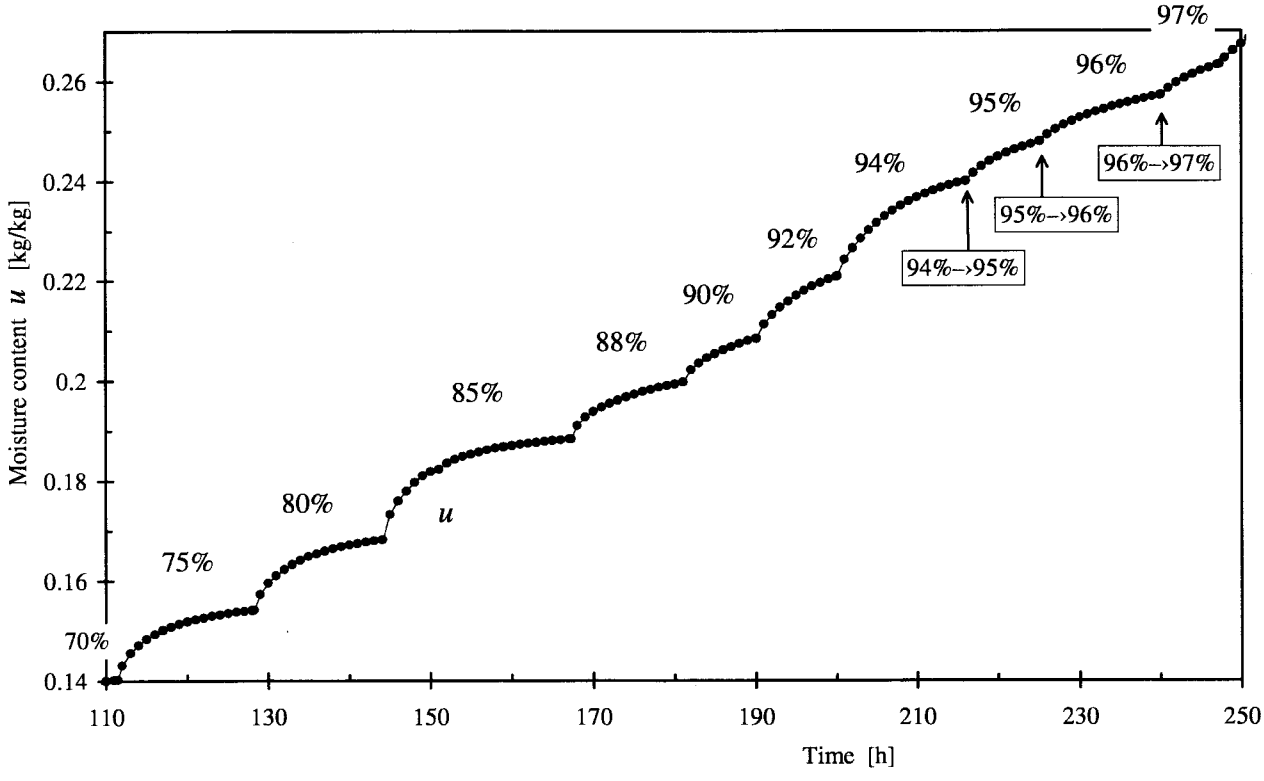

Figure 6.26 Sorption response, Sample 3, 70% –› 97% RH-interval.

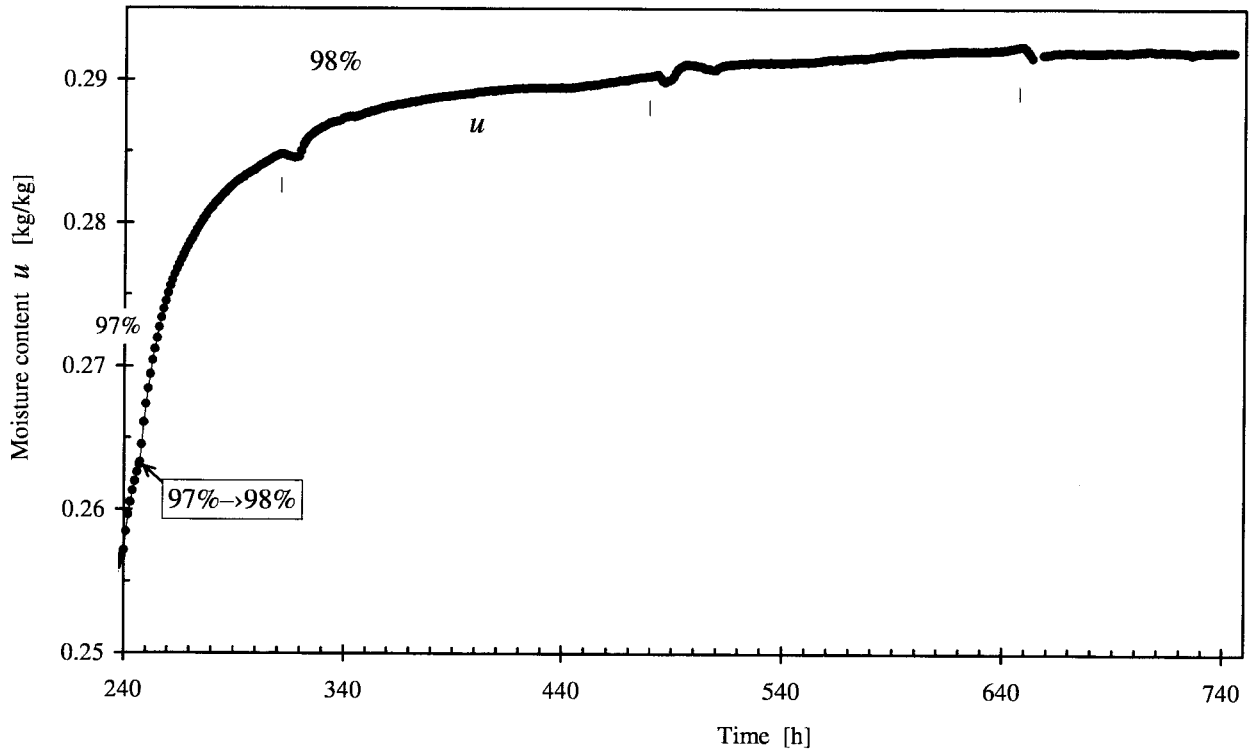

Figure 6.27 Sorption response, Sample 3, 97% → 98% RH-step.

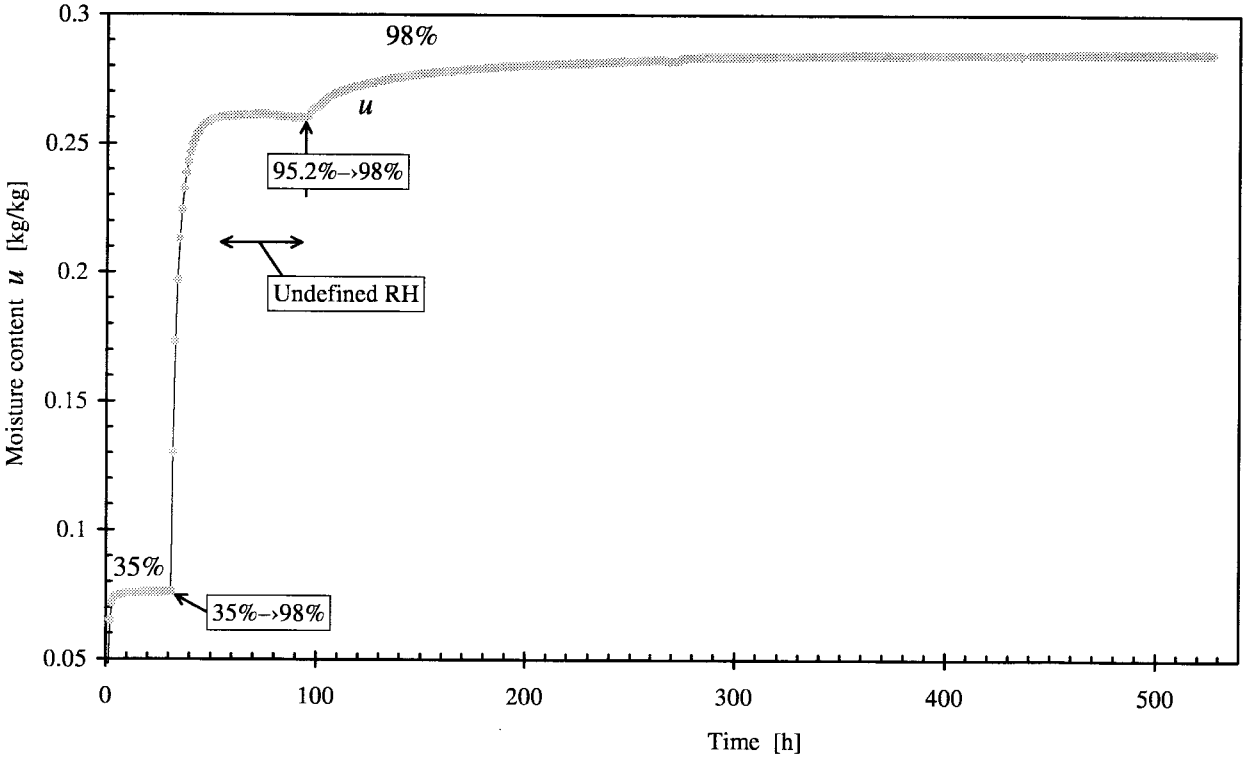

Figure 6.28 Sorption response, Sample 4, 35% → 98% RH-interval.

6.3.2 Desorption steps

Surveys of the desorption responses are shown in Figure 6.29 for Sample 3 and in Figure 6.30 for Sample 4. The desorption response curves for Sample 3 are shown in more detail in Figure 6.31 and in Figure 6.32. The desorption response curves for Sample 4 in Figure 6.33 and in Figure 6.34 were made in order to supplement the measurements in the second series, where data were lost due to recording problems.

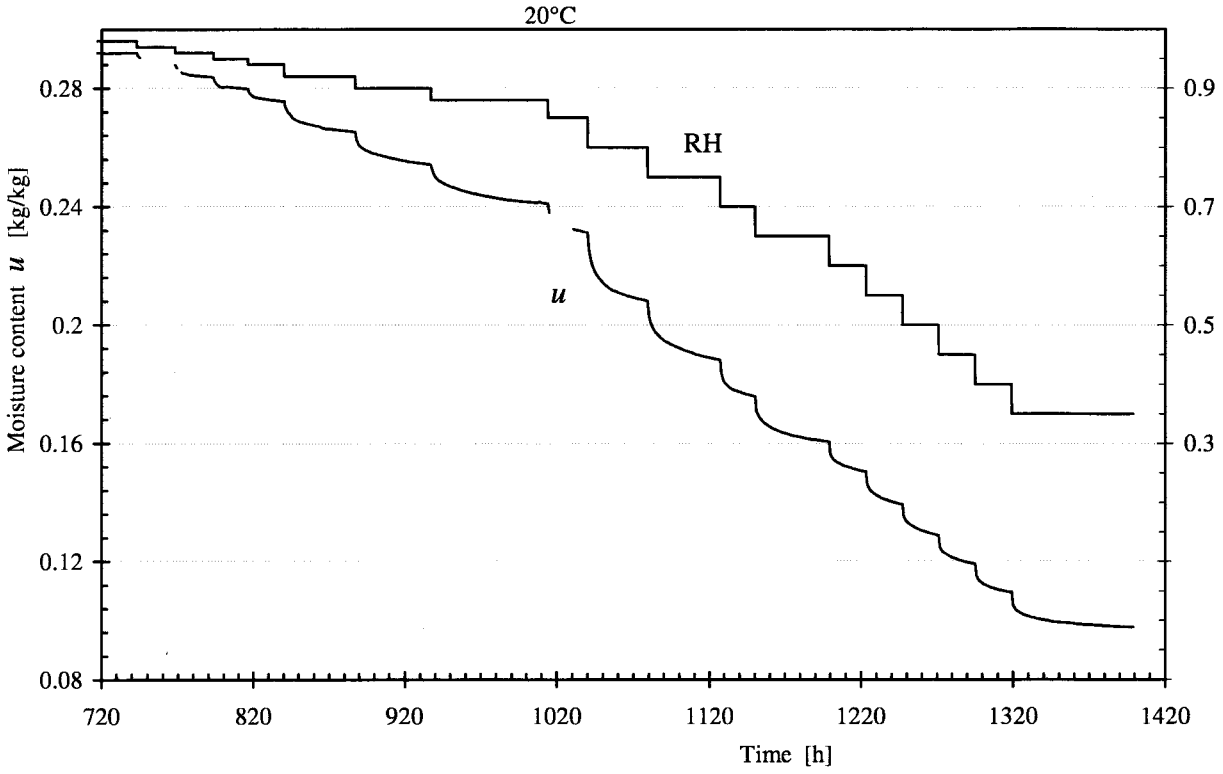

Figure 6.29 Survey of desorption response in the third series, Sample 3.

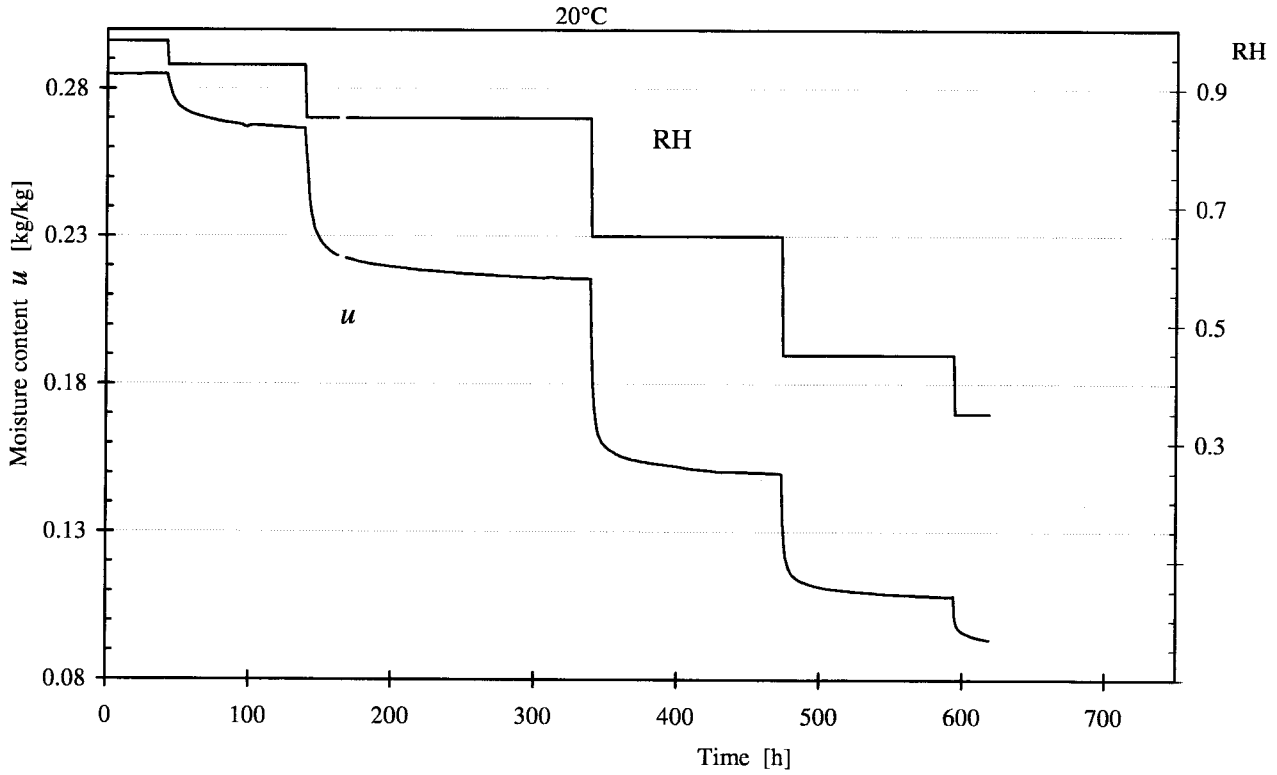

Figure 6.30 Survey of desorption response in the third series, Sample 4.

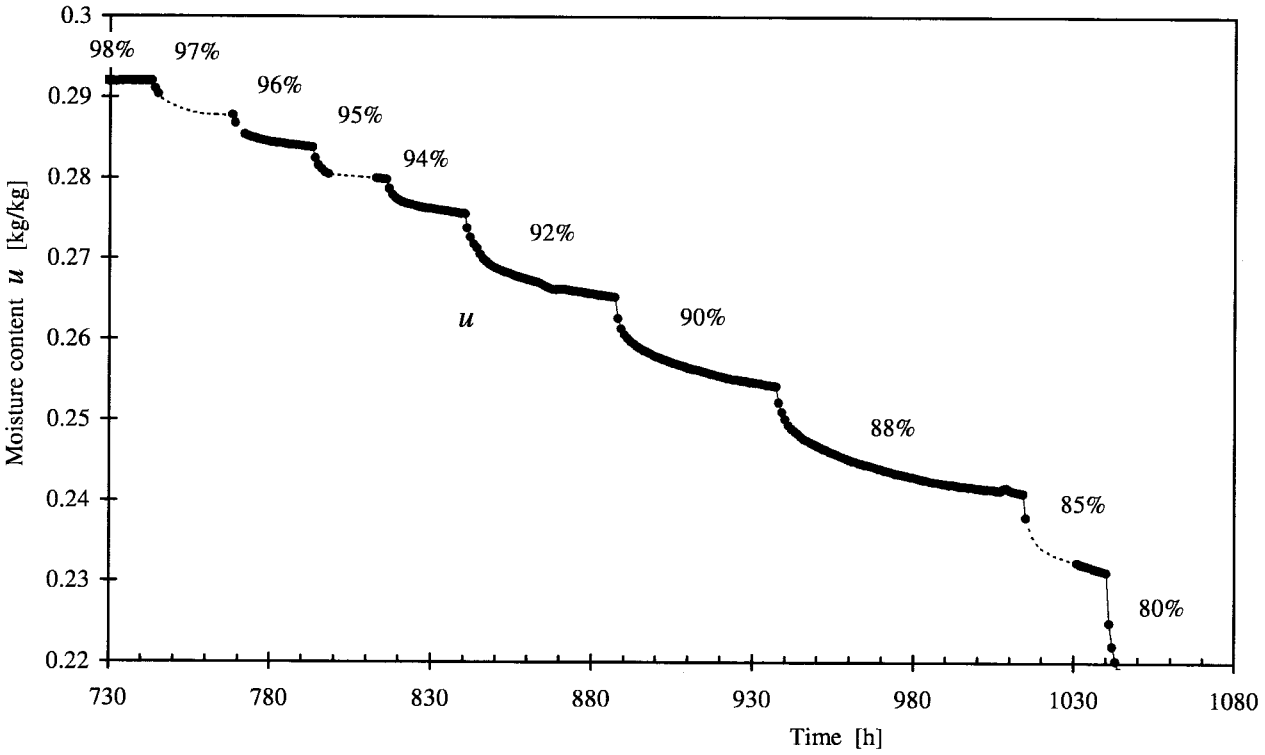

Figure 6.31 Sorption response, Sample 3, 98% → 85% RH-interval.

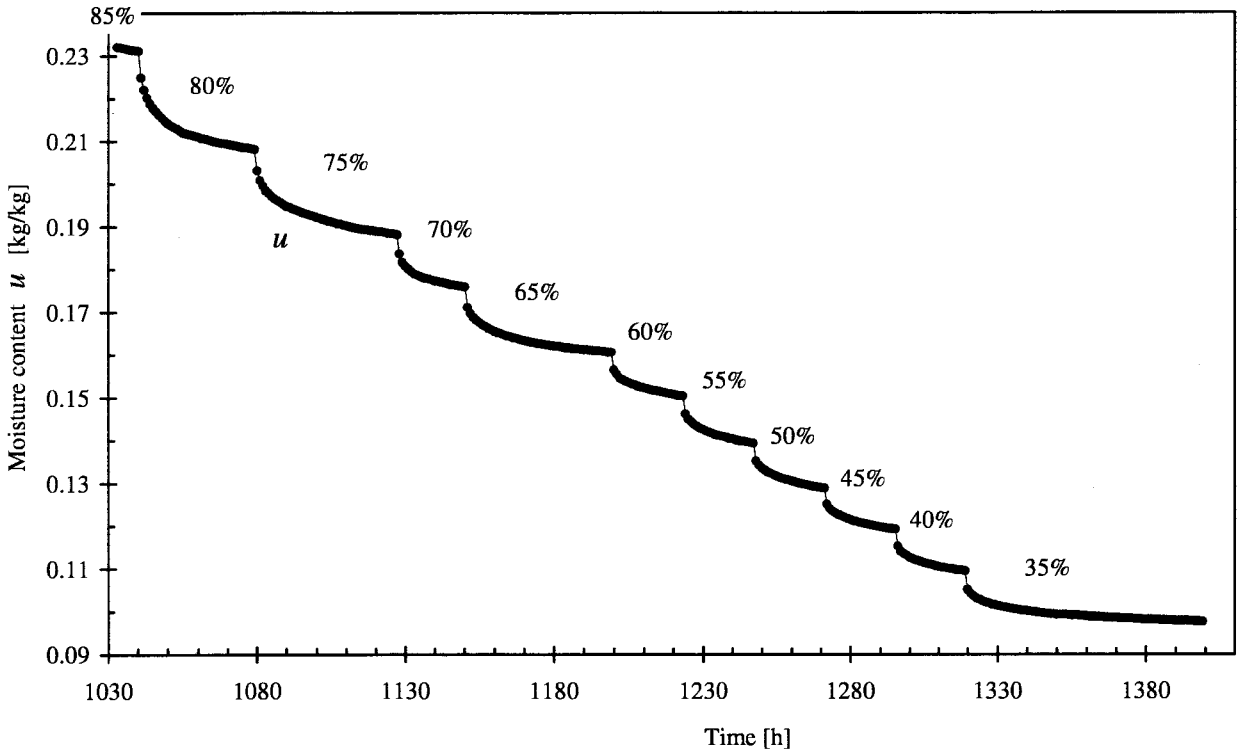

Figure 6.32 Sorption response, Sample 3, 85% → 35% RH-interval.

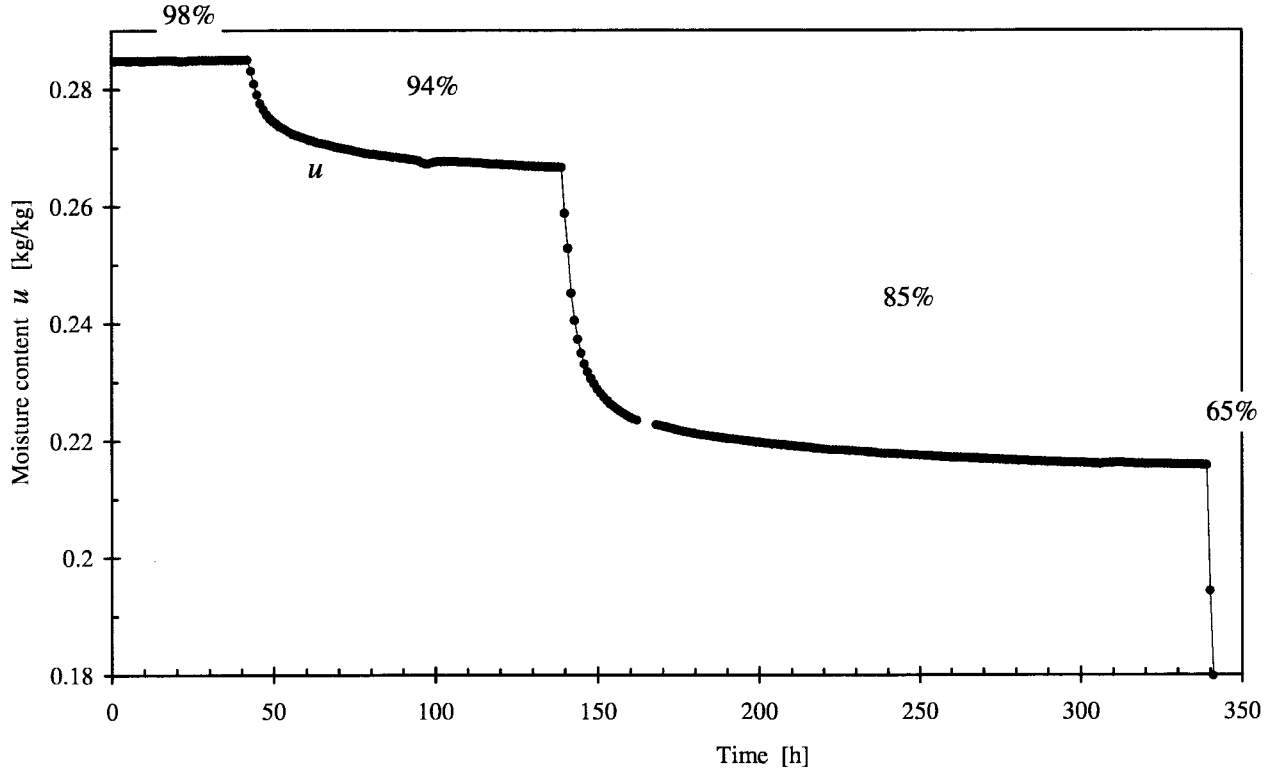

Figure 6.33 Sorption response, Sample 4, 98% → 85% RH-interval.

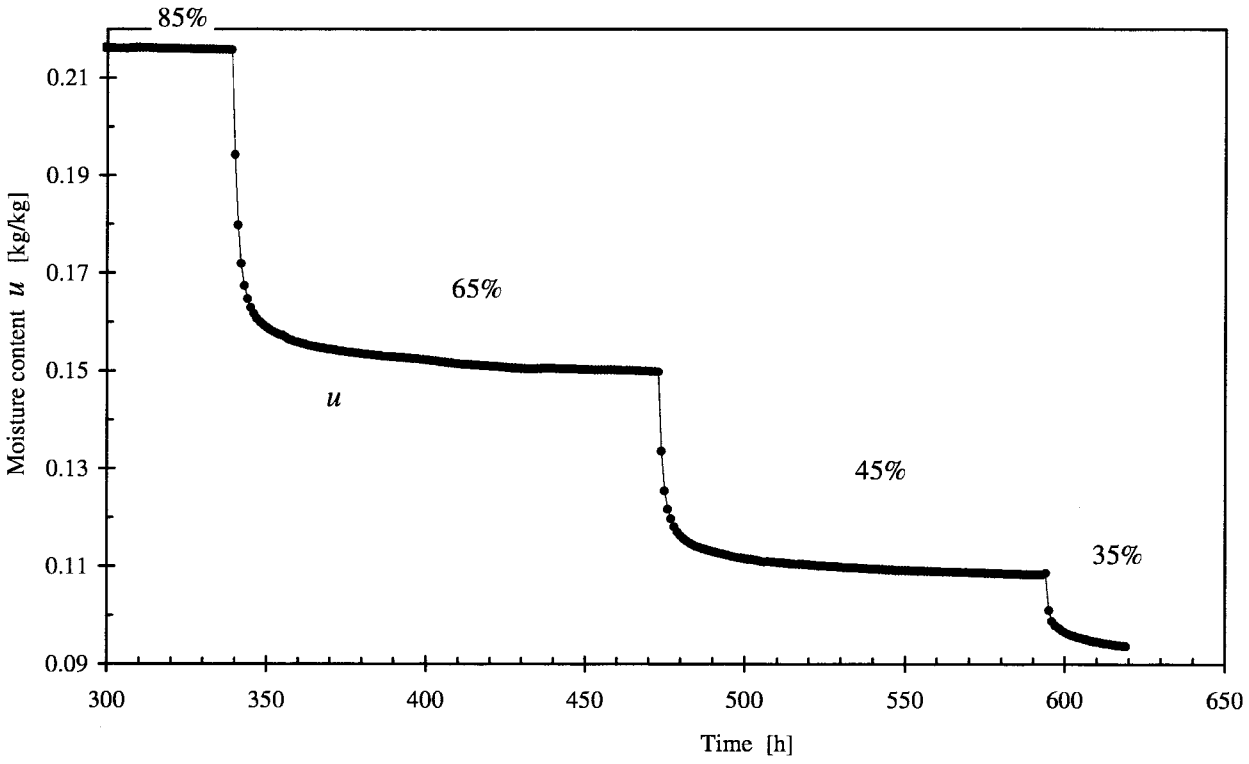

Figure 6.34 Sorption response, Sample 4, 85% –› 35% RH-interval.

6.3.3 Desorption followed by an absorption step

Figure 6.35 shows the last steps of sorption response in this series for Sample 3, including an absorption step.

Substantial retarded sorption effects were found during the desorption step to 35% RH. This was unexpected under such dry conditions. The time interval was extended to investigate this further.

After the wide desorption interval, starting at 98% RH, and the long equilibrium time at 35% RH, the opportunity to add an absorption step was used (35% to 45% RH). As seen in the figure, the sample comes to a much more distinct equilibrium during the last step, where desorption is followed by absorption.

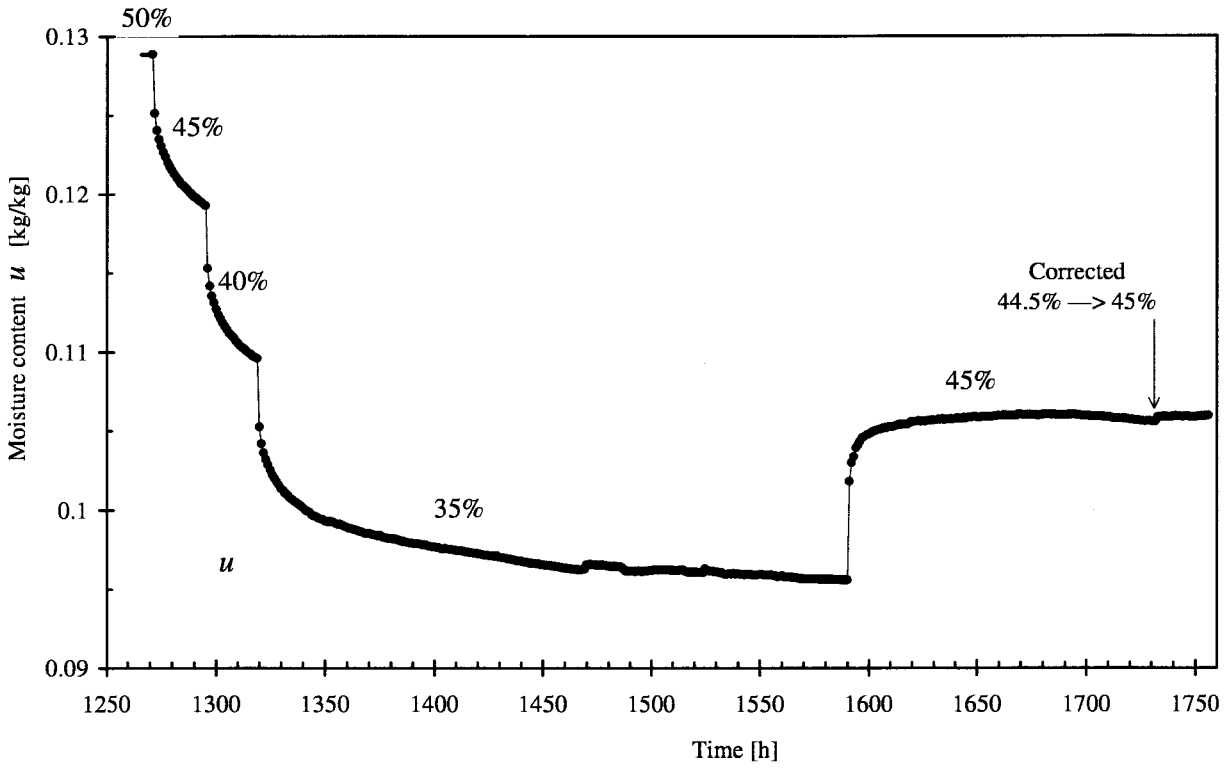

Figure 6.35 Sorption response, Sample 3, 45% –› 35% –› 45% RH-interval.

6.4 The fourth series

The sequence of relative humidities is shown in Figure 5.7. Those series of measurements are made on Samples 3 and 4 at 20°C as the previous series. Cyclic steps are introduced in this series. Also measurements of swelling are started, performed on separate samples, placed in the same chamber as Sample 3. The samples and the device for measurement of swelling are described in Section 2.4. A survey of the result of the sorption is shown in Figure 6.36 for sample 3 and in Figure 6.37 for sample 4.

The diagrams of the measured sorption responses for Sample 3 and Sample 4 are followed by a diagram with the measured swelling responses. Figure 6.40 is the first diagram of this type. Curves of tangential and radial swelling are shown in the same diagram. Thus allows comparison. Diagrams for the comparison of responses between swelling and sorption are given in Chapter 8.

The chamber containing Sample 3 and the samples for the swelling measurements has a short, very dry period (1993–09–02). This was due to an oversight to replenish the water in the saturation vessel for that chamber.

The time scale in the diagrams has got the year–month–day format in this series and the following ones. The primary ticks on the time scales are placed with 14 days interval and secondary ticks represent one day.

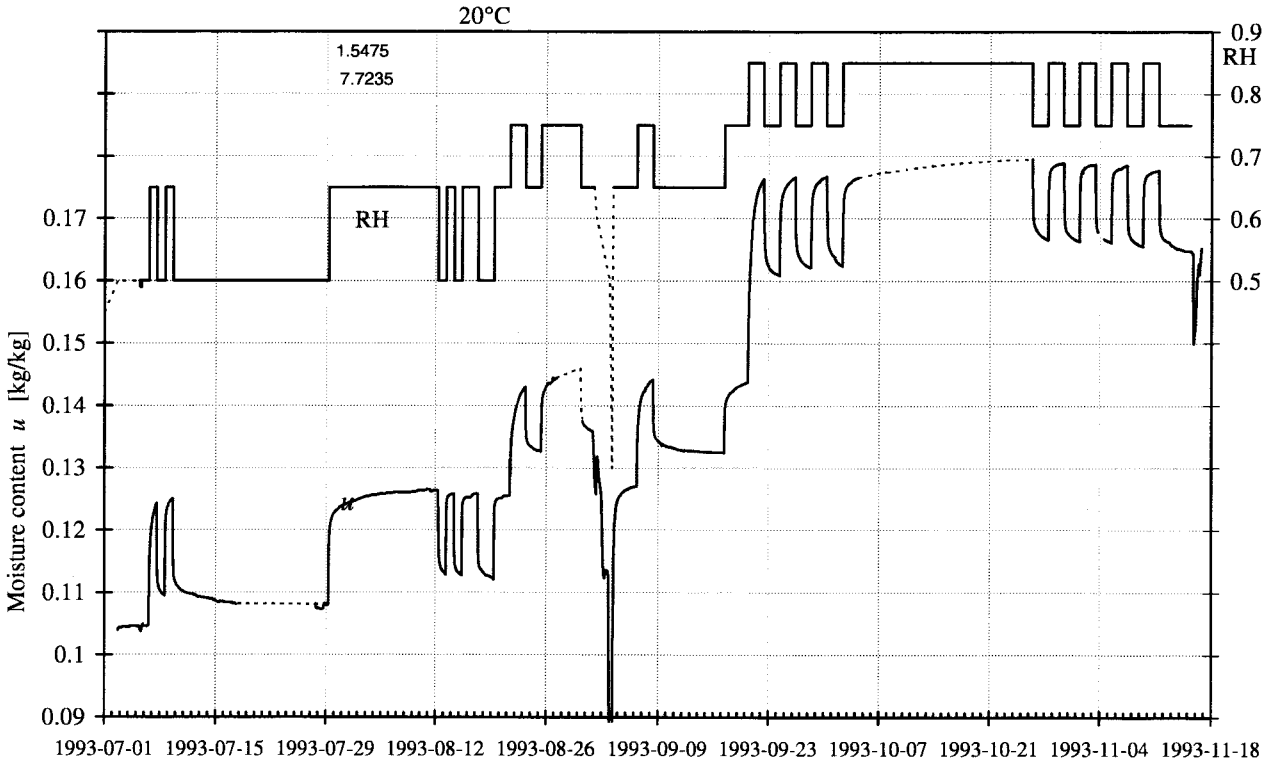

Figure 6.36 Survey of sorption response in the forth series, Sample 3.

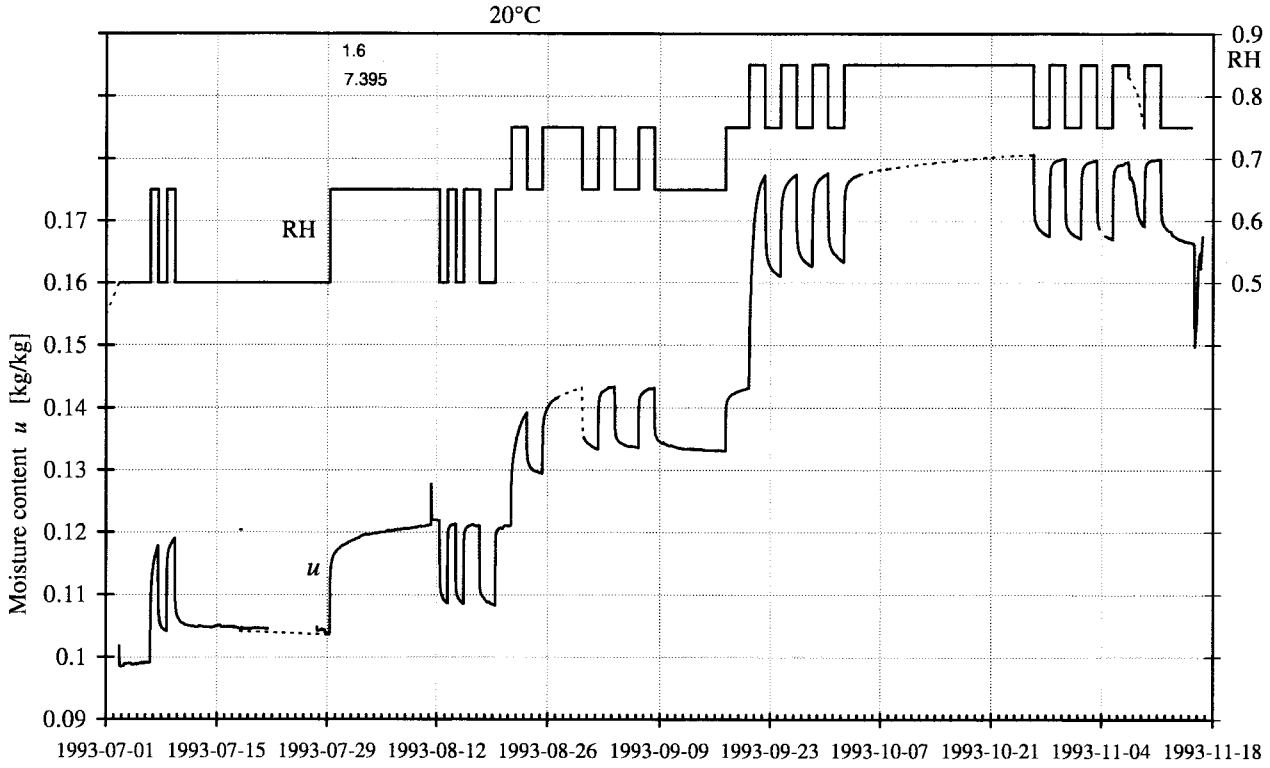

Figure 6.37 Survey of sorption response in the forth series, Sample 4, minor differences in RH from Sample 3 in Figure 6.36.

6.4.1 Cyclic steps between 50% to 65% and 65% to 75% RH

The conditions for the samples preceding this fourth series were as follows. Sample 3 was subjected to desorption to 35% RH followed by an absorption step to 45% RH in the third series. It was then exposed to room climate for 1½ months (an average RH of 50% is estimated). Sample 4 had desorption to 45% RH, and was then exposed to room climate for 2 months.

The sorption responses are shown in Figure 6.38 for Sample 3 and in Figure 6.39 for Sample 4. The swelling responses are shown in Figure 6.40.

The first parts of the series involve cycles between 50% and 65% RH. They were performed with a daily step change. After a few steps, the RH-level was kept constant at 50% for a longer period. A part of this time the control of the RH was left unattended and deviations were later found, but the RH-level was closely monitored some hours before the next step to 65% RH. This level was then kept for a long period. After that, cycles between 50% and 65% RH with a daily step change were repeated, followed by the same RH-steps with two days interval. The cycle time was thus 96 hours. This cycle time was chosen to be suitable and have been widely used in the following measurements.

After the cycles between 50% and 65%, cycles were performed at a higher level, 65% to 75% RH. Due to a mistake, the chamber containing Sample 3 together with the samples for swelling measurements got a short, very dry period (1993–09–02). However, the chamber containing Sample 4 was not affected. Comparison can be made for the subsequent sorption responses with different preconditions.

Generally, absorption steps to a previously not attained RH-level have resulted in large effects of retarded sorption. This is for instance the case for the step to 75% RH for the first time in this part of the measurements.

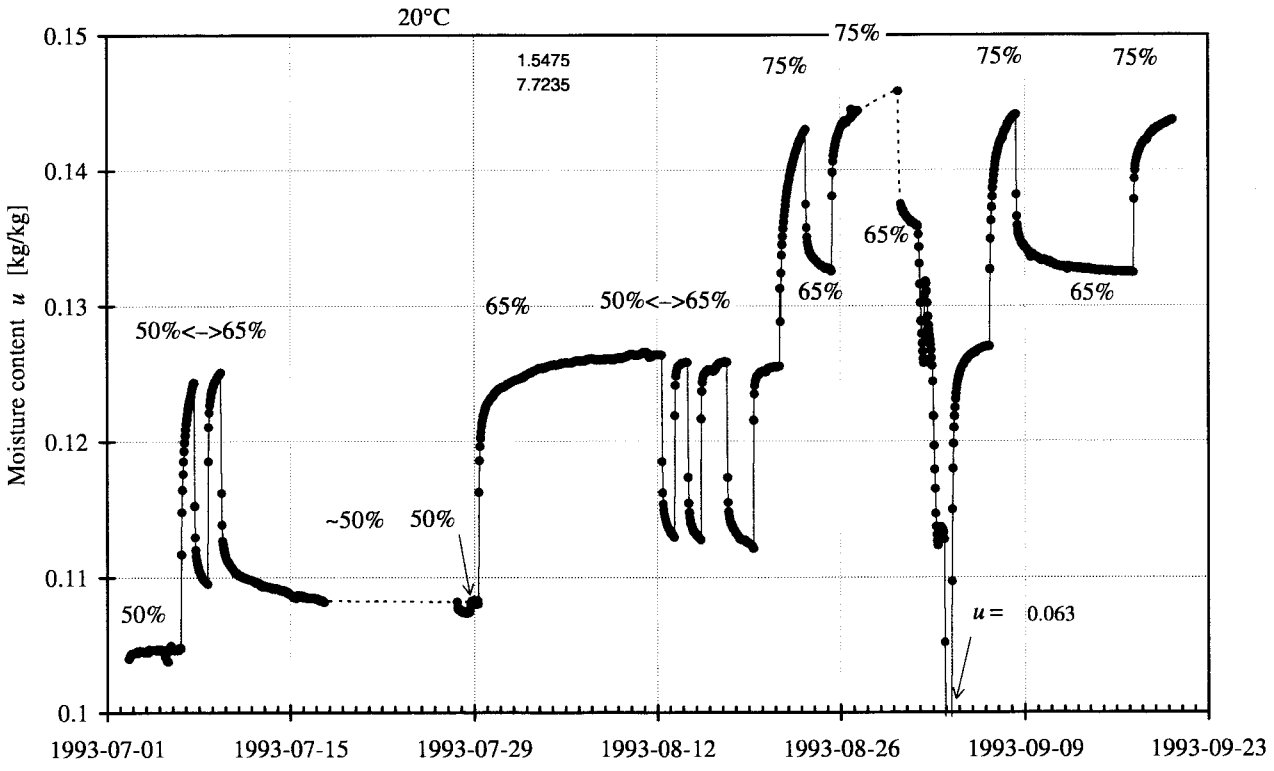

Figure 6.38 Sorption response, Sample 3, 50% ‹–› 65% and 65% ‹–› 75% cyclic RH-steps.

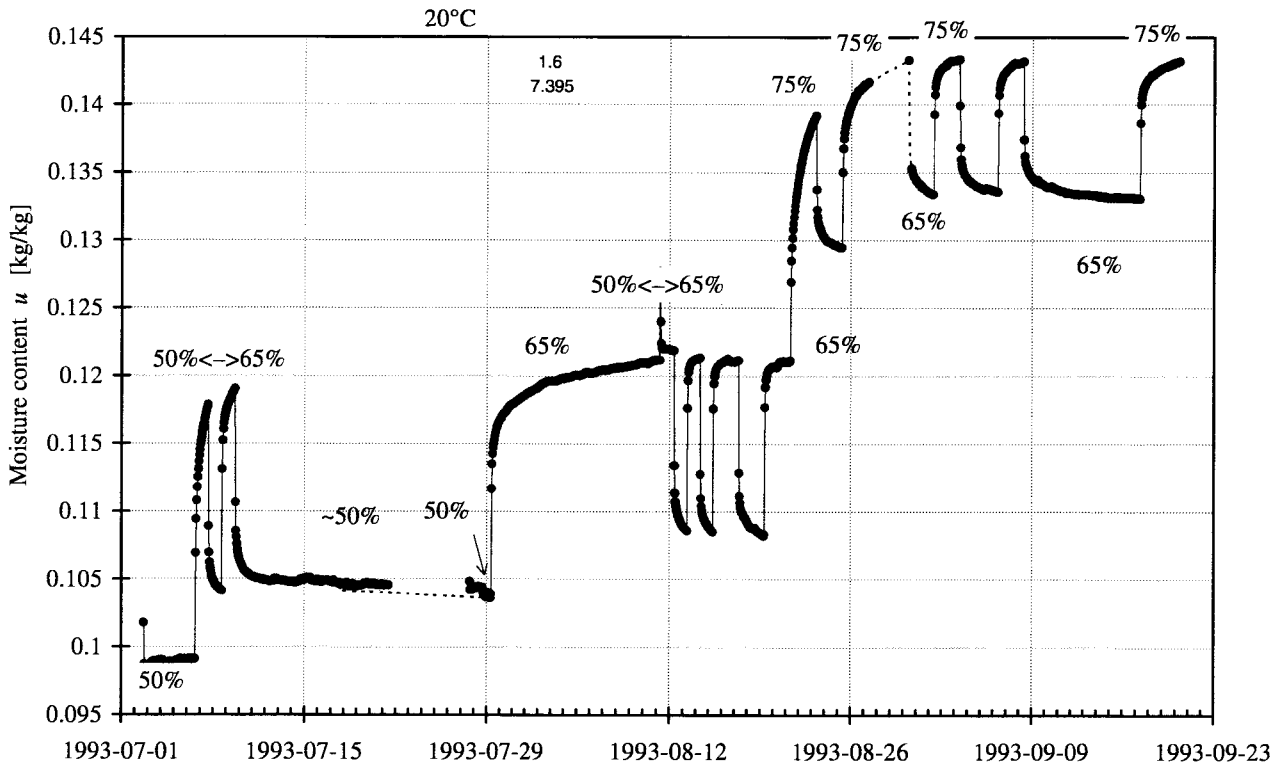

Figure 6.39 Sorption response, Sample 4, 50% ‹–› 65% and 65% ‹–› 75% cyclic RH-steps.

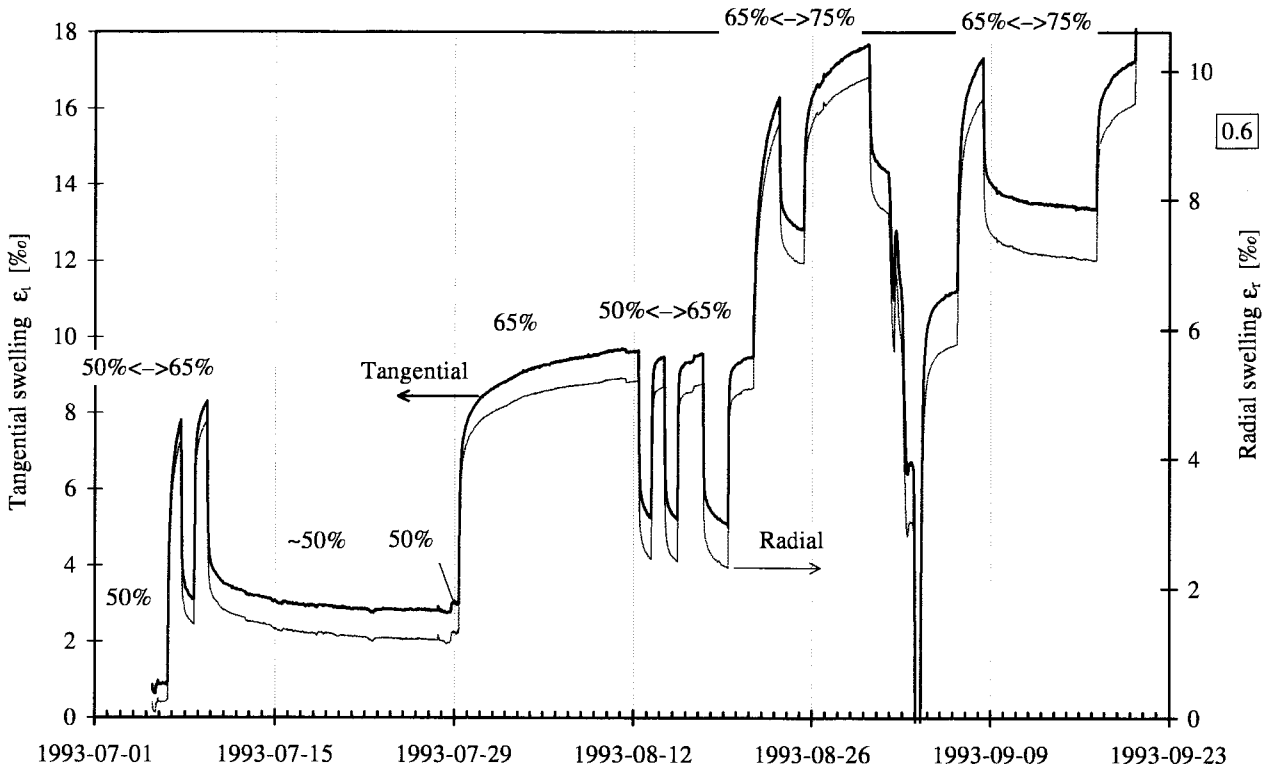

Figure 6.40 Tangential and radial swelling responses, 50% ‹–› 65% and 65% ‹–› 75% cyclic RH-steps.

6.4.2 Cyclic steps between 75% and 85% RH

In this part of the series, several cycles of steps between 75% and 85% RH were performed. The sorption responses are shown in Figure 6.41 for Sample 3 and in Figure 6.42 for Sample 4. The swelling responses are shown in Figure 6.43. The first cycles were preceded by an absorption step and the last cycles was preceded by a long period at 85% RH. The shapes of the sorption response curves are different for these two situations. A diagram with parallel comparison with these two cycles are made in Section 7.1.

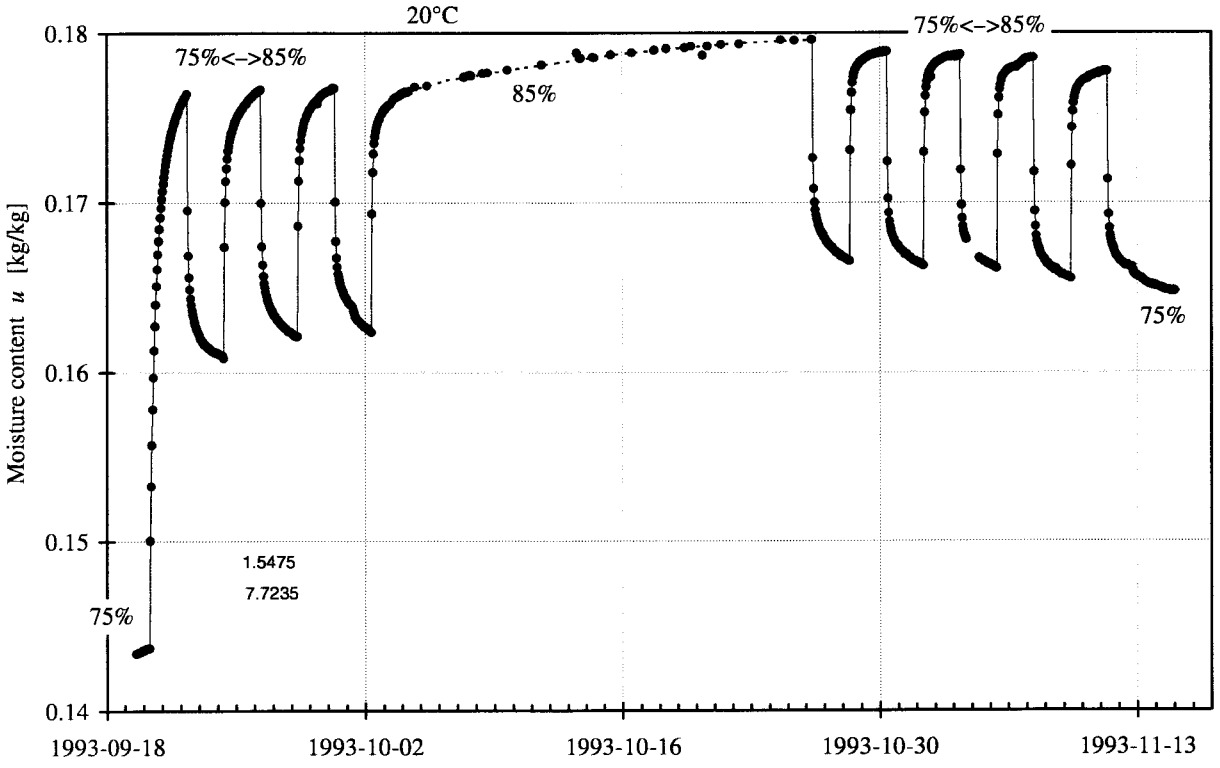

Figure 6.41 Sorption response, Sample 3, 75% ↔ 85% cyclic RH-steps.

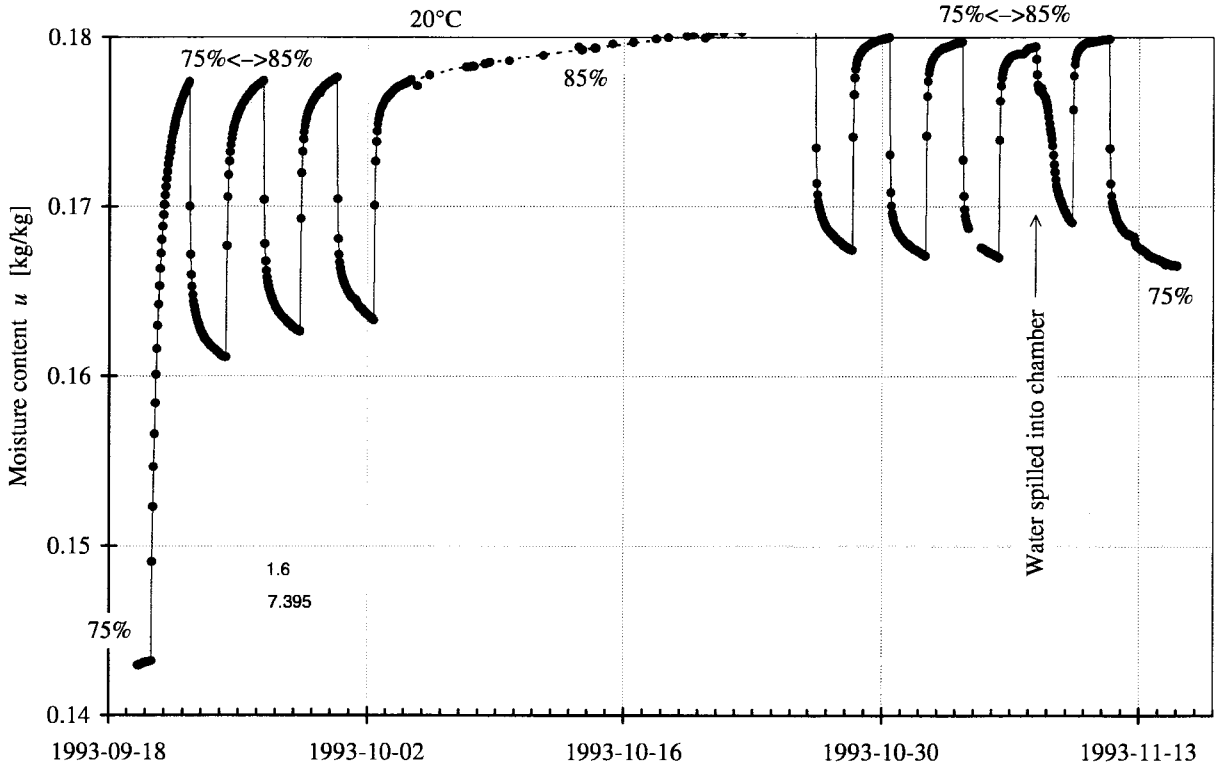

Figure 6.42 Sorption response, Sample 4, 75% <–> 85% cyclic RH-steps.

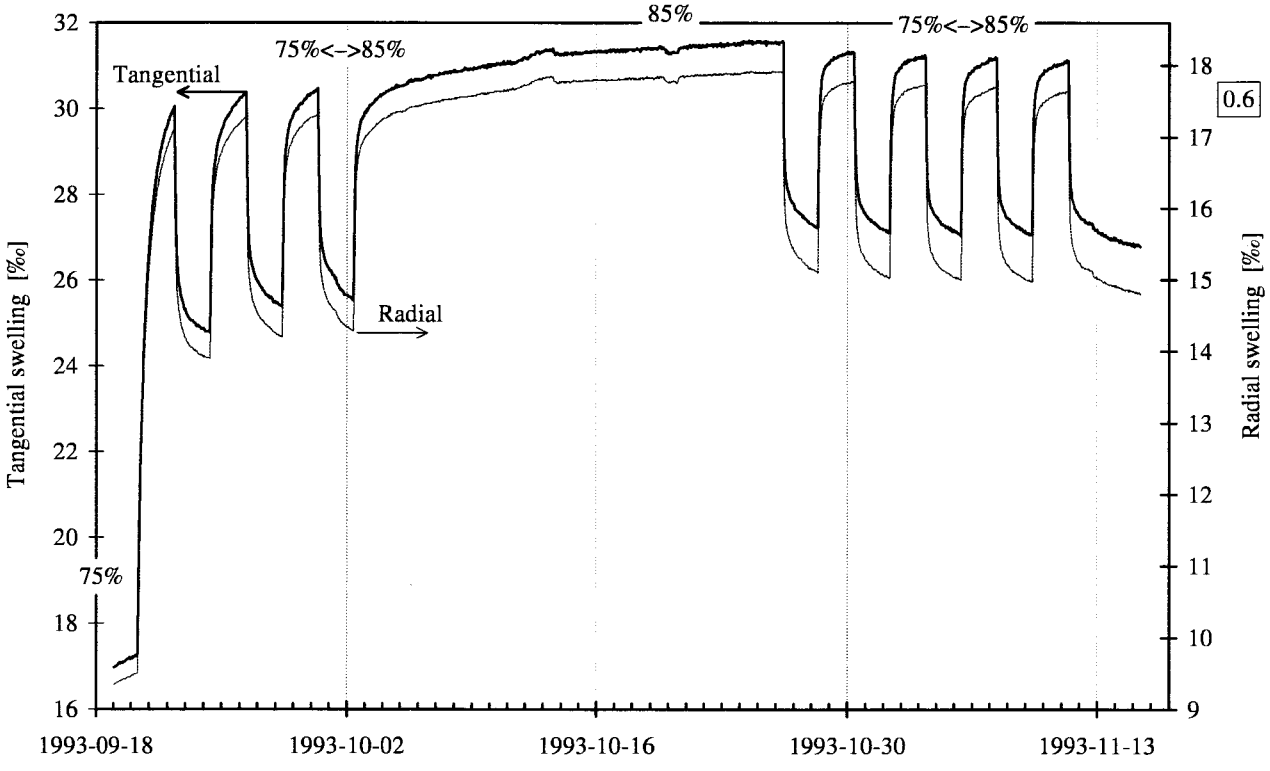

Figure 6.43 Tangential and radial swelling responses, 75% <–> 85% cyclic RH-steps.

6.5 The fifth series

New in the following fifth series compared to the previous ones is that the measurements were performed at 5°C instead of at 20°C. The sequence of relative humidities is shown in Figure 5.8. The RH-levels are comparatively high. This, in combination with the low temperature, results in profound effects of retarded sorption. Overviews of the sorption response is shown in Figure 6.44 for Sample 3 and in Figure 6.45 for Sample 4. The series is a direct continuation of the fourth, but starts with an unintentional dip in RH when the cooling device was started up for the first time.

An uneven temperature in the water bath, surrounding the chambers and condensers, resulted in a drop in the RH at the start-up of an external cooling system. This could be explained in the following way. An outline of the two-pressure RH-generator is shown in Figure 2.6. The cause of the drop in humidity is that, when one part of the condenser is cooler than the rest, the saturated air is depleted of moisture when passing the cool part and the saturation moisture content in the air is from then on determined by the lowest temperature during the passage. The connecting tubing to the water bath was too narrow to allow sufficient circulation to the external cooling system. The restricting tubing to the water bath was increased, and it was possible to use the full capacity of the circulation pump in the external cooling system. This was not totally sufficient however, to achieve full circulation in the water bath inside the apparatus. This was not discovered until the temperature was changed at the beginning of the sixth series.

The compressor for the air supply had a breakdown (1993-12-31), and no air entered the chambers for three days. Judging from the recorded changes in moisture contents, the RH-levels was only falling gradually with an estimated four percent, when the RH-control again was restored.

The same RH-sequence was intended for both samples. Water was however spilled into the chamber containing Sample 4 (Due to an ill-placed pressure gage of the water-column type, and the arrangement of the top lid). The chamber was opened and Sample 4 was subjected to room climate for 5 minutes, during which time the water in the chamber was wiped off.

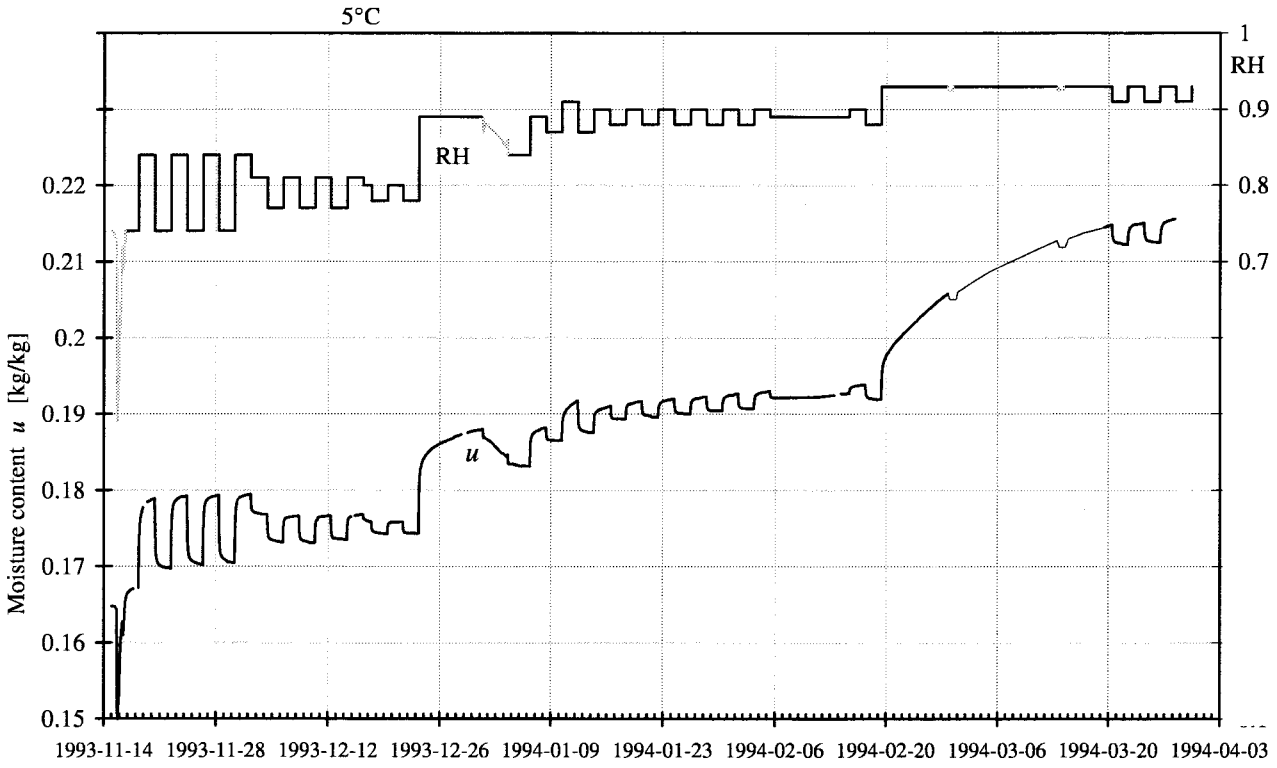

Figure 6.44 Survey of sorption response in the fifth series, Sample 3.

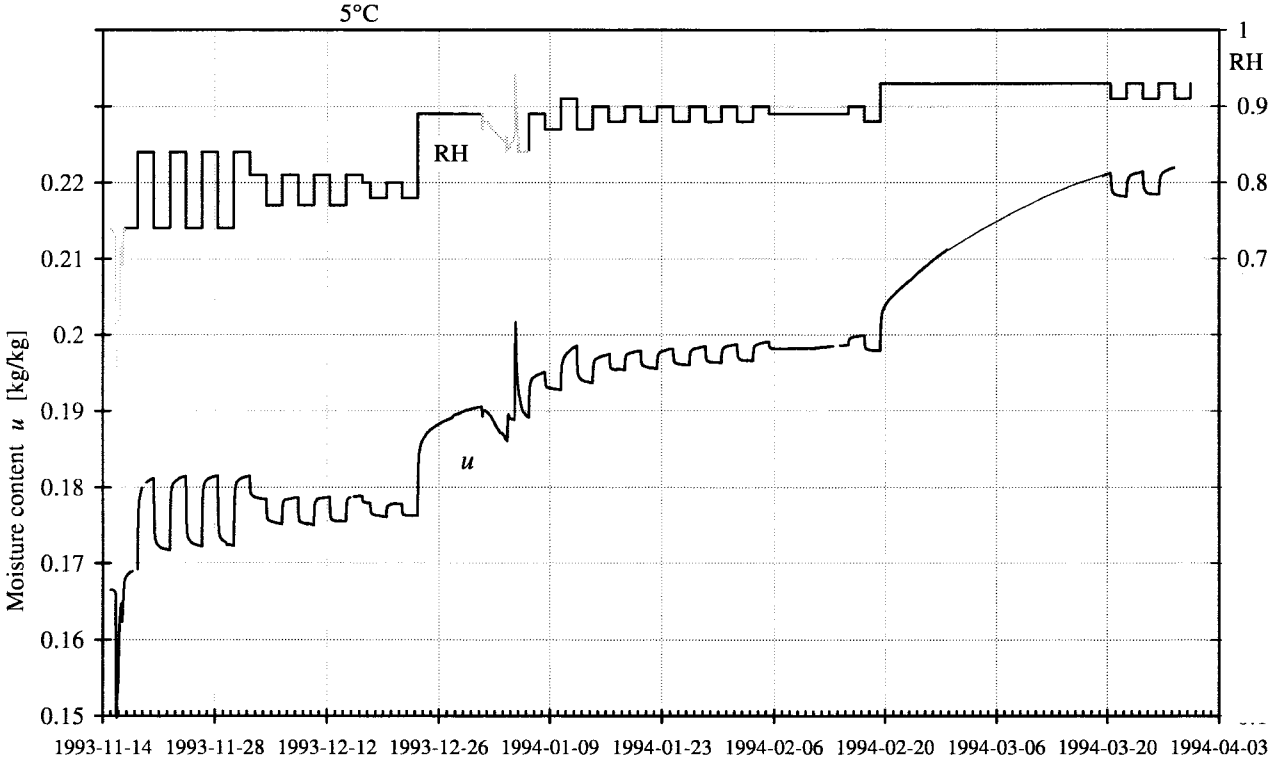

Figure 6.45 Survey of sorption response in the fifth series, Sample 4, minor differences in RH from Sample 3 in Figure 6.44.

6.5.1 Cyclic steps of different amplitude

After the unintentional low RH, cyclic steps were performed with three different amplitudes, but with the same average of relative humidity, 79%. See Figure 6.46 and Figure 6.47. The tangential and radial swelling is shown in Figure 6.48. After the cyclic steps, a single absorption step to 89% RH was kept for a longer period. The period was interrupted by a breakdown of the supplying air compressor, but the samples still could stay protected inside the chambers with little RH-change. To some extent, this was a test that the exit openings from the chambers not were excessively wide.

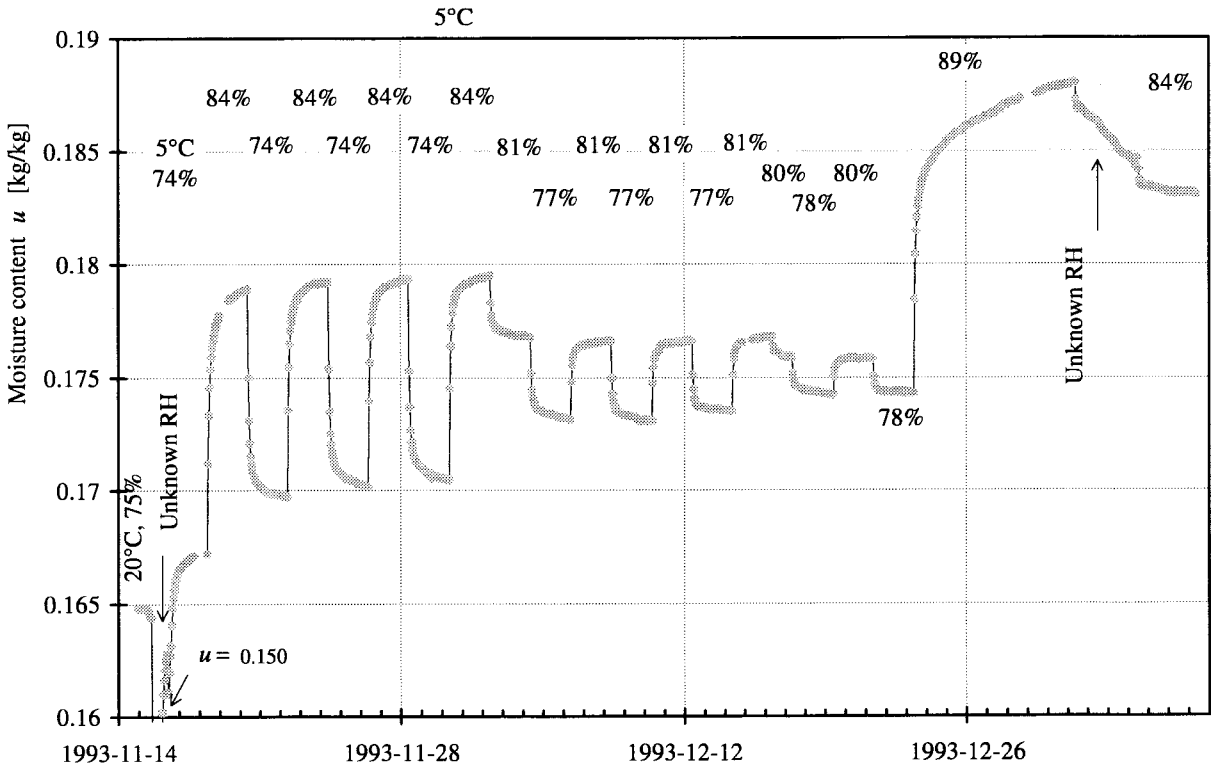

Figure 6.46 Sorption response, Sample 3, 74% ‹–› 84% and 77% ‹–› 81% cyclic RH-steps.

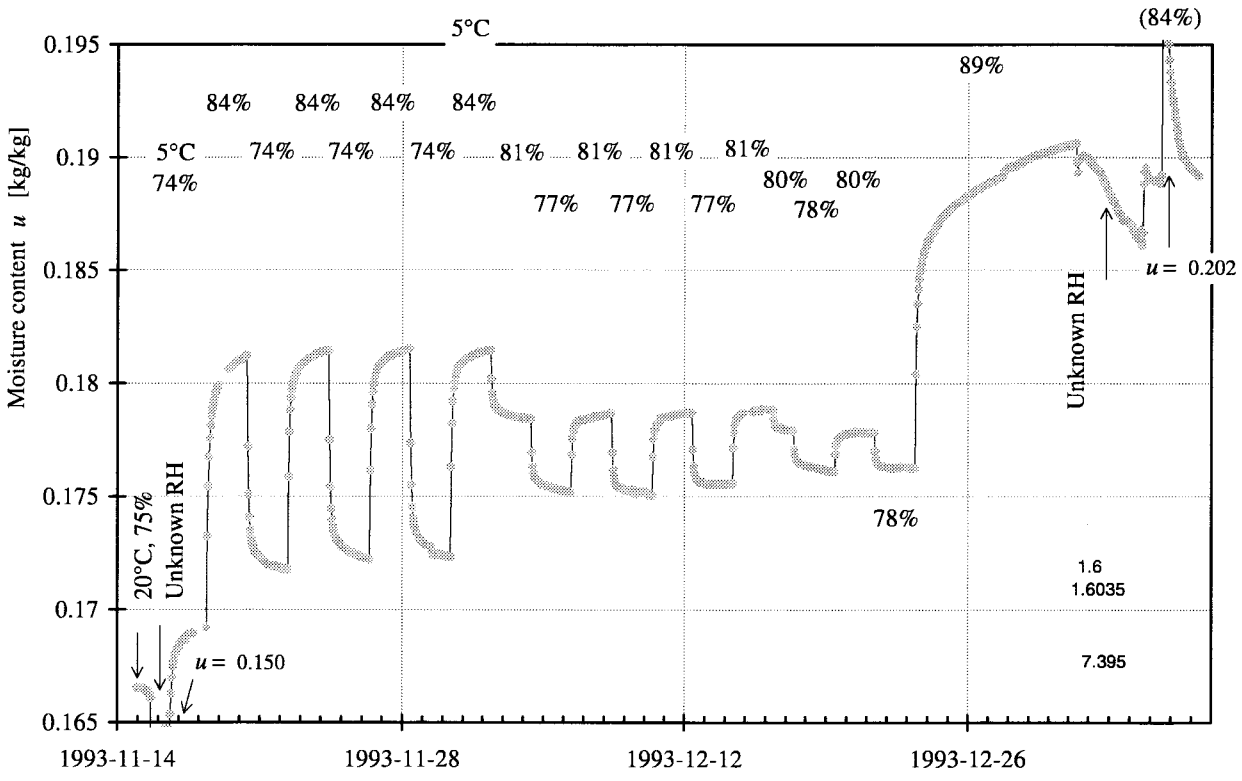

Figure 6.47 Sorption response, Sample 4, 74% ‹–› 84% and 77% ‹–› 81% cyclic RH-steps.

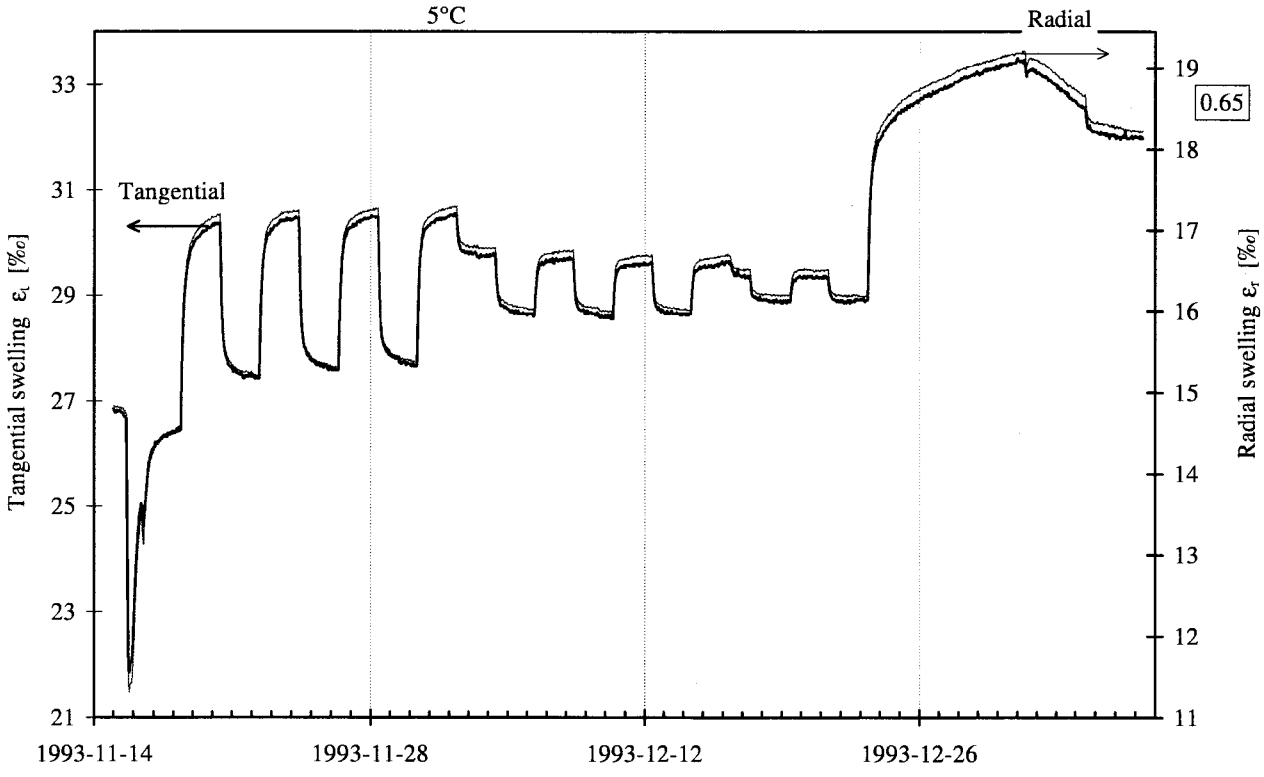

Figure 6.48 Tangential and radial swelling responses, 74% ‹–› 84% and 77% ‹–› 81% cyclic RH-steps.

6.5.2 Small cyclic steps at high RH

The sorption response curves for the sequence of small cyclic steps at high relative humidity are shown in Figure 6.49 for Sample 3 and in Figure 6.50 for Sample 4. The response curves for swelling are shown in Figure 6.51.

The temperature and moisture pulse at the start of the response for Sample 4 in Figure 6.50 was unintentional and caused by spilled water. The chamber had to be opened and Sample 4 was subjected to room climate during 5 minutes, while the water was wiped off. The very high peak in moisture uptake after that the sample was put back into the chamber is unexpected, but it could not be ruled out that a thin water film still was remaining on the surfaces of the chamber. The sorption responses for Sample 4 is compared with Sample 3 in a diagram in order to evaluate the impact from the pulse in chapter 7, Figure 7.9.

Cyclic steps, mainly between 88% and 90% RH, were performed. The samples had earlier been subjected to absorption in general terms for a long period. This seems to be reflected in the drift towards a higher moisture content, on which the cyclic step responses are superimposed. This is also the precondition for the following single step to 93% RH in the next section.

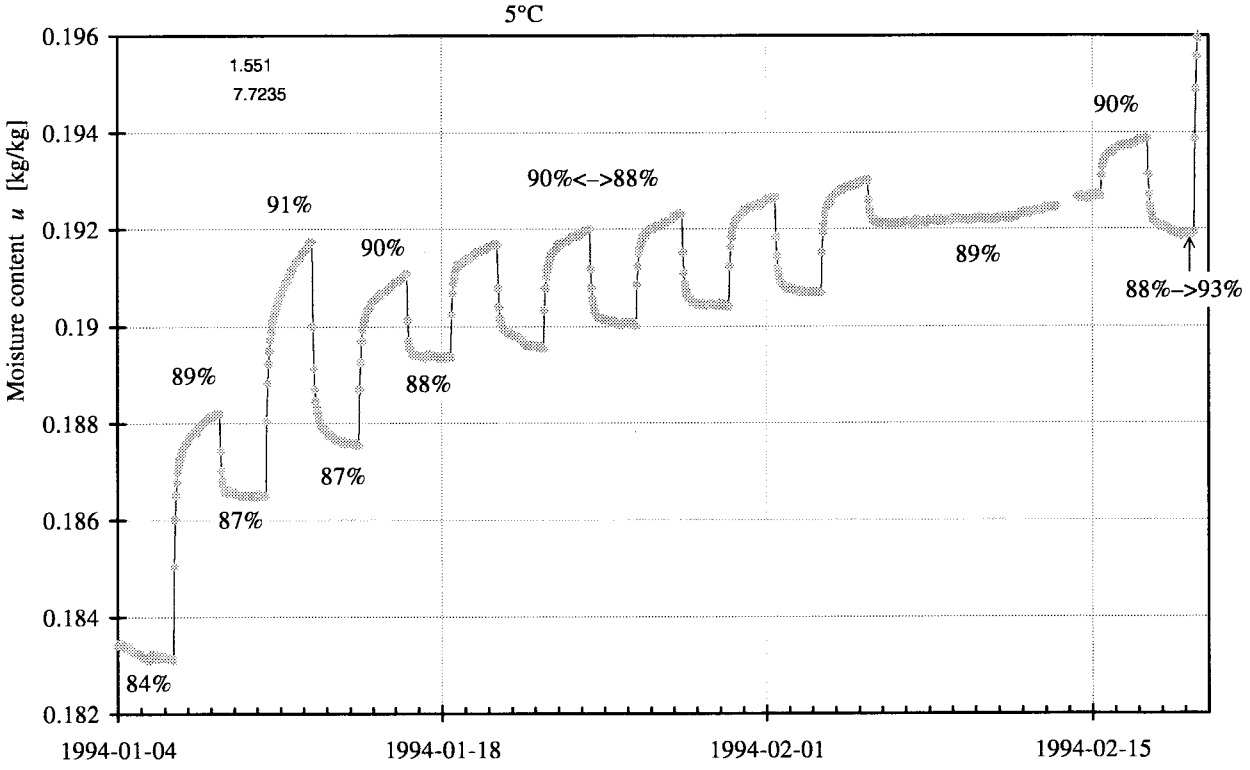

Figure 6.49 Sorption response, Sample 3, 88% <–> 90% cyclic RH-steps.

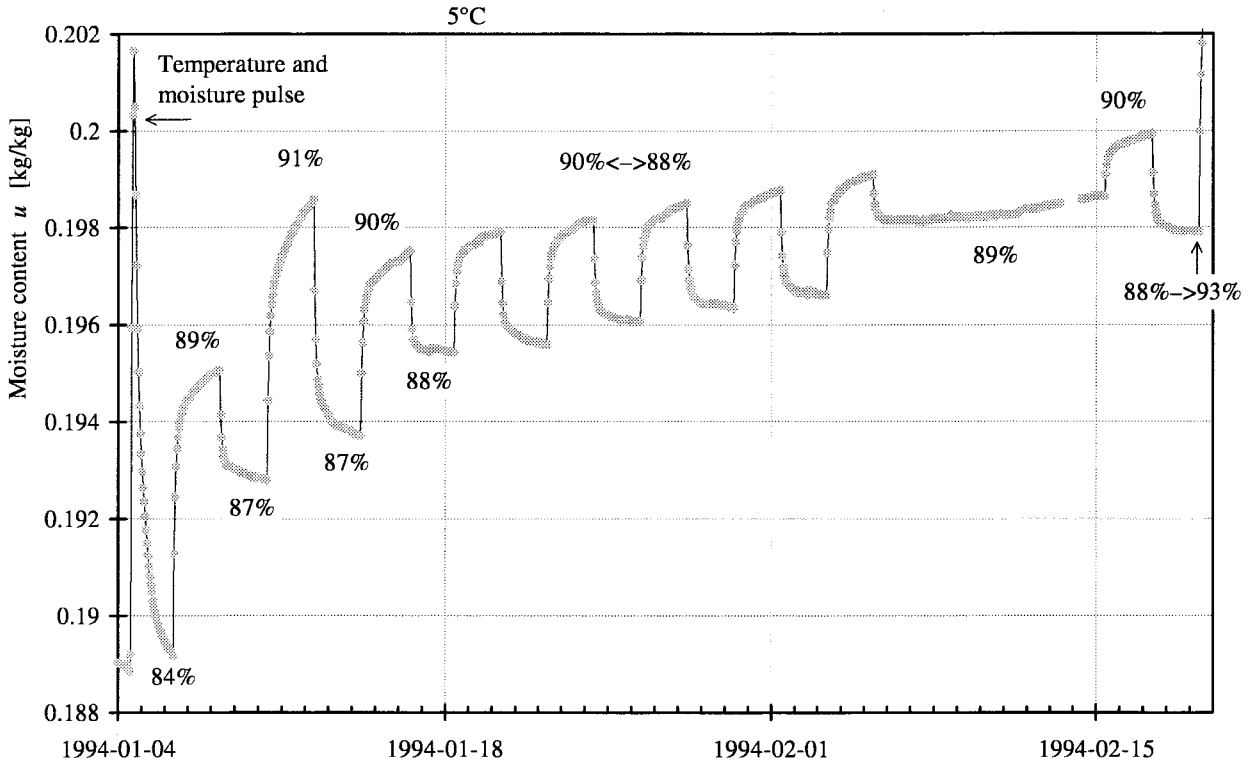

Figure 6.50 Sorption response, Sample 4, 88% ↔ 90% cyclic RH-steps.

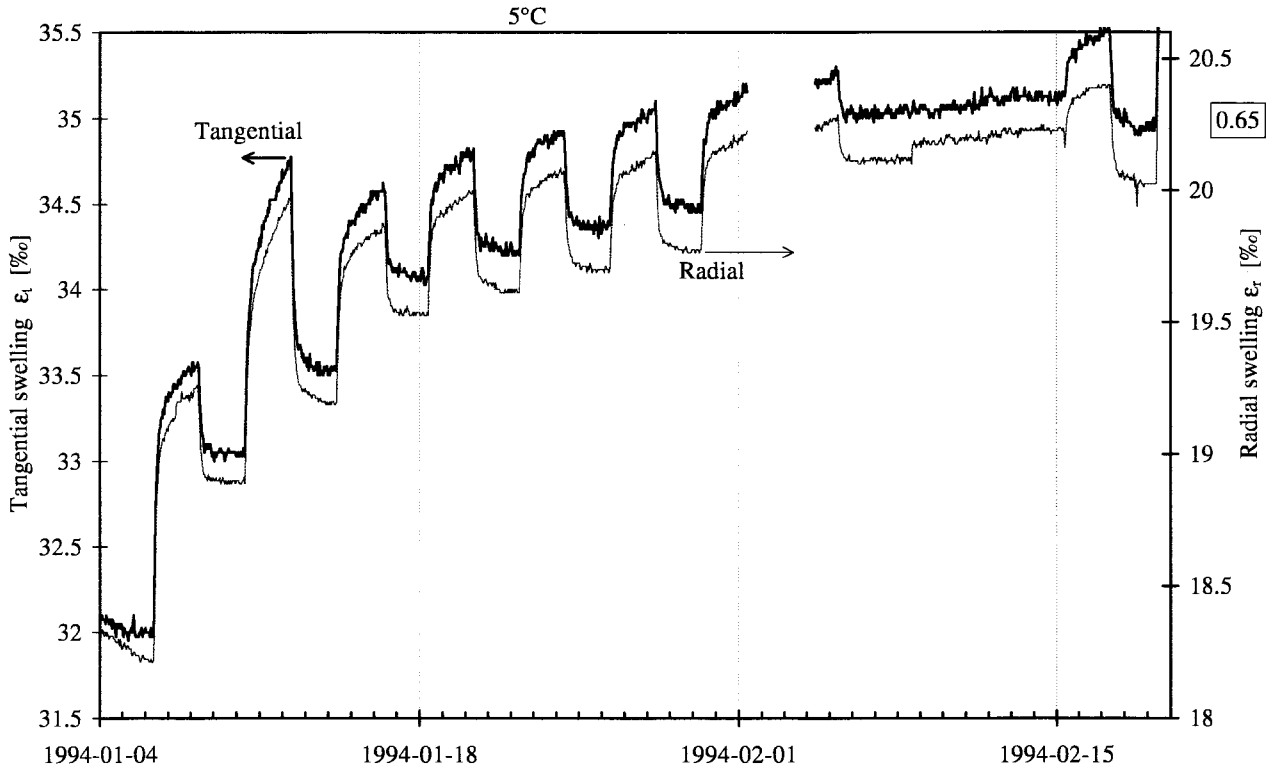

Figure 6.51 Tangential and radial swelling responses, 88% ↔ 90% cyclic RH-steps.

6.5.3 A single step at high RH

The response curves for the last part in this series is shown in Figure 6.52 for Sample 3 and in Figure 6.53 for Sample 4. The response curves for swelling are shown in Figure 6.54.

The sorption response was followed for a long time (29 days). The retarded sorption is very large. It seems as the combined action of low temperature, high relative humidity and a step to a previously not attained RH is the cause of this. Two small disturbances in the RH-level occurred for Sample 3. During the last part of the single step, the sorption was only recorded manually at irregular intervals, the swelling was however logged continuously.

The cyclic steps at the end of the series are described in the next series, where temperature shifts are made.

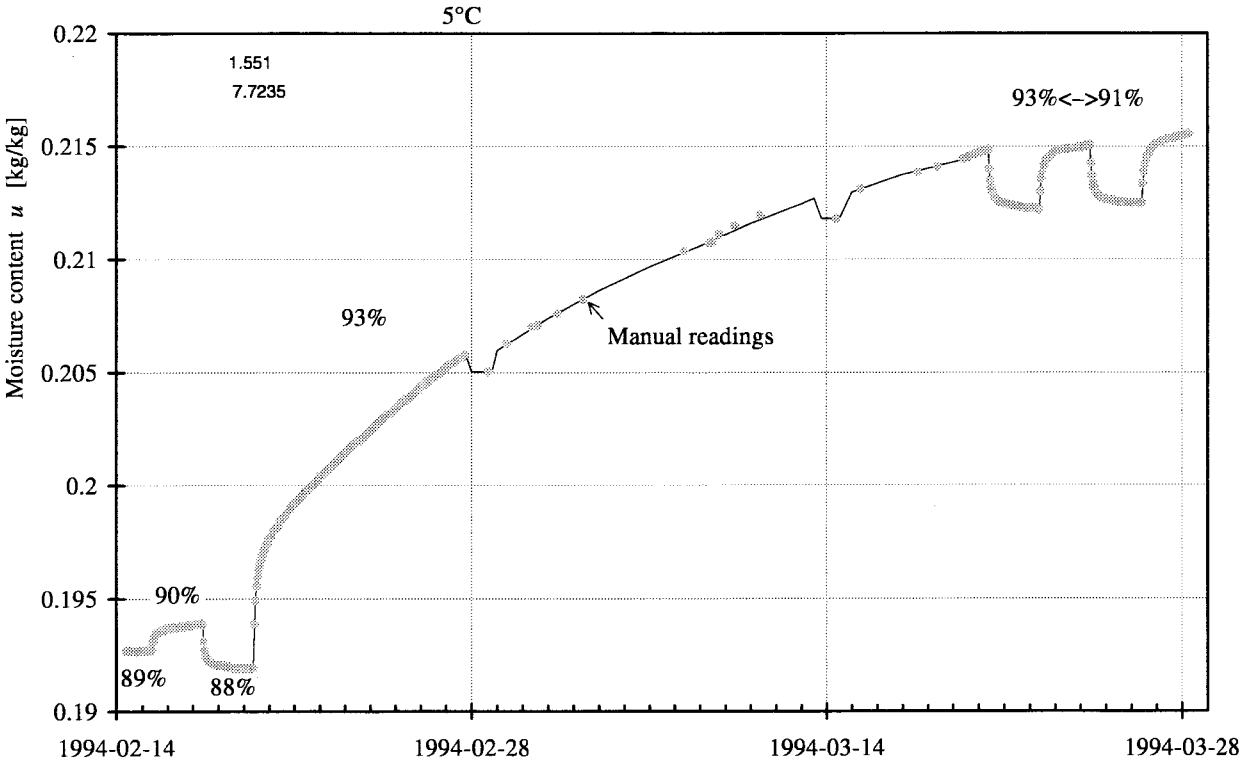

Figure 6.52 Sorption response for an absorption step to 93%, Sample 3.

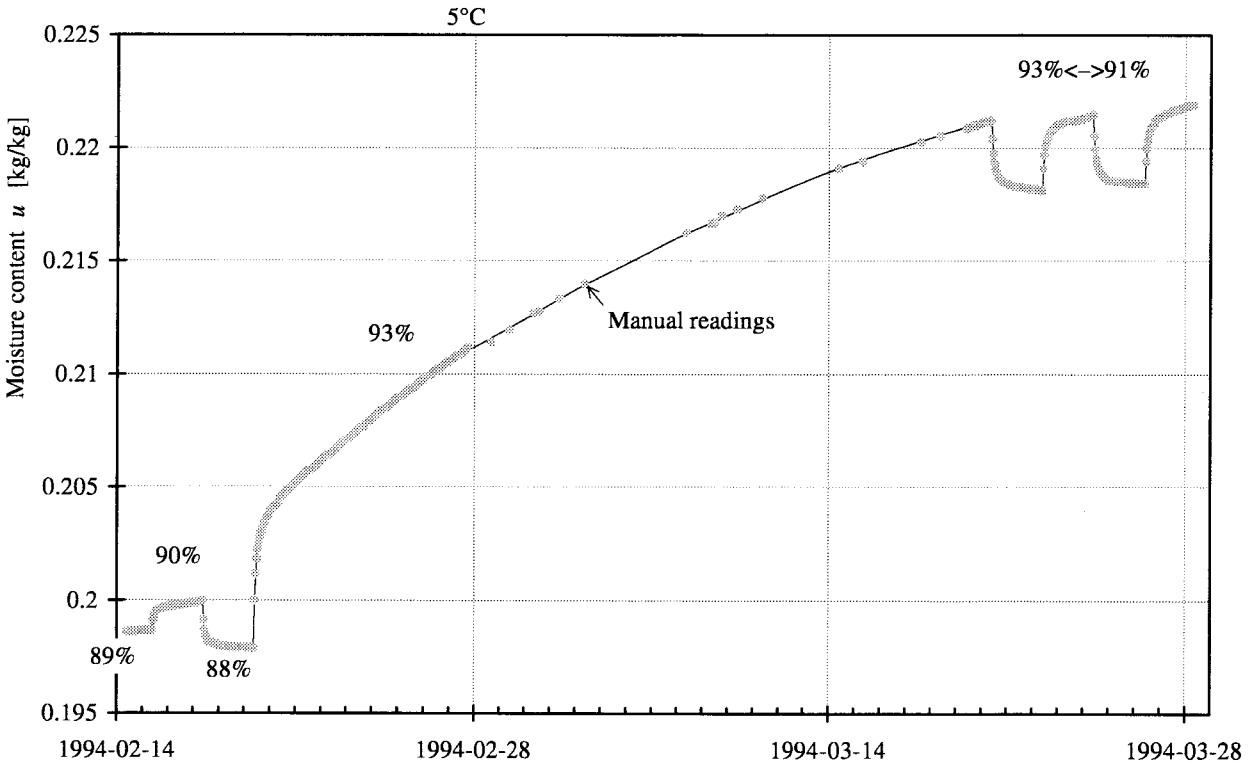

Figure 6.53 Sorption response for an absorption step to 93%, Sample 4.

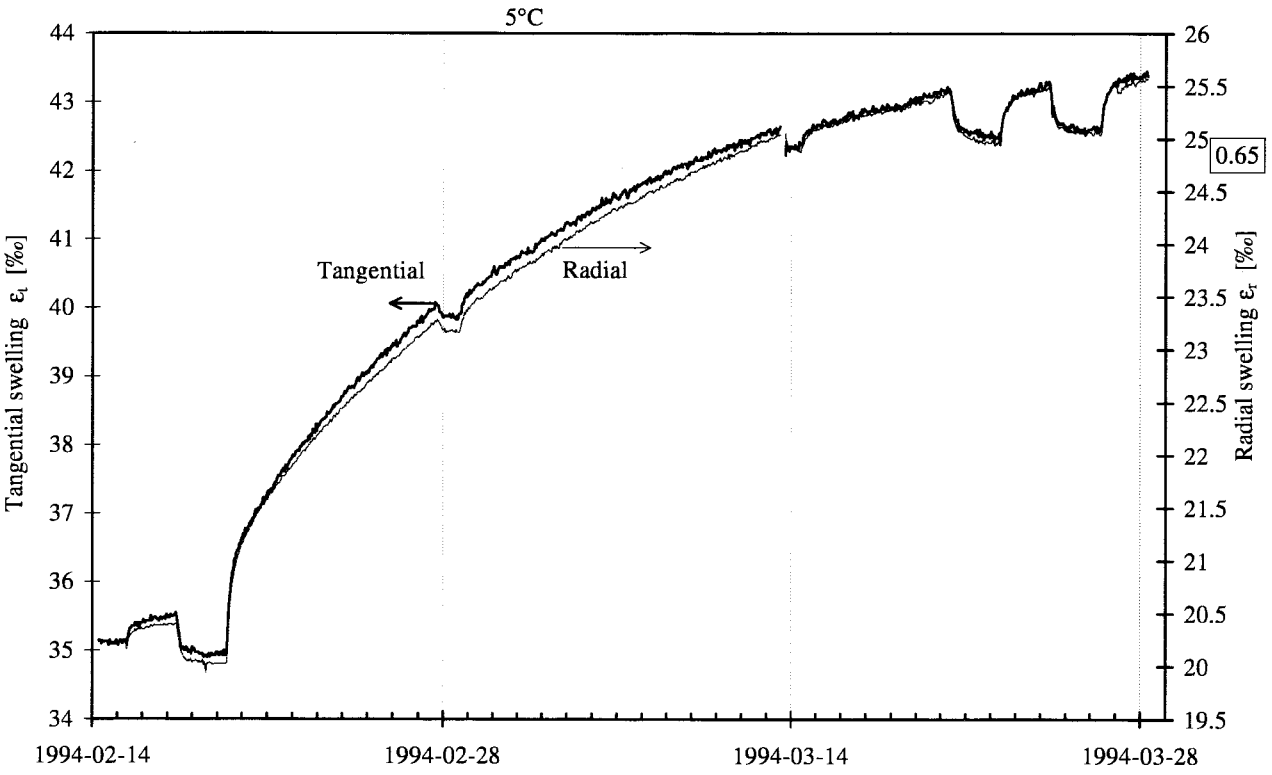

Figure 6.54 Tangential and radial swelling responses for an absorption step to 93%.

6.6 The sixth series

In the sixth series, primarily the influence on the sorption from temperature and temperature shifts was investigated. Overviews of the results from the measurements are shown in Figure 6.55 and in Figure 6.56. In the first part of the measurements, repeated cyclic steps were made: at 5°C, at 20°C and finally again at 5°C. This part is discussed in Section 6.6.1.

After this and a few desorption steps, the temperature dependence of the equilibrium moisture sorption curve was studied by making temperature shifts from 5°C to 20°C and back to 5°C. The RH was maintained at 85%. Substantial sorption effects were obtained.

At the end of the series, another temperature shift was made. This time the RH-level was adjusted according to an assumed temperature dependence for the sorption isotherm, so that a close to zero sorption during the shift was achieved. This gives an estimate in an other way of the temperature dependence of the sorption isotherm.

In this series, the measurements of swelling were failing.

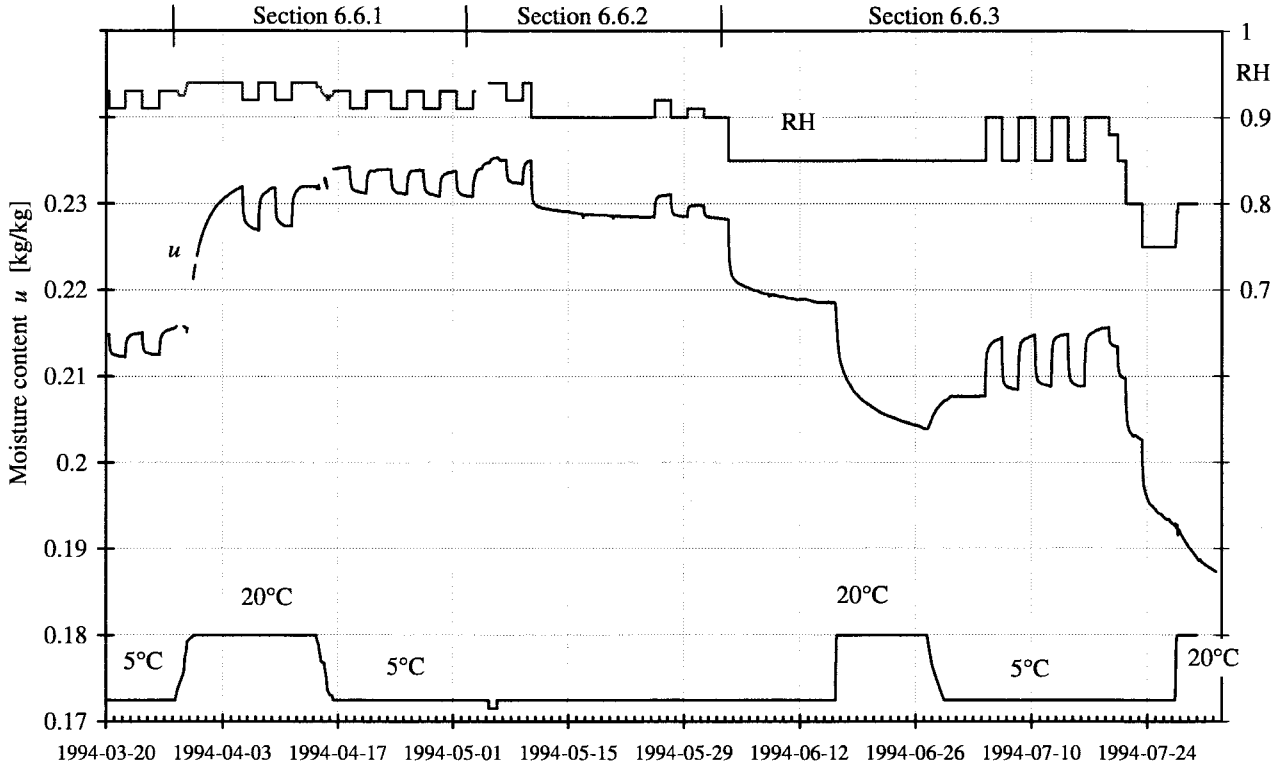

Figure 6.55 Survey of sorption response in the sixth series, Sample 3.

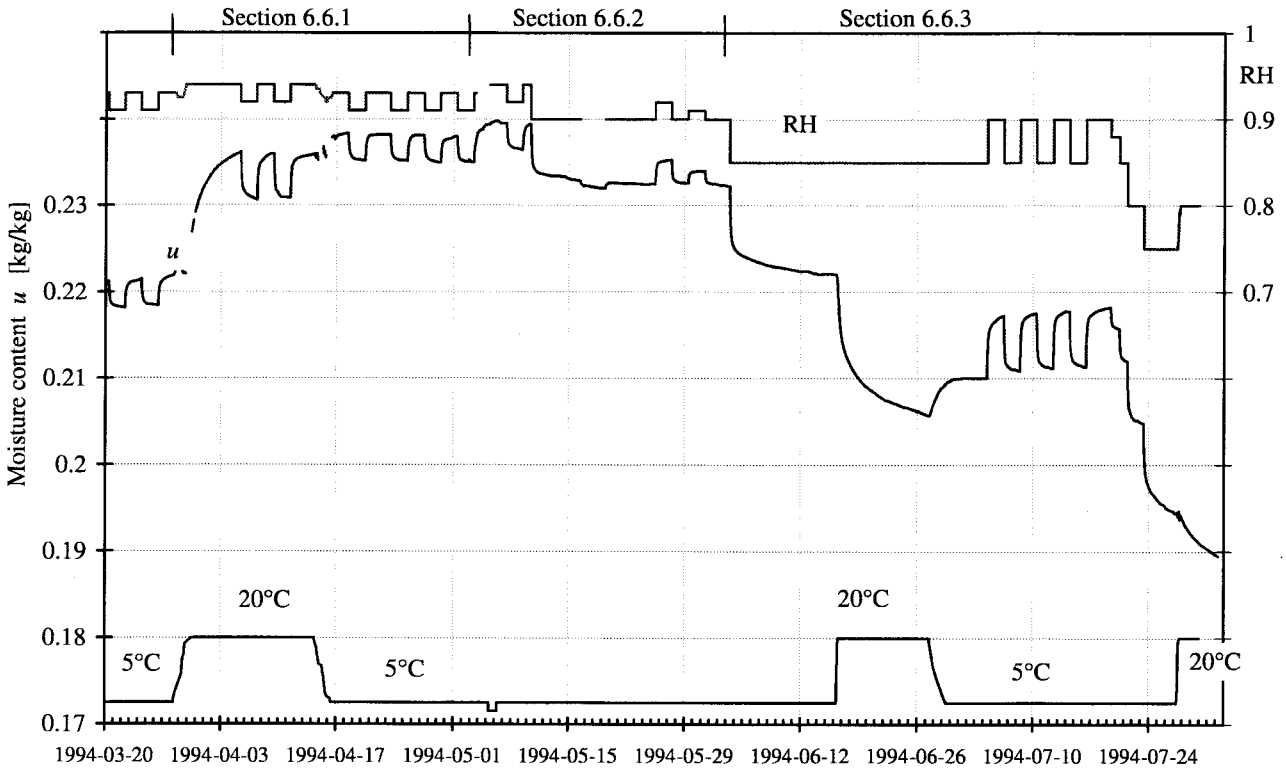

Figure 6.56 Survey of sorption response in the sixth series, Sample 4, minor differences in RH from Sample 3 in Figure 6.55.

6.6.1 Cycles at different temperature levels

This section starts by a temperature rise from 5°C to 20°C. At this temperature the same cycles as earlier were repeated. The temperature was again lowered to 5°C and the same cycles repeated once again.

When the temperature was changed to as low as 5°C for the first time, it was discovered that the mixing in the water bath was inadequate. The circulation from the cooling device was then enhanced. When the temperature was changed back to 20°C in this series, the RH still dropped somewhat. This is explained by uneven temperature distribution in the water bath surrounding the chambers and condensers, as described in Section 6.5. It was apparent that the entrance orifice to the water bath was not capable of inducing circulation. This was taken care of later, described in the next Section 6.6.2.

Based on the temperature dependence of the moisture equilibrium sorption curve, a higher temperature is expected to give a lower moisture content at the same RH. In this case the opposite takes place. Rising the temperature results in a large absorption, as seen in Figure 6.57 and Figure 6.58. When the same low temperature and the same cycles in RH are repeated (the last cycles in the diagrams), the level of the moisture content is much higher. It seems as the temperature shifts have triggered the wood to come to a different type of equilibrium.

There is an interesting difference of the shape of the response curves for cyclic steps at low and high temperature. All steps have a 2% amplitude in relative humidity, still the sorption amplitude is much larger at the higher temperature. Diagrams with parallel comparison with these two cycles at different temperatures are made in Chapter 7, Figures 7.7 and 7.8.

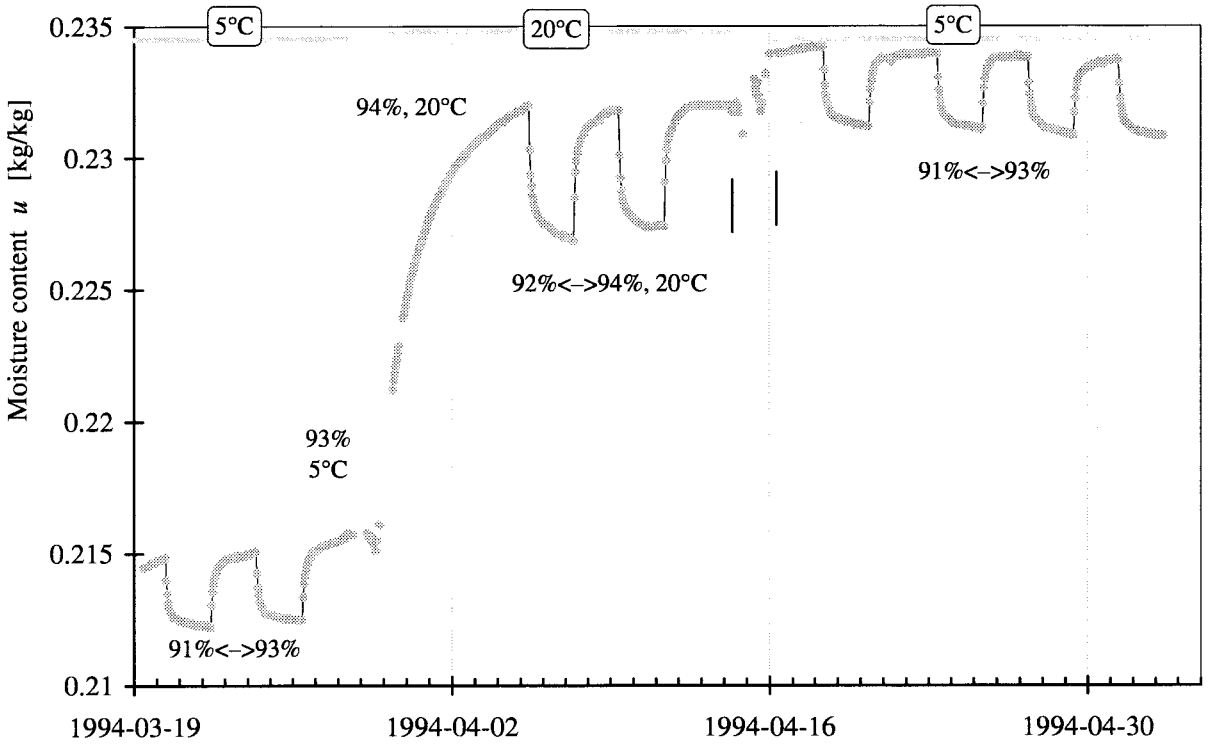

Figure 6.57 Sorption response for cyclic RH-steps with temperature shifts, Sample 3.

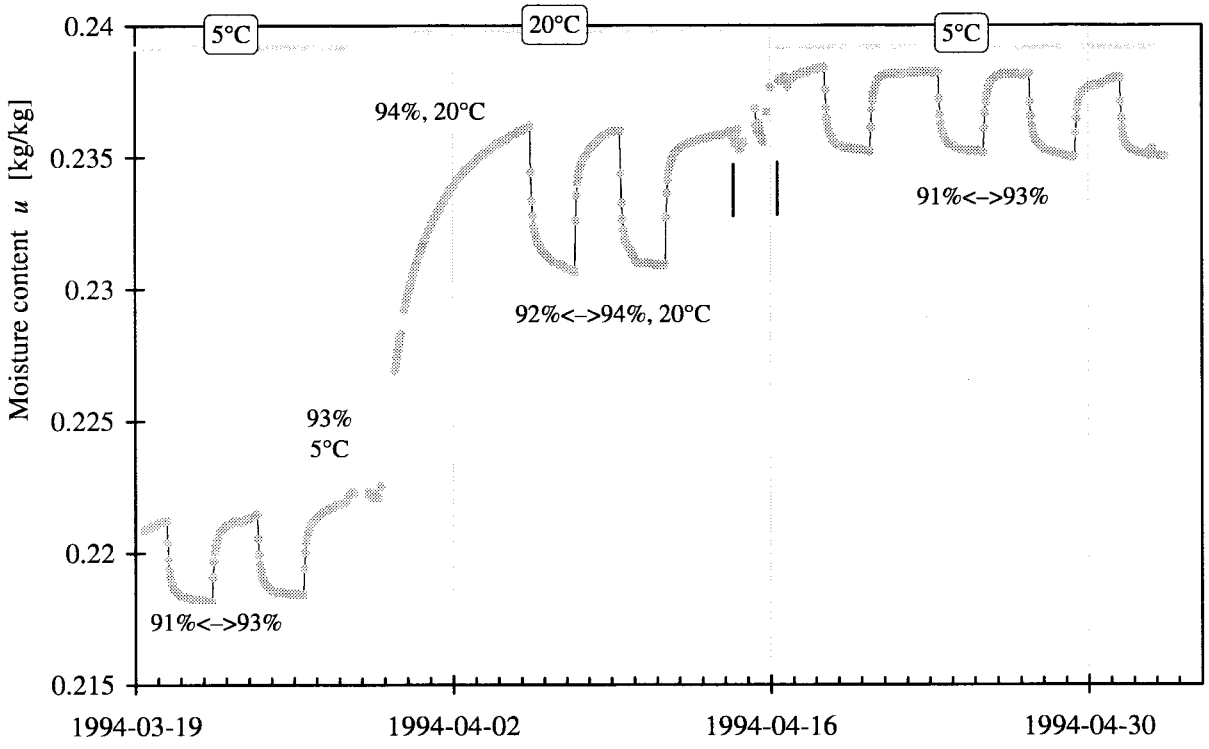

Figure 6.58 Sorption response for cyclic RH-steps with temperature shifts, Sample 4.

6.6.2 A few sorption steps at 5°C

In this section adjustment was made to the apparatus and sorption took place that basically was an indication of the function of the apparatus. The samples reached the highest moisture content and a desorption step was made that was followed for a rather long time.

During the measurements in this section the problem with inadequate circulation in the water bath surrounding the chambers was taken care of. The circulating water from the pump in the cooling device was injected through a tube with tapered section into the central part of the water volume. The water is leaving the end of the tube at high speed and is inducing an effective agitation in the water volume. A short change in temperature from 5°C to 3°C and back, was made to verify that the cooling worked properly.

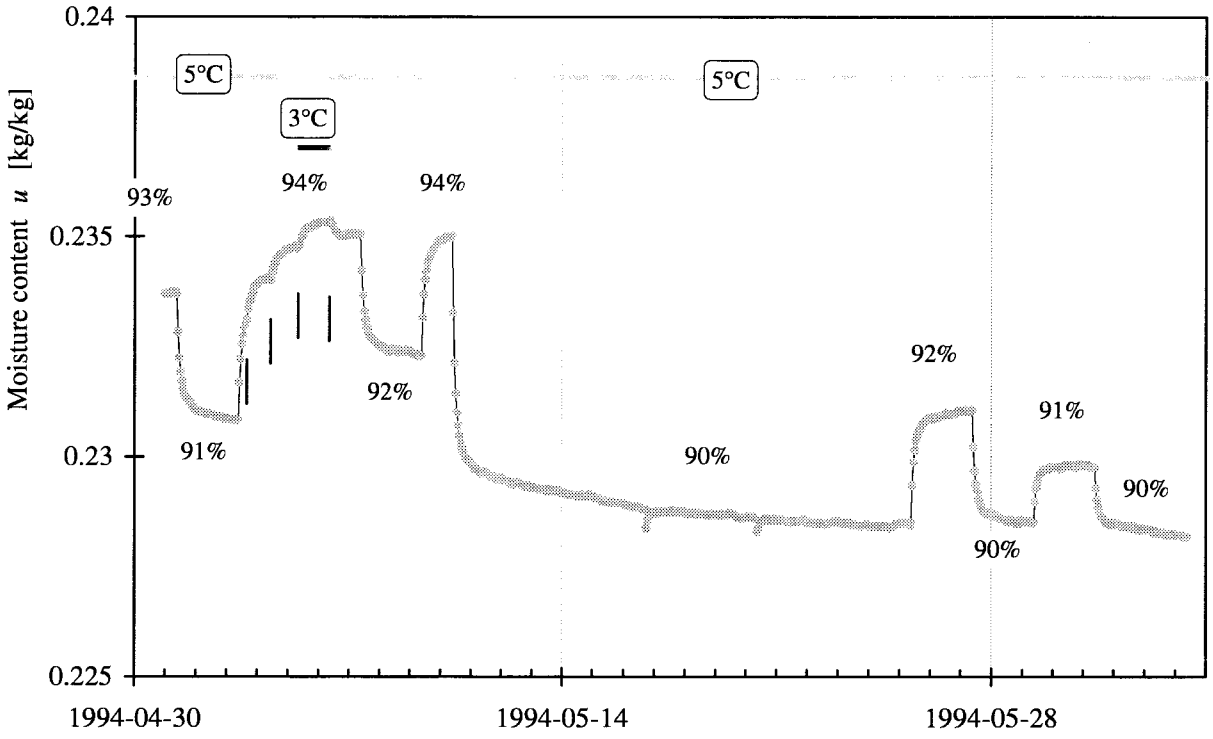

Figure 6.59 Sorption response for cyclic RH-steps in the 90% – 94% interval, 5°C, Sample 3.

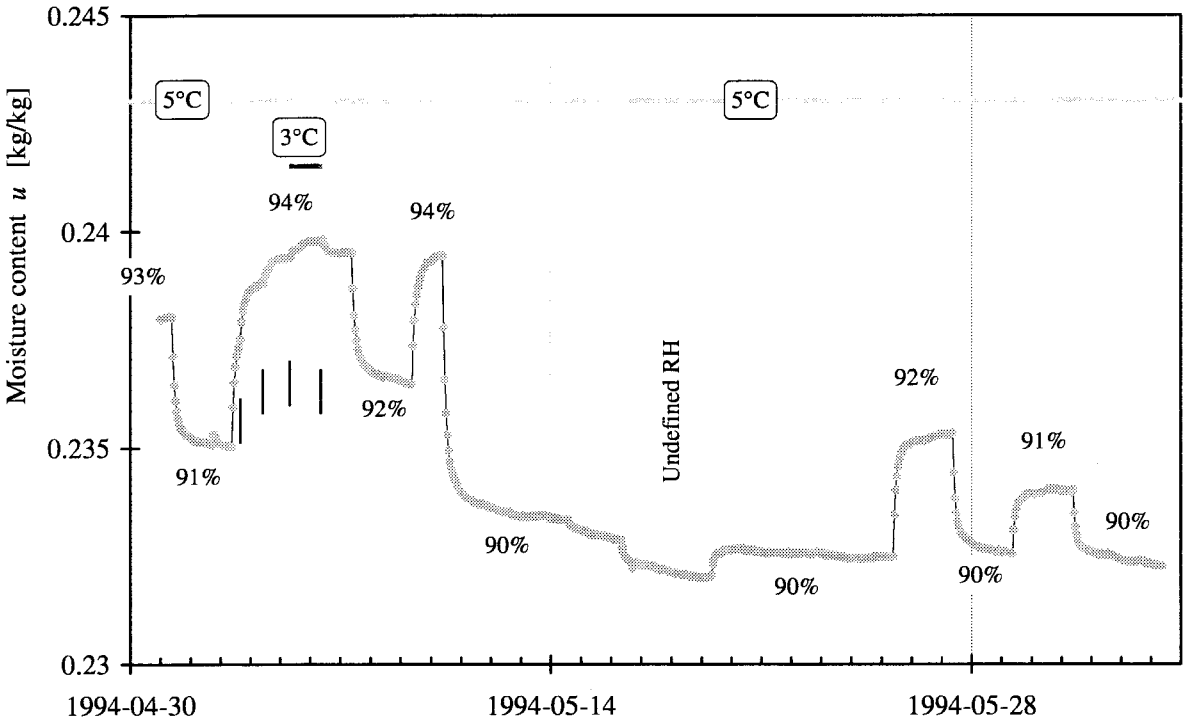

Figure 6.60 Sorption response for cyclic RH-steps in the 90% – 94% interval, 5°C, Sample 4.

6.6.3 Temperature shifts at constant RH and at adjusted RH to obtain zero sorption

The starting point for this section is marked at the top of the survey diagrams in Figure 6.55 and Figure 6.56.

The result from this part of the measurements are shown in Figure 6.61 for Sample 3 and Figure 6.62 for Sample 4. The desorption step in the previous measurements was continued by another desorption step from 90% to 85% RH. After 13 days, a shift in temperature from 5°C to 20°C was made. The relative humidity was maintained at 85%. The shift required 4 hours to do. A distinct and large desorption step with substantial drift was achieved. After 11 days the temperature was changed back to 5°C, still at constant RH. The shift took as long as 65 hours to accomplish, due to the large volume in the water bath and poor cooling capacity (ice temporarily forming?). The sorption came to a distinct equilibrium at a low moisture content shortly after the temperature shift was completed. This can be contrasted against the previous sorption response behaviour at the same temperature and RH, where the temperature shift was preceded by desorption steps.

The equilibrium at 85% RH was followed by several cyclic steps between 85% and 90% RH. This was followed by several desorption steps ending at 75% RH. The temperature was then shifted from 5°C to 20°C. As the temperature changed, the setting for the RH was manually altered according to the temperature dependence of the sorption isotherm. The assumed temperature dependence was 5% RH per 15°C. The purpose for this was to obtain zero sorption. This was successful, because the curves meet if they are extrapolated to a point at the time of change.

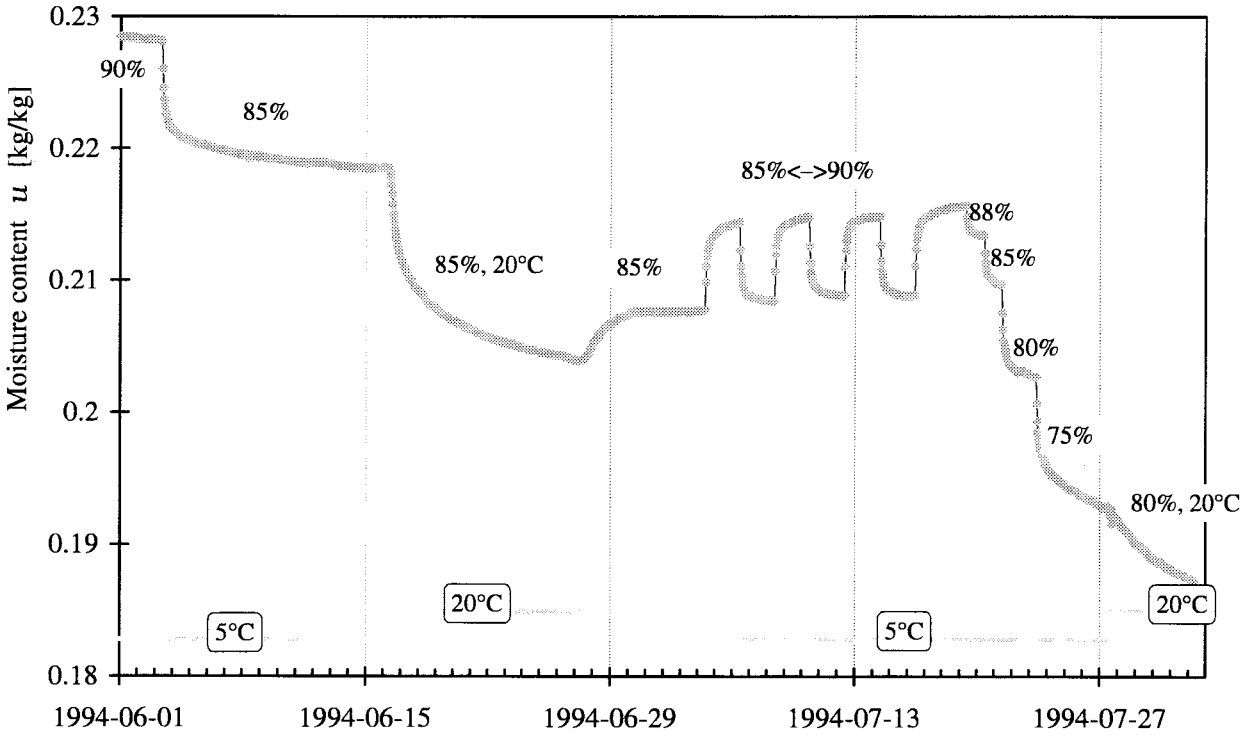

Figure 6.61 Sorption response for temperature shifts without change in RH, and combined with change in RH, Sample 3.

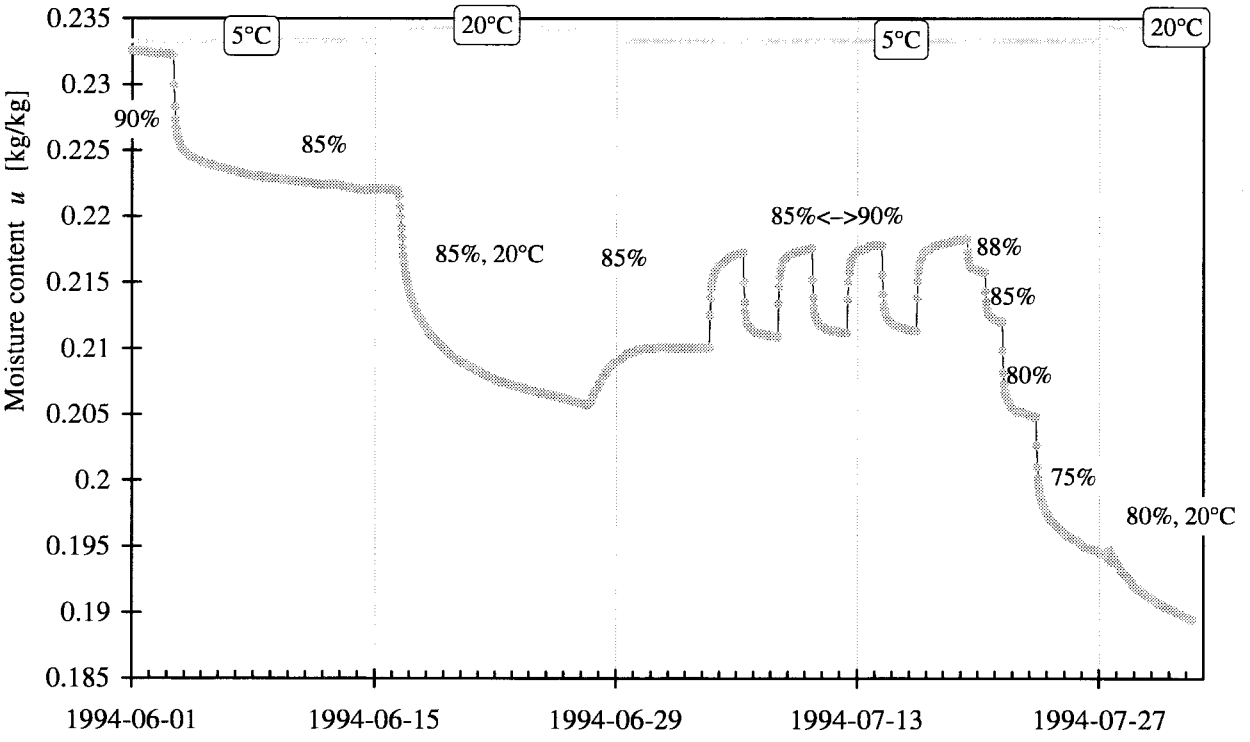

Figure 6.62 Sorption response for temperature shifts without change in RH, and combined with change in RH, Sample 4.

7 Particular analyses

The measurements reported in Chapter 6 show many things. In this chapter, a few observations, comparisons and analyses of details of measurements are presented.

7.1 Influence from moisture history on cyclic steps

The sorption and its development in time have proved to have an intricate dependence on the moisture history. A first example concerns the influence of moisture history on periodic sequences of steps. An overview of the two sequences that are selected from the fourth series of measurements to illustrate the influence from the prehistory is shown on Figure 7.1. The selected sequential periodical steps of sorption are marked with a thicker line. In Figure 7.2, the two sorption sequences are compared. They have the same cycles between 75% and 85% at 20°C, and only differing by the previous moisture history.

Let us look at the first sorption sequence in the overview. The RH-level is kept at 65% for 9 days, followed by a step to 75% for 3 days and a step to 85% for 2 days. The last step to 85% is to a previously not reached level, which has proved to give especially large proportion of retarded sorption. Two days are, by good margin, sufficient to let the sample come to equilibrium according to traditional Fickian theory. Substantial drift is taking place when a desorption step to 75% RH is made at 96 h on the time axis in Figure 7.2. One marked feature is that the previous absorption drift is not superimposed on the new desorption step.

The two sequences with repeated periods of cyclic steps have clearly different absorption patterns as seen in Figure 7.2. The prehistory for sequence 2 is a constant level at 85% RH kept for 24 days, whereas sequence 1 is reaching this level for the first time. The difference between patterns is repeated for several periods, and it is only gradually diminishing.

When a desorption step is made at 96 h, one marked feature is that the rising absorption slope of the response curve before the step not is superimposed on the new desorption step.

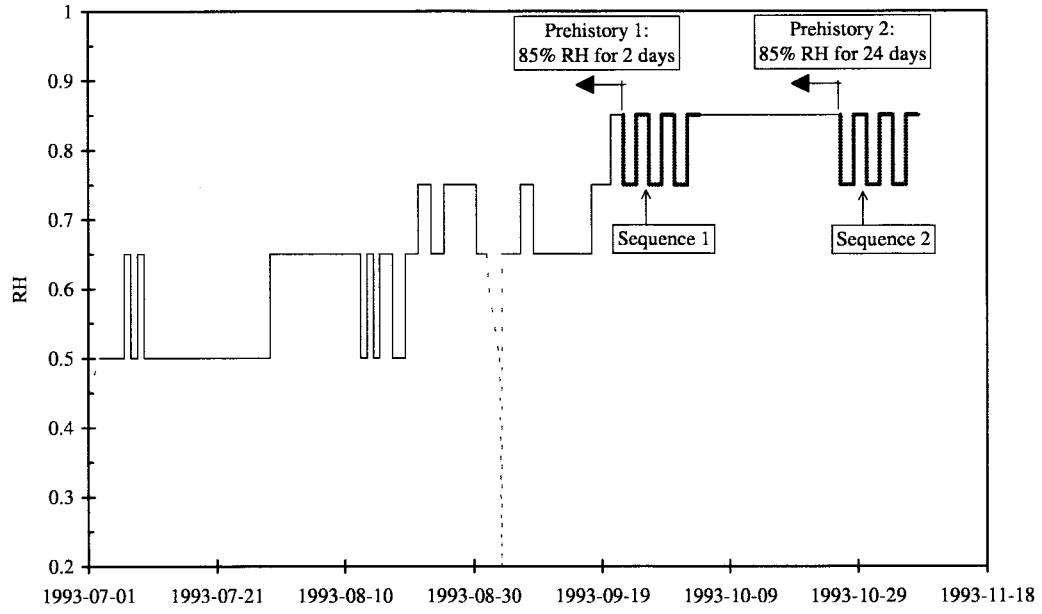

Figure 7.1 Survey of the prehistory for two sequences of RH-steps described in Figure 7.2

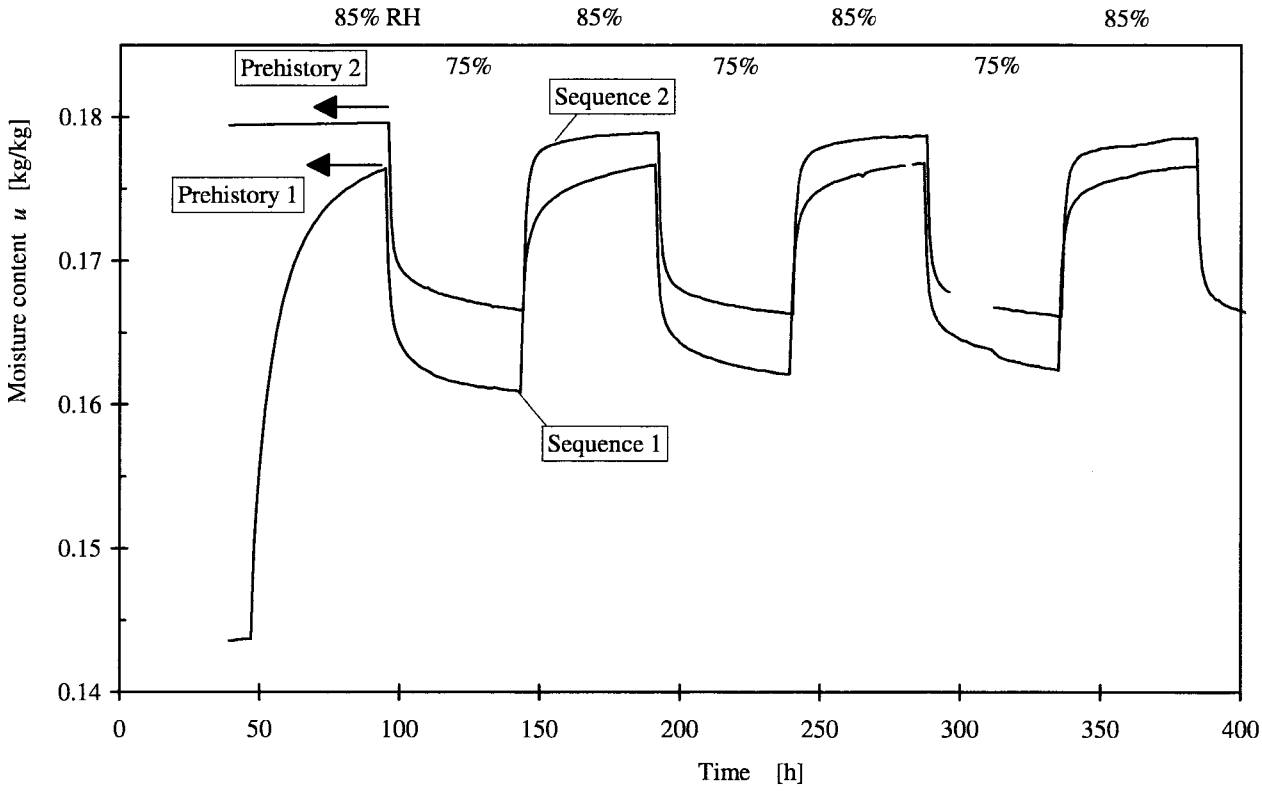

Figure 7.2 Sorption responses for two sequences with prehistory according to Figure 7.1.

7.2 Repeated cyclic steps

In Figure 7.4 comparisons between consecutive cycles are made. An overview of the preceding steps is shown in Figure 7.3. The cycles are between 75% and 85% RH and the temperature is 20°C.

A corresponding comparison for another sequence is made in Figure 7.6 with the overview of the preceding steps in Figure 7.5.

For both sequences of repeated cycles there is a tendency of diminishing moisture exchange with the number of cycles. The division between an initial fast phase and a phase with slow change, becomes more distinct with the number of cycles.

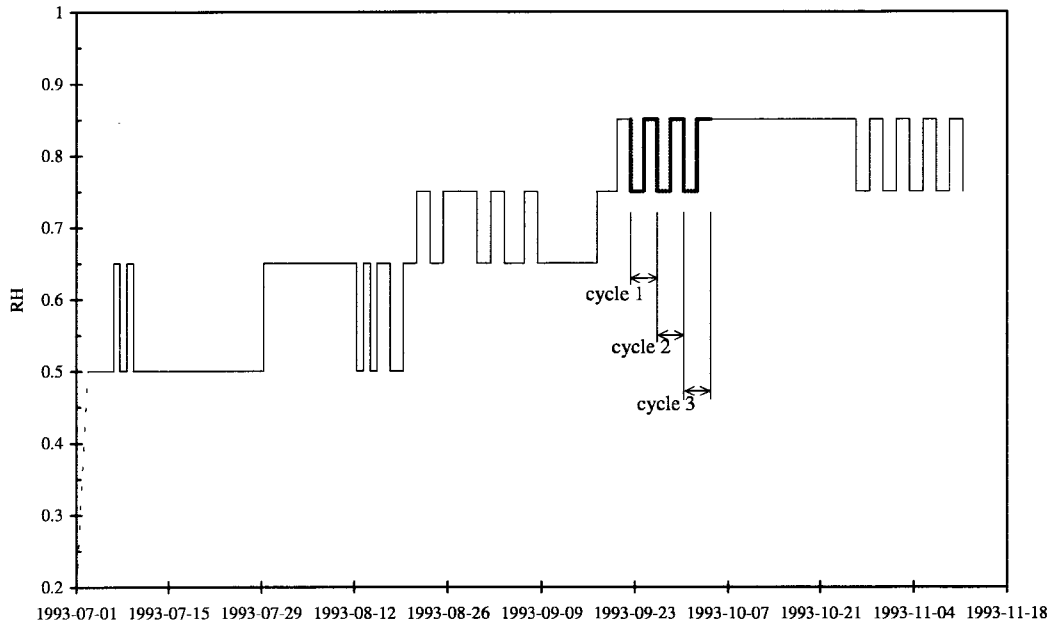

Figure 7.3 Survey of the RH-steps in Figure 7.4

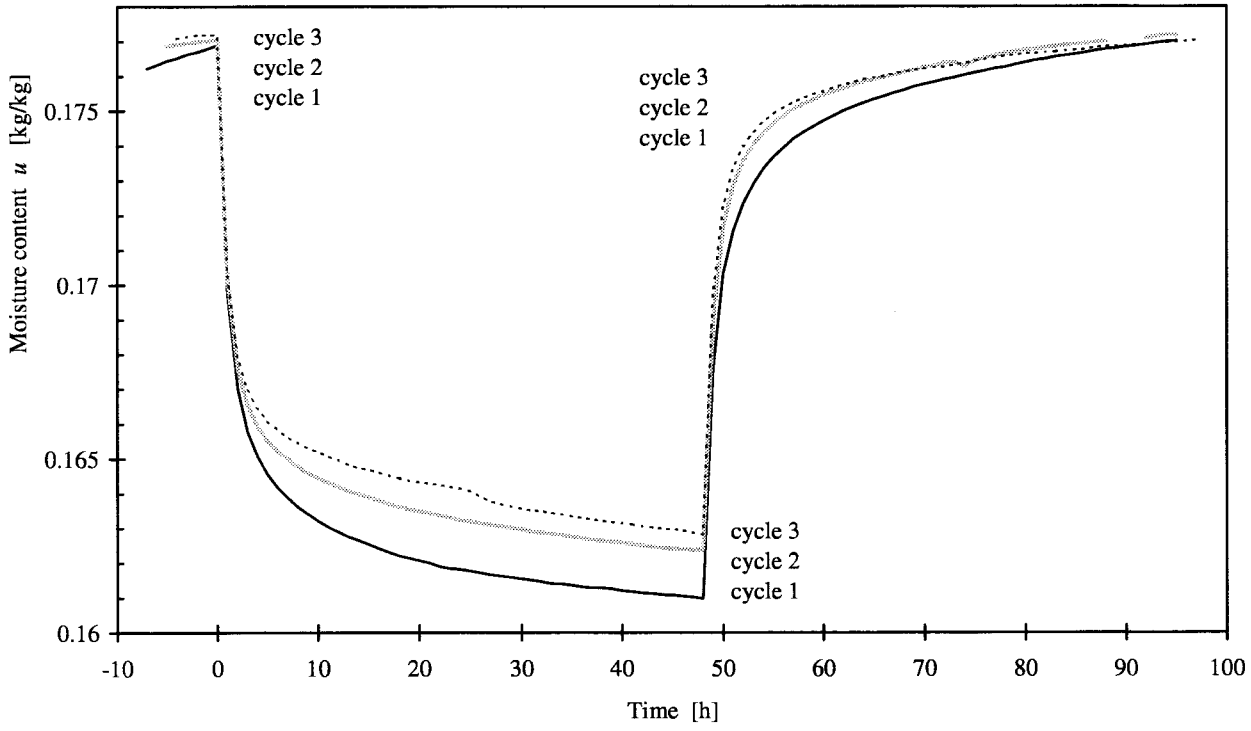

Figure 7.4 Sorption responses for consecutive cycles

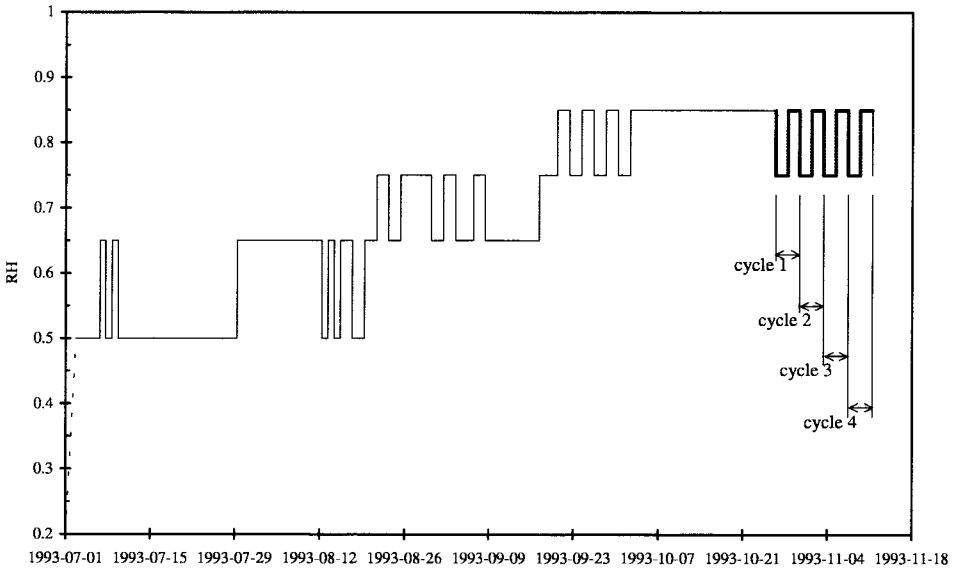

Figure 7.5 Survey of the RH-steps in Figure 7.6

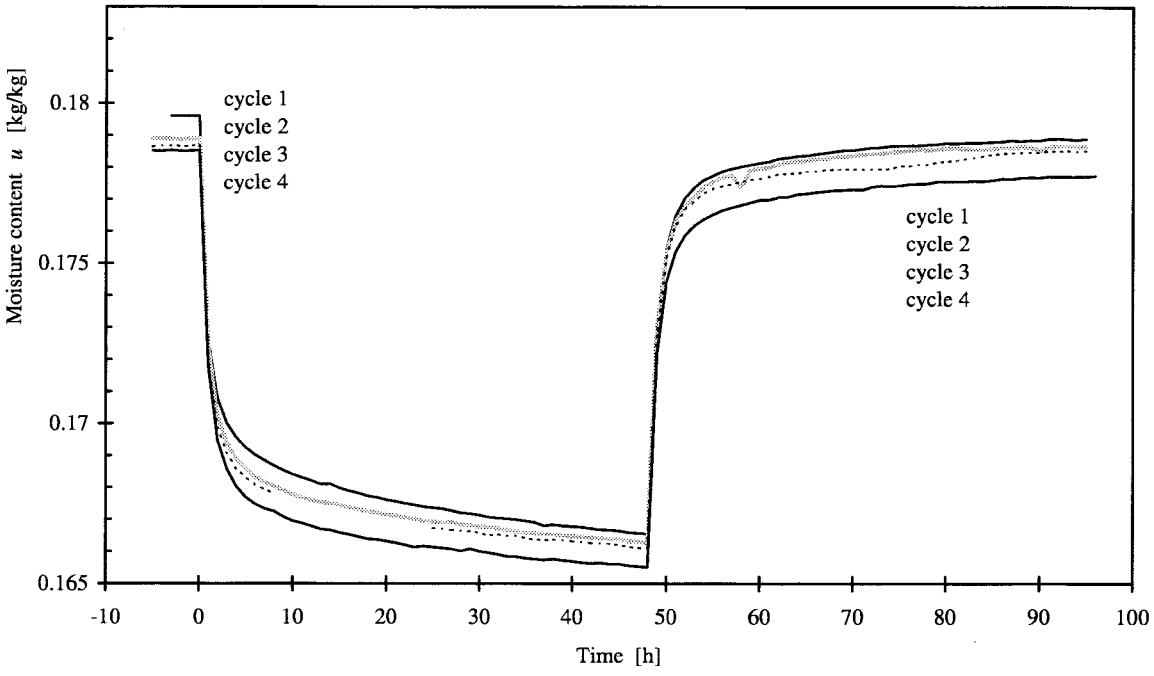

Figure 7.6 Sorption responses for consecutive cycles

7.3 Comparison between the sorption responses at 20°C and 5°C

In Figure 7.7 and Figure 7.8 response cycles with the same amplitude in RH, but at different temperature are shown together. In both cases the moisture exchange over the cycle is less at 5°C than at 20°C. At the lower temperature, there is a more distinct division between the initial fast phase after a step and the phase of slow retarded sorption.

One interpretation of the cause of the difference of shape on the response curves is that the time scale for the retarded sorption is greatly extended at the lower temperature.

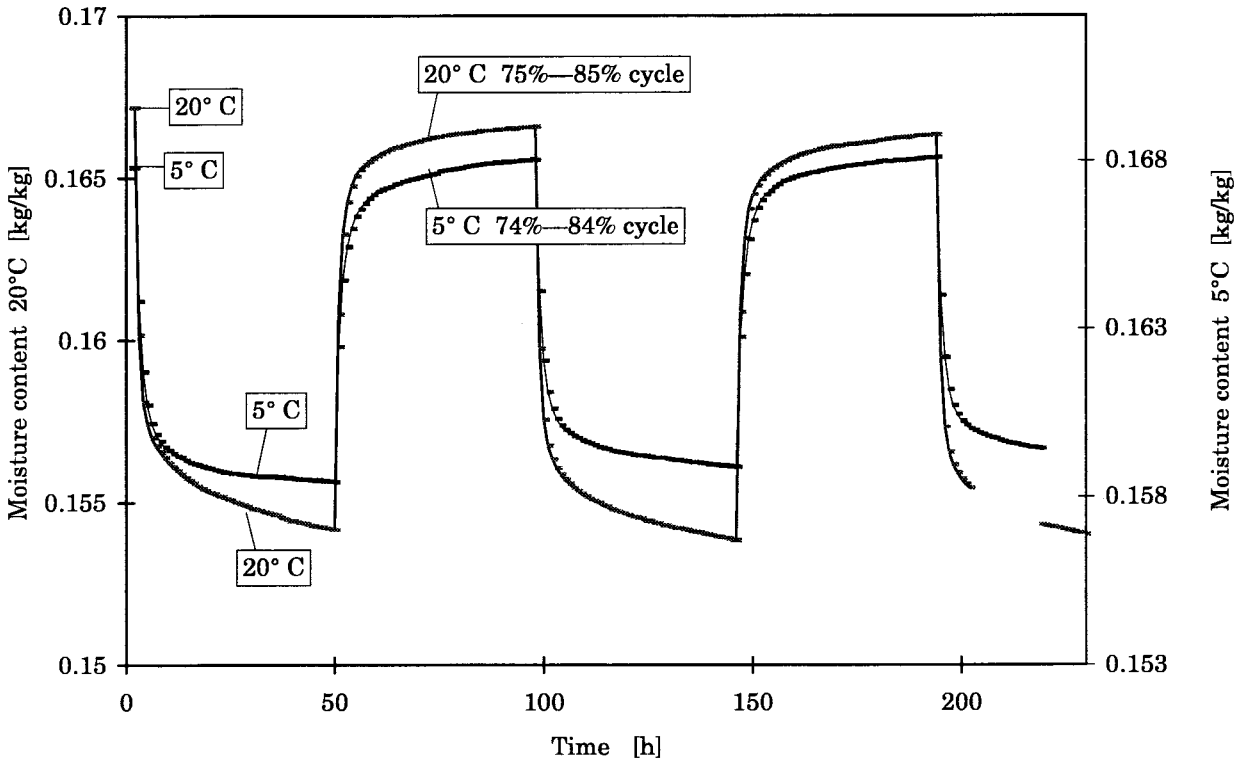

Figure 7.7 Sorption responses for cyclical steps at 5°C and 20°C.

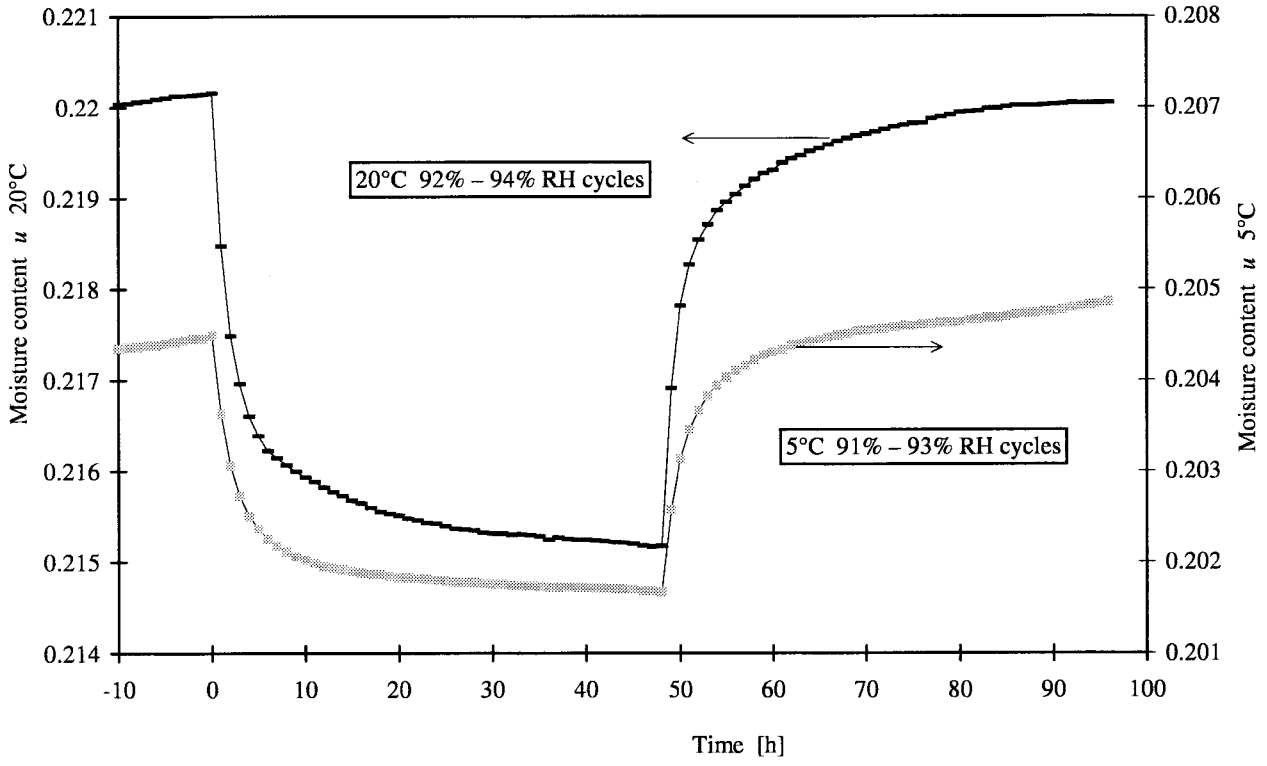

Figure 7.8 Sorption responses for cyclical steps at 5°C and 20°C.

7.4 Influences from temperature shifts on the sorption responses

By mistake, Sample 4 was subjected to a temperature and moisture pulse. This is described in more detail in Section 6.5.2 and indicated in Figure 6.50. Sample 3 was unaffected and allows comparison. In Figure 7.9 the sorption responses for the two samples are shown. The existing small difference of moisture content between the samples before the pulse is increased after the pulse and this difference is maintained for a long period, also after that the moisture content is exceeding that of the time of the moisture pulse. At the end of the sequence in the diagram, a temperature shift from 5°C to 20°C is made. The difference between the samples was substantially reduced after this event. It seems as if the temperature shifts triggers the samples to come to a more genuine equilibrium. By this interpretation, Sample 3 is deviating more from a true equilibrium, as it was not subjected to a temperature shift in the beginning of the diagram.

The influence from temperature shifts on the sorption is further dealt with in Section 7.7, where comparisons with a permanent equilibrium are made.

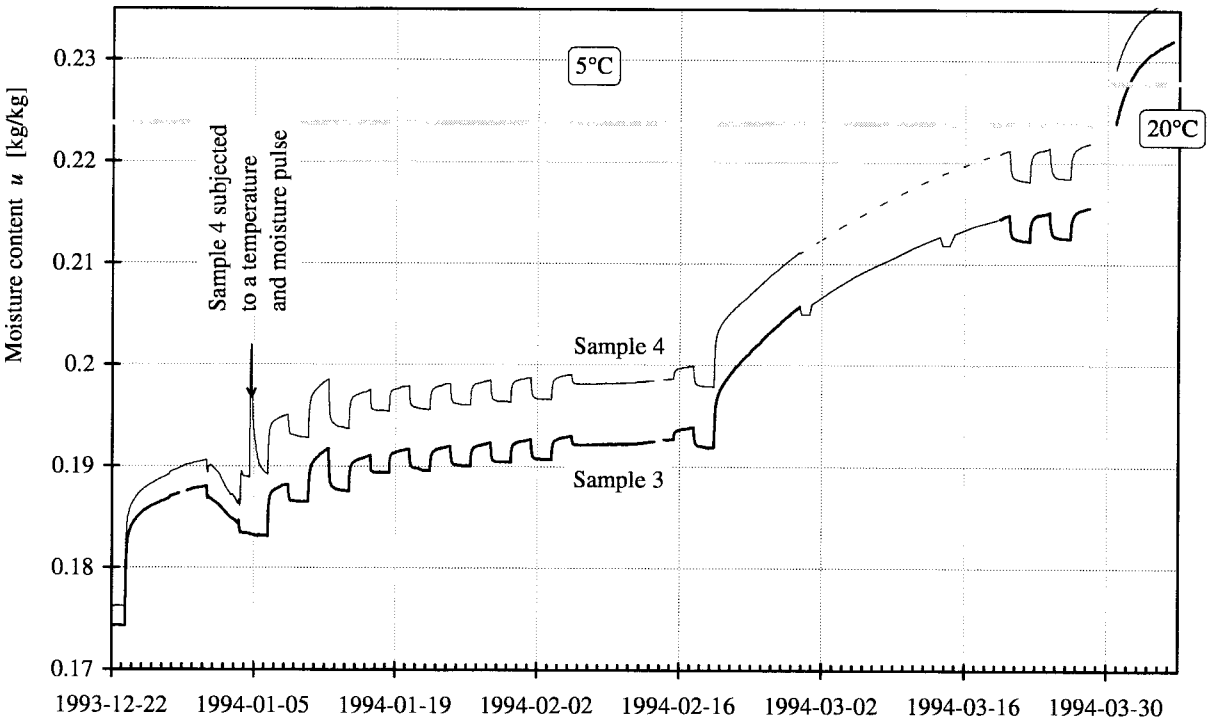

Figure 7.9 Sorption response following a temperature and moisture pulse (Sample 4) compared to the same undisturbed sequence (Sample 3).

7.5 Comparison between steps of different amplitudes

In the first and second series, tests of step responses were made with two samples simultaneously in the same interval of RH. The difference was that one sample was subjected to the entire interval in one step, whereas the interval for the other sample was divided into two steps. In most of the diagrams of sorption responses in Chapter 6.1 and 6.2 the two response curves are shown together. A typical example of the difference of the response curves is given

in Figure 6.10. One rather consistent feature of these measurements is that the slope, after that the first fast sorption after the step has taken place, of the two sorption responses are similar, regardless of the amplitude of the RH-step. Another feature is a tendency that the amount of sorption is less for the sum of two smaller steps compared to one larger step.

In the third series the interval was divided further into four steps for one sample. The step responses for desorption in the interval from 94% to 85% RH for Sample 3 in the third series is shown in Figure 7.10. The corresponding single step for Sample 4 is also shown. We see that the amplitude for the large steps is much larger than the sum of the four small steps.

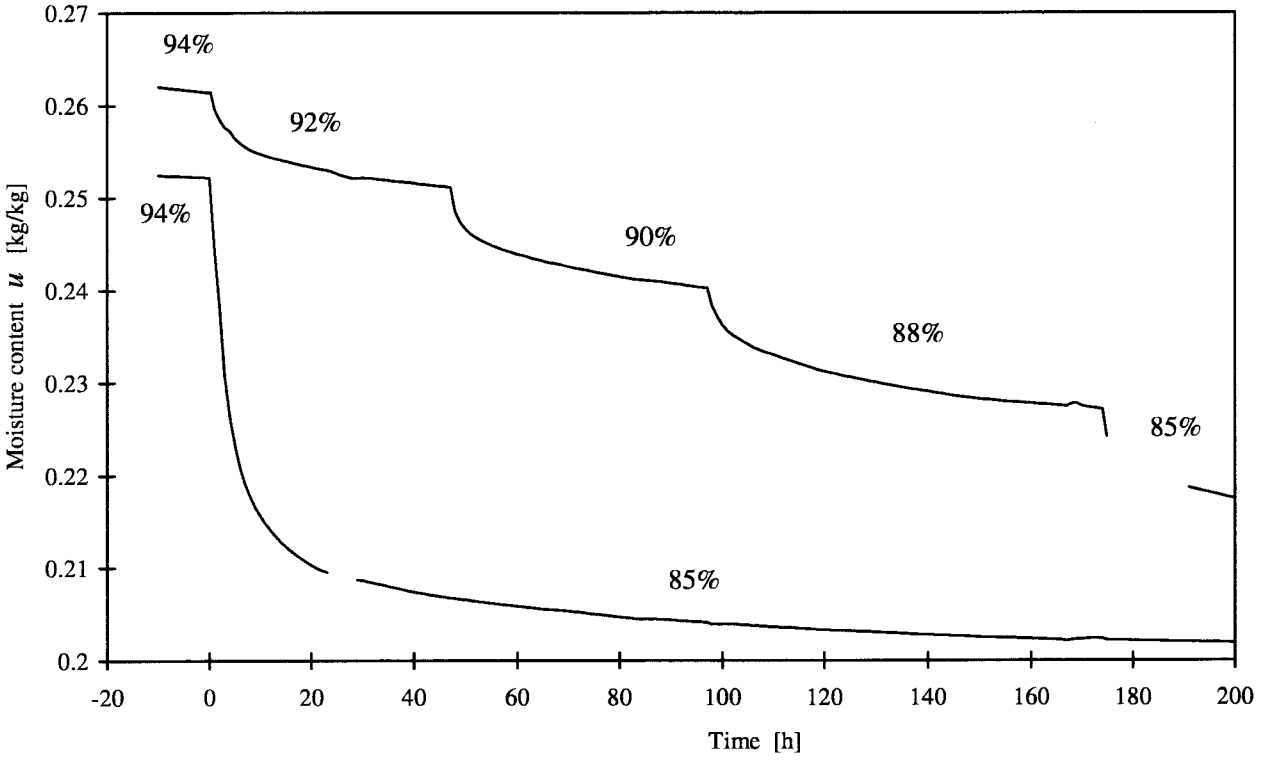

Figure 7.10 Sorption responses from one single step together with a corresponding sequence of four smaller steps.

7.6 Comparison between cyclic steps of different amplitude

In Figure 7.11 the sorption for cyclic steps of different amplitude is compared. The curve for 10% RH amplitude is taken from the first part of Figures 6.46 and 6.47 and the curve for 4% in the late part of the same figures. The relationship between the respective scales in the diagram for moisture content for the two curves is given the same relationship as the moisture content on an assumed equilibrium sorption curve for the respective RH-intervals. The equilibrium sorption curve in Section 10.5 was used. The same assumed equilibrium sorption curve is also used in Section 7.7. The average from two samples and two cycle sequences are used to increase the precision.

There is a slight tendency of reduced moisture capacity for the RH-cycles with small amplitude.

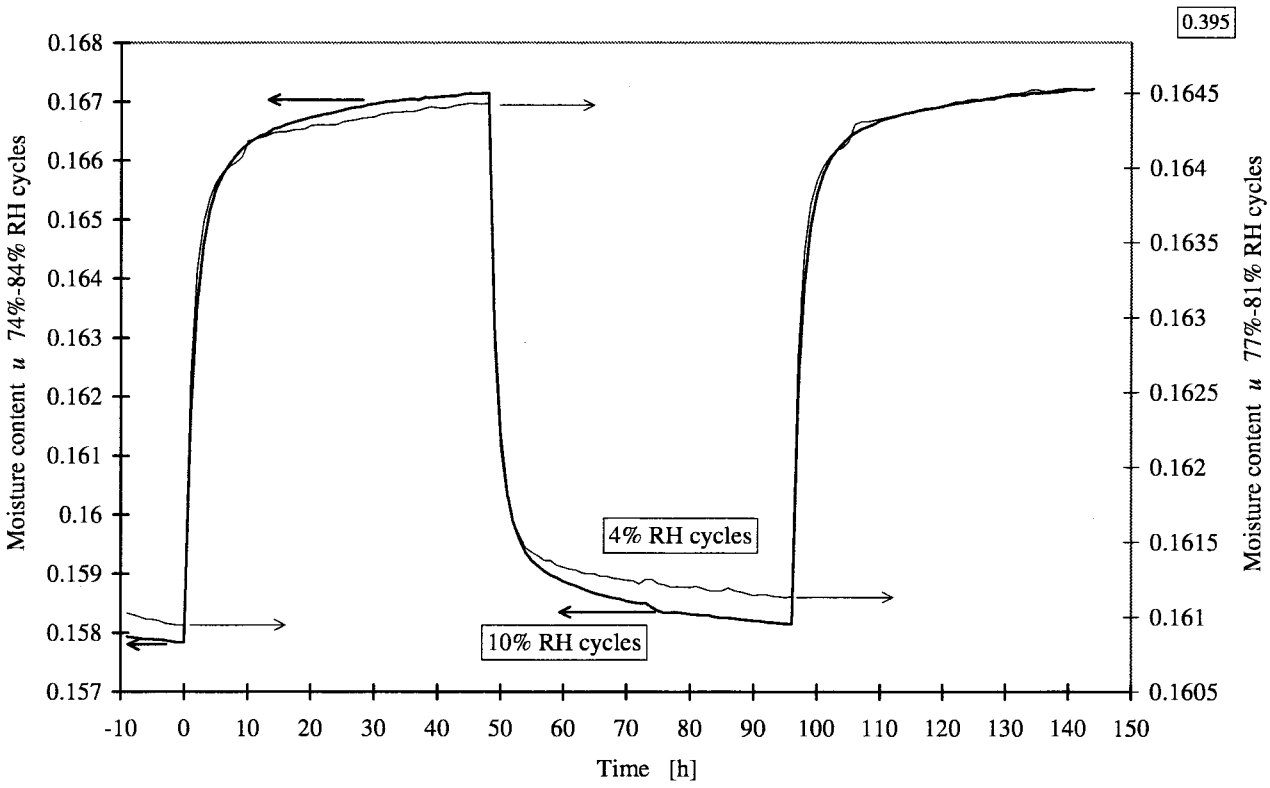

Figure 7.11 Sorption responses from cyclic steps of different amplitude.

7.7 Comparison between a sorption equilibrium curve and measured points

The sorption curve (or curves) relates moisture content u to relative humidity, φ . In the measurements we know $u(t)$ and $\varphi(t)$. It is quite instructive to plot these as points in a u - φ diagram together with the equilibrium sorption curve.

In this section comparisons are made between such measured points of sorption (which change slowly in time) and an assumed equilibrium moisture sorption curve. The points are selected at different times after a step and with different prehistory. This is one way to, with help of diagrams, illustrate the effects from retarded sorption, which result in deviations from a supposedly true equilibrium in different situations.

The points are consecutive and taken from the last part of the fifth series and the whole of the sixth series. Sections 7.7.1 to 0 show different features of the retarded sorption.

7.7.1 Sorption response at 5°C with a large portion retarded sorption

This section concerns the sequence A-B-C-D-E in Figure 7.12. Corresponding measured points are shown in Figure 7.13 with one value each day.

Absorption steps to a previously not attained RH-level have resulted in large effects of retarded sorption. This is especially true for this selected step in Figure 7.12 at high RH and low temperature.

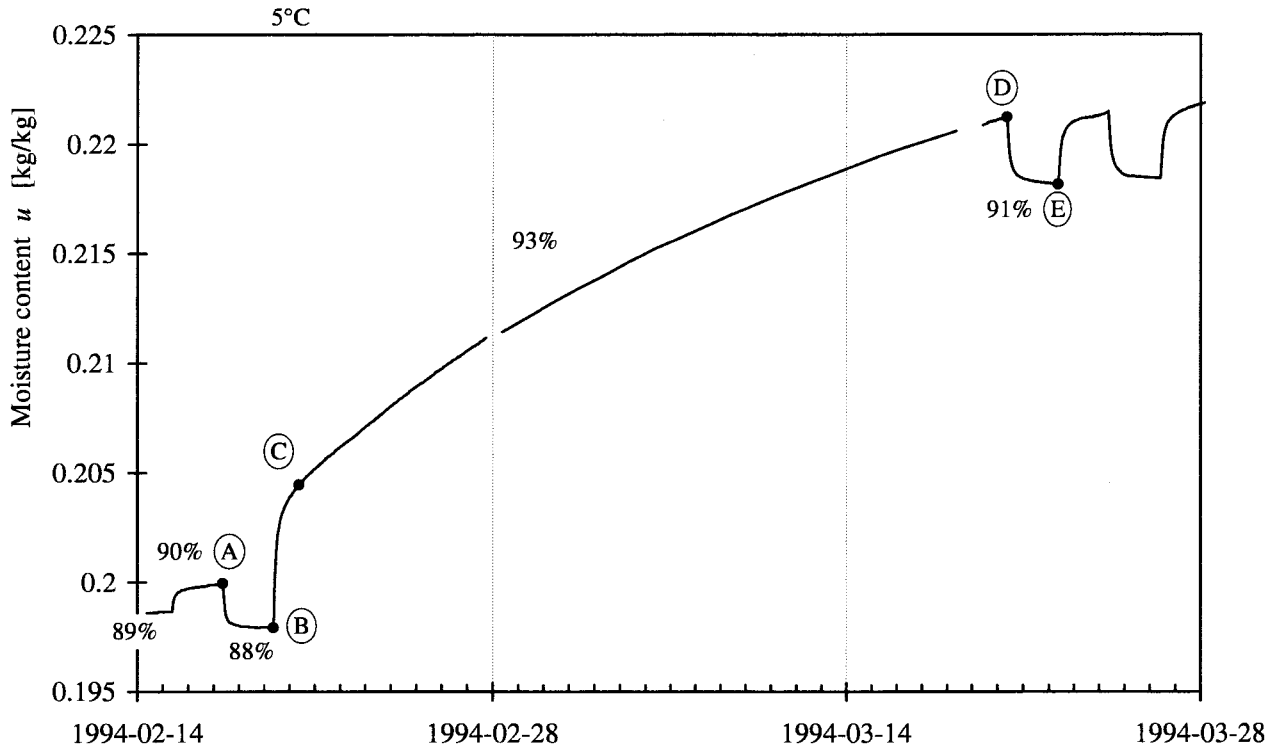

Figure 7.12 Sorption response at 5°C with a large portion retarded sorption.

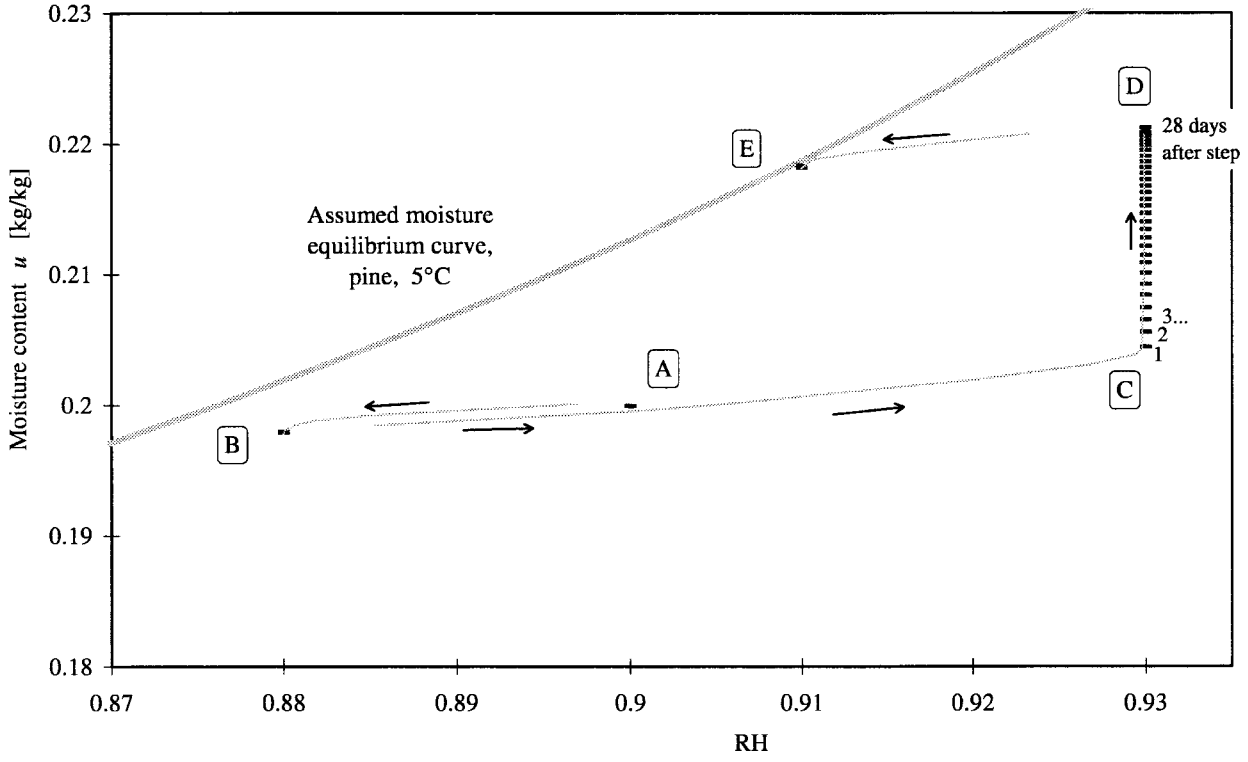

Figure 7.13 Measured sorption points obtained from the sequence of Figure 7.12 compared to a equilibrium sorption curve.

7.7.2 Cyclic sorption response with shifts of increasing and decreasing temperature

This section concerns the sequence E-F-G-H-I-J in Figure 7.14 and corresponding point in Figure 7.15.

In this sequence, cyclic steps with 2% amplitude in relative humidity are performed. These cycles are made before and after a temperature shift from 5°C to 20°C and again after a shift back to 5°C. This is described in more detail in Section 6.6.1. The sorption responses from the sequence of steps are shown in Figure 7.14. In Figure 7.15 the selected points are related to the equilibrium sorption curve.

The prehistory for this sequence is shown in Figure 7.12. In Figure 7.13 the deviation from the equilibrium sorption curve is illustrated. This gives the prehistory for the temperature changes here. After the temperature change from 5° to 20°C, a very large absorption took place at practically constant RH. This despite the fact that the temperature dependence for the moisture equilibrium curve is giving a desorption. This is illustrated in Figure 7.15, where point F is far under the corresponding moisture equilibrium curve at 5°C in contrast to point G that is above its moisture equilibrium curve at 20°C.

The amplitudes of moisture content are somewhat higher at 20°C, which is seen for instance on the slope of the line connecting the two levels of the step in Figure 7.15.

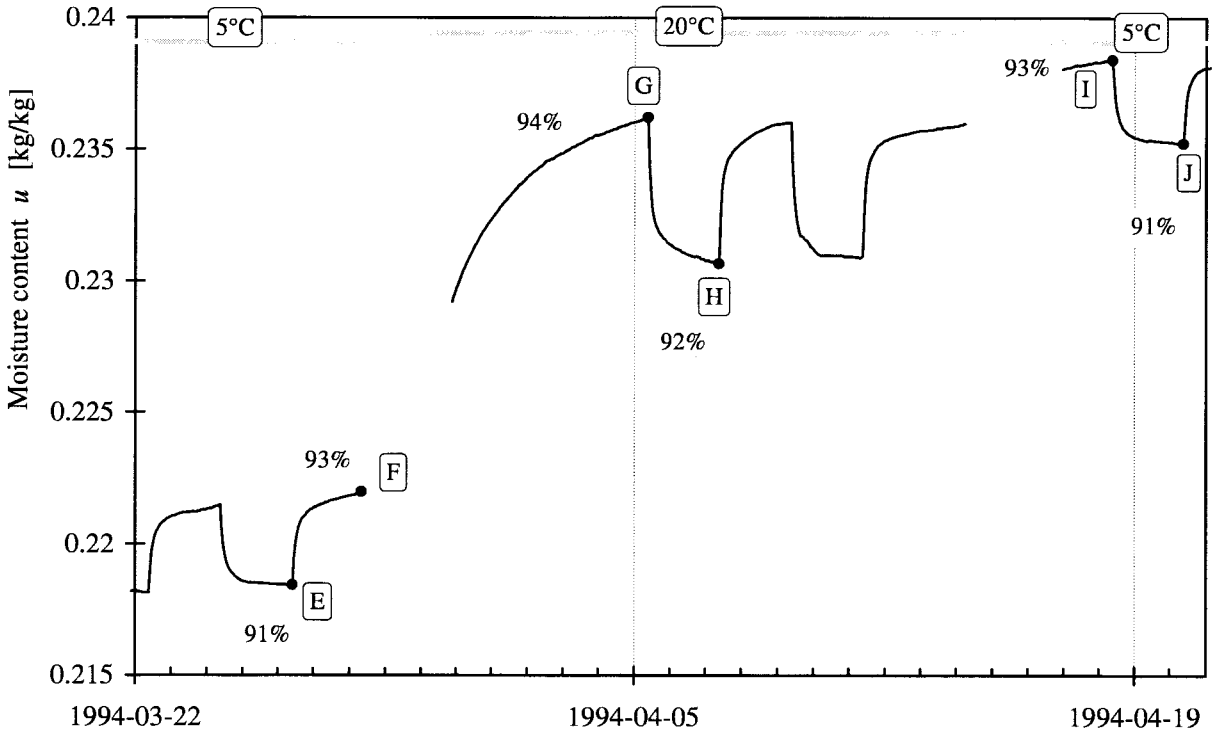

Figure 7.14 Sorption response with temperature shifts from 5°C to 20°C and back to 5°C.

rf_ko2.xls 4K1

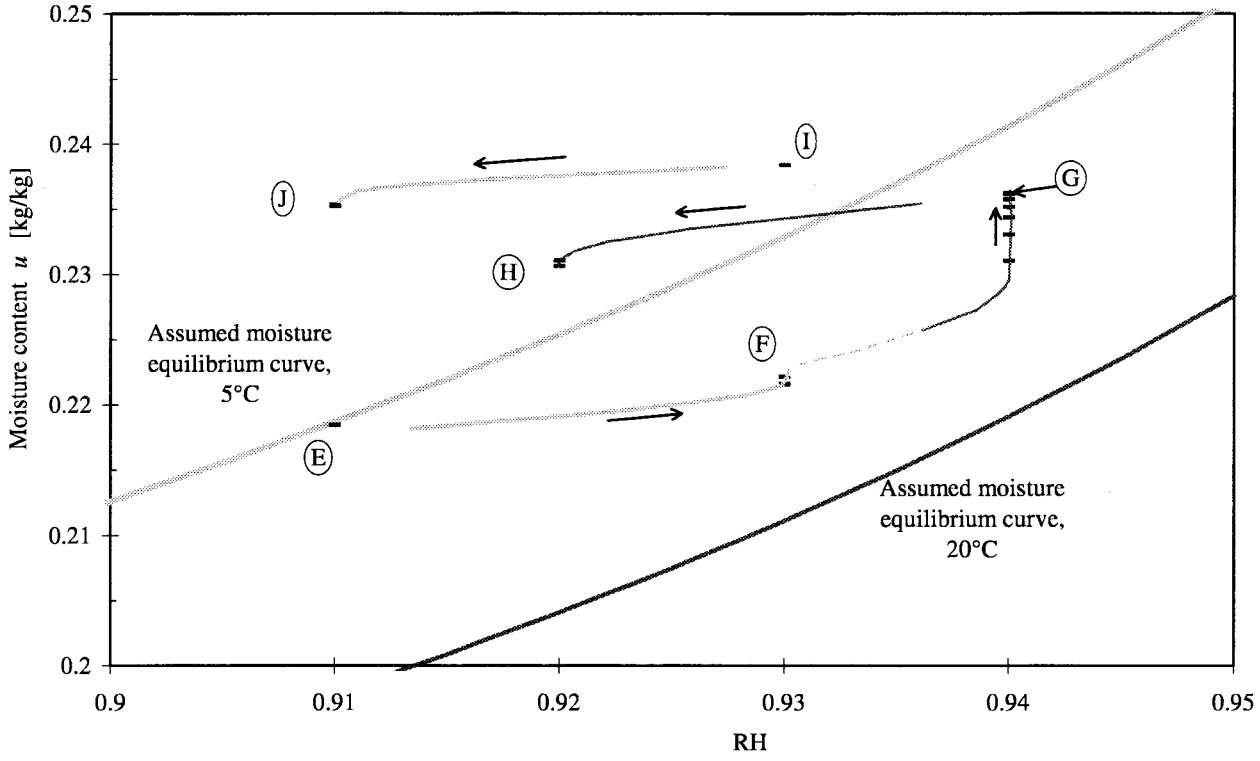

Figure 7.15 Measured sorption points obtained from the sequence of Figure 7.14 compared to equilibrium sorption curves for 5°C and 20°C.

7.7.3 Desorption response with shifts of increasing and decreasing temperature

This section concerns sequence M-N-O-P-Q-R in Figure 7.16. The measured points are shown in Figure 7.17.

The sorption response curve in Figure 7.16 starts with a desorption step from 90% to 85% RH (M–›N). This step was preceded by cycles in the 94% to 90% RH range. An overview of the preceding steps is shown in Figure 6.55. The 85% RH level is continuing for a rather long time to obtain reasonable equilibrium. At point O a temperature change is made at constant RH. This results in a desorption, quite according to the temperature dependence of the moisture equilibrium curve. The drift of the moisture content is rather large in point P as long as 11 days after the temperature step. At point P, a change back to 5°C is made. Still, the 85% RH level is maintained. The temperature step took 65 hours to complete (due to peculiarities with the apparatus). After the temperature step no drift of the moisture content is detectable for any of the two samples (this is the only time for all the measurements that this is the case).

It seems as if temperature shifts speed up the retarded sorption so the wood comes closer to a more genuine equilibrium. It could however be argued for this case that it was the effect of the desorption – absorption cycle O-P-Q in Figure 7.16.

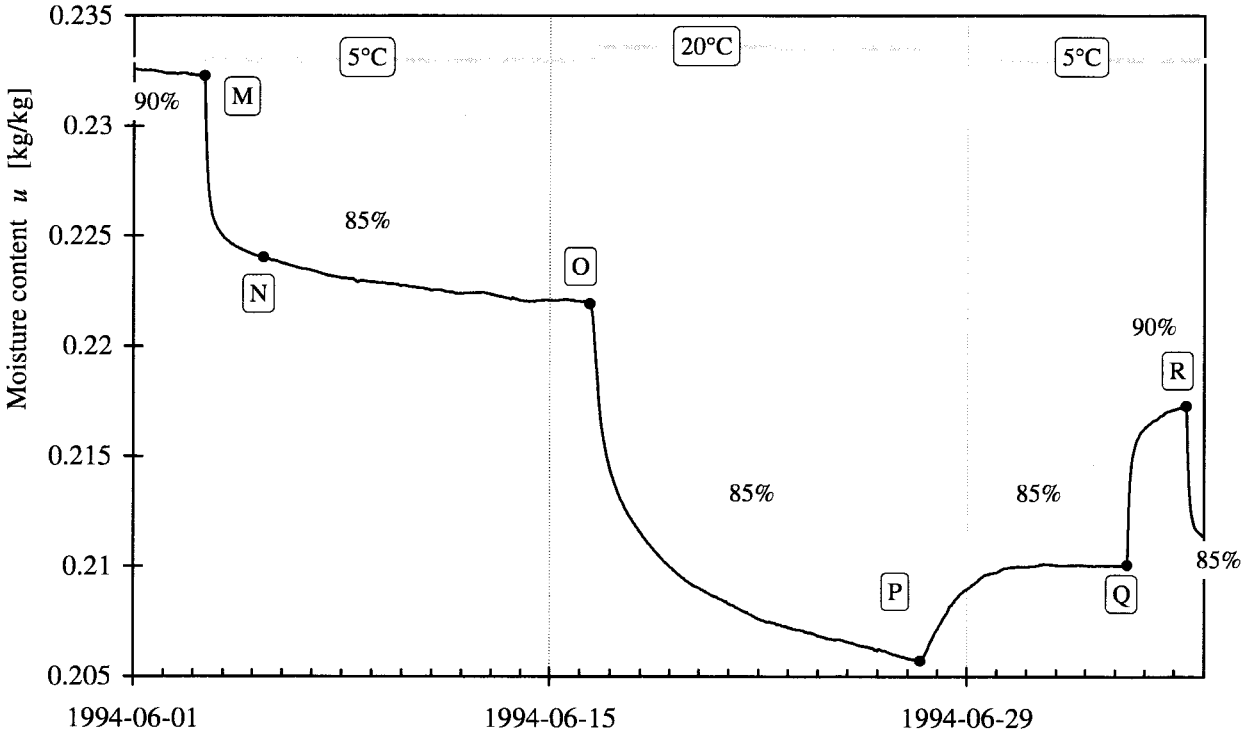

Figure 7.16 Desorption response with temperature shifts from 5°C to 20°C and back to 5°C.

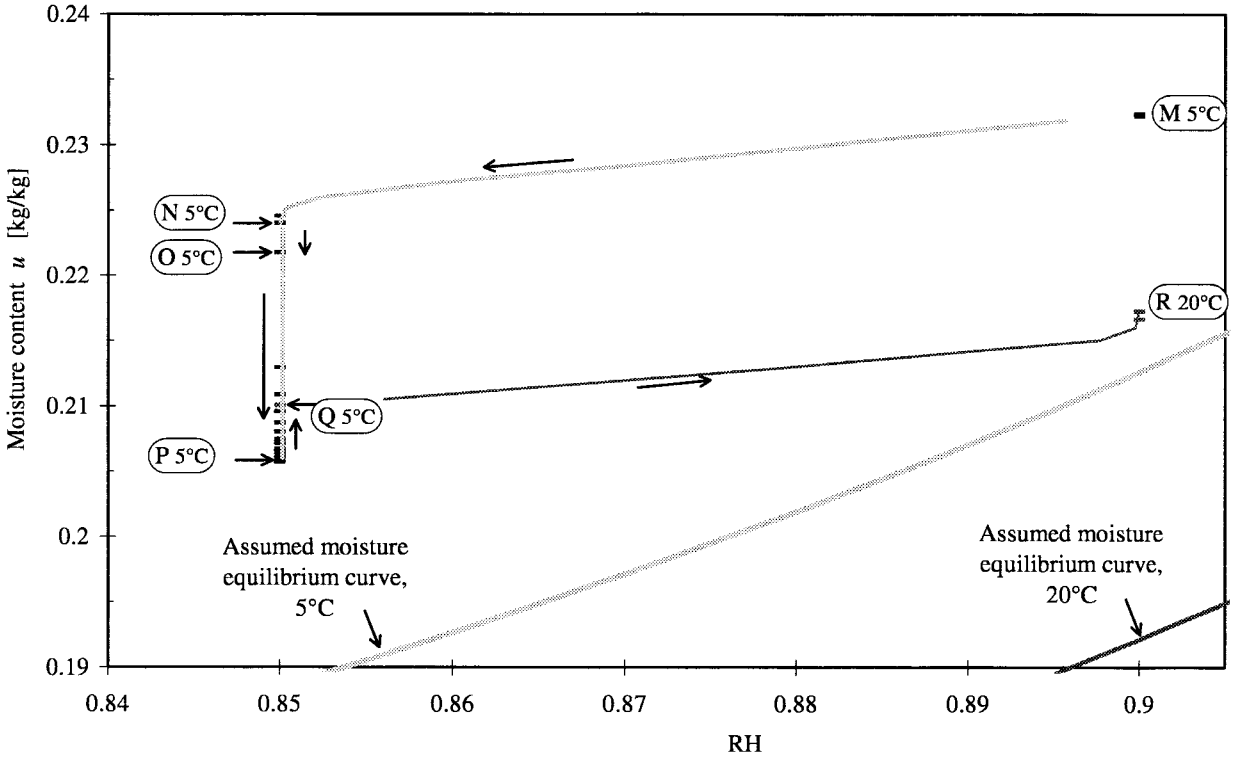

Figure 7.17 Measured sorption points obtained from the sequence of Figure 7.16 compared to equilibrium sorption curves for 5°C and 20°C.

7.7.4 The RH compensated to obtain zero sorption during a temperature shift

This section concerns sequence S-T-U-V-X-Y in Figure 7.18. The measured points are shown in Figure 7.19.

In this selected sequence, an assured desorption was established by a rather swift succession of desorption steps, sorption points S to V in Figure 7.18. After that, a temperature shift from 5°C to 20°C was made. Simultaneously with the temperature change, the RH was changed accordingly, with the ambition to attain zero sorption. The relation used was a 5% RH increase to compensate a 15°C temperature increase. The assumed temperature dependence was close to the indirectly measured, since the curves meet if they are extrapolated to a point between point V and X where the change took place.

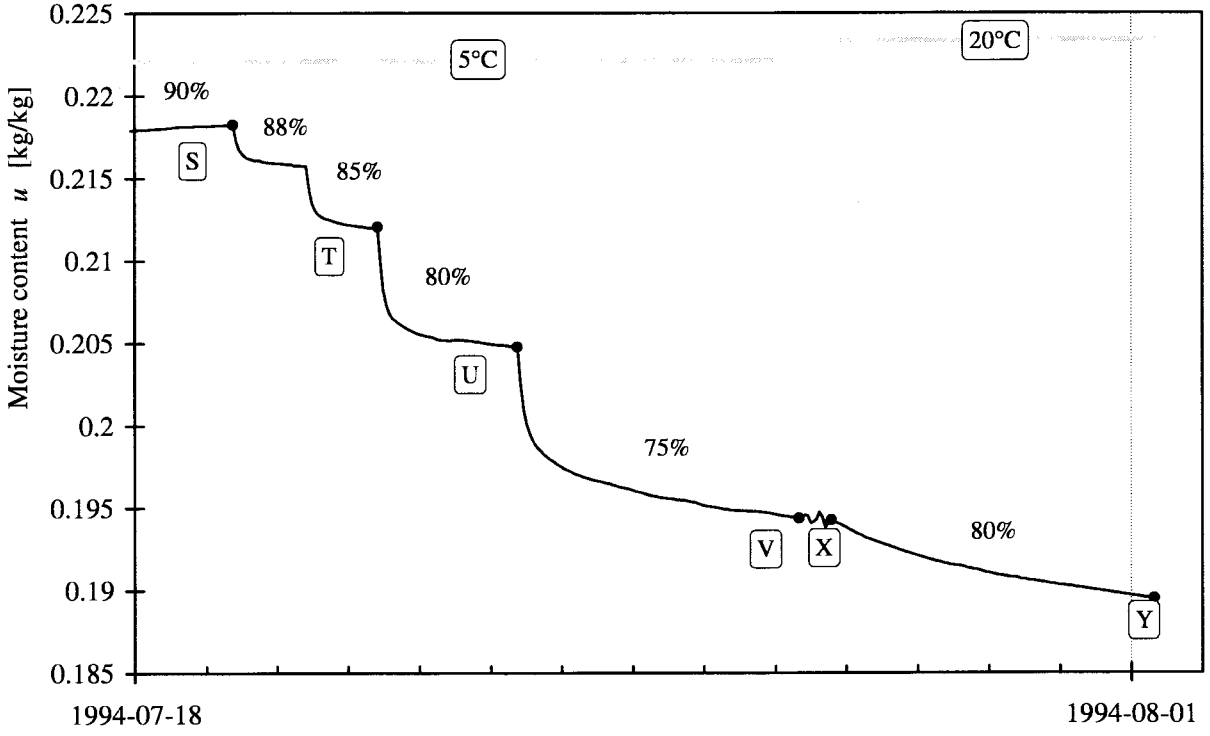

Figure 7.18 Sorption response with a temperature shift from 5°C to 20°C, the RH compensated to zero sorption during the shift.

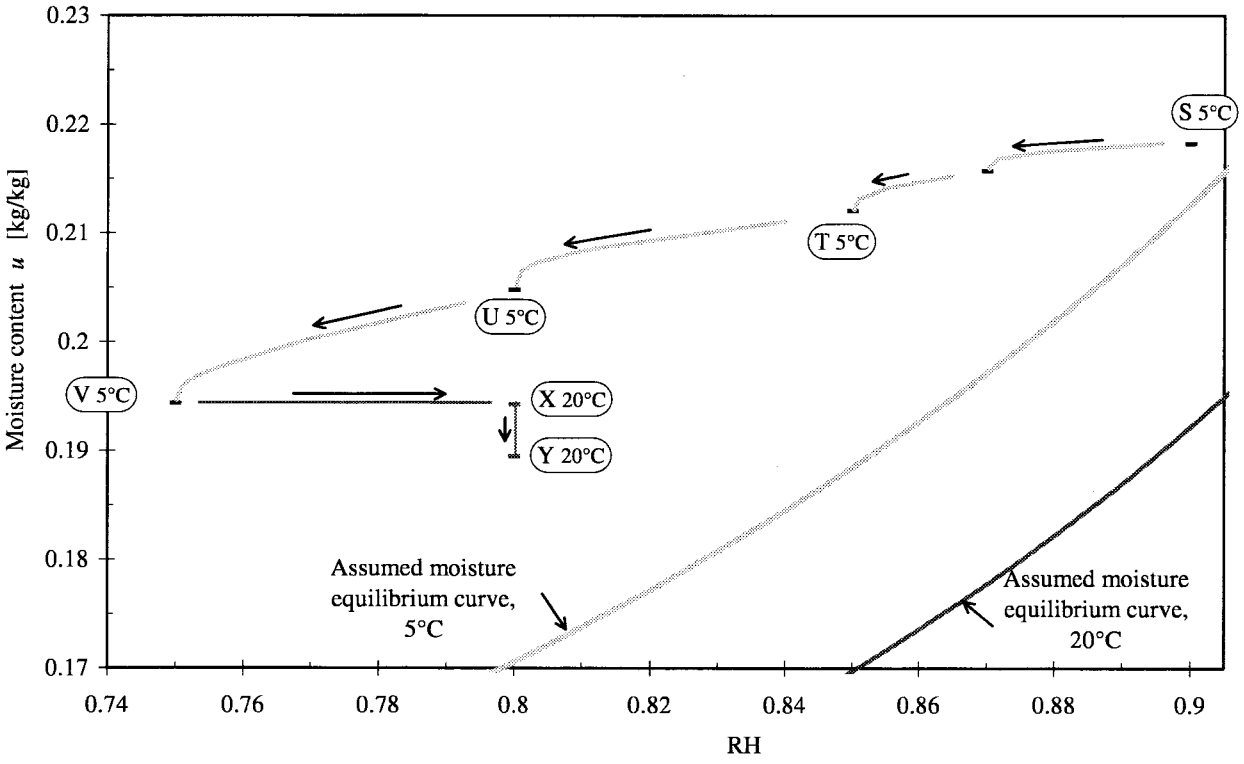

Figure 7.19 Measured sorption points obtained from the sequence of Figure 7.18 compared to equilibrium sorption curves for 5°C and 20°C.

8 Analyses of swelling

The free, moisture-related dimensional changes involving swelling and shrinkage are in this report called swelling. Also shrinkage is implied. Measured data of swelling are obtained from the forth and fifth series.

8.1 Comparison between tangential and radial swelling

Tangential and radial swelling, ε_t and ε_r , are presented together in the same diagram in the results presented in sections in Chapter 6, Sections 6.4 to 6.5. They follow each other very well during the various sequences. See Figures 6.40, 43, 48, 51 and 54. The ratio $\varepsilon_r(t) / \varepsilon_t(t)$ is quite constant. The scales in the diagrams for the two directions were adjusted for a representative value of $\varepsilon_r / \varepsilon_t$. For the forth series of measurements at 20°C the relationship $\varepsilon_r / \varepsilon_t$ is set to 0.6 as a representative value. The relationship is changed to 0.65 for the measurements at 5°C. These measurements have predominantly taken place at higher relative humidities than those at 20°C. It is therefore not possible clearly to relate the change in ratio to temperature or to RH-level.

Comparison can also be made in diagrams in the following section. See Figures 8.3, 5, 8, 11, 13, 16 and 19. In these diagrams the tangential swelling is plotted as a function of the radial swelling.

8.2 Comparison between sorption and swelling

In this section the tangential swelling step response is compared to the sorption response. Measured data of swelling are obtained from the forth and fifth series.

The comparison between sorption and swelling is made in three types of diagrams in this section. In the first type the swelling and sorption response curves are compared together as a function of time, where the sorption is designated with a thicker curve related to the left axis, and the tangential swelling to the right axis. An example of a diagram of this type is Figure 8.1. The relation between the scale for tangential swelling [m/m] and sorption [kg_{water}/kg_{wood}] is set at 0.32 for all diagrams. This is based on a rough fitting made at the initial phase of the step responses. The starting points for the scales are not accumulated from the previous diagram with the factor 0.32, but slightly adjusted to an even number for the individual diagram. The axes are also adjusted so the curves come close together to facilitate comparison. This means that the right-hand scale is shifted somewhat from one diagram to the next one. This applies for all the diagrams with a right hand scale.

In the second type of diagram the tangential swelling as a function the moisture content is directly compared in points and the progression of time is shown by a trajectory line. An example of a diagram of this type is Figure 8.2. The time between the selected points is six hours. The selected points are adjusted so the five hour measurements after a step not are included. This is because the samples for measurement of moisture content are placed closer to the jet of incoming air than the samples for swelling measurement. The jet is agitating the air, reducing the surface resistance. This has given a slightly faster response for the sorption samples, noticeable the first hour or two after a step.

The diagrams in all the figures illustrate that the patterns of response are rather similar for tangential swelling and the moisture uptake. This pattern also includes the retarded sorption. There is however a consistent tendency that this retarded response is somewhat larger for the swelling than the sorption. This is perhaps especially visible in the diagrams where swelling is plotted against moisture content.

The relationship between *radial* swelling and moisture uptake is not directly illustrated in diagrams. Instead a comparison has to be done in two stages. Radial and tangential swelling are shown together in diagrams in Chapter 6.4 to 6.5. In this chapter moisture content and tangential swelling are shown together in diagrams. However, the tangential and radial swelling are proportional to one another, or in some instances close to proportional.

An alternative way to compare tangential and radial swelling is a third type of diagram in this section, starting with Figure 8.3. In this type of diagram tangential swelling is plotted against radial swelling. The progression of time is shown by a trajectory line.

The axial swelling is not measured.

The measurements of swelling are getting very noisy after the fifth series in Chapter 6.5 and are assessed not to be credible. It seems that the position for the optical sensors have fallen out of the core of the light source, due to an unfortunate design. See Figure 2.5. This is remedied in the next version of position sensor, based on a laser diode as a light source, creating a stationary disc-shaped beam of light. The optical positioning sensor is moving in this stationary beam, connected to the sample.

8.2.1 The first part of the fourth series

The measurements in the fourth series are divided in two parts. The first part comprises a lower range of moisture contents and the second a higher one.

The measurements of sorption $u(t)$ and tangential swelling $\varepsilon_t(t)$ from the first part of the fourth series are shown in Figure 8.1. In Figure 8.2 tangential swelling is plotted against moisture content. The progression of time is shown by a thin trajectory line. Only the 50% – 65% RH cycles from Figure 8.1 are shown in Figure 8.2 and the rest is shown in Figure 8.4. In corresponding diagrams in Figure 8.3 and Figure 8.5 the tangential swelling is plotted against the radial swelling for the sequence in Figure 8.1.

The precondition for the samples for sorption measurements was room conditions for 1½ months (an average RH of 50% is estimated) preceded by roughly half a month at 35% RH (Sample 3 in the third series). The wood used to make the swelling samples had been kept at room climate for a long time.

The initial step in Figure 8.1 exhibits a different response patterns between sorption and swelling. In later steps in the same range the response patterns are very similar. This is clearly seen in Figure 8.2, where the moisture content is plotted versus the swelling. The conditions during the initial step can be described as a step outside the limits of earlier attained moisture content. This concept is used in mechano-sorption to describe special effects found during those conditions, Mårtensson (1992). The 65% – 50% RH cycles preceded by a period of 65% RH for as long as 14 days, exhibit a very close similarity between sorption and tangential swelling as the upper scanning curves in Figure 8.2 illustrate. The scanning curves for these cycles follow the ε_t / u ratio of 0.32 very closely for the whole sequence of repeated cycles.

The trajectory for the time describes a counter-clockwise pattern for the initial cycle in Figure 8.2. This means that a part of the tangential swelling is lagging behind compared the sorption. This can be compared to the diagrams in Section 7.7 where the sorption is lagging

behind the relative humidity. There it is however much more pronounced. In Figure 8.3 there is the same tendency of a counter-clockwise trajectory between tangential and radial swelling. A pattern of the time-delays of the different responses emerges. The largest time-delay is connected with the tangential swelling. The time-delay for radial swelling is somewhat smaller and the time-delay for sorption a bit smaller still. This pattern is consistent in the measurements (whenever a difference occurs).

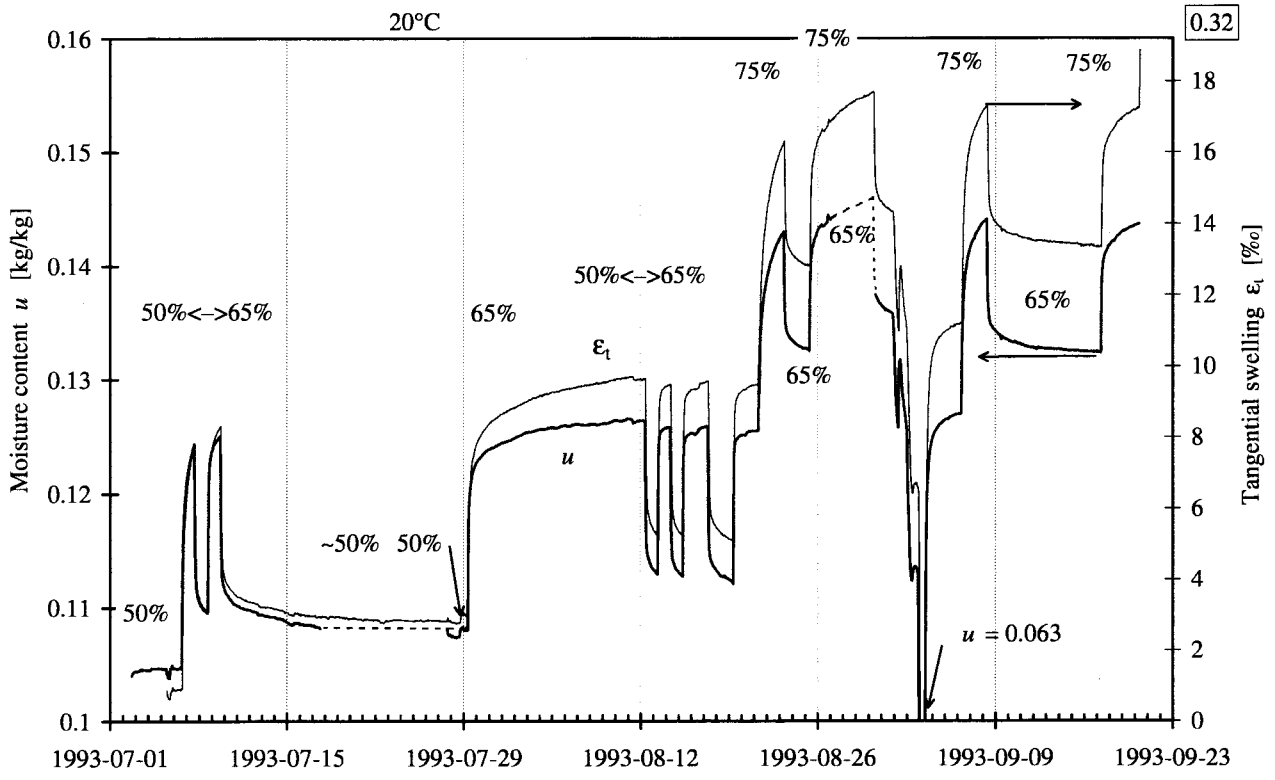

Figure 8.1 Sorption response compared with tangential swelling response, from the first part of the fourth series.

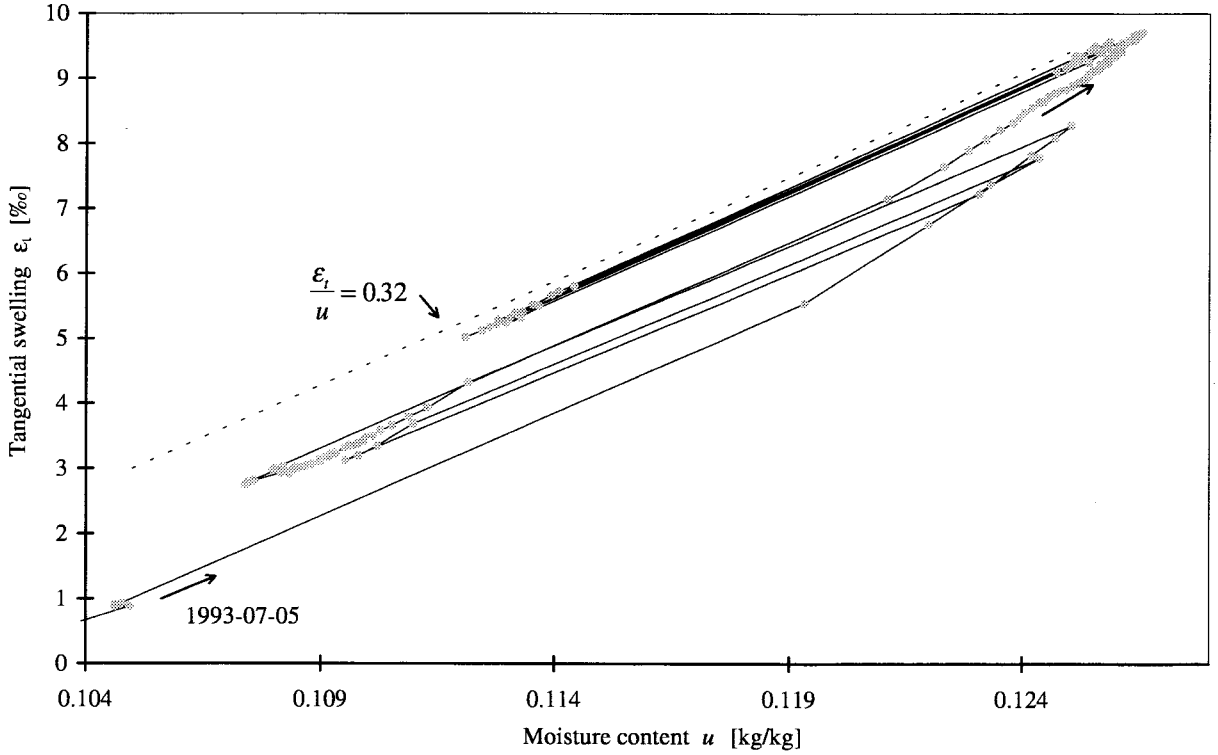

Figure 8.2 *Tangential swelling ε_t as a function of moisture content u. Consecutive points in time are connected with a thin line. From the 50% – 65% RH cycles in Figure 8.1.*

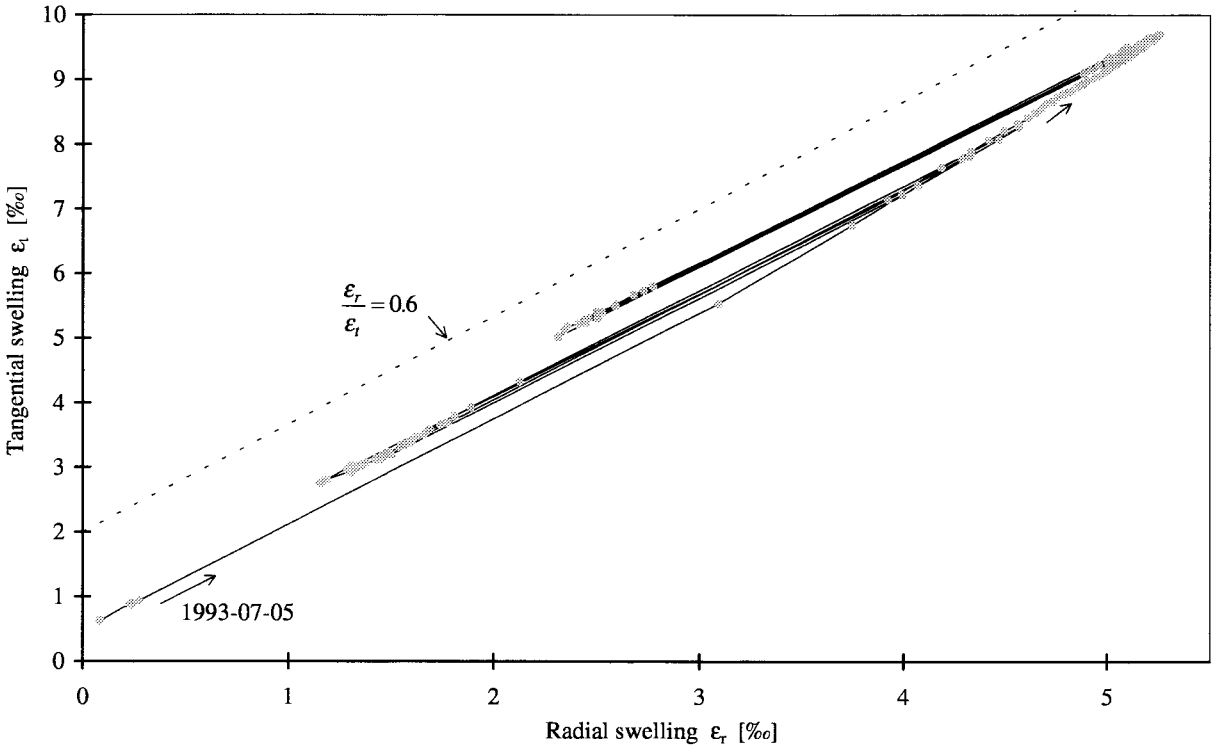

Figure 8.3 *Tangential swelling ε_t as a function of radial swelling ε_r. Consecutive points in time are connected with a thin line. From the 50% – 65% RH cycles in Figure 8.1.*

4\ 3&.xls Diagr2

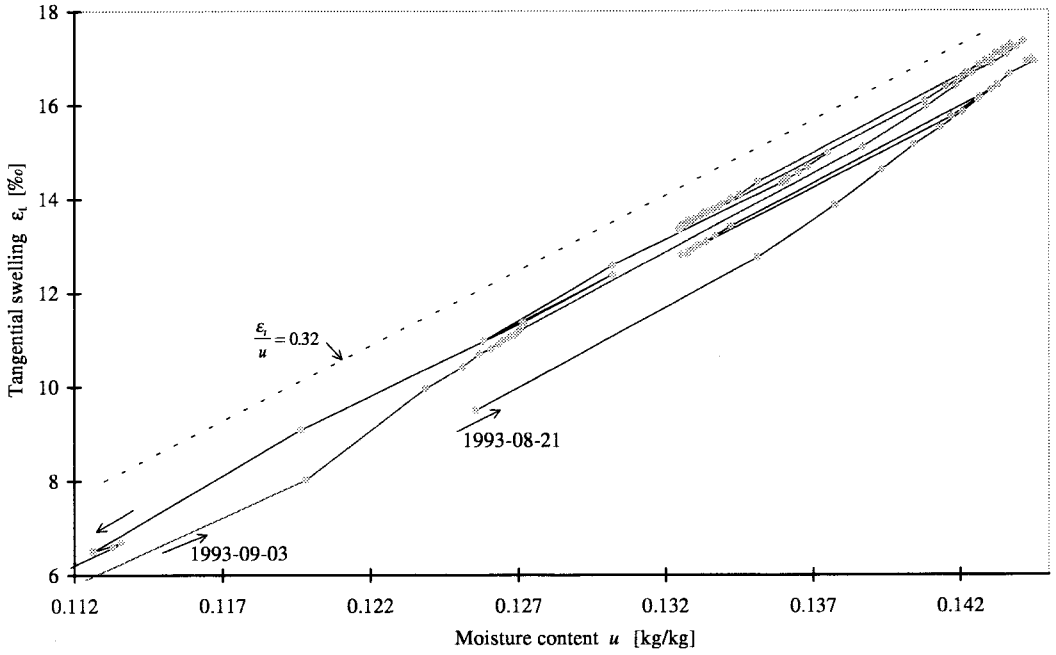

Figure 8.4 Tangential swelling ε_t as a function of moisture content u. Consecutive points in time are connected with a thin line. From the 65% – 75% RH cycles in the last part of Figure 8.1.

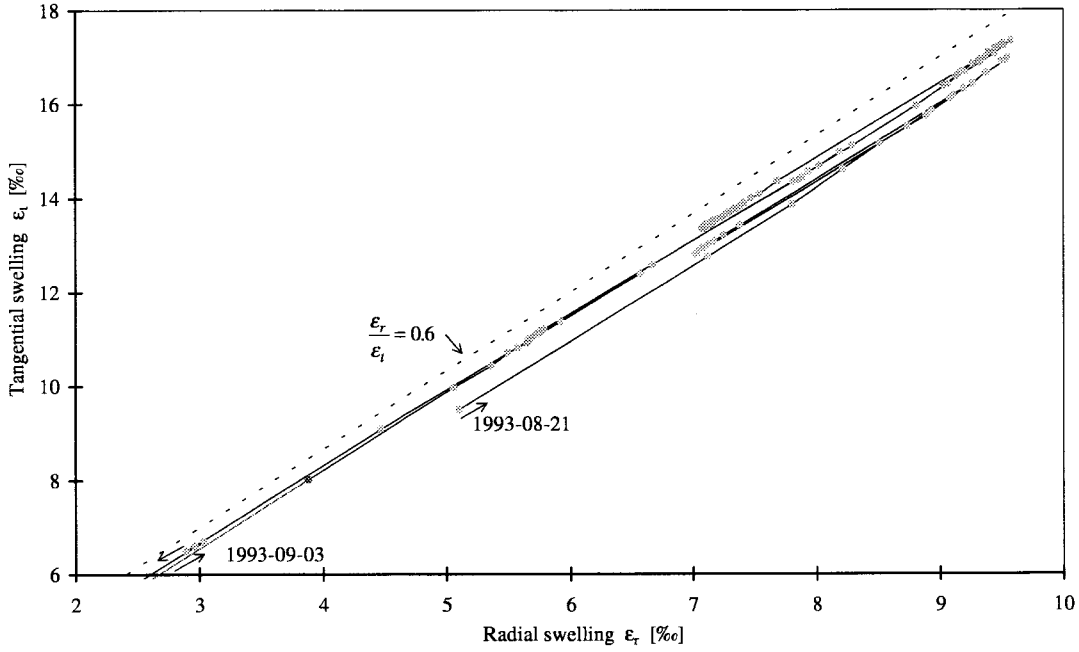

Figure 8.5 Tangential swelling ε_t as a function of radial swelling ε_r. Consecutive points in time are connected with a thin line. From the 65% – 75% RH cycles in the last part of Figure 8.1.

8.2.2 The last part of the fourth series

In Figure 8.6 to Figure 8.8 measurements of swelling from cycles between 75% and 85% are presented. The measurements of sorption $u(t)$ and tangential swelling $\varepsilon_t(t)$ are shown in Figure 8.6.

In Figure 8.7 tangential swelling is plotted against moisture content. The same pattern for the initial step to a previously not reached level is seen as in Figure 8.2. The initial step in the figure has a proportionally larger swelling than sorption. The remaining cycles in Figure 8.7 have only a slight drift towards higher tangential swelling compared to moisture content.

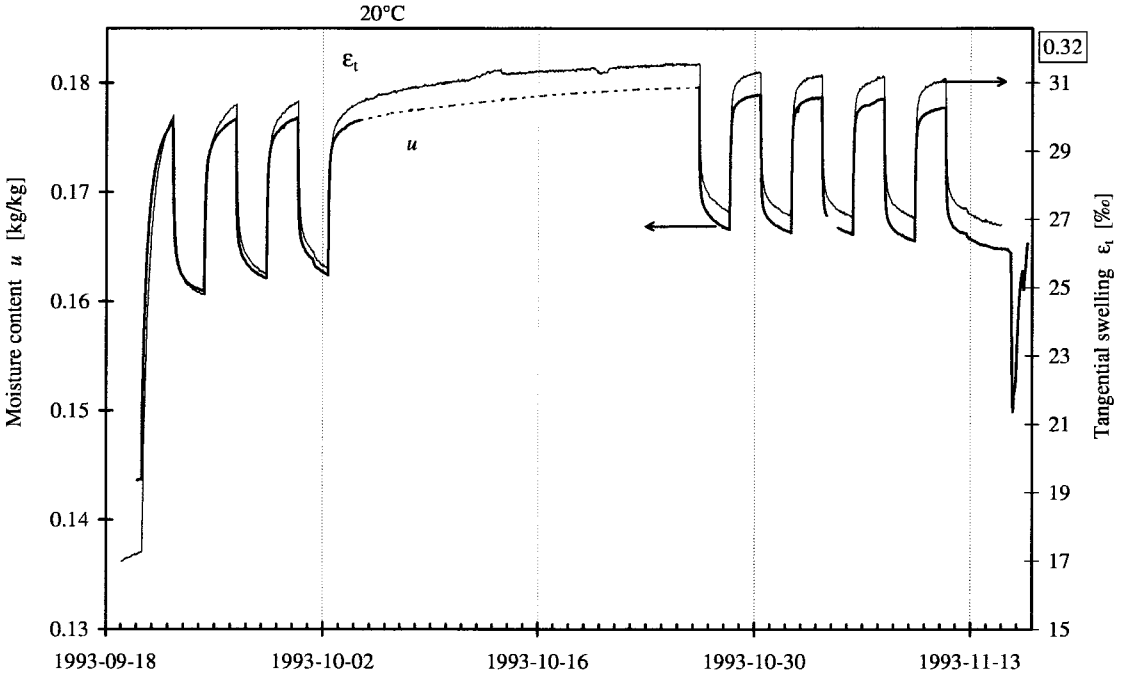

Figure 8.6 Sorption response compared with tangential swelling response, from the last part of the fourth series. 75% – 85% RH cycles.

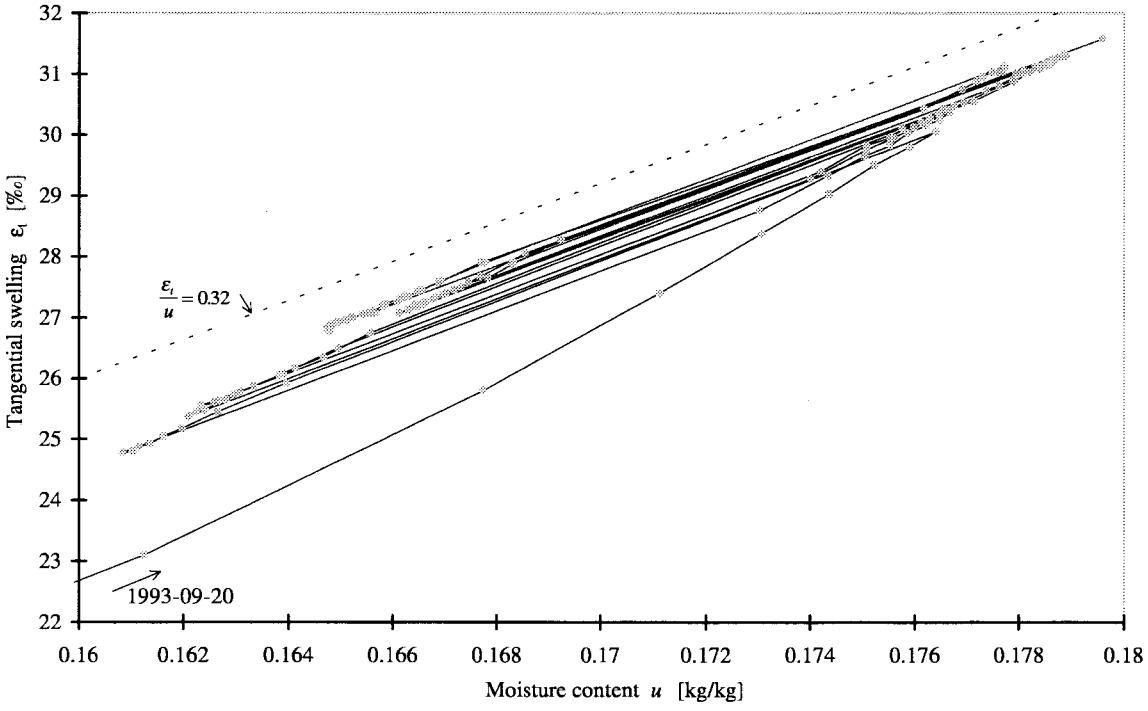

Figure 8.7 Tangential swelling ε_t as a function of moisture content u. Consecutive points in time are connected with a thin line. 75% – 85% RH cycles from Figure 8.6.

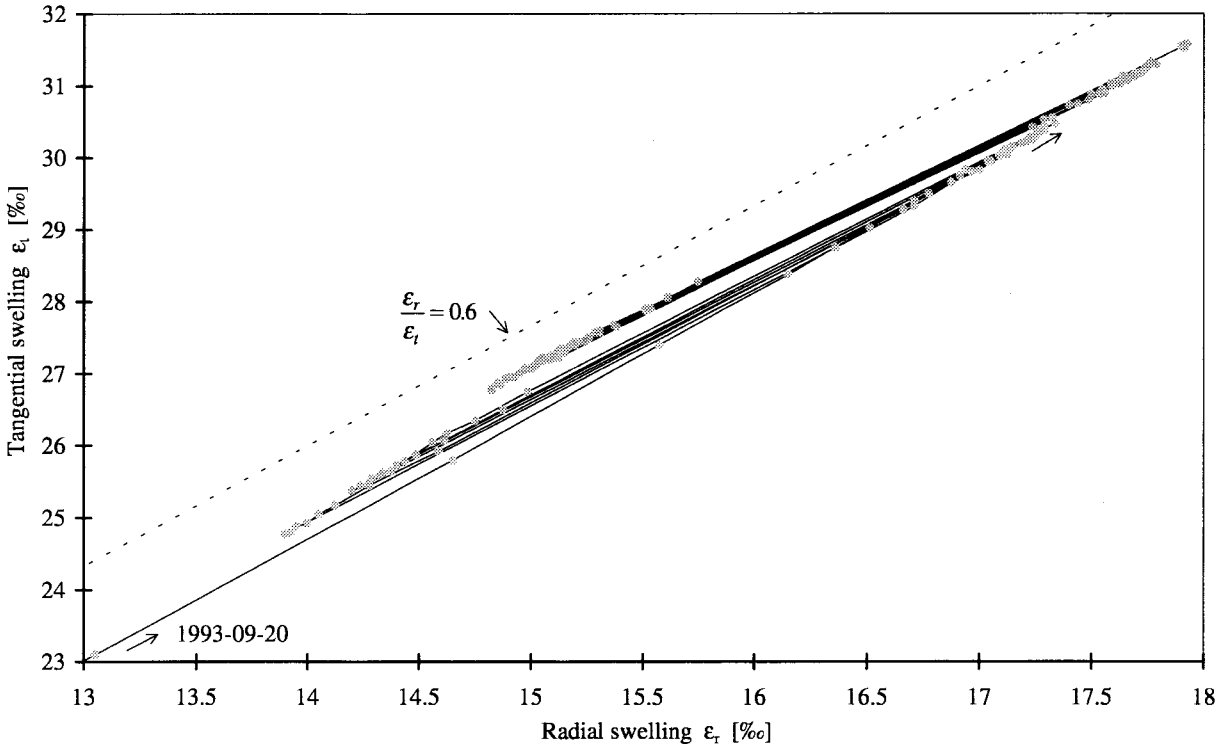

Figure 8.8 Tangential swelling ε_t as a function of radial swelling ε_r Consecutive points in time are connected with a thin line. 75% – 85% RH cycles from Figure 8.6.

8.2.3 The first part of the fifth series

The measurements of the fifth series are divided in three parts here. The first part includes the first cyclic steps in the fifth series. The second part describes cyclic steps at a higher RH level. The third part is a step to a high RH level maintained for a long time.

The measurements of sorption $u(t)$ and tangential swelling $\varepsilon_t(t)$ from the first part of the fifth series are shown in Figure 8.9. During the shift from 20°C to 5°C at the start of the fifth series an unintentional dip in RH was produced. This is shown at the beginning of the curves in Figure 8.9.

In Figure 8.10 the tangential swelling is plotted against moisture content for the cycles between 74% to 84% RH and for the following smaller cycles. In a corresponding diagram in Figure 8.11 the tangential swelling is plotted against the radial swelling. The large difference in swelling at the start of Figure 8.10 can be explained by thermal expansion.

In Figure 8.12 the tangential swelling is plotted against moisture content for a step to a previously not attained level (to 89% RH). We see the same pattern as in Figure 8.2 and Figure 8.7 before with proportionally larger swelling than sorption when RH is reaching beyond a previously not attained level.

In Figure 8.13 the tangential swelling is plotted against the radial swelling for the same sequence as Figure 8.12.

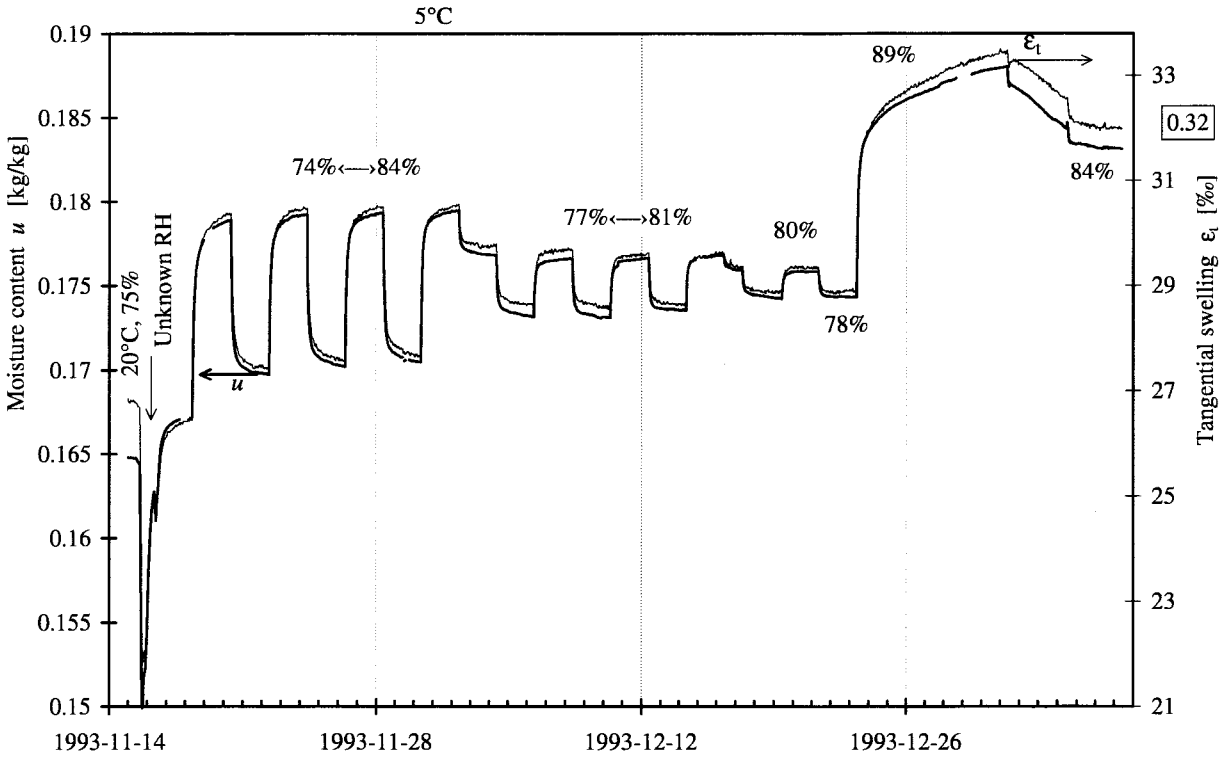

Figure 8.9 Sorption response compared with tangential swelling response, from the first part of the fifth series.

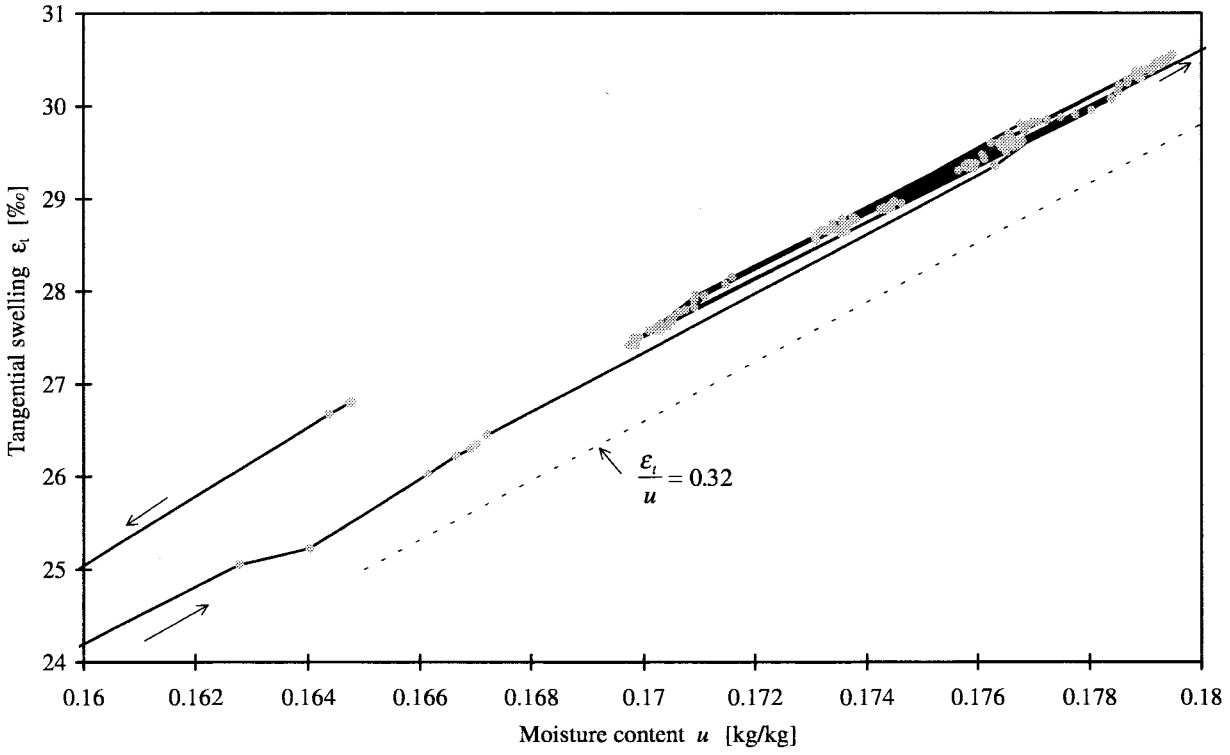

Figure 8.10 Tangential swelling ε_t as a function of moisture content u. Consecutive points in time are connected with a thin line. From the first part of Figure 8.9.

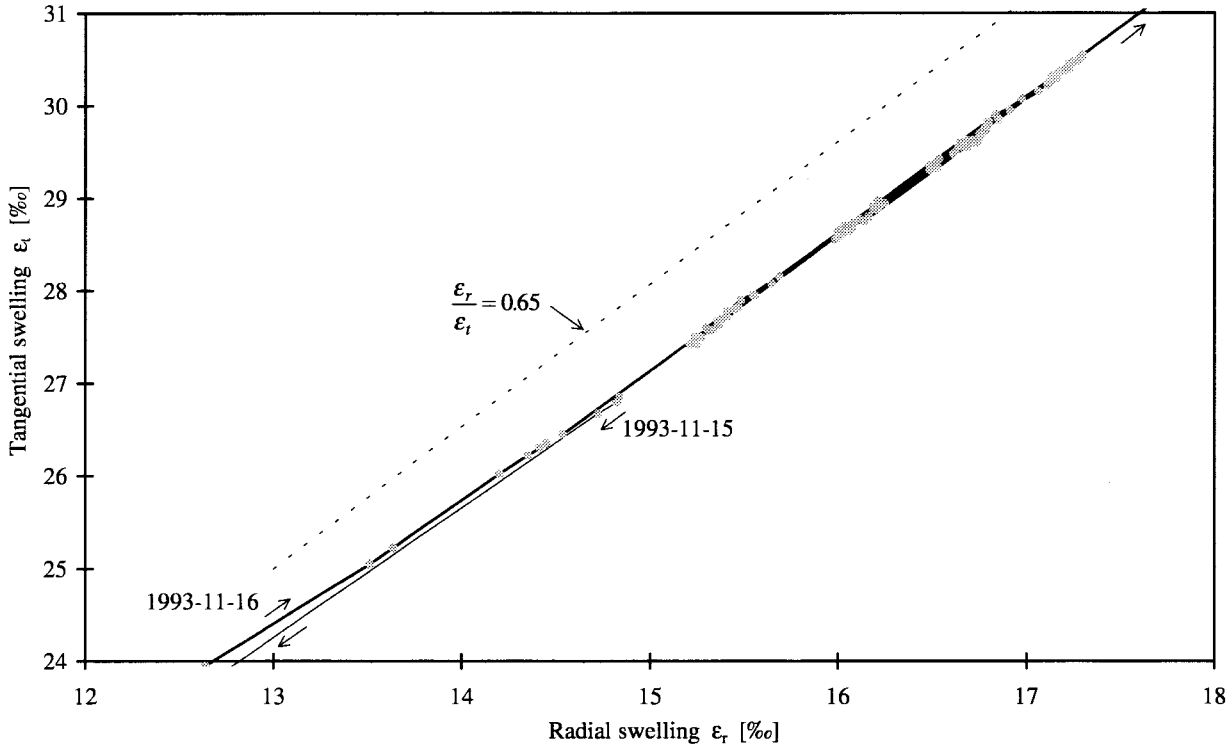

Figure 8.11 Tangential swelling ε_t as a function of radial swelling ε_r. Consecutive points in time are connected with a thin line. From the first part of Figure 8.9.

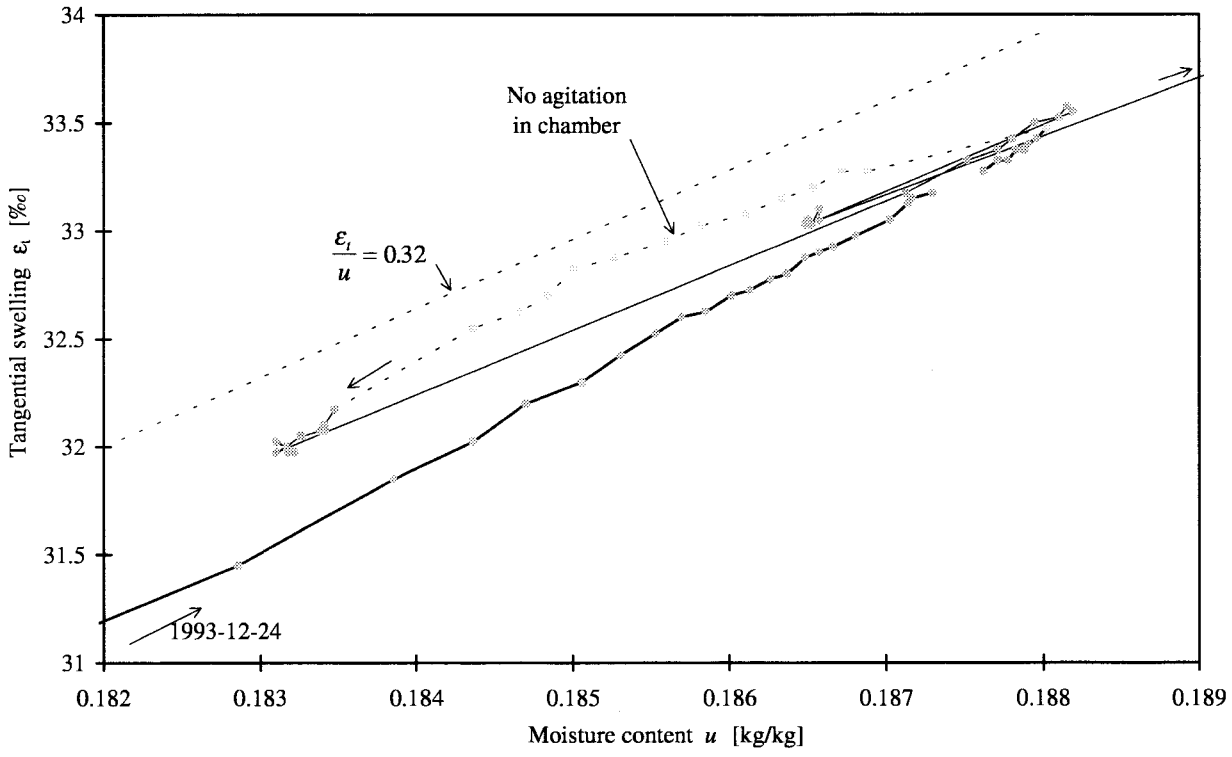

Figure 8.12 Tangential swelling ε_t as a function of moisture content u. Consecutive points in time are connected with a thin line. From the step to 89% RH and onwards in Figure 8.9.

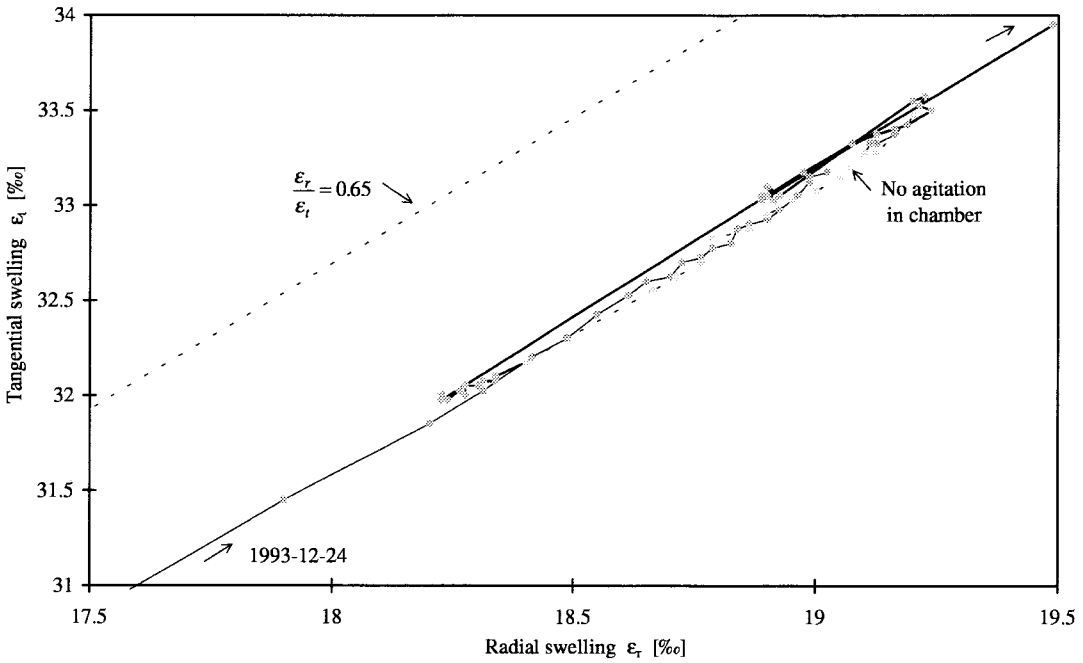

Figure 8.13 Tangential swelling ε_t as a function of radial swelling ε_r. Consecutive points in time are connected with a thin line. From the step to 89% RH and onwards in Figure 8.9.

8.2.4 Small cyclic steps in the fifth series

In Figure 8.14 to Figure 8.16, a number of small steps at a relatively high RH are made. For the smaller steps at the end of the sequence in Figure 8.15 the ε_t/u ratio is somewhat less than 0.32, indicated by the dashed line.

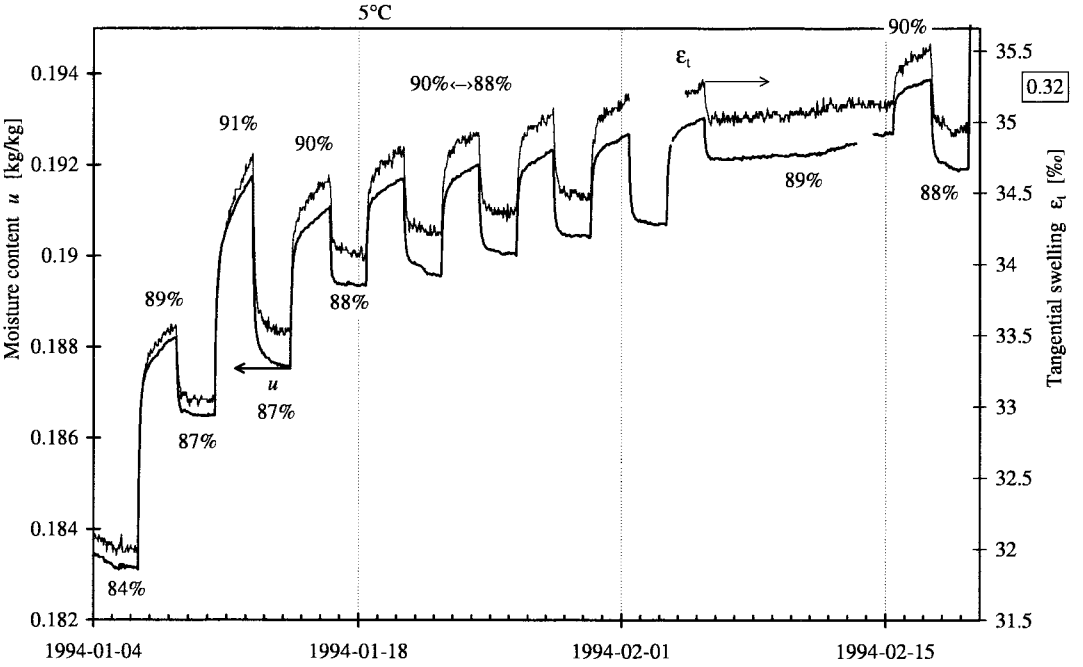

Figure 8.14 Sorption response compared with tangential swelling response, small cyclic steps in the fifth series.

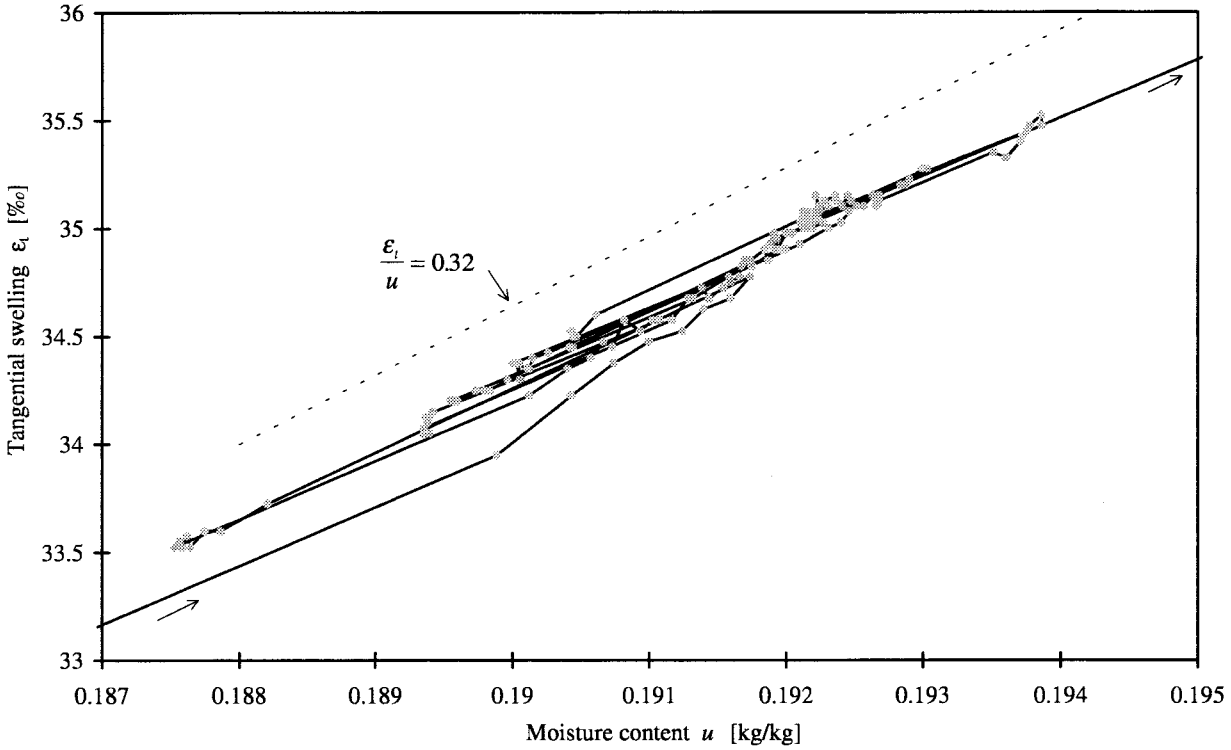

Figure 8.15 Tangential swelling ε_t as a function of moisture content u. Consecutive points in time are connected with a thin line. From Figure 8.14.

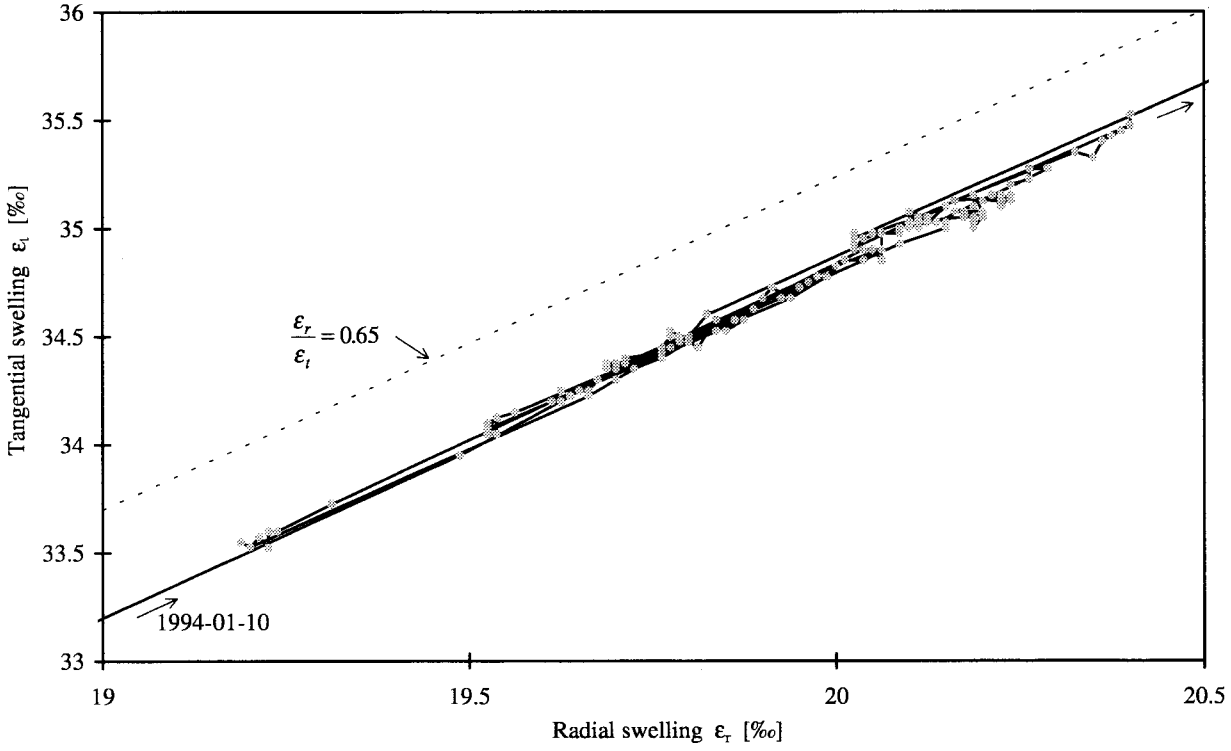

Figure 8.16 Tangential swelling ε_t as a function of radial swelling ε_r. Consecutive points in time are connected with a thin line. From Figure 8.14.

8.2.5 The last part of the fifth series

Finally, Figure 8.17 to Figure 8.19 describes a step to a high (93%) RH, followed by a few cyclic steps. The single step is maintained for a long time. We see in Figure 8.18 that the ε_t/u ratio is larger than 0.32 for the single step and smaller than 0.32 for the following cycles. The single step is reaching a previously not attained level.

Figure 8.19 shows that the same ratio as before between tangential and radial swelling is maintained for this part of the sequence at high RH.

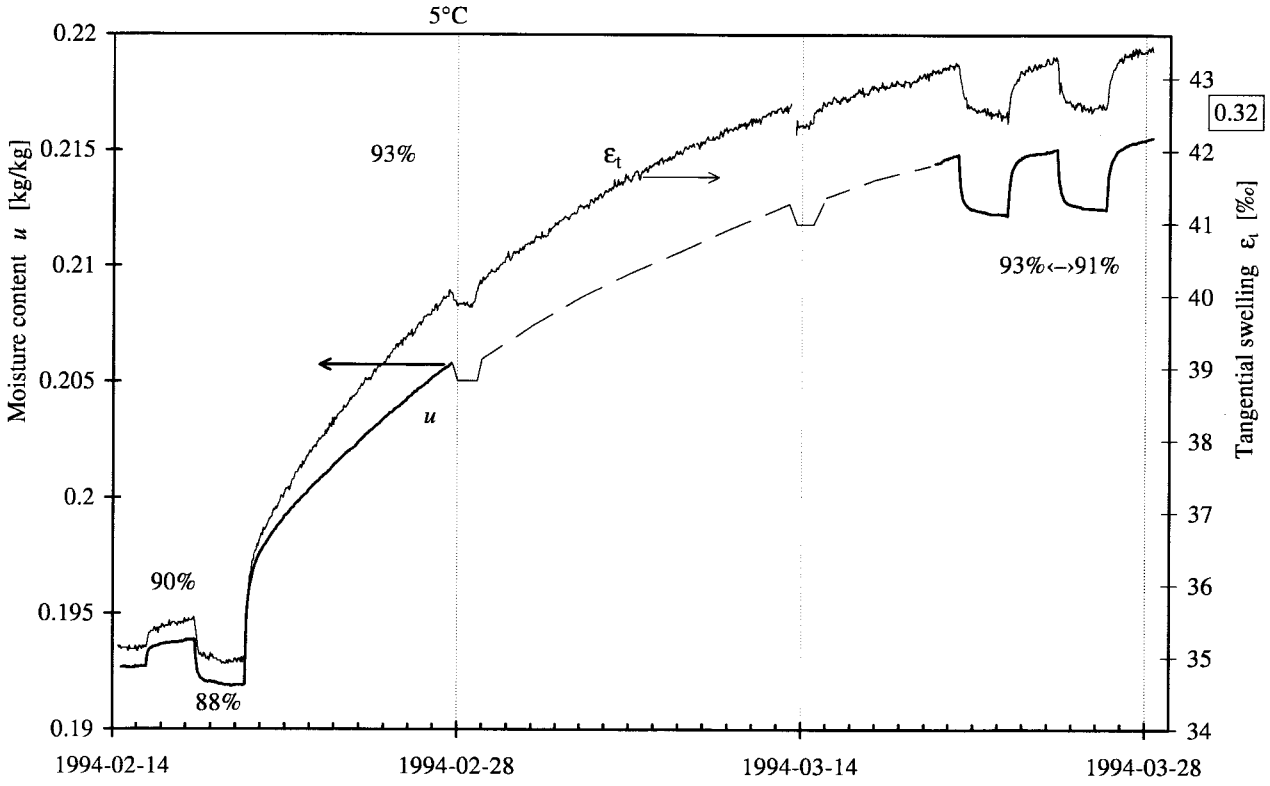

Figure 8.17 Sorption response compared with tangential swelling response, from the last part of the fifth series.

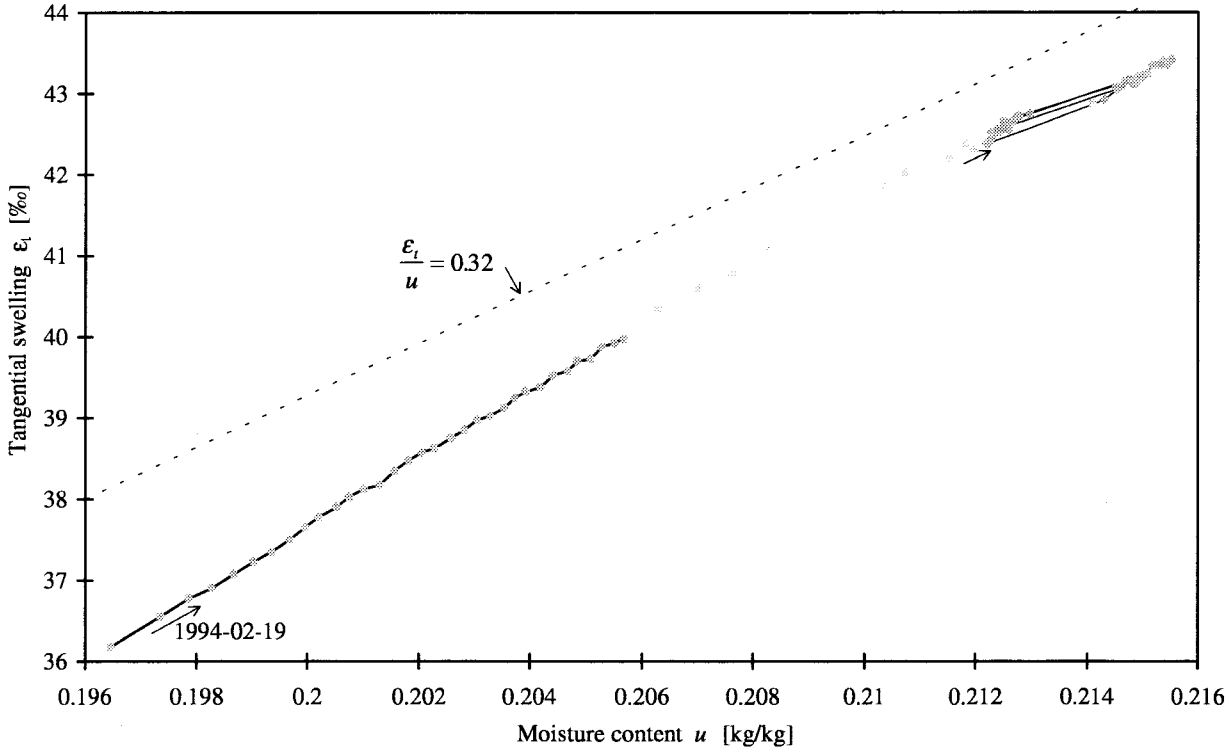

Figure 8.18 Tangential swelling ε_t as a function of moisture content u. Consecutive points in time are connected with a thin line. From Figure 8.17.

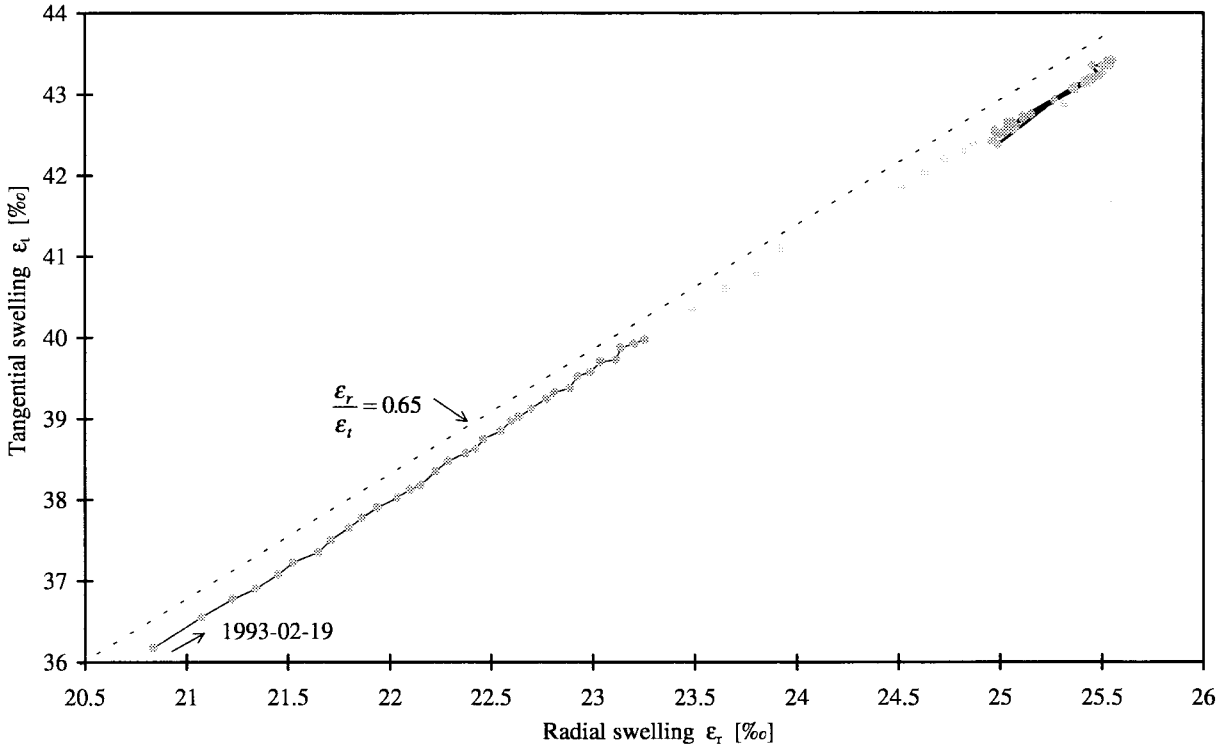

Figure 8.19 Tangential swelling ε_t as a function of radial swelling ε_r. Consecutive points in time are connected with a thin line. From Figure 8.17.

8.3 Volumetric swelling

Based on the measurements, an estimate of the relationship of the volumetric swelling and the volume of the sorbed water is made in the following way.

For small values, the volumetric relative swelling is the sum of the swelling in the three orthogonal directions:

$$\varepsilon_v = \varepsilon_t + \varepsilon_r + \varepsilon_l \qquad [m^3/m^3_{wood}]$$

An estimated average value for the relationship between $\varepsilon_r / \varepsilon_t$ is 0.65 for the fourth and fifth series. The longitudinal swelling was not measured, but the contribution is small and it is estimated to $\varepsilon_l = 0.05 \cdot \varepsilon_t$. The volumetric relative swelling is:

$$\varepsilon_V = \varepsilon_t + 0.65\varepsilon_t + 0.05\varepsilon_t = 1.7\varepsilon_t \qquad [m^3/m^3_{wood}]$$

The volume change of 1 m^3 of wood is $\varepsilon_V = 1.7 \cdot \varepsilon_t$. Let Δu denote the corresponding change of water content. The dry density of wood is $\rho_{dry} = 530$ kg/m^3. This means that $530 \cdot \Delta u$ kg water is added. The density of water is $\rho_{water} = 1000$ kg/m^3. The added water volume ΔV_w is then (if it were "free"):

$$\Delta V_w = \frac{\Delta u \cdot 530}{1000} \qquad [m^3_{water}/m^3_{wood}]$$

A representative value from the measurements for the ratio $\varepsilon_t / \Delta u$ is 0.32. The relationship between the volumetric relative change of the wood and the volume of the added water is.

$$\frac{\varepsilon_V}{\Delta V_w} = \frac{1.7 \cdot \varepsilon_t}{0.53 \cdot \Delta u} \cong \frac{1.7 \cdot 0.32 \cdot \Delta u}{0.53 \cdot \Delta u} = 1.026$$

One interpretation, since this relationship is close to one, is that the volume of the pores is unaffected and that the remaining wood is increasing in volume corresponding to the volume of the water.

8.4 Conclusions

In all different situations in the measurements, the tangential and radial swelling have rather similar step responses as the sorption. This means that roughly the same proportion between a fast response and a retarded response was measured. There is however a small difference. The fraction with retarded response is proportionally larger for swelling than for sorption. There is a pattern of order. The tangential swelling has most retarded response, closely followed by radial swelling, which in turn is followed by sorption. This pattern is consistent in the measurements (whenever a difference occurs).

Part III A non-linear model for retarded sorption

9 Characteristics of retarded sorption observed in measurements

Many observations and characteristics of the retarded sorption are presented in Chapter 6 and 7. In this chapter, some features are analysed further. Based on all this a tentative model to account for retarded sorption will be presented in Chapter 10.

9.1 Immediate moisture capacity

Figure 9.1 shows a typical moisture uptake $u(t)$ for a step-change of RH. The measured curve is the from the fifth series, Figure 6.52 (in this section somewhat incorrect dry weights have been used and the moisture contents vary from those in Chapter 6). There is a more or less exponential response during a first period. This is to be expected since the sample is very thin. But there is also a slow long-time increase.

The moisture sorption in the single cell wall may therefore be divided into two parts. The first part will be called the *immediate sorption* and the other part the *retarded sorption*. This distinction is not too precise. In conventional descriptions all moisture is assumed to be sorbed immediately if the sample is small enough.

This division into two parts is more pronounced at low temperatures. During the first hours after a step change, the time scale of the sorption is close to the conventional theory of diffusion, but with only a certain, often small fraction of the theoretical moisture capacity involved.

The following method has been used to estimate the immediate moisture capacity from the measurements. It is based on the fact that the sorption of a small sample after a step change, calculated with conventional theory, follows an exponential decline rather closely when half of the sorption has taken place. The measured moisture content u at t = 1, 2 ..6 hours after a step-change have been fitted to the following equation for exponential decline:

$$u(t) = u_1 - c \cdot e^{-t/t_0} \qquad (9.1)$$

It should be noted that the value u_0 at $t = 0$ is not included in the fitting.

The three adjusted variables are:

- u_1 final value for moisture content for the fitted fraction
- c constant
- t_0 time constant for a Fickian, single node response

A non-linear regression method has been employed to fit the constants with a least square criterion. An example of a graph of Eq. (9.1) fitted to measured points, is shown in Figure 9.1.

In the Eq. (9.2) below the final value u_1 from the fitted equation and the initial value u_0 are used to estimate the immediate moisture capacity $\Delta u_{im} / \Delta\varphi$:

$$\frac{\Delta u_{im}}{\Delta\varphi} = \frac{u_1 - u_0}{\varphi_1 - \varphi_0} \qquad (9.2)$$

Here , φ_0 and φ_1 are the RH-range of the step.

The calculated immediate moisture capacities are quite the same for absorption and desorption. An example of this can be seen in Figure 9.2 where the absorption step response is markedly different from the following desorption step response of the same RH-amplitude. The calculated immediate moisture changes, Δu_{im} , are on the other hand very similar. This example is taken from the fifth series, Figure 6.49.

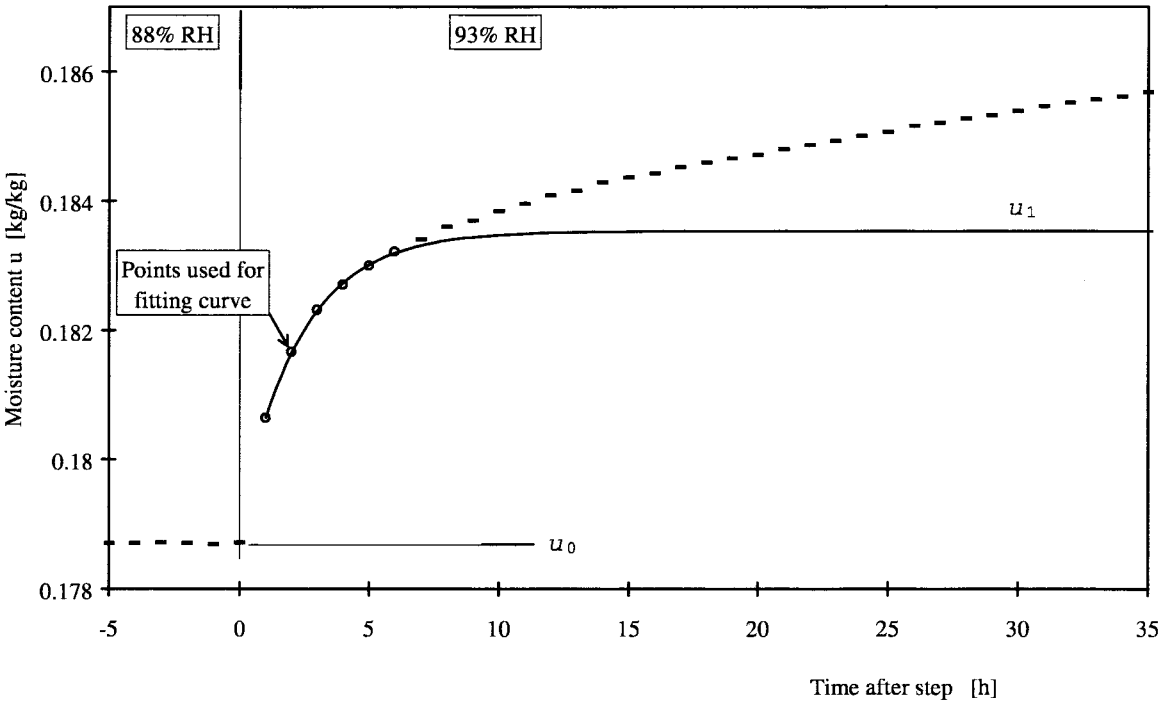

Figure 9.1 Exponential curve (9.1) fitted to the first part of the step response.

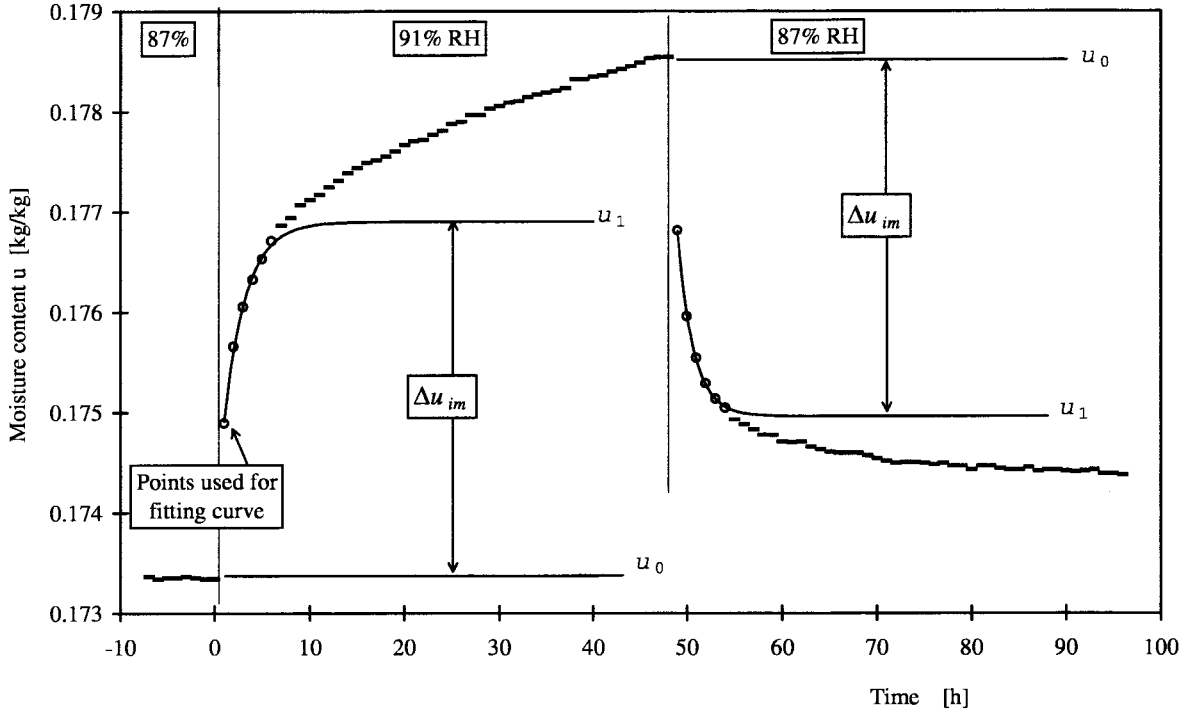

Figure 9.2 An example of almost equal immediate moisture capacity during absorption and desorption.

The immediate moisture capacities have been calculated for all measured step responses performed at 5°C. The result is shown in a survey in Figure 9.4. The two steps in Figure 9.2 have number 22 and 23 in the survey. Note that the axis represents order of events of the steps and not time. Some intervals are much longer than the most frequent 48 hours. Most of the measured sorption sequence at 5°C is shown in Figure 11.2.

Consecutive steps have similar immediate capacity, which seems to be independent of amplitude of step, interval between steps and absorption/desorption.

The time constants t_0 from the same calculations are shown in Figure 9.5. The time constant lies mainly in the interval from 1.5 h to 2.5 h with an average value for all time constants of 1.96 h.

These fitted time constants may be compared to what a simple model gives. See Figure 9.3, where the material in the sample is assumed to be lumped into one point. Here φ_{inlet} denotes the RH of the incoming air into the chamber. The total conductance K_0 is obtained from three resistances as described in Section 10.1.4. The dampening effect of the limited air supply, the surface resistance between the air and sample and the average resistance in the material. The immediate moisture capacity of the sample is denoted $\left.\frac{du}{d\varphi}\right|_{im}$.

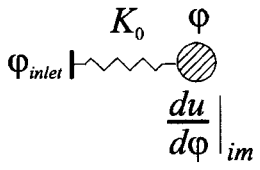

Figure 9.3 A simplified network for the immediate moisture capacity.

The moisture flux over the total conductance K_0 equals the moisture uptake:

$$\left.\frac{du}{d\varphi}\right|_{im} \cdot \frac{d\varphi}{dt} = K_0 \cdot (v_{inlet} - v)$$

Using the relation $v = \varphi \cdot v_{sat}(T)$, we get:

$$\frac{\left.\frac{du}{d\varphi}\right|_{im}}{v_{sat}(T) \cdot K_0} \cdot \frac{d\varphi}{dt} = \varphi_{inlet} - \varphi$$

This is a differential equation in $\varphi(t)$. The factor before $d\varphi/dt$ corresponds to the time constant t_0 :

$$t_0 = \frac{\left.\frac{du}{d\varphi}\right|_{im}}{v_{sat}(T) \cdot K_0} \qquad (9.3)$$

Inserting the above average value for t_0 and using the average value of $\Delta u_{im} / \Delta\varphi$ for $\left.\frac{du}{d\varphi}\right|_{im}$ we get:

$$K_0 = \frac{\left.\frac{du}{d\varphi}\right|_{im}}{t_0 \cdot v_{sat}(T)} = \frac{0.0945}{1.96 \cdot 3600 \cdot 6.80 \cdot 10^{-3}} = 0.00197 \qquad [m^3/(kg_{wood} \cdot s)]$$

there, $v_{sat}(T)$ is the saturated moisture content at the used 5°C.

This conductance may be compared to the value for the experimental set-up, which is given in Section 10.1.4. This value, which accounts for the moisture capacity of the air in the chamber, the sample surface resistance and ordinary diffusion in the thin sample. The value calculated for the experimental set-up, $K_0 = 0.0035$ [$m^3/(kg_{wood} \cdot s)$], is roughly twice as big. It corresponds to a time constant $t_0 \cong 1$ hour. This means that what is called here immediate sorption is influenced to a smaller extent by retarded effects.

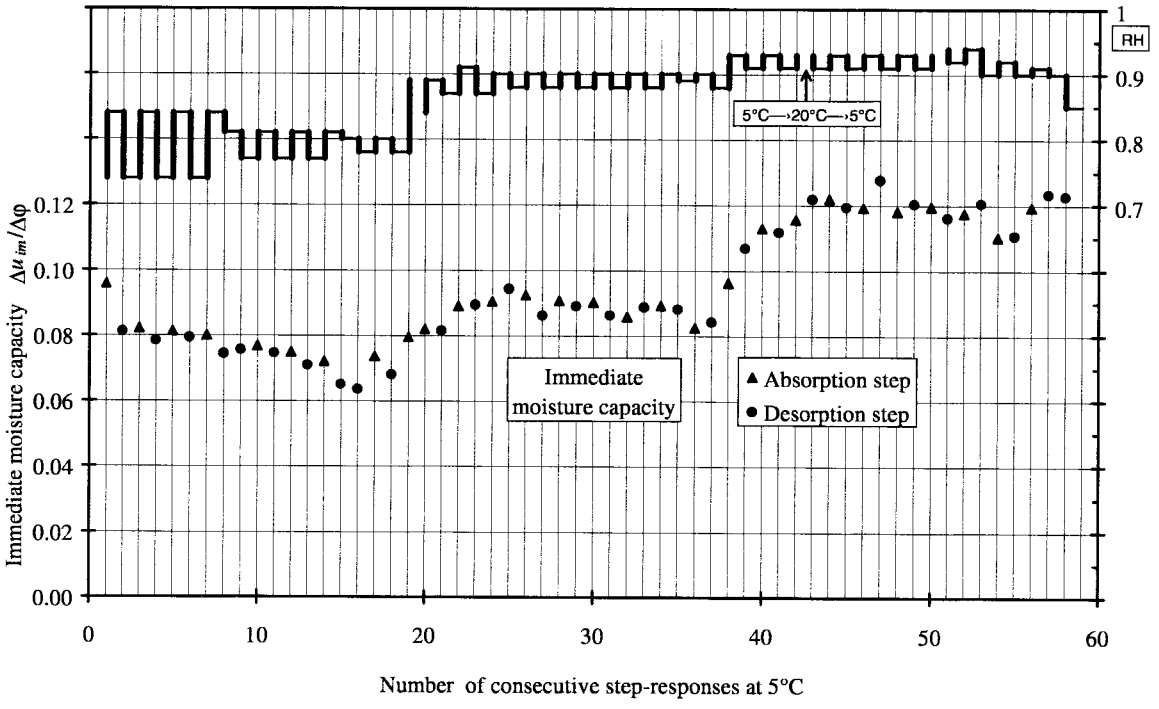

Figure 9.4 Survey of immediate moisture capacity calculated by exponential fitting, Eq. (9.1), for all measurements at 5°C.

An average value of the immediate capacities in Figure 9.4 all step changes is of interest. This value is 0.0945 [$kg_{water}/(kg_{wood} \cdot 100\%$ RH)] .

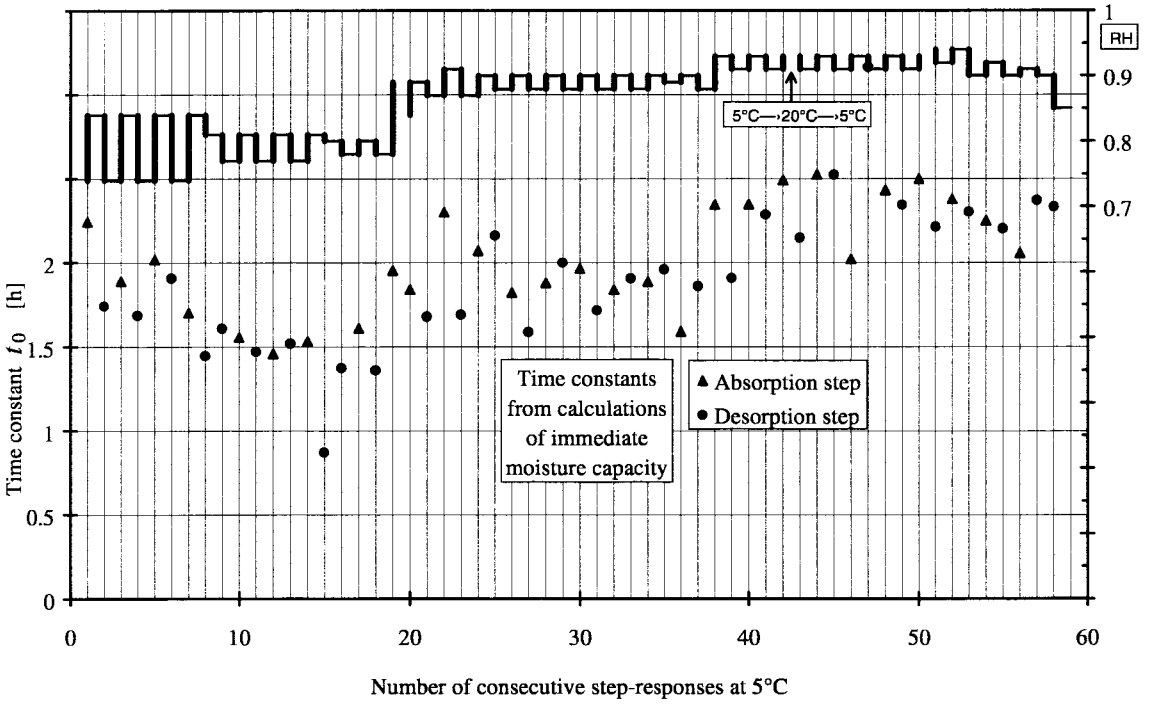

Figure 9.5 *Survey of time constants calculated by exponential fitting, Eq. (9.1), for all measurements at 5°C.*

The variation of immediate capacity with the RH-level is of interest. Figure 9.6 shows the estimated immediate capacity from all the sorption steps measured at 5°C to give the RH-dependence of the immediate capacity. An average between the two levels of RH in a step has been used for each point in the diagram. When consecutive periodic steps are made in the same interval however, a small alteration of RH has been done in order to be able to distinguish the individual points in the diagram.

Comparison can be made with the total moisture capacity in the same diagram derived from the slope of a moisture equilibrium curve. The immediate moisture capacity is rather constant over the measured RH-interval with only a slight increase at high RH, whereas the total moisture capacity is strongly increasing at high RH. Only a small fraction of the moisture capacity is immediate at high RH. This also illustrates that retarded sorption is more dominant at higher RH.

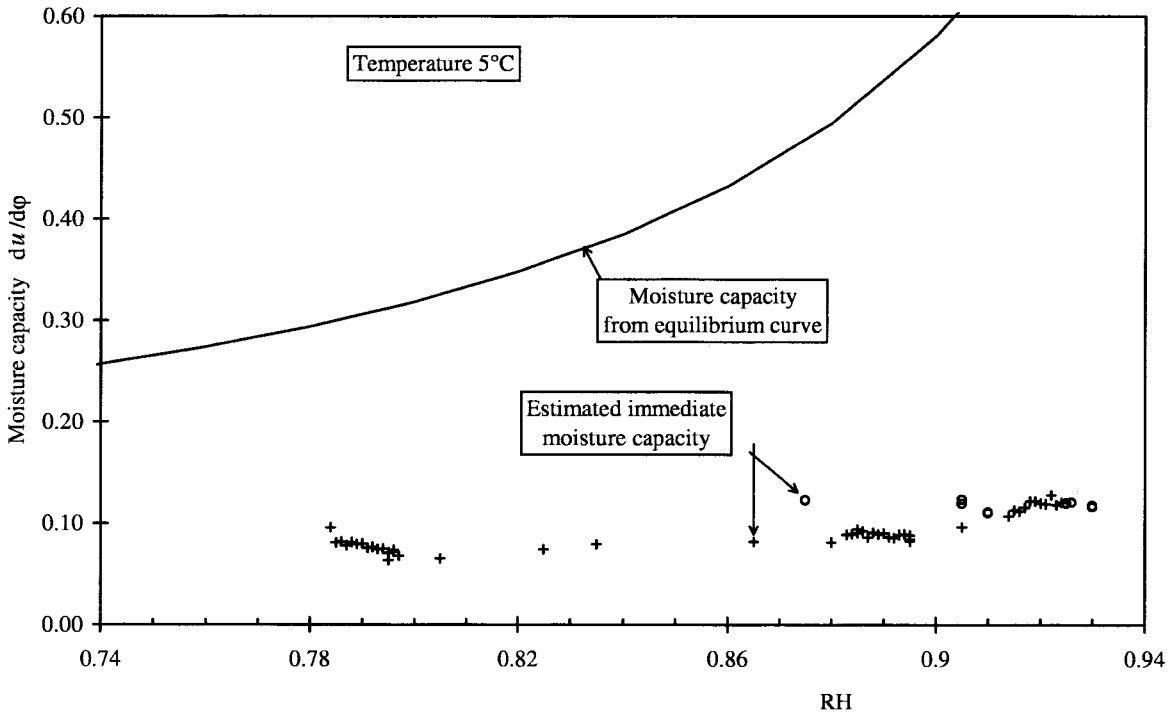

Figure 9.6 Immediate and total moisture capacity as a function of RH.

Another illustration of the fact that the immediate capacity can be small compared to the total is to look at measurements from periodic steps at low temperature and high RH and compare them with simulations based on traditional theory. This is made in Section 11.1.1, Figure 11.8.

9.2 Fitting the sorption curves using a few time constants

The sorption response can not be fitted by a single exponential function. The next step is to try a sum of exponentials with different time constants. The magnitude of each exponential component has to be fitted. Figure 9.7 shows an absorption response for a step in RH from 78% to 89% (Sample 4, the fifth series). A curve composed of three terms of exponential decline functions with assumed time constants has been fitted to the measured step response. A linear regression method has been used to determine the magnitude of each exponential function. The assumed time constants are 3, 20 and 150 hours. (The shape of the three components are shown in the figure. The sum is shown as 'Fitted curve'.) A good fit is possible and an extrapolation to an equilibrium is obtained.

This approach has been tested on many of the sorption responses from the tests of thicker samples (3 mm) in the first series and with longer intervals between steps. Up to seven time constants from 2h to 1000 h have been used. The magnitude of each exponential was determined for the best fit. There was not any regular pattern.

In view of the different step responses that have been recorded a more complex model is needed. The step response seems to be dependent on the amplitude of the step. A non-linear model that is able to take this into account is tested in Chapter 11, Section 11.2 and onwards.

The different measured step responses however show a variety of patterns seemingly depending on the previous conditions. This makes extrapolating a single curve of response to a

true equilibrium precarious. Such calculations are very sensitive to the assumed conditions and have failed to produce consistent equilibrium results.

In view of the many types of step responses that have been recorded a more complex model that is able to forecast the time pattern based on the previous history could be expected to be needed to find a more true equilibrium.

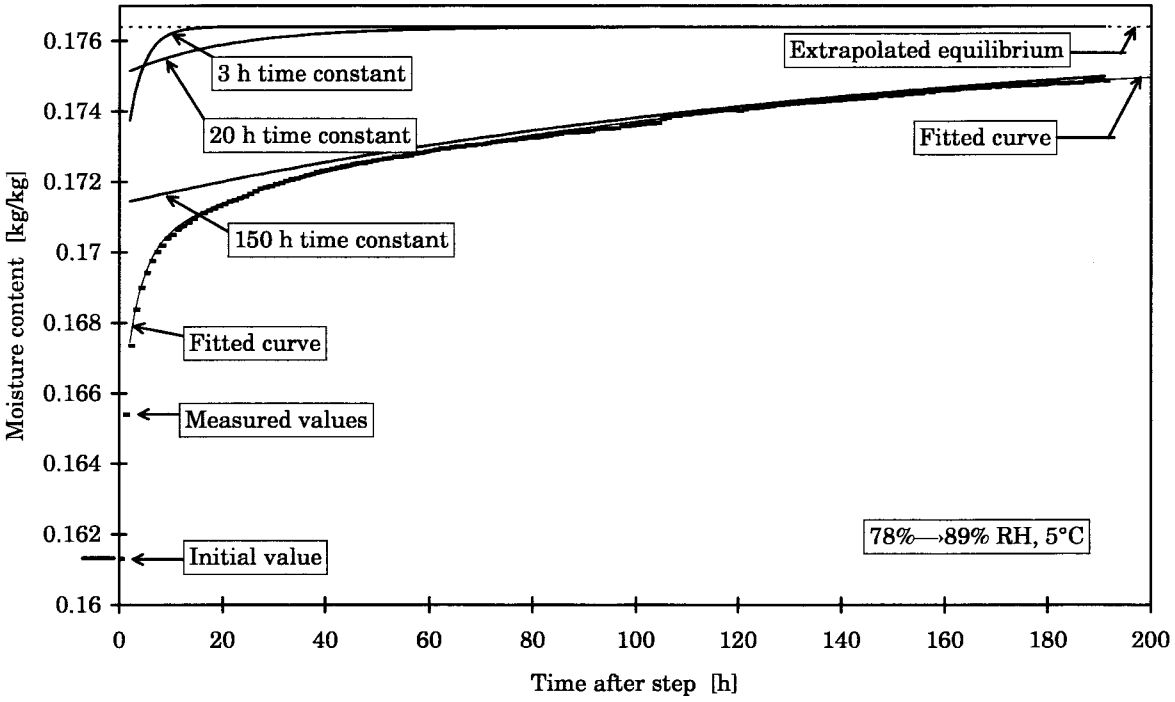

Figure 9.7 Fitting of measured response using exponential functions.

9.3 Blocking of moisture capacity in the cell wall

The retarded sorption has several features that could be described as a blocking of the moisture capacity. This blocking alters according to the conditions. It can be built up when RH and temperature are limited to a small range. This can be seen when a sample is subjected to repeated RH-cycles with small amplitude. An example is shown in Figure 9.8 where the step is from 85% to 90% RH taken from the sixth series, Figure 6.61. The moisture exchange is small with a decreasing tendency with the number of cycles.

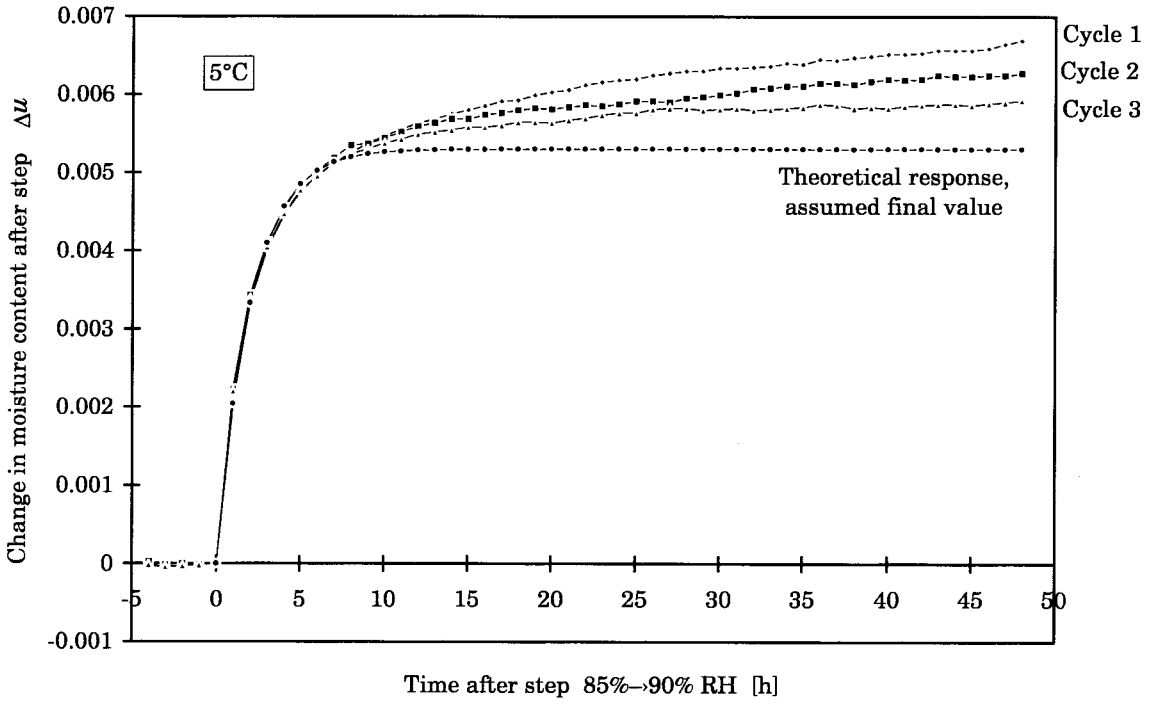

Figure 9.8 Calculated step response with assumed moisture capacity.

The blocking diminishes considerably when a large abrupt change of RH is made. If the previous strong blocking has caused the sorption to deviate significantly from a true equilibrium and if the new large step has the absorption-desorption direction to interact with it, a large sorption takes place. One such example is when cyclic steps are made and they are followed by a step to a previously not attained limit. The time scales of these large sorption responses seem to vary in a wide range in the measurements. This could to some extent be attributed to the wide range of moisture capacities over the used RH-interval since the timescale of the response is proportional to the capacity. The driving forces for the moisture uptake are proportional to the saturated vapour content that are strongly increasing with temperature. Simulations with a model that takes this into account can be expected to get a better overview of the specific parameters influencing the retarded sorption.

The total moisture capacity, represented by the slope of the moisture equilibrium curve, is strongly increasing with high RH for wood. The immediate capacity has been found rather constant over the RH range as mentioned earlier. Thus the reminder of the capacity which then carries the retarded properties, is much more dominating at high RH.

The step response is influenced by the previous moisture history. An example is when an absorption step has been executed outside previously attained limits, where a larger proportion of the sorption is retarded.

9.4 Superposition of step responses

When two small step responses from the measurements are superimposed, the result is clearly different from a response in the same interval where the change is made in a single step. This illustrates that the sorption is non-linear. This is demonstrated in Figure 9.9, Figure 9.10 and Figure 9.11 where the dotted line represents the two superimposed step responses. The complete measurement sequences are shown in Section 6.1. A general experience from the measurements is that the retarded part of the sorption is proportionally larger with small steps. There is also a tendency that the sorption is larger when it is made in few larger steps even when the response is extrapolated to equilibrium.

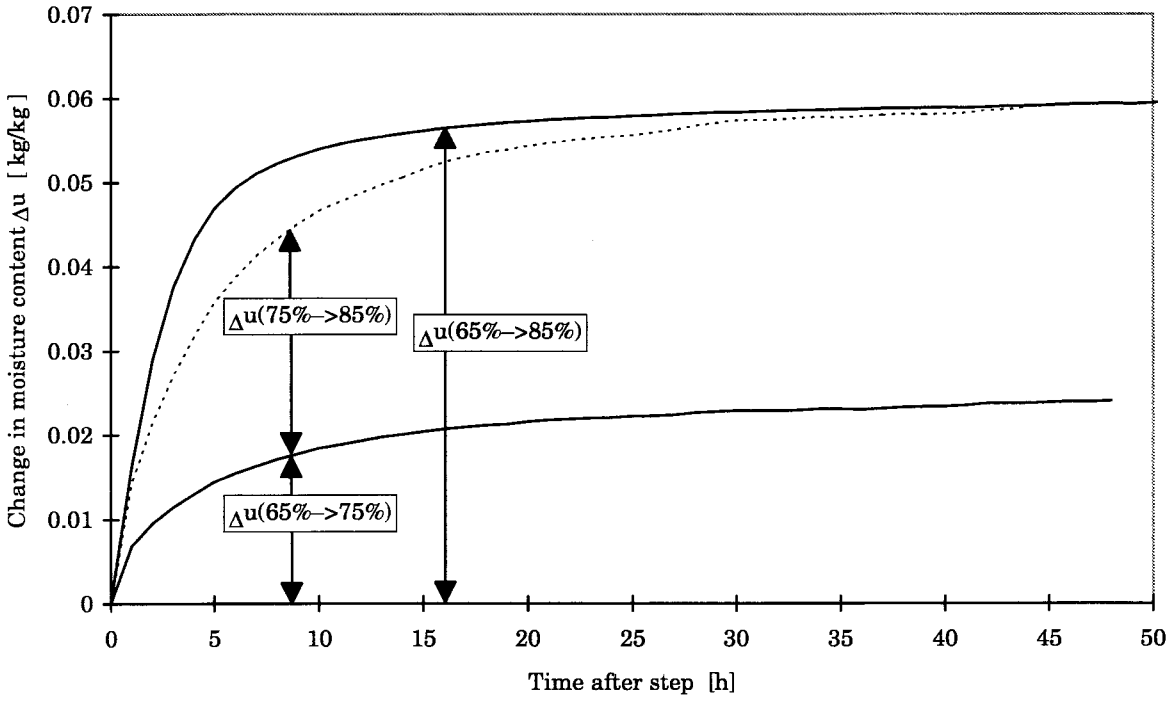

Figure 9.9 Two superimposed step responses compared to a single step. Absorption, 1.7 mm samples.

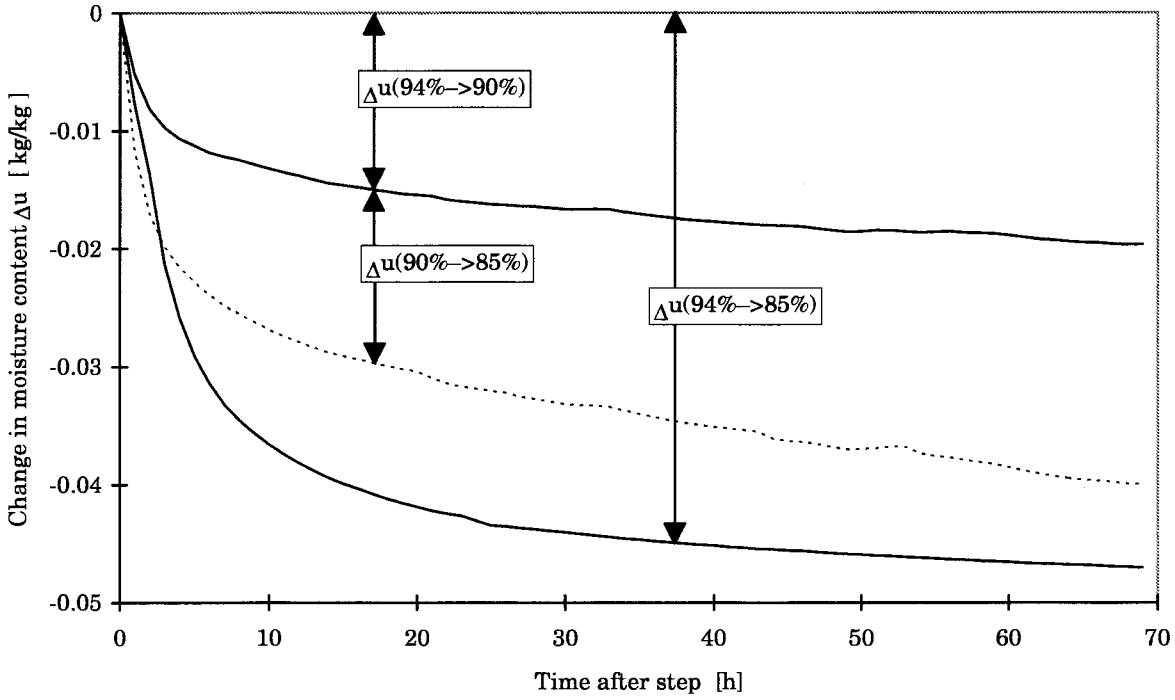

Figure 9.10 Two superimposed step responses compared to a single step. Desorption, 1.7 mm samples.

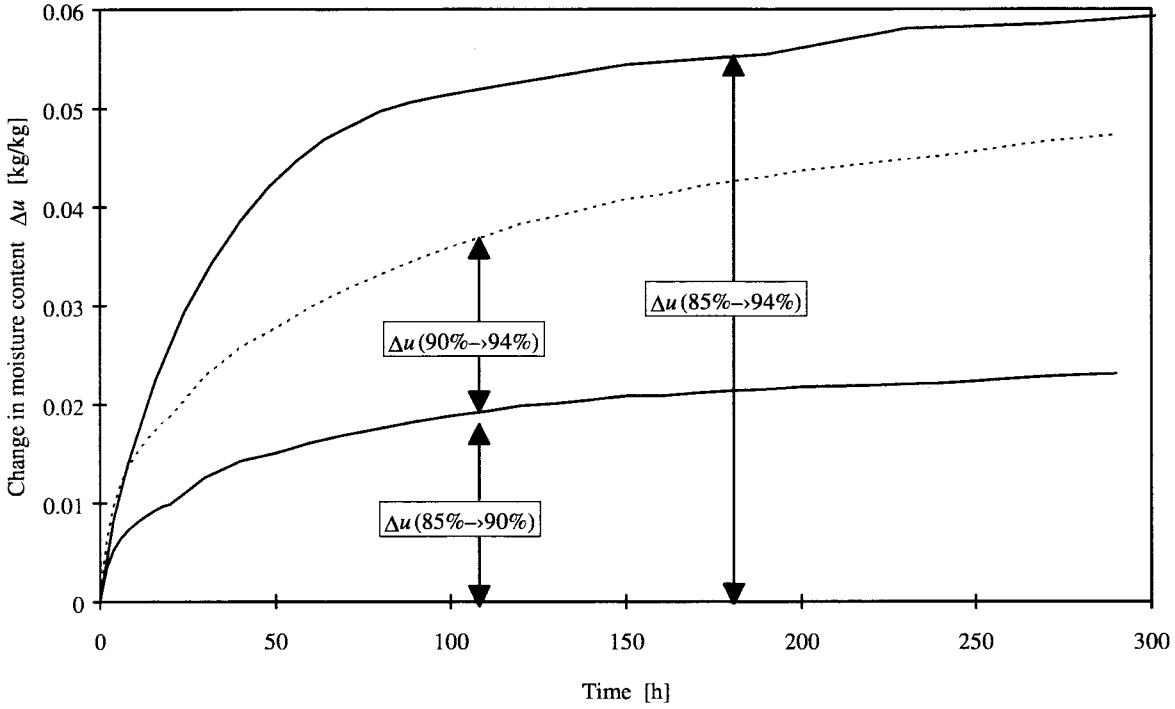

Figure 9.11 Two superimposed step responses compared to a single step. Absorption, 3 mm samples.

9.5 Temperature dependence of the retarded sorption

At lower temperatures the effects from the retarded sorption are more prominent and the sorption is more distinctly divided into immediate and retarded parts. The time-scales of the responses are also greatly increased. In cyclic steps the moisture exchange is significantly lower at 5°C than at 20°C.

An example of the influence of temperature change on retarded sorption can be seen in Figure 9.12 covering an 80-day period. This period has been preceded by a long period of slow absorption in steps at 5°C upon which cycles with small amplitude have been added. Then one larger absorption step from 88% to 93% RH is made to an previously not attained level. (At 1994-02-19 in Figure 9.12). This gives a remarkably large portion of retarded sorption. Even 30 days after the step a considerable drift is observed and only 68% of the sorption has taken place according to an estimation by extrapolation. (An exponential decline with a single time constant is assumed in this extrapolation and the last 20 days has been used in the calculation).

After some additional small cycles (91% ↔ 93% RH), the temperature is shifted to 20°C. According to the temperature dependency of the moisture equilibrium curve, 93% RH at 5°C gives a higher moisture content than 94% RH at 20 °C, but nevertheless an essential absorption occurs. The sorption unmistakably defies the traditional theory for the moisture equilibrium in this situation. At least for a part of the sorption, an explanation could be that the earlier ongoing process of slow retarded sorption is strongly accelerated.

The temperature is once again shifted to 5°C at 1994-04-15 and the same small cycles are repeated. The moisture content is now much higher and no drift is observed after the impact of the temperature cycle from 5°C to 20°C and back to 5°C.

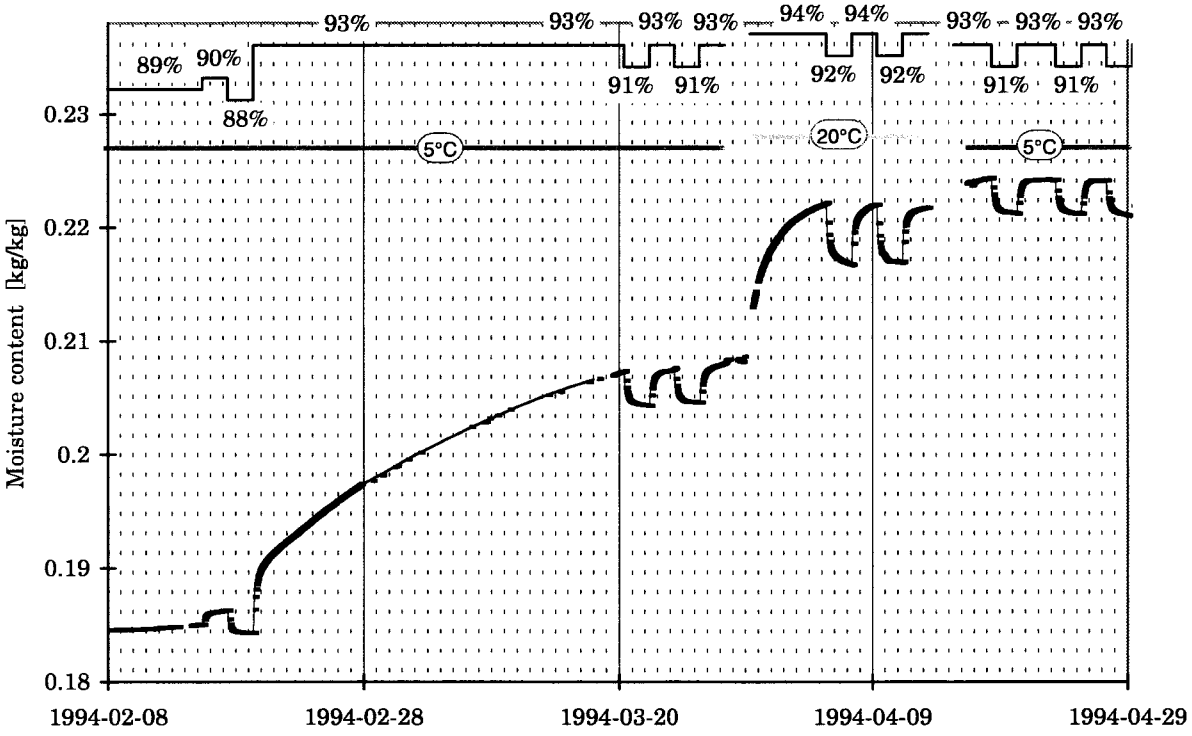

Figure 9.12 Sorption sequence with temperature shifts.

9.6 True sorption equilibrium

A unique moisture content versus RH at equilibrium is assumed for continuous absorption in conventional models. Any dependence on previous moisture history (except hysteresis) is not accounted for. Many measurements contradict this assumption. It has been reported that larger absorption steps give higher final moisture content than corresponding smaller ones. See for example Christensen (1965). However, since the sorption time-scales for the smaller RH-steps have proved to be much longer, an interpretation could be that the final moisture contents are the same if it was possible to wait sufficiently long time.

9.7 Modelling of layers in the cell wall

One pronounced feature of the retarded sorption is the small moisture exchange when the wood is subjected to RH-cycles. One possibility is to associate this to a limited penetration depth in the cell wall depending on the duration of the cycles. In a discrete model this depth corresponds to levels connected in series. A model with many levels can provide the gradually longer time-scales for the sorption which invariably have been observed after a step change. As each level has its own RH, the complexity of the model is increased by the number of levels. A model with several layers will be able to hold more intrinsic information about the moisture history of the sample.

Another possibility for a model to have a small moisture exchange if subjected to cycles, is if it is based on a hysteresis moisture equilibrium curve. One example of such a curve is seen in Figure 11.47. Here the intermediate curves which run between the absorption curve and the desorption curve designated 'pivot line', applies for the cyclic sorption case. The intermediate lines can be constructed to be much more horizontal than the upper desorption line or the lower absorption curve in the same RH-interval, to adopt to a desired lower moisture capacity.

Measurements have been made where the sample has been subjected to cycles that are followed by a larger absorption step outside previously attained limits. On these occasions a comparatively larger amount of moisture is activated by the large step, compared to the previous cyclic steps. In a model with a hysteresis moisture equilibrium curve this situation with cyclic steps corresponds to cycles on path c–›d in Figure 11.49 with low moisture capacity. When followed by a larger step, this corresponds to path d–›e in Figure 11.50 on the absorption curve, with a higher moisture capacity. The measurements show that the sorption is large when this last larger step is made, and it is distinctly retarded with long time-scales. This illustrates that the hysteresis seems not to be coupled to the immediate level in the model, but to have a stronger connection to deeper levels.

9.8 Non-linear retarded sorption

The retarded part of the sorption shows non-linear characteristics. When comparing the step response from one large step with the sum of two smaller steps, the larger step results in larger sorption with a proportionally smaller part retarded sorption.

To simulate the retarded sorption the models used here are composed of discrete conductances and capacities. If these components are linear a superposition of the responses would produce the same result, independent of how the division of steps is made. Thus, the conductances must be non-linear, i. e. they must depend on the moisture conditions of the internal levels.

10 Selected model

The aim of the extensive measurements is to study the effects of retarded sorption and to establish an experimental base for models of this transient sorption. The final goal is to be able to simulate the retarded sorption with sufficient accuracy with the simplest possible model. This is a complicated task. The efforts reported here should be regarded as tentative first models.

10.1 Model structure

An introductory presentation of the contemplated model of the retarded sorption and its coupling to the complete moisture process in wood is given in Section 1.1.5. Figure 1.3 showed the conceptual moisture flow network. See also Figure 10.2. In a conventional numerical solution we divide the porous material in nodes. Each node has a moisture capacity. The moisture flow is determined by the moisture conductances between the nodes. We get a moisture flow network with capacities that are coupled to neighbouring nodes and boundary nodes by conductances. A conventional model for a one-dimensional process with four nodes is shown in Figure 10.1.

Figure 10.1 Conventional, one-dimensional model (four nodes).

The model designed to simulate the retarded sorption consists of a number of internal nodes coupled to an outer node. The macroscale flow occurs in a conventional network between these outer nodes. In Figure 10.2 two internal nodes in series are added.

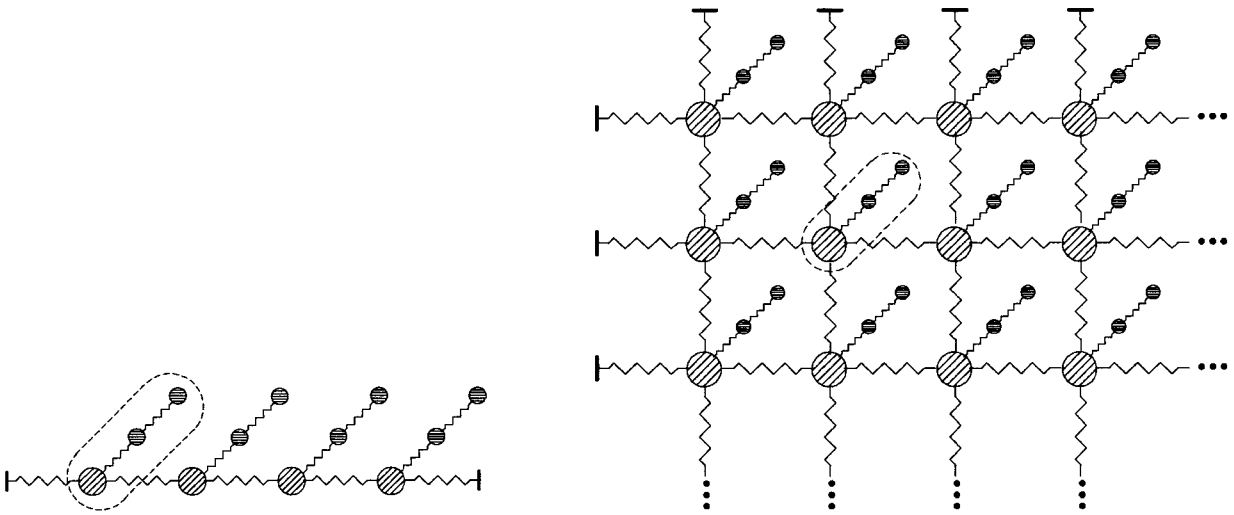

Figure 10.2 One- and two-dimensional moisture flow networks. The retarded sorption is modelled by internal nodes (enclosed by the dashed lines).

The model for retarded sorption involves only the outer node and its "appendix" of inner nodes. This part of the total network is enclosed by dashed lines in Figure 10.2. In the following we will only deal with this part, and omit the conventional network.

The thin samples used in the experiments are designed to register the internal moisture uptake in the cell wall. But the samples interaction with the climate chambers must be accounted for by a moisture conductance. Figure 10.3 shows the conceptual model of the experiments. The inlet water vapour content $v_{inlet}(t)$ acts over a moisture conductance on the outer node, which is in contact with inner nodes by conductances in series.

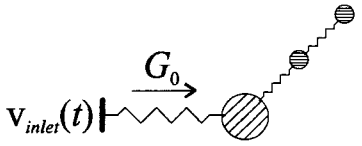

Figure 10.3 Network for the thin samples of the experiments. Outer node in contact with the climate chamber and two internal levels.

10.1.1 Moisture distribution in levels

To model the retarded sorption, N internal levels are added to an outer layer in direct contact to the cell lumen. The internal levels are thought to be situated deeper in the cell wall, and the macro-scale moisture flow may be assumed to take place in the outer layer only.

Thus the moisture content u is assumed to be distributed in $N + 1$ levels, where N levels are internal in the cell wall:

$$u(\varphi) = u_0(\varphi) + u_1(\varphi) + \ldots + u_N(\varphi) \qquad (10.1)$$

The total retarded sorption [kg_{water}/kg_{wood}] is given by the sum $u_1(\varphi) + \ldots + u_N(\varphi)$ of all internal nodes. The outer node with its part $u_0(\varphi)$ of the total capacity $u(\varphi)$ represents immediate or rapidly accessible moisture capacity.

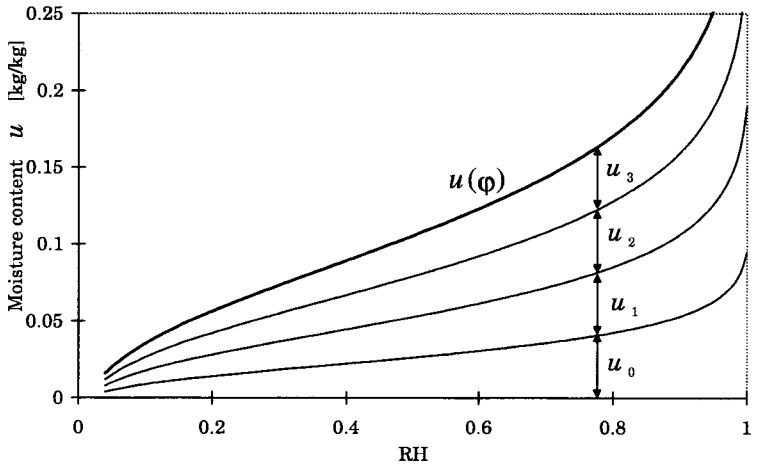

Figure 10.4 Distribution of the moisture content $u(\varphi)$ in an external part u_0, and N internal parts to represent retarded sorption. N = 3.

10.1.2 Internal moisture flows

The total moisture flow to the sample is denoted G_0 [kg_{water} / s]. We consider the whole sample with its mass m. The moisture flow from level n-1 to n is denoted G_n , n = 1,... N. See Figure 10.5. Here, the moisture flow conductances are represented by a new, more "wavy" symbol. This is done in order to emphasise that the conductance may be non-linear, i. e. not constant but dependent on the moisture state of the two adjacent nodes.

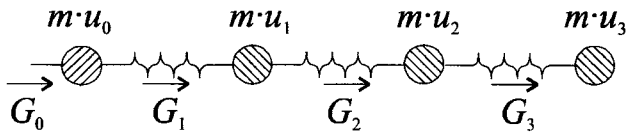

Figure 10.5 Network for the moisture flows between internal levels in the cell wall for the sample with mass m.

The dry mass of the sample is m [kg_{wood}]. The moisture flows per *unit dry mass* between internal levels are denoted g_n .

$$G_n = m \cdot g_n \qquad n = 0, 1... N$$

The moisture network related to a unit dry mass of the sample is shown in Figure 10.6.

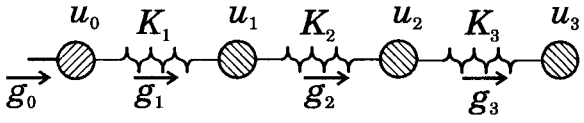

Figure 10.6 Network for the selected model for a unit dry mass of the sample.

The moisture flow between nodes depends on the differences in moisture state. We will use water vapour content v as state variable. The water vapour content in the outer node is v_0 and it is v_n in node n. Let K_n [$m^3/(kg_{wood} \cdot s)$] denote the moisture conductance between node $n-1$ and n. See Figure 10.6. These conductances have vapour content as driving potential, and they concern a unit mass of the wood sample. We have:

$$g_n = K_n \cdot (v_{n-1} - v_n) \qquad n = 1, ... N \qquad (10.2)$$

We assume in general that the internal conductance K_n depends on the two adjacent vapour contents v_{n-1} and v_n :

$$K_n = K_n (v_{n-1}, v_n)$$

An important case is of course constant values K_1,... K_n . The model is then linear. In the non-linear case we will test a power law of the following type:

$$K_n = k_n \cdot |v_{n-1} - v_n|^{\gamma} \qquad (10.3)$$

The choice of the constants k_n and γ is described in Section 10.4.2.

10.1.3 Mass balance equations

Mass balance equations for the $N + 1$ levels are:

$$\frac{du_0}{dt} = g_0 - g_1$$

$$\frac{du_1}{dt} = g_1 - g_2$$

$$\vdots$$

$$\frac{du_N}{dt} = g_N - 0,$$

or:

$$\frac{du_n}{dt} = g_n - g_{n+1} \qquad n = 0,\ldots N \quad (g_{N+1} = 0) \qquad (10.4)$$

Insertion of (10.2) gives:

$$\frac{du_n}{dt} = g_n - g_{n+1} = K_n \cdot (v_{n-1} - v_n) - K_{n+1} \cdot (v_n - v_{n+1}) \qquad (10.5)$$

The moisture content u_n depends on the relative humidity φ_n :

$$\frac{du_n}{dt} = \frac{du_n}{d\varphi_n} \cdot \frac{d\varphi_n}{dt}$$

Using $v_n = \varphi_n \cdot v_s(T)$, we get the following equation for the relative humidity $\varphi_n(t)$:

$$\frac{du_n}{d\varphi_n} \cdot \frac{d\varphi_n}{dt} = v_s(T) \cdot \left[K_n \cdot (\varphi_{n-1} - \varphi_n) - K_{n+1} \cdot (\varphi_n - \varphi_{n+1})\right] \qquad (10.6)$$

10.1.4 External moisture flow

The external moisture flow $G_0 = m \cdot g_0$ is related to the conditions in the precision chamber. The involved variables, which are shown in Figure 10.7, are:

$\dot{V}_{air}$ supply air flow [m^3/s]
V_{ch} volume of chamber [m^3]
v_{inlet} water vapour content in inflowing air [kg/m^3]
v_{ch} water vapour content in mixed air in chamber [kg/m^3]
v_{surf} water vapour content on surface of sample [kg/m^3]
G_0 moisture uptake [kg_{water} / s)]
m dry mass of sample, [kg_{wood}]
$g_0 = G_0/m$

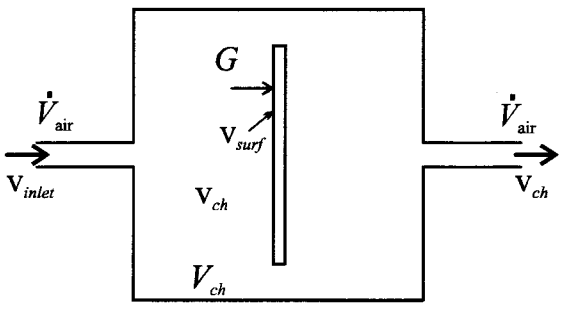

Figure 10.7 Variables for external moisture exchange to sample in chamber

The moisture balance for the air in the chamber is:

$$(v_{inlet} - v_{ch}) \cdot \dot{V}_{air} = G_0 = g_0 \cdot m \qquad (10.7)$$

Here the moisture capacity of the air, which may be of importance for rapid variations, is neglected. This is discussed further in Section 10.1.5.

Let β [m/s] denote the air-to-surface moisture transfer coefficient, and A [m^2] the total exposed area of the sample (both sides). The moisture balance of the surface becomes:

$$(v_{ch} - v_{surf}) \cdot \beta \cdot A = G_0 = g_0 \cdot m \qquad (10.8)$$

Let L_{eq} denote an estimated average length for the diffusion within the sample, and let D_v denote the vapour transport coefficient. See Figure 10.8. Then we have:

$$D_v \frac{v_{surf} - v_0}{L_{eq}} \cdot A = G_0 = g_0 \cdot m \qquad (10.9)$$

The length L_{eq} is shown in Figure 10.8. The choice $L_{eq} = 0.8 \cdot L$, where L is half the thickness of the sample, will be used below.

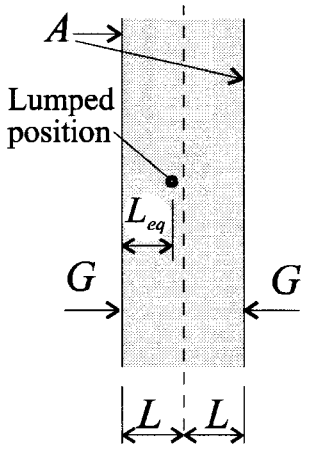

Figure 10.8 Estimated average diffusion length into the sample

The above three equations Eqs. (10.7) – (10.9) may be written in the following way:

$$v_{inlet} - v_{ch} = g_0 \cdot \frac{m}{\dot{V}_{air}} \qquad (10.10)$$

$$v_{ch} - v_{surf} = g_0 \cdot \frac{m}{\beta \cdot A} \qquad (10.11)$$

$$v_{surf} - v_0 = g_0 \cdot \frac{m \cdot L_{eq}}{A \cdot D_v} \qquad (10.12)$$

The factors after g_0 define three moisture resistances. See Figure 10.9.

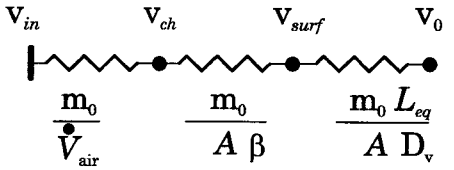

Figure 10.9 Moisture resistances between v_{in}, v_{ch}, v_{surf} *and* v_0

Addition of the three equations (10.10) – (10.12) gives:

$$v_{inlet} - v_0 = g_0 \cdot \left(\frac{m}{\dot{V}_{air}} + \frac{m}{A \cdot \beta} + \frac{m \cdot L_{eq}}{A \cdot D_v} \right)$$

The three moisture resistances of Figure 10.9 are added. The total moisture conductance between v_{inlet} and v_0 is given by the inverse of the total resistance:

$$K_0 = \frac{1}{\frac{m}{\dot{V}_{air}} + \frac{m}{A \cdot \beta} + \frac{m \cdot L_{eq}}{A \cdot D_v}} \quad [\, m^3 / (kg_{wood} \cdot, s) \,] \qquad (10.13)$$

It should be noted that A denotes the total surface area on both faces of the sample.

The conductance K_0 determines the external flow g_0 :

$g_0 = K_0 \cdot (v_{inlet} - v_0)$

The conductance K_0 for the external flow depends on the *experimental set-up* and the geometry of the sample. It is not dependent on the assumptions for the internal levels in the cell wall.

10.1.5 Data for external conditions in the measurements

Capacity of air in chamber

The moisture capacity of the volume of air in the chamber is neglected in Eq. (10.7). An estimate is made if this is reasonable. A worst case with a small sample and a low moisture capacity (at RH = 40%) for wood is selected.

The total moisture capacity of the air volume is:

$$\frac{dW_{air}}{d\varphi} = V_{ch} \cdot v_{sat} = 0.022 \cdot 6.80 \cdot 10^{-3} = 0.15 \cdot 10^{-3} \quad [kg_{water} / 100\% \text{ RH}]$$

Here V_{ch} [m^3] is the volume of the chamber, and v_{sat} [kg_{water}/m^3] is the moisture content of saturated air at 5°C.

The moisture capacity of the sample is:

$$\frac{dW}{d\varphi} = m \cdot \frac{du}{d\varphi} = 0.0077 \cdot 0.15 = 1.2 \cdot 10^{-3} \qquad [\mathrm{kg_{water}}/100\%\ \mathrm{RH}]$$

As seen from the two figures, the moisture capacity for the sample is dominating over the capacity in the volume of air.

Data for the conductance K_0

Characteristic values for the conductance K_0 for the external flow are calculated for the conditions in the actual measurements.

A low moisture transport coefficient has been selected, relevant for the dryer parts of the simulations. The transport direction in the wood is longitudinal.

The conductance K_0 consists of three resistances in series as described in Section 10.1.4, Eq. (10.10) – (10.12). Eq. (10.13) reads:

$$K_0 = \frac{1}{\frac{m}{\dot{V}_{air}} + \frac{m}{A \cdot \beta} + \frac{m \cdot L_{eq}}{A \cdot D_v}} \qquad [\mathrm{m^3}/(\mathrm{kg_{wood}} \cdot \mathrm{s})]$$

Two examples are considered. The first one concerns the first sequence simulated in Chapter 11 with longer intervals between steps in RH and at 20°C. (Samples 1 and 2, Thickness 3 mm). The following figures are obtained:

$$\frac{m}{\dot{V}_{air}} = \frac{0.054}{0.066 \cdot 10^{-3}} = 820 \qquad [(\mathrm{kg_{wood}} \cdot \mathrm{s})/\mathrm{m^3}]$$

$$\frac{m}{A \cdot \beta} = \frac{0.054}{0.005 \cdot 0.062} = 174 \qquad [(\mathrm{kg_{wood}} \cdot \mathrm{s})/\mathrm{m^3}]$$

$$\frac{m \cdot L_{eq}}{A \cdot D_v} = \frac{0.054 \cdot 0.8 \cdot 1.5 \cdot 10^{-3}}{0.062 \cdot 4 \cdot 10^{-6}} = 260 \qquad [(\mathrm{kg_{wood}} \cdot \mathrm{s})/\mathrm{m^3}]$$

The moisture conductance between v_{in} and v_0 becomes:

$$K_0 = \frac{1}{820 + 174 + 260} = 0.00080 \qquad [\mathrm{m^3}/(\mathrm{kg_{wood}} \cdot \mathrm{s})]$$

The second example concerns the second sequence simulated in Chapter 11 with shorter periods between steps in RH and at 5°C. (Samples 3 and 4, Thickness 1.7 mm). The following figures are used in the simulation:

$$\frac{m}{\dot{V}_{air}} = \frac{0.0077}{0.066 \cdot 10^{-3}} = 117 \qquad [(\mathrm{kg_{wood}} \cdot \mathrm{s})/\mathrm{m^3}]$$

$$\frac{m}{A \cdot \beta} = \frac{0.0077}{0.0178 \cdot 0.005} = 86 \qquad [(\mathrm{kg_{wood}} \cdot \mathrm{s})/\mathrm{m^3}]$$

$$\frac{m \cdot L_{eq}}{A \cdot D_v} = \frac{0.0077 \cdot 0.8 \cdot 0.85 \cdot 10^{-3}}{0.0178 \cdot 4 \cdot 10^{-6}} = 74 \qquad [(\mathrm{kg_{wood}} \cdot \mathrm{s})/\mathrm{m^3}]$$

The moisture conductance between v_{inlet} and v_0 becomes:

$$K_0 = \frac{1}{117 + 86 + 74} = 0.0036 \qquad [\mathrm{m^3}/(\mathrm{kg_{wood}} \cdot \mathrm{s})]$$

The resistance representing the thickness of the sample is only a rather small fraction of the total resistance $1/K_0$ in these two measurement cases. This means that that the assumed simplification to lump all of the material in one point is reasonable.

Figure 9.3 in Section 9.1 shows a simple network for the moisture response over a conductance K_0. The response to a step change becomes exponential, Eq. (9.1), with a time constant given by Eq. (9.3). For the second example above this gives, using the average moisture capacity from Section 9.1 obtained by Eq. (9.2):

$$t_0 = \frac{0.0945}{6.80 \cdot 10^{-3} \cdot 0.0036} = 3860 \text{ [s]} \cong 1.1 \text{ [h]}$$

Here t_0 is the time scale for the response for the sample in the precision chamber.

The figure for the resistance emanating from the limited supply of conditioned air is relative high. This means that the experimental set-up is not allowing steep step changes. However one advantage is that the layers of wood with different distances from the surface experience rather closely the same RH-change simultaneously with only small differences. This could be thought to increase the precision in analysing the retarded sorption, but at the same time not activating the fast components of the phenomenon. The step change in the material has taken place with a time constant in the order of two hours in the fast series of experiments.

10.2 Complete network for the model

Figure 10.10 shows the complete network with an outer node u_0 and N internal nodes. The outer conductance between v_{in} and v_0 is K_0, while K_1 ,... K_N are the conductances between the internal nodes. All equations refer to a unit mass of the sample.

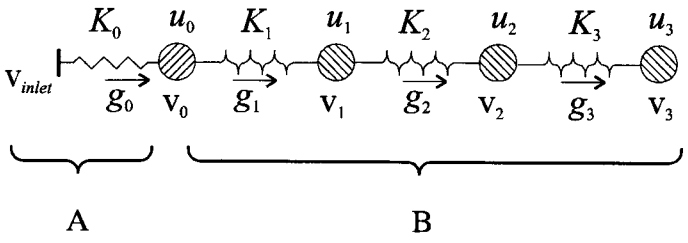

Figure 10.10 Network for the model. $N = 3$. A: Conductance calculated from physical conditions around the sample and transport into the sample. B: Conductances based on assumptions for a process acting locally in the cell wall.

The mass balance equations (10.4) are:

$$\frac{du_n}{dt} = g_n - g_{n+1} \qquad n = 0, .. N \quad (g_{N+1} = 0)$$

The final equations for the relative humidities $\varphi_0(t)$... $\varphi_N(t)$ are, Eq. (10.6):

$$\frac{du_n}{dt} = \frac{du_n}{d\varphi_n} \cdot \frac{d\varphi_n}{dt} = v_s(T) \cdot \left[K_n \cdot (\varphi_{n-1} - \varphi_n) - K_{n+1} \cdot (\varphi_n - \varphi_{n+1})\right]$$

$$\frac{du_n}{dt} = \frac{du_n}{d\varphi_n} \cdot \frac{d\varphi_n}{dt} = v_{sat}(T) \cdot \left[K_n \cdot (\varphi_{n-1} - \varphi_n) - K_{n+1} \cdot (\varphi_n - \varphi_{n+1})\right] \qquad (K_{N+1} = 0)$$

The system is driven by the inlet vapour content $v_{in}(t) = v_{sat}(T) \cdot \varphi_{in}(t)$.

10.3 Computer model

The numerical calculations to solve Eq. (10.6) are based on the method of explicit finite differences. For each time-step the following procedure is used.

1. v_n -values are calculated from φ_n -values and $v_s(T)$

$$\varphi_n = \frac{v_n}{v_s(T)}$$

2. The current values of the conductances K_n are calculated as a given function of $|v_{n-1}-v_n|$, Eq. (10.17). The factors for the variation of conductances between the levels are described by Eq. (10.17). The moisture capacity values, $du_n/d\varphi_n$, are computed from an algorithm described in Section 10.5, Eq. (10.18). The distribution of capacity between the levels are described in Section 10.4.1, Eqs. (10.14) – (10.16).

3. For each level, a stable time-step Δt_n is calculated:

$$\Delta t_n = \frac{du_n}{d\varphi_n} \cdot \frac{1}{v_s(T)\cdot(K_n + K_{n+1})} \quad (n = 0, ..N\text{-}1)\ ;\ \Delta t_N = \frac{du_N}{d\varphi_N} \cdot \frac{1}{v_s(T)\cdot K_N}$$

The smallest time-step from the levels is selected as the stable time-step Δt .
Since the values of the conductances are dynamically changing in the simulation of the non-linear models, the stable time-step is recalculated for each new time-step.

4. The quantity of moisture exchanged between the levels during a time-step is calculated:
$M_n = \Delta t \cdot K_n \cdot (v_{n-1}-v_n) \quad (n = 1, ..N)\ ; \quad M_0 = \Delta t \cdot K_0 \cdot (v_{in}-v_0)$

5. The sum of the quantities of moisture through adjacent conductances are divided with the moisture capacity for each level to form the calculated change in φ during a time-step.

$$\varphi_n^{new} = \varphi_n^{old} + \frac{M_n - M_{n+1}}{\frac{du_n}{d\varphi_n}} \qquad \varphi_N^{new} = \varphi_N^{old} + \frac{M_N}{\frac{du_N}{d\varphi_N}}$$

The relative humidities for all levels are shown in the diagram of simulation to illustrate the progress of the potentials for the retarded sorption.

6. An algorithm for the moisture equilibrium curve calculates the value of the moisture content for each level and a total u can be summed up to give the output for the time-step in the simulation program.

$$u^{new} = \sum_{n=0}^{N} u_n(\varphi_n) \qquad (n = 0, ..N)$$

The program is written in Visual Basic within Excel and with a spreadsheet as an interface. Desired output times and RH are entered as inputs on the spreadsheet and total moisture content and the RH for each level are calculated by the program. Diagrams are linked to the spreadsheet and comparison with measured values can easily be made in the Excel environment.

10.4 Specific assumptions

10.4.1 Moisture distribution in the assumed levels

The total moisture capacity is strongly increasing with high RH for wood. This is seen by the steep slope of the moisture equilibrium curve at high RH. The immediate sorption responses in the measurements the first hours after a step have proven rather proportional to the RH-step independent of RH-level. This is reflected in the used models by giving the immediately accessible level (designated 0) a constant capacity. This is seen in the assumed moisture equilibrium curve in Figure 10.11, where this capacity is represented by a straight line.

A constant moisture capacity is assumed in level 0:

$$u_0(\varphi) = c_0 \cdot \varphi \qquad (10.14)$$

The reminder of the moisture capacity is distributed over the N levels by factors α_n:

$$u_n(\varphi) = \alpha_n \cdot (u(\varphi) - u_0(\varphi)) \qquad \sum_{n=1}^{N} \alpha_n = 1 \qquad (10.15)$$

In order to get a manageable number of parameters it is assumed that the factors α_n are given by a geometrical series:

$$\alpha_n = \alpha_1 \cdot (b_u)^{n-1} \qquad n = 1,\ldots N \qquad (10.16)$$

The sum of the factors is 1, so we have:

$$1 = \sum_{n=1}^{N} \alpha_n = \alpha_1 \cdot \left(1 + b_u + \ldots + b_u^{N-1}\right) = \alpha_1 \cdot \frac{1 - b_u^N}{1 - b_u}$$

From this we have:

$$\alpha_n = \frac{1 - b_u}{1 - b_u^N} \cdot b_u^{n-1} \qquad n = 1,\ldots N$$

For any given total moisture equilibrium curve $u(\varphi)$, the above model uses three parameters, c_0, N, b_u to get the moisture capacities $u_n(\varphi)$, $n = 0,\ldots N$

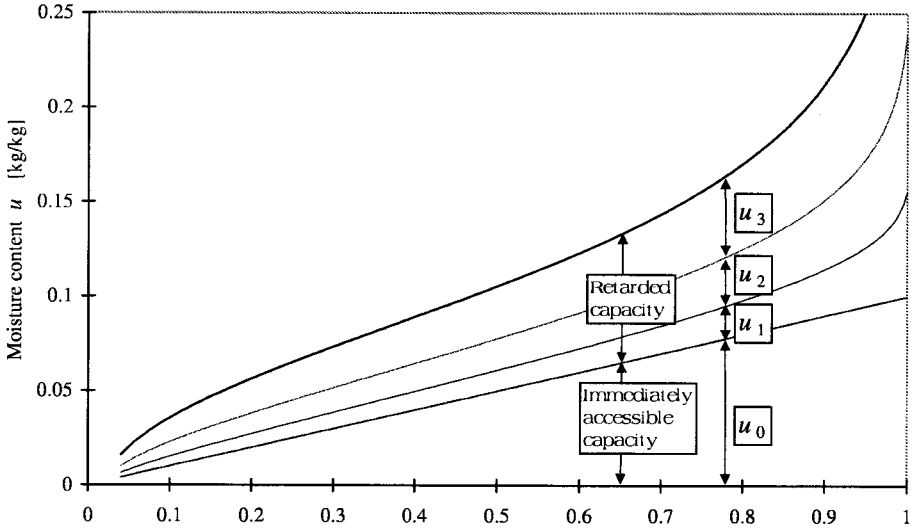

Figure 10.11 Distribution of moisture capacity in model with three internal levels.

10.4.2 Conductances $K_n(v_{n-1}, v_n)$

The conductances K_n between the different levels are determined by constants k_n given by a geometric series:

$$K_n = k_n \cdot |v_{n-1} - v_n|^{\gamma} \qquad k_n = k_1 \cdot (b_k)^{n-1} \qquad (b_k < 1) \qquad (10.17)$$

The values $\gamma = 1$ and $\gamma = 2$ are used in the models. Constant conductances are also tested. They are also given by the geometric series:

$K_n = K_1 \cdot (b_k)^{n-1}$ $(b_k < 1)$.

The model thus uses three parameters k_1, b_k and γ to determine the conductances $K_1, \ldots K_N$.

10.5 Sorption isotherm

In Chapter 4.2.1 a formula for the sorption isotherm was presented. An earlier simpler formula for the sorption isotherm has been used for the simulations of retarded sorption and in the comparison with the measurements.

The formula for the sorption isotherm is given by Eq. (10.18). The φ-interval is limited since the function is not finite at $\varphi = 0$. In the simulations of the measurements, values for low φ's are not needed and the low interval can be excluded.

$$u(\varphi) = \frac{A - \ln(C - \ln(\varphi))}{B} \qquad \frac{du}{d\varphi} = \frac{1}{\varphi B \left(C - \ln(\varphi)\right)} \qquad (10.18)$$

The following values have been used at 20°C:

$$u(\varphi) = \frac{1.37 - \ln(0.005 - \ln(\varphi))}{18.6} \qquad 0.08 \le \varphi \le 1$$

A temperature dependency is added:

$$u(\varphi, T) = \frac{(1.47 - 0.005 \cdot T) - \ln\{(0.007 - 0.0001 \cdot T) - \ln(\varphi)\}}{16.6 + 0.1 \cdot T} \qquad (10.19)$$

$0.08 \le \varphi \le 1 \quad 0°C \le T \le 30°C$

This isotherm is shown in Figure 10.12. This formula is used in Chapter 7 to 11. In Section 11.3 the algorithm has been supplemented with a hysteresis function.

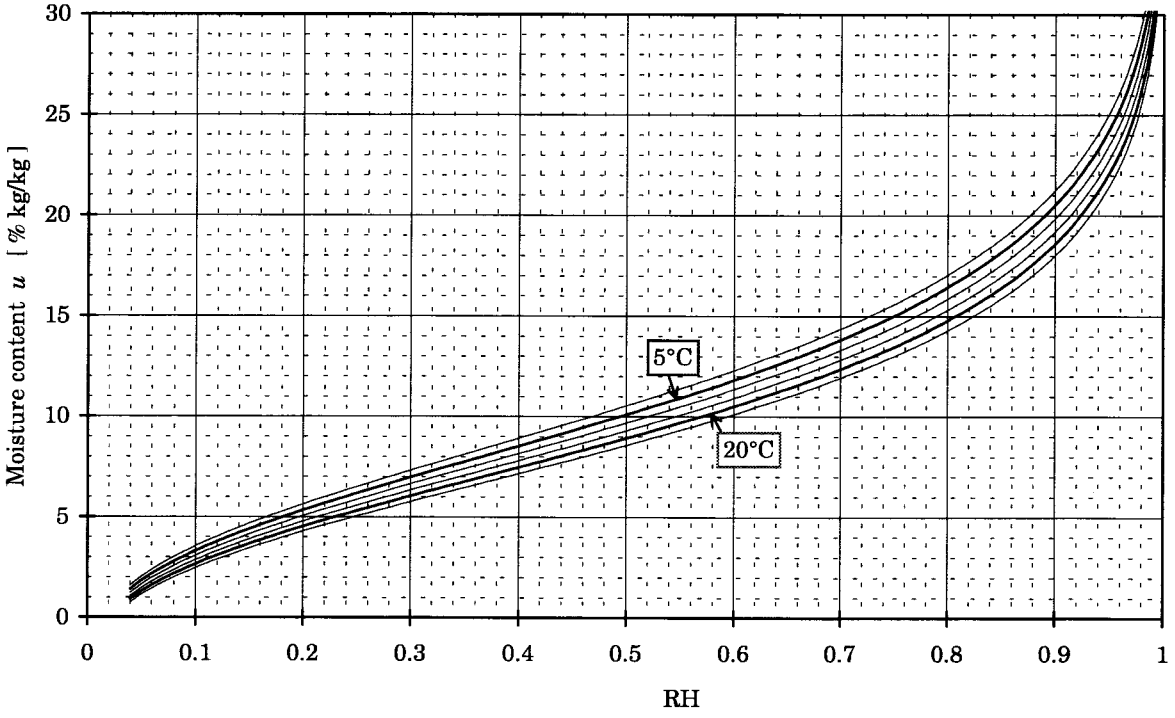

Figure 10.12 Moisture equilibrium curve from the formula (10.19).

10.6 Temperature dependence of moisture flow

In the discussion in Section 9.3, blocking was defined as the varying obstruction that made parts of the moisture capacity inactive. There are several indications that the blocking increases strongly with decreasing temperature.

One way to achieve temperature dependence is to use water vapour content (or alternatively vapour pressure) as the driving force for the relaxation of moisture between the internal levels in the model. A vapour difference Δv is connected to a difference in RH, $\Delta\varphi$, by the saturated vapour content v_{sat}

$$\Delta v = \Delta\varphi \cdot v_s$$

In the main, non-linear model the internal moisture flow g is related to the vapour difference Δv.

$$g = \text{constant} \cdot \Delta v \cdot |\Delta v|^{\gamma} \qquad \gamma = 1$$

$$\varphi = \frac{v}{v_{sat}(T)}$$

By using the non-linear model, the temperature effect for the retarded sorption is enhanced. At 20°C and 5°C respectively, the ratio between the saturated vapour contents v_{sat} is 2.55. With the non-linear model the corresponding ratio for the internal moisture flow becomes

$$\frac{g_{20°}}{g_{5°}} = \frac{(v_{sat}(20)\cdot\Delta\varphi)^{\gamma+1}}{(v_{sat}(5)\cdot\Delta\varphi)^{\gamma+1}} = \left(\frac{17.29\cdot10^{-3}}{6.80\cdot10^{-3}}\right)^2 = 2.55^2 \cong 6.5$$

This ratio gives the increased speed with which the retarded sorption relaxes at 20°C compared to 5°C in the used main non-linear model.

11 Simulations of measured sequences

Two measured sequences have been selected for the simulations with the objective to cover a wide range of conditions. The aim is to test different models and to fit the parameters of the models.

The sequences are starting at a point where the retarded sorption is considered small to minimize the influence of the necessary assumed initial values in the internal nodes of the models.

The first sequence, which consists of the main part of the first series of measurements described in Section 6.1, concerns a measurement for a time of almost one year. The temperature is 20°C . See Figure 11.1. The first part consists of absorption in steps to 98% RH. It is followed by corresponding desorption steps. The results from the measurements are shown in Section 6.1.

The absolute levels of the moisture content for the first sequence is somewhat uncertain. During the long measuring time, dust may have collected on the sample etc. Drying in oven was not been performed prior to the measurements, in order not to destroy the sample. Instead the dry weight of the sample was temporarily estimated for the results to the first report in Swedish. Later the samples were dried at a higher temperature and the dry weight used here.

The second sequence which consists of the main part of the fifth series of measurements described in Section 6.5, consists of periodic steps interspersed with single larger absorption steps for longer periods. The temperature is 5°C. The sequence is taken from Section 6.5 . The results from the measurements are shown in Figure 11.2.

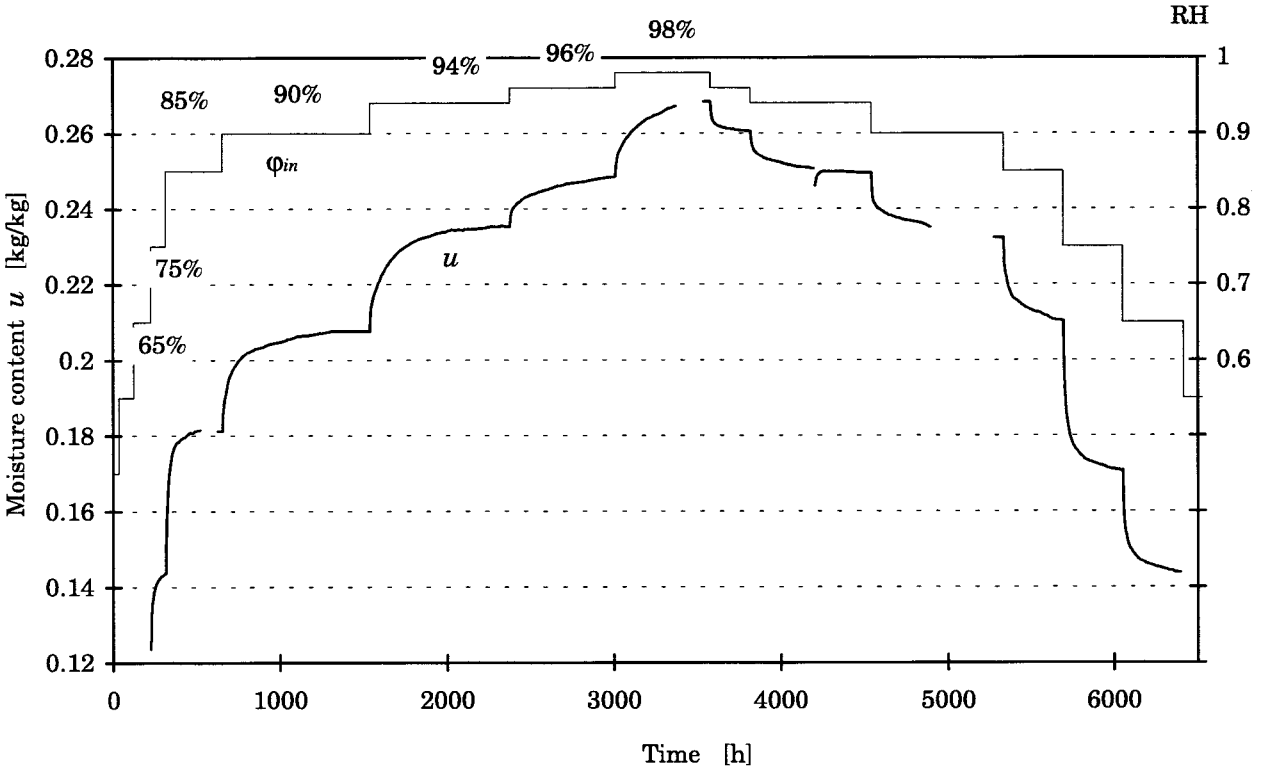

Figure 11.1 Measured sequence at 20°C used to test different models (from the first series of measurements described in Section 6.1).

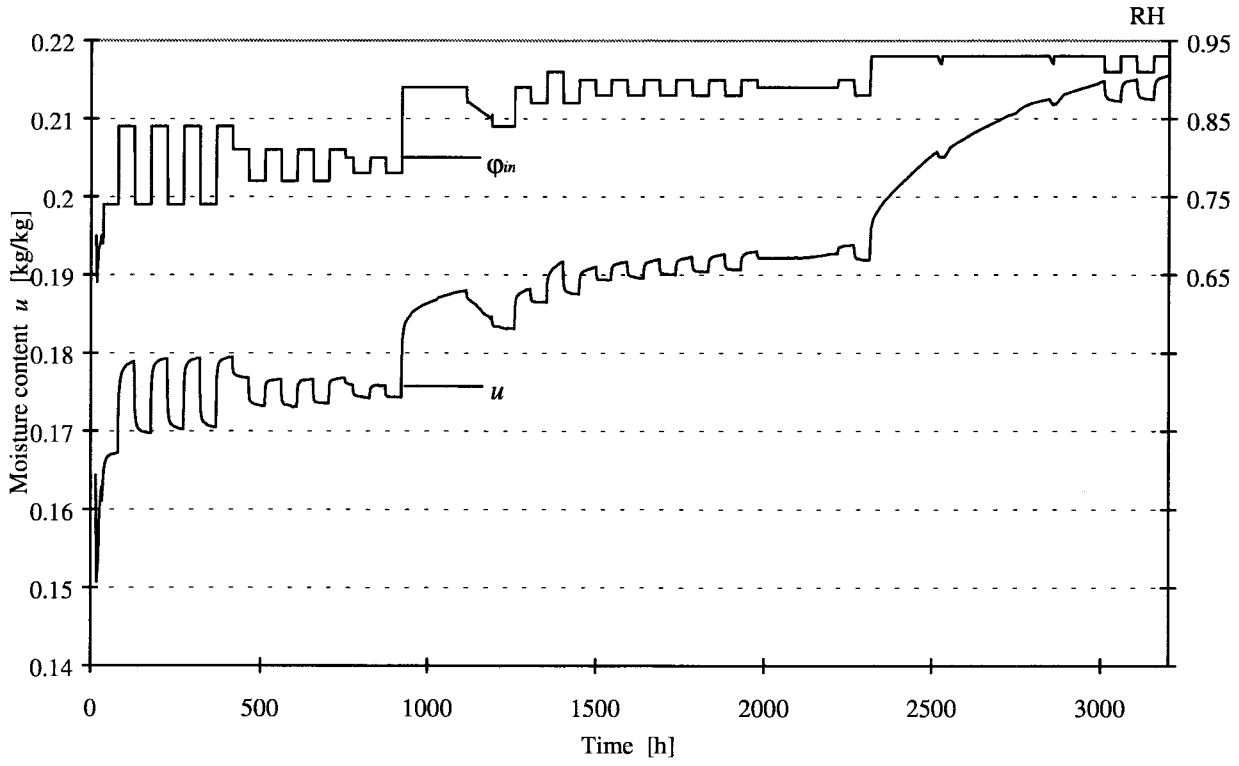

Figure 11.2 Measured sequence at 5°C used to test different models (from the fifth series of measurements described in Section 6.5).

For each section in this chapter a new variant of model is tested. The parameters in the model are kept the same in the two simulated sequences. The first two diagrams in each section show the simulation results for the two sequences together with the relative humidity in the outer level or node and in the internal levels. This makes it possible to get an overview of the progress of the RH-potentials in the assumed levels and compare with the simulated moisture content. In the rest of the diagrams in each section, the simulation result is shown together with the measured values.

11.1 Linear models

We will first test linear models, i. e. models with constant conductivities K_n, $n = 1,\ldots N$.

11.1.1 Fickian

The first simulations are made with a model based on traditional theory where all of the moisture content is assumed to be immediately accessible in a local point in the material.

Figure 11.3 shows a moisture flow network for this model. The sample is very thin so the 'Fickian' diffusion on a macro-scale is not significant. The essential process is the moisture uptake from the incoming air into the precision chamber to the cell walls.

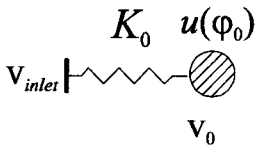

Figure 11.3 Network for a Fickian process for a very thin sample.

The values for the components constituting K_0 are described in Section 4.1.5. K_0 is dependent of the thickness of the sample. The values are $K_0 = 0.00083$ [m^3 /(kg_{wood} ·s)] for the thicker sample (20°C sequence), and $K_0 = 0.0035$ [m^3 /(kg_{wood} ·s)] for the thinner sample (5°C sequence). Theses values are used for all the models in this chapter.

The moisture capacity is given by the moisture equilibrium curve in Section 10.5.

Figure 11.4 shows the result from the simulation of the sequence at 20°C. The upper curve in the diagram is the calculated RH in node 0, which is the only node in this Fickian model. In Figure 11.5 the same simulation for the sequence at 5°C is shown.

In Figure 11.6, comparison for the sequence at 20°C is made. Figure 11.7 shows two step-responses at high RH from the previous figure more in detail. We can see how fast the traditional Fickian model reaches a distinct equilibrium after a step-change. The measured response never reaches equilibrium during the measured intervals. The sorption responses show a wide range of time-scales.

In Figure 11.8 and Figure 11.9 comparison with the measurements from the second sequence at 5°C involving cyclic steps is made. The difference between the Fickian model and measurements is very big, in particular for the cyclic variations.

It is clear that a Fickian model cannot reproduce the measured values.

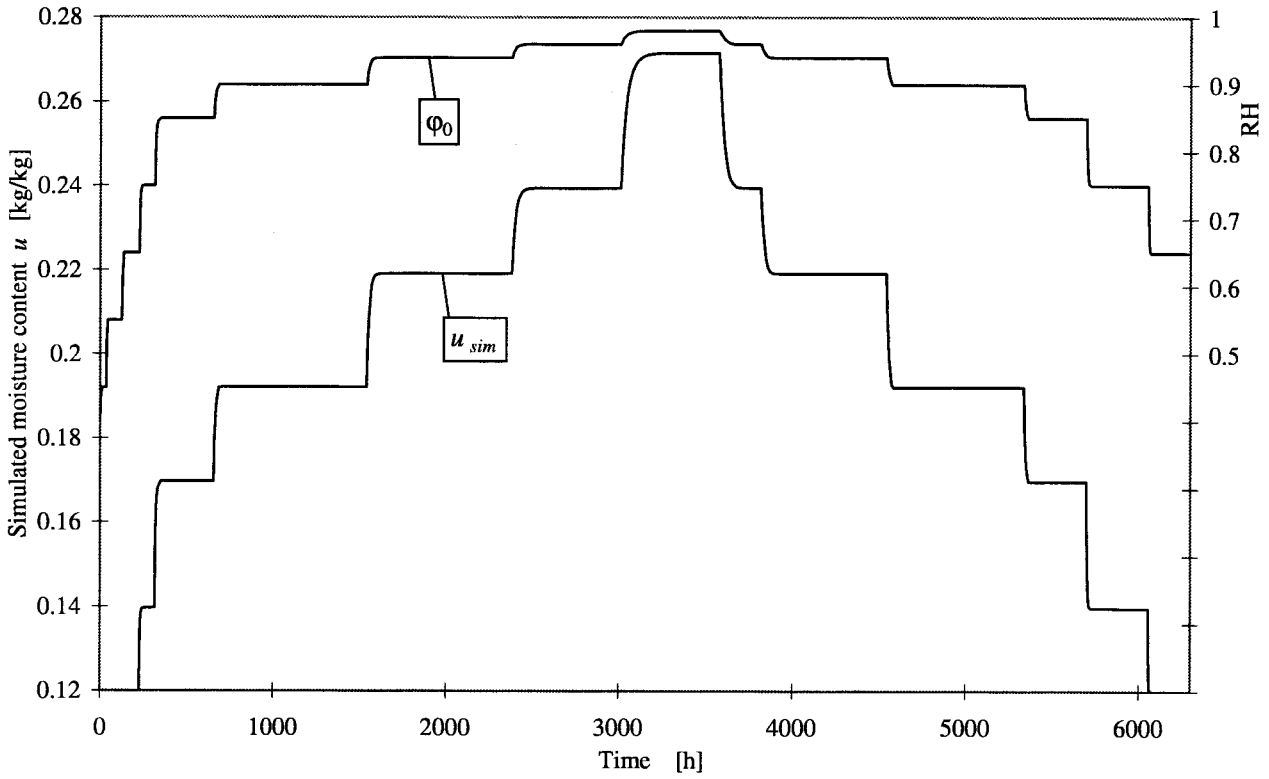

Figure 11.4 Simulation of the sequence at 20°C.

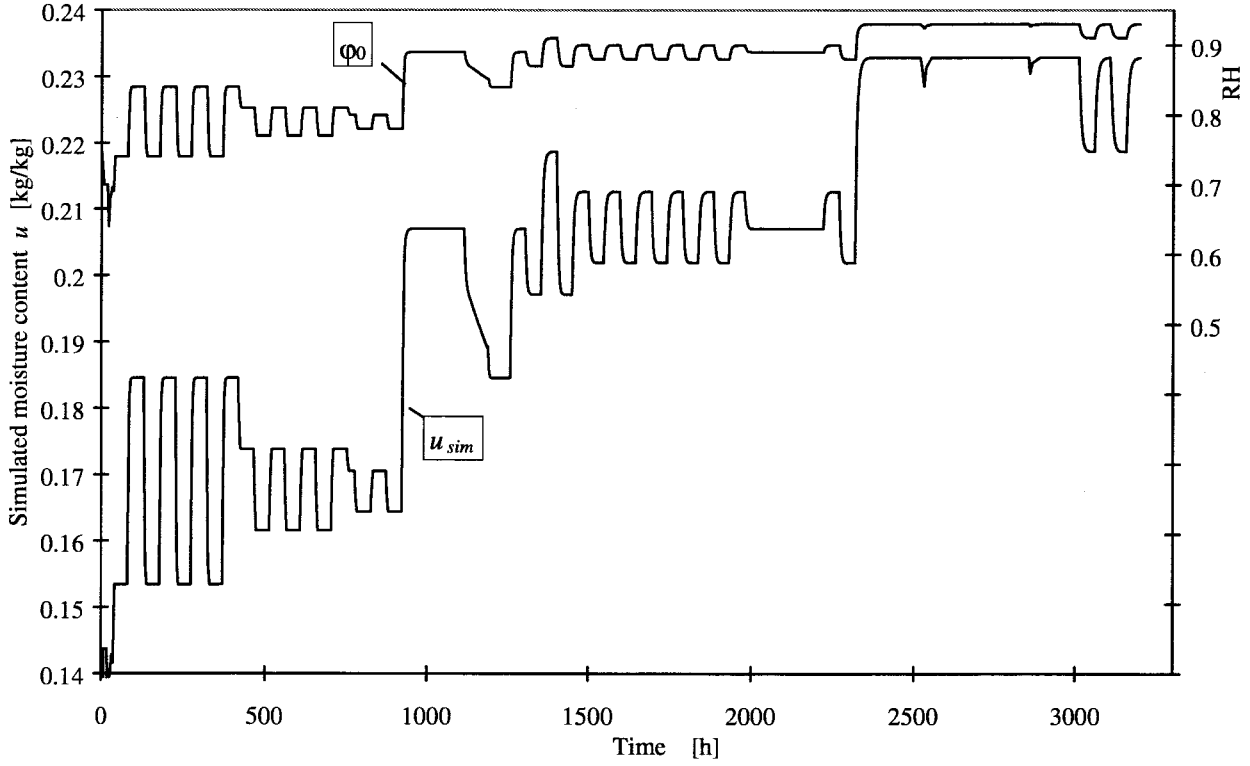

Figure 11.5 Simulation of the sequence at 5°C.

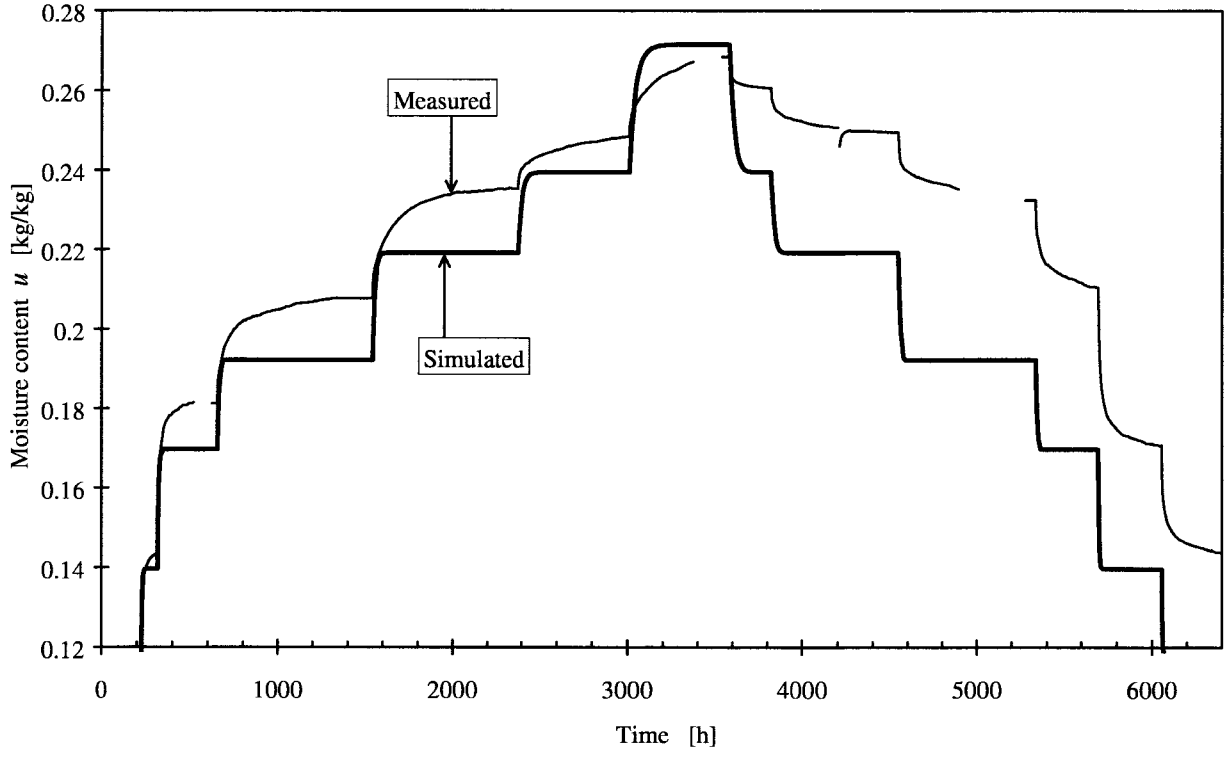

Figure 11.6 Simulation compared to measurements for the sequence at 20°C.

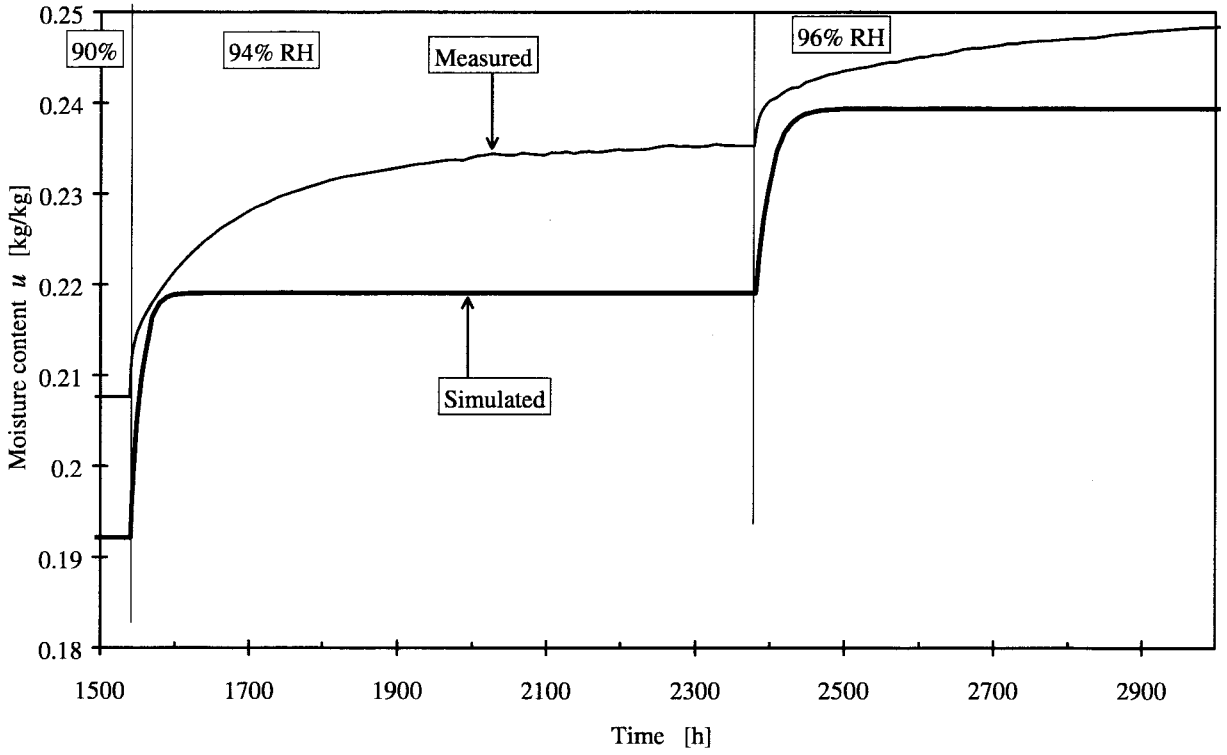

Figure 11.7 Simulation compared to measurements at 20°C. Detail from Figure 11.6.

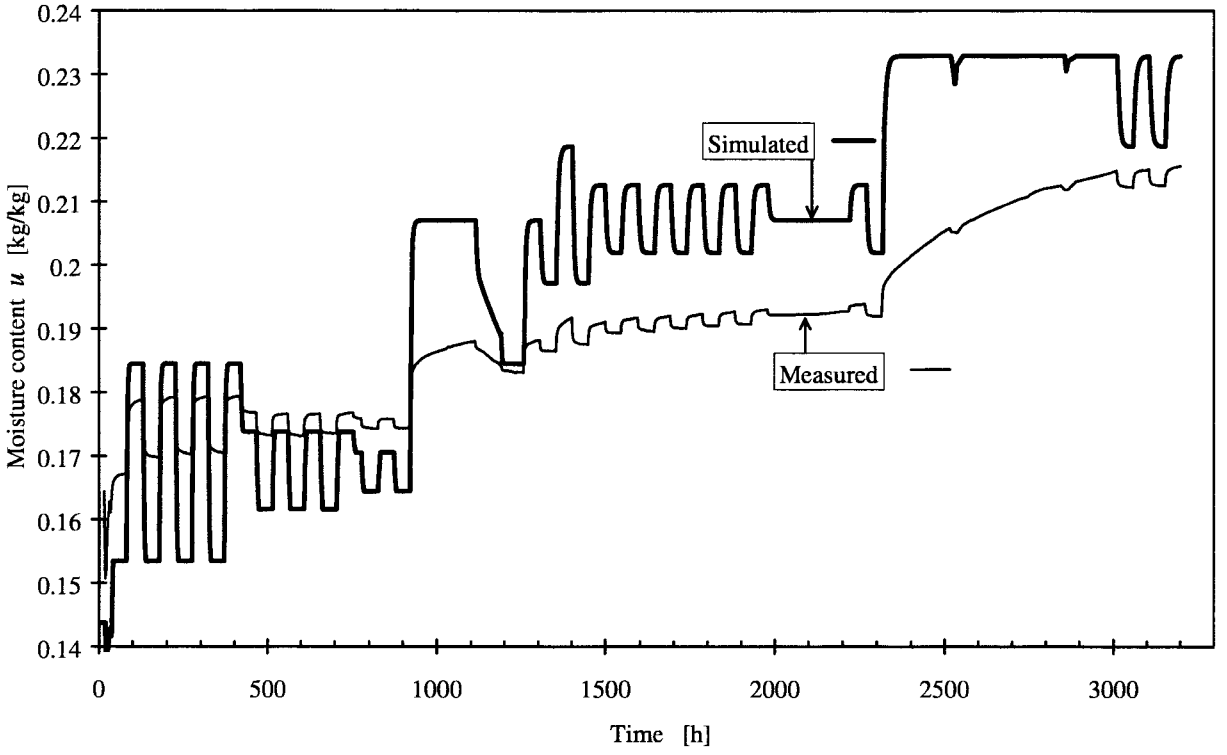

Figure 11.8 Simulation compared to measurements at 5°C.

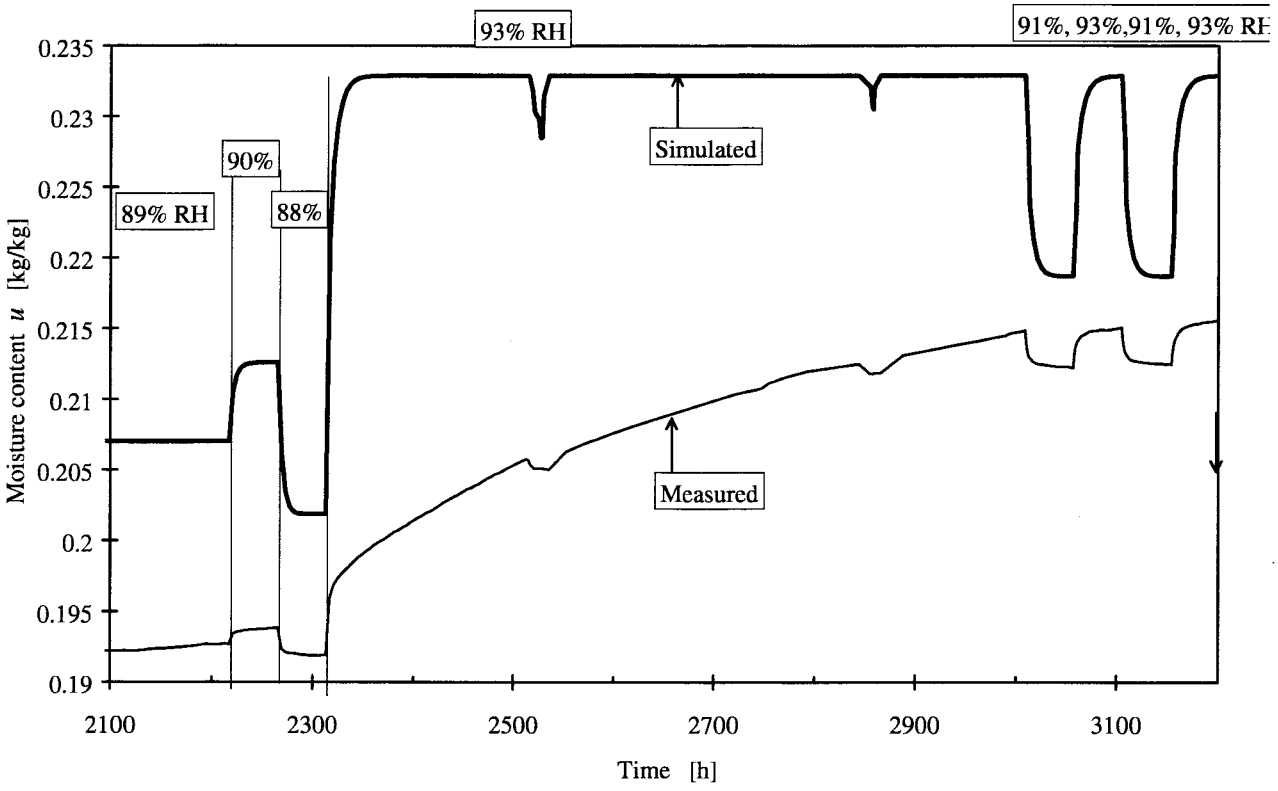

Figure 11.9 Simulation compared to measurements at 5°C. Detail from Figure 11.8.

11.1.2 One internal level in the cell wall

A simple model with only internal level ($N = 1$) is tested. Figure 11.10 shows a moisture flow network for this model.

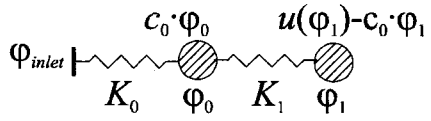

Figure 11.10 Network using one internal level.

The corresponding non-linear model with one internal level is studied in Section 11.2.1. In Section 11.3.3 the corresponding non-linear model including hysteresis is studied.

The outer level 0 has been given a constant capacity c_0, independent of RH, based on observations made in Section 9.1. The method gives level 0 a constant capacity versus RH and makes the capacity of the other levels all the more varying. This is described in 10.4.1. From Figure 9.4 the following value of c_0 in Eq. (17) is chosen:

$$u_0(\varphi) = c_0 \cdot \varphi$$

$$c_0 = 0.08 \quad [\mathrm{kg_{water}/kg_{wood}}]$$

This value, which is somewhat uncertain, is used in all models for both 5°C and 20°C in this chapter (except for the model in Section 11.1.3 with its special assumptions). The value is based on analyses on measurements at 5°C only.

The internal moisture transport coefficient K_1 concerns -a unit mass of wood, and it refers to water vapour as gradient. By fitting one of the first step responses at 20°C, the following value was obtained:

$K_1 = 5 \cdot 10^{-4}$ [m^3 /(kg_{wood} , s)]

Figure 11.11 shows the result from the simulation of the sequence at 20°C. In figure 11.12 the same simulation for the sequence at 5°C is shown. The two upper curves in the diagrams are the calculated relative humidities in the nodes. The thicker line designates $\varphi_0(t)$.

In Figure 11.13 comparison with the measurements at 20°C is made. Figure 11.14 shows two step-responses from the previous figure more in detail. The amplitudes of the steps are decreasing from 4% in the first step to 2% RH in the second one. We can see that the second measured response is very different from the simulated both in shape and amplitude. These steps will later be compared in Figure 11.39 for a non-linear model with 5 internal levels.

In Figure 11.15 the result of the simulation for the sequence at 5°C is shown. Figure 11.16 shows a part in more detail. The simulation cannot at all reproduce the sorption response for the cyclic steps. The magnitude of the moisture exchange for the cyclic steps are however reduced to some extent compared to the Fickian model (Figure 11.8 versus Figure 11.15).

One situation, where all tested linear models for retarded sorption and models with just one internal level have failed, are seen at the end in Figure 11.16. Here the simulated values has come close to equilibrium (at 93% RH) and then a number of cyclic steps are added in the simulation. The moisture level is drifting for each new cycle in the simulation. This sequence will later be compared in Figure 11.41 for a non-linear model with 5 internal levels.

A linear model with one extra internal level improves the agreement between simulation and measurement by introducing a second, large time-scale. But the measured responses contain many and varied time scales. All the time-scales cannot be accounted for by this type of model. It is clear that more complex models are needed.

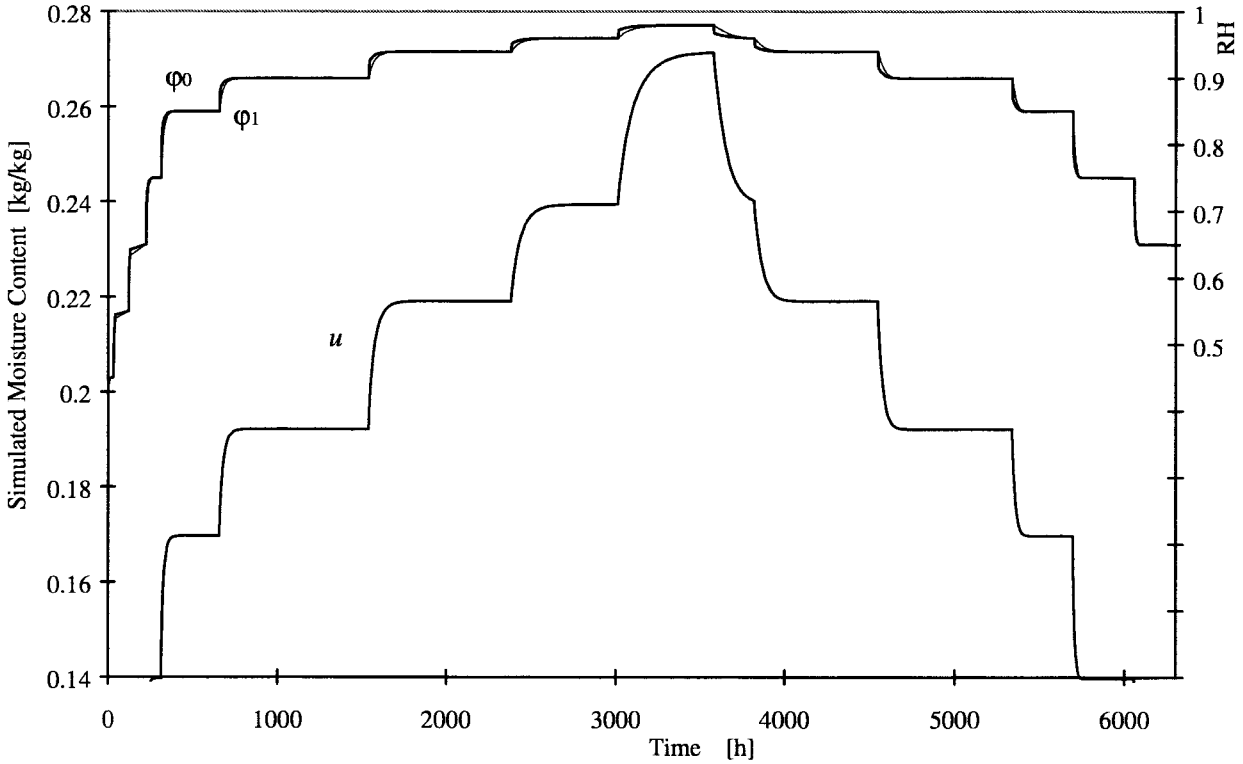

Figure 11.11 Simulation of the sequence at 20°C.

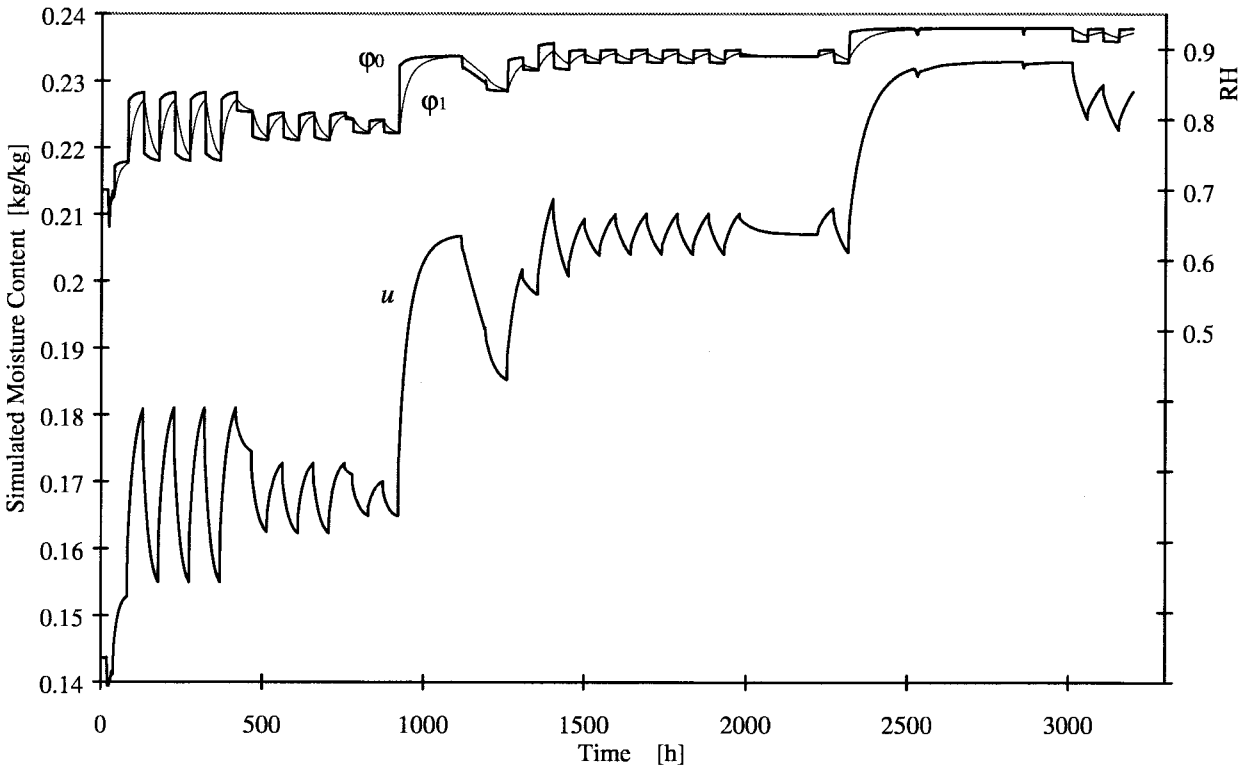

Figure 11.12 Simulation of the sequence at 5°C.

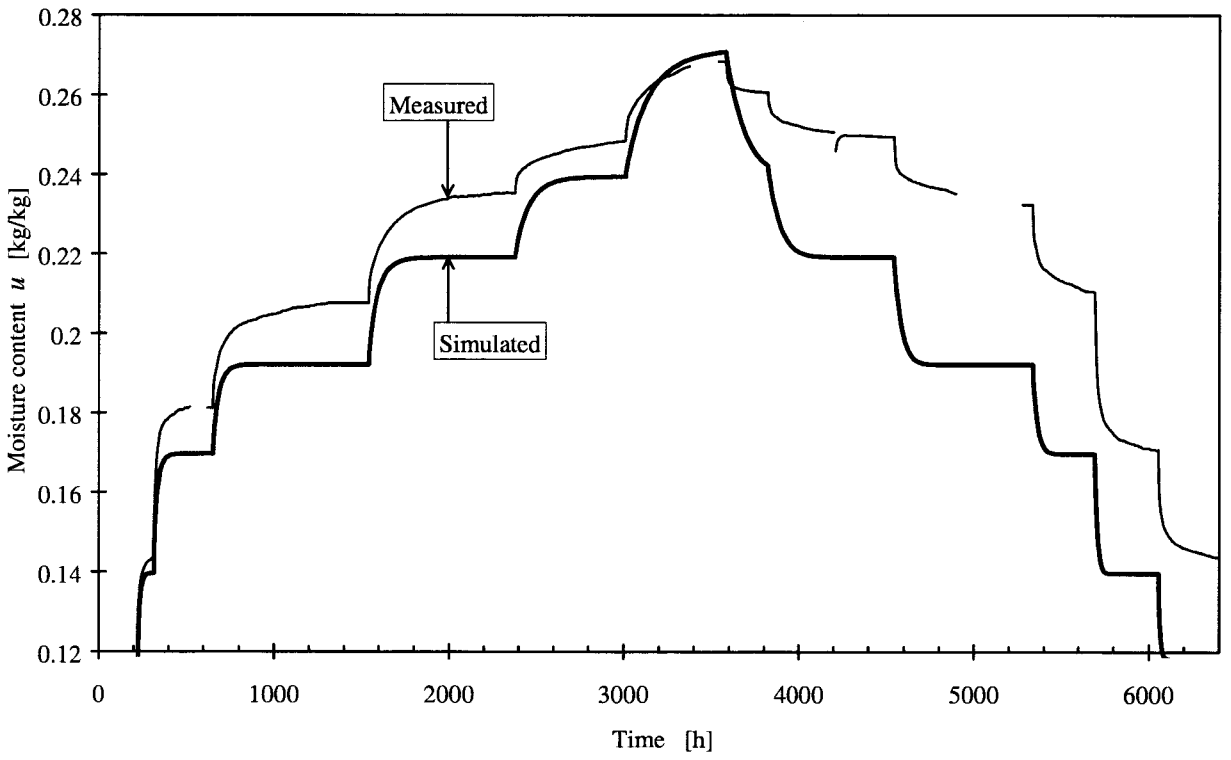

Figure 11.13 Simulation compared to measurements at 20°C.

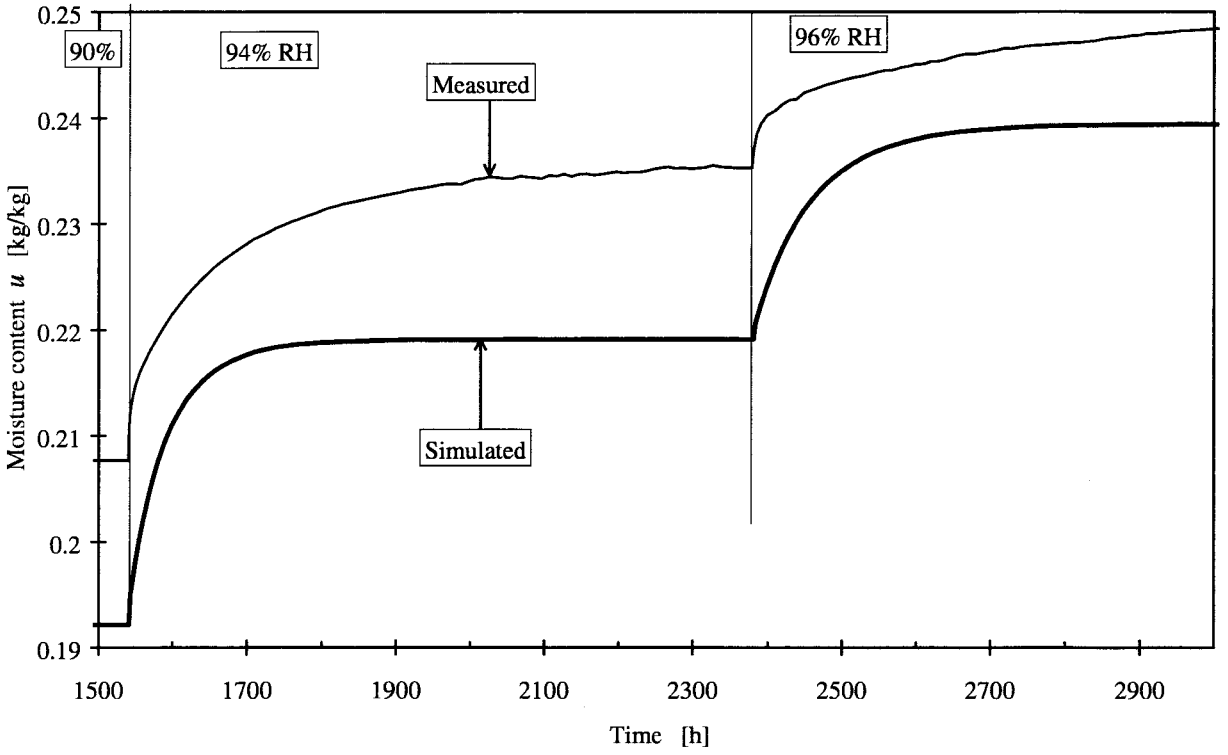

Figure 11.14 Simulation compared to measurements at 20°C. Detail from Figure 11.13.

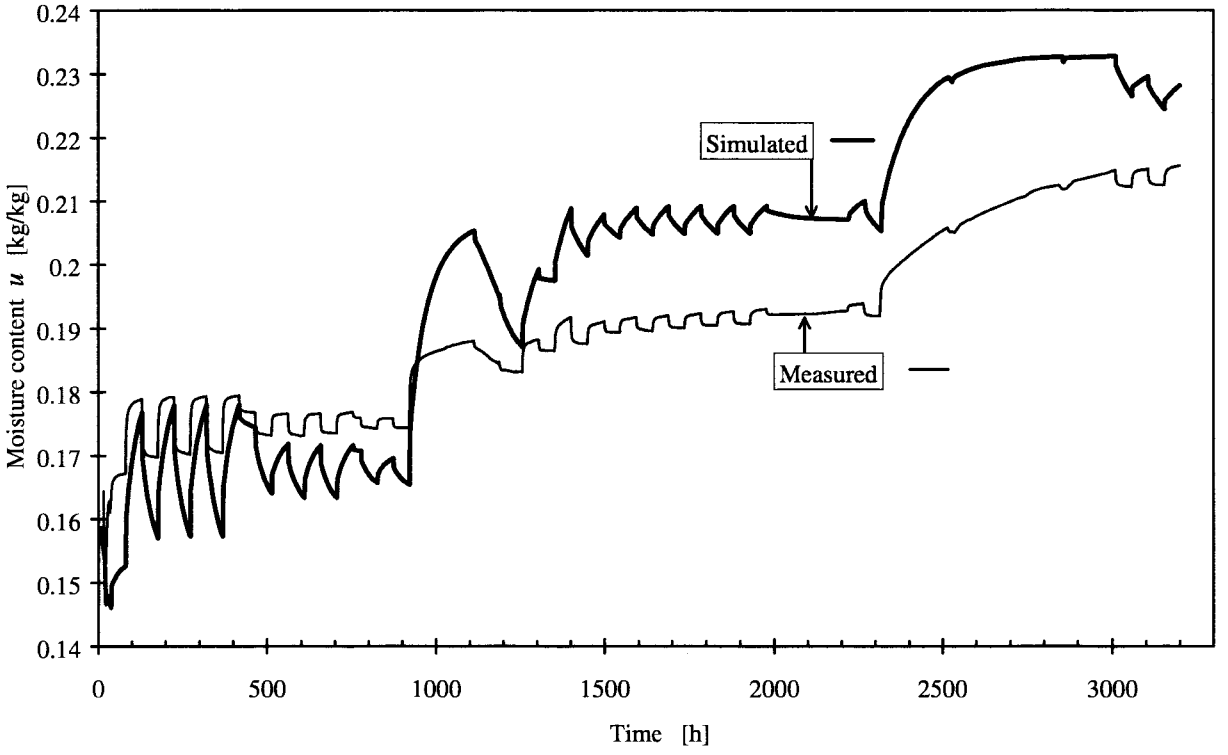

Figure 11.15 Simulation compared to measurements at 5°C.

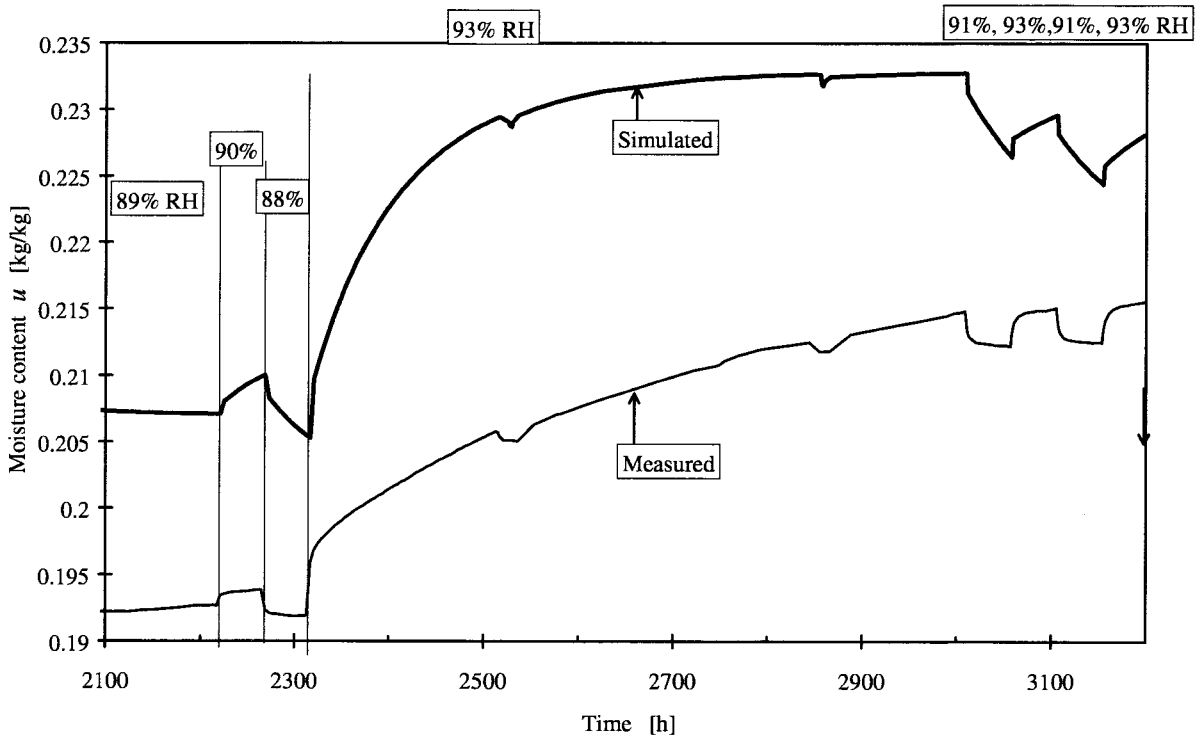

Figure 11.16 Simulation compared to measurements at 5°C. Detail from Figure 11.15.

11.1.3 Constant conductances in cell wall

The next level of model complexity is to use several internal levels. The cell wall is imagined to consist of N layers. In particular we will consider $N = 6$. See Figure 11.17. There is normally another cell wall to the right. The flux to the right is therefore by symmetry zero. The complete moisture flow network is indicated in Figure 11.18.

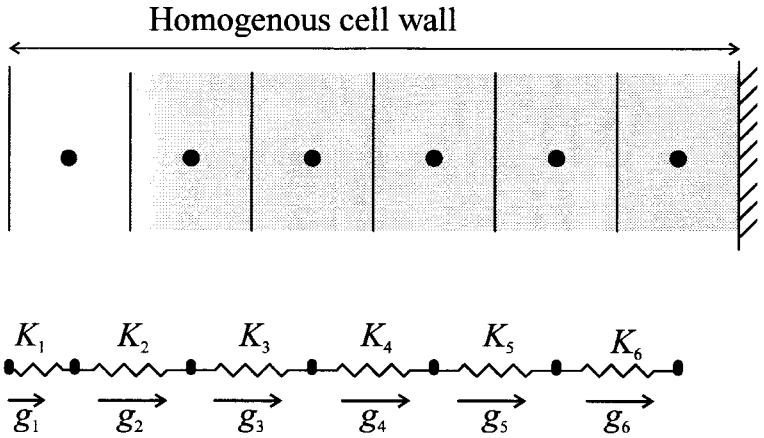

Figure 11.17 Model of cell wall with 6 internal levels.

The total $u(\varphi)$ is divided in one fraction p_0 of the moisture content that is directly accessible for the outer pore system. The rest, $1\text{-}p_0$, is distributed proportional to layer thickness in the cell wall. For a *homogenous* material and layers of constant thickness, this gives:

$u_0 = p_0 \cdot u(\varphi)$ $u_n = p_1 \cdot u(\varphi)$ $n = 1, \ldots N$

$1\text{-}p_0 = p_1 \cdot N$

Here $N = 6$ is used, and $p_0 = 0.4$ has been chosen for a rough balance between immediate and retarded sorption. Note that the RH-dependence is the same for the outer capacity $u_0(\varphi)$, as for the inner $u_n(\varphi)$. In all other models with internal nodes, level 0 has been given a constant capacity, based on direct observations from the measurements.

The conductances are chosen in proportion to the thickness of the layers in the cell wall. Let K_1 be the conductance of the first half layer in Figure 11.17. Then the other conductances become:

$K_n = 0.5 \cdot K_1 \qquad n = 2, \ldots N$

The chosen value of the total conductance for the cell wall, K_1 /(2·N) , is $15 \cdot 10^{-6}$ [m^3 /(kg_{wood} , s)]. This gives $K_1 = 180 \cdot 10^{-6}$ [m^3 /(kg_{wood} , s)] for $N = 6$. The choice is made to roughly fit the long time-scales for the steps at high RH in the first sequence with its long intervals.

The only parameters in this model that are adjusted to fit the measured response are p_0 and K_1 .

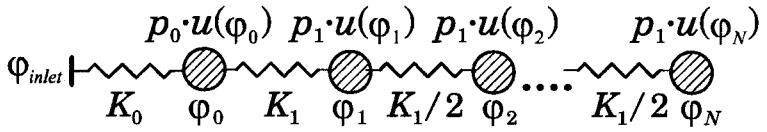

Figure 11.18 Network for a homogenous cell wall using 6 internal levels.

The results of the simulations of the two sequences are shown in Figure 11.19 and Figure 11.20 together with the RH in the different levels. This gives a possibility to follow the progress of the change of RH and moisture in the cell wall for this model.

In Figure 11.21, Figure 11.22 and Figure 11.23 the results of the simulations are compared to the measurements.

A low conductance in the cell wall has been used to model the long time-scale for the sorption at high RH. This gives far to slow sorption at mid-range RH in the beginning of the simulation. The shape of the sorption response curves are also very different from the shapes in the measured sequence . When RH is kept constant for a long period all the nodes arrive at near equilibrium and the sorption stops, whereas retarded sorption always is present in the measured sequences. See in particular Figure 11.21.

It is clear that this model, where the internal conductances are the same, is not sufficient.

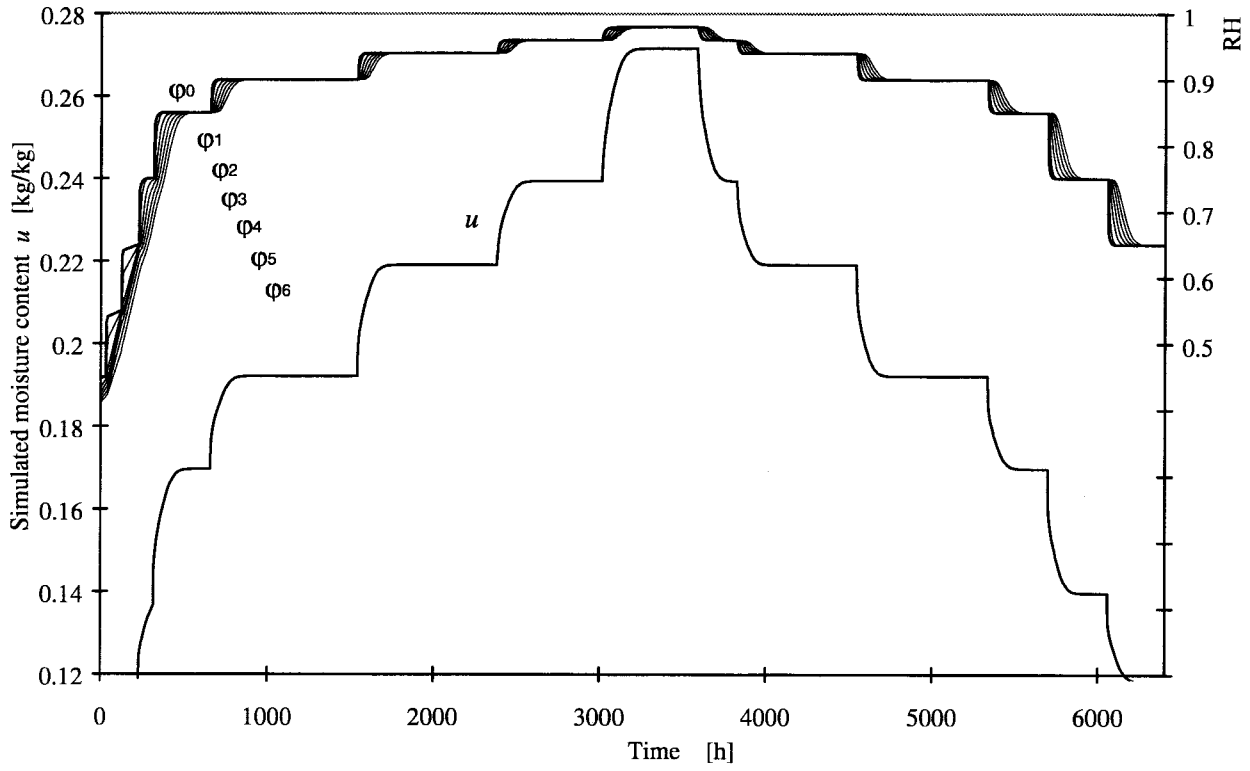

Figure 11.19 Simulation of the sequence at 20°C.

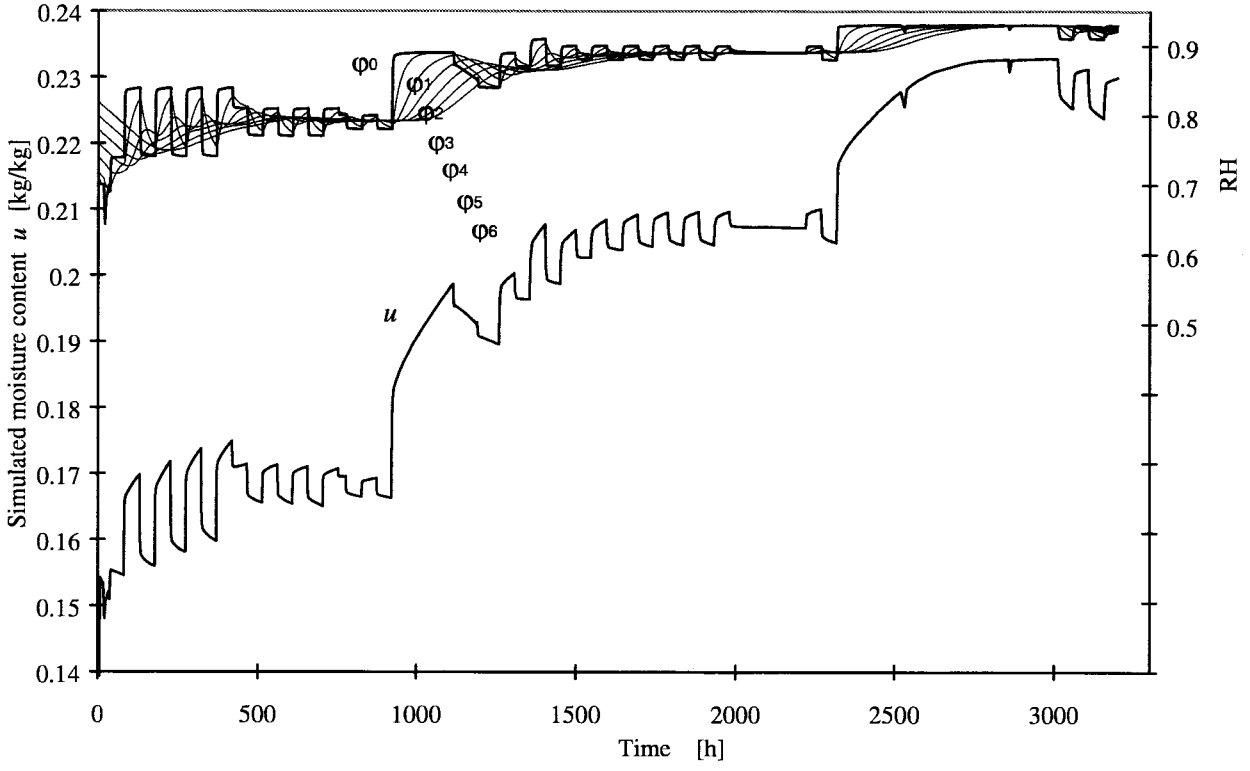

Figure 11.20 Simulation of the sequence at 5°C.

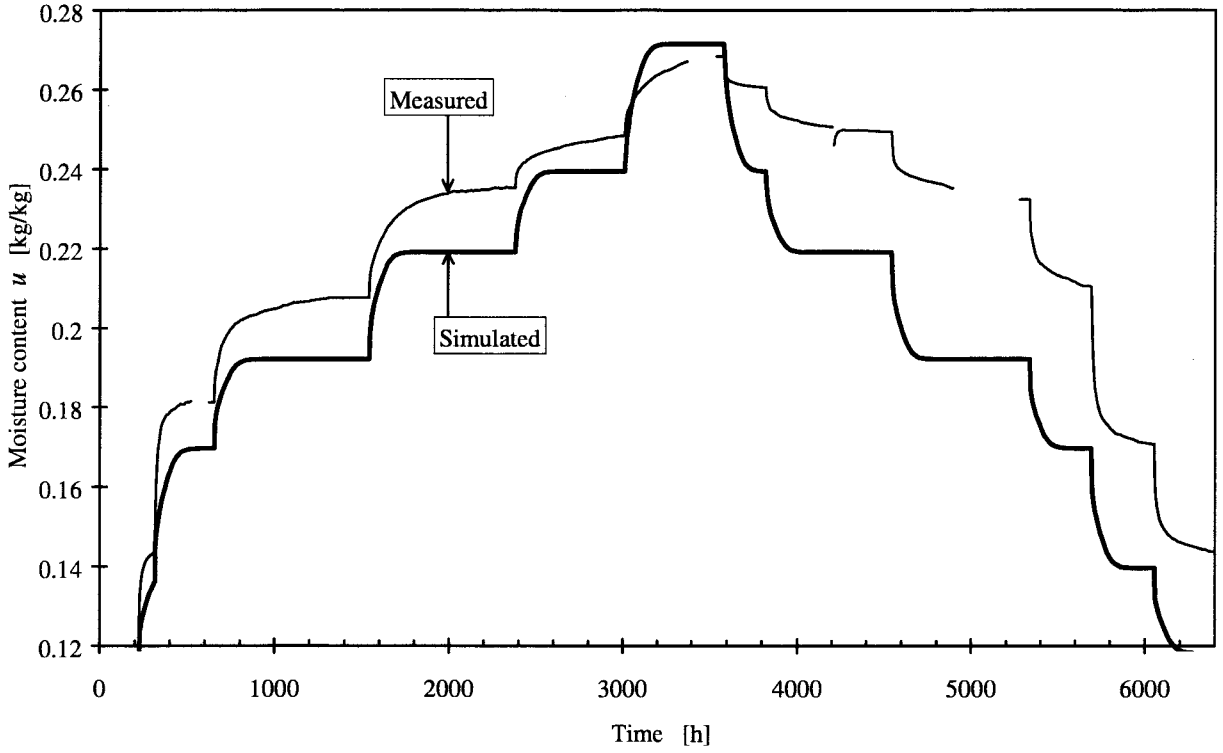

Figure 11.21 Simulation compared to measurements at 20°C.

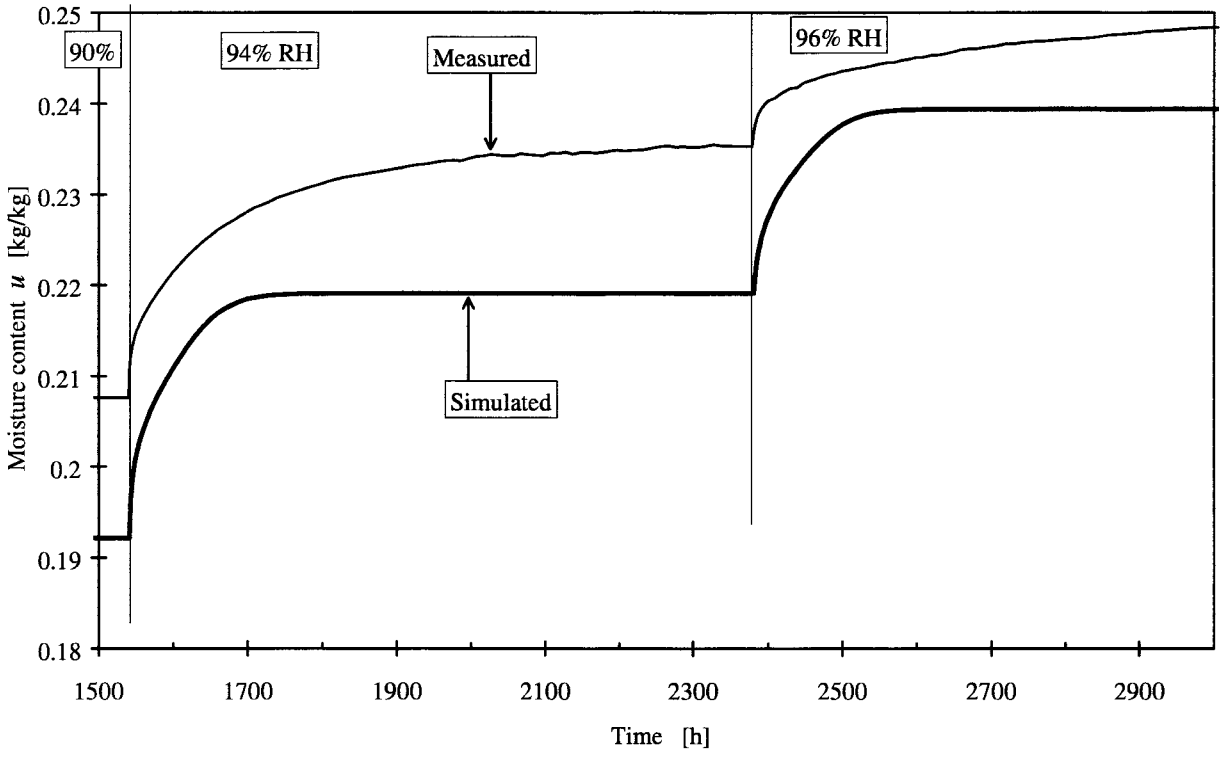

Figure 11.22 Simulation compared to measurements at 20°C. Detail from Figure 11.21.

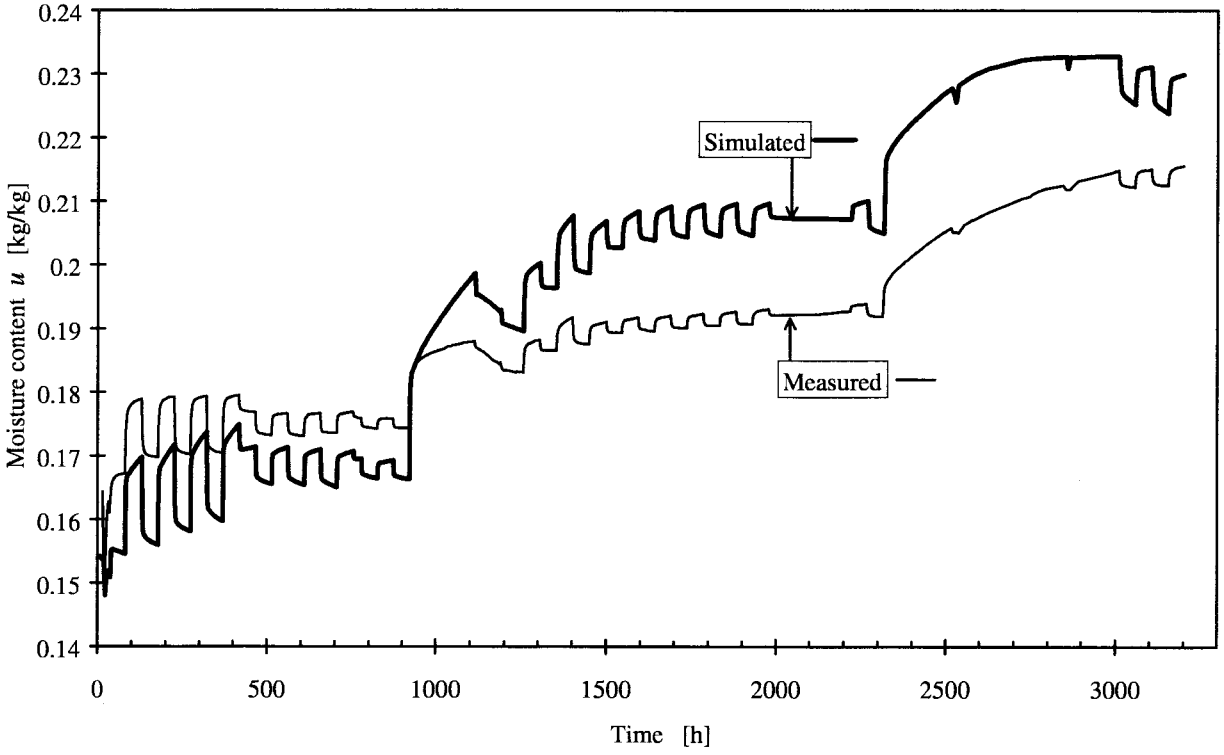

Figure 11.23 Simulation compared to measurements at 5°C.

11.1.4 Variable conductances in cell wall

The next step of complexity in the model is to consider different internal conductances.

This model is similar to the model in Section 11.1.2, but instead of one internal level this model has five (N = 5). The conductances between the levels are progressively decreasing unlike the previous model in Section 11.1.3, where the conductances were the same to describe a homogenous cell wall. Figure 11.24 shows a moisture flow network for this model.

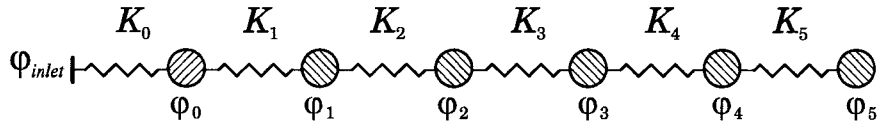

Figure 11.24 Network using five internal levels and variable conductances

As described in Section 10.1.4 and used for the model in Section 11.1.2, the moisture capacity in level 0 has been given a constant value.

$c_0 = 0.08$ [kg_{water}/kg_{wood}] $\qquad u_0(\varphi) = c_0 \cdot \varphi$

The reminder of the moisture capacity is distributed in the N = 5 internal layers as a geometric series according to Eqs. (10.14)-(10.16) in Section 10.4.1:

$u_n(\varphi) = \alpha_n \cdot (u(\varphi) - u_0(\varphi))$

$\alpha_n = \alpha_1 \cdot (b_u)^{n-1} \qquad n = 1,... N$

The factor α_1 is determined by b_u, Eq. (10.16). After a few tests $b_u = 1.4$ has been chosen, which results in $\alpha_1 = 0.091$, $\alpha_2 = 0.128$, $\alpha_3 = 0.179$, $\alpha_4 = 0.252$, $\alpha_5 = 0.351$.

The conductances K_n between the different levels are also varied as a geometric series:

$K_n = K_1 \cdot (b_k)^{n-1}$ $\quad (b_k < 1)$,

After a few tests, $b_k = 0.6$ and $K_1 = 1 \cdot 10^{-3}$ $[m^3/(kg_{wood}, s)]$ has been chosen.

The results of the simulations of the two sequences are shown in Figure 11.25 and Figure 11.26 together with the RH in all levels.

In Figure 11.27, Figure 11.28 and Figure 11.29, the results of the simulations are compared with the measured values.

A difference for the two simulation sequences at different temperatures can be noted. At 20°C as seen in Figure 11.27, the assigned value for the conductances appear too small and the retarded sorption is too dominating. Comparison can be made with a simulation with the same assumed conductances for the 5°C sequence, Figure 11.28. Here on the other hand, a stronger blocking of the capacity seems to be needed to reduce the sorption amplitudes and to make the time-scales longer. In the non-linear models a reduction of the conductances by temperature is attained by the temperature dependence of the vapour contents as described in Section 10.6.

Level 0 has been given a constant capacity versus RH in this model, in contrast to the internal levels. Comparison can be made with the homogenous cell wall model in Section 11.1.3, which has the same capacity variations for all levels. The retarded sorption is far too pronounced at low RH in the homogenous cell wall model seen in Figure 11.19 of the simulation at 20°C. Comparison can be made with the corresponding Figure 11.25 with this model. This demonstrates indirectly the need to assign a different RH-dependence for the immediate sorption. The immediate capacity was analysed more directly in Section 9.1.

Figure 11.27 contains steps where absorption is followed by desorption. This linear model is very poor in reproducing the first two step-responses after the turn at 98% RH. The corresponding simulation with a non-linear model is in Section 11.2.2, Figure 11.38 will later show a much better agreement.

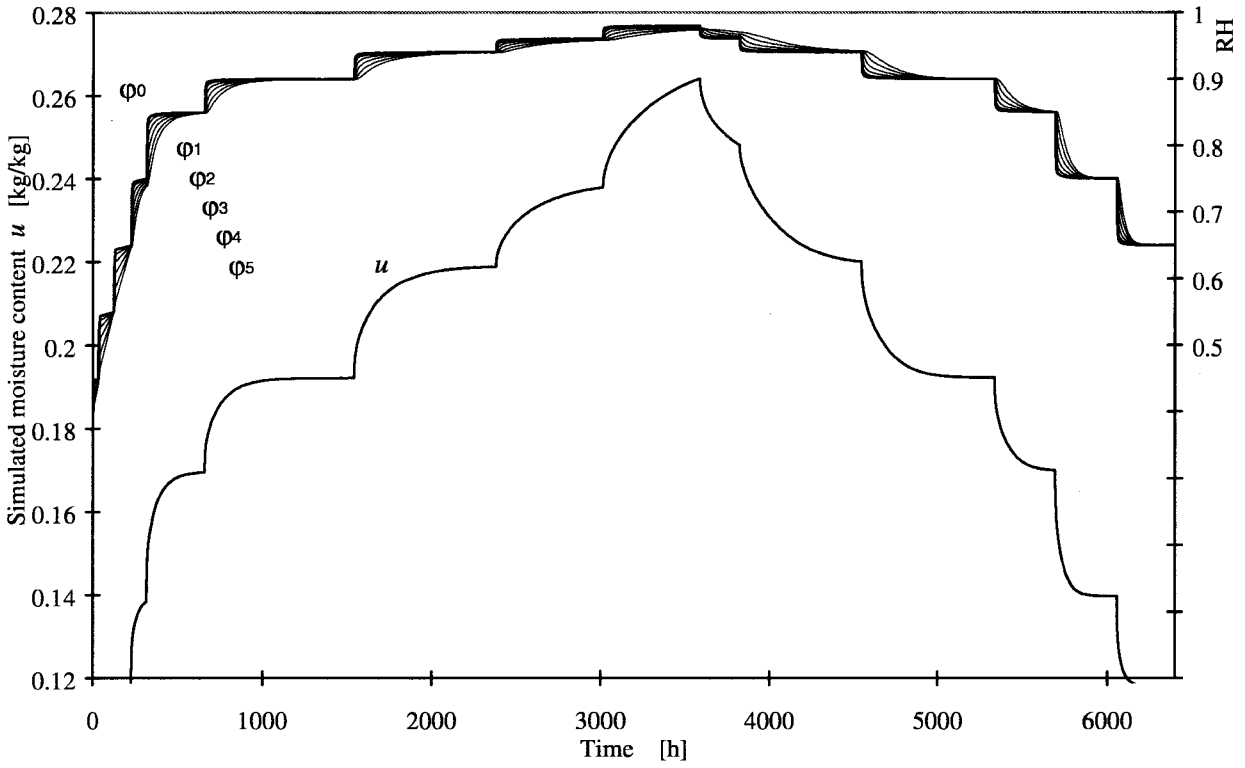

Figure 11.25 Simulation of the sequence at 20°C.

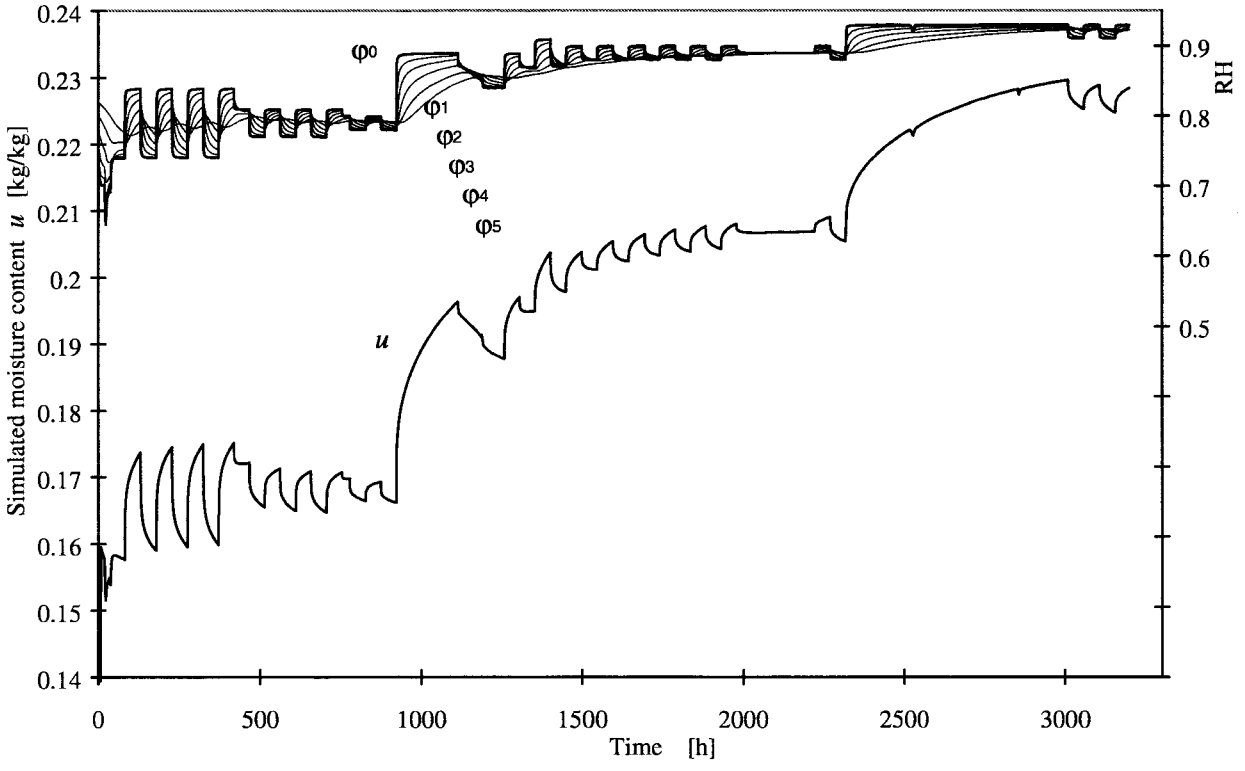

Figure 11.26 Simulation of the sequence at 5°C.

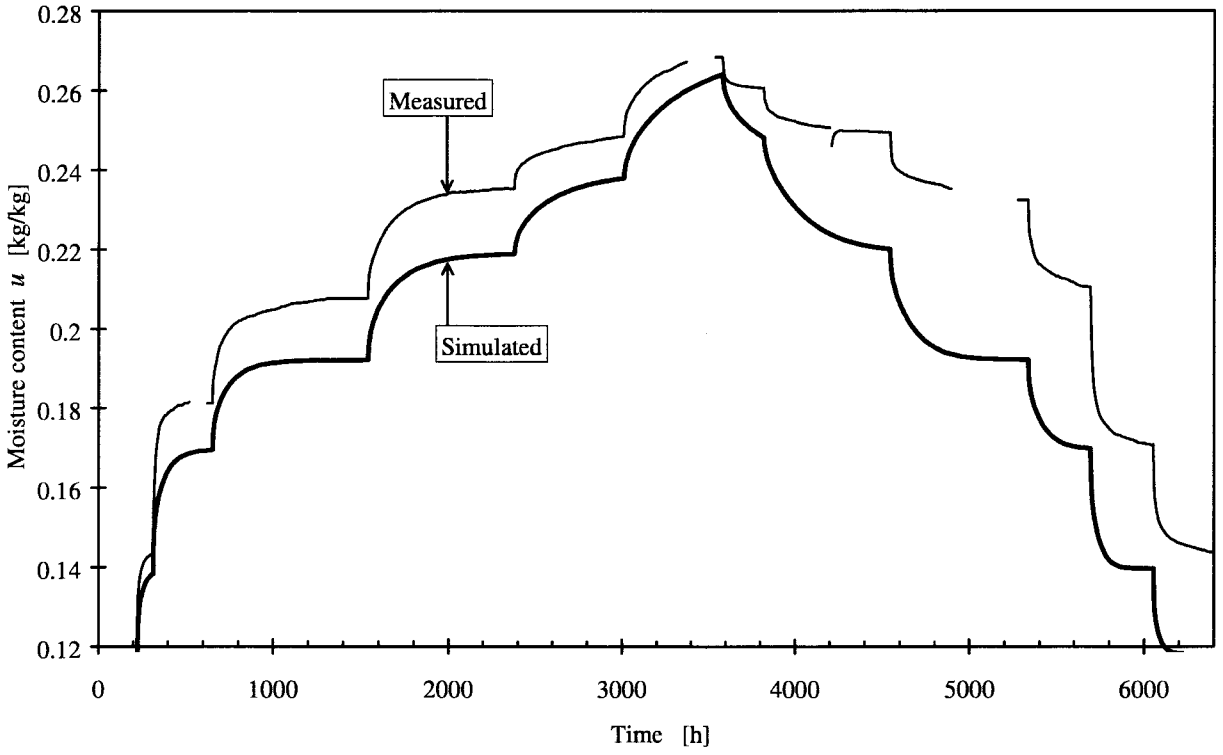

Figure 11.27 Simulation compared to measurements at 20°C.

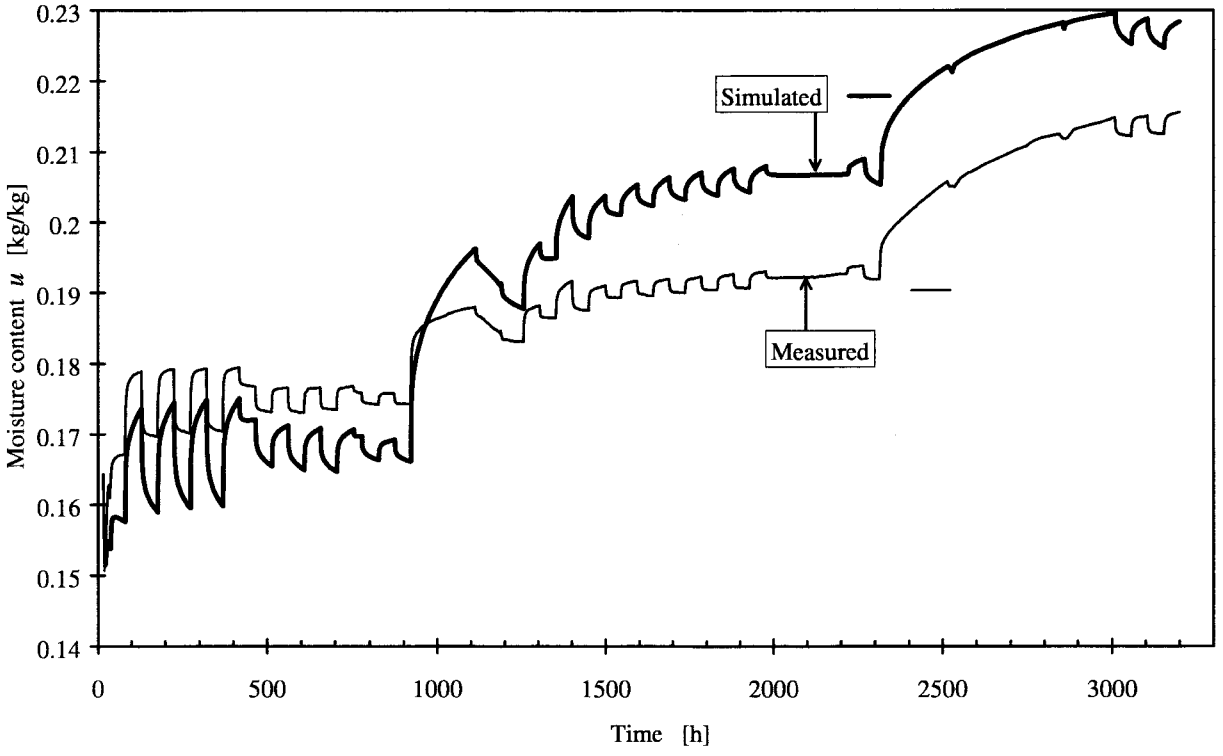

Figure 11.28 Simulation compared to measurements at 5°C.

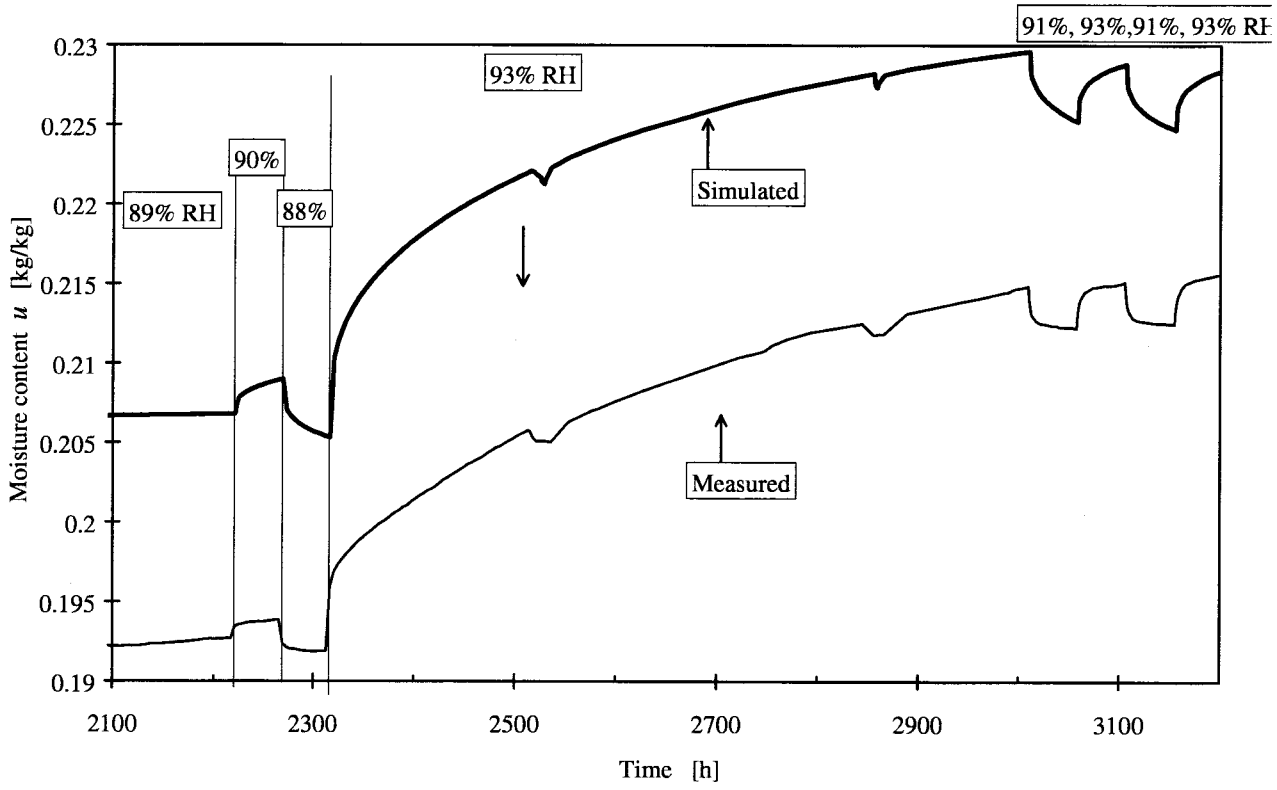

Figure 11.29 Simulation compared to measurements at 5°C. Detail from Figure 11.28.

11.2 Non-linear models

The previous models in Section 11.1 with their increasing complexity are all linear. They could simulate parts of the various complex responses. But very clear discrepancies between measured and simulated responses are still remaining. It is clear that non-linear models are needed.

In the networks a non-linear conductance is given a special symbol:

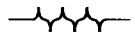 non-linear conductance

11.2.1 One internal level in cell wall

A non-linear model with one internal level ($N = 1$) is tested. Its linear counterpart is discussed in Section 11.1.2. Figure 11.30 shows a moisture flow network for this model.

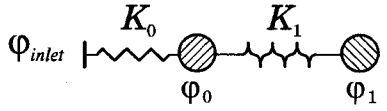

Figure 11.30 Non-linear network using one internal level.

As earlier, the moisture capacity in level 0 has been given a constant value:

$c_0 = 0.08$ [kg_{water} /kg_{wood}]

The conductance K_1 from Eq. (10.17) in Section 10.4.2 contains two parameters, k_1 and γ:

$$K_1 = k_1 \cdot | v_0 - v_1 |^{\gamma}$$

The exponent for the non-linearity of the internal conductances is $\gamma = 1$. This means that the internal moisture flow is proportional to the square of the applied difference of vapour content over the conductance.

By fitting one of the first step-responses with long intervals, the following value was obtained:

$k_1 = 0.5$ [m^6 /(kg_{wood} , $kg_{water} \cdot s$)] $\gamma = 1$

The fitting was made for the same intervals as the fitting in the corresponding linear model in Section 11.1.2.

The result of the simulations of the two sequences are shown in Figure 11.31 and Figure 11.32 together with RH of the two levels.

In Figure 11.33 and Figure 11.34, the results of the simulations are compared with the measured values. One improvement in the result from this non-linear model compared to the corresponding linear model in Section 11.1.2 can be studied in steps with small amplitude in RH. If the simulation result for the steps 94%–›96%–›98% RH (2380 h to 3600 h on the time axis) in Figure 11.13 is compared to the result in Figure 11.33, the non-linear model can block and delay the sorption somewhat better. In the simulation of periodic steps, Figure 11.15 compared to Figure 11.34, the shape of the responses are better for the non-linear model.

Cycles of larger amplitude have produced proportionally slightly larger sorption than cycles with smaller RH amplitude. This model exaggerates this effect. This can be seen in Figure 11.34, where the simulated sorption for the 74%–84% RH cycles, to the left in the figure, is far too big. This can be compared to the 88%–90% RH cycles in the centre of the diagram.

The model is not able to simulate the different time-scales present in the 5°C sequence. Generally, the models with just one internal level are too crude to be able to simulate both short and long intervals between steps.

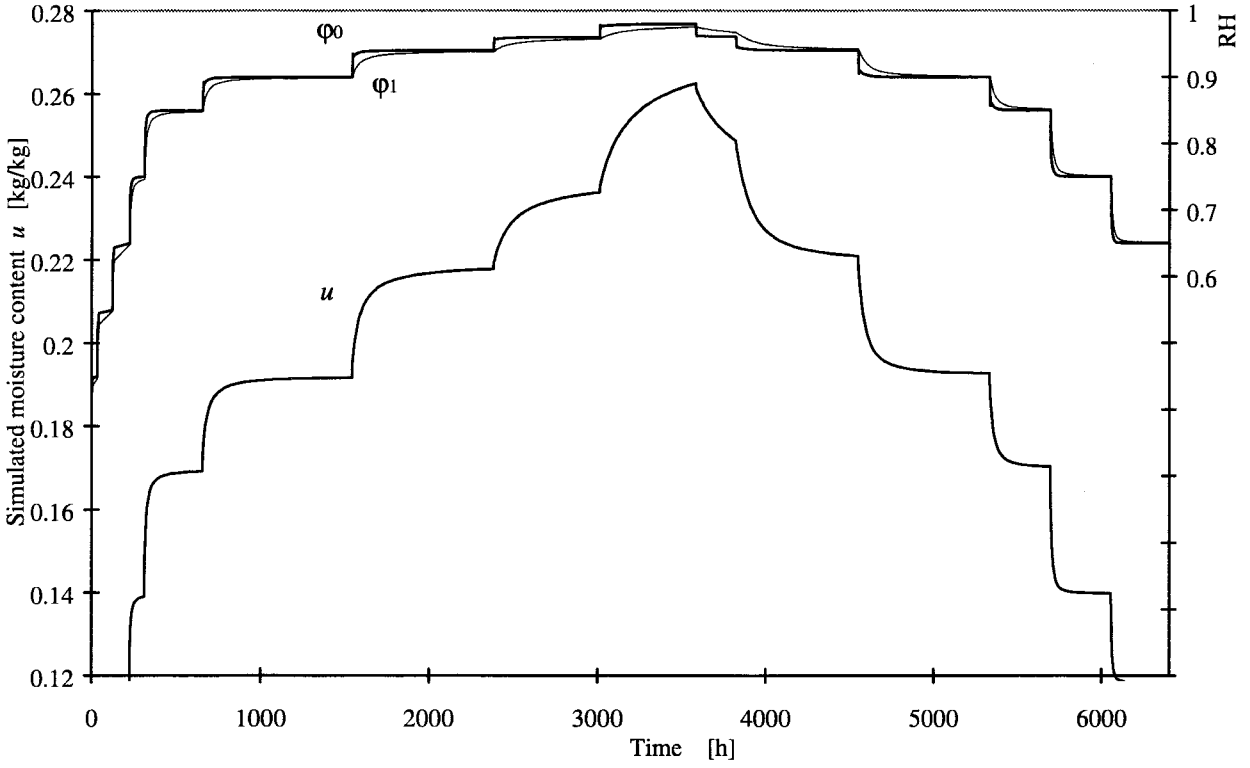

Figure 11.31 Simulation of the sequence at 20°C.

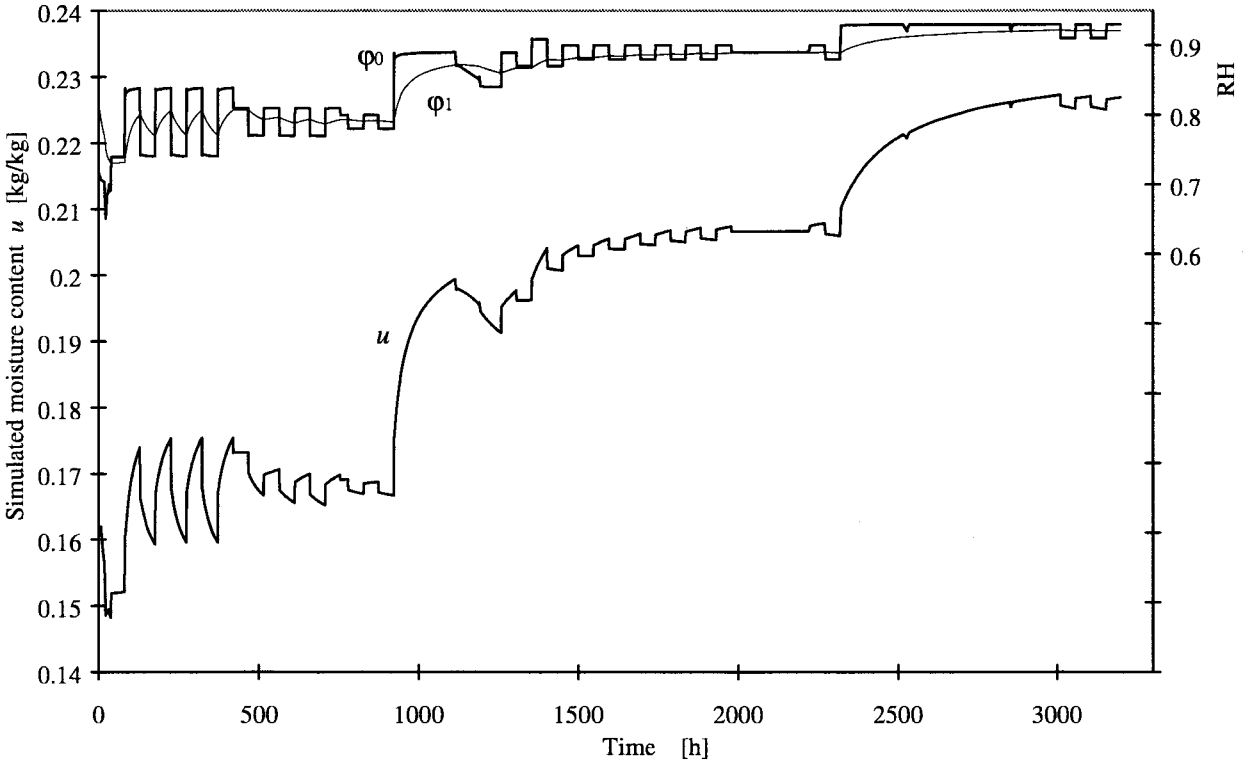

Figure 11.32 Simulation of the sequence at 5°C.

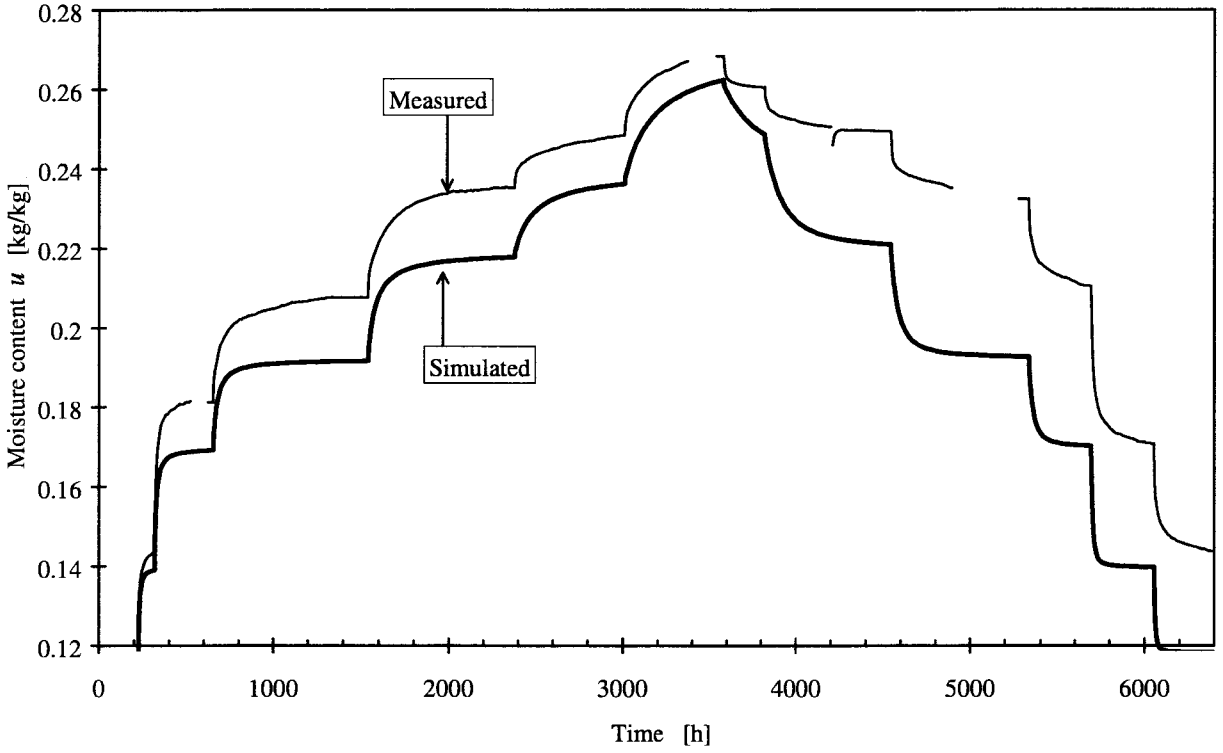

Figure 11.33 Simulation compared to measurements at 20°C.

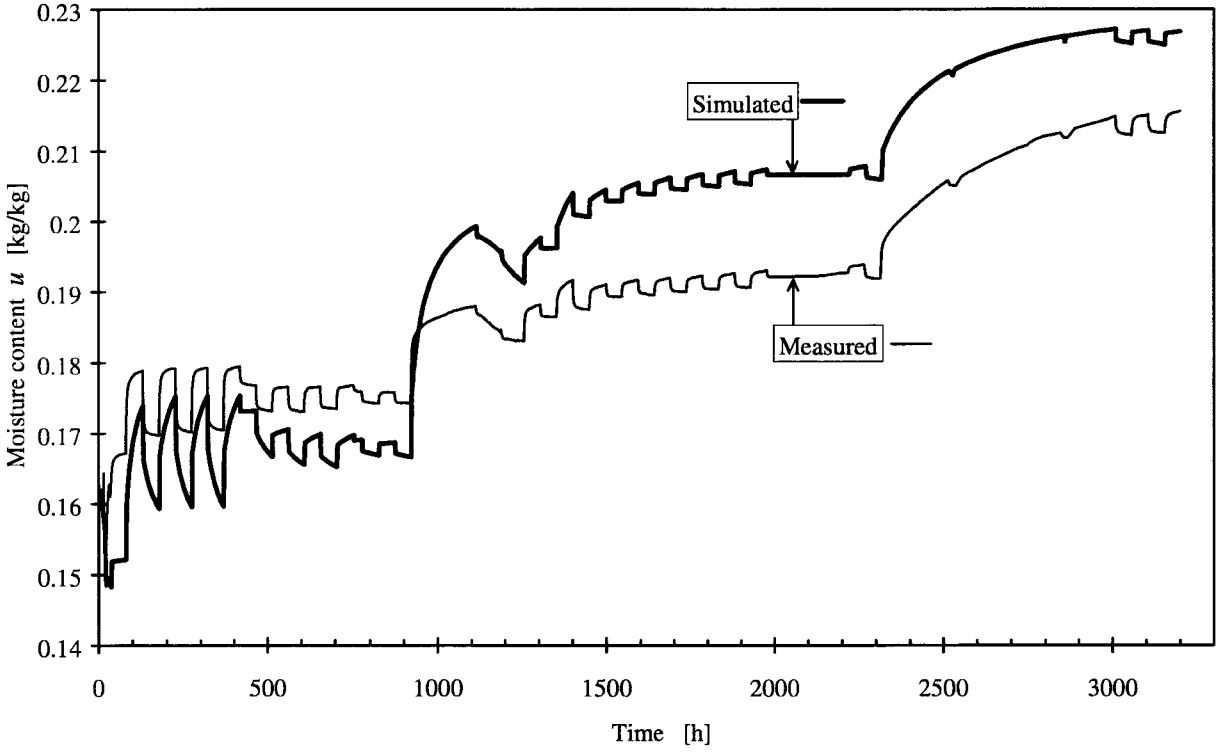

Figure 11.34 Simulation compared to measurements at 5°C.

11.2.2 5 internal levels in cell wall

The previous non-linear model, with just one internal level, showed some improvement on the corresponding linear model. In this model non-linear conductances are combined with several internal levels. Its linear counterpart is described in Section 11.1.4. Figure 11.35 shows a moisture flow network for this model with five internal levels.

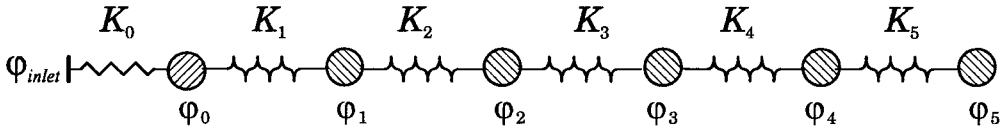

Figure 11.35 Non-linear network using five internal levels.

As earlier, the moisture capacity in level 0 has been given a constant value.

$c_0 = 0.08$ [kg_{water} /kg_{wood}] $u_0(\varphi) = c_0 \cdot \varphi$

The reminder of the moisture capacity is distributed in the $N = 5$ internal layers as a geometric series according to Eqs. (10.14)-(10.16) in Section 10.4.1:

$u_n(\varphi) = \alpha_n \cdot (u(\varphi) - u_0(\varphi))$

$\alpha_n = \alpha_1 \cdot (b_u)^{n-1}$ $n = 1,... N$

The same value $b_u = 1.4$ as the model in Section 11.1.4 has been chosen.

The conductances are proportional to factors k_n , Eq. (10.17) in Section 10.4.2:

$K_n = k_n \cdot | v_{n-1} - v_n |^{\gamma}$ $\gamma = 1$

$k_n = k_1 \cdot (b_k)^{n-1}$ $n = 1,... N$

For a good over-all agreement, the value $k_1 = 2$ [m^6 /(kg_{wood} ·kg_{water} ·s)] was chosen. The same value $b_k = 0.6$ as the model in Section 11.1.4 is used.

The result of the simulations of the two sequences are shown in Figure 11.36 and Figure 11.37 together with RH for all levels.

In Figure 11.38 to Figure 11.41, the results of the simulations are compared with the measured values. This model exhibits considerable improvements compared to the previous ones. Responses are fairly well reproduced, both with long and short time-scales. Proportions between the sorption at different amplitude also show good agreement. The model can also handle combinations of steps. One example is an absorption step kept constant for a long period followed by small cyclic steps. See Figure 11.41. Another example is a long succession of absorption steps followed by a desorption step in Figure 11.38.

As a general conclusion, the measurements have shown, that the sorption after a step is dependent on the previous moisture history. A model that consists of several layers connected with non-linear conductances opens the possibility of having the desired properties for a sorption that is dependent on the previous history in a way that is observed in the measurements. Take as an example a case where slow absorption has taken place over a long period. Here the model with non-linear conductances allows a small but significant difference of potential between the levels to be built up. The retarded sorption can still be slow. If then another absorp-

tion step is added, the differences of potential are increased. This results in higher conductances and a substantial retarded sorption takes place.

The simulation of the first desorption step in Figure 11.38 gives rather good agreement (3600 h to 3800 h on the time axis). The model blocks much of the sorption for this first desorption step. Comparison can be made with the corresponding simulation in Figure 11.27 with a linear model. Here too much sorption is activated.

Despite the generally good agreement, there are still some discrepancies between model simulations and measurements. The major discrepancy occurs when the sequence has scanned over a wide range of absorption and desorption. This is apparent when the third desorption step is made in the first sequence seen in Figure 11.38 (4500 h on the time axis and onwards).

This model has a counterpart with a hysteresis function selected as the model with the best over-all agreement described in Section 11.3.5. In the second sequence (5°C), the hysteresis in the model is hardly activated, since the hysteresis components in the deeper levels of the model almost entirely are exposed to absorption. The outcome of the simulations are then almost identical.

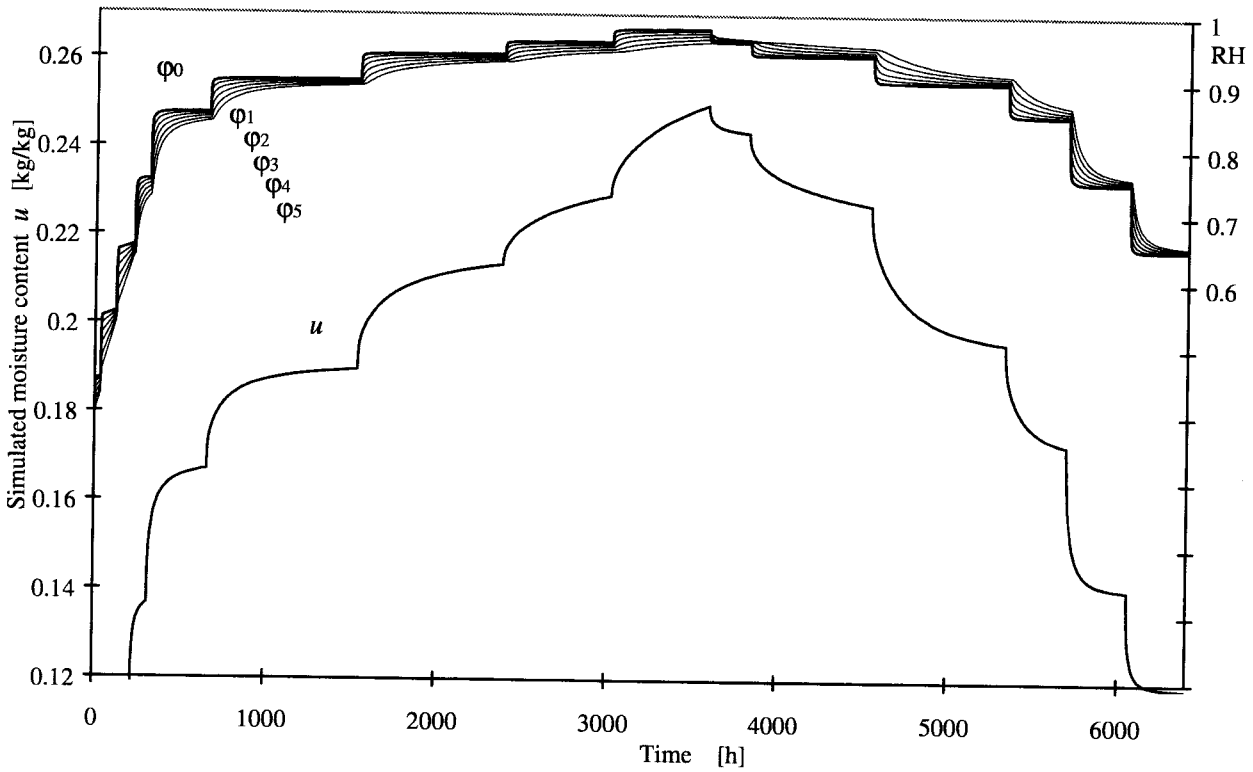

Figure 11.36 Simulation of the sequence at 20°C.

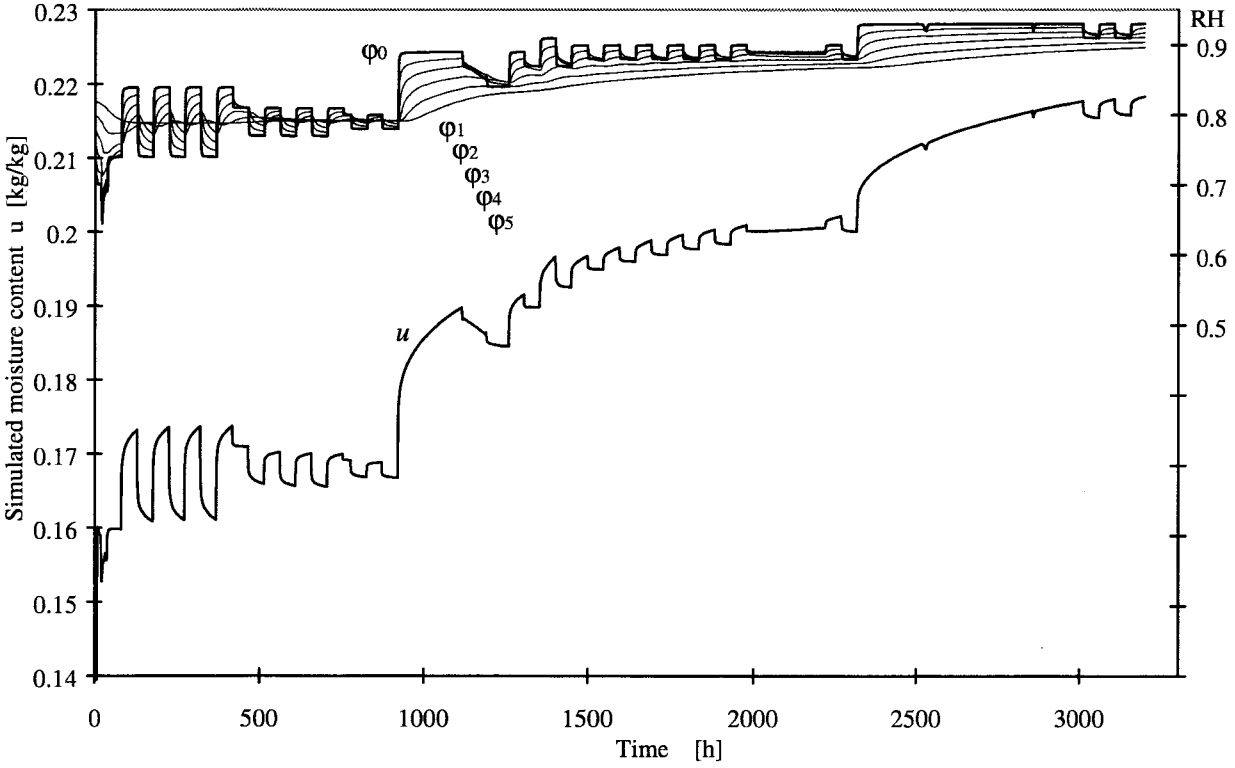

Figure 11.37 Simulation of the sequence at 5°C.

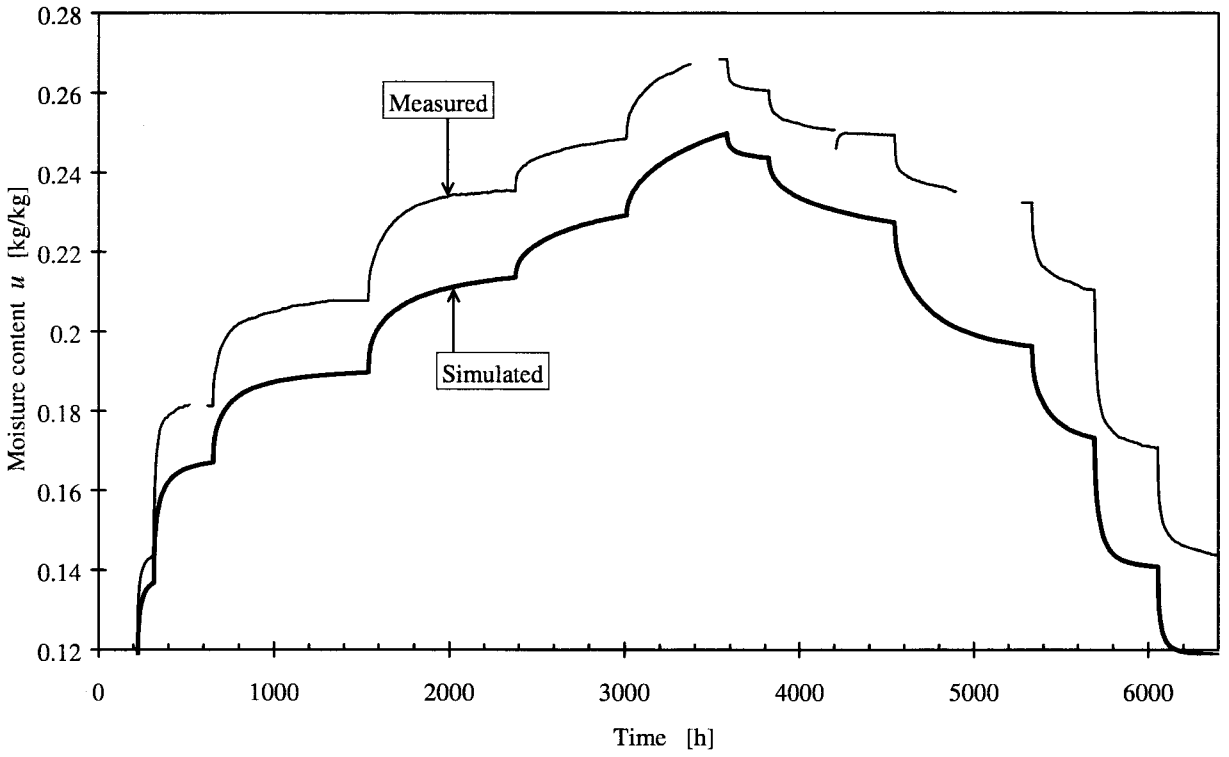

Figure 11.38 Simulation compared to measurements at 20°C.

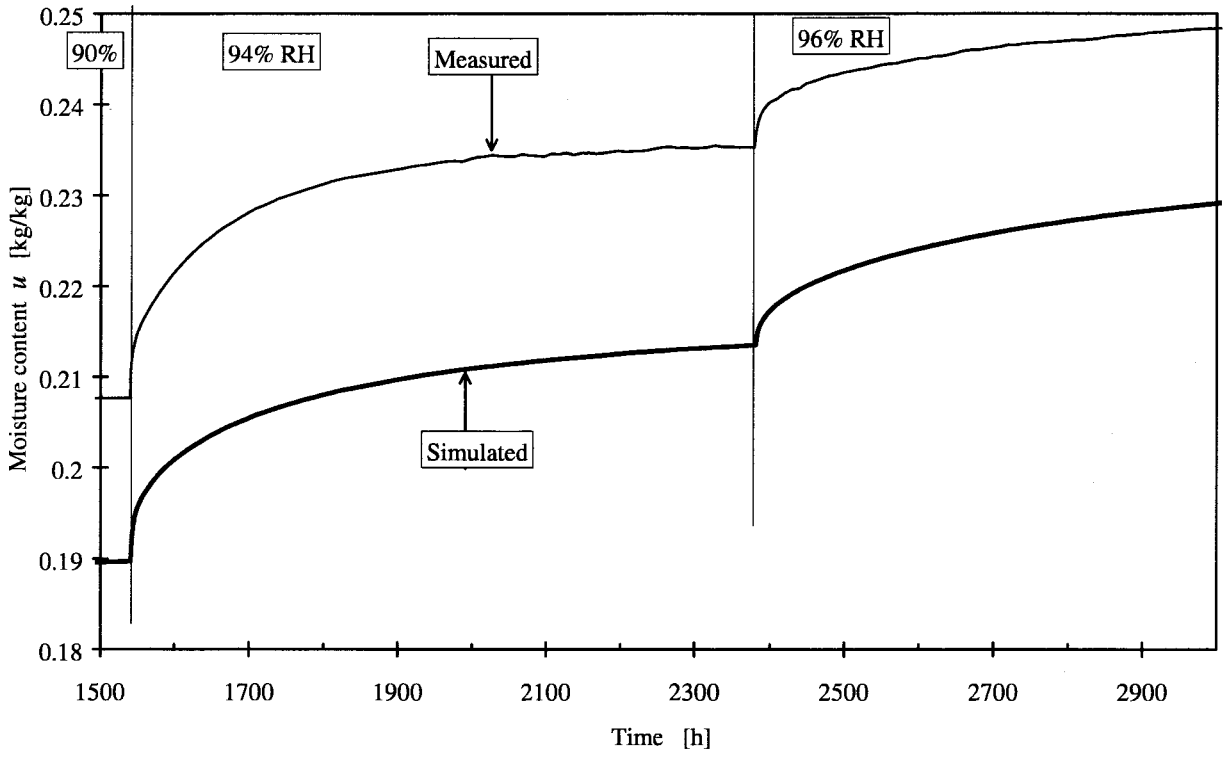

Figure 11.39 Simulation compared to measurements at 20°C. Detail from Figure 11.38.

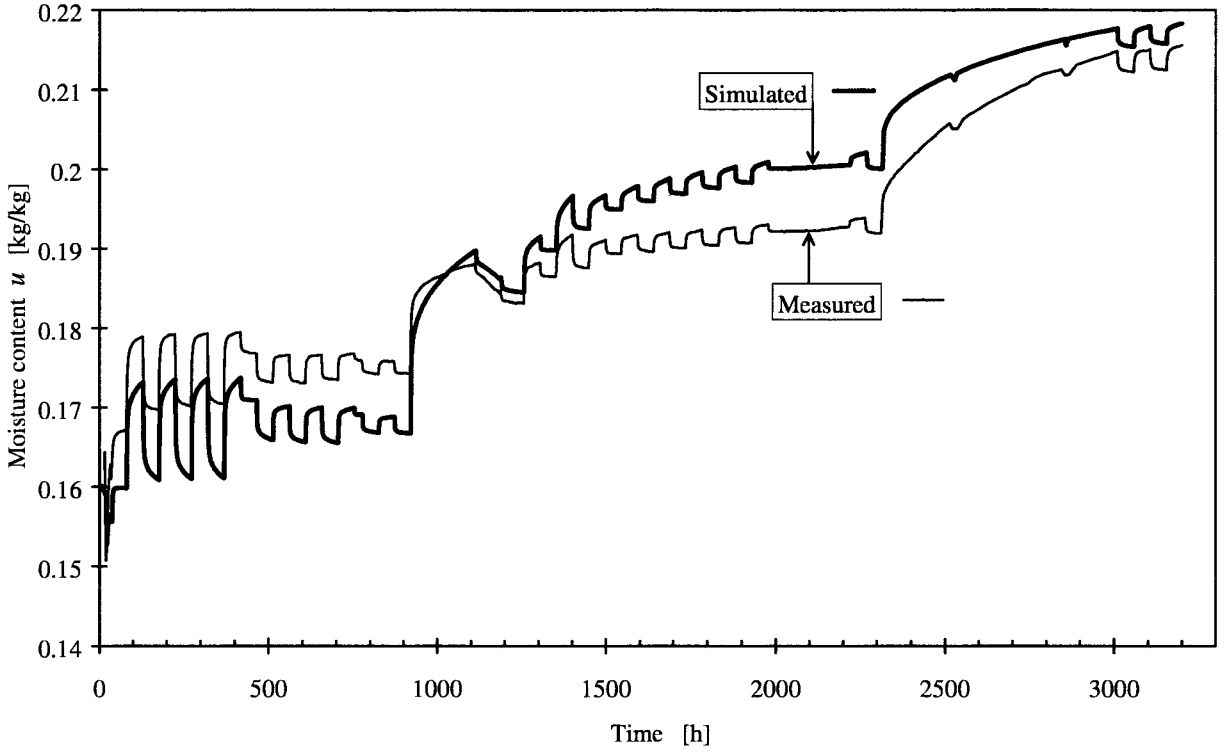

Figure 11.40 Simulation compared to measurements at 5°C.

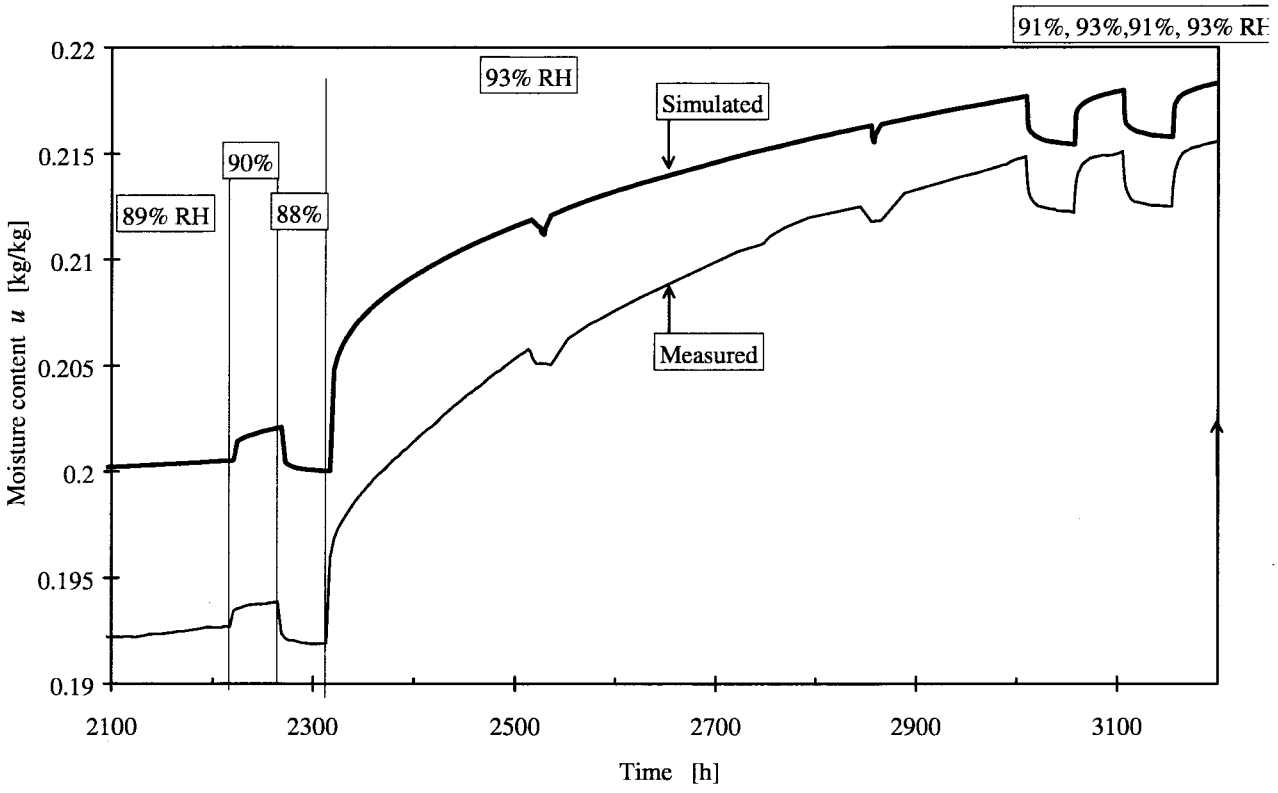

Figure 11.41 Simulation compared to measurements at 5°C. Detail from Figure 11.40.

11.2.3 Conductances with stronger non-linearity

To investigate the influence from a stronger non-linear modelling a variant of the previous model in Section 11.2.2 is tested. Instead of $\gamma = 1$ for the exponent in the equation for the conductances, $\gamma = 2$ has been tested. The same moisture flow network with the same number of nodes as in Figure 11.35 is used.

The capacities are the same as in the compared model in Section 11.2.2:

$c_0 = 0.08$ [kg_{water} /kg_{wood}] $b_u = 1.4$

The conductances are proportional to factors k_n from Eq. (20):

$K_n = k_n \cdot | v_{n-1} - v_n |^{\gamma}$, $\gamma = 2$

$k_n = k_1 \cdot (b_k)^{n-1}$ $n = 1,... N$ $(N = 5)$

After a few tests, $k_1 = 100$ [m^9 /(kg_{wood} , $(kg_{water})^2$, s)] and $b_k = 0.7$ was chosen.

The result of the simulations of the two sequences are shown in Figure 11.42 and Figure 11.43 together with RH for all levels.

In Figure 11.44 and Figure 11.45 the results of the simulations are compared with the measured values.

Comparison can be made with the result for the corresponding earlier model with weaker non-linearity. Figure 11.38 can be compared to Figure 11.44 and Figure 11.40 to Figure 11.45. No direct disadvantage can be seen when using this strongly non-linear model. It is however hard to get an overview of the impact from changes of the parameters in these non-linear models. It is then hard to estimate how good the parameters for the two individual tests are fitted.

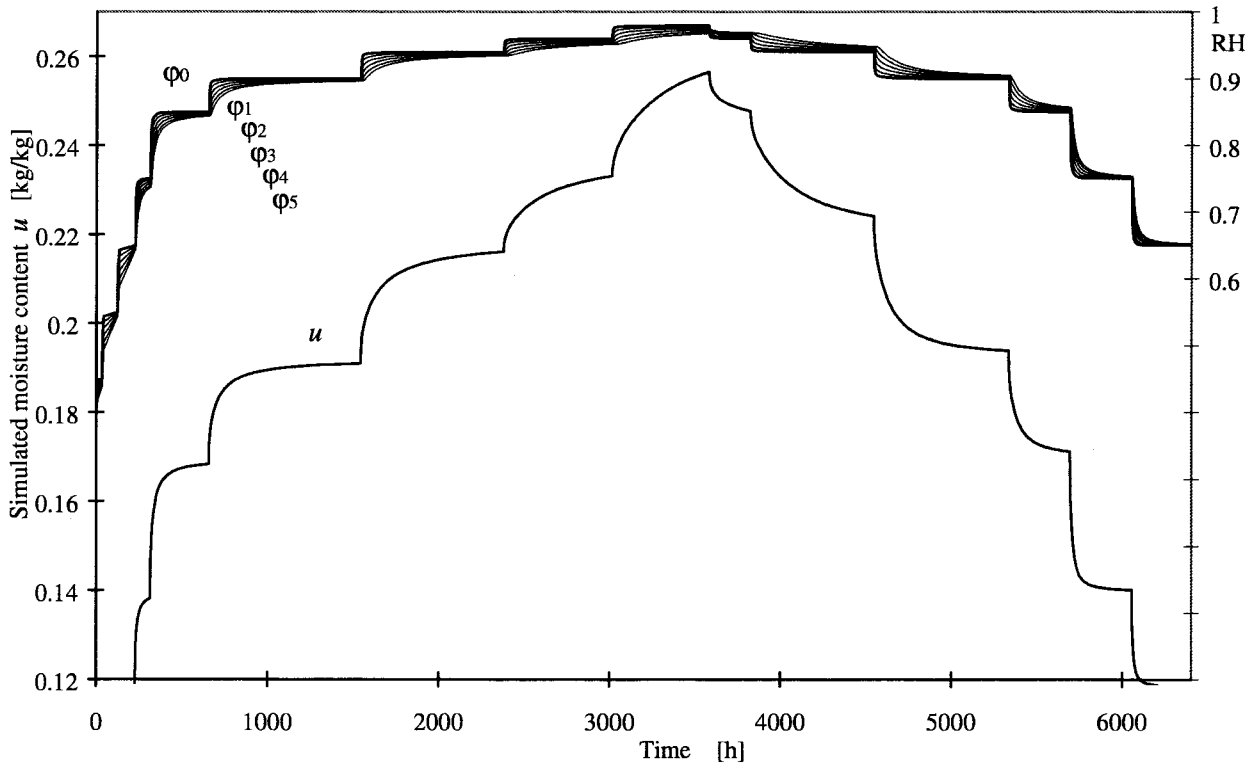

Figure 11.42 Simulation of the sequence at 20°C.

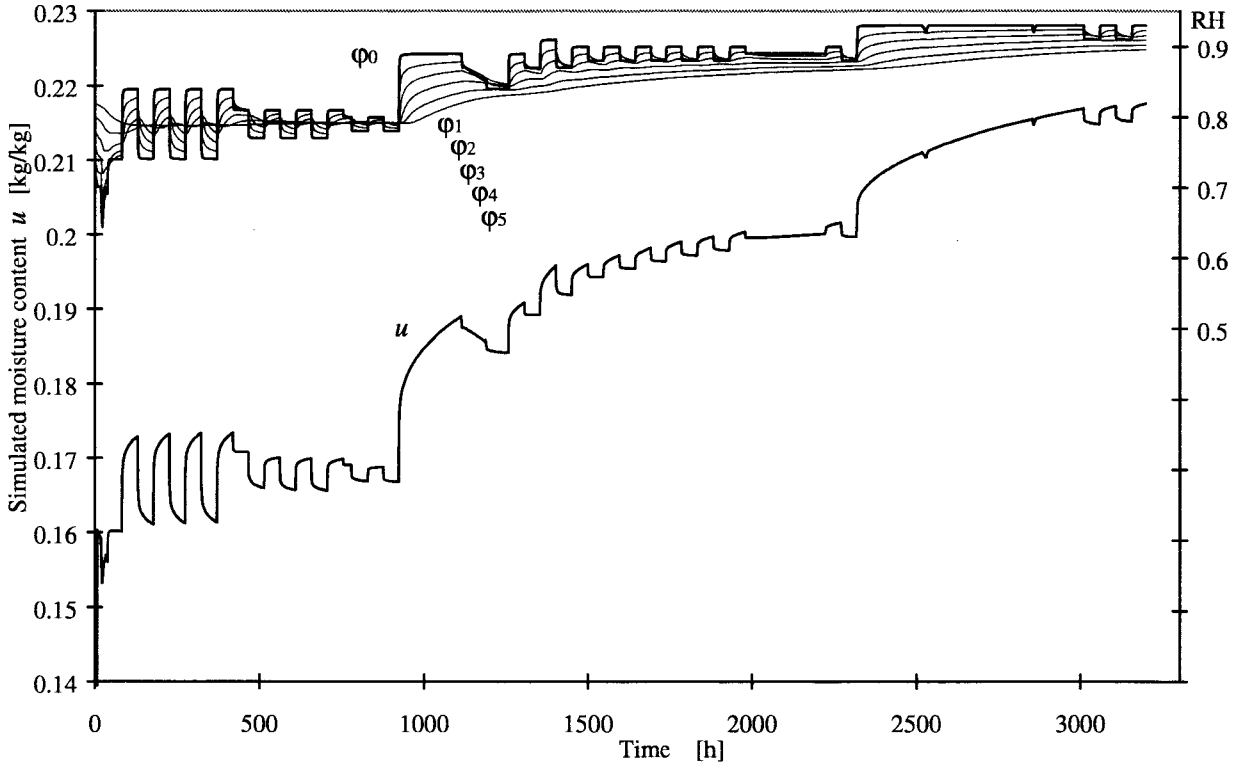

Figure 11.43 Simulation of the sequence at 5°C

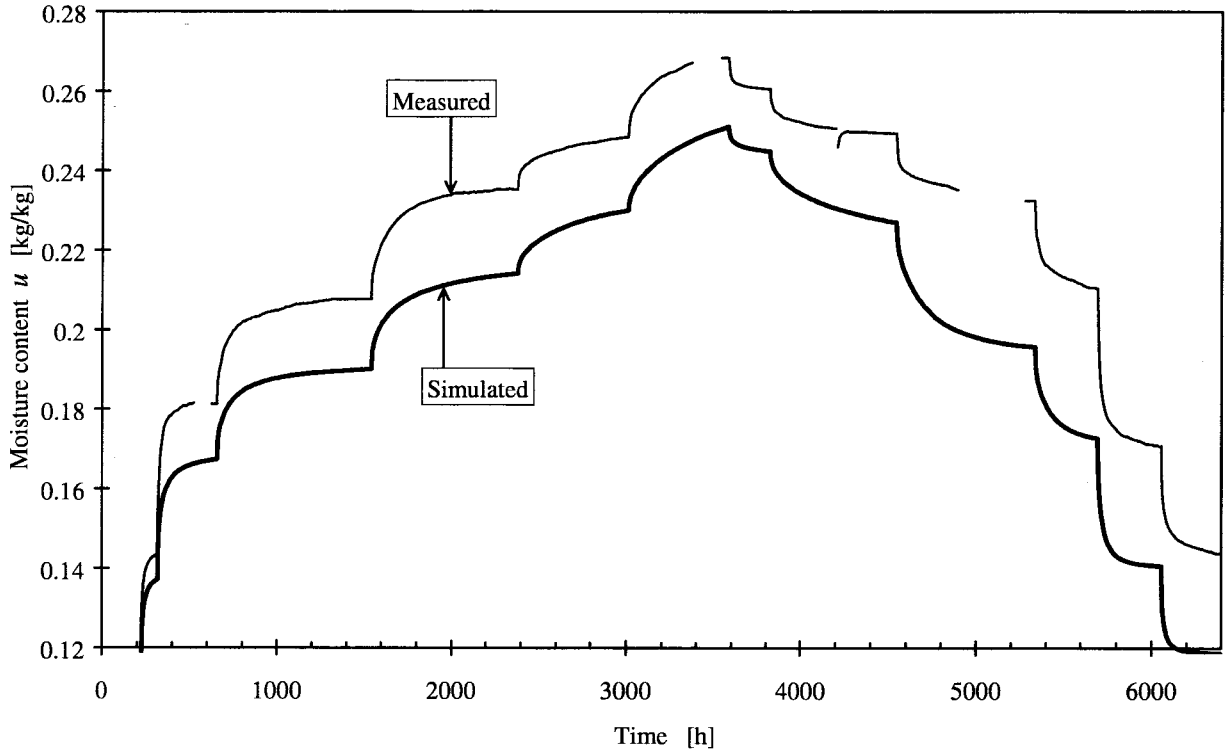

Figure 11.44 Simulation compared to measurements at 20°C.

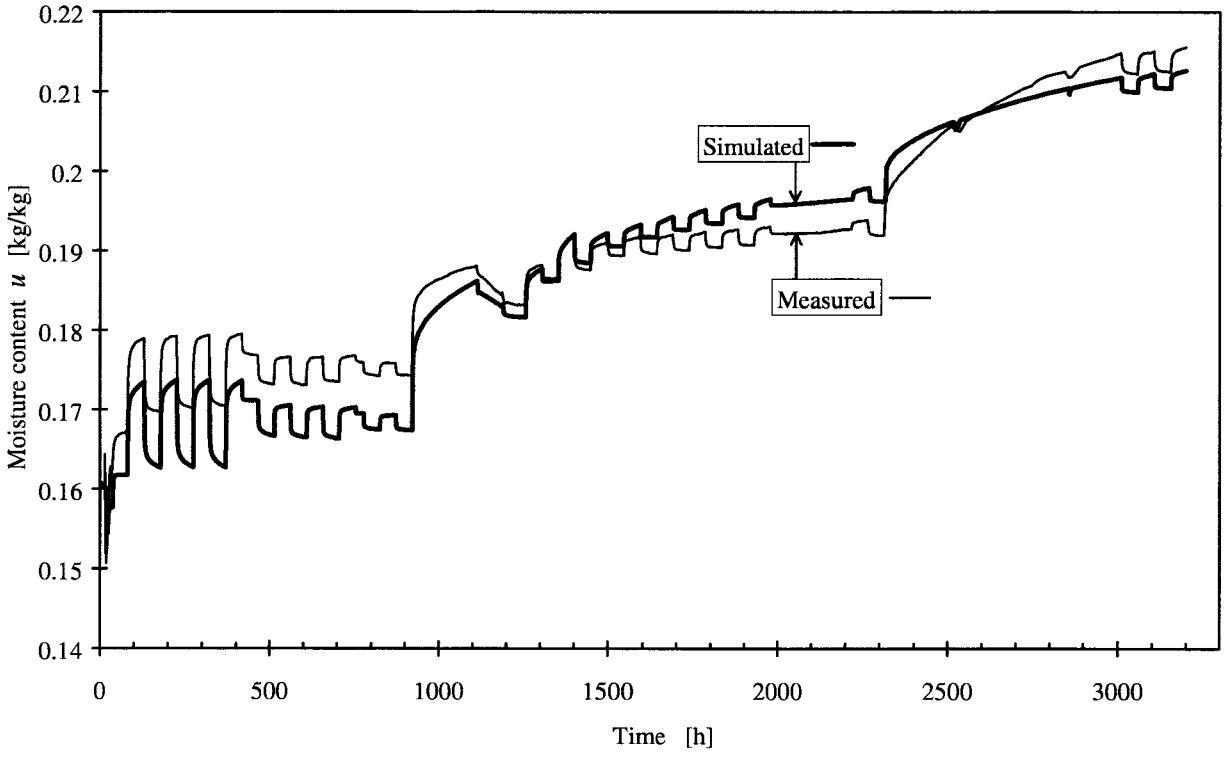

Figure 11.45 Simulation compared to measurements at 5°C.

11.3 Models including hysteresis

11.3.1 Sorption hysteresis function

In order to investigate the influence of sorption hysteresis in the models for retarded sorption, a set of moisture equilibrium curves with the following characteristics has been used.

The hysteresis results in so called scanning curves. This means that the moisture content u follows a new curve after each turn between absorption and desorption. The properties of the hysteresis function used in the model is described in steps for an example below.

Consider first an initial absorption from dry conditions. The moisture equilibrium curve for initial absorption is followed, $u_{in.ab.}$. A fraction $(1- \alpha_{hyst})$ of this curve is assumed not to be influenced by hysteresis. This fraction can be altered to give the desired strength of hysteresis for the total moisture capacity. For the models in this paper $\alpha_{hyst} = 0.351$ has been used after a rough fitting.

This separation in two parts is illustrated in figure 11.46. The fraction above the horizontal axis influences the hysteresis, while the fraction under the axis represents a constant contribution, independent of hysteresis.

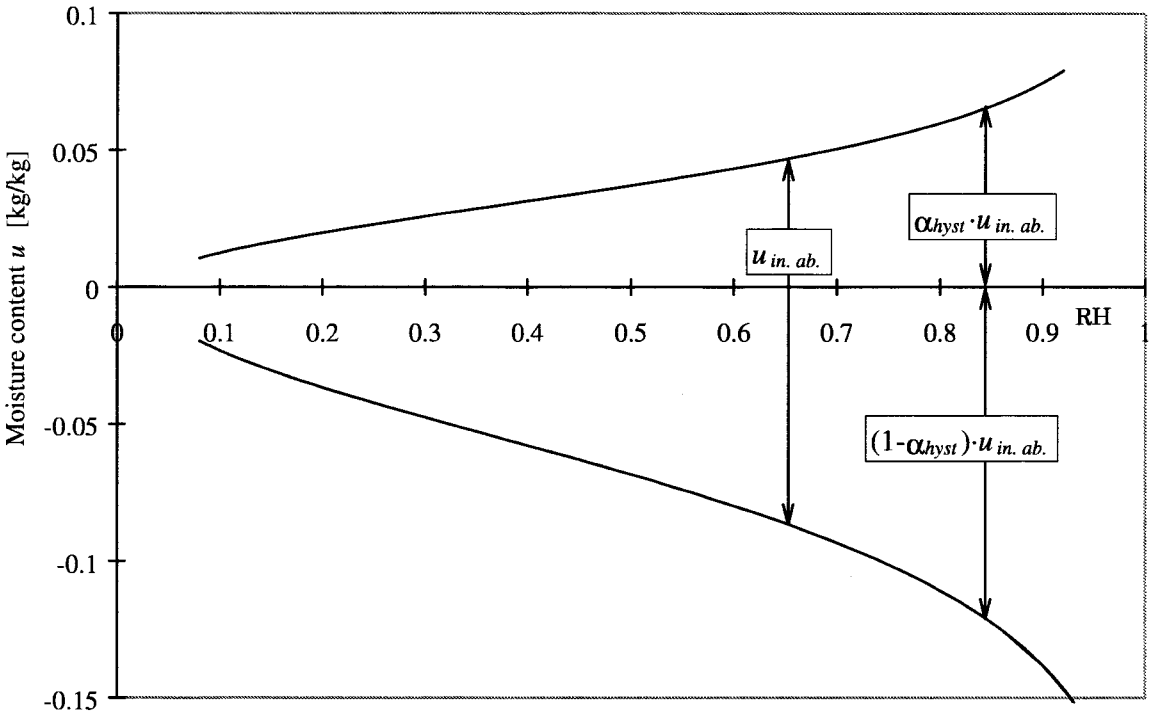

Figure 11.46 Division of the moisture equilibrium curve in two components. The fraction above the horizontal axis influences the hysteresis, while the fraction under the axis represents a constant contribution, independent of hysteresis.

Figure 11.47 illustrates the principles of the hysteresis model. The lower full curve is the hysteresis part of the initial adsorption curve, i. e. the curve above the horizontal axis in Figure 11.46. We consider any sequence of increasing and decreasing RH. We start at low RH φ_0 , then RH is increased to φ_1 , then decreased to φ_2 , increased to φ_3 , etc. Let φ_{max}

denote the largest RH in the sequence (up to the considered time). A so called pivot line is drawn from this φ_{max} on the absorption curve, to a suitably chosen pivot point. See Figure 11.47. The hysteresis part of the moisture content is enclosed between the absorption curve and the pivot line. The absorption curve may be followed for increasing RH, and the pivot line may be followed for decreasing RH. At intermediate points the dotted lines with a less steep slope are followed in both directions. A complication occurs when φ_{max} is exceeded by a new higher RH. Then a new pivot line is created. This is illustrated in Figure 11.50.

We will illustrate how this works with a few examples. In Figure 11.48 to Figure 11.53, a sequence a, b,... to j is followed.

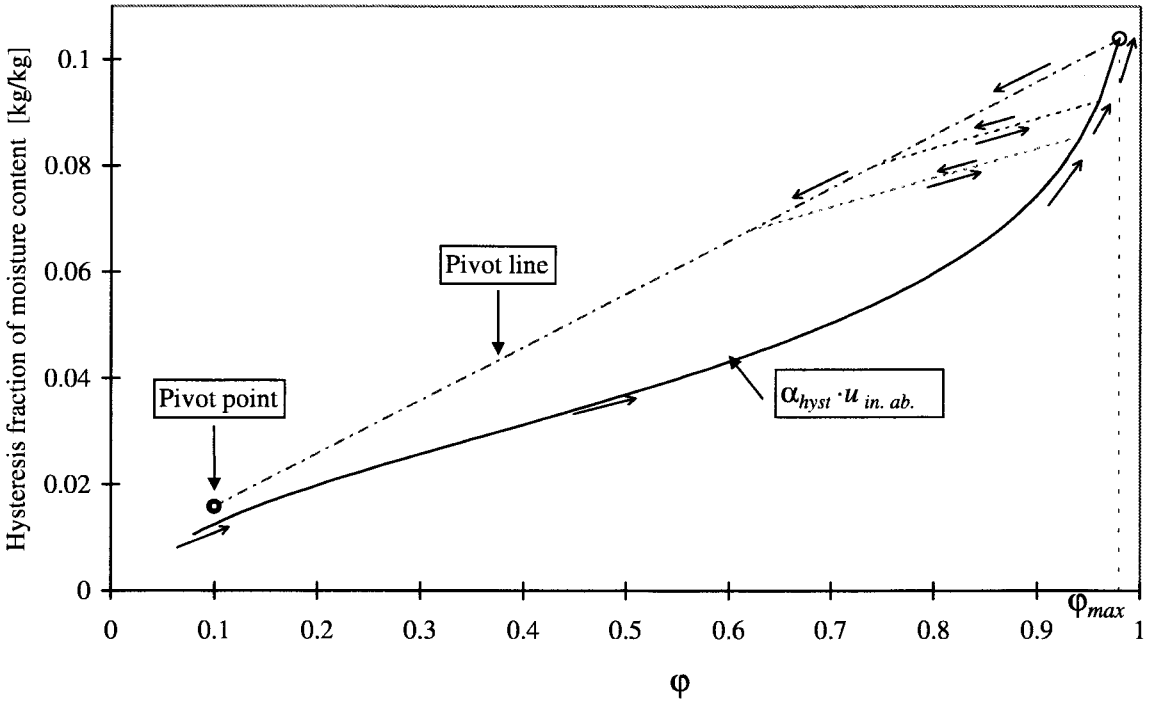

Figure 11.47 Principles for the hysteresis model.

1 a–>b–>c

Consider first a desorption that follows after the initial absorption. The situation is illustrated in Figure 11.48. Curve 1 shows the hysteresis part, $\alpha_{hyst} \cdot u_{in.ab.}$, of the initial absorption curve, i. e. the curve above the RH-axis in Figure 11.46.

The absorption starts in point a. The next event in this example is when the sorption reaches a maximum value and a desorption starts, point b. The desorption is assumed to follow a straight line to a fixed point, named pivot point in the figure. The position of this pivot point is selected to be above any tangents of the absorption moisture equilibrium curve. At the same time it is rather close to the tangents for the curve in the medium range of RH. This results in the desired small hysteresis effects in this range.

The line from the maximum reached RH sorption point to the pivot point is called pivot line. This line defines the ceiling for subsequent scanning curves until the current maximum RH is exceeded.

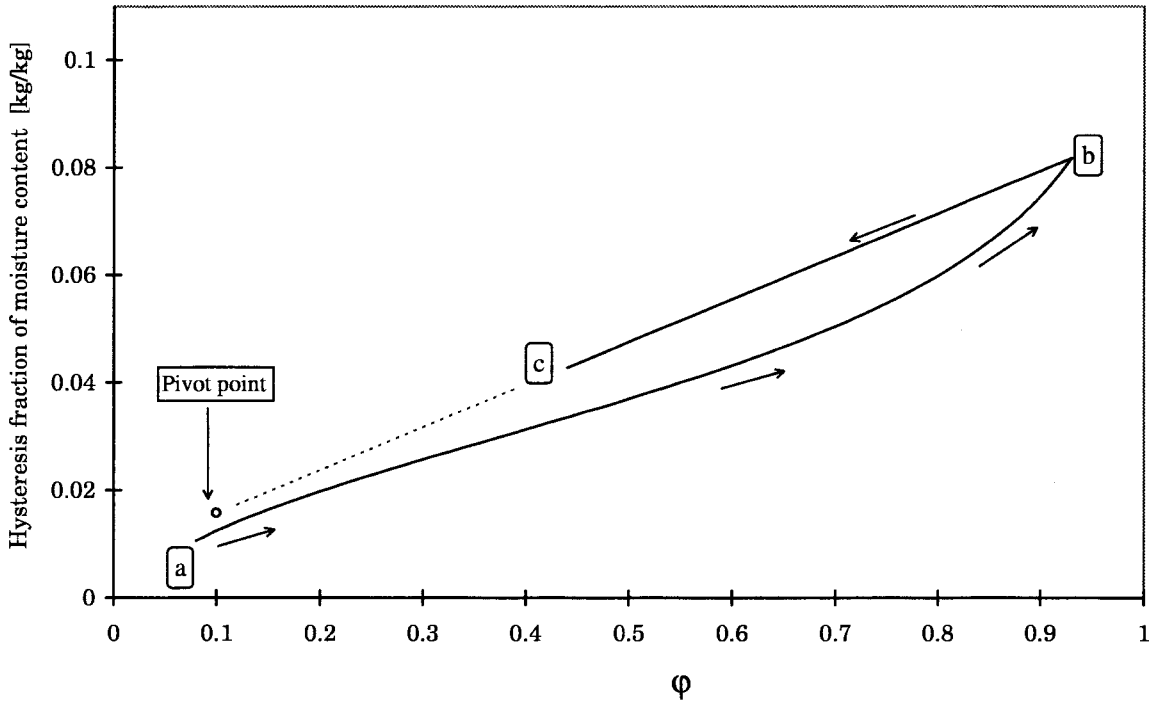

Figure 11.48 Example for an initial absorption followed by desorption, a–›b–›c.

2 a–›b–›c–›d

The next level of complication is to consider a second absorption that starts from the pivot line type 2, point c in Figure 11.49. A constant slope is used for this intermediate curve. Roughly the same slope has been used as the slope in the inflection point of the absorption moisture equilibrium curve. This type of curve is allowed to continue until it meets the initial absorption curve, point d in Figure 11.49.

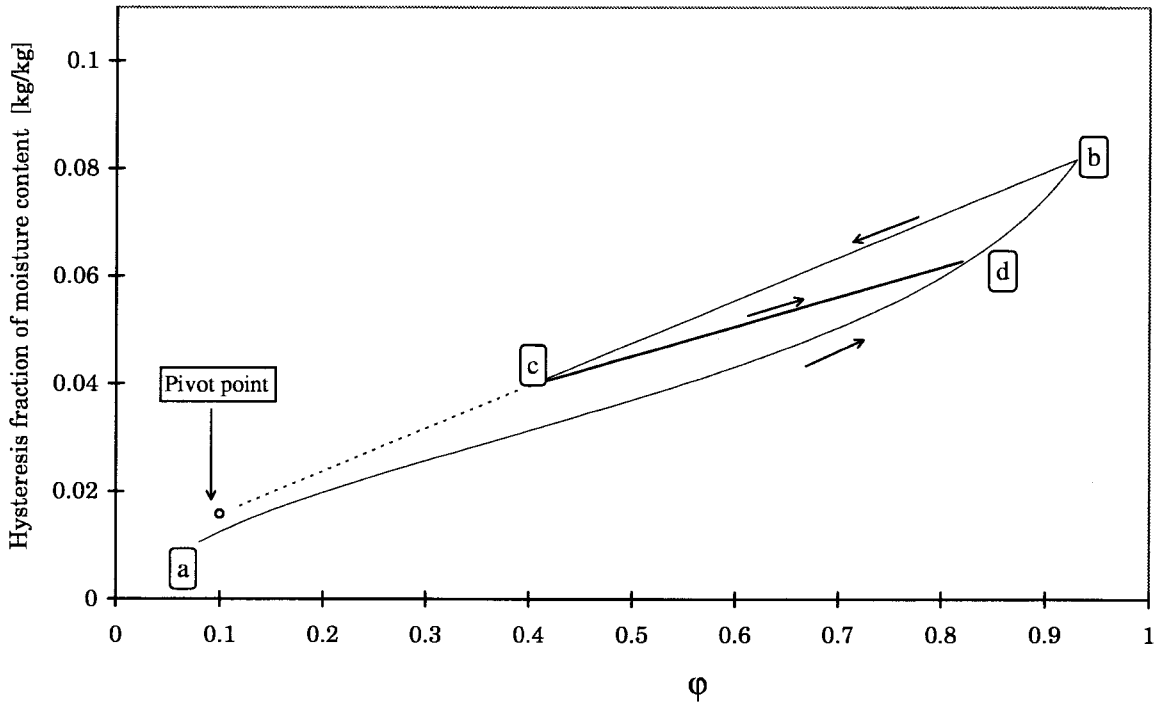

Figure 11.49 A second absorption curve, c–›d.

3 a–›b–›c–›d–›e–›f–›g

An absorption-›desorption–›absorption cycle is added. The added curves are shown in Figure 11.50, (d–›e–›f–›g). The previous φ_{max} is exceeded, $\varphi_e > \varphi_b$. A new pivot line is created.

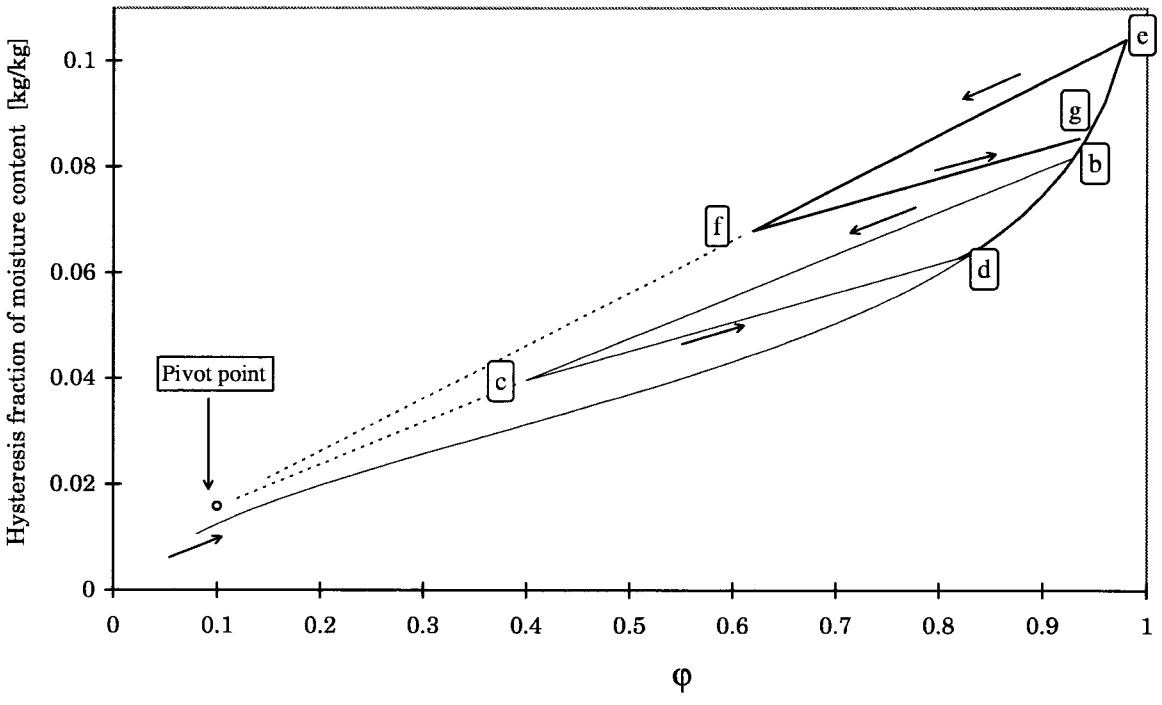

Figure 11.50 Two cycles added to the previous cycle, d–›e–›f–›g.

4 a–›b–›c–›d–›e–›f–›g–›h–›i–›j

A last absorption–›desorption cycle in this example is added and it is shown in Figure 11.51, f–›g–›h–›i–›j. At the turning point in h, a previous scan has reached a higher level. In this case the desorption follows an intermediate line with the same constant slope as curve c–› d and f–›g. The curve continues until it joins the previously established pivot line, in point i.

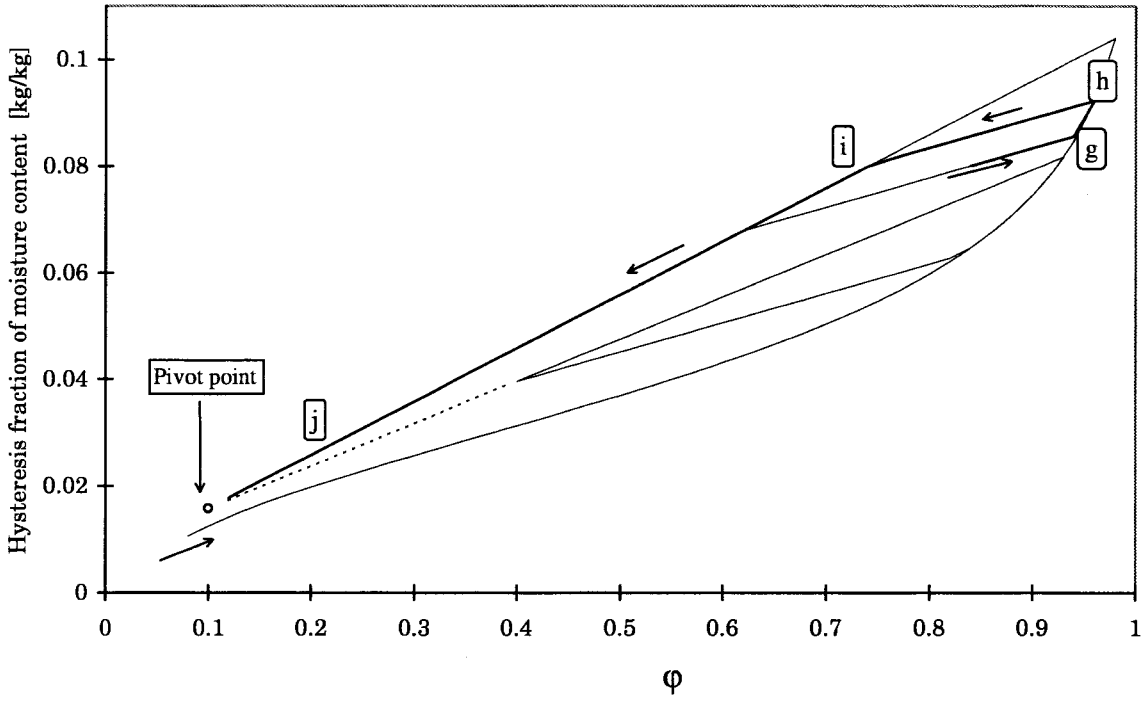

Figure 11.51 The final cycle in the example, g–›h–›i–›j.

To sum up, the rules for the hysteresis function are: The sorption is not allowed to exceed a envelope created by the initial absorption curve and a desorption line (pivot line) from the maximum reached RH-level. Within this envelope the scanning curves have constant slope.

The hysteresis component of the scanning curve for the whole above example is shown in Figure 11.52. This component, combined with the part not influenced by hysteresis, results in the total moisture equilibrium curve in Figure 11.53.

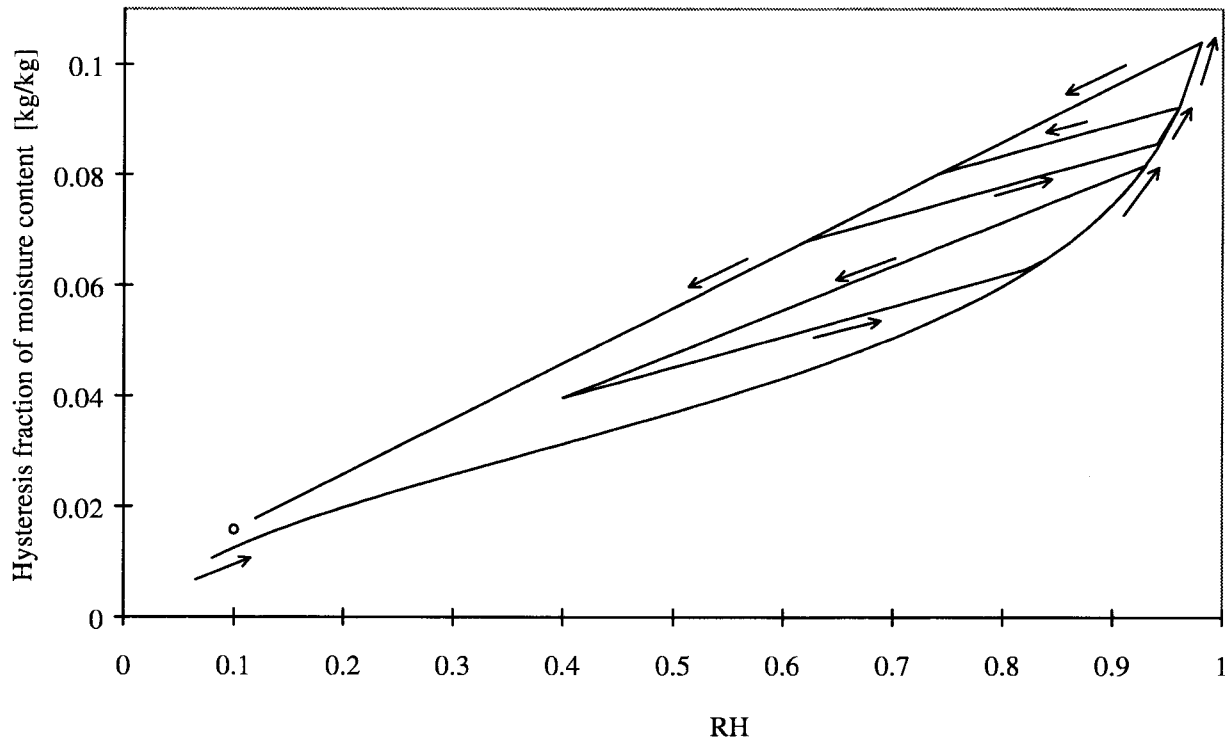

Figure 11.52 Hysteresis component in the moisture equilibrium curve.

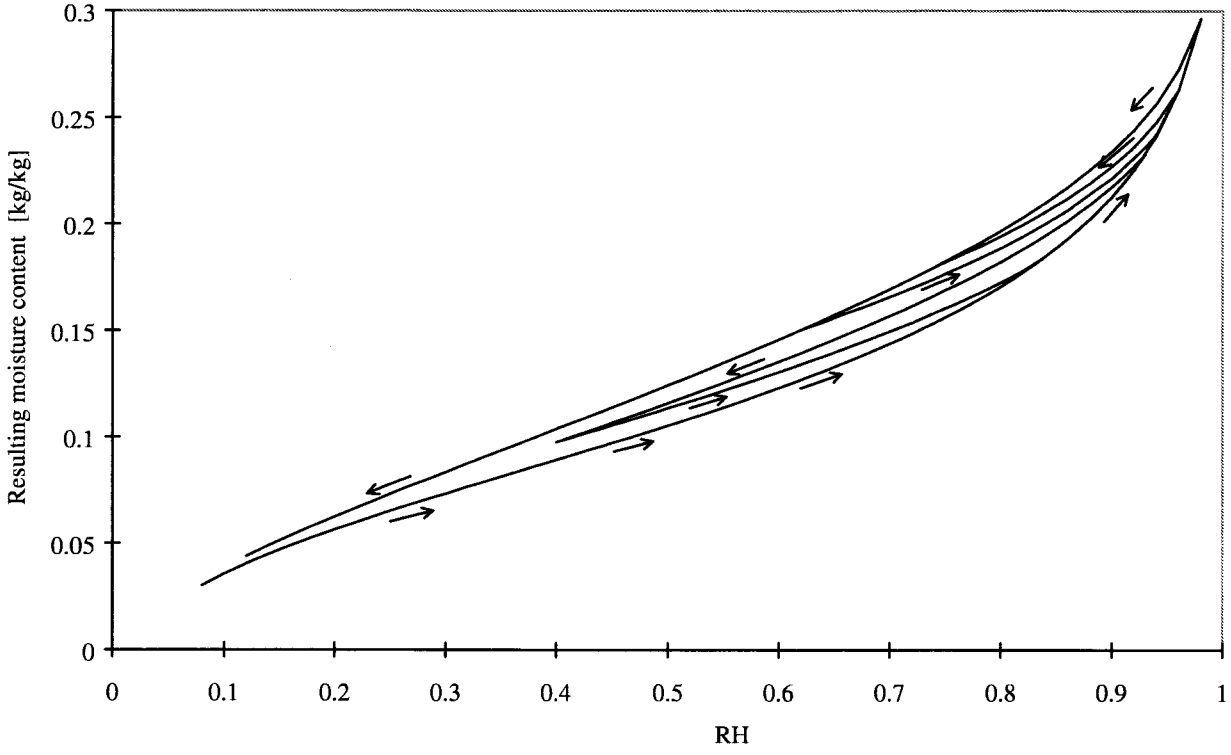

Figure 11.53 The resulting total moisture equilibrium curve.

11.3.2 Fickian model with hysteresis

This model is identical to the model in Section 11.1.1 except that the moisture capacity includes hysteresis. A moisture flow network for the model is shown in Figure 11.54. A special symbol is used for the moisture capacity of a node with hysteresis according to the model in Section 11.3.1.

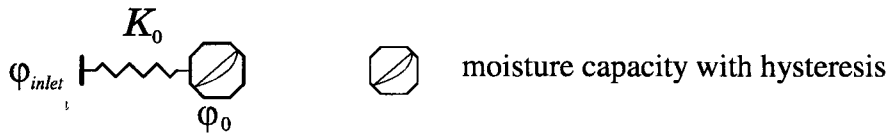

Figure 11.54 Network for a Fickian process including hysteresis.

The above model for hysteresis is used with $\alpha_{hyst} = 0.351$. This fraction is also used in the following models in Section 11.3.3, 11.3.4, and 11.3.5. The construction of the hysteresis functions is described in Section 11.3.1.

The result of the simulations of the two sequences are shown in Figure 11.55 and Figure 11.56 together with RH in level 0, which is the only node in this Fickian model.

In Figure 11.57, Figure 11.58 and Figure 11.59 the results of the simulations are compared with the measured values.

The Fickian model reaches an equilibrium very fast compared to the long intervals used in the sequence in Figure 11.57. During these periods of equilibrium the levels of sorption are the same as the corresponding points in the moisture equilibrium curve including hysteresis. The effect of hysteresis at equilibrium is seen by comparing with the result from the Fickian model without hysteresis in Section 11.1.1 (Figure 11.6 and Figure 11.57, and the details in Figure 11.7 and Figure 11.58).

The cyclic steps in Figure 11.59 can be compared with the corresponding Figure 11.8, in Section 11.1.1. Only a modest improvement compared with the non-hysteresis model is achieved for the sorption amplitudes.

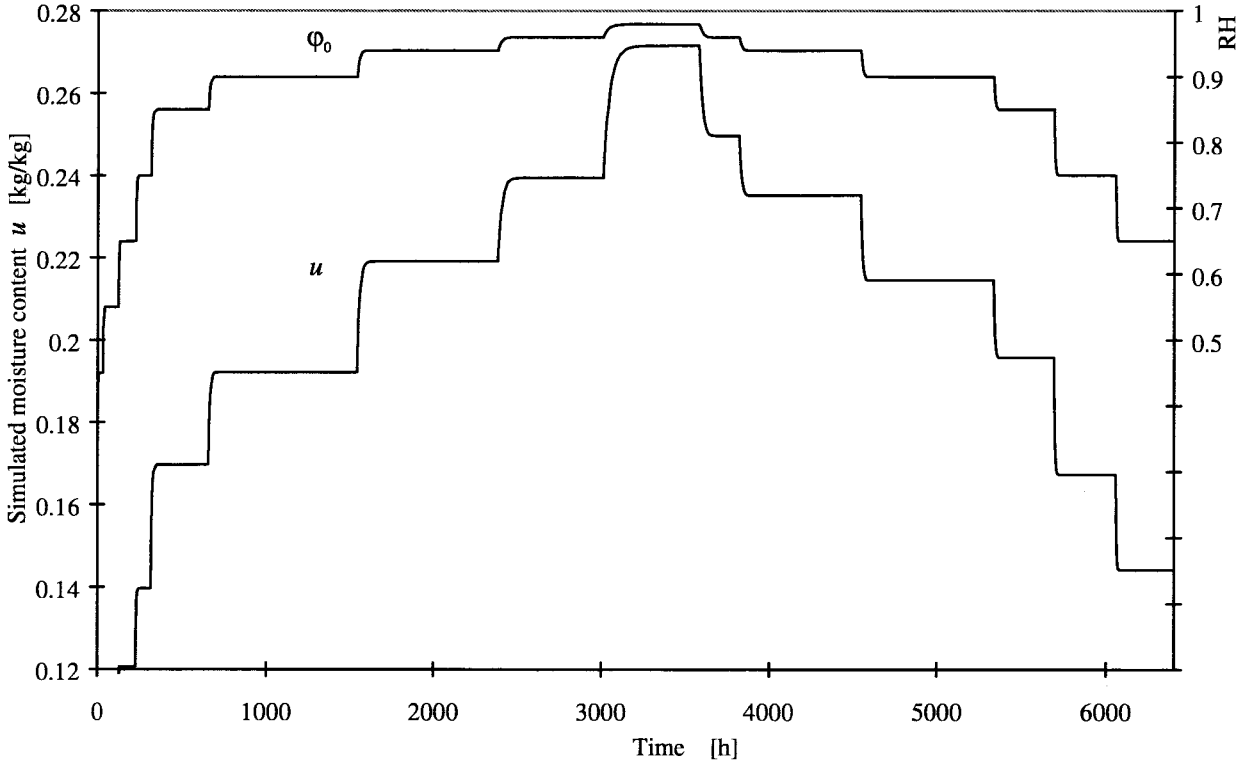

Figure 11.55 Simulation of the sequence at 20°C.

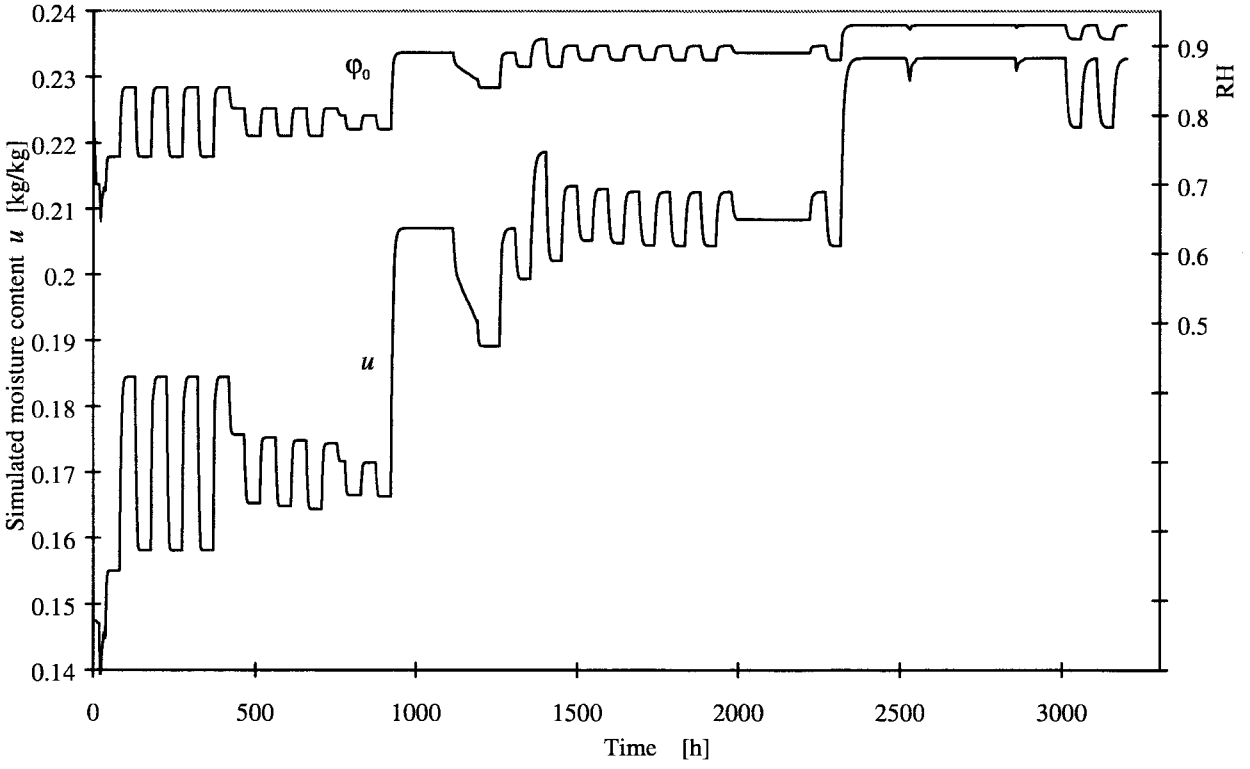

Figure 11.56 Simulation of the sequence at 5°C.

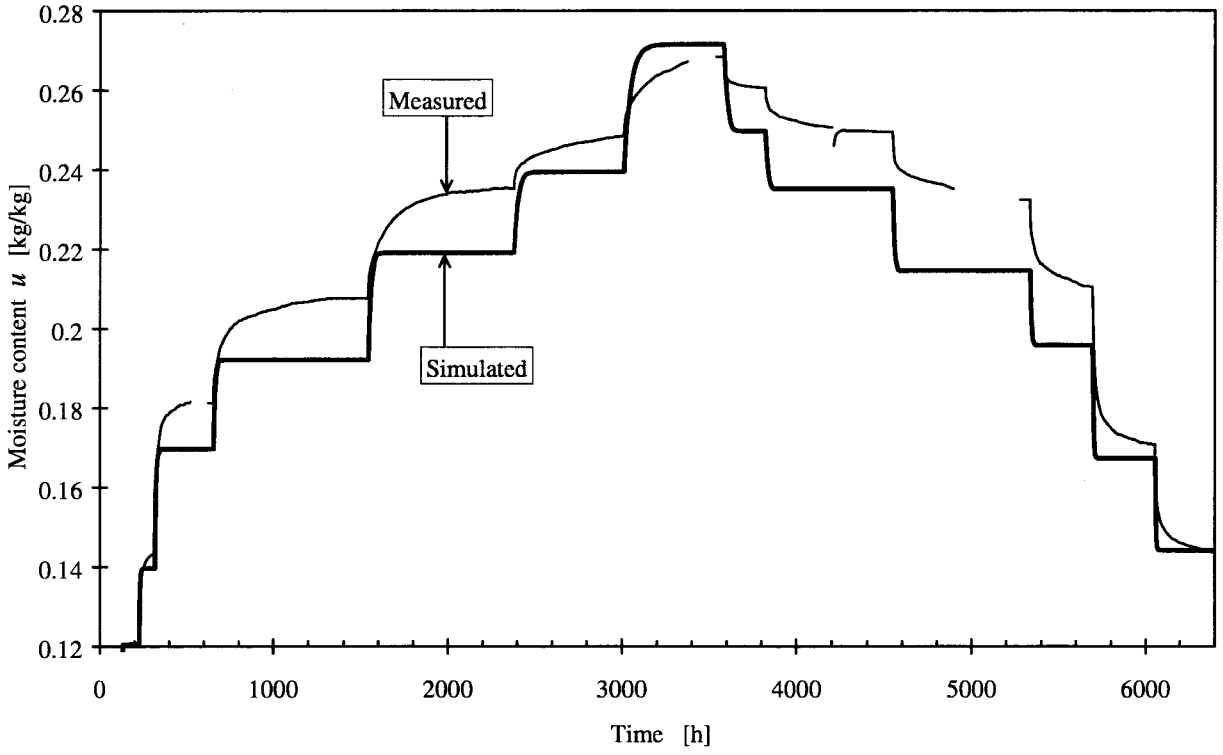

Figure 11.57 Simulation compared to measurements at 20°C.

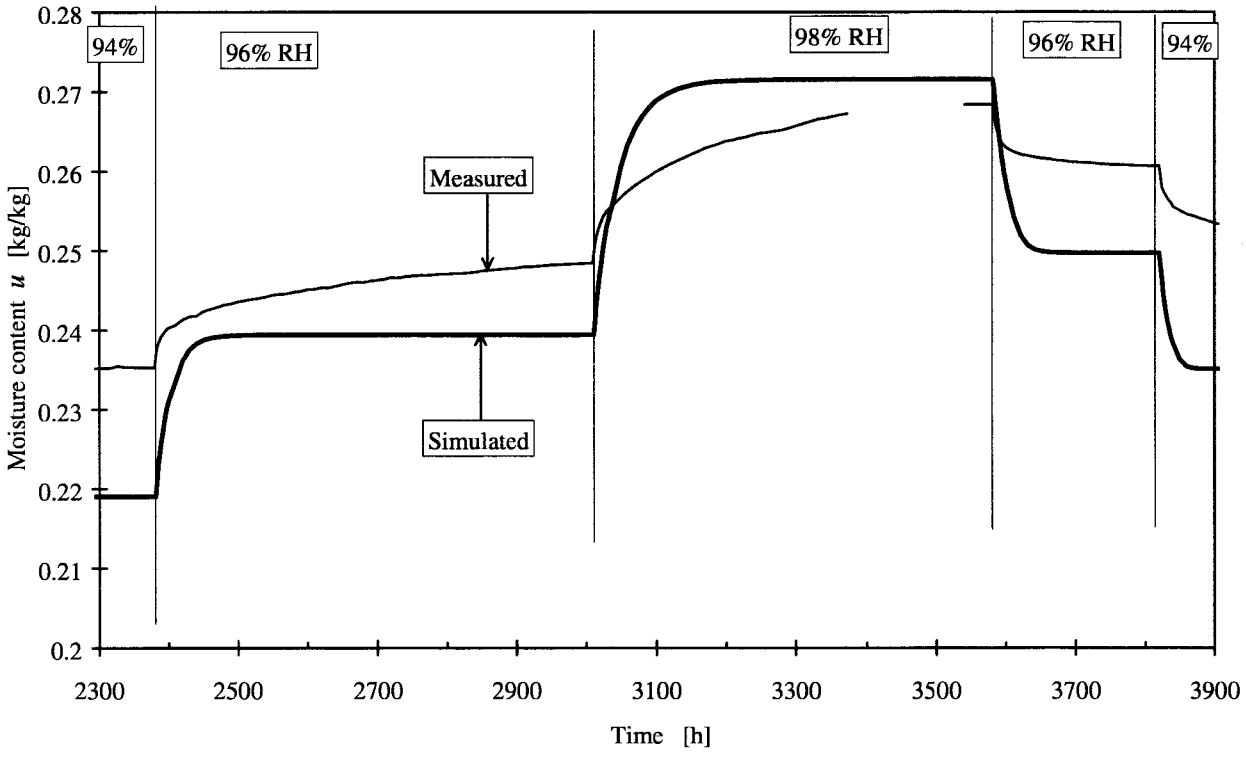

Figure 11.58 Simulation compared to measurements at 20°C. Detail from Figure 11.57.

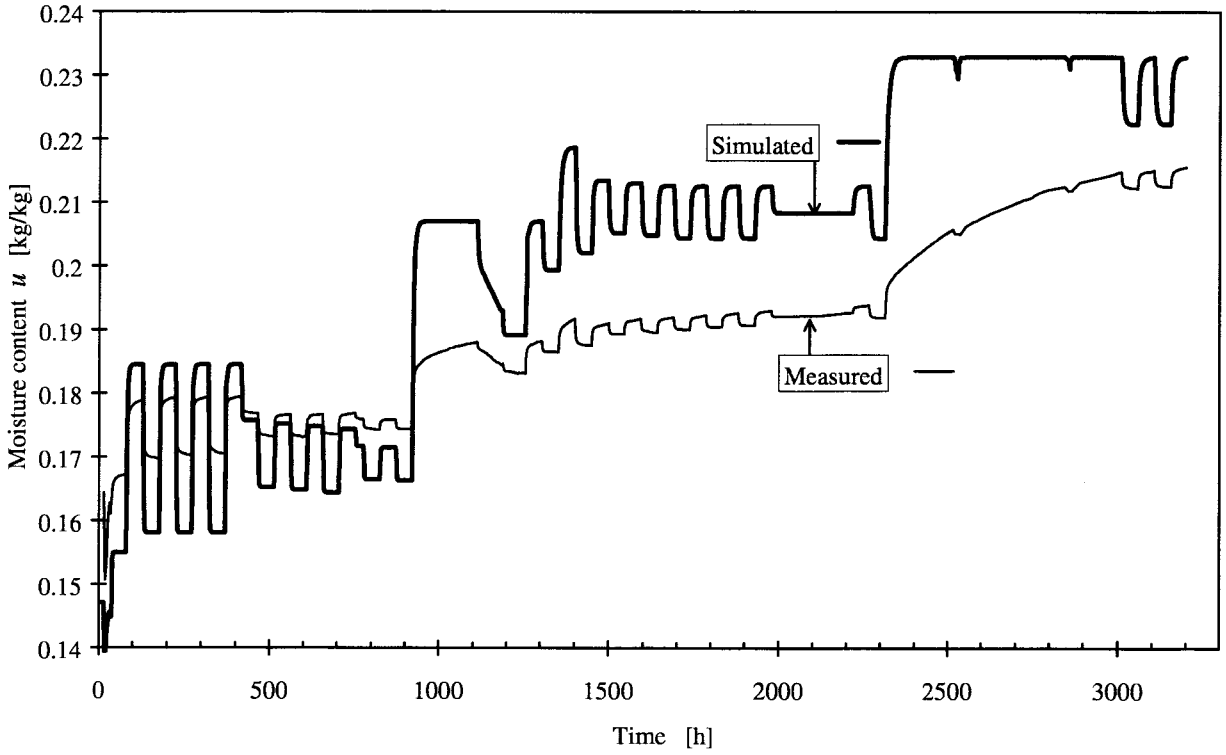

Figure 11.59 Simulation compared to measurements at 5°C

11.3.3 Hysteresis and one internal level in cell wall

This model is intended to illustrate the effect of hysteresis combined with non-linearity. Comparison can be made with the model in Section 11.2.1, which also has one internal level and the same non-linear conductance. The moisture flow network is shown in Figure 11.60. The same symbol for the hysteresis has been used as in Section 11.3.2.

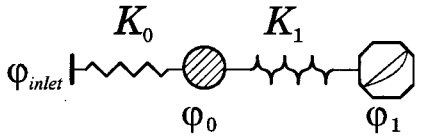

Figure 11.60 Network using one internal level including hysteresis.

As before, the moisture capacity in level 0 has been given a constant value:

$c_0 = 0.08$ [kg_{water} /kg_{wood}]

The model for hysteresis is used for the internal node 1. The initial absorption curve is reduced to $u_{in.\,ad.} - c_0 \cdot \varphi$, since $c_0 \cdot \varphi$ is attributed to level 0. The fraction $\alpha_{hyst} = 0.351$ of this reduced initial absorption is used in the hysteresis part.

The conductance is proportional to a factor k_1 from Eq. (10.17) in Section 10.4.2.

$K_1 = k_1 \cdot | v_0 - v_1 |^{\gamma}$

The same k_1 and exponent γ as in the model in Section 11.2.1 are used:

$k_1 = 0.5$ [m^6 /($kg_{wood} \cdot kg_{water} \cdot s$)] $\gamma = 1$

The simulations are shown in Figure 11.61 and Figure 11.62 together with the RH for the two levels. Measured and simulated values are compared in Figure 11.63 to Figure 11.65.

Hysteresis is included in this model. In other respects it is the same as the model in Section 11.2.1. In the simulated consecutive absorption steps in the first sequence (20°C), the hysteresis function follows a absorption curve, and the two simulations are identical. The diagrams concerned are Figure 11.33 and Figure 11.63. The amplitudes of the following desorption steps in the same first sequence have a better agreement for the model with hysteresis. The poor reproduction of the responses remains. The first desorption steps have small steps in RH, and the responses are modelled too slow. The opposite applies for the larger steps in RH at the end of the sequence.

The same comparison between the two models can be made for the second sequence, (5°C) in Figure 11.34 and Figure 11.64. This model, with hysteresis included, simulates the first cycles in the beginning with slightly better agreement. The development for the RH in the inner node φ_1 for these cycles can be followed in Figure 11.62. The RH for this node is here scanning in absorption/desorption and the available moisture capacity is then less for the hysteresis alternative. For the smaller cycles in the centre of the diagrams, φ_1 is much more static. This is due to the fact that the non-linear conductance in the model is smaller when subjected to smaller amplitudes.

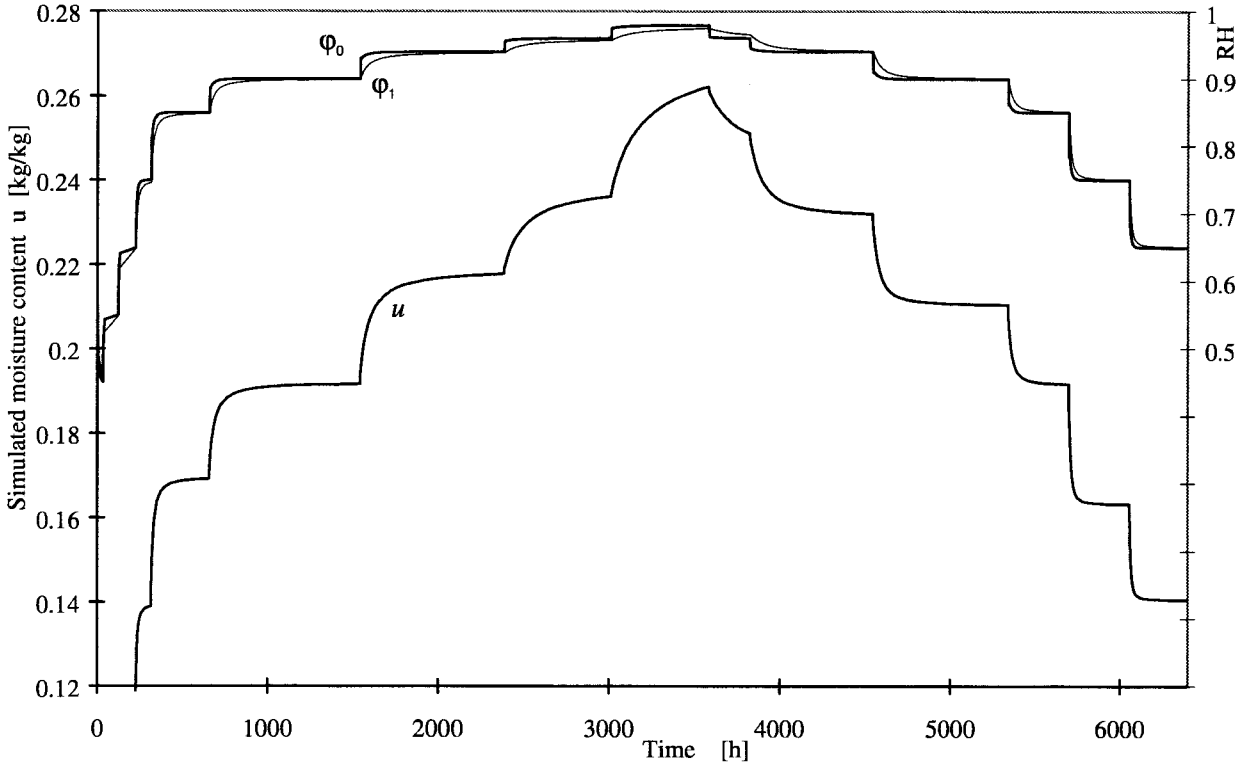

Figure 11.61 Simulation of the sequence at 20°C.

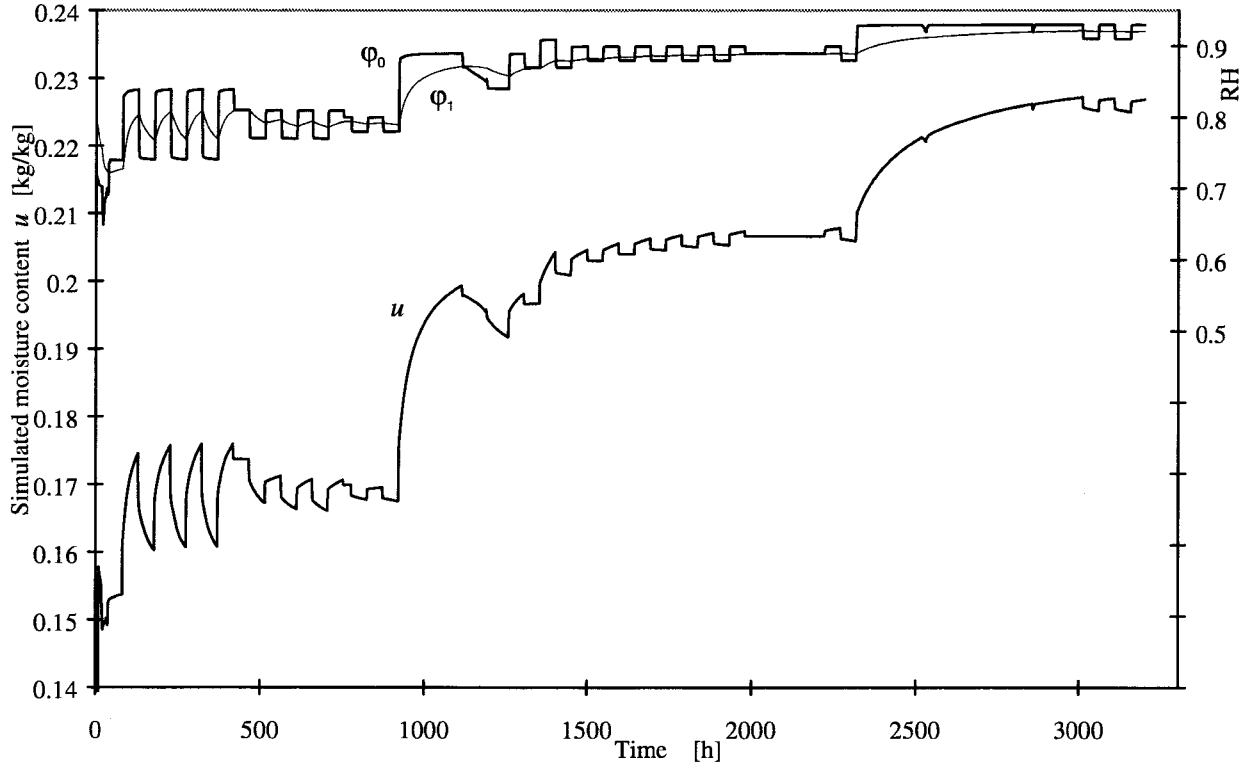

Figure 11.62 Simulation of the sequence at 5°C.

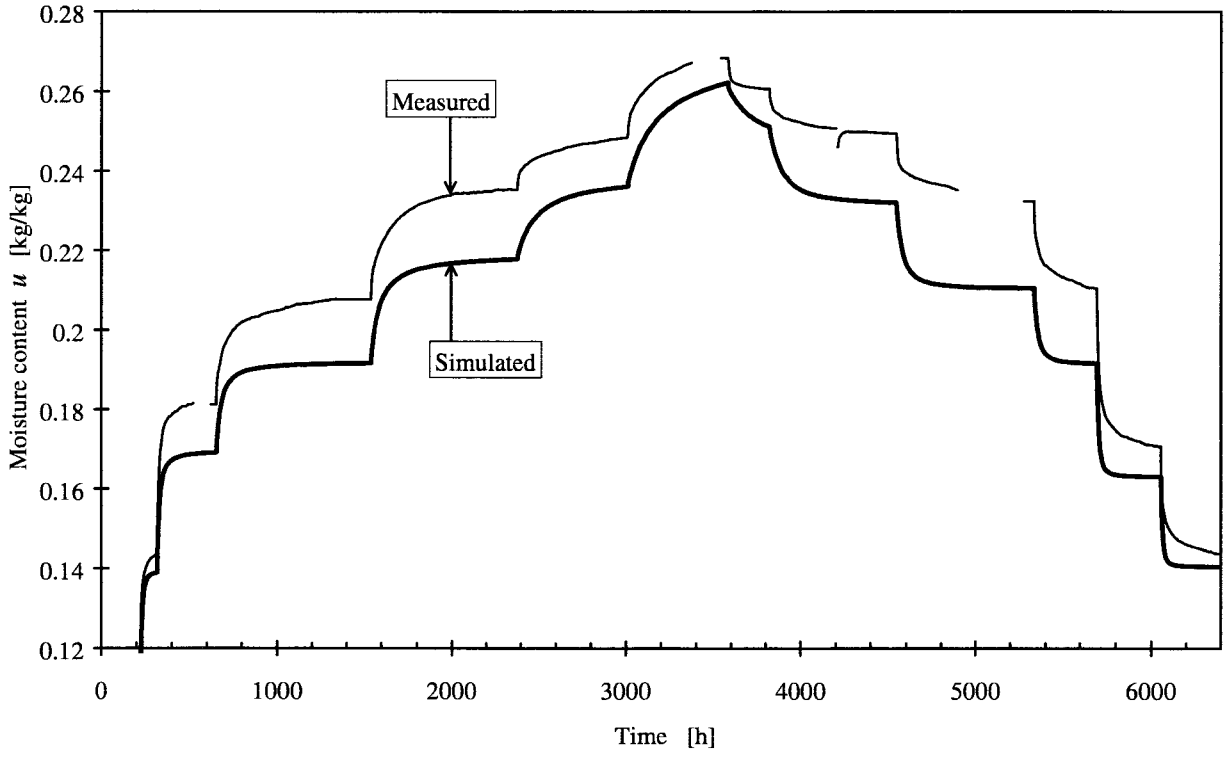

Figure 11.63 Measured sequence at 20°C.

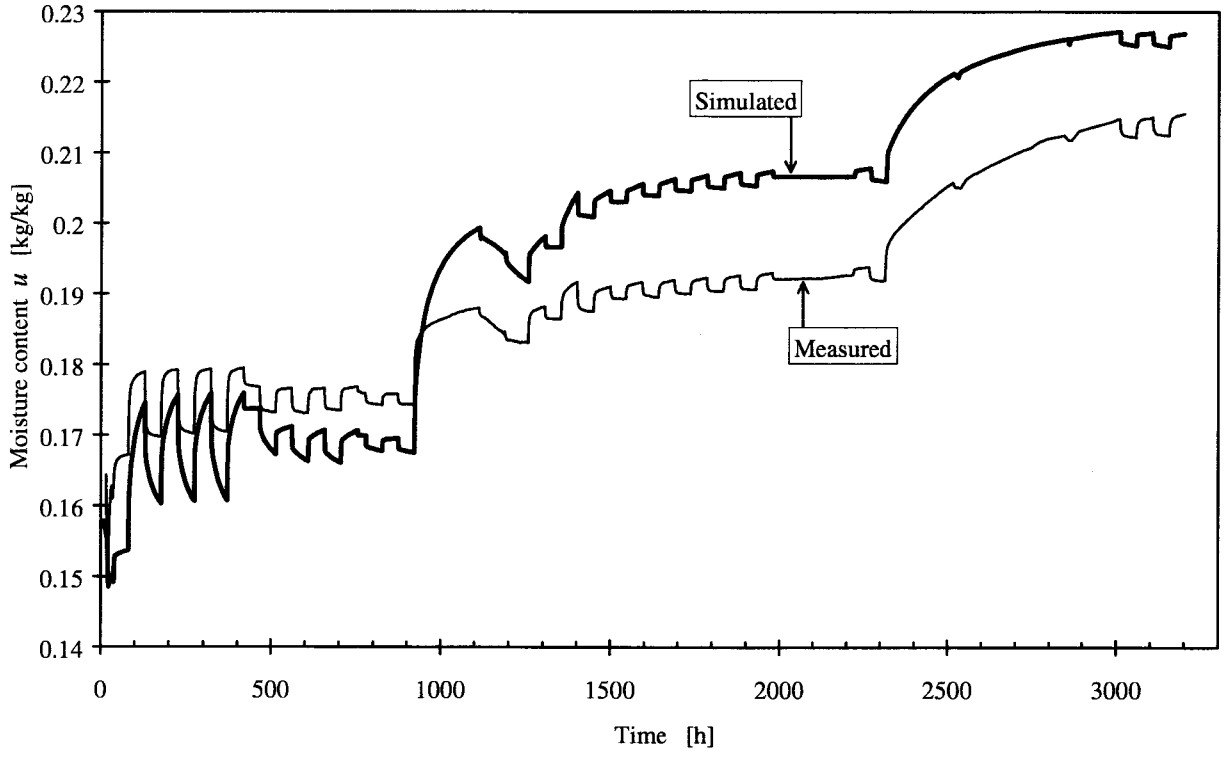

Figure 11.64 Simulation compared to measurements at 5°C.

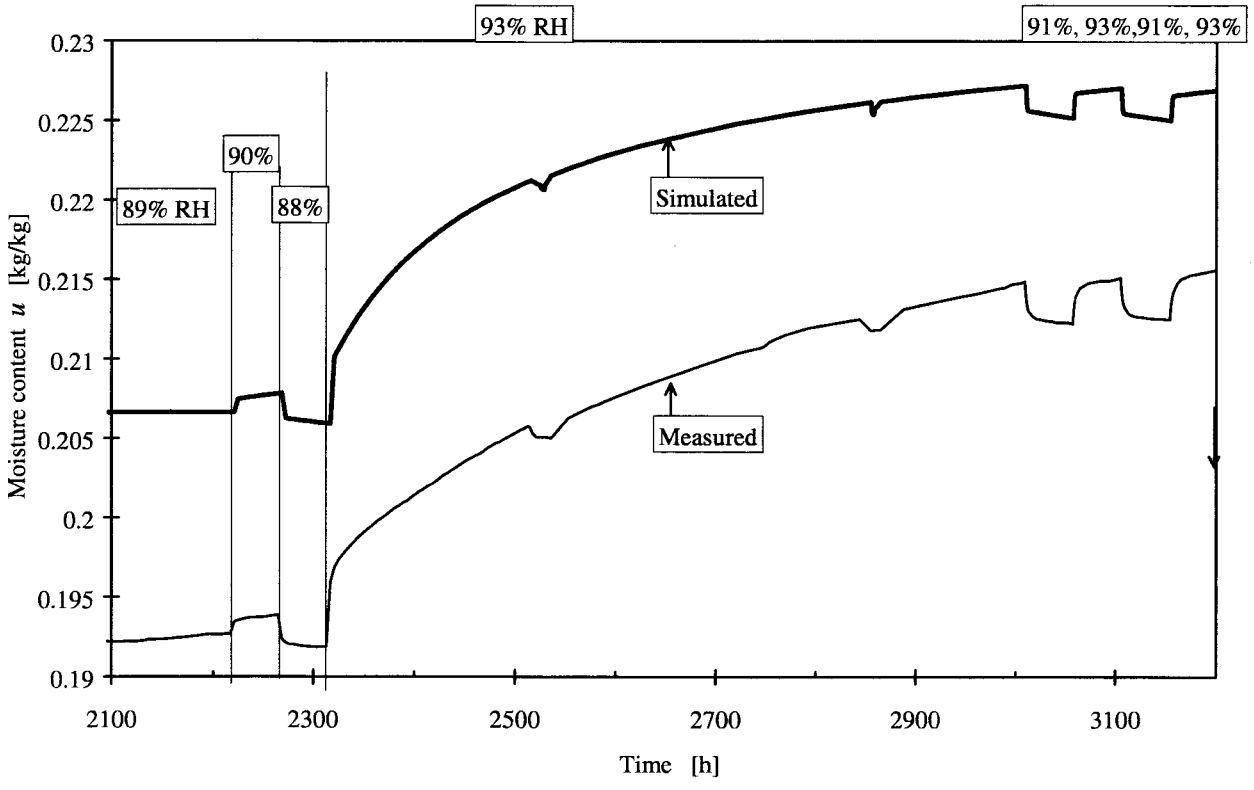

Figure 11.65 Simulation compared to measurements at 5°C. Detail from Figure 11.64.

11.3.4 Hysteresis and 5 internal levels in cell wall

The model with good agreement from Section 11.2.2 is here supplemented with hysteresis. The model is non-linear and has five internal levels.

As before, the moisture capacity in level 0 has been given a constant value.

$c_0 = 0.08$ [kg_{water} /kg_{wood}]

The model for hysteresis is used for the internal nodes 1 to 5. The initial absorption curve is reduced to $u_{in.\,ab.} - c_0 \cdot \varphi$, since $c_0 \cdot \varphi$ is attributed to level 0. The fraction $\alpha_{hyst} = 0.351$ of this reduced initial absorption is used in the hysteresis part. This capacity is distributed between the internal levels in the same way as in all models with five internal levels in this study.

The conductances have been assigned the same values, ($k_1 = 2$ [m^6 /(kg_{wood} ·kg_{water} ·s)], $b_k = 0.6$) and function of non-linearity ($\gamma = 1$) as in the simulation in Section 11.2.2. A moisture flow network for the model is shown in Figure 11.66.

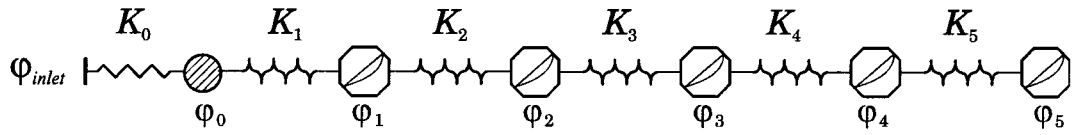

Figure 11.66 Network using five internal levels with hysteresis.

The simulations are shown in Figure 11.67 and Figure 11.68 together with RH for all levels. Measurements and simulations are compared in Figure 11.69 and Figure 11.70.

In the simulation of the sequence at 20°C with the corresponding model without hysteresis, Figure 11.38, the response of the first desorption step is rather similar to the measured. The following desorption steps show however poor agreement, both in magnitude and shape. This model with hysteresis included shows a better agreement for these step responses. See Figure 11.69. The step response for this model is however simulated too fast for these steps.

The effect from hysteresis is small for the two simulated sequences. The result of the simulation at 5°C is shown in Figure 11.68 together with the RH in the levels. The levels are mostly subjected to absorption. The effect from hysteresis is here almost negligible, at least with the used hysteresis model. The result of the simulation is compared to measured values in Figure 11.70 and is almost identical to Figure 11.40 for the corresponding model without hysteresis.

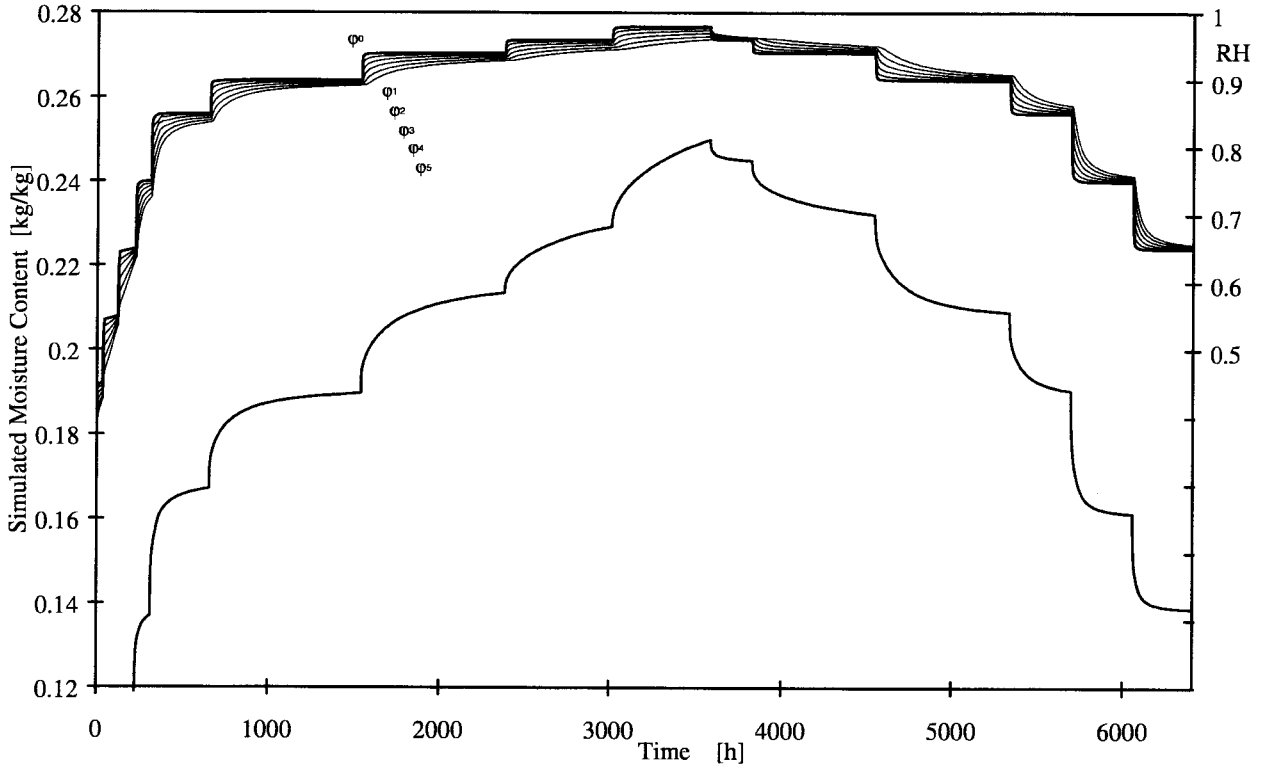

Figure 11.67 Simulation of the sequence at 20°C.

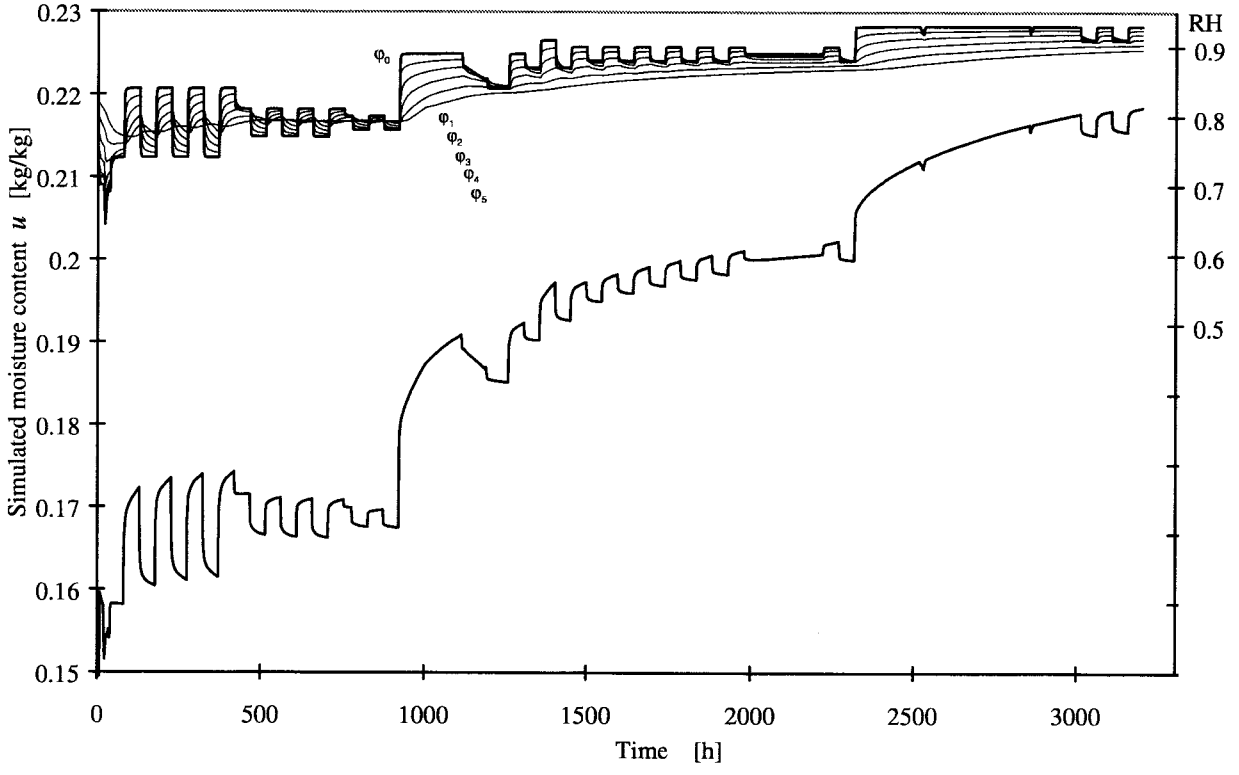

Figure 11.68 Simulation of the sequence at 5°C.

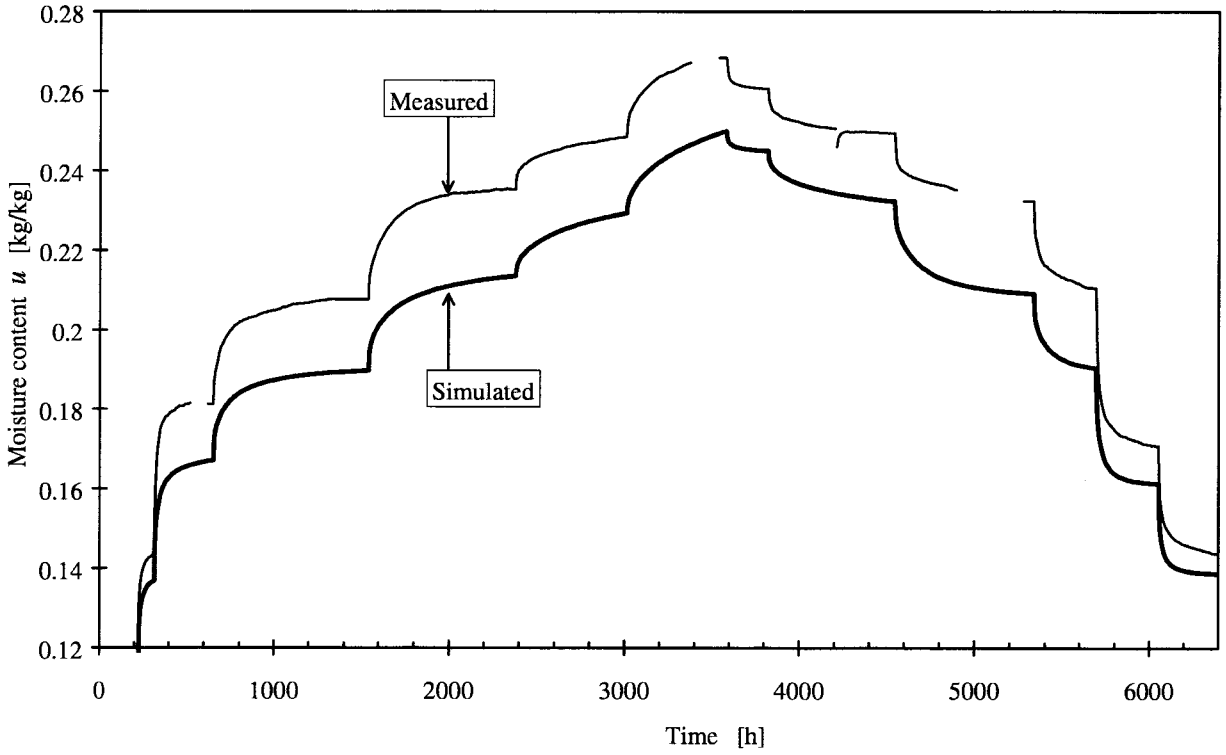

Figure 11.69 Simulation compared with measurement at 20°C.

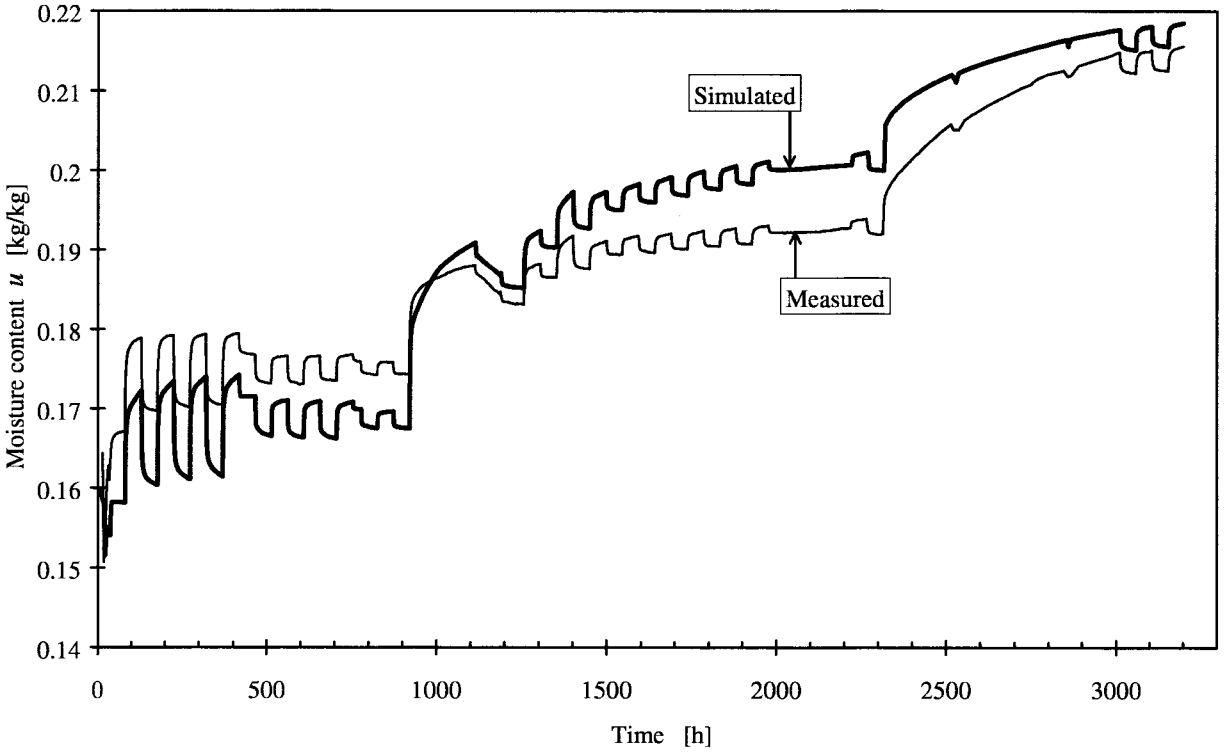

Figure 11.70 Simulation compared with measurement at 5°C.

11.3.5 Hysteresis only in the innermost internal level

The simulations for desorption in the first sequence (20°C) for the previous model in Section 11.3.4 were found to result in too fast step responses. This applies generally for the desorption steps. See Figure 11.69. The present model tests the alternative to concentrate the hysteresis function to the innermost level. See Figure 11.71. One advantage for such a model is that the numeric computing is reduced, since the extra variables for the hysteresis are restricted to one level. The same hysteresis for the total moisture equilibrium curve as for the other models is used.

The nodes 0 to 4 have been designated the same moisture capacity as the model without hysteresis in Section 11.2.2. The sum of the capacity for these nodes corresponds to the curve under the axis in Figure 11.46. The remaining fifth node corresponds to the curve over the axes and carries the hysteresis. This is so because the fraction for distribution between the internal levels for level 5, $\alpha_5 = 0.351$, has the same value as the factor for the hysteresis part $\alpha_{hyst} = 0.351$. In this way the same hysteresis is used as for the other models but is concentrated in the innermost level.

The conductances have been assigned the same values ($k_1 = 2$ $[m^6/(kg_{wood} \cdot kg_{water} \cdot s)]$ $b_k = 0.6$) and function of non-linearity ($\gamma = 1$) as in the simulations in Section 11.2.2 and 11.3.4 .

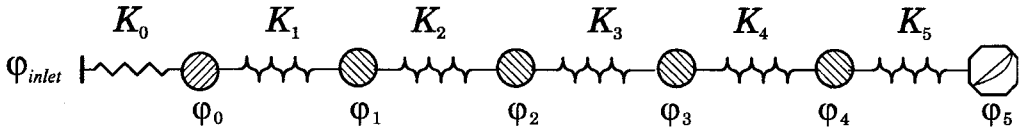

Figure 11.71 Network using five internal levels with all hysteresis in the innermost level.

The simulation for the first sequence, (20°C), is shown in Figure 11.72 together with the RH in the levels. Comparison with the measured values is made in Figure 11.74. The result from the second sequence, (5°C), is shown in Figure 11.73. The effect of hysteresis negligible for this sequence.

The time-scales for the desorption steps in Figure 11.74 show a good agreement. Comparison can be made with the previous model, with the hysteresis function evenly distributed in the layers, in Figure 11.69 in Section 11.3.4. Especially the first desorption step responses are to fast modelled and the model of this section in Figure 11.74 shows better agreement.

Figure 11.75 is practically identical to Figure 11.70 for the previous model and Figure 11.40 for the corresponding model without hysteresis.

It follows from all above comparisons that this model has the best general agreement.

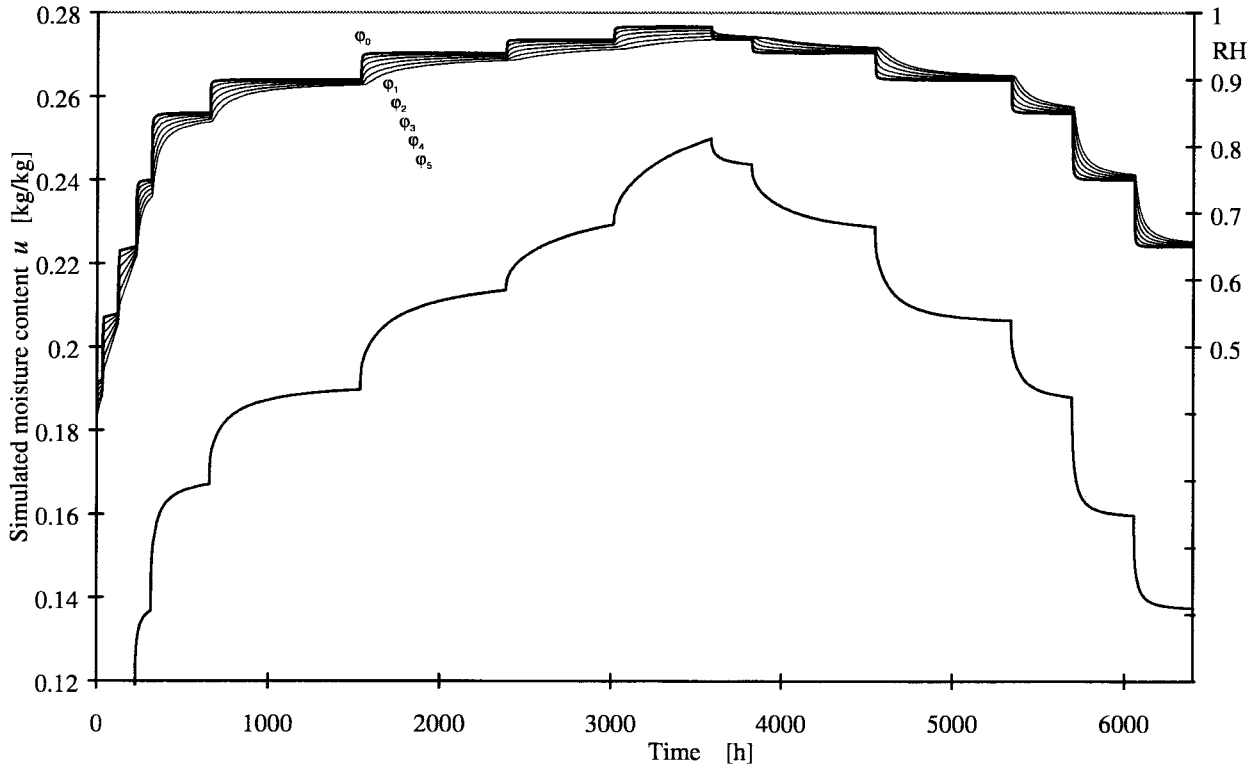

Figure 11.72 Simulation of the sequence at 20°C.

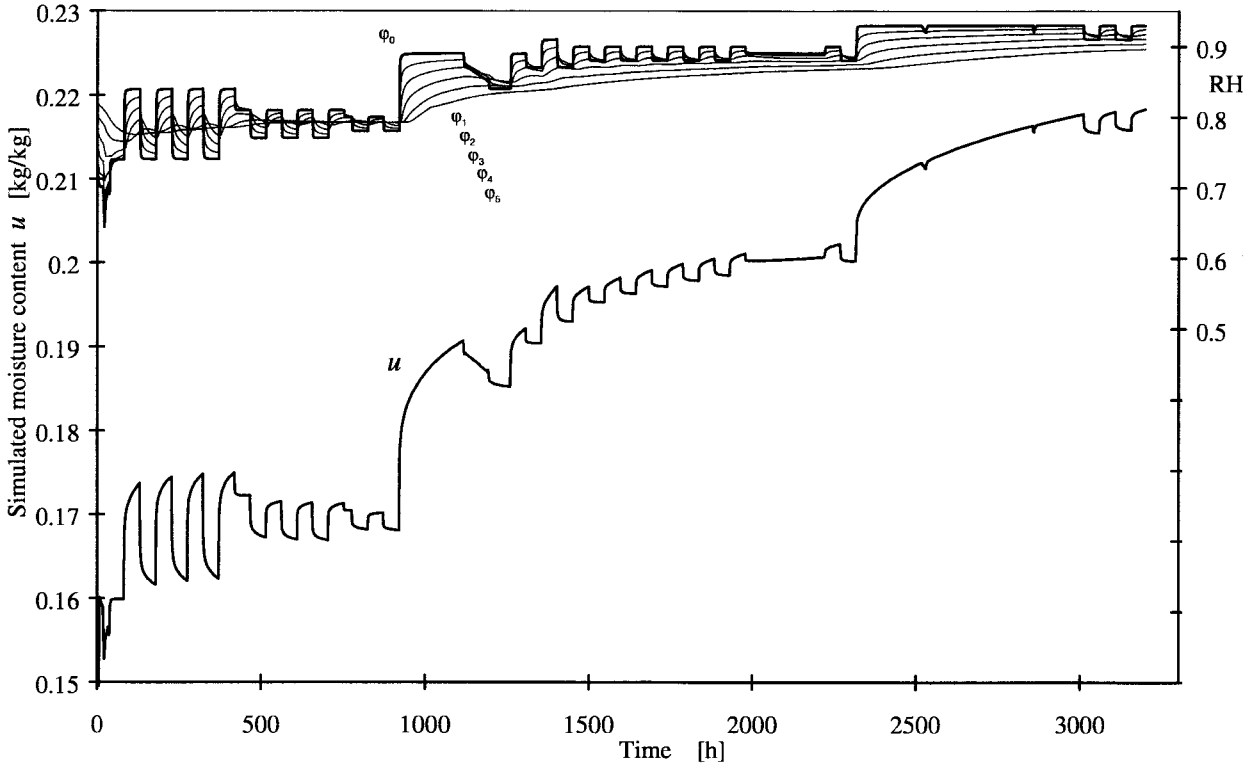

Figure 11.73 Simulation compared with measurement at 5°C.

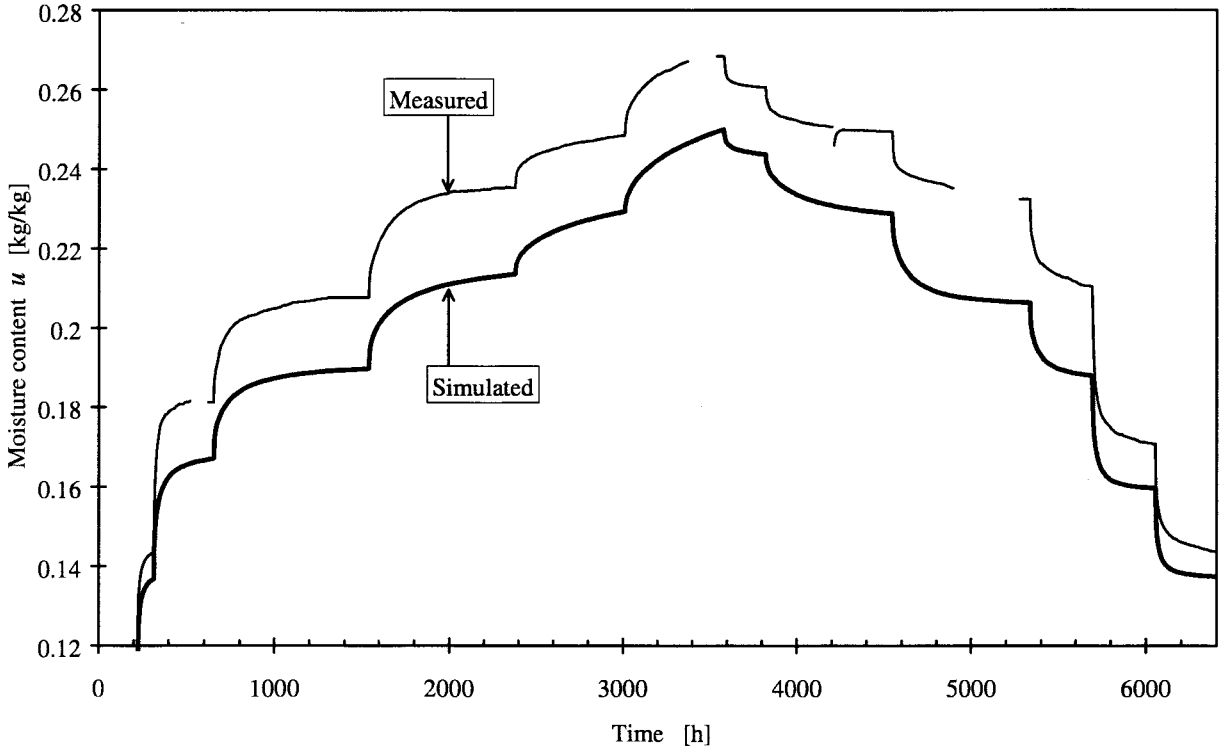

Figure 11.74 Simulation compared with measurement at 20°C.

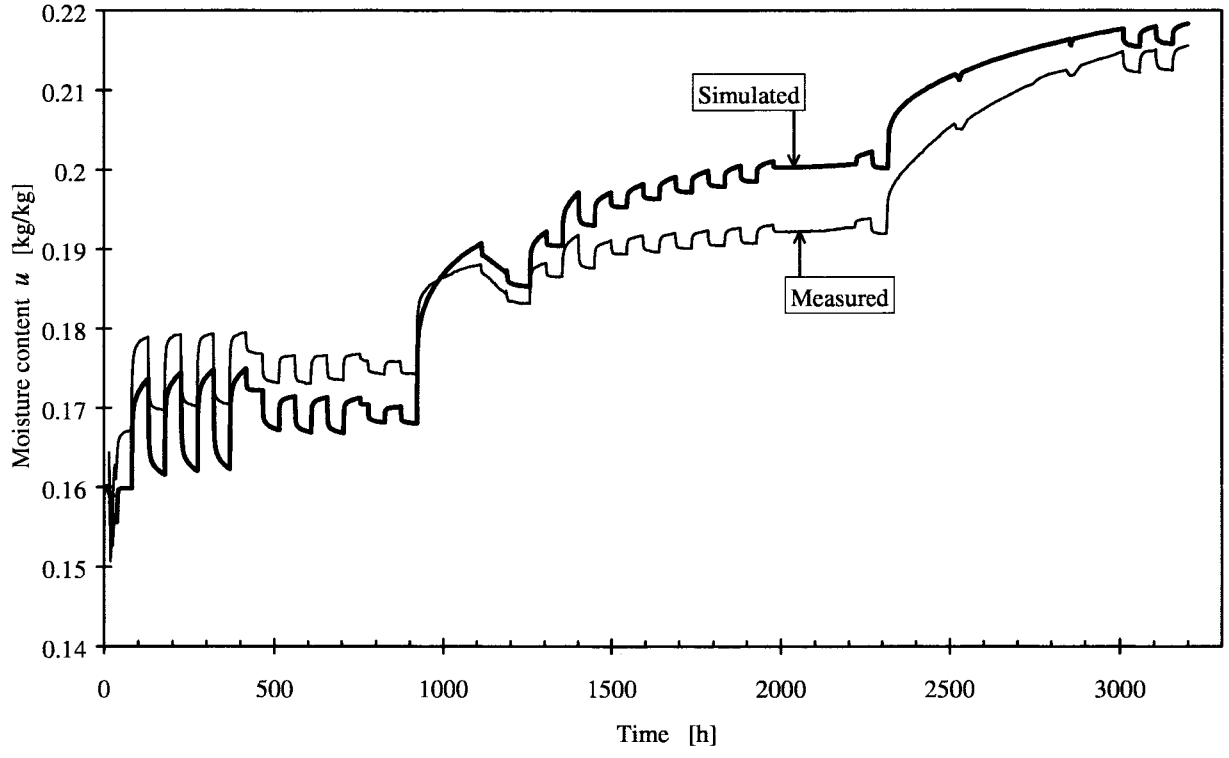

Figure 11.75 Simulation compared with measurement at 5°C.

11.4 Simulations for two special cases

11.4.1 Simulation of superposition of step-responses

In Section 9.4 dealing superposition of step-responses, it is described how the sum of two superimposed measured step responses is different of the response in the same interval made in one step. Figure 9.11 shows an example of this. Corresponding responses from the simulations are shown in Figure 11.76. The model in Section 11.2.2 (non-linear, five nodes) is used. The same tendencies are found in the simulated responses, but less pronounced.

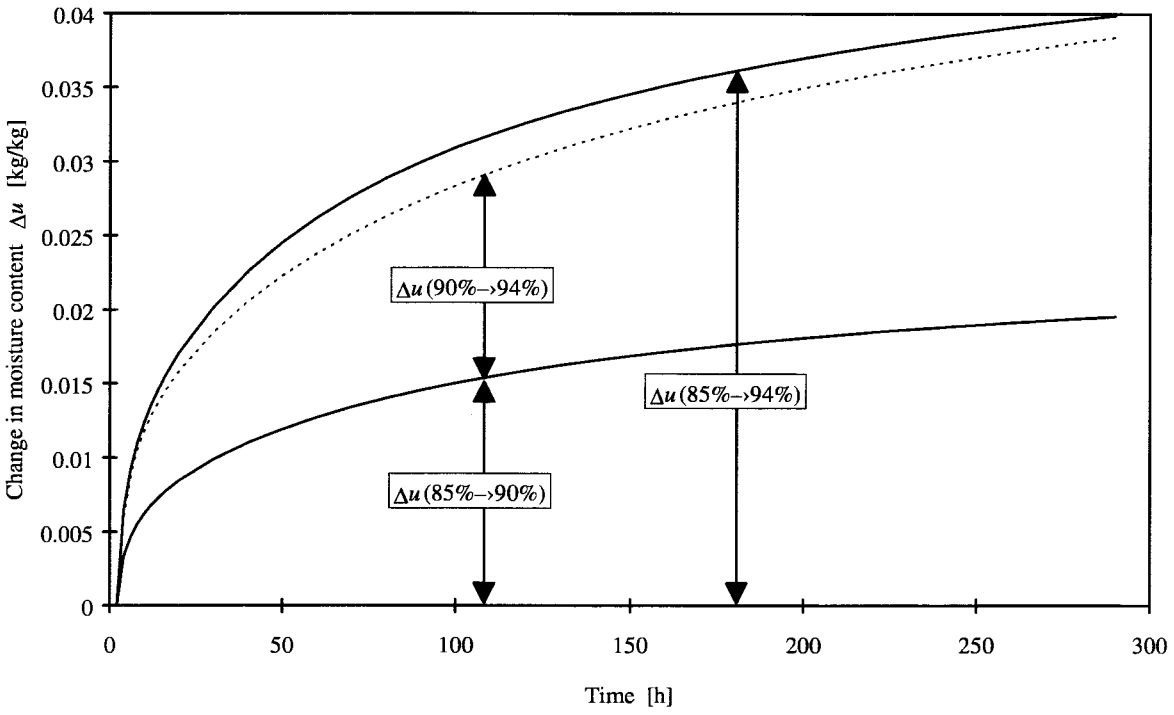

Figure 11.76 Simulation of two superimposed step responses compared to a single step. Corresponding measured responses are shown in Figure 9.11.

11.4.2 Simulation of temperature shift

Measurements shown in Figure 9.12, Section 9.5, involve the situation when the sample is subjected to large temperature shifts. Figure 11.77 shows a simulation with the model from Section 11.2.2 on a sequence with a temperature shift from 5°C to 20°C.

The computer model is not adapted to have the temperature as a dynamic input but the RH-potentials for the levels at the end of the simulation of the sequence at 5°C have been recalculated as an input for the initial values for a consecutive simulation of the sequence at 20°C.

As anticipated in Section 10.6, a non-linear model with water vapour content as the driving force gives a much faster relaxation speed at 20° than at 5°C. The difference is however not at all sufficient compared to the measurement.

When a large shift in temperature takes place, it seems as some kind of process is acting to nullify the internal potential differences that are the source of the retarded sorption. This phenomenon is different from the non-linear blocking described by the model.

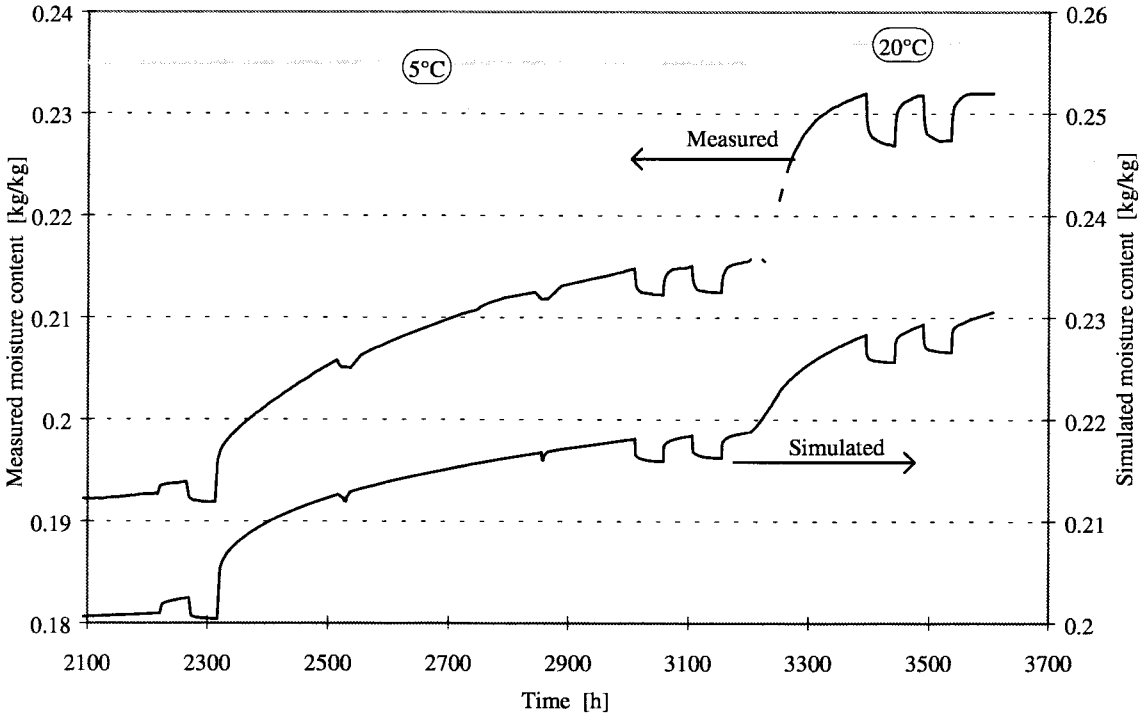

Figure 11.77 Simulation of change of temperature.

11.5 Conclusions

It is only the models with non-linearity *combined* with several internal nodes that have been able to reproduce reasonably well all situations in the tested sequences.

Measurements that include a wide absorption-desorption range have been simulated. In this case the model needs an included hysteresis function for the moisture equilibrium curve. In cases with just a small desorption change, a non-linear model has been able to reproduce the measured response.

It seems as hysteresis for the moisture equilibrium curve is associated with the same structures that are responsible for the retarded sorption. This is indicated by the good results from simulations where the hysteresis function is confined to the innermost level of the model. Another more direct indication is, that the immediately available moisture capacity seems unaffected by the direction of absorption-desorption.

The immediately available moisture capacity shall have a different (smaller) variation versus RH than the capacity for the remaining retarded sorption. In the simulations a constant capacity is chosen for the immediate capacity.

The non-linear model is able to simulate the different behaviour of the retarded sorption at the two investigated temperature levels without changing of assumed parameters in the model. However, when a larger temperature shift is done, a process takes place that seems to nullify the temporary deviation from equilibrium that is characteristic of the retarded sorption. The proposed model cannot fully reproduce the response to a large temperature shift.

12 Sorption, swelling /shrinkage and mechano-sorption

The interaction between the variations of moisture content and mechanical loading is often called mechano-sorption. This topic is not dealt with in this thesis, but there are several points of connection between mechano-sorption on one hand, and retarded sorption and swelling on the other.

Mechano-sorptive effects are not found on synthetically produced, hygroscopic polymers, Hunt (1989). The reason for this may lie in the origin of wood as a biologically created material, which gives it a number of special properties, distinguishing it from synthetic polymers. Wood has orthotropic properties. The swelling has a different transient behaviour in the transverse direction than in the longitudinal one. In the following some tentative thoughts and ideas about the background for these special properties are put forward.

Wood consists to a large degree of polymers. Wood has a complicated structure that spans over a range of levels, from the possibility of an orderly organisation of molecules to the dimensional variations over the tree trunk. The strongly orthotropic character of wood both in moisture transport characteristics, moisture related movements, and mechanical properties is another example of the organised structure.

The structure reflects the different functions that the wood has to perform in the living tree, for instance as a conveyer of water and nutrients as well as support.

The living tree is adapting to the circumstances and is able to do so by for instance creating so called reaction wood when subjected to abnormal compression stress. Some characteristics are however rather constant. The equilibrium moisture content, calculated per mass of wood, shows little variation for practically all kinds of wood whereas the densities vary much.

The wood derives much of its longitudinal stiffness and strength from microfibrils in the cell wall. A way for the living tree to adapt to structural needs over the tree trunk is to change its density but also to change angle of the microfibrils. The microfibrils are spiralling around the centre cavity in the wood cell in a tubular layer, S_2 , in the middle of the cell wall. Differences in the microfibril angle have a large influence on the moisture-related strains in the three directions in the trunk.

A particularity for wood is that it is highly hygroscopic with large swelling. The bulk volymetric expansion is about the same as the volume of the absorbed water. Some of the sorption sites could be thought to exist as potential for sorption rather than present voids.

During the work with these experiments and the thesis, a number of observations were made. Some of these may also have a bearing on mechano-sorption.

The retarded sorption is large at high humidities. The mechano-sorptive effects are also large for high humidities. The retarded sorption is especially prominent for a step to a previously not attained humidity level. This is also a situation when the mechano-sorptive effects are large.

Tangential and radial swelling was measured together with sorption. The result is analysed in Chapter 8. The tangential and radial swelling responses were close to proportional with the sorption responses. However, when a step to a previously not attained level was performed, the swelling was consistently larger.

For cyclic humidity variations, the value of the available moisture capacity together with a transport coefficient is a determining factor for the actual RH-gradient in moisture calculation over the thickness of a body. Mechano-sorption is most affected by cyclic variations, and a correct description of the dynamic moisture (humidity) transport is essential to calculate the strains resulting from the moisture gradient.

In Figure 1.11 taken from Hunt (1989), a peak in the longitudinal strain occurs already 0.15 hours after a step at high RH-level. The relative humidity is thought to be the driving potential for the moisture transport. The distribution of relative humidity has far from reached equilibrium at that time, even though the samples are thin, 0.5 mm. The longitudinal strain has a development in time, seemingly faster than RH. A way a mechanism could work to achieve this is by being driven by a difference between RH in an outer pore system and another moisture state in an inner system.

Another observation is the following one. The immediate part of the sorption has the same available moisture capacity for sorption and absorption. Longitudinal swelling has an immediate response pattern. The longitudinal swelling does not show any noticeable hysteresis between absorption and desorption. See Figure 1.12 taken from Hunt(1990). These above phenomena for immediate sorption and longitudinal swelling seem to be connected and driven by the relative humidity only.

A further observation is that both the retarded part of the sorption and tangential /radial swelling are in some way connected with hysteresis.

13 Concluding summary

Moisture sorption in wood is, as wee have seen, a complicated process. In Section 1.1, discrepancies between conventional Fickian models and experimental data are reported. In many cases, the calculated change of moisture content is much faster than what is observed in the experimental studies. Possible explanations of the discrepancies are discussed. It is proven that a surface resistance could not be the cause.

In conventional Fickian models, the sorption at a point or a small part in the wood material is supposed to be immediate. The moisture content at the present relative humidity is assumed to be given by the moisture equilibrium curve $u = u(\varphi)$.

It is the main proposition in this thesis that the slow sorption in many experimental situations is due to a so-called *retarded sorption.* This means that the moisture uptake even for a very small piece of wood, in particular a single fibre cell wall, involves time delays. It is not sufficient to use the moisture equilibrium curve only in order to describe (and model) the process. Part of the sorption is more or less immediate, while the remaining part up to the full value of the moisture equilibrium curve is retarded. This retarded sorption involves a wide range of time scales.

We need laboratory experiments, where the transient moisture change is determined by weighing for so small pieces of wood that the single cell wall is, as directly as possible, exposed to a variable moisture climate. Therefore, very thin samples (1.7 mm) cut perpendicular to the fibre direction are used. The sample in the climate chamber is exposed to a strong air current in order to minimize moisture flow resistance between air and sample. The samples are exposed to a well-defined relative humidity in the precision climate chamber. This relative humidity is changed in steps and kept strictly constant between the steps. The moisture uptake is measured by continuous weighing.

A model of time-dependent moisture flow processes in wood must be able to account for these measured processes, where a cell wall is exposed to a sequence of relative humidities. The experimental set-up is designed so that this local process is isolated from the macroscale moisture flow process on a level above the single wood cell.

The idea is to measure carefully the response in characteristic situations with different sequences of relative humidity. This is done in Part II. Then this internal process is to be modelled in a suitable way. Different models are tested in Part III. Unfortunately, the measurements show many complications. The models tend to become quite intricate. It has not been possible, within the limits of this thesis, to find a model that accounts for all effects. But it is shown that all major effects may be modelled.

The apparatus to measure the response after step changes in relative humidity has some unavoidable time delays due to limited capacity of supply of humid air, air-to-sample moisture flow resistance, etc. In order to distinguish between immediate and retarded sorption, it is necessary to know these time scales inherent in the experimental set-up. One particular complication is that the temperature change due to the heat of condensation /evaporation may influence the process.

In Chapter 3, a detailed model of the combined moisture and thermal process for the small and thin samples is presented. The two coupled, non-linear equations are solved numerically (in Mathcad). The model is based on conventional theory with immediate sorption according to the moisture equilibrium curve. It shows the time scales in a conventional case without retarded sorption. In Chapter 4, the model is applied for the experimental situation. It is found

that the response times for a step change is of the order of a few hours. At high relative humidity and low temperature the response time may increase to half a day. If distinctly longer time scales for the sorption response to a step change are measured, then we have a case of retarded sorption and internal processes in the cell wall that cannot be explained without modifications of conventional theory.

The measurement response times are in many of the experimental situations distinctly larger than those of conventional theory. We have then very clear instances of retarded sorption.

An overview of the measurements is presented in Chapter 5. Six long series of measurements with sequences of steps in relative humidity have been made. Two samples are tested independently in the twin chambers. The first series for sample 1 involved 8 absorption steps followed by 8 desorption steps. The humidities lie between 45% and 98%. The time between steps lies in the range of 90 to 900 hours. The total period of continuous weighing is almost one year (6900 h). The number of steps were halved for Sample 2 so that two consecutive steps for Sample 1 together were equal to one step for Sample 2. From this it is possible to test whether steps may be superimposed as in a linear model. We have found that this was not the case in many instances. This means that the sorption process is not linear. This is a considerable complication.

In the second series for the thinner samples 3 and 4, the same steps in relative humidity were performed as in the first series. The time between step changes is relatively small compared to the first series. The total time was 1600 hours.

In the third series for Sample 3 the previous 8 steps were halved into 16 steps. The steps were performed in a rather fast succession. But the time at the highest relative humidity, 98%, was 400 hours. This was followed by 16 fast desorption steps. A single large step from 35% to 98% was made for Sample 4. The following desorption steps were a repetition of those in the second series to supplement failing parts of measurements.

In the fourth series, cyclic steps were introduced. This type of process, where the relative humidity changes between two levels, is quite important, since this occurs frequently in many natural situations.

The four first series were performed at room temperature, 20°C. In the fifth series cyclic steps at 5°C were tested. Then, at the end of the fifth series, and in the sixth series a few temperature shifts between 5°C and 20°C were tested.

In Chapter 6, all measured results are presented in 62 detailed diagrams. The moisture content is shown in the diagrams as function of continuous time, so evaluation of the prehistory from previous diagrams is possible. The sorption was recorded with one-hour intervals and the recorded moisture content is represented by a dot in the diagrams. This facilitates evaluation of the first, steep parts of the step responses.

In Chapter 7, observations, comparisons and analyses of the measured results are presented. There is a clear and occasionally intricate dependence of the moisture history. An example is a periodic sequence of steps. The response contains more retarded sorption, if the cyclic steps follow immediately after a step to a new higher level. Another effect is that the moisture difference between the two levels diminish with the number of cycles. This amplitude of the moisture exchange also diminishes with decreasing temperature. The amplitude between the same two RH levels is distinctly smaller at 5°C than at 20°C.

Swelling (and shrinkage) due to moisture changes have been measured in the fourth and fifth series. Tangential and radial swelling follow each other very well during the various sequences of RH. The ratio between radial and tangential strain is close to 0.60 at 20°C. A representative value of the ratio at 5°C is 0.65.

The tangential swelling $\varepsilon_t(t)$ is compared to the sorption $u(t)$ in Section 8.2. The measured points in an u–ε_t diagram fall on lines with quite constant slope. In the fourth and fifth series, cyclic steps were performed. The slope of the lines is quite close to 0.32 for these cyclic steps. The slope becomes higher in case of prominent retarded sorption caused by a step to a previously not attained level of humidity.

A major aim of this thesis is to study models for the retarded sorption. This is done in part III. The measurements impose various requirements on such a model. The immediately available moisture content is analysed in Section 9.1. From exponential fitting, it is concluded that the immediately available moisture content has a rather constant capacity as a function of relative humidity. This is contrary to the moisture equilibrium curve, for which the capacity increases strongly for high humidities. It is clear from the measurements that the sorption responses involve many time scales. It is natural to test functions that contain a number of exponentials with different decline times. This is done in Section 9.2. The amplitude of the exponentials are fitted to the sorption response curve. But it was not possible to get any consistent results. Based on this and on analyses of superposition of pulses, it is clear that a non-linear model must be used. It is also clear that it is necessary to use a number of internal nodes.

A sequence of models with increasing complexity has been tested. This is reported in Chapter 11. The Fickian model attains equilibrium very rapidly. The measured sorption, on the other hand, always exhibits changes during longer times, even during long intervals between steps. The measured sorption amplitude for cyclic steps is much smaller than the result from the Fickian model.

One internal node, connected by a constant conductance to the original outer node with its immediately accessible moisture capacity, is added. This gives a new time scale, which may be adjusted by changing the value of the conductance. Only one time scale for the response is obtained. But the measured responses contain many and varied time scales and the model is not sufficient.

The next step is to consider a model with a number of nodes in the cell wall and constant conductances between these. This model reaches a distinct equilibrium in simulations with long periods between steps. This behaviour is not reflected in the measurements.

It is clear that the conductances between the internal nodes must decrease inwards. This type of model gives acceptable results for most amplitudes of sorption, and it can also produce varied time scales. It is often poor in reproducing irregular combinations of steps. One such combination is a desorption step preceded by a series of absorption steps.

The above internal conductances are independent of the moisture difference between the nodes. This means that the models are linear. In the next kind of tested models, the conductances were made to depend on this difference. The models are non-linear, and the response becomes faster for large steps.

The non-linear model with one internal node produces rather erratic output for the cyclic steps, depending on the step amplitude. A model with five internal nodes and non-linear conductances gave quite good results. Responses are well reproduced both for the long and short time scales and with different combinations of steps. The model can also handle absorption-desorption scans of moderate amplitude.

The last type of model to be tested allowed for hysteresis also. The hysteresis is assumed to be dependent on the maximum attained RH-level. The previously tested non-linear models combined with hysteresis capacity functions were tested. These models performed better when the hysteresis was concentrated to the innermost node.

The overall best result was obtained for the non-linear model with five internal nodes and hysteresis in the innermost node.

References

Ahlgren L. (1972)
Moisture fixation in porous building materials. Report 36. Dept.of Building Materials, Lund University, Sweden.

Amdur E.J. White R.W. (1965)
Two-pressure relative humidity standards. *Humidity and Moisture*. Ed. Wexler A., New York Reinhold Publ., 3 445-454.

Avramidis S. Siau J. (1987)
An investigation of the external and internal resistance to moisture diffusion in wood. *Wood Sci. Tech.* 21, 249-256.

Barkas W. W. (1949)
The swelling of wood under stress. *HMSO*, London.

Basant Z. P. (1985)
Constitutive equation of wood at variable humidity and temperature. *Wood Sci. Tech.* 19, 159-177.

Bejan A. (1993)
Heat Transfer. John Wiley & Sons, Inc. , New York.

Boyd J. (1982)
New perspectives in wood anatomy. Nijhoff and Junk, 171-222.

Choong E. T. Skaar C . (1969)
Separating internal and external resistance to moisture removal in wood drying. *Wood Sci.* 1, 200-202.

Choong E. T. Skaar C . (1972)
Diffusivity and surface emissivity in wood drying. *Wood and Fibre Sci.* 4, 80-86.

Christensen G.N. (1959)
The rate of sorption of water vapor by wood and pulp. *Appita* 13, 112-123.

Christensen G.N. (1960)
Kinetics of sorption of water vapour by wood. *Austral. J. Appl. Sci.* 11:2, 295-304.

Christensen G.N. (1965)
The rate of sorption of water vapor by thin materials. *Humidity and Moisture*, Ed. Wexler A., New York Reinhold Publ., 4, 279-293.

Christensen G.N. (1967)
Sorption and Swelling within Wood Cell Walls. *Nature*, 13, 782.

Christensen G.N. Hergt H.F.A. (1969)
Effect of Previous History on Kinetics of Sorption By Wood Cell Walls. *J.of Polymer Sci.*, 7:2, 2427-30.

Christensen G.N. Kelsey K.E. (1959)
Die Geschwindigkeit der Wasserdampfsorption durch Holz. *Holz als Roh- und Werkstoff* 17, 178-188.

Claesson J. (1997)
Mathematical modelling of moisture transport. *Proc. from COST Action E8, Mechanical performance of Wood and Wood products, Theme: Wood – water relations.* Dept. of Structural Engineering and Materials. Technical University of Denmark.

Claesson J. Hagentoft C.-E. (1994)
Basic building physics. Mathematical modelling. Dept. of Building Physics, Lund University, Sweden.

Claesson J. Håkansson H. (1993)
Modelling of Moisture Flow in Wood. Fundamental Experiments and Analyses. *Proc. of the 3rd symposium, Building Pysics in the Nordic Countries,* Thermal Insulation Laboratory, Tech. Univ. of Denmark.

Claesson J. Håkansson H. (1996)
Modelling, measurements and analyses of transient sorption and moisture flow in wood. *Proc. of the 4th symposium, Building Pysics in the Nordic Countries,* VTT Building Technology, Espoo, Finland.

Claesson J. Håkansson H. Arfvidsson J. (1996)
Modelling of moisture flow in coated wood – recent results. *Proc. from a Nordic Conference, Wood – Paint – Moisture*, Stockholm, Sweden.

Comstock G. L. (1963)
Moisture diffusion cefficients in wood as calculated from adsorption, desorption and steady-state data. *Forest products J.* 13, 151-168

Cunningham M. J. (1995)
A model to explain 'anomalous' moisture sorption in wood under step under step function driving forces. *Wood and Fiber Sci.* 27, no. 3, 265-277.

Grigull U. (editor) (1979)
Properties of Water and Steam in SI-Units. Springer-Verlag, Berlin.

Eckert E. R. G. Drake R. M. Jr. (1959)
Heat and Mass Transfer. McGraw-Hill Book Co. New York

Hunt D.G. (1989)
Two classical theories combined to explain anomalies in wood behaviour. *J. Materials Sci.*, 8, 1474-76

Hunt D.G. (1990)
Longitudinal shrinkage – moisture relations in softwood. *J. Materials Sci.* 25, 3671-76.

Håkansson H. (1994a)
Experimentella studier av transient sorption i cellväggen i trä. (Experimental studies of transient sorption in the cell wall of wood) .(Report TABK--94/3021). Lund Institute of Technology, Dept. of Building Science.

Håkansson H. (1994b)
Time-dependent sorption and swelling in wood. *Proc. from Nordic Workshop, Moisture in Building materials and Constructions,* Trondheim, Norway.

Håkansson H. (1995a)
Experimentella studier av transient sorption i cellväggen i trä. Del II —Fortsatta mätningar. (Experimental studies of transient sorption in the cell wall of wood. Part II —Continued measurements). (Report TABK--95/3030). Lund Institute of Technology, Dept. of Building Science.

Håkansson H. (1995b)
A non-linear model for time-dependent moisture sorption in wood. (Report TABK--95/3031). Lund Institute of Technology, Dept. of Building Science.

Håkansson H. (1995c)
Time-dependent moisture sorption in wood. (Report TABK--95/1005). Lund Institute of Technology, Dept. of Building Science.

Håkansson H. (1995d)
Measurements of time-dependent sorption in wood. *Proc. from W40 Symposium on Moisture problems in Building Walls*, Porto, Portugal.

Håkansson H. (1995e)
Time-dependent sorption in wood. *Proc. from a Nordic Conference, Wood – Paint – Moisture*, Skellefteå, Sweden.

Kelly M. W. and Hart A. C. (1970)
Water vapour sorption rates by wood cell walls. *J. Materials Sci.* 1, 270-283.

Kelsey (1957)
The sorption of water vapour by wood. *Austral. J. Appl. Sci.*

Kielsgaard-Hansen K. (1986)
Sorption isotherms. A catalogue. Building Materials Laboratory. The Technical University of Denmark.

Krischer O. (1963)
Die Wissenschaftlichen Grundlagen der Trocknungstechnik. Springer-Verlag, Berlin.

McNamara S. W. Hart C. A. (1971)
An analysis of internal and average diffusion coefficients for unsteady-state movement of moisture in wood. *Wood Sci. Tech.* 4, 37-45.

Meylan B. A. (1972)
The influence of microfibril angle on the longitudinal shrinkage-moisture content relationship. Wood Sci. Tech., 6, 293-301.

Mårtensson A (1992)
Mechanical behaviour of wood exposed to humidity variations. Ph.D. Dissertation, Dept. of Structural Eng., Lund University, Sweden.

Nevander L.-E. Elmarsson B. (1994)
Fukthandbok. Svensk Byggtjänst, Stockholm, Sweden.

Nilsson L.-O. (1988)
Fukttransportegenskaper hos trä och träbaserade skivor, (Properties of moisture transport for wood and wood-based boards) P-88:4 Dept. of Building Materials, Chalmers University, Sweden.

Nilsson L.-O. (1990)
Fukttransportegenskaper hos furu, gran och träbaserade skivor. (Properties of moisture transport for pine, spruce and wood-based boards) P-90:5, Dept. of Building Materials, Chalmers University, Sweden.

Park G. S. (1968)
The glassy state and slow process anomalies. Diffusion in polymers, New York, Academic press.

Persson K. (1997)
Modelling of wood properties by a micro-mechanical approach. Div. of Structural Mechanics. Lund Univ. Sweden.

Petersson H. Dahlblom O. Ormarsson S. Persson K. (1997)
Moisture distortion modelling of wood and structural timber. *Proc. from COST Action E8, Mechanical performance of Wood and Wood products, Theme: Wood – water relations*. Dept. of Structural Engineering and Materials. Technical University of Denmark.

Pitts D. R. Sissom L. E. (1977)
Theory and Problems of Heat Transfer. McGraw-Hill Book Co. New York.

Prichananda C. (1966)
A study of some aspects of sorption dynamics in wood. Ph.D. Dissertation SUNY-CESF.

Rogers C. E. (1965)
Physics and chemistry of organic solid state. Vol II, New York, Interscience Publishers.

Siau J. F. (1984)
Transport processes in wood. Springer-Verlag, Berlin.

Skaar C. (1988)
Wood -water relations. Springer-Verlag, Berlin.

Stamm A. S. (1964)
Wood and cellulose science. The Ronald Press Company, New York.

Svensson S. (1997)
Intenal Stress in Wood Caused by Climate Variations, Ph.D. Dissertation, Dept. of Structural Eng., Lund University. Sweden.

The Institute of Measurement and Control (1996)
A guide to the measurement of humidity. ISBN 0-904457-24-9 London.

Time B. (1998)
Hygroscopic Moisture Transport in Wood. Ph.D. Dissertation, Norwegian University of Science and Technology, Dept. of Building and Construction Engineering, Trondheim.

Toratti T. Svensson S. (1998)
Mechano-sorptive experiments perpendicular to grain under tensile and compressive loads. *Wood Sci. and Tech.* Submitted for publication.

Wadsö L. (1993)
Studies of Water Vapor Transport and Sorption in Wood. Ph.D. Dissertation, Dept.of Building Materials, Lund University, Sweden.

Wadsö L. (1994)
Describing non-Fickian water-vapour sorption in wood. *J. Materials Sci.* 29, 2367-2372.

Wadsö L. (1997)
Sorption på lignocelluloser. (in Swedish) Tech. Univ. of Denmark, Dept. of Struct. Eng. and Materials.

Villadsen J. (1993)
Water vapour transmission properties of wood - Determined by the cup method. *Proc. of the 3rd symposium, Building Pysics in the Nordic Countries,* Thermal Insulation Laboratory, Tech. Univ. of Denmark.

Appendix A

Solution of coupled equations for moisture content $u(t)$ and temperature $T(t)$ for a small body.

Non-linear general solution according to Section 3.3.

Expression for sorption isotherm. (0<T<80°C)

Constants:

$$A(T) := 1.7 - 0.01 \cdot T \qquad B(T) := 19.1 + 0.00025 \cdot T^2 \qquad u_{max}(T) := 0.52 - 0.001 \cdot T$$

Constants C and D, derived from A(T) , B(T) and u_{max}

$$C(T) := e^{-e^{A(T) - B(T) \cdot u_{max}(T)}} - e^{-e^{A(T)}} \qquad D(T) := e^{-e^{A(T)}}$$

Sorption isotherm:

$$u(\varphi, T) := \frac{(A(T) - \ln(-\ln(C(T) \cdot \varphi + D(T))))}{B(T)}$$

Inverse of sorption isotherm:

$$\varphi(u, T) := \frac{1}{C(T)} \cdot \exp(-\exp(A(T) - B(T) \cdot u)) - D(T)$$

Derivatives: ($\frac{du}{d\varphi}$ is designated dudφ)

$$dud\varphi(\varphi, T) := \frac{C(T)}{B(T)} \cdot \frac{1}{-\ln(C(T) \cdot \varphi + D(T))} \cdot \frac{1}{C(T) \cdot \varphi + D(T)}$$

$$d\varphi du(u, T) := \frac{B(T)}{C(T)} \cdot \exp(A(T) - B(T) \cdot u - \exp(A(T) - B(T) \cdot u))$$

Expression for water vapour content in saturated air. (0<T<80°C)

$$a_1 := -6050 \quad a_2 := 14.835 \quad a_3 := -0.0268 \quad a_4 := 0.0000172 \quad a_5 := 1.43$$

$$v_{sat}(T) := \exp\left[\frac{a_1}{T + 273.15} + a_2 + a_3 \cdot (T + 273.15) + a_4 \cdot (T + 273.15)^2 + a_5 \cdot \ln(T + 273.15)\right]$$

Vapour content v(u,T) :

$$v(u, T) := v_{sat}(T) \cdot \varphi(u, T)$$

Primary input data:

$$T_{inlet} := 20 \qquad \varphi_{inlet} := 0.85 \qquad T_{init} := 20 \qquad \varphi_{init} := 0.75 \qquad m := 0.0077$$

$$A_{surf} := 0.0178 \qquad D_v := 4 \cdot 10^{-6} \qquad L_{eq} := 0.68 \cdot 10^{-3} \qquad c := 2000 \qquad h_{evap} := 2.26 \cdot 10^{6}$$

$$\alpha_c := 12 \qquad \alpha_r := 4 \qquad \alpha_{tot} := \alpha_c + \alpha_r \qquad \beta := \frac{\alpha_c}{1200} \qquad Vdot := 0.066 \cdot 10^{-3}$$

Auxiliary data:

$\alpha_{tot} = 16$ $\beta_{vtot} := \frac{1}{\frac{A_{surf}}{Vdot} + \frac{1}{\beta} + \frac{L_{eq}}{D_v}}$ $\beta_{vtot} = 1.8529 \cdot 10^{-3}$

$v_{sat}(T_{init}) = 0.01729$ $\frac{d}{dT_{inlet}} v_{sat}(T_{inlet}) = 1.0124 \cdot 10^{-3}$ $dud\varphi(\varphi_{inlet}, T_{init}) = 0.3759$

$u_{inlet} := u(\varphi_{inlet}, T_{init})$ $u_{init} := u(\varphi_{init}, T_{init})$ $u_{inlet} = 0.1733$ $u_{init} = 0.1436$

$v_{inlet} := v(u_{inlet}, T_{inlet})$ $v_{init} := v(u_{init}, T_{init})$ $v_{inlet} = 0.0147$ $v_{init} = 0.013$

Coupled differential equations for u(t) and T(t):

Initial conditions in vector y: $y_1 = u$ $y_2 = T$.
Differential equations with respect to t in vector D.

$y_1 := u_{init}$ $y_2 := T_{init}$

$$D(t,y) := \begin{bmatrix} \frac{\beta_{vtot} \cdot A_{surf}}{m} \cdot (v_{inlet} - v(y_1, y_2)) \\ \frac{\alpha_{tot} \cdot A_{surf}}{m \cdot c} \cdot (T_{inlet} - y_2) + \frac{\beta_{vtot} \cdot A_{surf} \cdot h_{evap}}{m \cdot c} \cdot (v_{inlet} - v(y_1, y_2)) \end{bmatrix}$$

The function rkfixed(y, 0, tmax, N, D) is solving the equations based on the Runge-Kutta method. The endpoints of the evaluated interval are 0 and tmax. N is the number of points at which the solution is to be approximated.

Solution:

$N := 1800$ $tmax := 18000$ $Z := rkfixed(y, 0, tmax, N, D)$ $i := 1 .. N$ $t_i := Z_{i,1}$ $u_i := Z_{i,2}$ $T_i := Z_{i,3}$

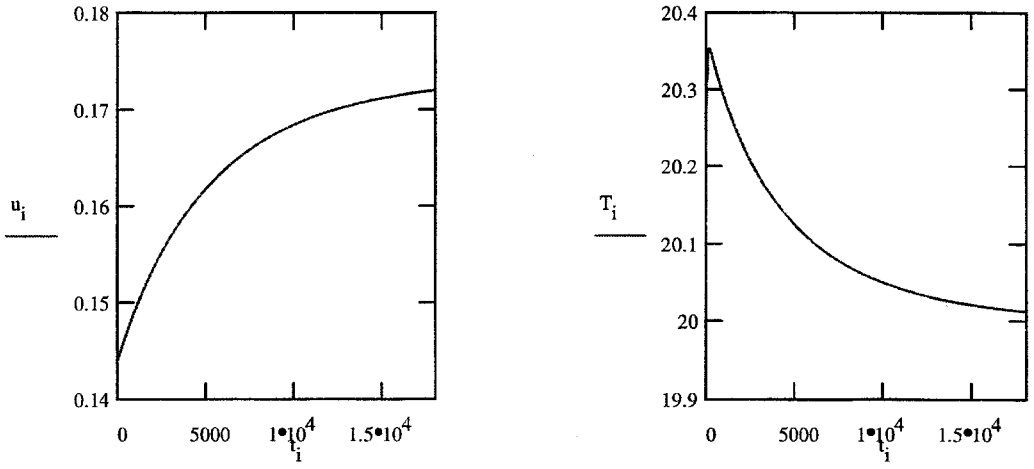

The moisture content u(t) and the temperature T(t) during 5 h

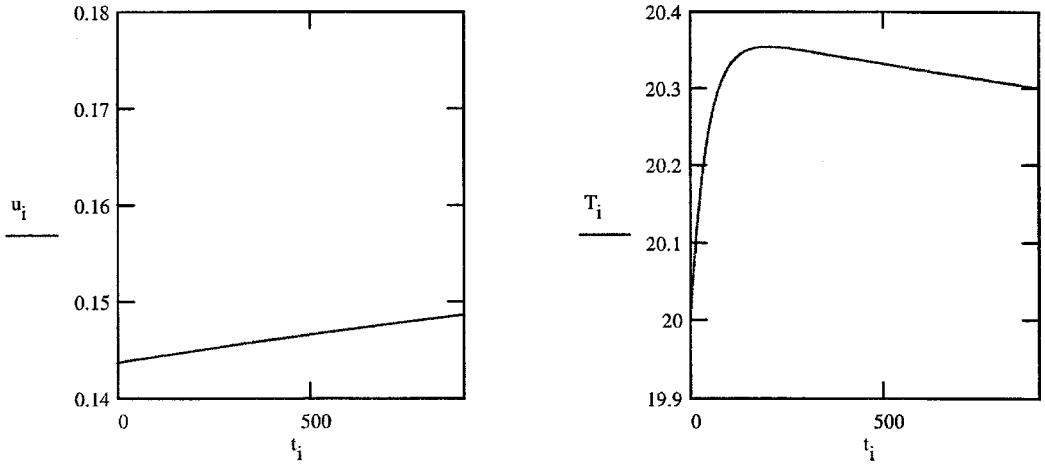

The moisture content u(t) and the temperature T(t) for the initial period

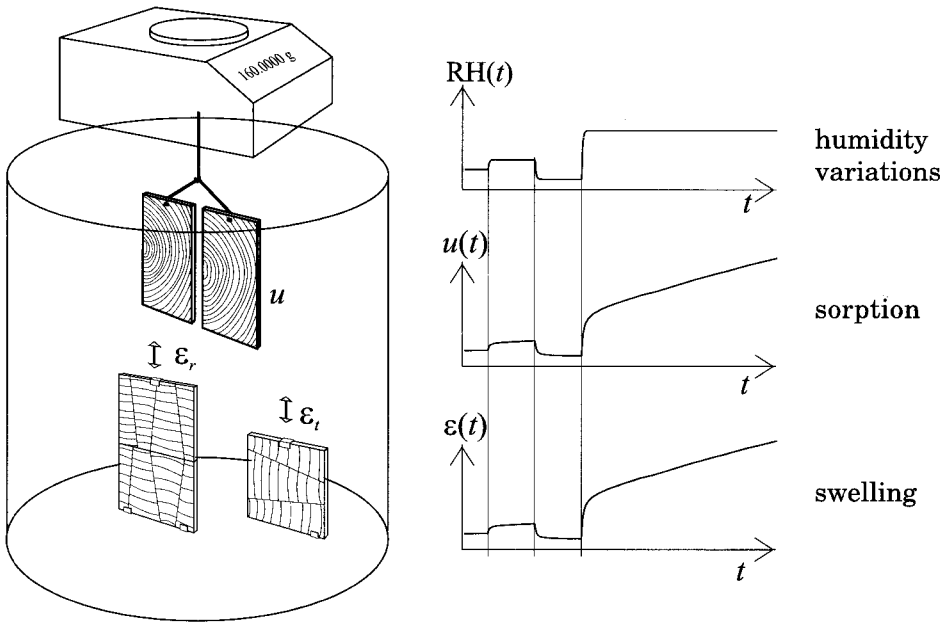

ISRN LUTADL/TABK--1012--SE